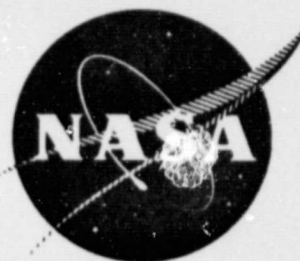


N O T I C E

THIS DOCUMENT HAS BEEN REPRODUCED FROM
MICROFICHE. ALTHOUGH IT IS RECOGNIZED THAT
CERTAIN PORTIONS ARE ILLEGIBLE, IT IS BEING RELEASED
IN THE INTEREST OF MAKING AVAILABLE AS MUCH
INFORMATION AS POSSIBLE

NASA CR-135266
R76AEG379-1



QUIET CLEAN SHORT-HAUL EXPERIMENTAL ENGINE
(QCSEE)

**ACOUSTIC TREATMENT
DEVELOPMENT AND DESIGN**

MAY 1979

by

ART CLEMONS

(NASA-CR-135266) QUIET CLEAN SHORT-HAUL
EXPERIMENTAL ENGINE (QCSEE): ACOUSTIC
TREATMENT DEVELOPMENT AND DESIGN (General
Electric Co.) 353 p HC A16/MF A01 CSCL 21E

N80-15122

Unclas
G3/07 33505

Prepared For

National Aeronautics and Space Administration

NASA-Lewis Research Center
NAS3-18021



1. Report No. NASA CR-135266	2. Government Accession No.	3. Recipient's Catalog No.	
4. Title and Subtitle QUIET CLEAN SHORT-HAUL EXPERIMENTAL ENGINE (QCSEE) Acoustic Treatment Development and Design		5. Report Date May 1979	
		6. Performing Organization Code	
7. Author(s) Art Clemons		8. Performing Organization Report No. R76AEG379-1	
		10. Work Unit No.	
9. Performing Organization Name and Address General Electric Company Aircraft Engine Group Cincinnati, Ohio 45215		11. Contract or Grant No. NAS3-18021	
		13. Type of Report and Period Covered Contractor Report	
12. Sponsoring Agency Name and Address National Aeronautics and Space Administration Washington, D.C. 20546		14. Sponsoring Agency Code	
15. Supplementary Notes Acoustic Treatment Design Report Project Manager: C.C. Ciepluch, QCSEE Project Office Technical Adviser: Irv Loeffler, NASA-Lewis Research Center, Cleveland, Ohio 44135			
16. Abstract Acoustic treatment designs for the QCSEE engines are defined in this report. The procedures used in the development of each noise-source suppressor device are presented and discussed in detail. A complete description of all treatment concepts considered and the test facilities utilized in obtaining background data used in treatment development are also described. Additional supporting investigations that are complementary to the treatment development work are presented. The expected suppression results for each treatment configuration are given in terms of ASPL versus frequency and in terms of Δ PNdB.			
17. Key Words (Suggested by Author(s)) Acoustic Treatment, Engine System Noise, Constituents, Fan and Core Noise, Suppression Resonators, Frequency, Duct Height, Treatment Length			
19. Security Classif. (of this report) Unclassified	20. Security Classif. (of this page) Unclassified	21. No. of Pages 333	22. Price

* For sale by the National Technical Information Service, Springfield, Virginia 22151

TABLE OF CONTENTS

<u>Section</u>		<u>Page</u>
1.0	SUMMARY	1
2.0	INTRODUCTION	2
3.0	DEFINITION OF SUPPRESSION REQUIREMENTS	4
3.1	Unsuppressed UTW Engine Spectra	4
3.1.1	Fan Inlet Spectra	4
3.1.2	Fan Exhaust Spectra	9
3.1.3	Core Noise Spectra	9
3.2	Unsuppressed OTW Engine Spectra	9
3.2.1	Fan Inlet Spectra	9
3.2.2	Fan Exhaust Spectra	9
3.2.3	Core Noise Spectra	9
3.3	System Constituent Noise Levels and Suppression Level Requirements	17
3.3.1	UTW Engine Component Noise Levels and Required Suppression	17
3.3.2	OTW Engine Component Noise Levels and Required Suppression	26
4.0	SUMMARY OF PROGRAM ELEMENTS AND TEST FACILITIES	28
4.1	Fan Exhaust Duct Facilities and Tests	28
4.2	Fan Exhaust Treatment Testing on Scale Model Fan Vehicle	28
4.3	Fan Inlet Treatment Testing on Scale Model Fan Vehicle	34
4.4	Core Exhaust Duct Facility and Tests	34
5.0	FAN EXHAUST TREATMENT DEVELOPMENT AND DESIGN	42
5.1	Acoustic Duct Tests	42
5.1.1	Phased Treatment Concept	42
5.1.2	Porosity Optimization	42
5.2	Scale Model Rotor 55 Vehicle Tests	52
5.2.1	Constant-Depth Treatment Configurations	71
5.2.2	Variable-Depth Treatment Configurations	75
5.2.2.1	Constant Porosity	75
5.2.2.2	Mixed Porosity	75
5.2.3	Comparison of Variable and Constant-Depth Panel	81
5.2.4	Acoustic Splitter Simulation	81
5.2.5	Treatment Area Effectiveness	89
5.2.6	Variable-Depth Treatment Orientation	97

TABLE OF CONTENTS (Continued)

<u>Section</u>		<u>Page</u>
5.3	Engine Boilerplate Treatment Design and Suppression Estimates	101
6.0	FAN INLET TREATMENT DEVELOPMENT AND DESIGN	109
6.1	Scale Model Inlet Tests	109
6.1.1	Description of Inlet Treatment Configurations	109
	6.1.1.1 Accelerating Inlets	109
	6.1.1.2 Low Mach Inlets	109
6.1.2	Treatment Designs	118
	6.1.2.1 Accelerating Inlet Treatment	118
	6.1.2.2 Low Mach Inlet Treatment	120
6.1.3	Suppression Results	126
	6.1.3.1 Accelerating Inlet Suppression	126
	6.1.3.2 Low Mach Inlet Suppression	136
6.2	Engine Boilerplate Inlet Treatment Design and Suppression Estimates	148
6.2.1	Unsuppressed Spectra and Tuning Frequency Requirements	148
	6.2.1.1 Unsuppressed Spectra	148
	6.2.1.2 Noy-weighted Spectra-Treatment Tuning Frequency Requirements	153
6.2.2	Definition of Inlet Design and Predicted Suppression	158
7.0	CORE EXHAUST SUPPRESSOR DESIGN	169
7.1	Definition of Concepts to Be Evaluated	169
7.2	Acoustic Duct Tests	169
	7.2.1 Test Facilities	173
	7.2.2 Data Results	173
	7.2.2.1 Cold Flow Duct	173
	7.2.2.2 High-Temperature Duct	209
7.3	Definition of Engine Core Treatment Design and Suppression Estimates	224
	7.3.1 Suppressor Concept Selection	224
	7.3.2 Suppressor Design Definition	225
	7.3.3 Engine Suppression Estimates	231

TABLE OF CONTENTS (Concluded)

<u>Section</u>	<u>Page</u>
8.0	238
ADDITIONAL SUPPORTING INVESTIGATIONS	
8.1	238
Flow Noise Regeneration	
8.1.1	238
Preliminary Analysis	
8.1.2	241
Rotor 55 Flow Noise Investigation	
8.2	243
Composite Faceplate Materials	
8.2.1	247
Composite Materials Test	
8.2.2	247
Test Results	
8.3	257
Composite Nacelle Flexible Joint Transmission Loss Study	
8.3.1	257
Identification of Nacelle Flex Joints	
8.3.2	263
Transmission Loss Test Arrangement	
8.3.3	263
Transmission Loss Test Results	
8.3.4	263
Data Analysis and Application to Engine Configuration	
9.0	275
NOMENCLATURE	
APPENDIX A —	277
Sound Transmission Loss Tests Lab Report	
APPENDIX B —	285
Acoustic Design Procedure for Bulk Absorber Fan Inlet Treatment	
REFERENCES	332

LIST OF ILLUSTRATIONS

<u>Figure</u>		<u>Page</u>
1.	QCSEE Noise Goals.	5
2.	UTW Takeoff Fan Inlet Spectra, Hard-Wall Accelerating Inlet.	6
3.	UTW Approach Unsuppressed Fan Inlet Spectra, Baseline Bellmouth Inlet.	7
4.	UTW Reverse Thrust Unsuppressed Fan Inlet Spectra.	8
5.	UTW Takeoff Unsuppressed Fan Exhaust Spectra.	10
6.	UTW Takeoff Unsuppressed Predicted Core Noise Spectra.	11
7.	OTW Unsuppressed Fan Inlet Spectra at Takeoff Power.	12
8.	OTW Unsuppressed Fan Inlet Spectra at Approach Power.	13
9.	OTW Unsuppressed Fan Exhaust Spectra at Takeoff Power.	14
10.	OTW Unsuppressed Fan Exhaust Spectra at Approach Power.	15
11.	OTW Unsuppressed Core Noise Spectra.	16
12.	Summary Unsuppressed and Required Suppressed Levels of Noise Constituents for UTW Engine at Takeoff Power.	18
13.	Summary Unsuppressed and Required Suppressed Levels of Noise Constituents for UTW Engine at Approach Power.	19
14.	Summary UTW Reverse Thrust Unsuppressed and Required Suppressed Levels of Noise Constituents.	20
15.	Summary UTW Reverse Thrust Unsuppressed and Required Suppressed Levels of Noise Constituents.	21
16.	Summary Unsuppressed and Required Suppressed Levels of Noise Constituents for OTW Engine at Takeoff Power.	22
17.	Summary Unsuppressed and Required Suppressed Levels of Noise Constituents for OTW Engine at Approach Power.	23
18.	Summary Unsuppressed and Required Suppressed Levels of Noise Constituents for OTW Engine at Reverse Thrust.	24

LIST OF ILLUSTRATIONS (Continued)

<u>Figure</u>		<u>Page</u>
19.	Schematic of Rectangular Cold Flow Laboratory Duct Facility.	29
20.	Instrumentation of Rectangular Cold Flow Duct Facility.	30
21.	Schematic of the General Electric-Schenectady Anechoic Chamber, Fan Exhaust Test Configuration.	31
22.	Scale Model Fan Test Vehicle Schematic.	32
23.	Installed Test Vehicle Schematic.	33
24.	Schematic of General Electric Research and Development Center Anechoic Chamber.	35
25.	Photo of Anechoic Chamber.	36
26.	Cross Section of UTW Variable-Pitch Fan.	37
27.	Assembly of UTW Simulator Test Stand.	38
28.	High-Temperature Acoustic Duct Facility Component Details.	40
29.	Instrumentation of High-Temperature Acoustic Duct Facility.	41
30.	Definition of Duct Variable-Depth Treatment Configurations.	43
31.	Corrected Transmission Loss Vs. Frequency for Variable-Depth Treatment; Configuration with 12% Porosity.	44
32.	Corrected Transmission Loss Vs. Frequency for Variable-Depth Treatment; Configuration with 12% Porosity.	45
33.	Corrected Transmission Loss Vs. Frequency for Variable-Depth Treatment; Configuration with 12% Porosity.	46
34.	Corrected Transmission Loss Vs. Frequency for Variable-Depth Treatment; Configuration with 27% Porosity.	47
35.	Corrected Transmission Loss Vs. Frequency for Variable-Depth Treatment; Configuration with 27% Porosity.	48

LIST OF ILLUSTRATIONS (Continued)

<u>Figure</u>		<u>Page</u>
36.	Corrected Transmission Loss Vs. Frequency for Variable-Depth Treatment; Configuration with 27% Porosity.	49
37.	Corrected Transmission Loss Vs. Frequency for Variable-Depth Treatment, 12% and 27% Porosities.	50
38.	Definition of Acoustic Duct Constant-Depth Treatment Configurations.	51
39.	Corrected Transmission Loss Vs. Frequency for Mach Number Variations, 3.6% Porosity.	55
40.	Corrected Transmission Loss Vs. Frequency for Mach Number Variations, 5% Porosity.	56
41.	Corrected Transmission Loss Vs. Frequency for Mach Number Variations, 7.5% Porosity.	57
42.	Corrected Transmission Loss Vs. Frequency for Mach Number Variations, 10% Porosity.	58
43.	Corrected Transmission Loss Vs. Frequency for Mach Number Variations, 14.5% Porosity.	59
44.	Corrected Transmission Loss Vs. Frequency for Mach Number Variations, 5% Porosity.	60
45.	Corrected Transmission Loss Vs. Frequency for Mach Number Variations, 7.5% Porosity.	61
46.	Corrected Transmission Loss Vs. Frequency for Mach Number Variations, 10% Porosity.	62
47.	Corrected Transmission Loss Vs. Frequency for Mach Number Variations, 14.5% Porosity.	63
48.	Corrected Transmission Loss Vs. Frequency for Mach Number Variations, 22.7% Porosity.	64
49.	Corrected Transmission Loss Vs. Frequency for Mach Number Variations, 7.5% Porosity.	65
50.	Corrected Transmission Loss Vs. Frequency for Mach Number Variations, 10% Porosity.	66

LIST OF ILLUSTRATIONS (Continued)

<u>Figure</u>		<u>Page</u>
51.	Corrected Transmission Loss Vs. Frequency for Mach Number Variations, 14.5% Porosity.	67
52.	Corrected Transmission Loss Vs. Frequency for Mach Number Variations, 22.7% Porosity.	68
53.	Corrected Transmission Loss Vs. Frequency for Mach Number Variations, 27% Porosity.	69
54.	Optimum Faceplate Porosity Vs. H/λ_0 for an SDOF Configuration.	70
55.	Measured Suppression Vs. Porosity for Constant-Depth Liner.	72
56.	Measured Suppression Spectra at Two Fans Speeds, 12% Porosity for Constant Depth Liner.	73
57.	Measured Suppression Vs. Spectra at Two Fan Speeds, 27% Porosity for Constant Depth Liner.	74
58.	Predicted Vs. Measured Suppression Spectra: Constant Depth, 12% Porosity Panels.	76
59.	Measured Suppression Vs. Porosity for Variable-Depth Liner.	77
60.	Variable-Depth, Constant-Porosity and Variable-Depth, Variable-Porosity Configurations.	78
61.	Measured Suppression with Constant Vs. Variable Porosity.	79
62.	Suppression Spectra for Individual Panels Vs. H/λ_0 .	80
63.	Constant-Depth and Variable-Depth Treatment Configurations.	82
64.	Measured Suppression Spectra for Constant Vs. Variable Panel Depth.	83
65.	Predicted Vs. Measured Suppression Spectra: Variable-Depth, Mixed-Porosity Panels.	84
66.	Predicted Vs. Measured Suppression Spectra, Splitter Simulation, 12% Porosity Panels.	85

LIST OF ILLUSTRATIONS (Continued)

<u>Figure</u>		<u>Page</u>
67.	Constant Thickness, Variable-Depth, and Splitter Simulation Treatment Configurations.	86
68.	Splitter Simulation Vs. Constant-Depth Wall Treatment.	87
69.	Splitter Simulation Compared to Treatment with Variable Depth on Both Walls.	88
70.	Configurations With and Without Reduced Treatment Area.	90
71.	Suppressed and Unsuppressed Spectra for Different Treatment Areas.	91
72.	Predicted Vs. Measured Suppression Loss Resulting from Reduced Treatment Area.	92
73.	Suppression Vs. L/H (Actual).	93
74.	Measured Suppression for Rotor-OGV Treatment.	95
75.	Measured Suppression of Fully Treated Fan Exhaust With and Without Rotor-OGV Treatment.	96
76.	Thin/Thick Vs. Thick/Thin Variable-Depth Treatment Configurations.	98
77.	Effect of Treatment Orientation on Suppression.	99
78.	Suppression Spectra for Thin/Thick Vs. Thick/Thin Treatment.	100
79.	Rotor 55 and QCSEE UTW Rotor-OGV Treatment.	102
80.	Model and Engine Aft Duct Treatment Configurations.	103
81.	Adjusted Predictions Vs. Measured Suppressed Spectra, Variable-Depth, Mixed-Porosity Panels.	104
82.	Adjusted Prediction Vs. Measured Suppression Spectra, Splitter Simulation, 12% Porosity Panels.	106
83.	UTW Boilerplate No. 1 Treatment Configuration.	107
84.	UTW Boilerplate No. 1 Noy-Weighted Suppressed Fan Exhaust Spectrum.	108

LIST OF ILLUSTRATIONS (Continued)

<u>Figure</u>		<u>Page</u>
85.	Predicted Reverse Thrust UTW Engine Noise Spectra at 86% N_{FC} , 60° to Inlet.	112
86.	Reverse Thrust Acoustic Reactance Vs. Frequency for Accelerating Inlet Treatments A and B.	113
87.	Reverse Thrust Acoustic Reactance Vs. Frequency for Accelerating Inlet Treatments C and D.	114
88.	Forward Thrust Acoustic Reactance Vs. Frequency for Accelerating Inlet Treatments A and B.	115
89.	Forward Thrust Acoustic Reactance Vs. Frequency for Accelerating Inlet Treatments C and D.	116
90.	UTW Takeoff Fan Inlet Spectra, Hard-Wall Accelerating Inlet.	121
91.	Predicted Unsuppressed Forward Thrust UTW Fan Spectra at 100% N_{FC} , 60° to Inlet for the Low Mach No. Inlet.	122
92.	Forward Thrust Acoustic Reactance Vs. Frequency for Low Mach No. Inlet Treatments A and C.	124
93.	Reverse Thrust Acoustic Reactance Vs. Frequency for Low Mach No. Inlet Treatments A and C.	125
94.	Reverse Thrust PNL Directivity, All Accelerating Inlets at 86% N_{FC} .	127
95.	Reverse Thrust 1/3-OBSPL Spectra, All Accelerating Inlets at 86% N_{FC} , 60° to Inlet.	128
96.	Forward Thrust PNL Vs. Percent Fan Speed, Baseline Bellmouth Inlet and Accelerating Inlets, Hard Wall, Treatments B and D.	129
97.	Forward Thrust PNL Directivity, Accelerating Inlet Hard Wall, Treatments B and D at 0.79 (Takeoff) Throat Mach No.	131
98.	Forward Thrust 1/3-OBSPL Spectra, Accelerating Inlet Hard Wall, Treatments B and D at 0.79 (Takeoff) Throat Mach No., 60° to Inlet.	132

LIST OF ILLUSTRATIONS (Continued)

<u>Figure</u>		<u>Page</u>
99.	Forward Thrust 1/3-OBSPL Spectra, Accelerating Inlet Hard Wall, Treatments B and D at 0.79 (Takeoff) Throat Mach No., 70° to Inlet.	133
100.	Forward Thrust 1/3-OBSPL Spectra, Accelerating Inlet Hard Wall, Treatments B and D at 0.79 (Takeoff) Throat Mach No., 50° to Inlet.	134
101.	Forward Thrust PNL Directivity, Accelerating Inlet Hard Wall, Treatments B and D at 70% N _{FC} .	135
102.	Forward Thrust 1/3-OBSPL Spectra, Accelerating Inlet Hard Wall, Treatments B and D at 70% N _{FC} , 60° to Inlet.	137
103.	Forward Thrust PNL Vs. Percent Fan Speed, All Low Mach No. Inlets.	138
104.	Fwd Thrust Directivity, All Low Mach No. Inlets at 70% N _{FC} .	139
105.	Forward Thrust 1/3-OBSPL Spectra, All Low Mach No. Inlets at 70% N _{FC} , 60° to Inlet.	140
106.	Forward Thrust 1/3-OBSPL Spectra, All Low Mach No. Inlets at 98.5% N _{FC} .	141
107.	Forward Thrust 1/3-OBSPL Spectra, All Low Mach No. Inlets at 98.5% N _{FC} , 60° to Inlet.	142
108.	Forward Thrust 1/3-OBSPL Suppression Spectra, Low Mach No. Inlet Treatments A, B, and C at 70% N _{FC} , 60° to Inlet.	144
109.	Forward Thrust 1/3-OBSPL Suppression Spectra, Low Mach No. Inlet Treatments A, B, and C at 99.5% N _{FC} , 60° to Inlet.	145
110.	Reverse Thrust PNL Vs. Percent Fan Speed - All Low Mach No. Inlets.	146
111.	Reverse Thrust PNL Directivity, All Low Mach No. Inlets at 86% N _{FC} .	147
112.	Reverse Thrust 1/3-OBSPL Spectra, All Low Mach No. Inlets at 86% N _{FC} , 60° to Inlet.	149

LIST OF ILLUSTRATIONS (Continued)

<u>Figure</u>		<u>Page</u>
113.	Reverse Thrust 1/3-OBSPL Spectra, All Low Mach No. Inlets at 60% N_{FC} , 60° to Inlet.	150
114.	Reverse Thrust 1/3-OBSPL, All Low Mach No. Inlets at 100% N_{FC} , 60° to Inlet.	151
115.	Unsuppressed UTW Reverse Thrust Fan Spectra, Prediction Vs. Measured.	152
116.	Unsuppressed UTW Takeoff Thrust Fan Spectra, Prediction Vs. Measured.	154
117.	Unsuppressed UTW Approach Thrust Fan Spectra, Prediction Vs. Measured.	155
118.	Reverse Thrust Spectra.	156
119.	Hard-Wall Accelerating Inlet Spectra.	157
120.	Unsuppressed Spectra, Bellmouth Inlet.	159
121.	UTW Reverse Thrust Suppression Spectra.	160
122.	UTW Predicted Suppression Spectrum.	162
123.	UTW Forward Thrust Suppression Spectra.	163
124.	UTW Suppression Spectra.	164
125.	UTW Boilerplate No. 1 Fan Inlet Treatment Design.	166
126.	Predicted Acoustic Reactance Vs. Optimum Reactance.	168
127.	Predicted Core Noise Spectra.	170
128.	Compact Suppressor Concepts.	171
129.	Suppressor Envelope Definition.	172
130.	Schematic of Rectangular Cold Flow Duct Facility.	174
131.	Instrumentation of Rectangular Cold Flow Duct Facility.	175
132.	Schematic of High-Temperature Acoustic Duct Facility.	176

LIST OF ILLUSTRATIONS (Continued)

<u>Figure</u>		<u>Page</u>
133.	Instrumentation of High-Temperature Acoustic Duct Facility.	177
134.	Sketch of Quarter-Wave Suppressor Test Trays.	178
135.	Definition of Quarter-Wave Suppressor Configurations.	180
136.	Cold Flow Acoustic Duct Data, Hard-Wall Baseline Configuration 1.	181
137.	Cold Flow Acoustic Duct Data, Configuration 2 Folded Quarter-Wave Resonator, 12.7 cm (5.0 in.), Slots on One Side, L/H = 6.75.	182
138.	Cold Flow Acoustic Duct Data, Configuration 3 Folded Quarter-Wave Resonator, 12.7 cm (5.0 in.), Slots Forward, L/H = 6.75.	183
139.	Cold Flow Acoustic Duct Data, Configuration 4 Folded Quarter-Wave Resonator, 12.7 cm (5.0 in.), Slots Aft, L/H = 6.75.	184
140.	Cold Flow Acoustic Duct Data, Configuration 5 Folded Quarter-Wave Resonator, 12.7 cm (5.0 in.), Slots Forward, L/H = 4.05.	185
141.	Cold Flow Acoustic Duct Data, Configuration 6 Folded Quarter-Wave Resonator, 10.2 cm (4.0 in.), Slots Forward, L/H = 4.6.	186
142.	Cold Flow Acoustic Duct Data, Configuration 7 Folded Quarter-Wave Resonator, 7.62 cm (3.0 in.), Slots Forward, L/H = 3.8.	187
143.	Cold Flow Acoustic Duct Data, Configuration 8 Folded Quarter-Wave Resonator, 7.62 cm (3.0 in.), and 12.7 cm (5.0 in.), Slots Forward, L/H = 4.5.	189
144.	Definition of Dual-Layer SDOF Dissipative Treatment Test Configurations.	190
145.	Cold Flow Acoustic Duct Data, Configuration 2 Dual-Layer SDOF Treatment, L/H = 3.6.	191
146.	Cold Flow Acoustic Duct Data, Configuration 3 Dual-Layer SDOF Treatment, L/H = 3.6.	192

LIST OF ILLUSTRATIONS (Continued)

<u>Figure</u>		<u>Page</u>
147.	Cold Flow Acoustic Duct Data, Configuration 4 Dual-Layer SDOF Treatment, L/H = 3.6.	193
148.	Cold Flow Acoustic Duct Data, Configuration 5 Dual-Layer SDOF Treatment, L/H = 3.6.	194
149.	Cold Flow Acoustic Duct Data, Configuration 6 Dual-Layer SDOF Treatment, L/H = 2.4.	195
150.	Cold Flow Acoustic Duct Data, Configuration 7 Dual-Layer SDOF Treatment, L/H = 3.6.	196
151.	Cold Flow Acoustic Duct Data, Configuration 8 Dual-Layer SDOF Treatment, L/H = 3.6.	197
152.	Cold Flow Acoustic Duct Data, Configuration 9 Dual-Layer SDOF Treatment, L/H = 3.6.	198
153.	Summary of Dual-Layer SDOF Treatment Suppression Vs. Porosity.	2
154.	Cold Flow Acoustic Duct Data, Folded Quarter-Wave Suppressor (Two Sides Treated), Mach No. = 0.	201
155.	Cold Flow Acoustic Duct Data, Folded Quarter-Wave Suppressor (Two Sides Treated), Mach No. = 0.2.	202
156.	Cold Flow Acoustic Duct Data, Folded Quarter-Wave Suppressor (Two Sides Treated), Mach No. = 0.3.	203
157.	Cold Flow Acoustic Duct Data, Folded Quarter-Wave Suppressor (Two Sides Treated), Mach No. = 0.4.	204
158.	Cold Flow Acoustic Duct Data, Dual-Layer SDOF Treatment (Two Sides Treated), Mach No. = 0.	205
159.	Cold Flow Acoustic Duct Data, Dual-Layer SDOF Treatment (Two Sides Treated), Mach No. = 0.2.	206
160.	Cold Flow Acoustic Duct Data, Dual-Layer SDOF Treatment (Two Sides Treated), Mach No. = 0.3.	207

LIST OF ILLUSTRATIONS (Continued)

<u>Figure</u>		<u>Page</u>
161.	Cold Flow Acoustic Duct Data, Dual-Layer SDOF Treatment (Two Sides Treated), Mach No. = 0.4	208
162.	Cold Flow Acoustic Duct Data, Side-Branch Resonator (Treated on One Side), Mach No. = 0.	210
163.	Cold Flow Acoustic Duct Data, Side-Branch Resonator (Treated on One Side), Mach No. = 0.2.	211
164.	Cold Flow Acoustic Duct Data, Side-Branch Resonator (Treated on One Side), Mach No. = 0.3.	212
165.	Cold Flow Acoustic Duct Data, Side-Branch Resonator (Treated on One Side), Mach No. = 0.4.	213
166.	Schematic of Side-Branch Resonator Treatment Panel.	215
167.	Schematic of Dual-Layer SDOF Treatment Panel.	216
168.	PWL Spectrum for Duct Hard-Wall Configuration.	217
169.	PWL Spectrum for Side-Branch Resonator Configuration.	218
170.	PWL Spectrum for Dual-Layer SDOF Treatment Configuration.	219
171.	Suppression in Δ PWL for Side-Branch Resonator Treatment Configuration.	220
172.	Suppression in Δ PWL for Dual-Layer SDOF Treatment Configuration.	221
173.	Suppression in Δ SPL for Side-Branch Resonator Treatment Configuration.	222
174.	Suppression in Δ SPL for Dual-Layer SDOF Treatment Configuration.	223
175.	Suppression Spectra for Dual-Layer SDOF Vs. Side-Branch Resonator Treatment.	226
176.	Predicted Core Noise Spectra.	228

LIST OF ILLUSTRATIONS (Continued)

<u>Figure</u>		<u>Page</u>
177.	QCSEE Core Suppressor Tuning Frequencies Low-Frequency Combustor Treatment.	229
178.	QCSEE Core Suppressor Tuning Frequencies High-Frequency Turbine Treatment.	230
179.	UTW Boilerplate No. 1 Core Exhaust Treatment Definition.	232
180.	QCSEE Core Exhaust Outer Wall Acoustic Treatment.	233
181.	QCSEE Core Exhaust Inner Wall Acoustic Treatment.	234
182.	QCSEE Core Exhaust Plug Nozzle Assembly.	235
183.	QCSEE Core Exhaust Nozzle Assembly.	236
184.	UTW Boilerplate No. 1 Core Exhaust Dual-Layer SDOF Treatment Suppression.	237
185.	Normalized Spectrum of Strut Noise.	239
186.	UTW Suppressed Fan- and Flow-Generated Noise Spectra.	240
187.	Treatment Regenerated Flow Noise Configurations.	242
188.	Aft Suppression Spectra Change with Duct Mach Number Change.	244
189.	UTW Engine Total System Noise Suppression Level Vs. Predicted Flow Noise Floor, Takeoff Power.	245
190.	UTW Engine Total System Noise Suppressed Level Vs. Predicted Flow Noise Floor, Approach Power.	246
191.	Sketch of Composite Kevlar and Laser-Drilled Graphite Faceplate Materials.	248
192.	Duct Cavity Flow Resistance, Metal Perforate Faceplate.	250
193.	Duct Cavity Flow Resistance, Kevlar 3-Ply, Composite Faceplate.	251
194.	Duct Cavity Flow Resistance, Graphite 4-Ply, Composite Faceplate.	252

LIST OF ILLUSTRATIONS (Continued)

<u>Figure</u>		<u>Page</u>
195.	Duct Transmission Loss Results, Mach No. = 0.	253
196.	Duct Transmission Loss Results, Mach No. = 0.3.	254
197.	Duct Transmission Loss Results, Mach No. = 0.4.	255
198.	Normal Impedance Test Results.	256
199.	Engine Seal Locations.	258
200.	Outer Cowl/Inlet Attachment Forward of Fan Frame.	259
201.	Outer Cowl/Inlet Attachment Aft of Fan Frame.	260
202.	Nacelle/Pylon Hinge Seal Outer Cowl.	261
203.	Outer Cowl Rotary Latch Seal.	262
204.	Chevron Seal Test Configuration.	264
205.	Bulb Seal Test Configuration.	265
206.	Base Structure Vs. No Seal Transmission Loss.	266
207.	Base Structure Vs. No Chevron Transmission Loss.	267
208.	Base Structure Vs. No Bulb Seal Transmission Loss.	268
209.	Chevron Seal Vs. Bulb Seal Transmission Loss.	269
210.	Test Panel and Engine Sound Transmission Paths.	271
211.	QCSEE Fan Exhaust Suppression.	272
212.	QCSEE UTW Fan Exhaust Spectrum.	273
213.	Effect of Material Density on Acoustic Reactance of Scottfelt.	288
214.	Effect of Material Density on Acoustic Reactance of Kevlar 29.	289
215.	Comparison of Kevlar and Scottfelt Acoustic Reactance.	290

LIST OF ILLUSTRATIONS (Continued)

<u>Figure</u>		<u>Page</u>
216.	Effect of Thickness on Acoustic Reactance of Scottfelt 3-900.	292
217.	Measured Acoustic Reactance Vs. Frequency at Various Sound Pressure Levels for Scottfelt 3-900.	293
218.	Effect of Flow on Acoustic Reactance of Bulk Absorber Panel.	294
219.	Effect of Flow on Acoustic Reactance of SDOF Panel.	296
220.	Predicted Effects of Faceplate Porosity on Acoustic Reactance for SDOF and Bulk Absorber Panels.	297
221.	Measured Acoustic Reactance Vs. Frequency for Scottfelt 3-900 With and Without Faceplate.	298
222.	Effect of Material Density on Acoustic Resistance of Scottfelt.	300
223.	Effect of Material Density on Acoustic Resistance of Kevlar 29.	301
224.	Effect of Thickness on Acoustic Resistance of Scottfelt 3-900.	302
225.	Effect of Thickness on Acoustic Resistance of Kevlar 29.	303
226.	Measured Acoustic Resistance Vs. Frequency for Scottfelt 3-900 With and Without Faceplate.	305
227.	Correlation of Required and Measured Reactance for Bulk Absorber Treatment Panel.	306
228.	Bulk Absorber Thickness Requirement for Peak Suppression as a Function of Fan Diameter, Frequency, and Mach Number.	308
229.	Comparison of Predicted Vs. Measured Frequency of Peak Attenuation.	309
230.	Full-Scale Engine No. 1 Suppression Spectrum.	311
231.	Comparison of Predicted Vs. Measured Peak Suppression Frequencies for Full-Scale Engine No. 1.	312

LIST OF ILLUSTRATIONS (Continued)

<u>Figure</u>		<u>Page</u>
232.	Full-Scale Engine No. 2 Suppression Spectrum.	313
233.	Comparison of Predicted Vs. Measured Peak Suppression Frequencies for Full-Scale Engine No. 2.	314
234.	Scale Model Fan No. 1 Suppression Spectrum.	315
235.	Comparison of Predicted Vs. Measured Peak Suppression Frequencies for Scale Model Fan No. 1.	316
236.	Suppression Spectrum for Scale Model Fan No. 2 Data Scaled to Full-Scale Engine No. 1 Size.	317
237.	Comparison of Predicted Vs. Measured Peak Suppression Frequencies for Scale Model Fan No. 2 Data Scaled to Full-Scale Engine No. 1 Size.	318
238.	Inlet Treatment Suppression Rate Vs. Acoustic Resistance.	319
239.	Acoustic Resistance as a Function of Material Thickness and Density for Kevlar 29.	321
240.	Acoustic Resistance as a Function of Material Thickness and Density for Scottfelt Materials.	322
241.	Typical Bulk Absorber Treatment Panel.	324
242.	Noise Level Corrections Vs. Frequency for Obtaining Noy-Weighted Spectra.	325
243.	Typical Fan Inlet Noise Spectrum With and Without Noy-Weighting Factors.	326
244.	Bulk Absorber Thickness Requirement for Peak Suppression as a Function of Fan Diameter, Frequency, and Mach Number.	328
245.	Acoustic Resistance as a Function of Material Thickness and Density for Kevlar 29.	329
246.	Acoustic Resistance as a Function of Material Thickness and Density for Scottfelt Materials.	330

LIST OF TABLES

<u>Table</u>		<u>Page</u>
I.	Summary of UTW Noise Component Suppression Requirements.	25
II.	Summary of OTW Noise Component Suppression Requirements.	27
III.	Definition of Constant-Depth Treatment Configurations Tested for Porosity-Optimization Study.	53
IV.	Detail Definition of Faceplate and Core Cell Size for Constant-Depth Treatment Configuration Tested in Porosity-Optimization Study.	54
V.	Accelerating Inlet Treatment Designs.	110
VI.	Accelerating Inlet Designs, Acoustic Treatment Faceplate Definitions.	111
VII.	Low Mach Inlet Treatment Designs.	117
VIII.	Low Mach Inlet Faceplate Definitions.	119
IX.	Treatment Design Details.	167
X.	Design Frequencies.	167
XI.	QCSEE Core Suppression Estimates.	227

1.0 SUMMARY

Acoustic treatment was developed for the QCSEE UTW and OTW engines. Treatment design concepts were studied, and hardware designs were defined to meet the noise suppression level goals for several constituents that make up the total engine system noise level. Treatment configurations have been defined to suppress the forward and aft radiated fan-, turbine-, and combustor-generated noise levels.

During the development phase of the treatments, acoustic laboratory duct configurations and scale model test vehicles were utilized to obtain the necessary data to define and estimate the fan treatment design requirements in order to meet the engine noise-suppression objectives. Laboratory facilities were also used extensively in studying the various treatment concepts considered to have a high potential for reducing the core engine radiated noise level.

The UTW fan inlet treatment configuration, which has a total length-to-fan diameter ratio of 0.74, is predicted to give a total suppression of 4.5 PNdB for the reverse thrust fan operation. At takeoff power the treatment, combined with the high throat Mach number effect, is predicted to give a total suppression of 13.4 PNdB, of which 3 PNdB is a result of the treatment. Approximately 6 to 7 PNdB are expected from the treatment at the approach fan speed.

The UTW fan exhaust configuration, consisting of fan frame treatment plus treated walls and an acoustic splitter in the fan exhaust duct, is predicted to give approximately 13.4-PNdB suppression both at takeoff and at approach power settings.

The core exhaust treatment, which employs both high- and low-frequency suppression (turbine and combustor noise) in a "stacked treatment" concept, is predicted to give as much as 5-PNdB suppression of combustor noise and about 10-PNdB suppression of turbine noise.

For the OTW engine, the predicted suppressions for the inlet are 13.5 and 10.4 PNdB at takeoff and approach, respectively; for the exhaust, the suppression is expected to be 13.9 PNdB at both power settings.

The designs developed for each of the engine system noise constituents approach or exceed the suppression goals that were established in the early phase of the QCSEE program.

The results of additional supporting investigations complementary to the treatment development are also presented and discussed herein.

2.0 INTRODUCTION

In the Quiet Clean Short-Haul Experimental Engine (QCSEE) Program sponsored by NASA-Lewis, under Contract NAS3-18021 to the General Electric Company, two engines were designed and built to develop and demonstrate technology applicable to engines intended for future commercial short-haul turbofan aircraft. Details of the design rationale are available in References 8 and 9.

The Under-the-Wing (UTW) engine utilizes several low noise features, such as:

- Low fan tip speed
- Treated inlet with high inlet throat Mach number
- Rotor/stator spacing of 1.5 rotor tip chords
- Optimized vane/blade ratio to reduce fan second harmonic tone content
- Fan exhaust wall suppression
- An acoustic splitter in fan exhaust passage
- Core suppression which utilizes a thick low-frequency resonator with a thin high-frequency suppressor built into the low-frequency faceplate.

Reverse thrust on this engine is achieved by actuating the variable-pitch fan blades through stall. UTW acoustic design considerations are discussed in Reference 10.

The Over-the-Wing (OTW) engine incorporated many of the same acoustic design features as the UTW, including the high-throat-Mach-number inlet with bulk absorber treatment, 1.93 rotor tip chord spacing between the rotor and stator, fan wall treatment, acoustic splitter, and stacked core treatment. Reverse thrust was achieved by a target reverser. Details of the acoustic design criteria of the OTW engine are given in Reference 11.

Although the engines have been designed for very low unsuppressed noise levels, attainment of the very severe noise goal requires higher suppression levels than ever previously achieved.

The low-noise goal requires the suppression of several noise sources, namely: the fan inlet and exhaust, and the core (turbine and combustor) exhaust. Suppression of all these constituents is required for the engine operating conditions at takeoff, approach, and reverse thrust.

Since there are many noise-source elements that have to be considered, much emphasis has been directed toward developing a well-balanced suppression system in the fan inlet, fan exhaust, and core exhaust configurations. The engine system treatment design must also be integrated with the engine aerodynamic/mechanical design features; therefore, consideration must be given to those engine design features that introduce treatment design constraints. The treatment configurations developed herein are expected to meet the noise suppression goals.

3.0 DEFINITION OF SUPPRESSION REQUIREMENTS

The noise requirements for both the UTW and the OTW engine are specified in terms of total system noise level. The noise goals for the aircraft are given in the illustration presented in Figure 1. The noise levels at three specific engine operating conditions are:

- Takeoff 95 EPNdB on a 152.4 m
100% F_N (500 ft) sideline - 61 m (200 ft) altitude
- Approach 95 EPNdB on a 152.4 m
65% F_N (500 ft) sideline 61 m (200 ft) altitude
- Reverse Thrust 100 PNdB on a 152.4 m
35% F_N (500 ft) sideline

The noise levels pertain to an aircraft utilizing four engines.

3.1 UNSUPPRESSED UTW ENGINE SPECTRA

3.1.1 Fan Inlet Spectra

The estimated unsuppressed inlet noise spectra for the takeoff, approach, and reverse thrust operating conditions are presented in Figures 2 through 4 for the Under-the-Wing (UTW) engine. The takeoff and approach spectra are given for an acoustic angle of 60° on a 152.4-m (500-ft) sideline at an altitude of 61-m (200-ft).

The given spectra are estimates based on scale model data taken from 50.8-cm (20-in.) simulator tests (Reference 1) scaled to the full-size engine. The frequency was scaled directly as the fan speed ratio, full-size to model size; the level was scaled by 10 times the logarithm of the weight-flow ratio, full-size to model size. The spectrum given in Figure 2 is for the takeoff condition and includes the noise reduction resulting from the 0.79 inlet throat Mach number. Shown with the hard-wall spectra are the Noy-weighted spectra that depict the frequency range controlling the PNdB level of the spectrum. The Noy-weighted spectrum is essential if the treatment design is to be optimized to reduce the noise in terms of PNdB.

Figure 3 shows the unsuppressed spectrum for the approach condition. The condition is for $+5^\circ$ blade angle, (blade rotated 8° toward flat pitch from the nominal takeoff setting), 95% fan speed, which gives 65% of the forward thrust available. The Noy-weighted spectrum is also given. Figure 4 shows the spectrum at the maximum noise forward angle for the reverse thrust condition.

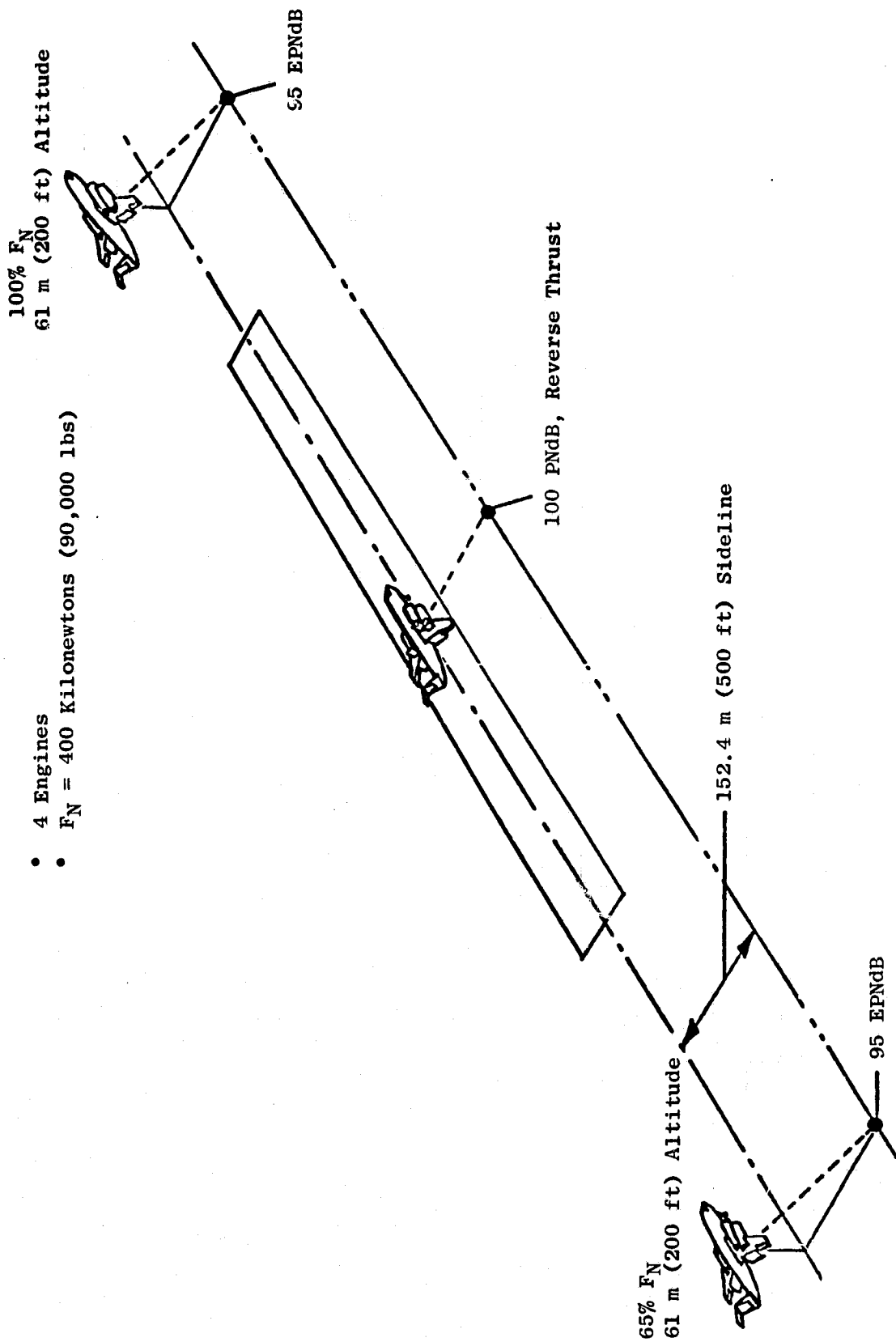


Figure 1. QCSEE Noise Goals.

- 60° Acoustic Angle
- 152.4 m (500 ft) Sideline at
61 m (200 ft) Altitude
- 0.79 Throat Mach Number

— Hard Wall
 - - - - Noy-Weighted Hard Wall

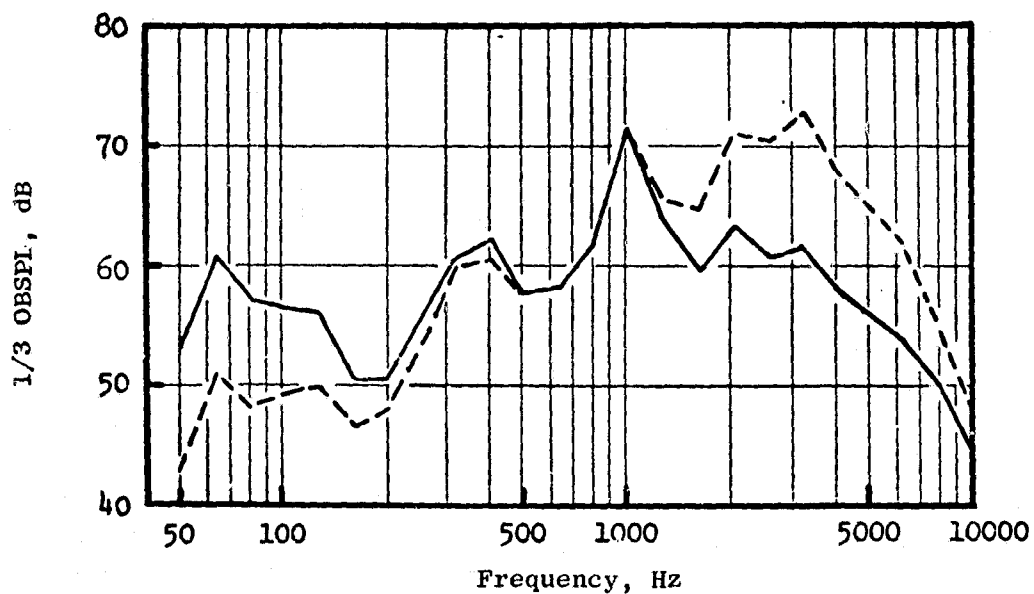


Figure 2. UTW Takeoff Fan Inlet Spectra,
 Hard-Wall Accelerating Inlet.

- 60° Acoustic Angle
- 152.4 m (500 ft) Sideline at
61 m (200 ft) Altitude
- +5° Blade Angle
- 65% of Takeoff Thrust
- 95% Corrected Fan Speed

—— Unsuppressed
 - - - - Noy-Weighted Unsuppressed

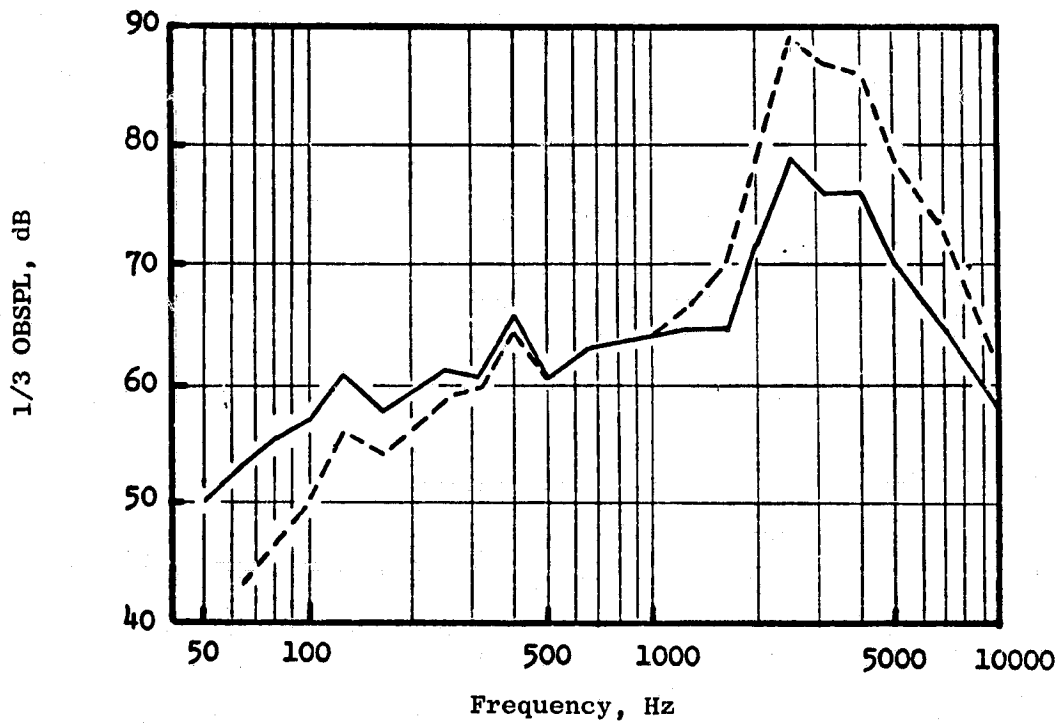


Figure 3. UTW Approach Unsuppressed Fan Inlet Spectra, Baseline Bellmouth Inlet.

- Max. Noise Forward Angle
- 152.4 m (500 ft) Sideline
- 35% of Takeoff Forward Thrust
- -100° Blade Angle
- 50.8 cm (20 in.) Simulator Data Scaled to Full Size
- 86% Corrected Fan Speed

————— Unsuppressed
 - - - - - Noy-Weighted Unsuppressed

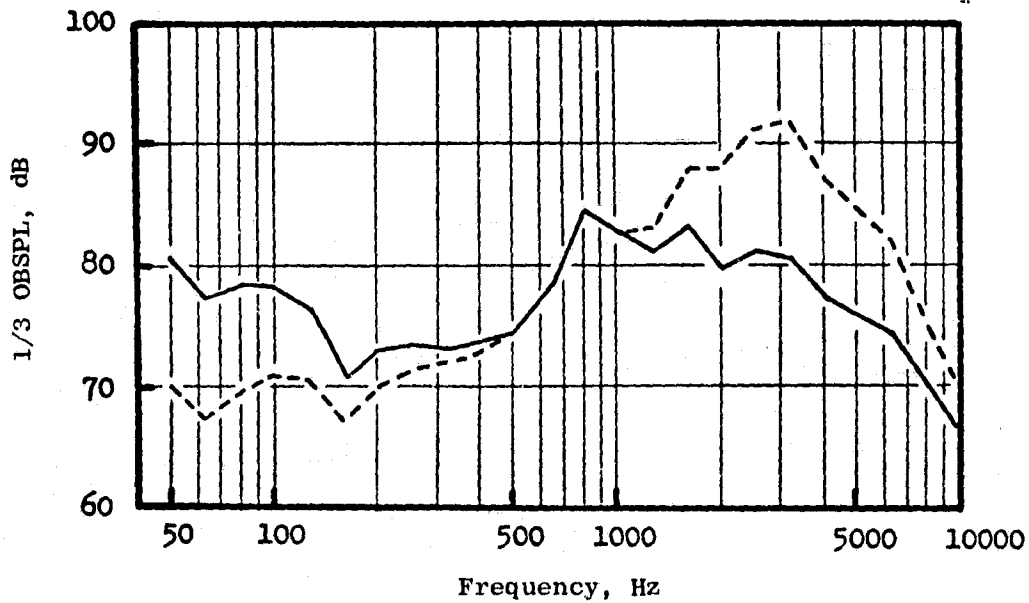


Figure 4. UTW Reverse Thrust Unsuppressed Fan Inlet Spectra.

3.1.2 Fan Exhaust Spectra

Figure 5 shows the aft fan unsuppressed noise spectra for the takeoff condition. The unsuppressed spectrum and the unsuppressed Noy-weighted-spectrum for the maximum aft acoustic angle on a 152.4-m (500-ft) sideline at an altitude of 61-m (200-ft) are shown. The unsuppressed spectrum is based on previous scale model and full-scale fan data scaled to the OTW engine by adjusting for weight flow, pressure ratio, rotor/stator spacing, vane/blade ratio, and fan tip speed. The approach spectrum is not shown since the fan rpm during approach is nearly the same as at takeoff and thus has the same spectrum shape.

3.1.3 Core Noise Spectra

Figure 6 shows the turbine and combustor unsuppressed spectra. The spectra shown are for the maximum aft acoustic angle on a 152.4-m (500-ft) sideline at 61-m (200-ft) altitude. The combined turbine and combustor noise spectrum, Noy-weighted, is also shown. The predicted unsuppressed spectra were obtained by the use of semiempirical prediction procedures developed by General Electric under separate contracts (Reference 2). The applicability of these predictions has been checked against measured data from a QCSEE-type engine (Reference 12) where near-field and far-field measurements were compared with the predicted spectra. Although the data are contaminated by other noise sources, the comparison does show that the prediction procedures for the turbine and the combustor spectra are adequate to define the level of core noise suppression required for the QCSEE engine.

3.2 UNSUPPRESSED OTW ENGINE SPECTRA

3.2.1 Fan Inlet Spectra

Figures 7 and 8 show the unsuppressed fan inlet spectra for the OTW engine at takeoff and approach conditions. These spectra are based on scale-model and full-scale fan data scaled to the OTW engine by adjusting for weight flow, pressure ratio, tip speed, and vane/blade ratio.

3.2.2 Fan Exhaust Spectra

The aft fan unsuppressed spectra for takeoff and approach conditions are shown in Figures 9 and 10. These spectra were also predicted using previously measured scale model and full-scale fan data scaled to the OTW engine by adjusting for weight flow, pressure ratio, tip speed, rotor/stator spacing and vane/blade ratio.

3.2.3 Core Noise Spectra

The OTW core noise spectra (turbine and combustor noise) are given in Figure 11. The spectra were predicted using the same procedure as previously described in Section 3.1.3.

- Max. Aft Angle
- 152.4 m (500 ft) Sideline at 61 m (200 ft) Altitude

— Unsuppressed
 - - - Noy-Weighted Unsuppressed

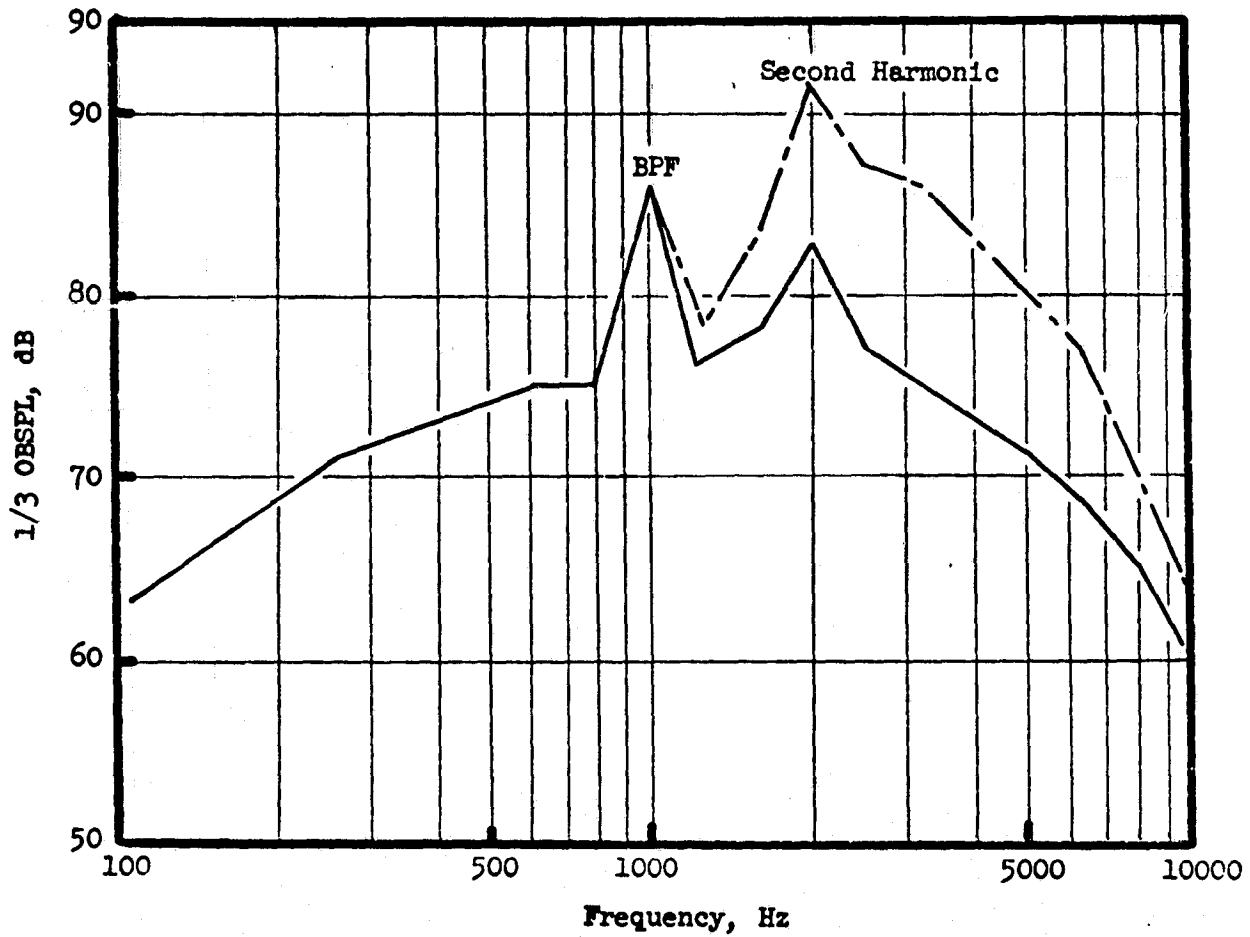


Figure 5. UTW Takeoff Unsuppressed Fan Exhaust Spectra.

- 120° Acoustic Angle
- 152.4 m (500 ft) Sideline at 61 m (200 ft) Altitude

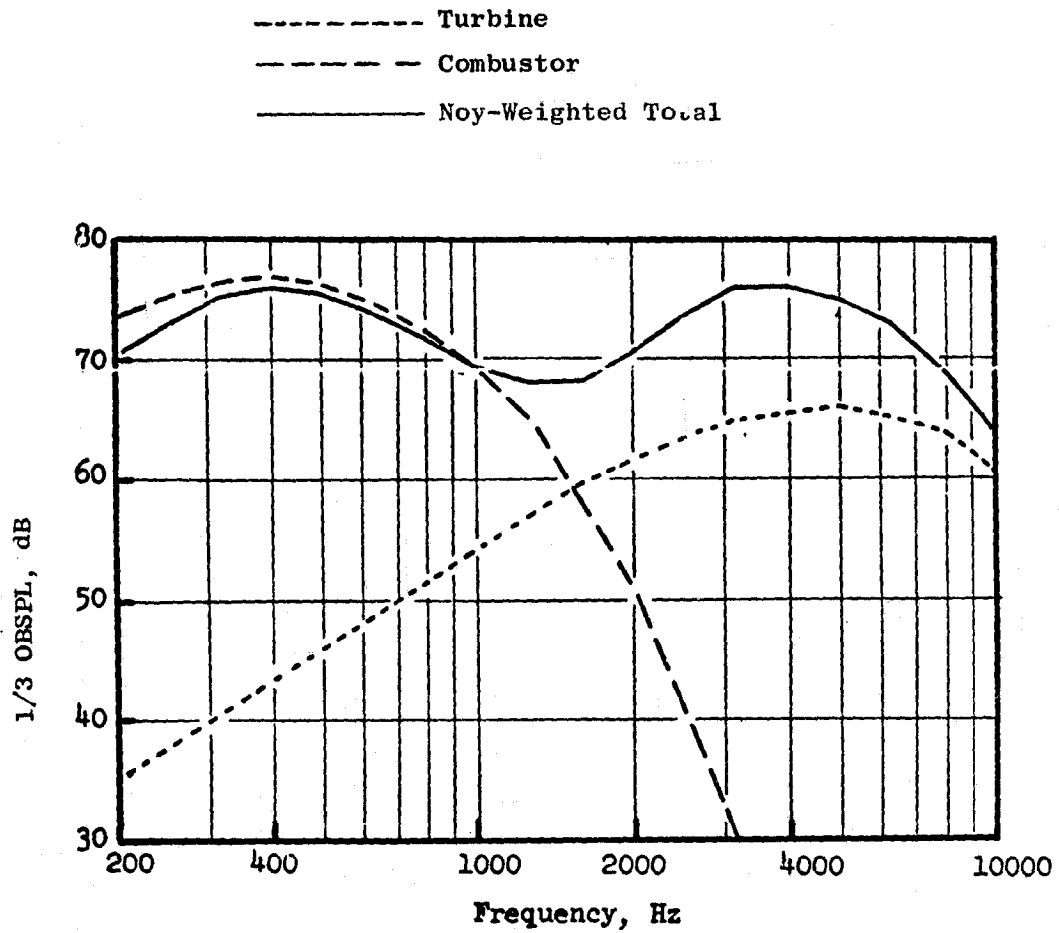


Figure 6. UTW Takeoff Unsuppressed Predicted Core Noise Spectra.

- Max. Forward Angle
- 152.4 m (500 ft) Sideline
at 61 m (200 ft) Altitude
- Takeoff Power

————— Unsuppressed
 - - - - - Noy-Weighted Unsuppressed

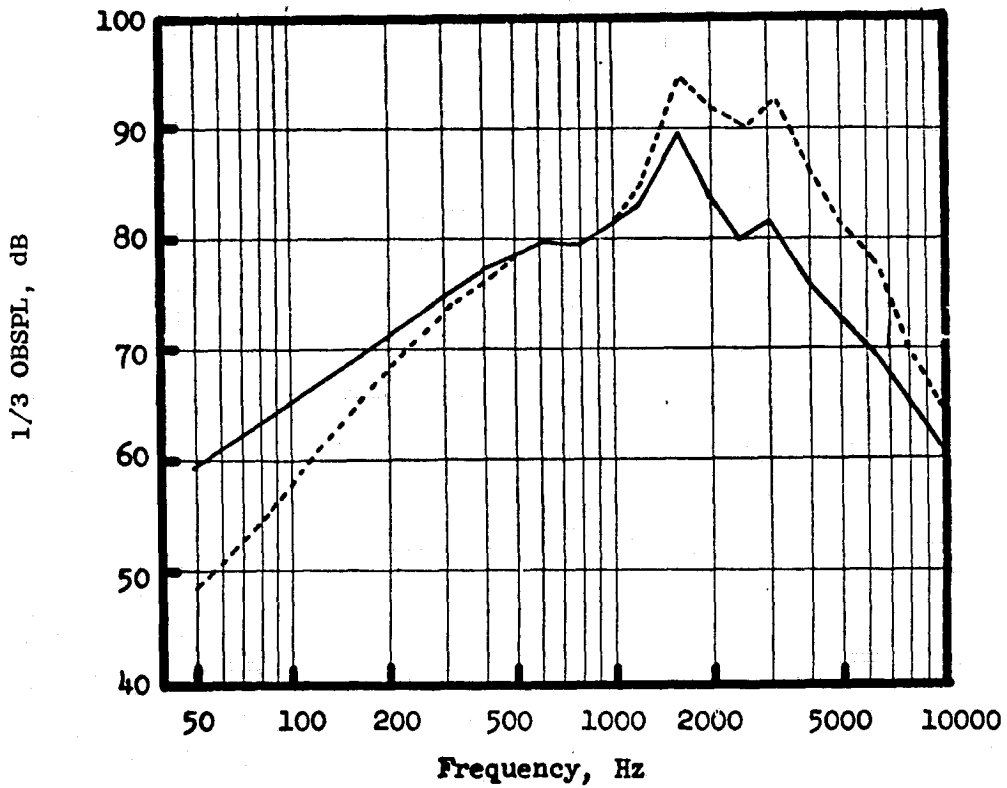


Figure 7. OTW Unsuppressed Fan Inlet Spectra at Takeoff Power.

- Max. Forward Angle
- 152.4 m (500 ft) Sideline
at 61 m (200 ft) Altitude
- Approach Power

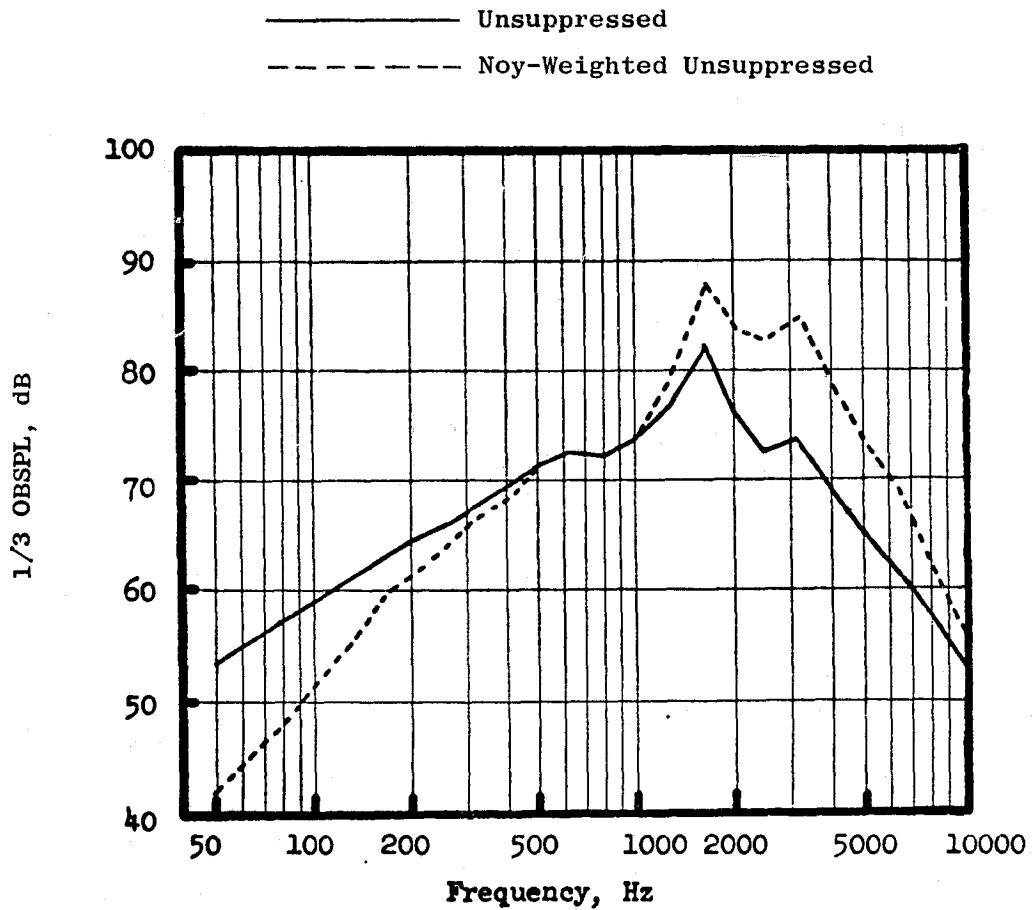


Figure 8. OTW Unsuppressed Fan Inlet Spectra at Approach Power.

- Max. Aft Angle
- 152.4 m (500 ft) Sideline
at 61 m (200 ft) Altitude
- Takeoff Power

————— Unsuppressed
 - - - - - Noy-Weighted Unsuppressed

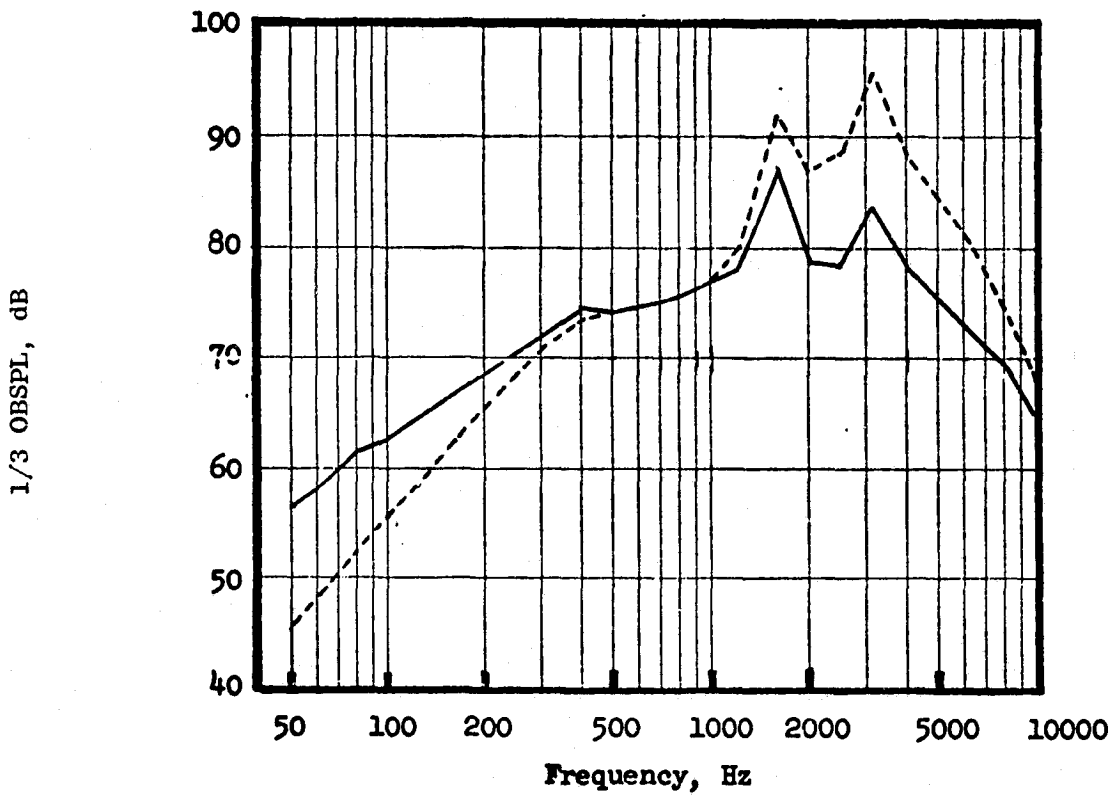


Figure 9. OTW Unsuppressed Fan Exhaust Spectra at Takeoff Power.

- Max. Aft Angle
- 152.4 m (500 ft) Sideline
at 61 m (200 ft) Altitude
- Approach Power

— Unsuppressed
 - - - Noy-Weighted Unsuppressed

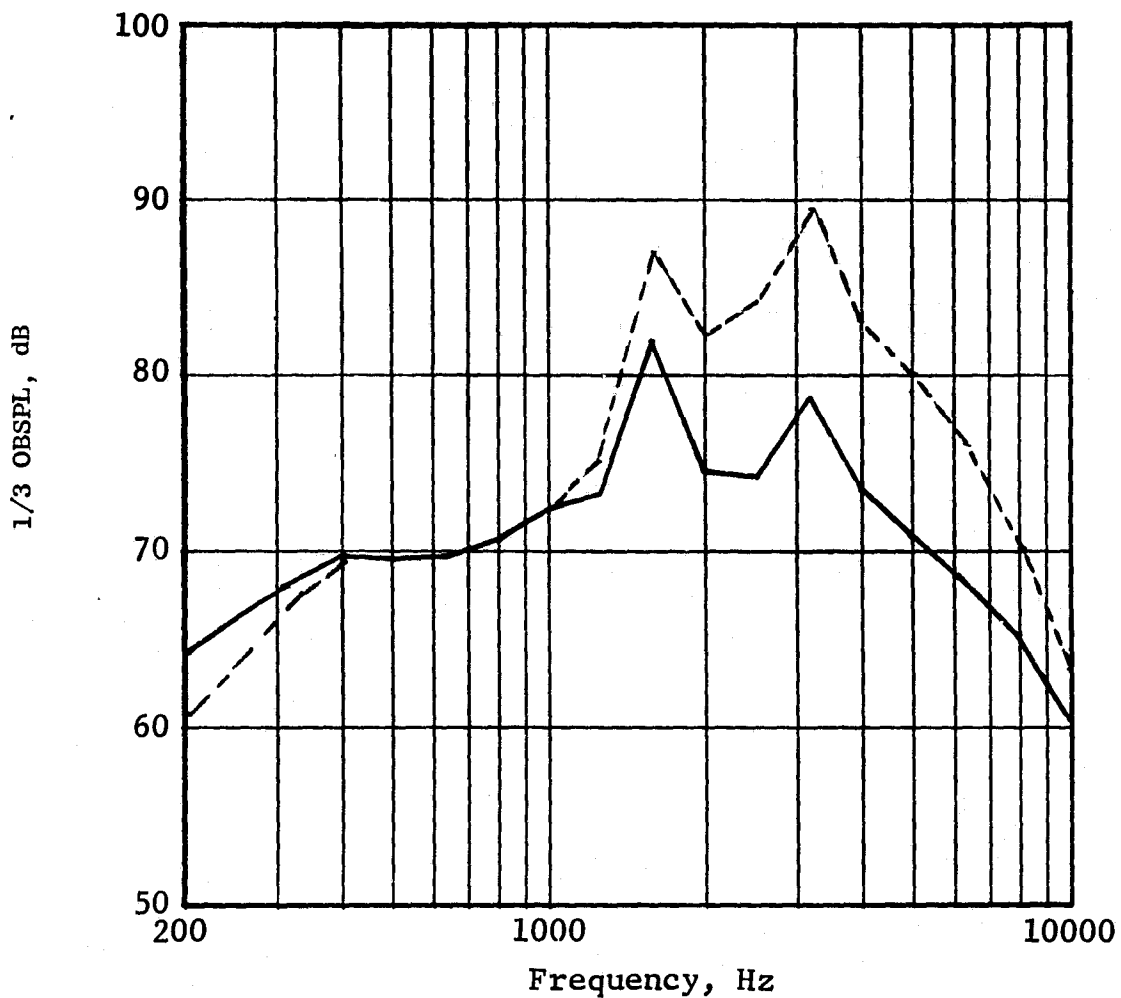


Figure 10. OTW Unsuppressed Fan Exhaust Spectra at Approach Power.

- Max. Aft Angle
- 152.4 m (500 ft) Sideline
at 61 m (200 ft) Altitude
- Takeoff Power

----- Turbine
 - - - - - Combustor
 _____ Noy-Weighted Total

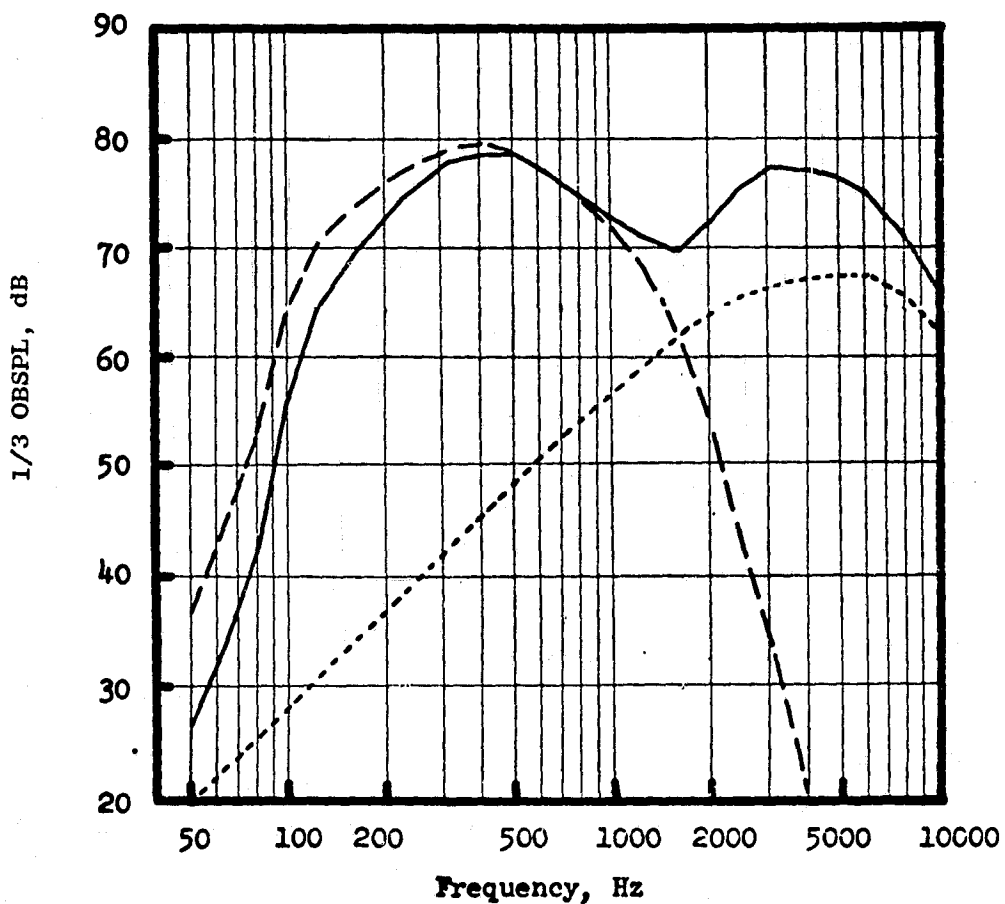


Figure 11. OTW Unsuppressed Core Noise Spectra.

3.3 SYSTEM CONSTITUENT NOISE LEVELS AND SUPPRESSION LEVEL REQUIREMENTS

3.3.1 UTW Engine Component Noise Levels and Required Suppression

The constituent noise levels for the UTW and the OTW engines are shown in Figures 12 through 18 in bar chart form. The fan inlet, fan exhaust, turbine, and combustor noise levels are given for maximum forward noise and maximum aft noise angles. The unsuppressed levels plus the suppression needed for the total system to reach the noise goal are shown.

The UTW component levels at the takeoff condition are shown in Figure 12. The levels are given for the maximum forward and the maximum aft acoustic angles on a 61-m (200-ft) sideline. The fan noise is seen to dominate the unsuppressed level in both the forward and aft quadrants. The suppressed levels indicate that the fan is still the controlling source in both quadrants; however, the turbine and combustor now contribute more to the total noise level. The bar charts show that, if left unsuppressed, the combined turbine and combustor levels would be higher than the suppressed fan. Therefore, for achieving the total system noise goal, a core noise suppressor system is clearly needed.

Figure 13 shows the UTW component noise levels for the approach power condition. The unsuppressed fan dominates the total noise level in both the forward and aft noise quadrants. The suppressed levels indicate that the fan noise still dominates in the forward quadrant; however, the aft quadrant shows a balanced level among fan, combustor, and turbine.

The noise components for the UTW reverse thrust operation are shown in Figures 14 and 15. The fan levels given in Figure 14 are based on the NASA QF9 (Reference 13) data scaled to QCSEE size. This comparison shows the total noise is fan-dominated in both quadrants. The suppression levels as designated were estimated to be sufficient to attain the 100 PNdB suppressed level goal on a 152.4-m (500-ft) sideline.

The levels given in Figure 15 are based on updated data relative to the levels given in Figure 14 which were used to set the suppression requirements for the reverse thrust condition. The updated levels show an unexpected increase (≈ 5.0 PNdB) in the forward fan noise unsuppressed level. This increase prevents the noise goal from being met without a substantial increase in the fan suppression. The reverse thrust fan levels are based on the 50.8-cm (20-in.) scale model fan data. Although the measured suppression in these tests is somewhat higher than predicted in Figure 15, the additional suppression is small compared to the source noise increase.

A summary of the UTW noise component suppression goals is given in Table I. These suppression values are based both on the total system noise levels (as given in Table I) for each condition and on the predicted component levels in the bar charts given in Figures 12 through 18.

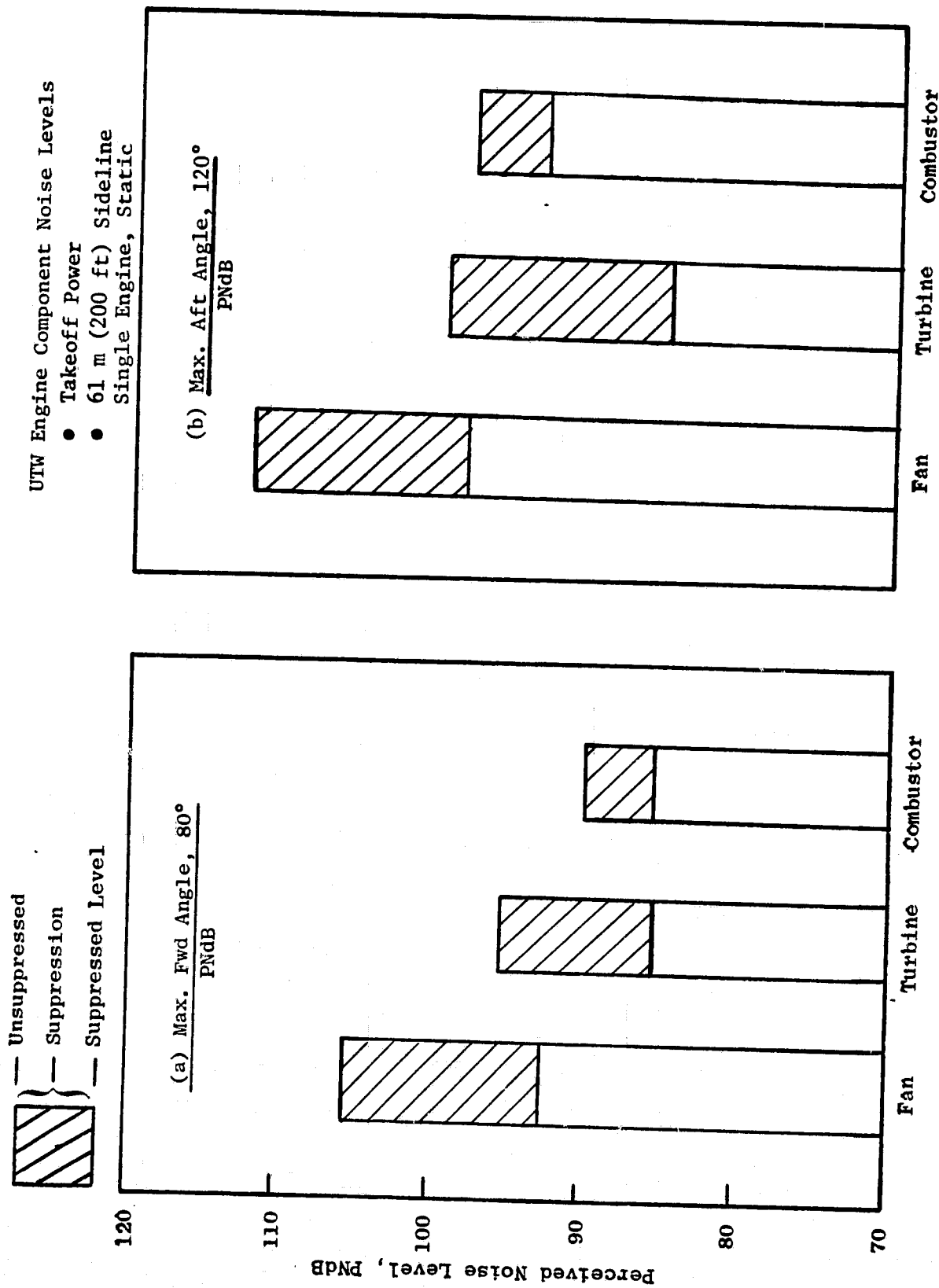


Figure 12. Summary, Unsuppressed and Required Suppressed Levels of Noise Constituents for UTW Engine at Takeoff Power.

UTW Engine Component Noise Levels

- Approach Power
- 61 m (200 ft) Sideline
- Single Engine, Static

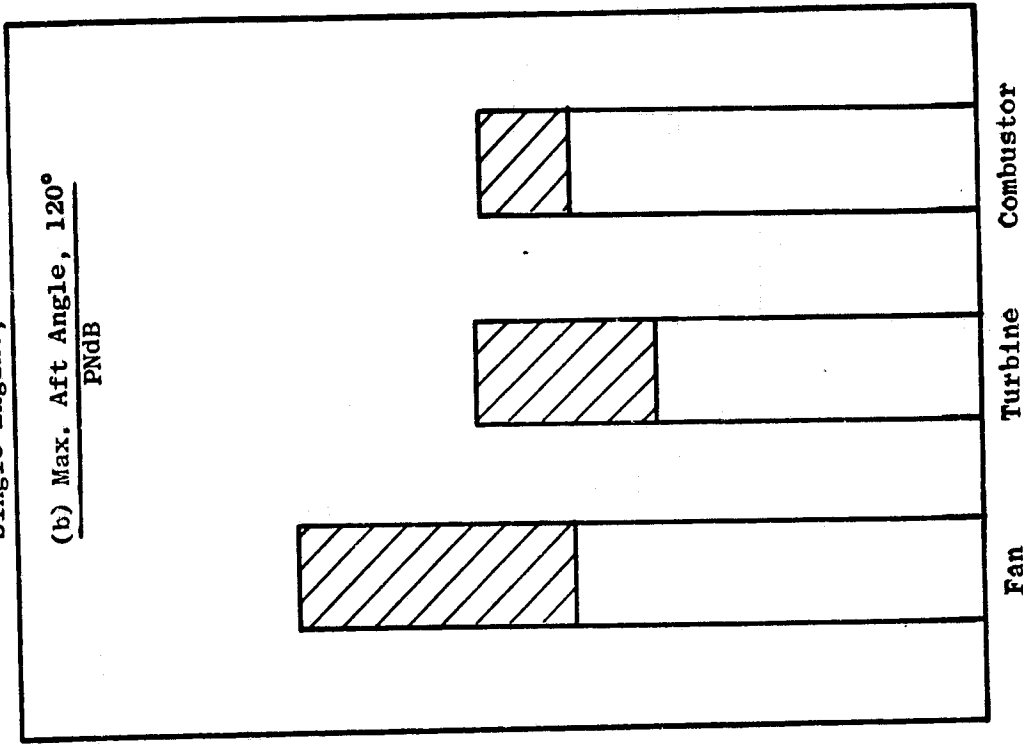
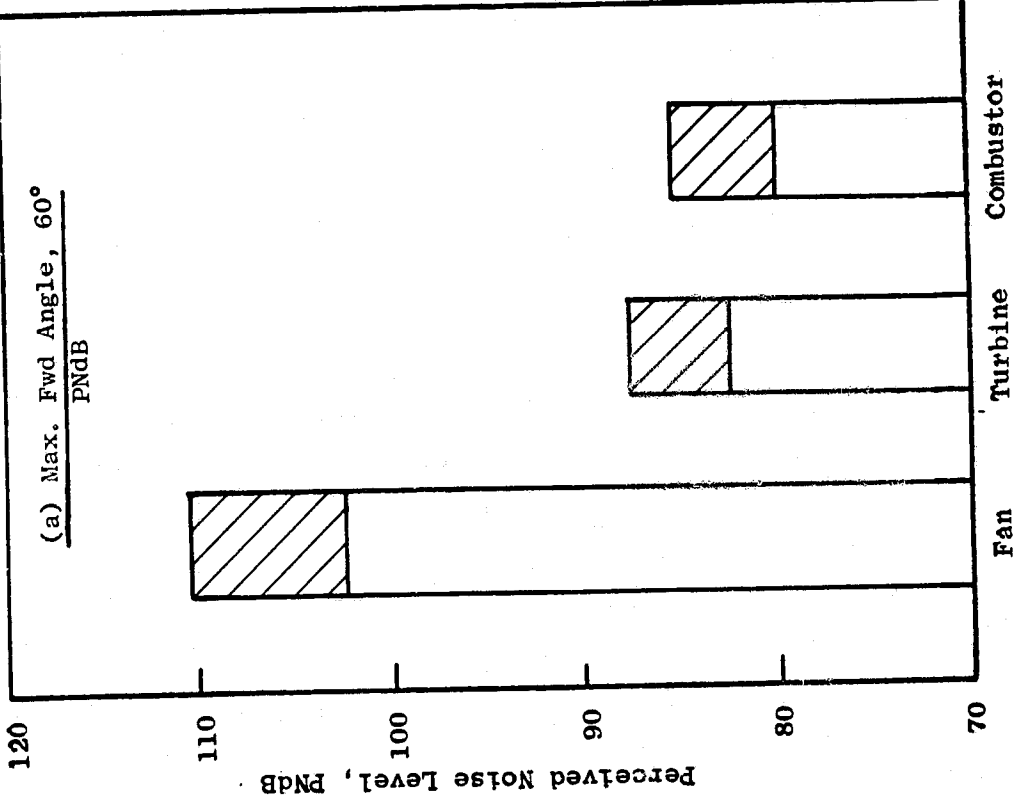
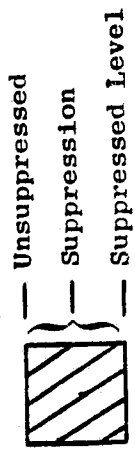


Figure 13. Summary, Unsuppressed and Required Suppressed Levels of Noise Constituents for Approach Power.

UTW Reverse Thrust Noise Constituents

- 152.4 m (500 ft) Sideline
- Through Stall, 90% N_f

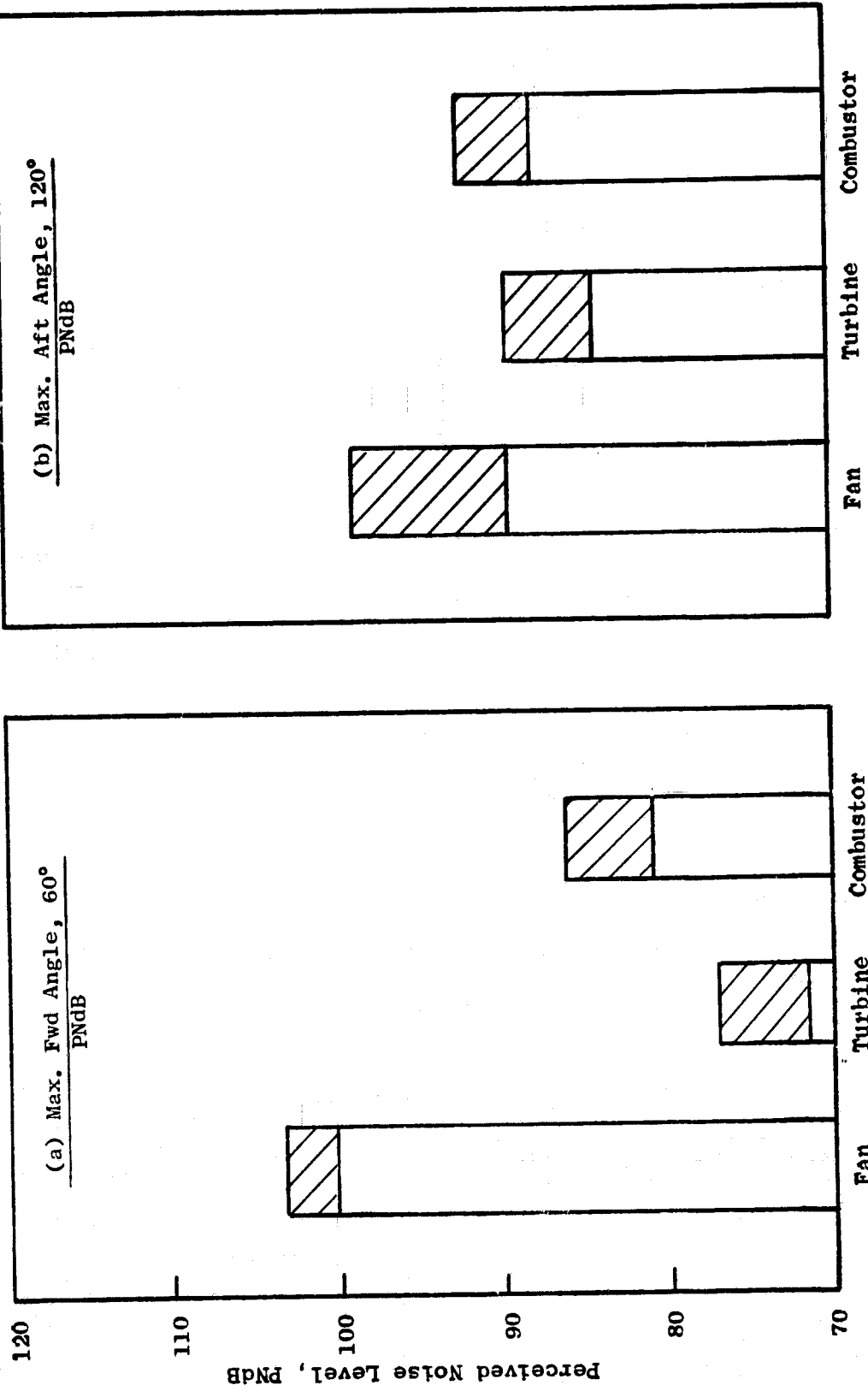
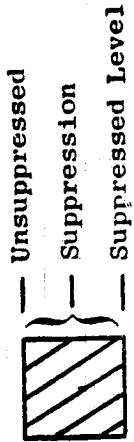


Figure 14. Summary, UTW Reverse Thrust Unsuppressed and Required Suppressed Levels of Noise Constituents (Fan Data Scaled from the NASA QF9 Fan, Reference 13).

UTW Engine Component Noise Levels

- Reverse Thurst
- 86% Corrected Fan Speed
- 100° Blade Angle

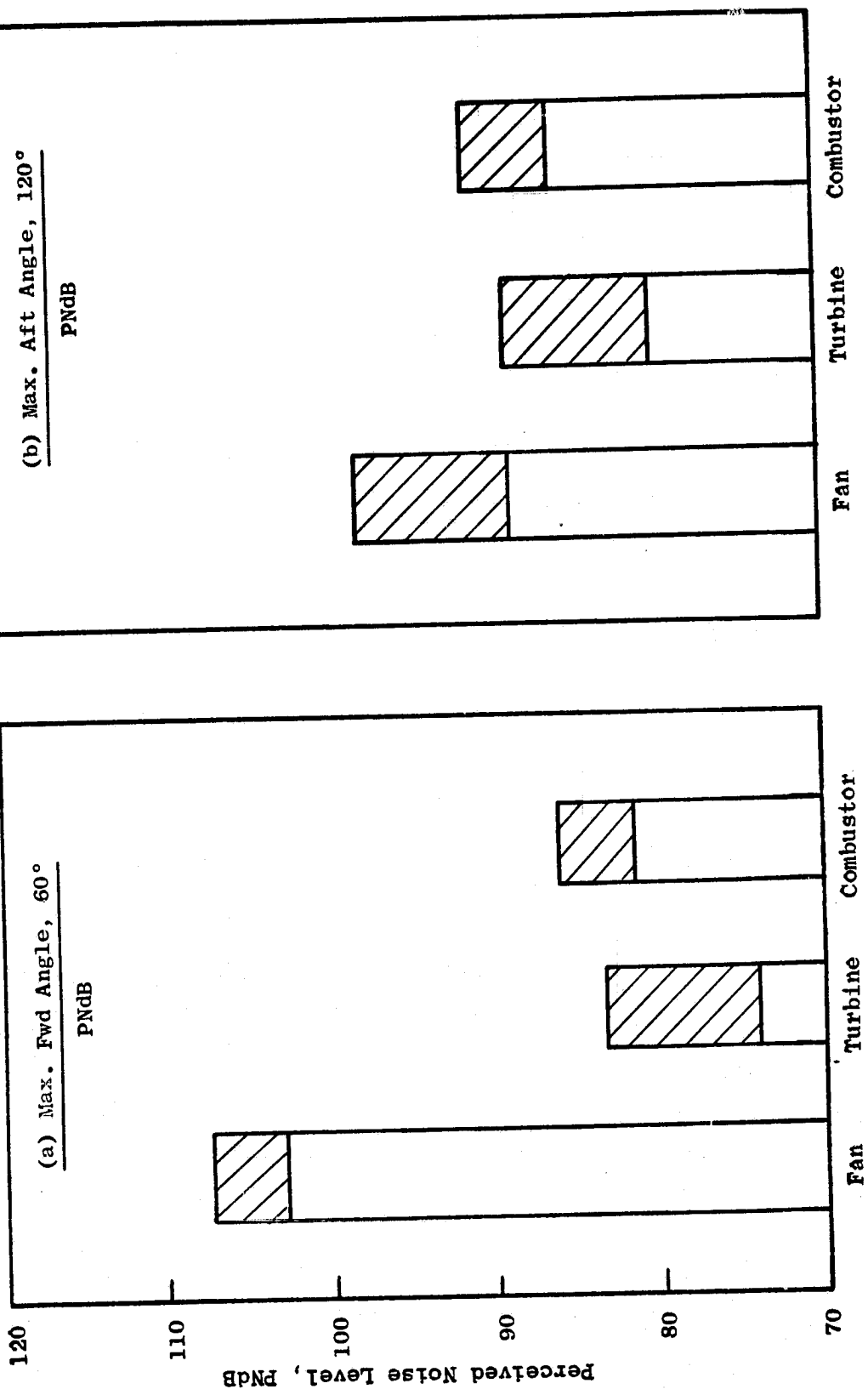
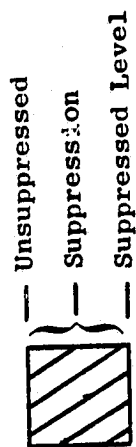


Figure 15. Summary, UTW Reverse Thrust Unsuppressed and Required Suppressed Levels of Noise Constituents (Based on Fan Data from This Program, Reference 16).

— Unsuppressed
 — Suppression
 — Suppressed Level

OTW Engine Component Noise Levels
 • Takeoff Power
 • 61 m (200 ft) Sideline
 • Single Engine, Static

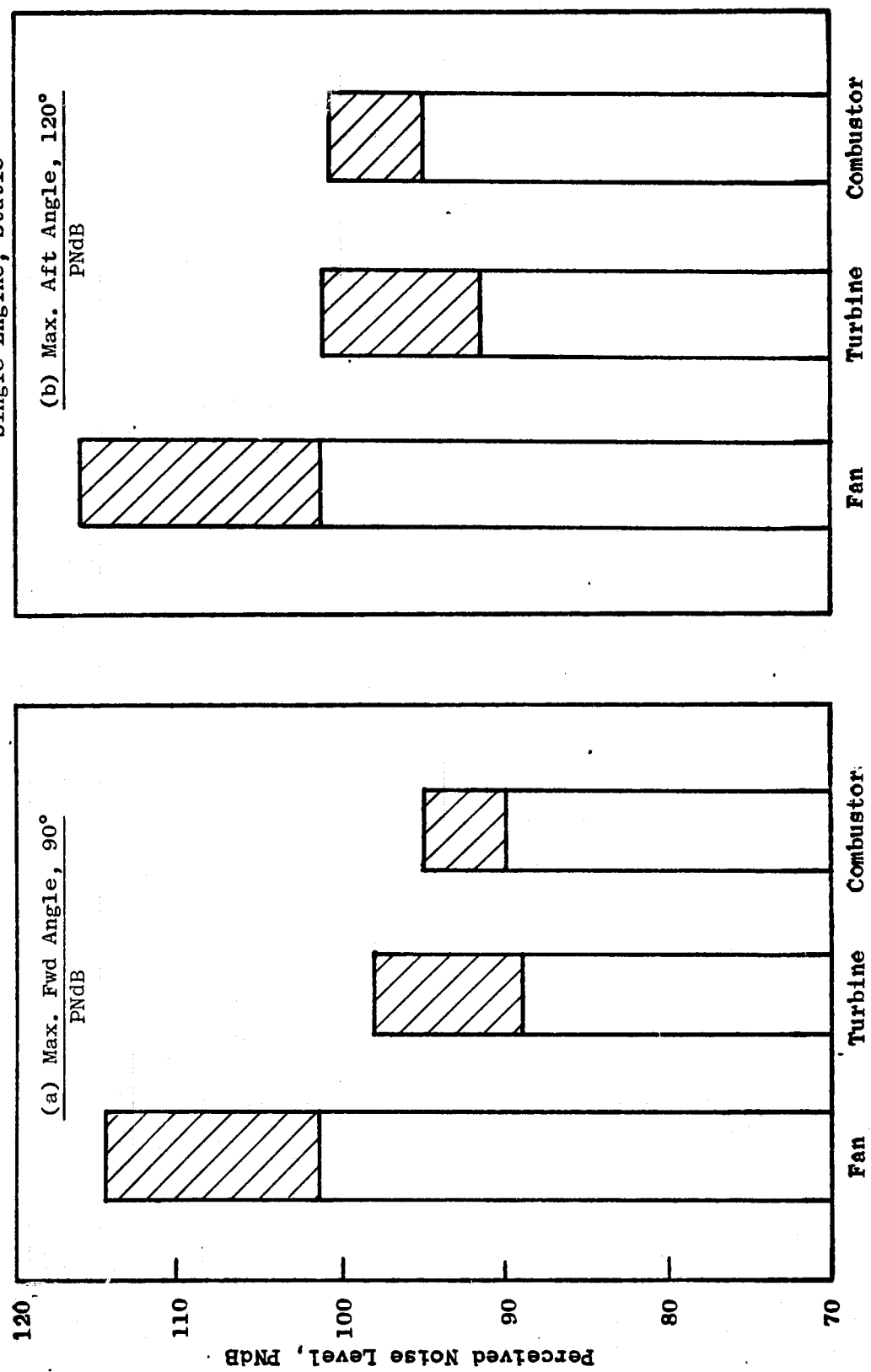


Figure 16. Summary, Unsuppressed and Required Suppressed Levels of Noise Constituents for OTW Engine at Takeoff Power.

OTW Engine Component Noise Levels

- Approach Power
- 61 m (200 ft) Sideline
- Single Engine, Static

Unsuppressed
 Suppression
 Suppressed Level

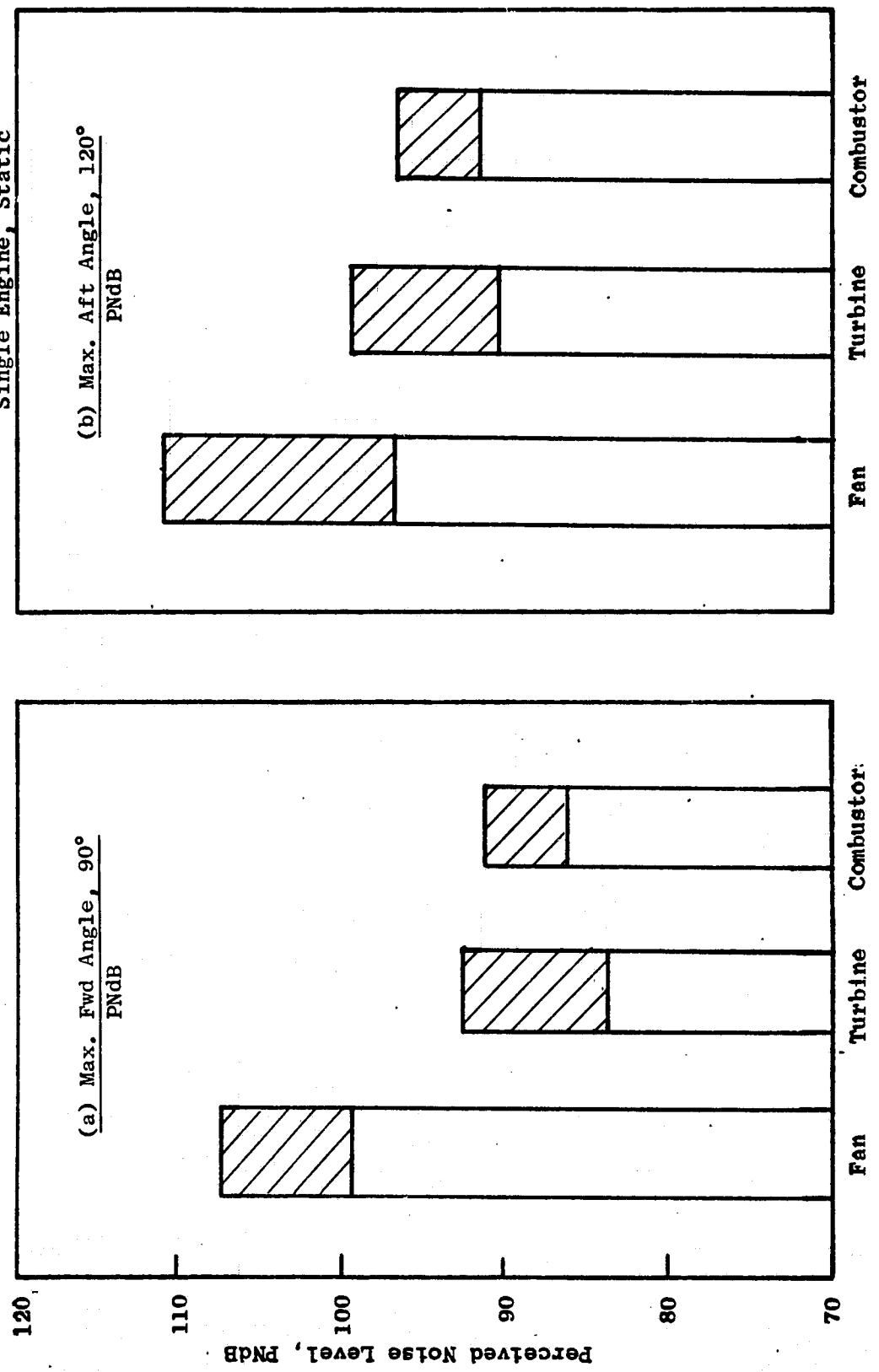


Figure 17. Summary, Unsuppressed and Required Suppressed Levels of Noise Constituents for OTW Engines at Approach Power.

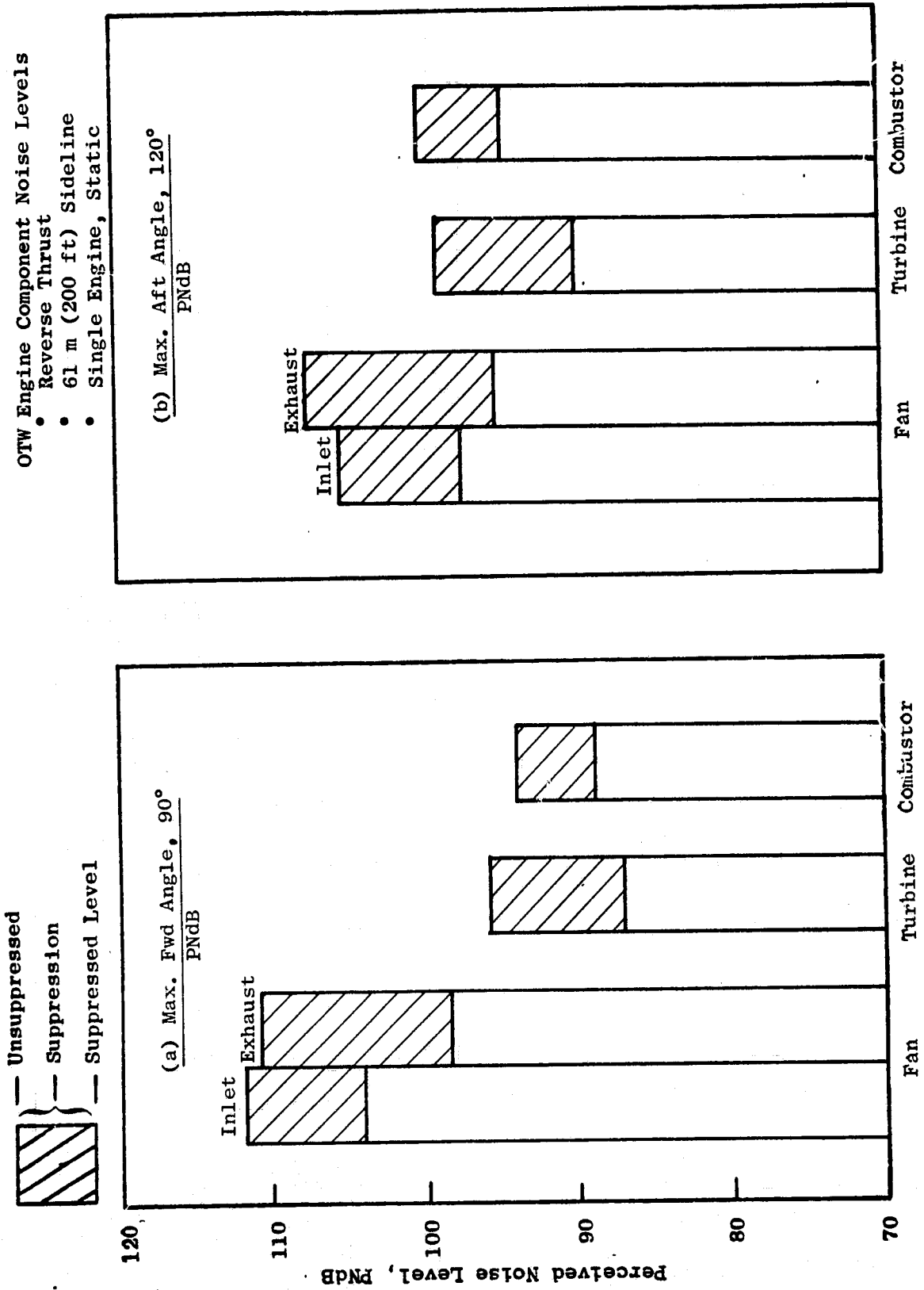


Figure 18. Summary, Unsuppressed and Required Suppressed Levels of Noise Constituents for OTW Engine at Reverse Thrust.

Table I. Summary of UTW Noise Component Suppression Requirements.

- Suppression in Δ PNdB
- Treatment Designed to Meet Takeoff 95-EPNdB Goal

	<u>Max. Fwd Angle</u>			<u>Max. Aft Angle</u>		
	<u>Fan</u>	<u>Turbine</u>	<u>Combustor</u>	<u>Fan</u>	<u>Turbine</u>	<u>Combustor</u>
Takeoff	13.5	9.8	5.1	14.5	9.8	5.1
Approach	8.0	9.8	5.1	14.5	9.8	5.1
Reverse Thrust	4.5	9.8	5.1	9.3	9.8	5.1

3.3.2 OTW Engine Component Noise Levels and Required Suppression

Noise component levels for the OTW engine are shown in Figures 16 through 18 in bar chart form. The levels are given for the maximum forward and maximum aft angles on a 61-m (200-ft) sideline.

Figure 16 shows that the OTW unsuppressed level is dominated by fan noise in the forward and aft quadrants. The suppressed levels indicate that the fan is still the dominant source in both quadrants. Figure 17 gives the approach levels. Here the fan also dominates at both unsuppressed and suppressed conditions.

Figure 18 gives the OTW reverse thrust noise levels. The comparison shows the fan noise to be the dominating source in both forward and aft quadrants. The thrust reverser noise level is not shown, but this noise source is predicted to dominate the total noise level.

A summary of the OTW noise suppression requirements for the fan inlet, fan exhaust, and core is given in Table II.

Table II. Summary of OTW Noise Component Suppression Requirements.

- Suppression in Δ PNdB
- Treatment Designed to Meet Takeoff 95-EPNdB Goal

	<u>Max. Fwd Angle</u>			<u>Max. Aft Angle</u>		
	<u>Fan</u>	<u>Turbine</u>	<u>Combustor</u>	<u>Fan</u>	<u>Turbine</u>	<u>Combustor</u>
Takeoff	13.0	9.8	5.1	14.5	9.8	5.1
Approach	7.7	9.8	5.1	14.5	9.8	5.1
Reverse Thrust	7.7	9.8	5.1	13.0	9.8	5.1

4.0 SUMMARY OF PROGRAM ELEMENTS AND TEST FACILITIES

4.1 FAN EXHAUST DUCT FACILITIES AND TESTS

The acoustic treatment design development for the QCSEE UTW and OTW engines consists of several elements, each aimed at providing essential data needed to define effective treatment designs for the fan inlet, fan exhaust, and core exhaust.

The designs of the aft fan acoustic treatment for the QCSEE engines are based on supporting data from acoustic duct and scale model fan test results. Acoustic lab tests were aimed at giving the required data base needed both to design new treatment concepts, such as phased and variable-depth treatment, and to optimize the faceplate porosity. A schematic diagram of the acoustic duct test facility is shown in Figure 19. The treatment location and the noise-source input positions are indicated. A Ling Electronics EPT-200 Electropneumatic Transducer acoustic driver is used as a noise source; it was operated in the mode that produced broadband noise over the entire spectrum of interest.

A schematic depicting the transmission-loss data acquisition system is given in Figure 20. The acoustic instrumentation used to record data in determining treatment suppression values included two acoustic waveguide probes located forward and aft of the treatment section as indicated in the figure. The sound level was measured by 1.27-cm (0.50-in.) B&K microphones attached to the end of each probe. The signal was filtered using a 1/3-octave-band analyzer and recorded using an X-Y plotter. Each probe was connected to an actuator system to provide a traverse at the upstream and downstream axial positions. Thus, a transverse map of the noise levels was recorded. The signal provided by the noise generator was introduced upstream of the treatment section. Aerodynamic instrumentation was included to determine the duct Mach number. Pitot-static probes were mounted in the duct mid-stream, and manometers were used in reading pressure levels.

4.2 FAN EXHAUST TREATMENT TESTING ON SCALE-MODEL FAN VEHICLE

The fan exhaust treatment configuration that acoustic duct tests found to best suppress noise was further evaluated. A test series, designated as the Scale Model Fan Test Program, was conducted in the General Electric Company, Schenectady, Anechoic Chamber. Aft radiated noise level effects were measured with the noise source provided by a low tip speed, low pressure ratio, 50.8-cm (20-in.) diameter NASA-Lewis-Research-Center Fan (designated Rotor 55). The test chamber and its sound field are shown schematically in Figure 21, while Figure 22 presents a schematic cross section of the test vehicle. A photograph of the installed vehicle is shown in Figure 23 with the location of the duct probes identified. More details of the test facility, test vehicle, data acquisition and data reduction systems can be found in Reference 3.

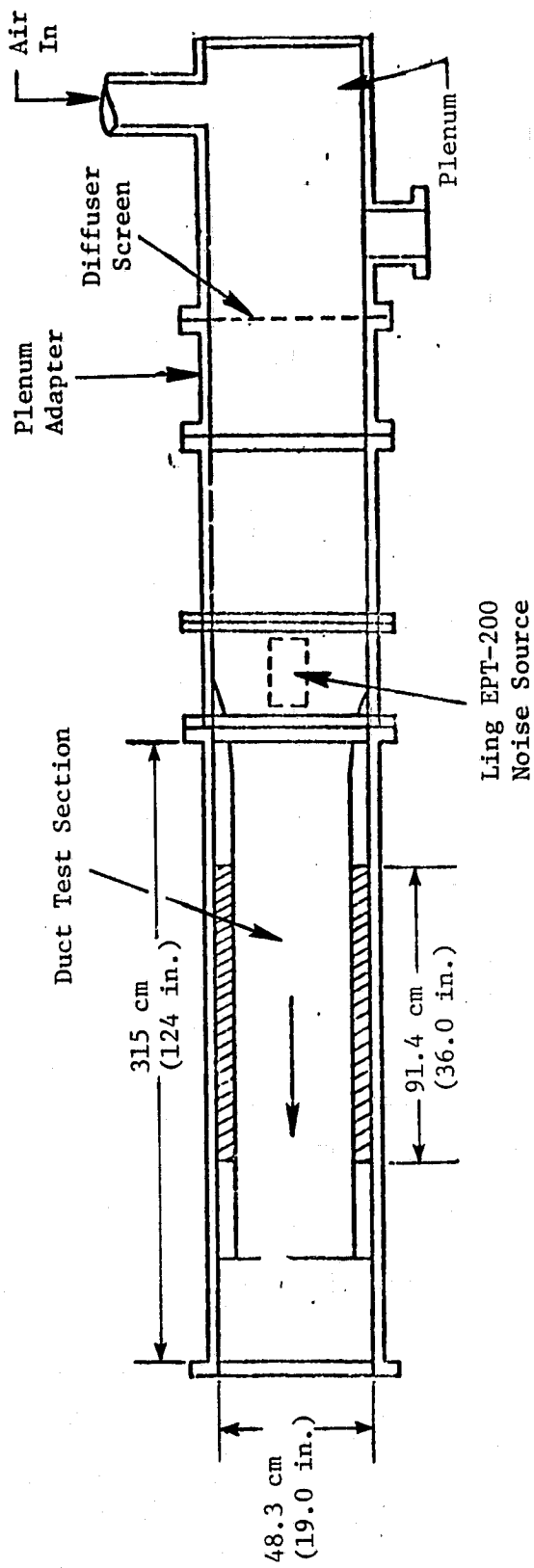


Figure 19. Schematic of Rectangular Cold Flow Laboratory Duct Facility.

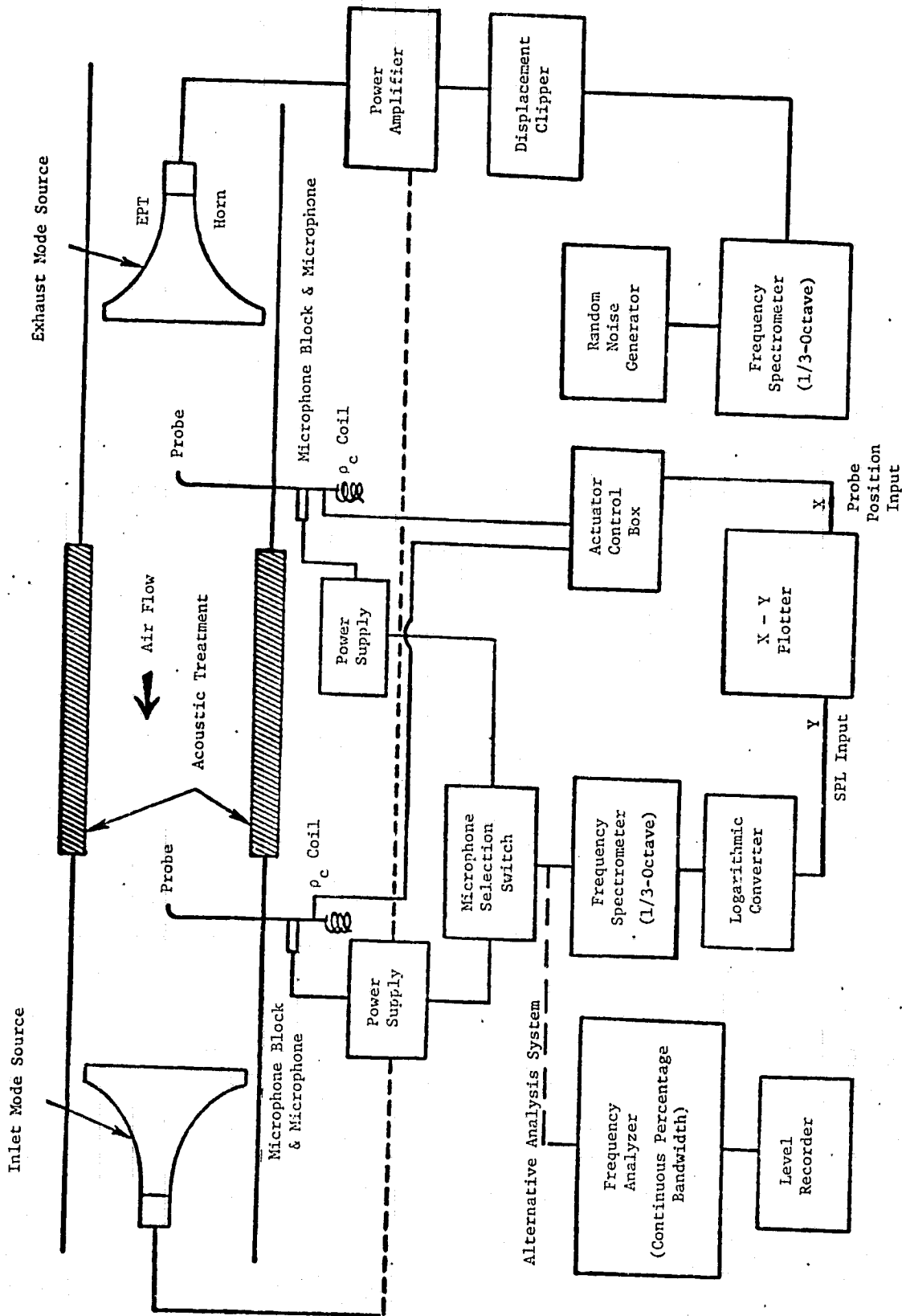


Figure 20. Instrumentation of Rectangular Cold Flow Duct Facility.

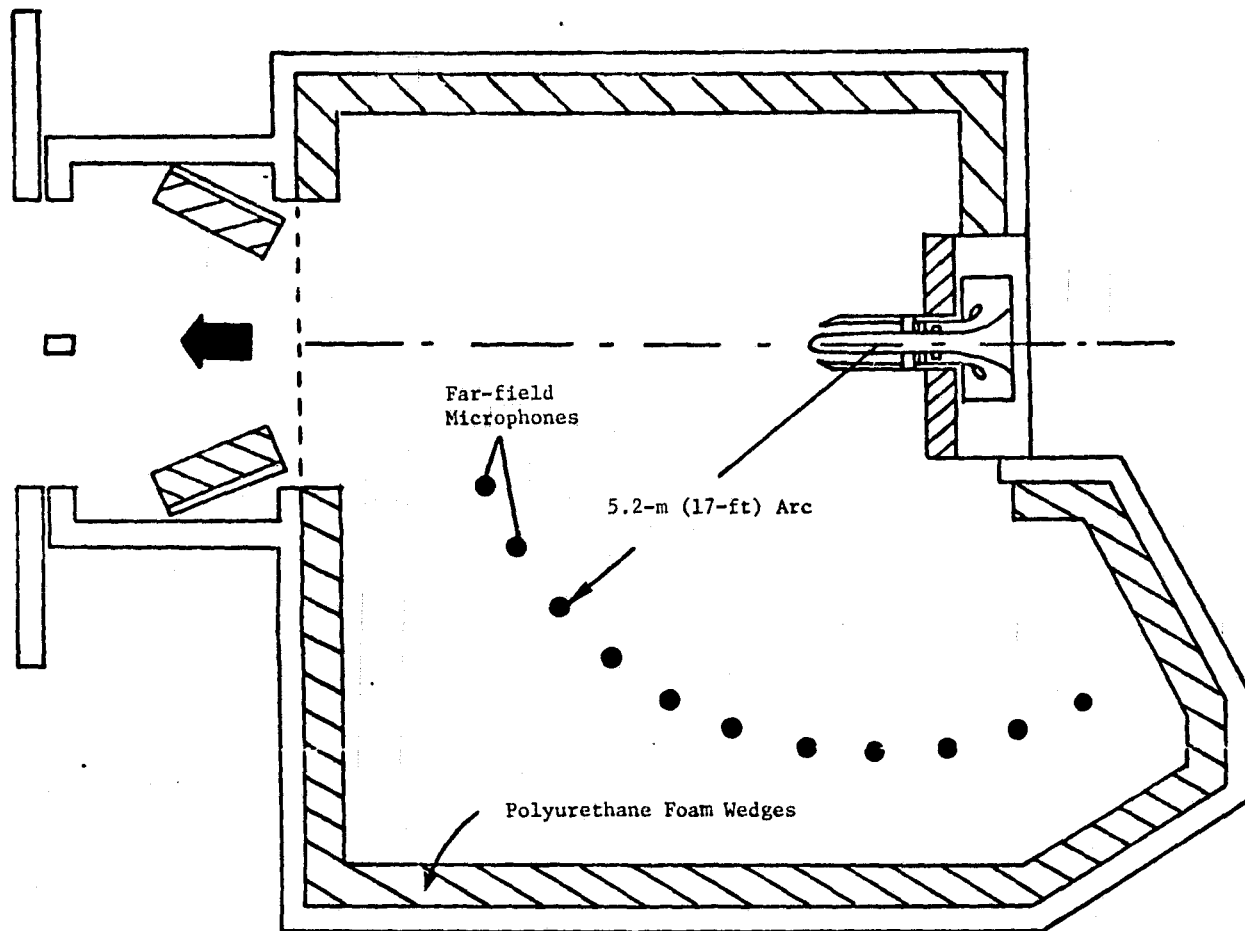


Figure 21. Schematic of the General Electric-Schenectady Anechoic Chamber, Fan Exhaust Test Configuration.

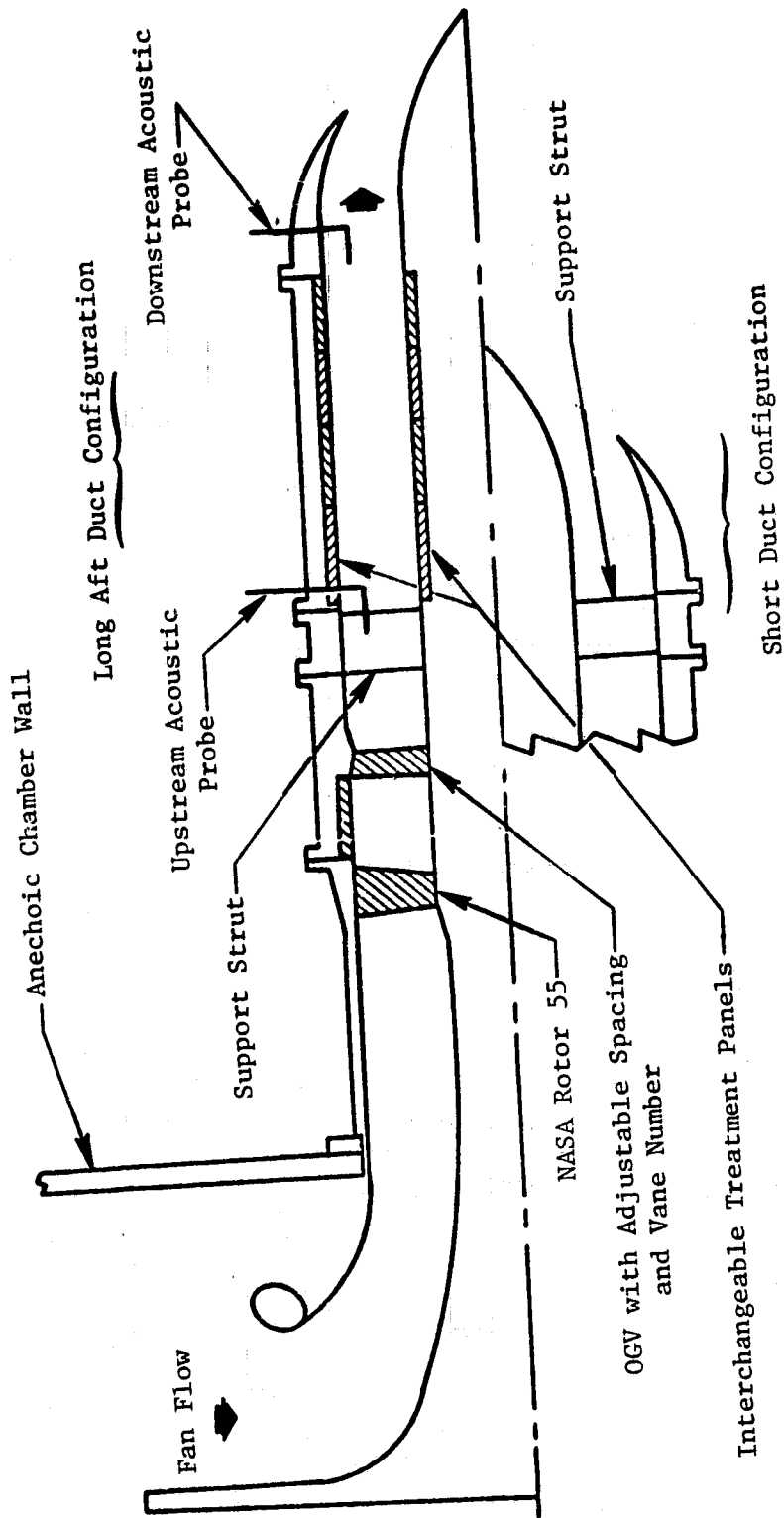


Figure 22. Scale Model Fan Test Vehicle Schematic.

REPRODUCIBILITY OF THE
ORIGINAL PAGE IS POOR

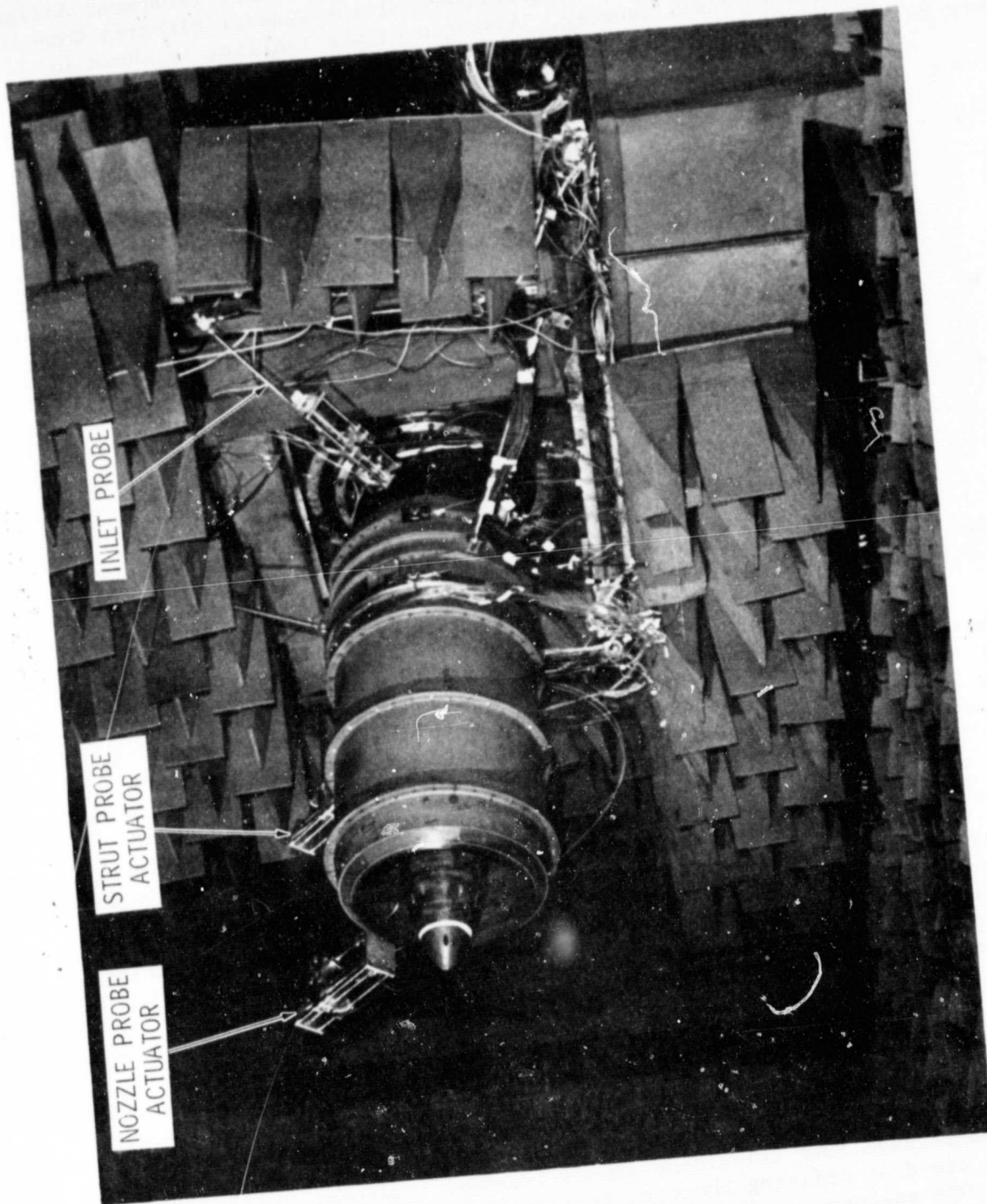


Figure 23. Installed Test Vehicle.

4.3 FAN INLET TREATMENT TESTING ON SCALE MODEL FAN VEHICLE

A series of tests selected to develop the required inlet treatment design was also conducted in the anechoic environment of the General Electric Company, Schenectady, Anechoic Chamber. A sketch of the facility is shown in Figure 24, and a photograph is presented in Figure 25. It is comprised of:

- A 2,500-hp drive system for speeds up to 15,000 rpm.
- An anechoic chamber approximately 10.67-m (35.0-ft) wide by 7.62-m (25.0-ft) long by 3.05-m (10.0-ft) high designed for less than ± 1 dB standing wave ratio at 200 Hz. All walls, floor, and ceiling are covered with an array of 71.1-cm (28.0-in.) polyurethane foam wedges.
- Porous walls for minimum inflow distortion to the fan when measuring inlet radiated noise.
- Ability to install the fan for evaluation of both forward and exhaust radiated noise.
- Far-field noise measurement on a 5.2-m (17.0-ft) arc from 0 to 110° relative to the inlet for inlet-radiated noise.

The sound field is set up with the center of the arc located at the fan face during tests of inlet-radiated noise levels.

The test vehicle (Figure 26) was an adjustable-pitch 50.8-cm (20-in.) diameter exact linear scale model (scale factor 20:71) of the QCSEE Under-the-Wing (UTW) variable-pitch fan. The scale model included the rotor, the nonaxisymmetric bypass OGV and pylon, the core stator, and the transition duct for the core flow. On the transition duct that guides the fan hub flow into the core compressor, a modification was made to permit the use of an existing facility drive shaft. The modification was regarded as minor.

There were 18 variable-pitch rotor blades with a solidity of 0.95 at the tip and 0.98 at the hub. The 50.8-cm (20-in.) simulator fan assembly on the test stand is shown in Figure 27. A fully adjustable discharge valve was used to vary the bypass exhaust nozzle area. The core flow was controlled by suction through two Fuller pumps.

4.4 CORE EXHAUST DUCT FACILITY AND TESTS

Acoustic duct testing was conducted in the cold flow and high-temperature acoustic duct facilities. Treatment concepts such as side-branch resonators and stacked SDOF (single-degree-of-freedom) treatment were evaluated in a program aimed at defining the core exhaust treatment for the QCSEE UTW as well as for OTW engines, which use a common core design.

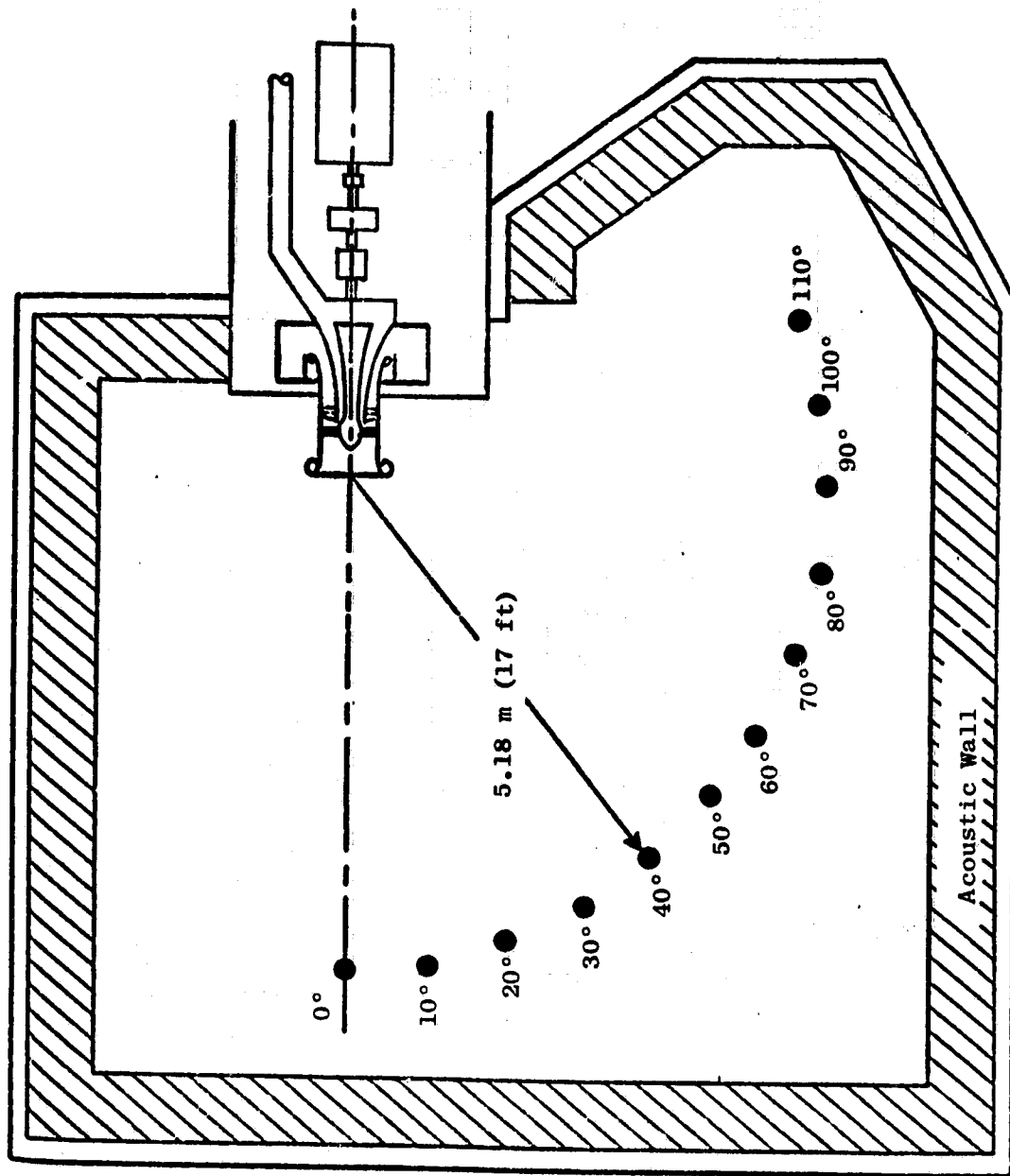


Figure 24. Schematic of General Electric Research and Development Center Anechoic Chamber.

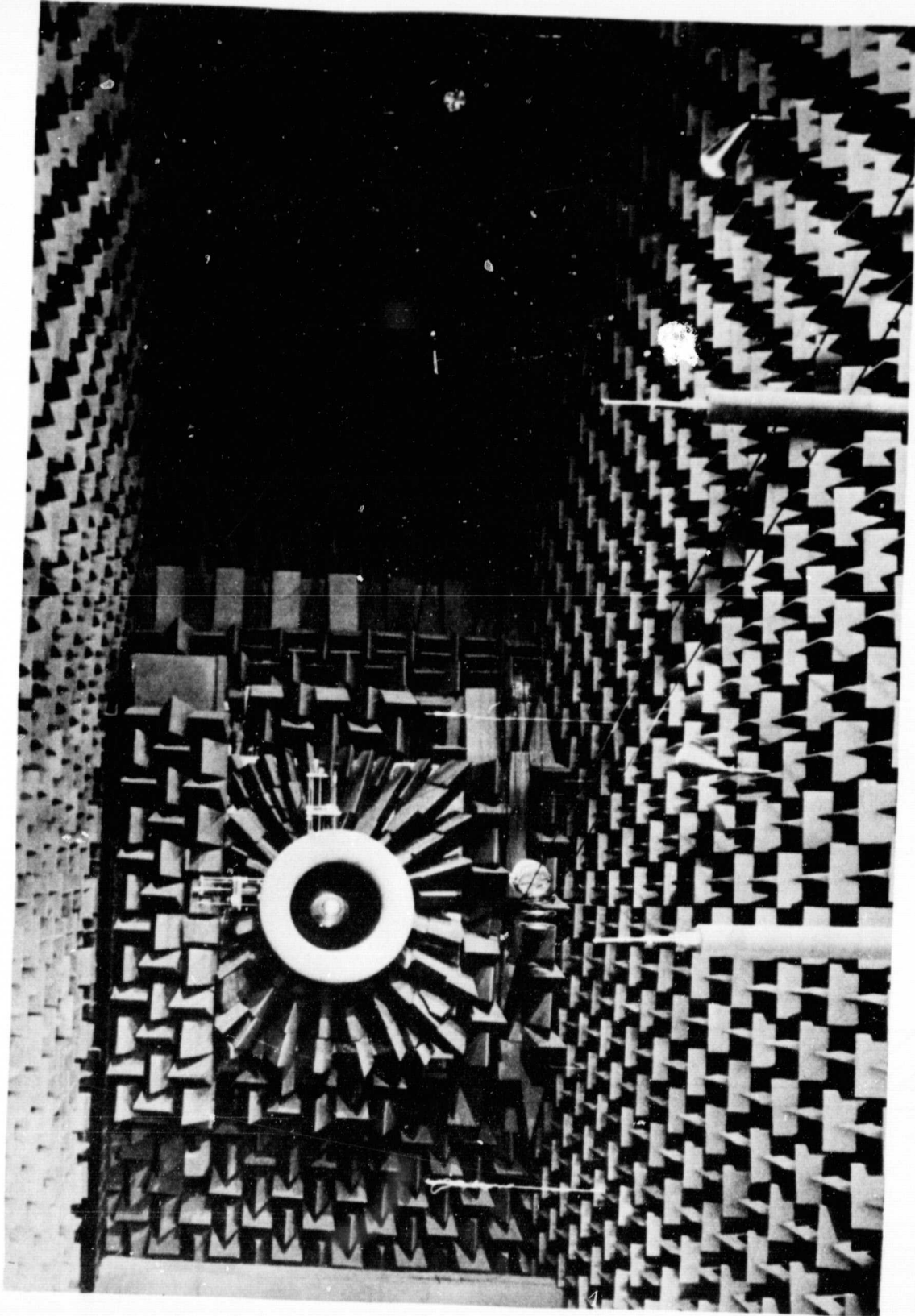
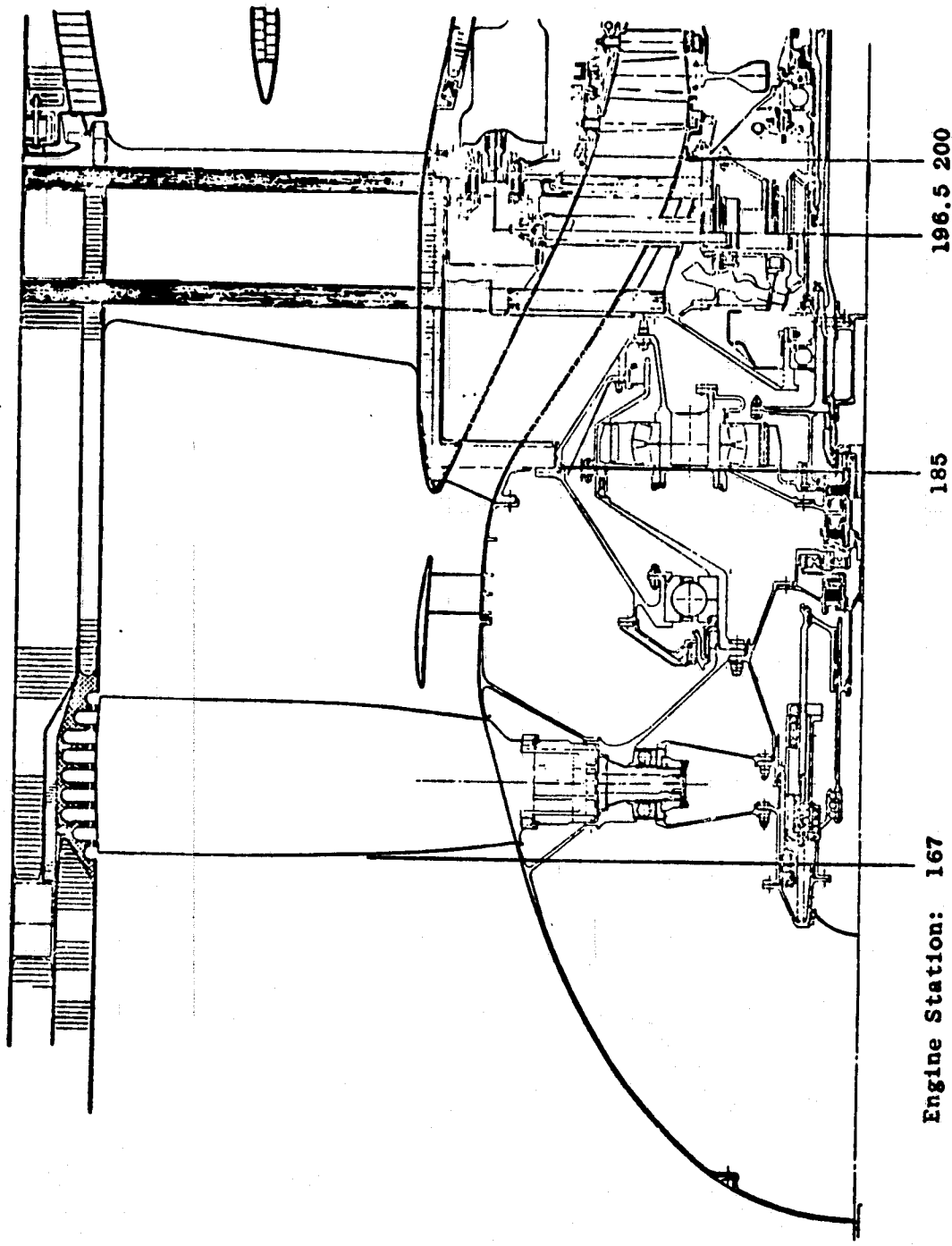


Figure 25. Photo of Anechoic Facility.



Engine Station: 167

185

196.5 200

Figure 26. Cross Section of UTW Variable-Pitch Fan.

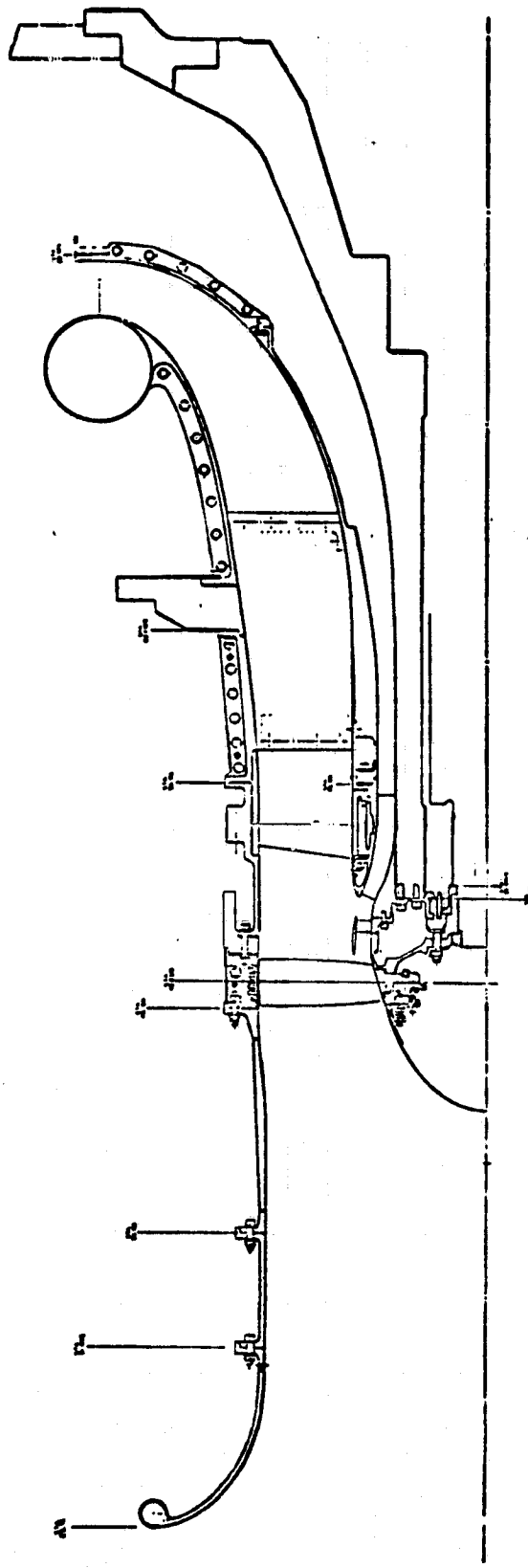


Figure 27. Assembly of UTW Simulator Test Stand.

The cold flow rectangular duct was used to test new concepts and evaluate candidates for testing in the High-Temperature Acoustic Duct Facility (HITAD). The HITAD testing enabled the evaluation of the proposed treatment concepts under the environmental conditions expected in the engine core exhaust, such as airflow and engine temperature.

The cold flow rectangular duct facility was described in Section 4.1. The HITAD facility is depicted in the photo on Figure 28. The test setup used to perform the duct transmission-loss measurements is schematically illustrated in Figure 29. The facility is capable of obtaining Mach numbers up to 0.5 and temperatures up to 1200° F. The acoustic treatment test panels were mounted in a 10.16-cm (4-in.) by 20.32-cm (8-in.) rectangular duct cross section with the treated surfaces 10.16-cm (4-in.) apart. Test panels up to 91.44-cm (36-in.) in length and 15.24-cm (6-in.) in depth can be tested. The instrumentation used in acquiring acoustic data and monitoring the test conditions is shown in Figure 29.

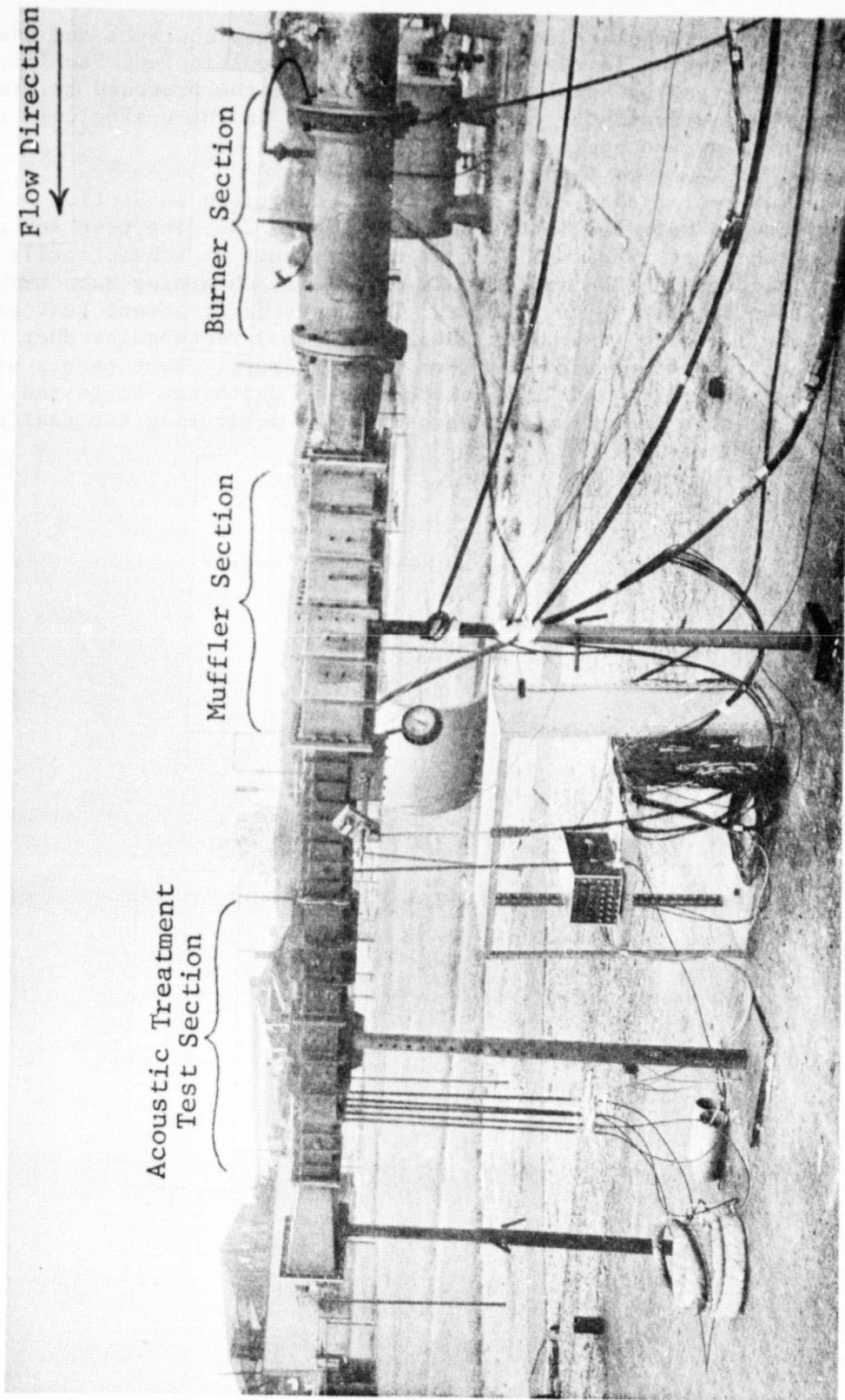


Figure 28. High-Temperature Acoustic Duct Facility Component Details.

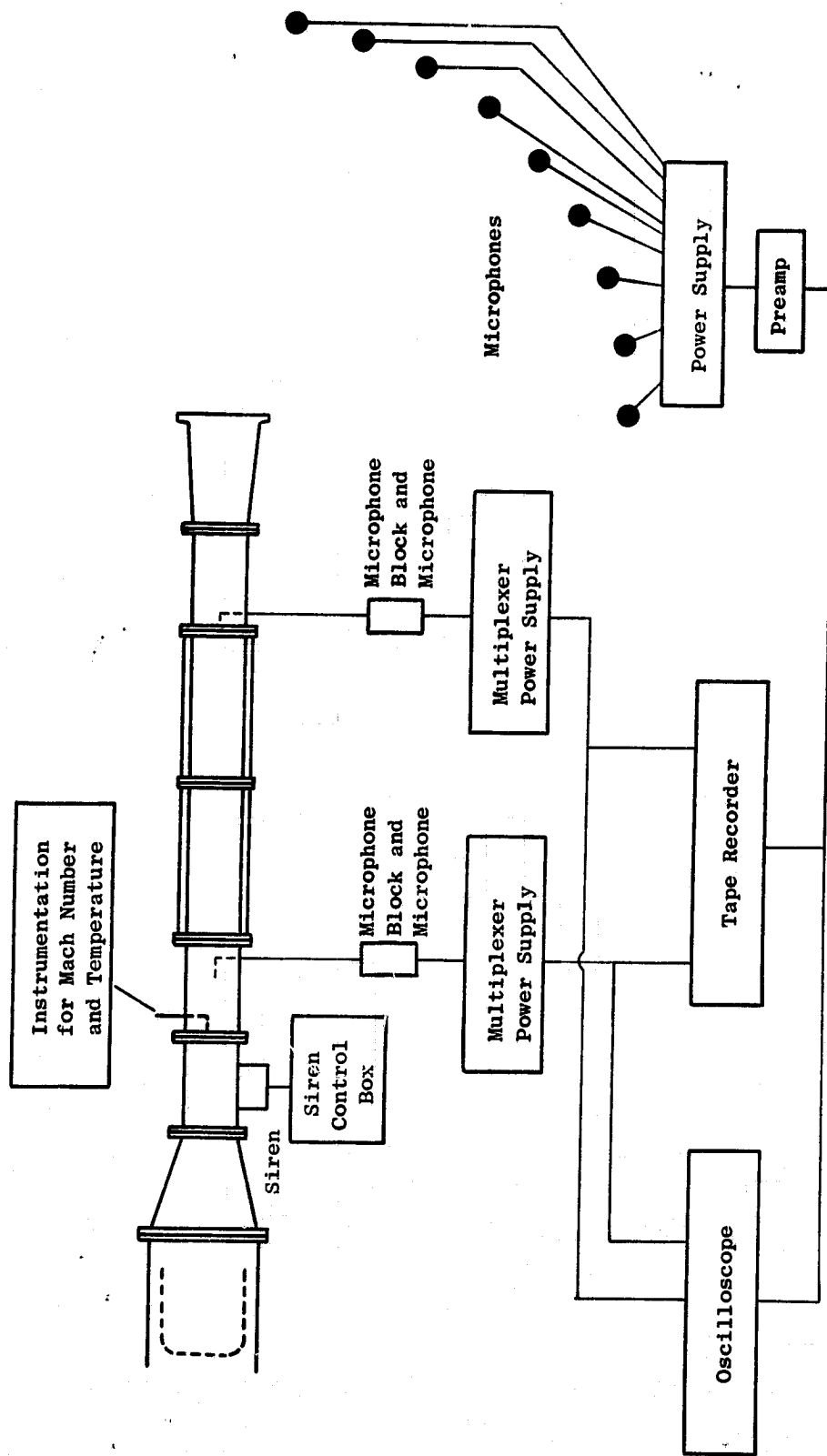


Figure 29. Instrumentation of High-Temperature Acoustic Duct Facility.

5.0 FAN EXHAUST TREATMENT DEVELOPMENT AND DESIGN

5.1 ACOUSTIC DUCT TESTS

A series of acoustic tests was conducted in the rectangular duct test facility in an effort to develop the treatment design technology needed to define the QCSEE fan exhaust treatment. A description of the test facility is given in Section 4.0 of this report. The duct tests were designed to provide the data needed to study the significance of several acoustic parameters felt to have an influence on the suppression characteristics of resonator-type treatment systems. Data were taken at different Mach numbers for each test configuration.

5.1.1 Phased Treatment Concept

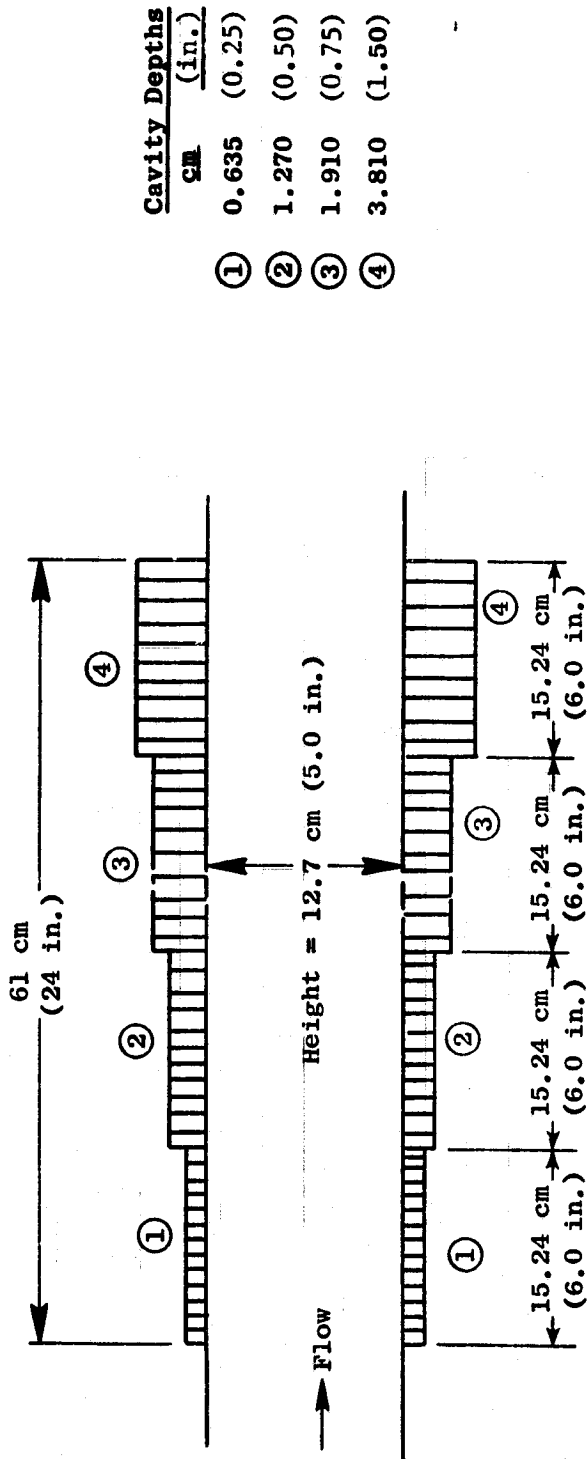
Acoustic duct tests were conducted for configurations with variable-depth panels rather than for the more conventional constant-depth design. This concept was evaluated extensively since potential suppression increases had been demonstrated by Zorumski of NASA. Two phased-treatment test configurations were derived in the laboratory duct from extensive empirical exploration of various possible combinations of the four different thicknesses of panels listed in Figure 30; each panel thickness was tested for both 12% and 27% faceplate porosities. The arrangement (sequence) of the different thicknesses which yielded the best result in the laboratory duct is also shown in Figure 30. The highest suppression was obtained with the 27% porosity case; the results for the 12% case are included for comparison.

Data results showing the measured corrected transmission-loss values for the low- (12%) and the high-porosity (27%) configurations for Mach numbers 0, 0.3, and 0.4 are given in Figures 31 through 36.

The corrected transmission loss spectra for the two configurations are compared in Figure 37 at a 0.4 Mach number condition. The comparison indicates a very significant increase in suppression at most of the 1/3-octave-band frequencies, with a difference of 8 dB shown at 4000 Hz. This substantial increase in the duct suppression level with the variable-depth treatment that had the high faceplate porosity value (27%) was the basis for choosing similar designs for further evaluation on the scale model fan vehicle. The designs and the resulting data are presented and discussed later in this section.

5.1.2 Porosity Optimization

In order to optimize the faceplate porosity, tests were run on several constant-depth treatment configurations having various faceplate porosities. Figure 38 shows a schematic defining the geometry of the test configurations.



Configuration 1 and 2 of QCSEE Cold Flow Rectangular Acoustic Duct Tests

Hole Diameter = 0.16 cm (0.0625 in.)
 Faceplate Thickness = 0.08 cm (0.032 in.)

Configuration
 1 12%
 2 27%
 Porosity

Figure 30. Definition of Duct Variable-Depth Treatment Configurations.

Rectangular Cold Flow Duct Suppression Spectra

- $L/H = 4.8$
- Configuration 1, 12% Porosity
- Duct Mach = 0

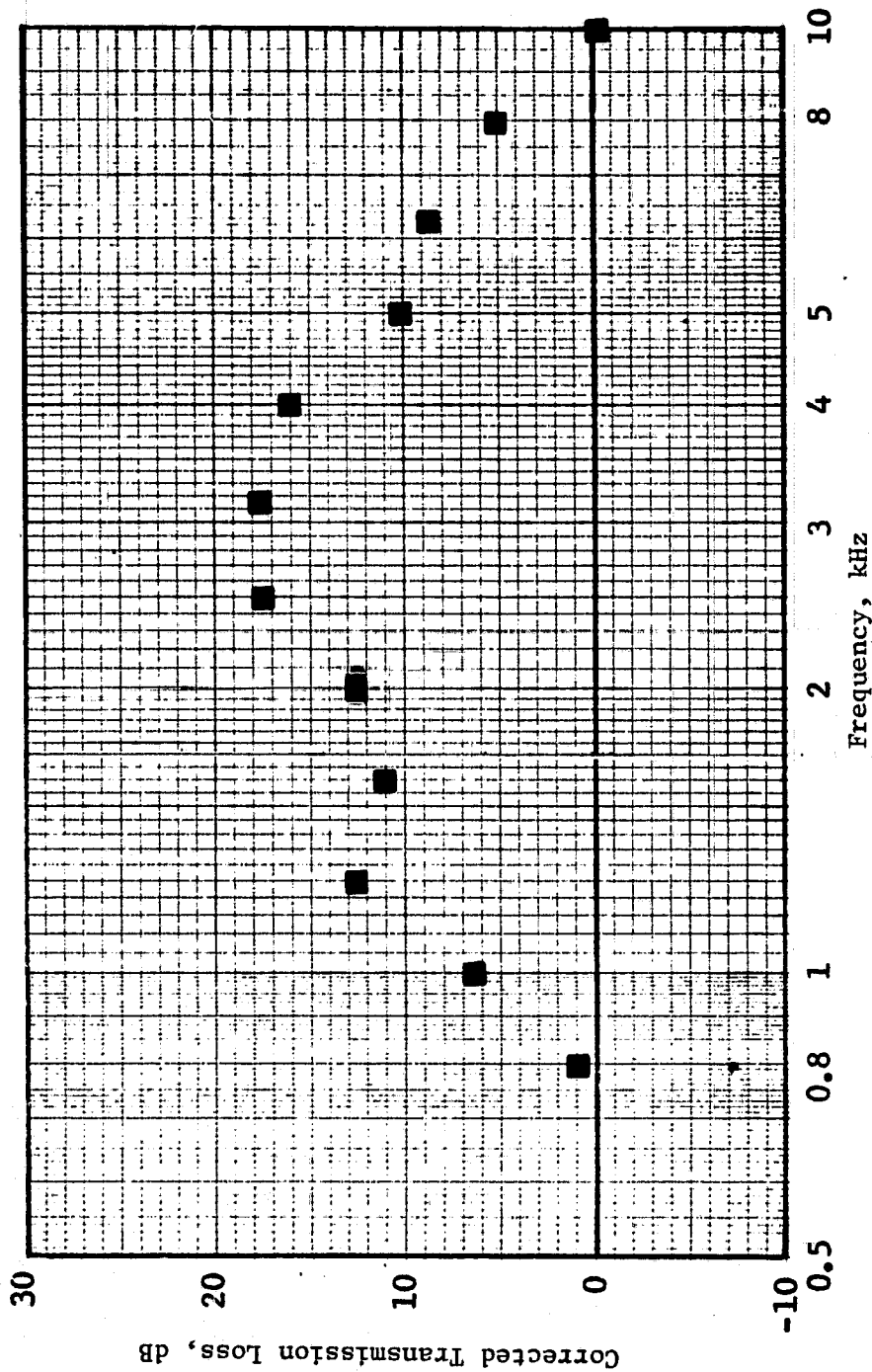


Figure 31. Corrected Transmission Loss Vs. Frequency for Variable-Depth Treatment; Configuration with 12% Porosity.

Rectangular Cold Flow Duct Suppression Spectra

- $L/H = 4.8$
- Configuration 1, 12% Porosity
- Duct Mach = 0.3

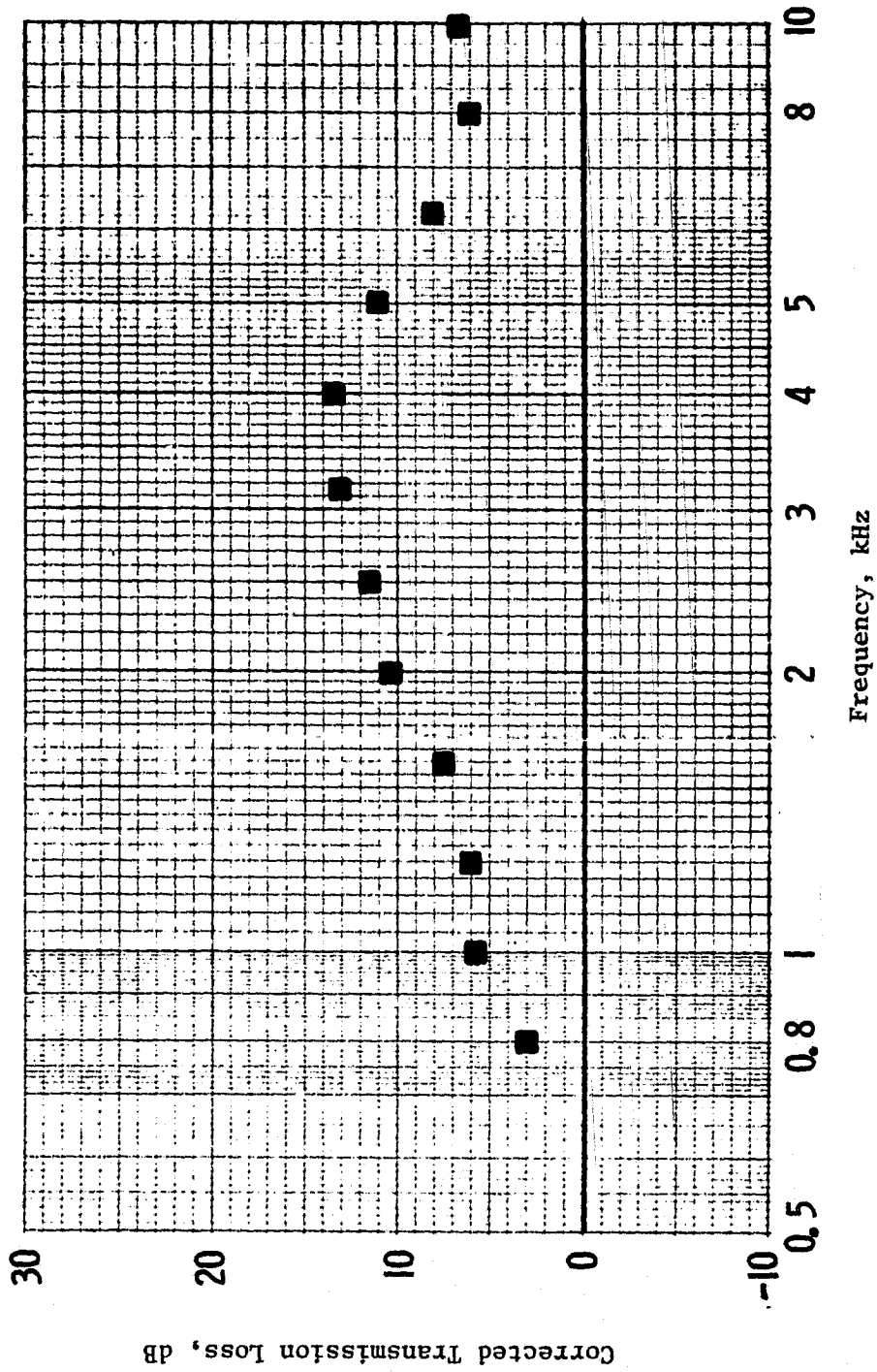


Figure 32. Corrected Transmission Loss Vs. Frequency for Variable-Depth Treatment; Configuration with 12% Porosity.

Rectangular Cold Flow Duct Suppression Spectra

- $L/H = 4.8$
- Configuration 1, 12% Porosity
- Duct Mach = 0.4

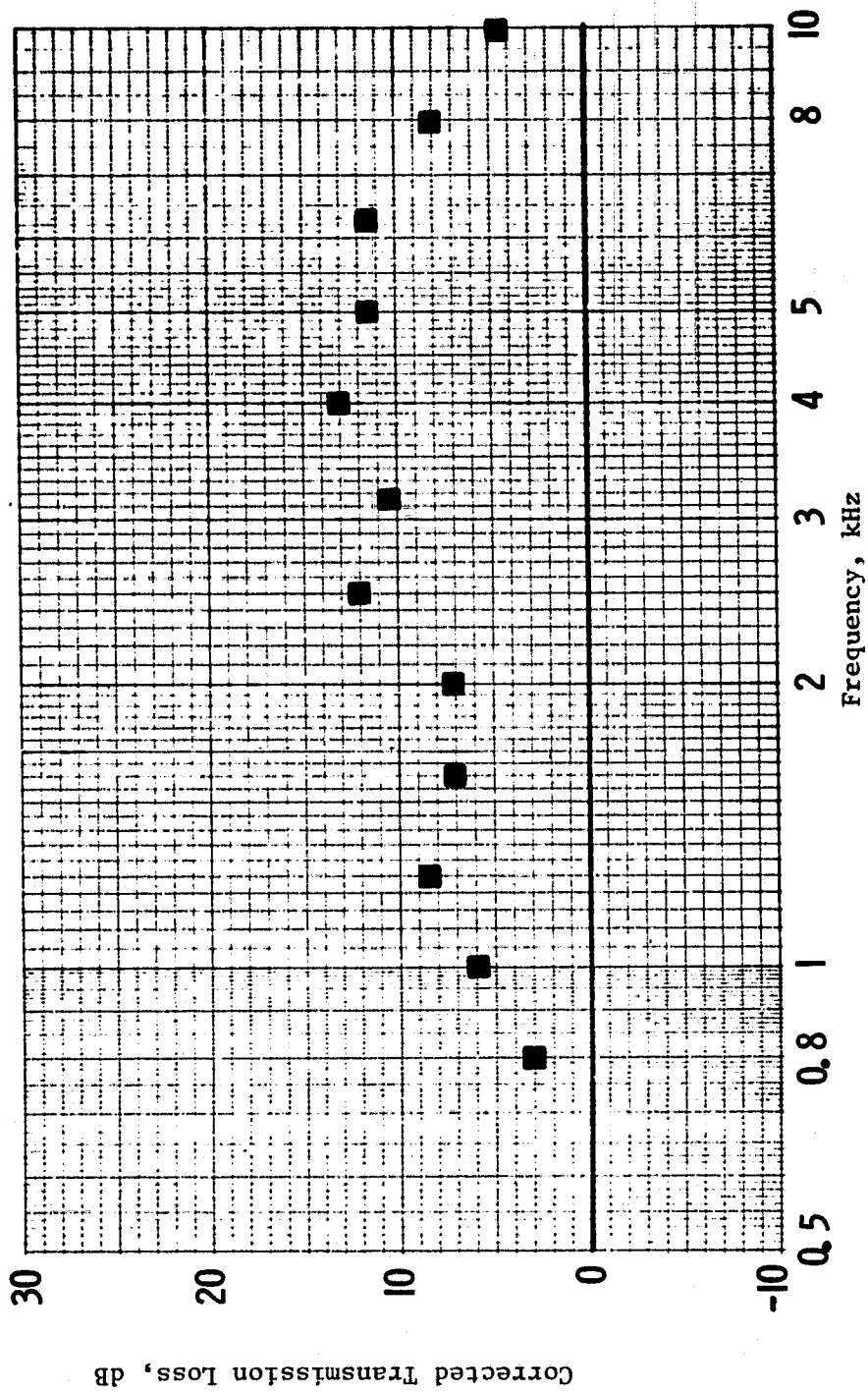


Figure 33. Corrected Transmission Loss Vs. Frequency for Variable-Depth Treatment; Configuration with 12% Porosity.

Rectangular Cold Flow Duct Suppression Spectra

- $L/H = 4.8$
- Configuration 1, 27% Porosity
- Duct Mach = 0

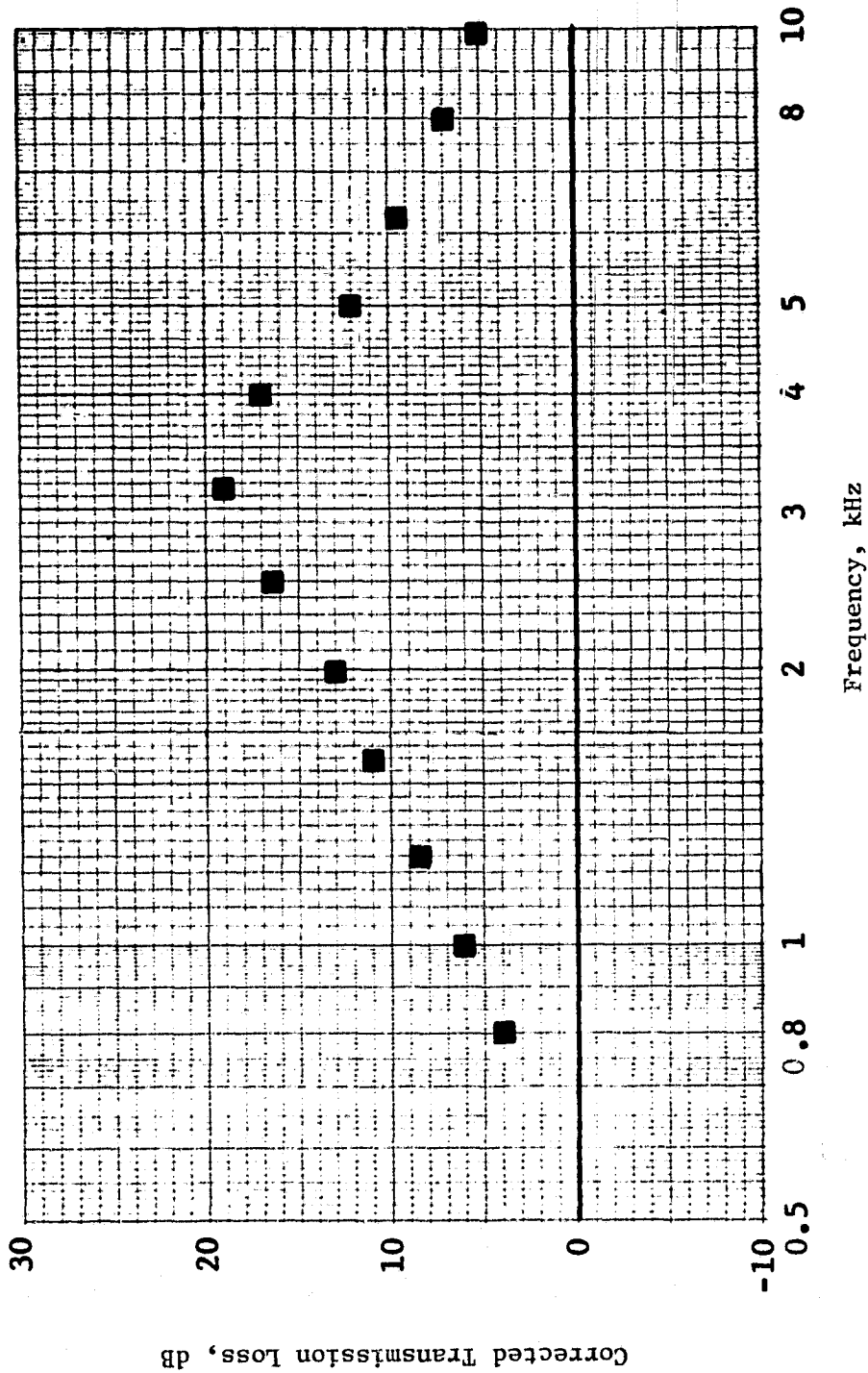


Figure 34. Corrected Transmission Loss Vs. Frequency for Variable-Depth Treatment; Configuration with 27% Porosity.

Rectangular Cold Flow Duct Suppression Spectra

- $L/H = 4.8$
- Configuration 2, 27% Porosity
- Duct Mach = 0.3

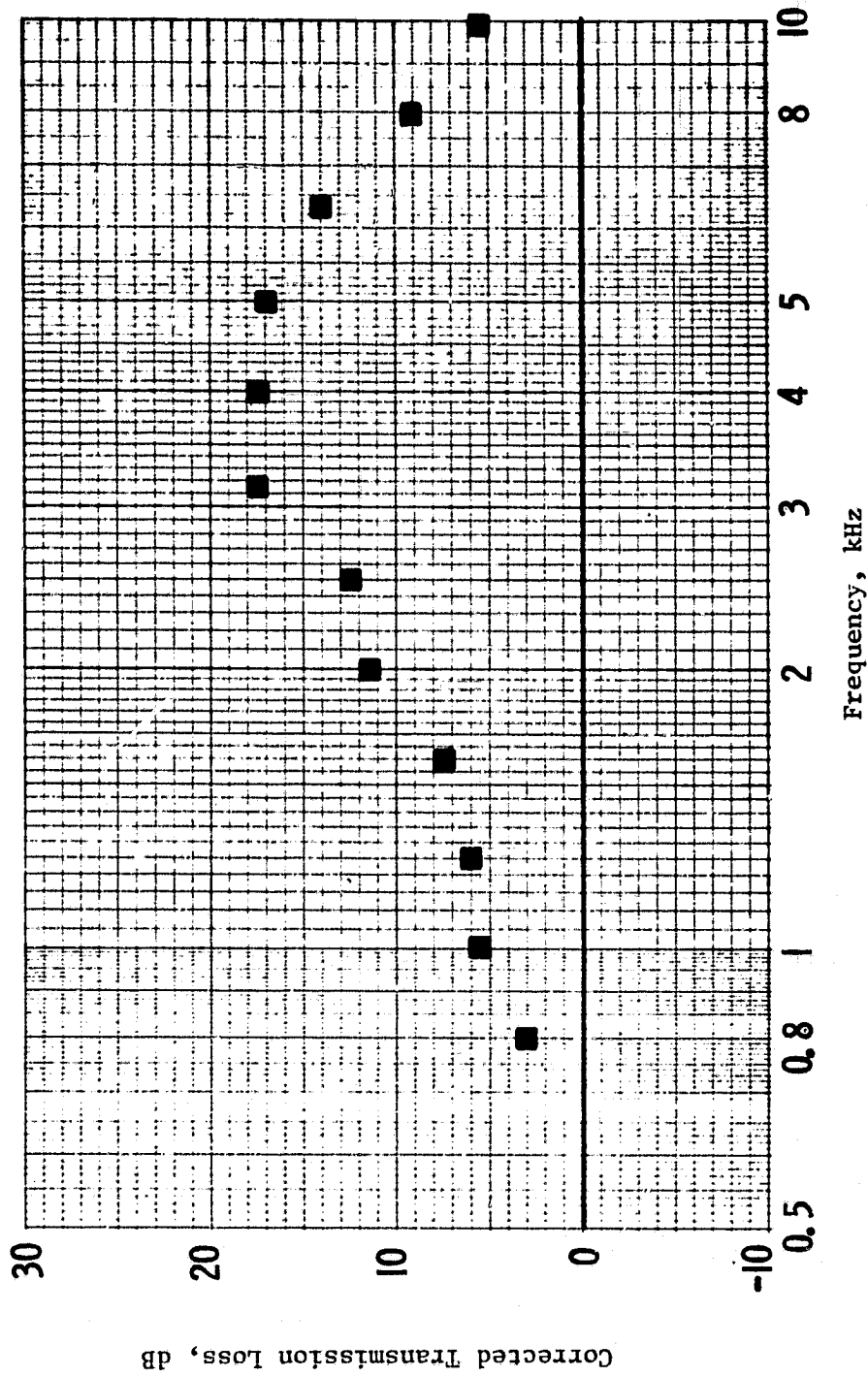


Figure 35. Corrected Transmission Loss Vs. Frequency for Variable-Depth Treatment; Configuration with 27% Porosity.

Rectangular Cold Flow Duct Suppression Spectra

- $L/H = 4.8$
- Configuration 2, 27% Porosity
- Duct Mach = 0.4

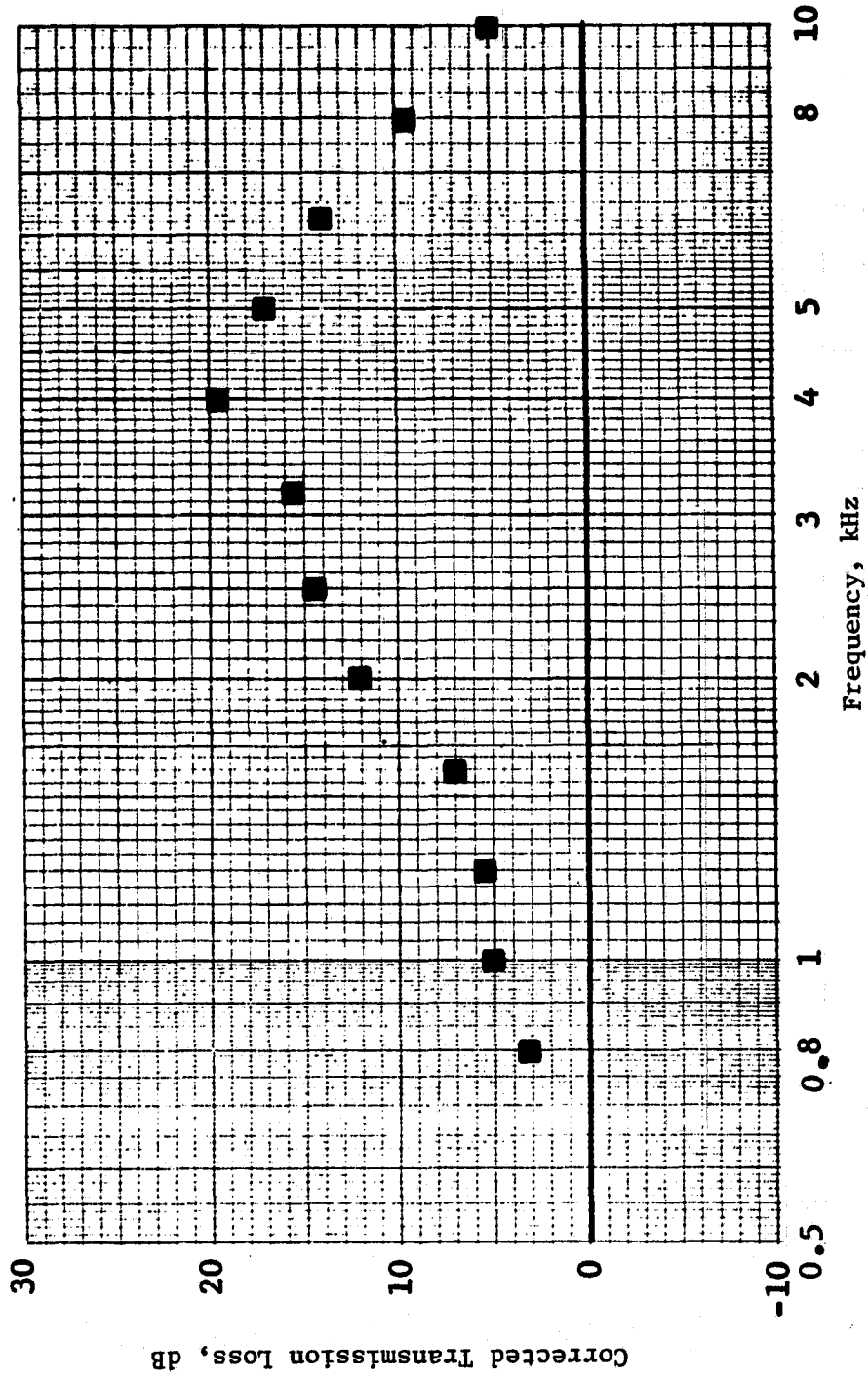


Figure 36. Corrected Transmission Loss Vs. Frequency for Variable-Depth Treatment; Configuration with 27% Porosity.

Rectangular Cold Flow Duct Suppression Spectra

- L/H = 4.8
- Duct Mach = 0.4

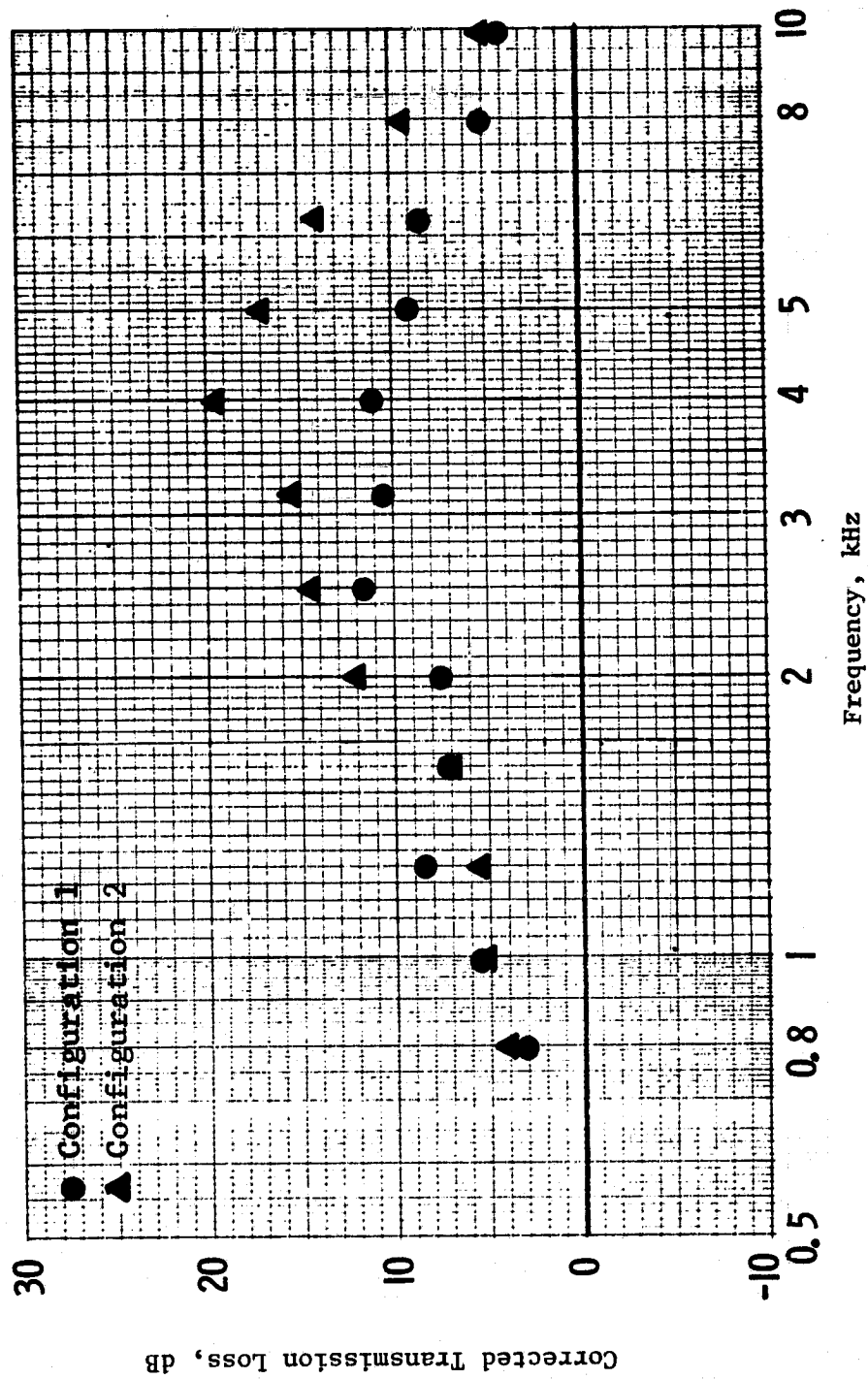


Figure 37. Corrected Transmission Loss Vs. Frequency for Variable-Depth Treatment; 12% and 27% Porosities.

Cold Flow Acoustic Duct Facility

• Straight Duct Geometry

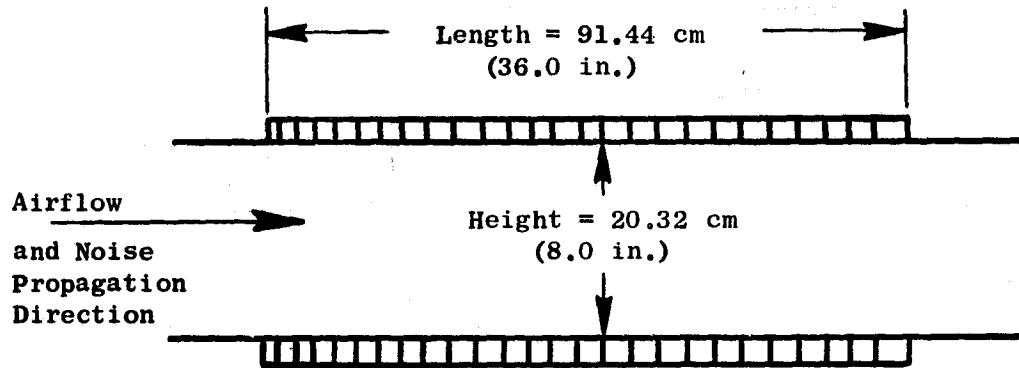


Figure 38. Definition of Acoustic Duct Constant-Depth Treatment Configurations.

For each configuration, the treatment length of 91.44-cm (36.0-in.) was maintained with a corresponding constant duct height of 20.32-cm (8.0-in.). Data were recorded at duct Mach numbers of 0, 0.3, and 0.4 for each treatment configuration tested.

The test matrix of SDOF configurations tested in the porosity optimization effort is given in Table III. Panel depths range from 0.635-cm (0.25-in.) to 4.44-cm (1.75-in.). A total of seven different porosity values were tested, from a low of 3.6% to a high of 27.0%. Table IV defines the faceplate and the honeycomb cell dimensions. In addition, a low-frequency case is included, using the data from configurations defined in Figure 144. The data itself are given in Figure 153.

The test results in terms of corrected transmission loss are given in Figures 39 through 53. Data are given for the no-flow condition and for duct Mach numbers of 0.3 and 0.4. The objective of these tests, as mentioned in the above discussion, was to identify the optimum face-sheet porosity. Figure 54 gives a correlation, developed from the data, that defines the optimum porosity versus the parameter H/λ_0 - the ratio of the duct height (H) to the wave length (λ_0) at which peak suppression occurred - that gives the highest peak suppression at 0.4 duct Mach number. The dashed lines define the sensitivity of peak suppression to faceplate porosity; the range of porosity within the lines will provide a suppression approximately within 5% of the peak. The curve was developed by determining the porosity and frequency at which the peak suppression occurred at a 0.4 Mach number. The frequency was then converted to H/λ_0 because of the theoretical dependence of optimum resistance upon this parameter.

5.2 SCALE MODEL ROTOR 55 VEHICLE TESTS

The Rotor 55 fan exhaust treatment evaluation tests were selected such that the design concepts defined in the acoustic duct could be further evaluated in an engine-type environment with a rotating fan vehicle serving as the noise source. Treatment configurations utilizing constant-depth and variable-depth panels were tested with various faceplate porosity combinations.

The variable-depth treatment designs had four different sections of treatment. Each of these sections was designed to have a different tuning frequency which produces a variation in the acoustic parameter H/λ_0 . Theoretically, the optimum acoustic resistance varies with this parameter. Thick acoustic liners tuned to low frequencies typically give low H/λ_0 values and require low resistance. Thus, a thick panel requires a higher porosity value than a thinner panel.

Various treatment depth combinations were evaluated at 12% and 27% porosities. All had a treated L/H value of 4.6 and were made up of four treatment panels. The different combinations tested were as follows (t is the depth and σ is the faceplate porosity):

Table III. Definition of Constant-Depth Treatment Configurations Tested for Porosity-Optimization Study.

• Test Matrix of SDOF Configurations
Tested in a 20.32-cm (8-in.) Duct

<u>Configuration</u>	<u>Depth</u>		<u>Porosity, %</u>
	<u>cm</u>	<u>in.</u>	
A	0.635	0.25	3.6
B	0.635	0.25	5.0
C	0.635	0.25	7.5
D	0.635	0.25	10.0
E	0.635	0.25	14.5
F	1.270	0.50	5.0
G	1.270	0.50	5.0
H	1.270	0.50	7.5
I	1.270	0.50	10.0
J	1.270	0.50	14.5
K	1.270	0.50	22.7
L	4.440	1.75	7.5
M	4.440	1.75	10.0
N	4.440	1.75	14.5
O	4.440	1.75	22.7
P	4.440	1.75	27.0

Table IV. Detail Definition of Faceplate and Core Cell Size for Constant-Depth Treatment Configuration Tested in Porosity-Optimization Study.

• Faceplate and Honeycomb Cell Dimensions

<u>Configuration</u>	<u>Faceplate Thickness</u>		<u>Hole Diameter</u>		<u>Honeycomb Cell Size</u>	
	<u>cm</u>	<u>(in.)</u>	<u>cm</u>	<u>(in.)</u>	<u>cm</u>	<u>(in.)</u>
A Through F	0.083	(0.0325)	0.159	(0.0625)	0.635	(0.250)
G	0.083	(0.0325)	0.159	(0.0625)	0.950	(0.375)
H Through O	0.083	(0.0325)	0.159	(0.0625)	0.635	(0.250)
P	0.046	(0.0180)	0.084	(0.0330)	0.635	(0.250)

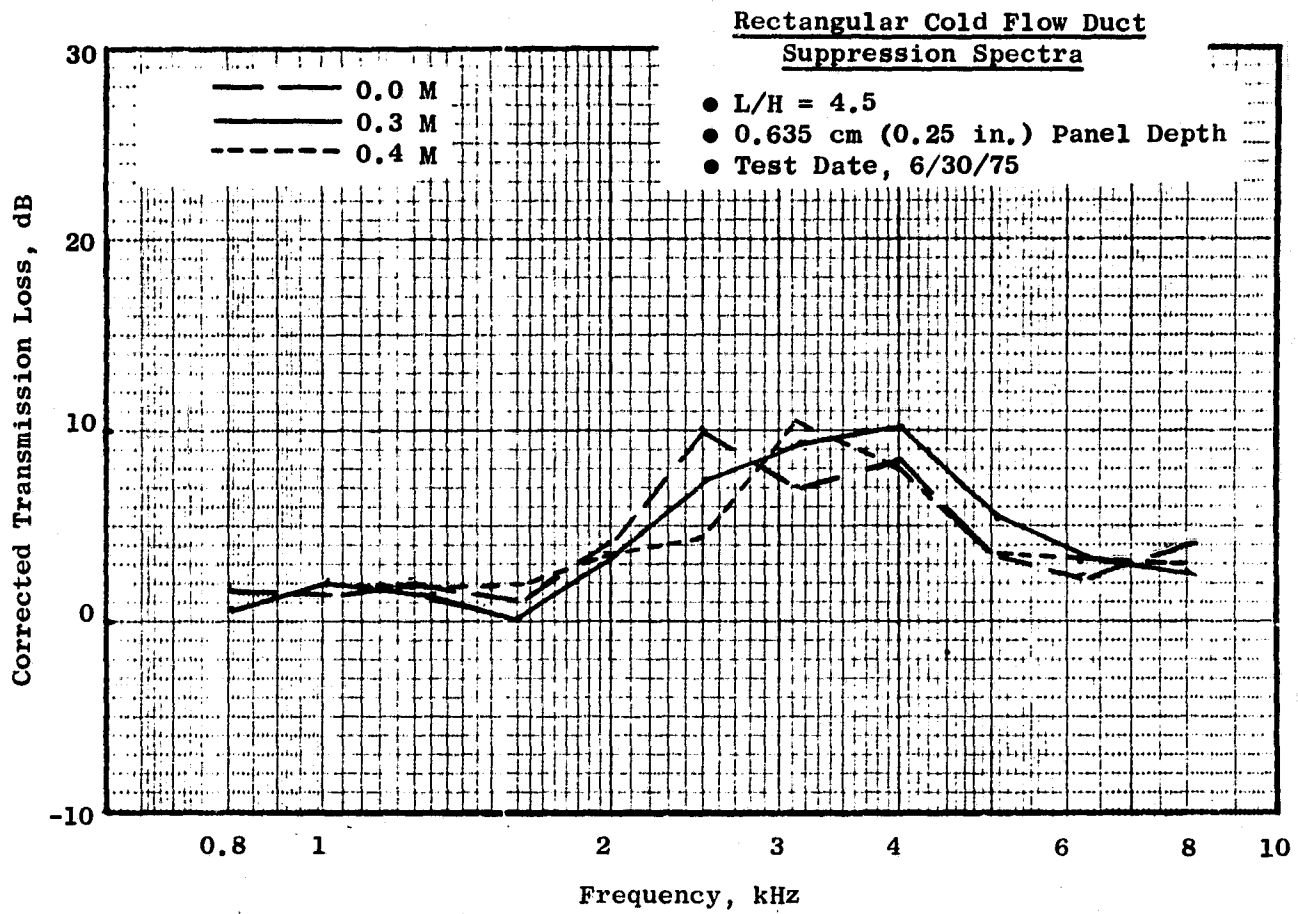


Figure 39. Corrected Transmission Loss Vs. Frequency for Mach Number Variations, 3.6% Porosity.

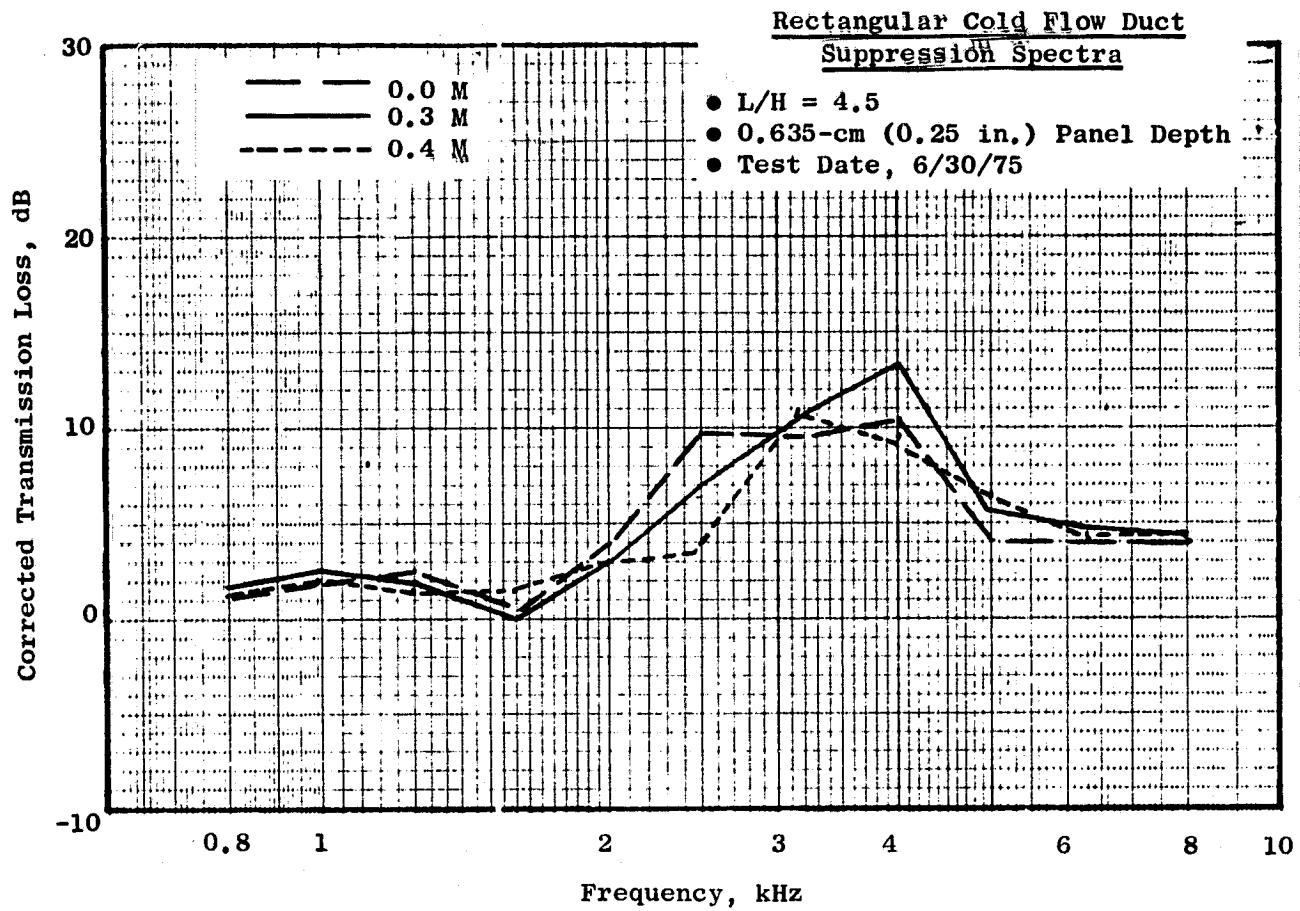


Figure 40. Corrected Transmission Loss Vs. Frequency for Mach Number Variations, 5% Porosity.

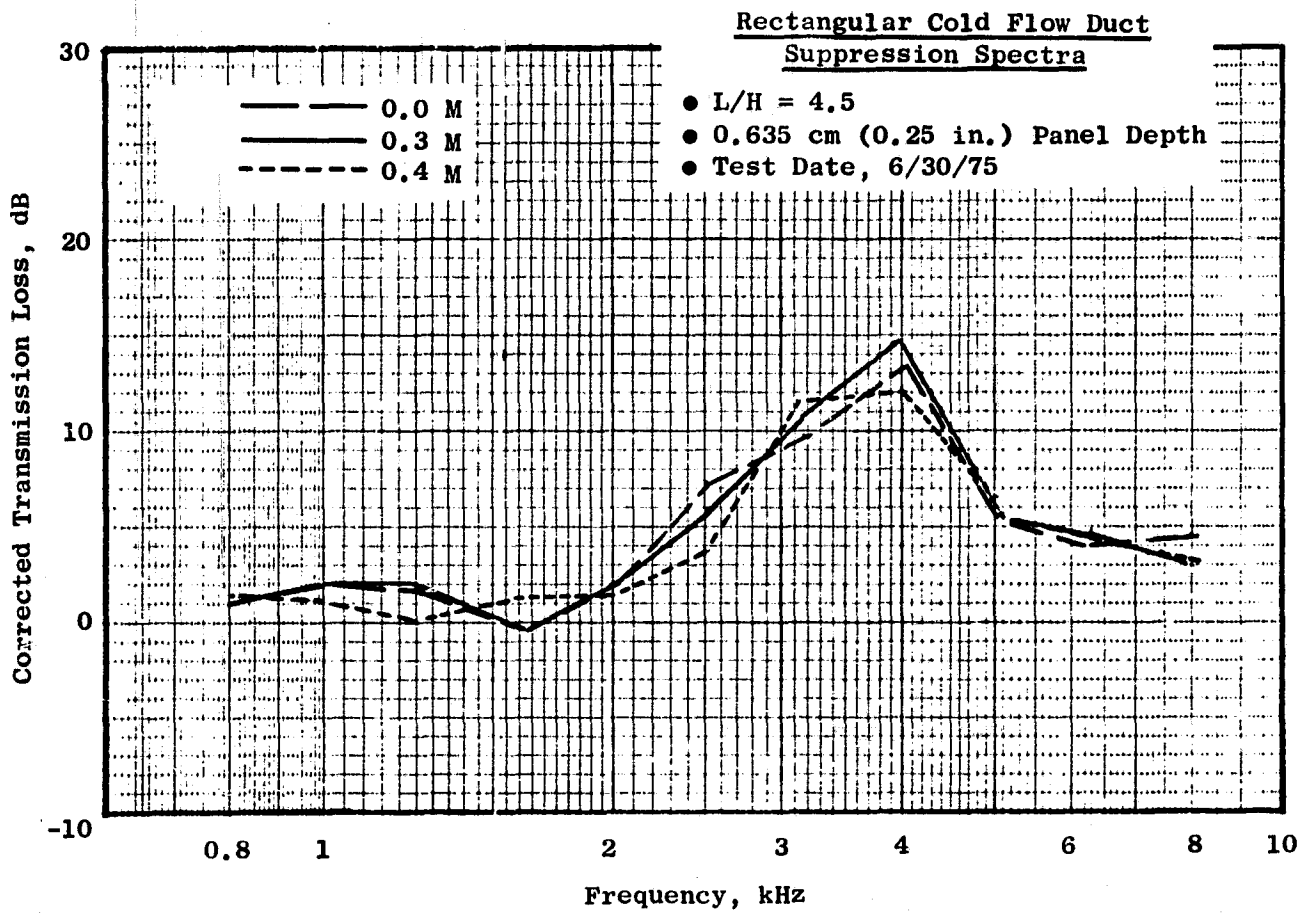


Figure 41. Corrected Transmission Loss Vs. Frequency for Mach Number Variations, 7.5% Porosity.

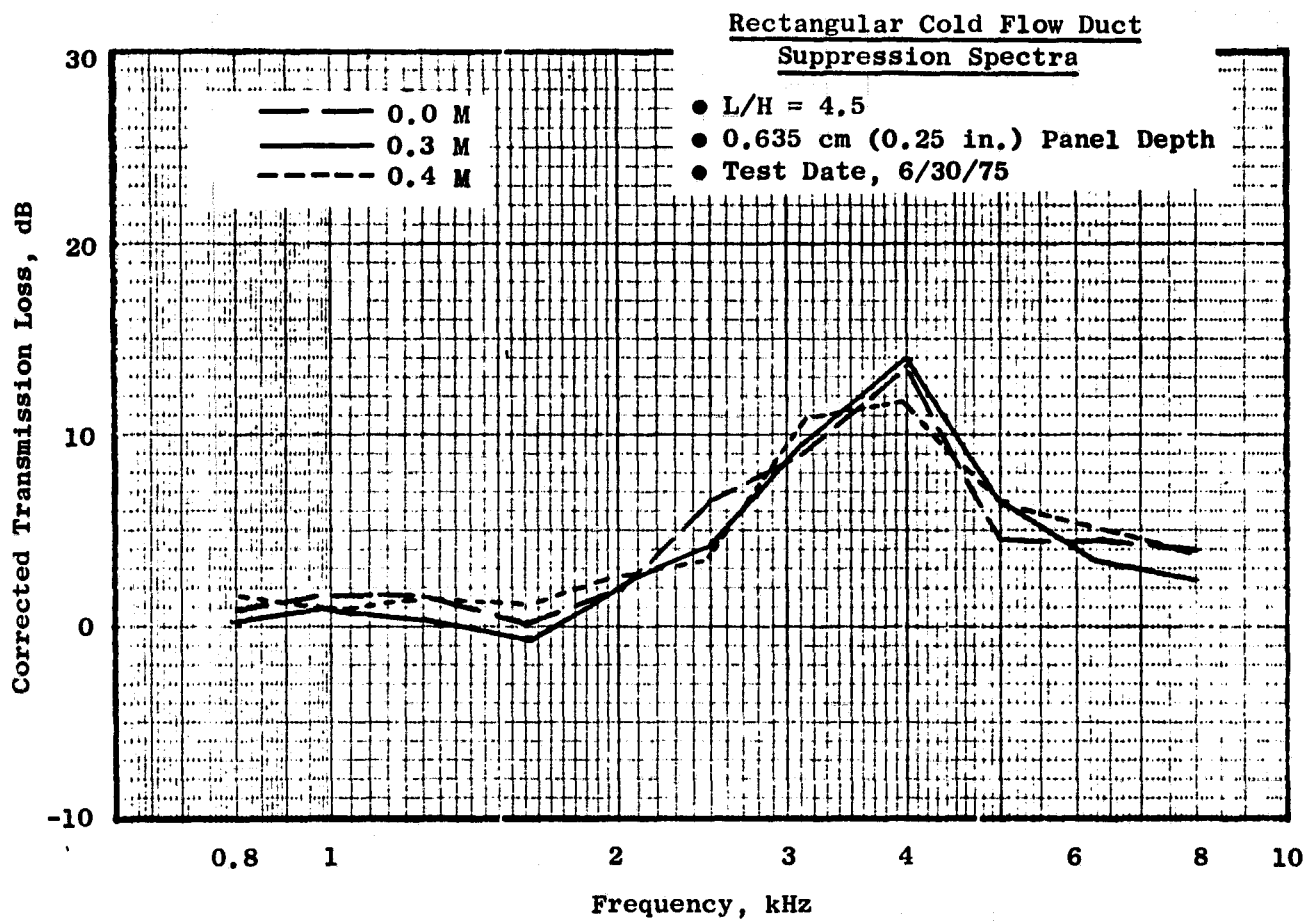


Figure 42. Corrected Transmission Loss Vs. Frequency for Mach Number Variations, 10% Porosity.

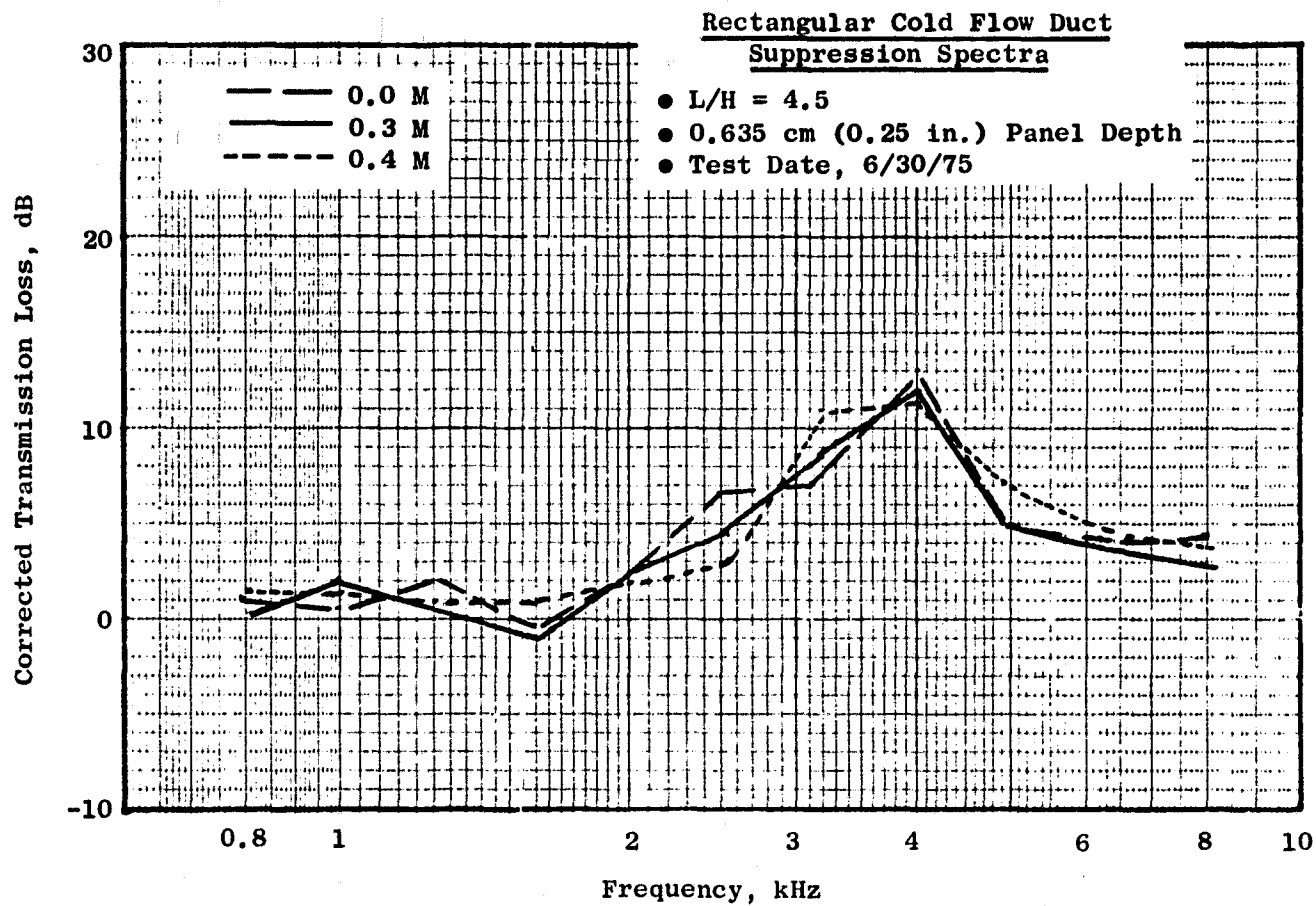


Figure 43. Corrected Transmission Loss Vs. Frequency for Mach Number Variations, 14.5% Porosity.

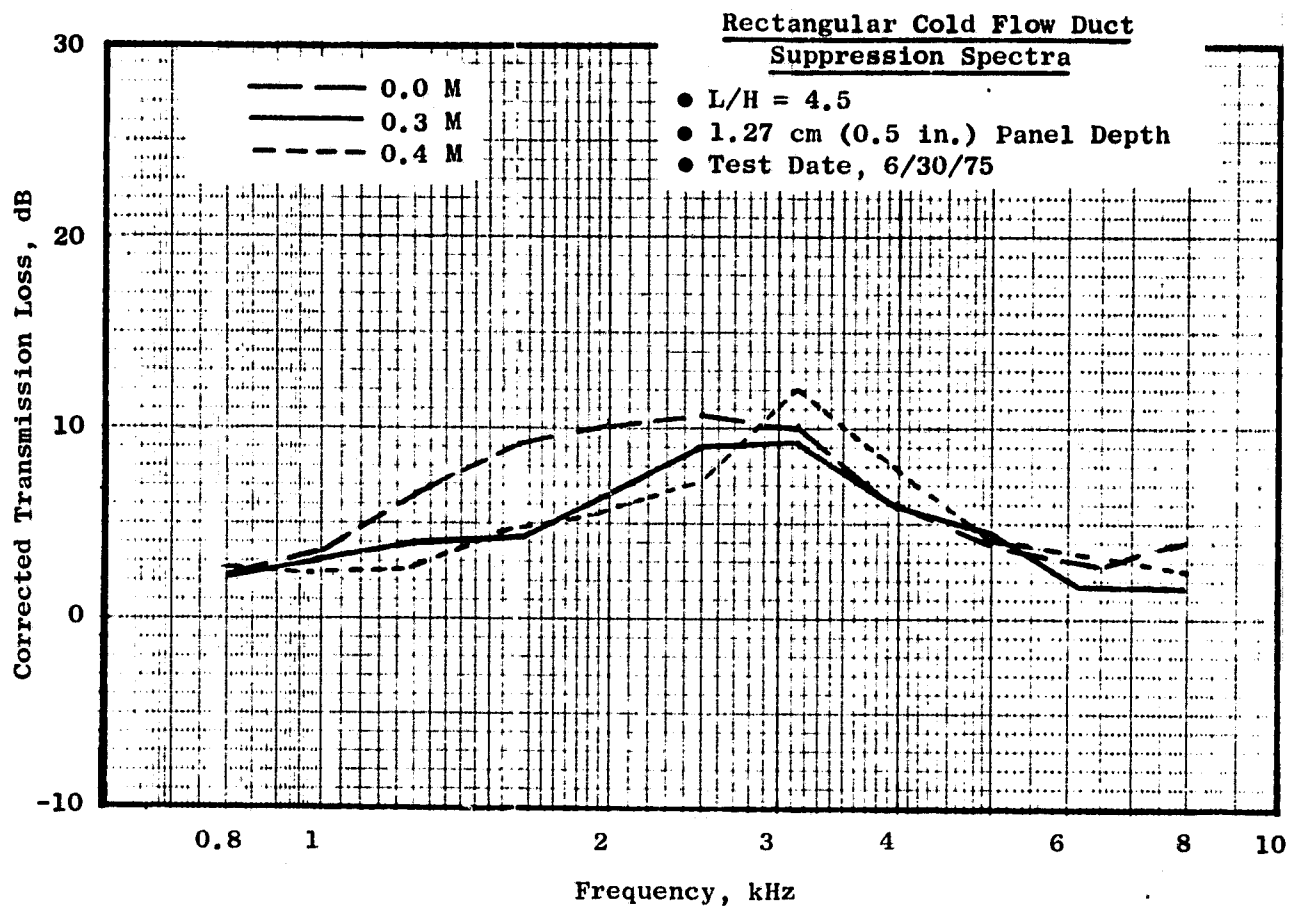


Figure 44. Corrected Transmission Loss Vs. Frequency for Mach Number Variations, 5% Porosity (Configuration G).

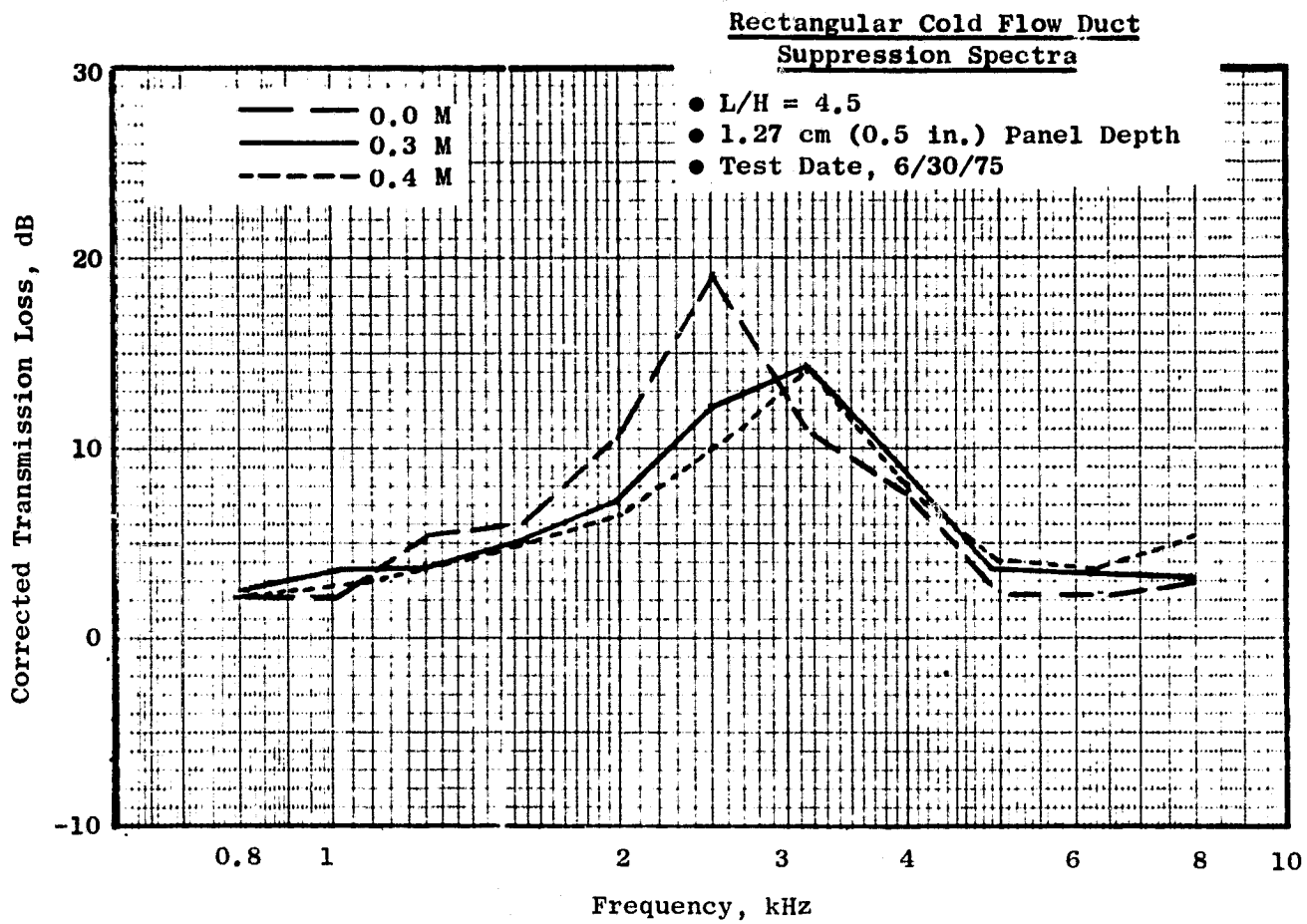


Figure 45. Corrected Transmission Loss Vs. Frequency for Mach Number Variations, 7.5% Porosity.

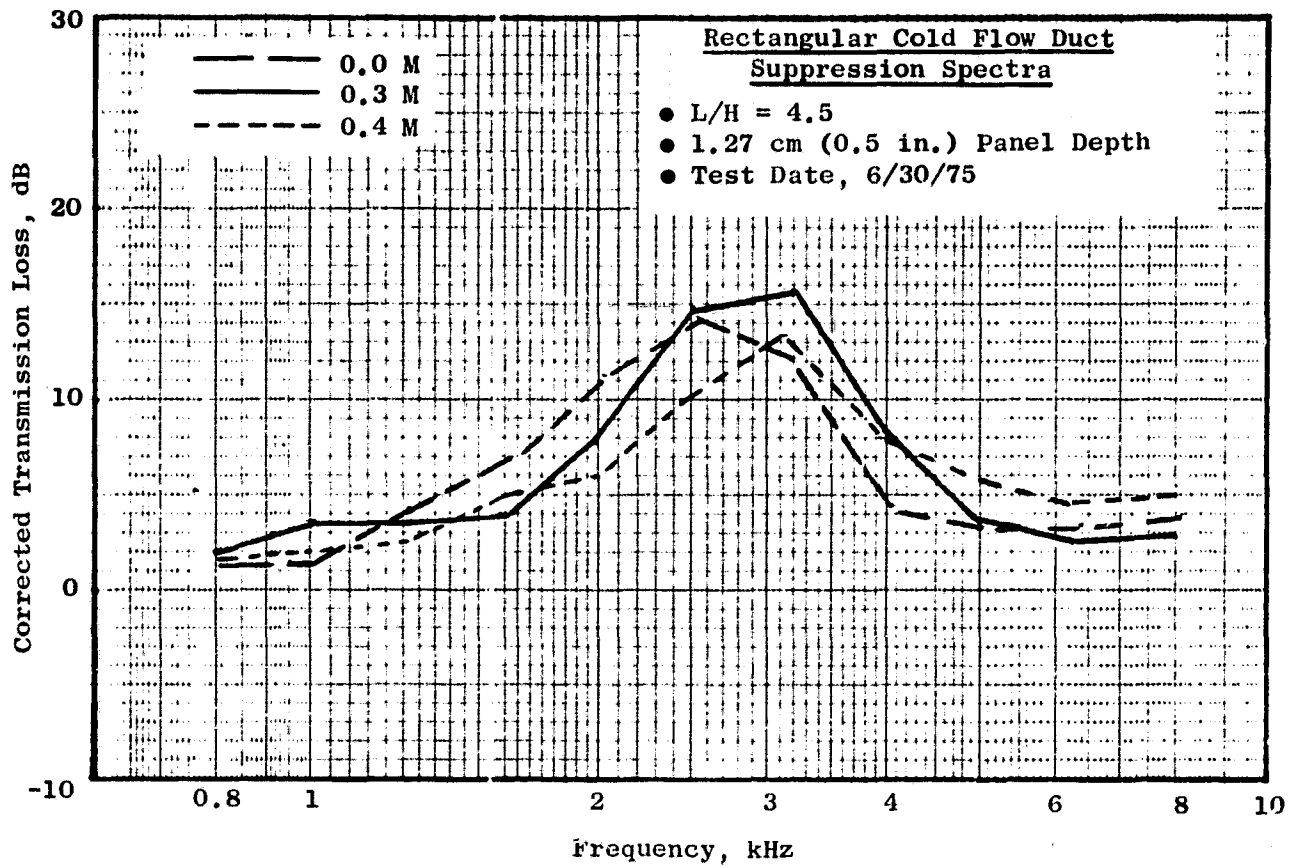


Figure 46. Corrected Transmission Loss Vs. Frequency for Mach Number Variations, 10% Porosity.

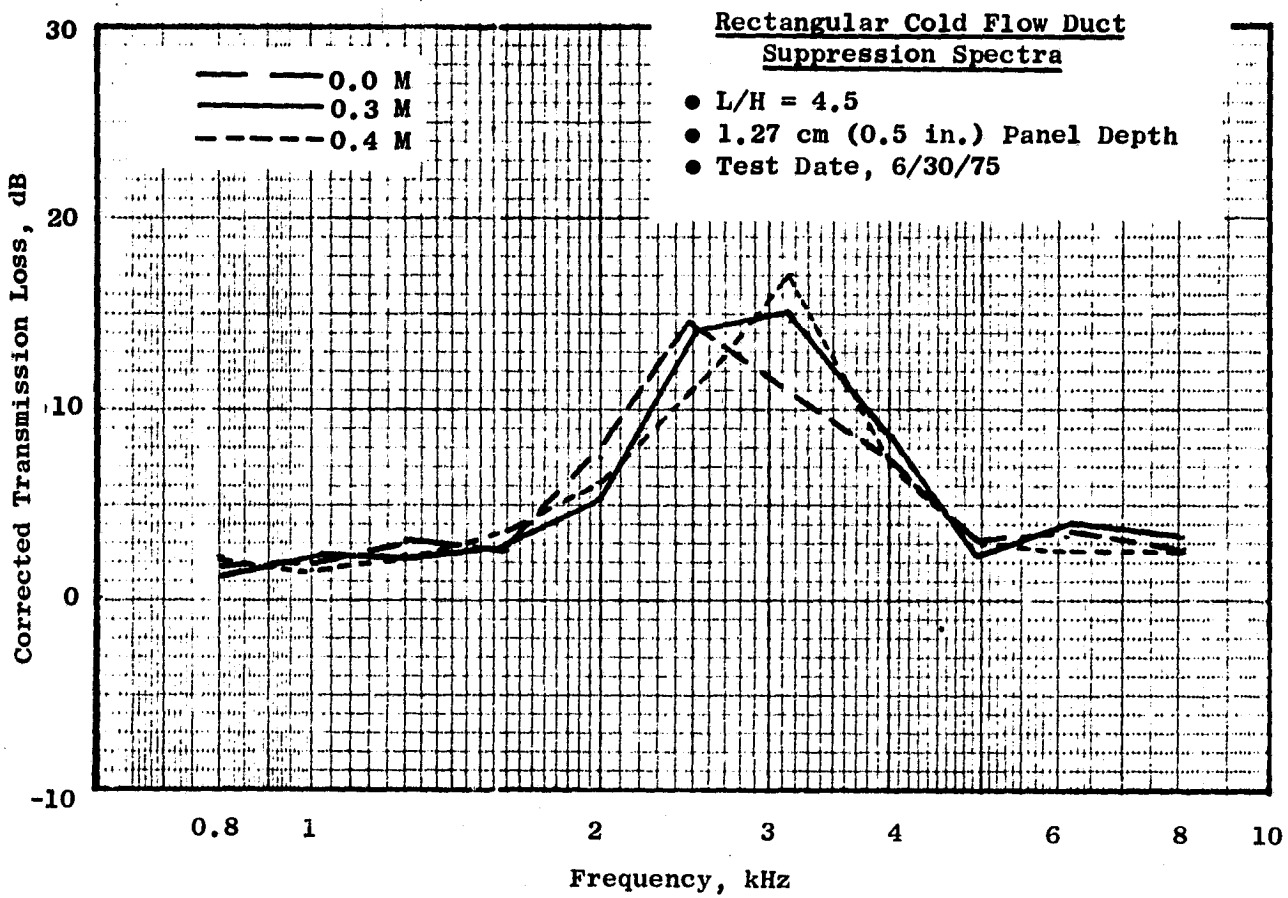


Figure 47. Corrected Transmission Loss Vs. Frequency for Mach Number Variations, 14.5% Porosity.

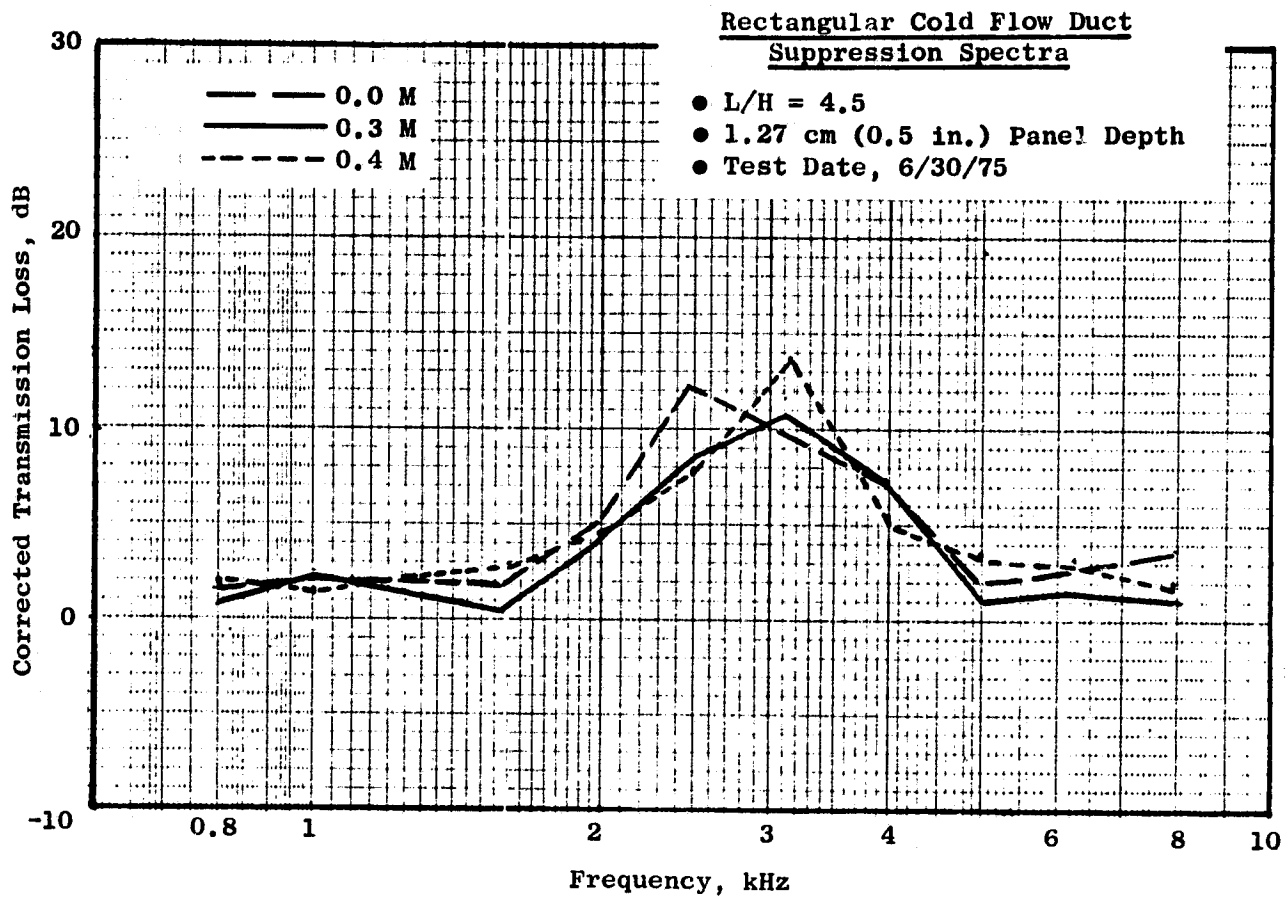


Figure 48. Corrected Transmission Loss Vs. Frequency for Mach Number Variations, 22.7% Porosity.

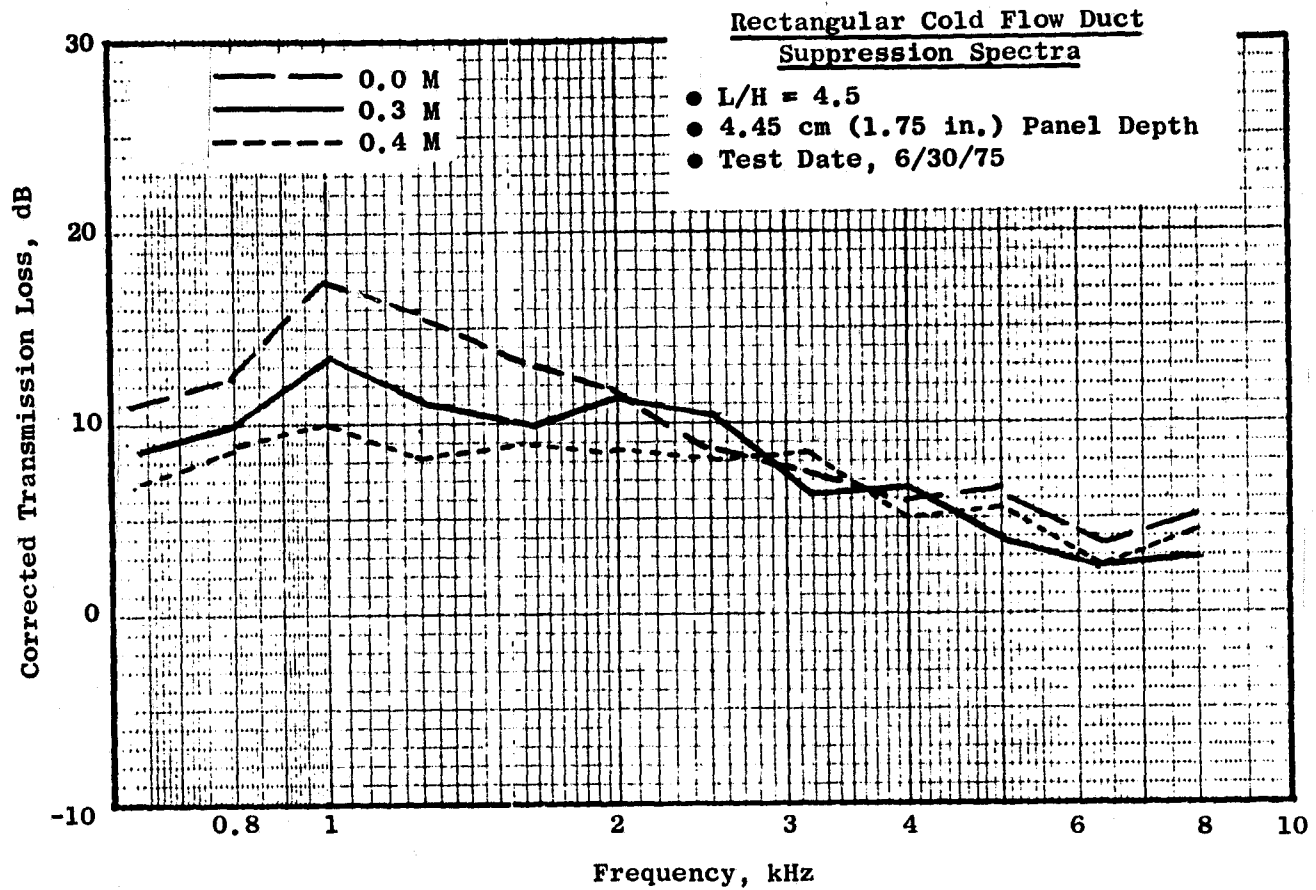


Figure 49. Corrected Transmission Loss Vs. Frequency for Mach Number Variations, 7.5% Porosity.

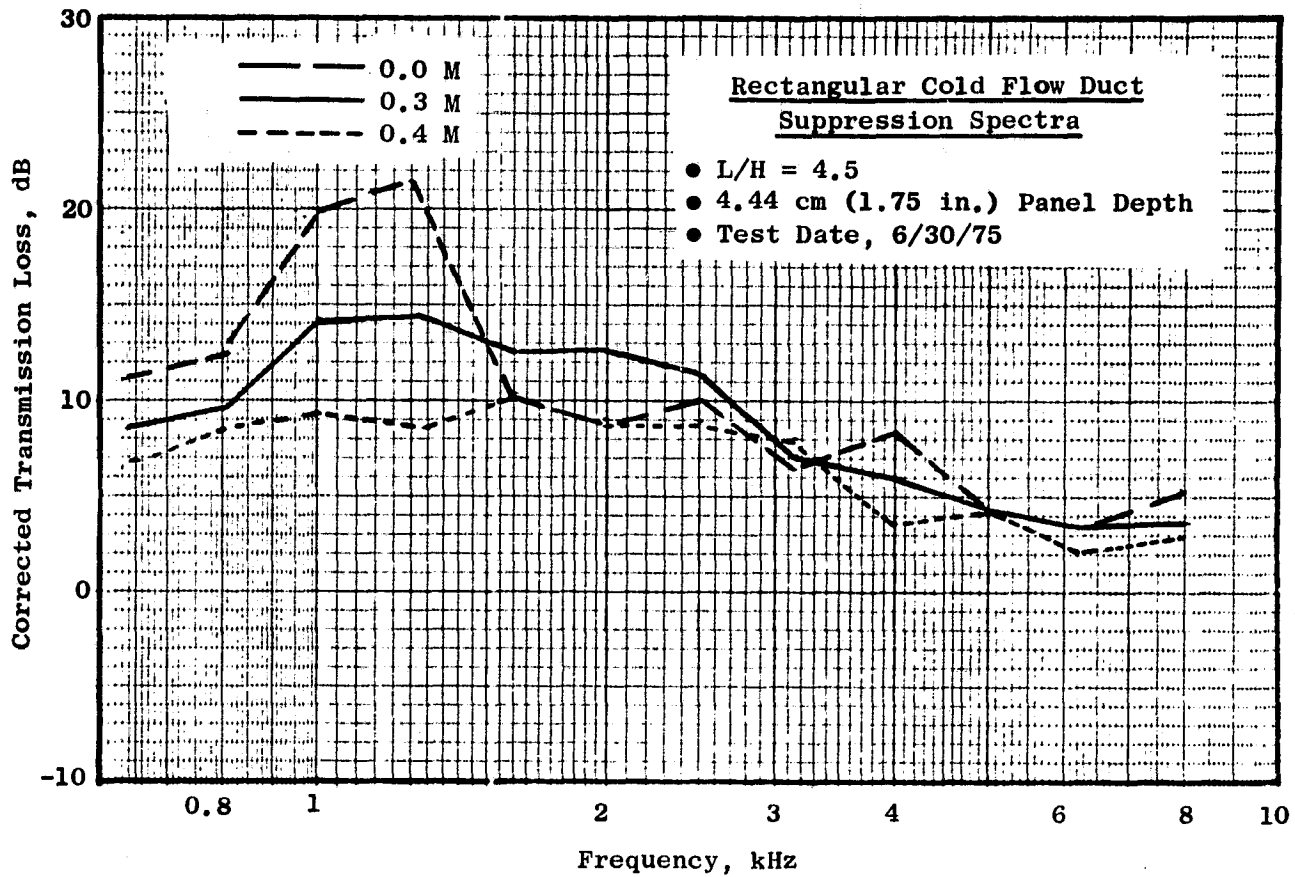


Figure 50. Corrected Transmission Loss Vs. Frequency for Mach Number Variations, 10% Porosity.

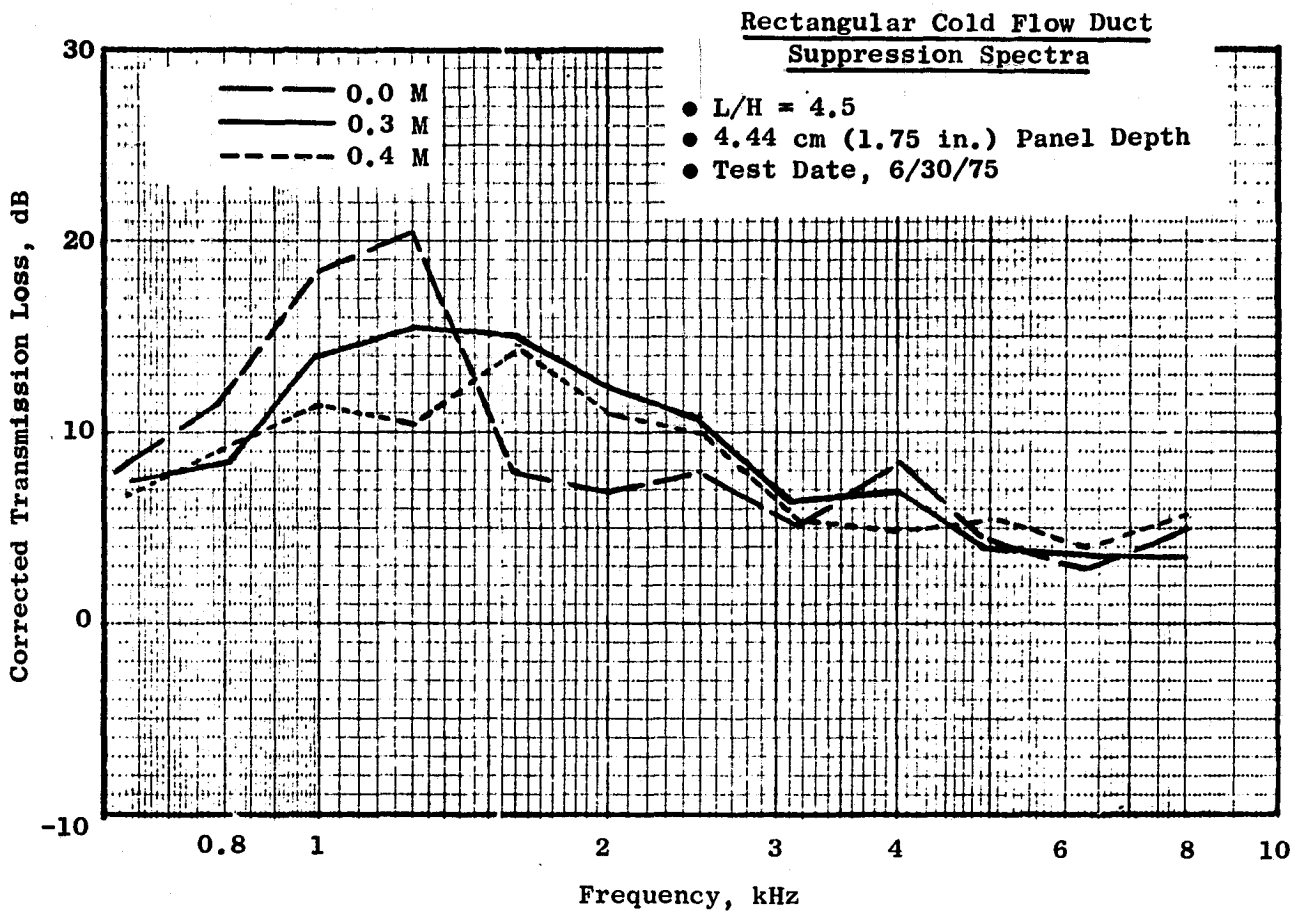


Figure 51. Corrected Transmission Loss Vs. Frequency for Mach Number Variations, 14.5% Porosity.

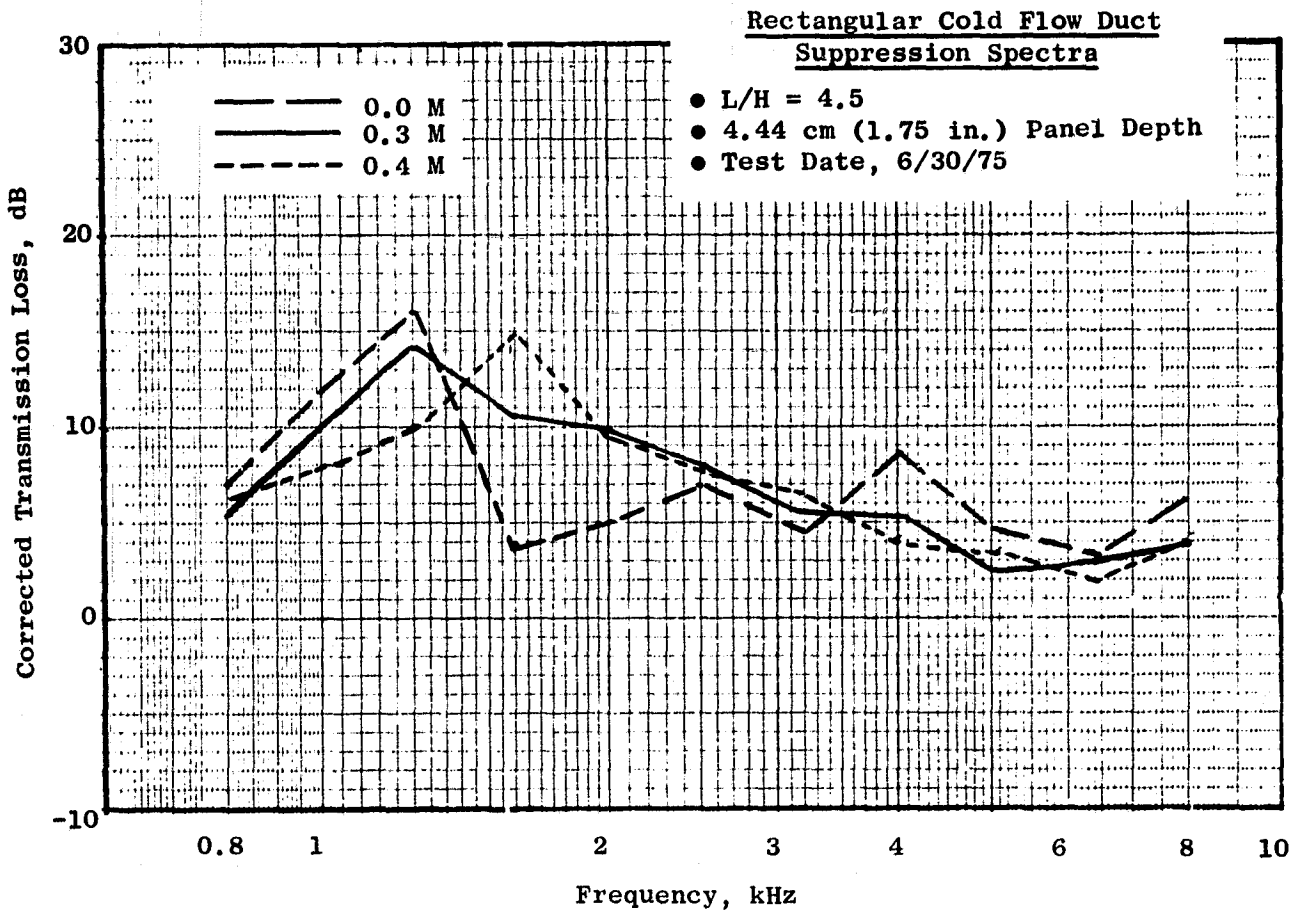


Figure 52. Corrected Transmission Loss Vs. Frequency for Mach Number Variations, 22.7% Porosity.

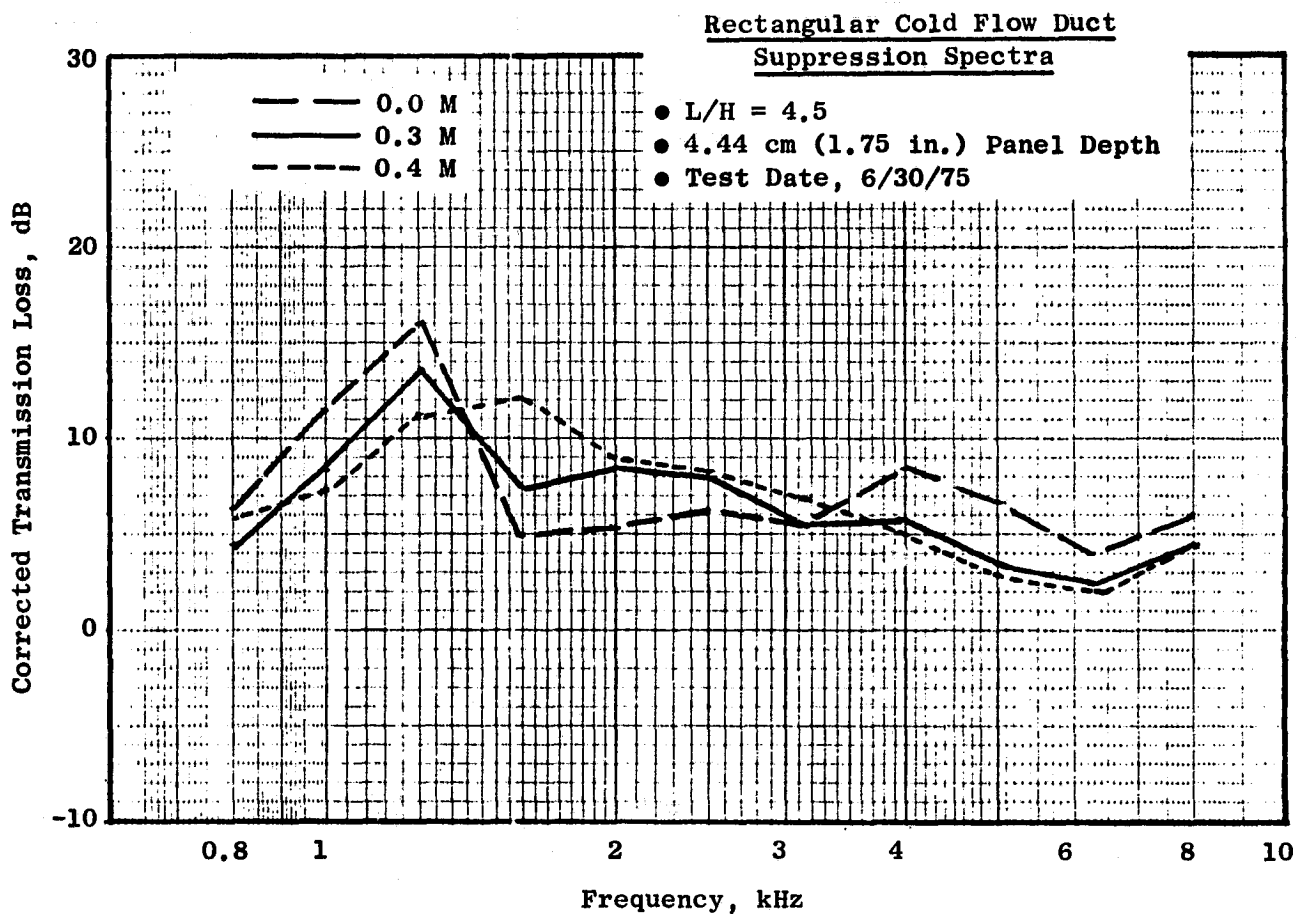


Figure 53. Corrected Transmission Loss Vs. Frequency for Mach Number Variations, 27% Porosity.

- Based on Acoustic Duct Data
- Duct Mach = 0.4

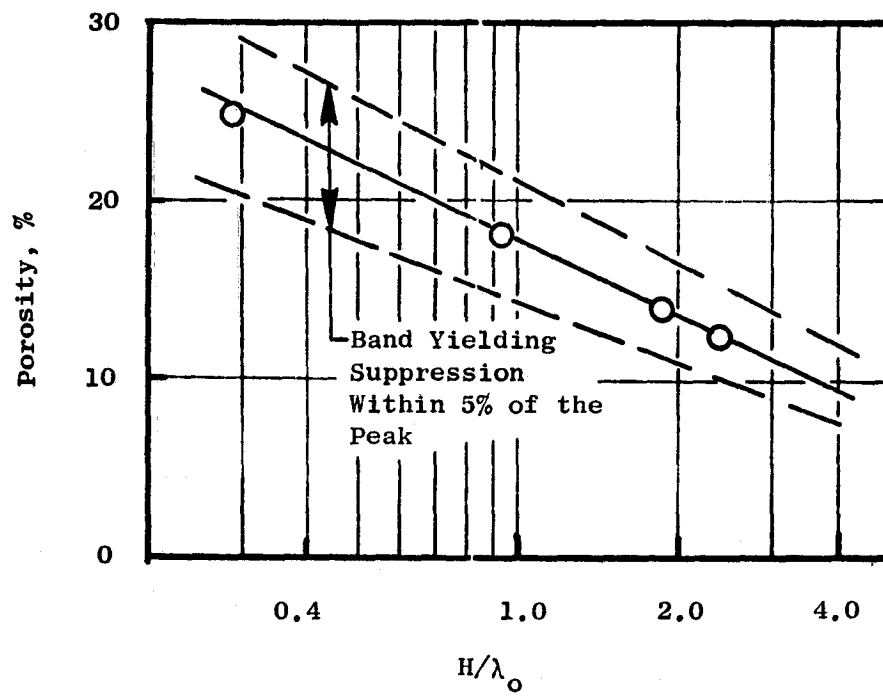


Figure 54. Optimum Faceplate Porosity Vs. H/λ_0 for an SDOF Configuration.

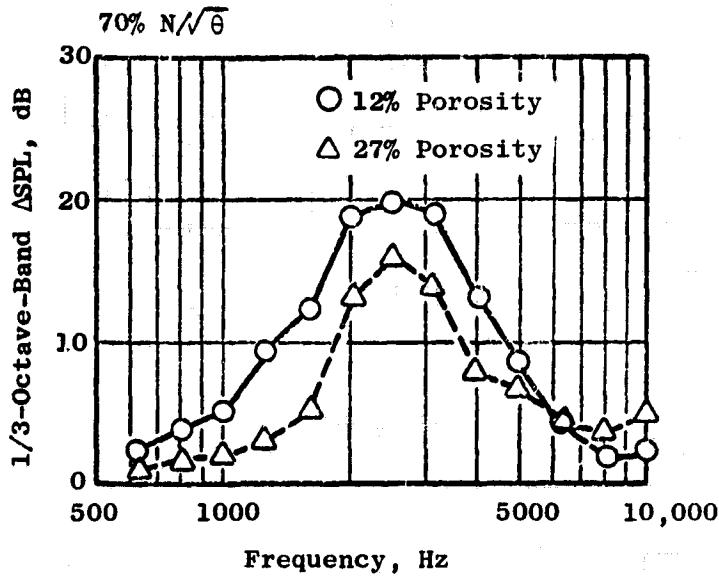
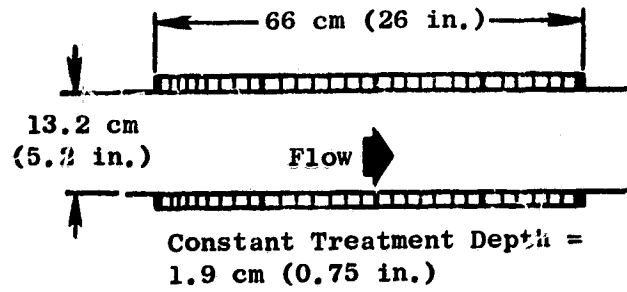
<u>Configuration</u>	<u>Treatment Panel</u>							
	<u>1</u>		<u>2</u>		<u>3</u>		<u>4</u>	
	<u>t,</u> <u>cm (in.)</u>	<u>σ,</u> <u>%</u>	<u>t,</u> <u>cm (in.)</u>	<u>σ,</u> <u>%</u>	<u>t,</u> <u>cm (in.)</u>	<u>σ,</u> <u>%</u>	<u>t,</u> <u>cm (in.)</u>	<u>σ,</u> <u>%</u>
Constant-Depth No. 1	1.9 (0.75)	12	1.9 (0.75)	12	1.9 (0.75)	12	1.9 (0.75)	12
Constant-Depth No. 2	1.9 (0.75)	27	1.9 (0.75)	27	1.9 (0.75)	27	1.9 (0.75)	27
Variable-Depth No. 1 Panels	0.6 (0.25)	12	1.2 (0.50)	12	1.9 (0.75)	12	3.8 (1.5)	12
Variable-Depth No. 2 Panels	0.6 (0.25)	27	1.2 (0.50)	27	1.9 (0.75)	27	3.8 (1.5)	27
Variable-Depth and Mixed-Porosity	1.27 (0.50)	12	1.9 (0.75)	12	0.635 (0.25)	12	3.8 (1.5)	27

5.2.1 Constant-Depth Treatment Configurations

The constant-depth treatment configurations had a panel depth of 1.9 cm (0.75 in.) with porosity values of 12% and 27%. The measured 1/3-octave-band suppression is given in Figure 55 for both the 12% and 27% faceplate porosities. The data are for the maximum aft acoustic angle (111°) for fan speeds of 70% and 100% $N/\sqrt{\theta}$.

The 12% porosity configuration gave a higher suppression level over the indicated frequency. This suggests that the acoustic resistance of the 12% porosity faceplate is closer to the optimum resistance value for the test conditions. The duct Mach number is 0.3 at 70% $N/\sqrt{\theta}$ and 0.42 at 100% $N/\sqrt{\theta}$. Figure 56 gives the suppression comparison for the 12% porosity configuration at the two fan speeds, 70% $N/\sqrt{\theta}$ and 100% $N/\sqrt{\theta}$. The peak suppression decreases 3.0 dB as the fan speed is increased from 70% $N/\sqrt{\theta}$ to 100% $N/\sqrt{\theta}$. This reduction could be a result of increasing the resistance of the resonator system above the optimum since the Mach number is increased from 0.3 to 0.42 for higher fan speed.

Figure 57 gives the same data comparison for the 27% porosity configuration. The peak suppression increases as the fan speed is increased, which could mean that the 27% porosity has a resistance below the optimum. The higher resistance resulting from the increased Mach number at the 100% $N/\sqrt{\theta}$ fan speed point improves suppression.



● Maximum Aft Angle, 110°

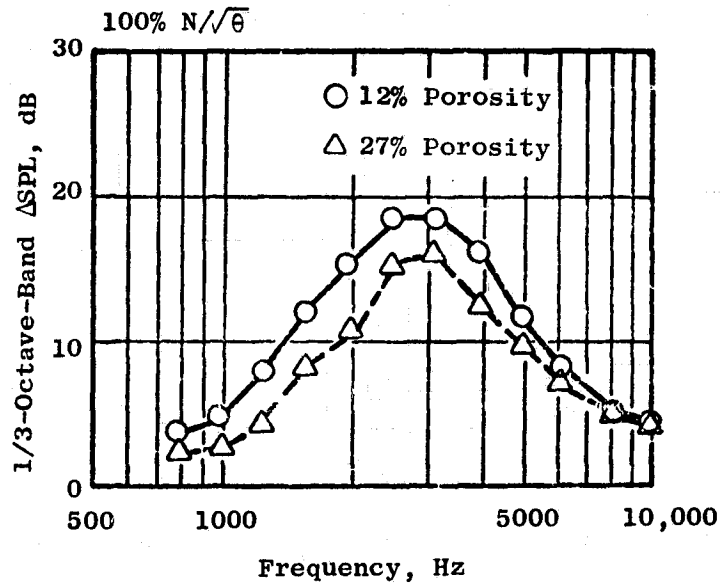


Figure 55. Measured Suppression Vs. Porosity for Constant-Depth Liner.

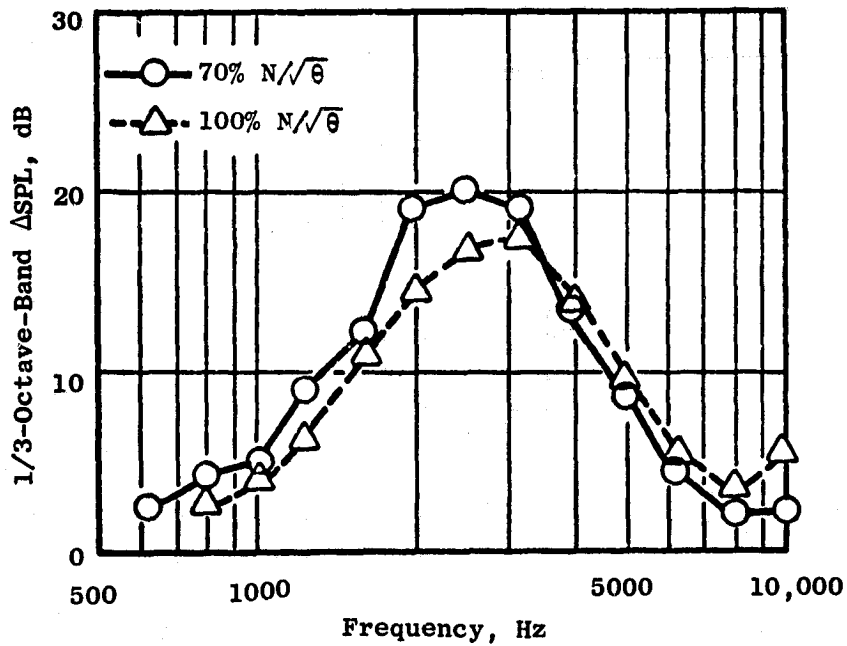
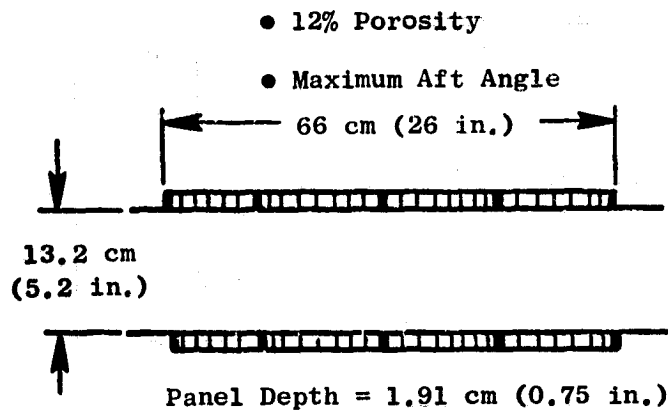


Figure 56. Measured Suppression Spectra at Two Fan Speeds, 12% Porosity for Constant Depth Liner.

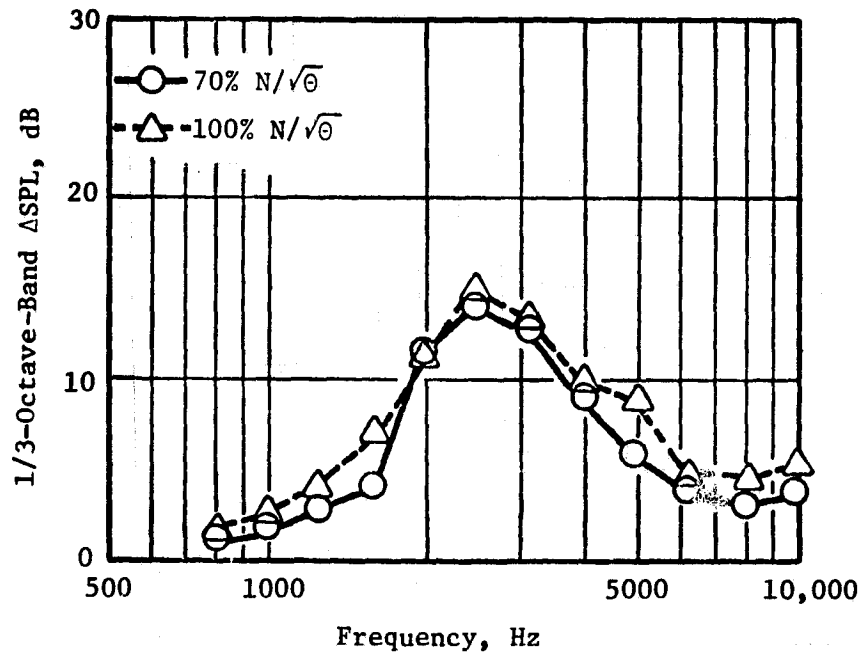
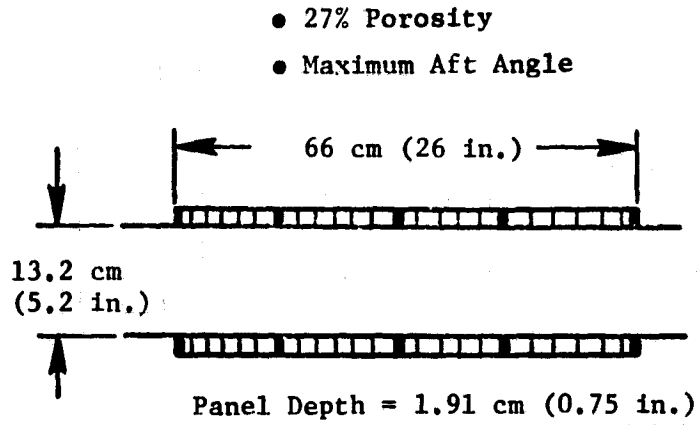


Figure 57. Measured Suppression Spectra at Two Fan Speeds, 27% Porosity for Constant Depth Liner.

Predicted Versus Measured Suppression

The measured suppression spectrum at 70% $N/\sqrt{\theta}$ fan speed is repeated in Figure 58 for the 12% porosity configuration. The suppression is compared with the predicted suppression spectrum, which was calculated from a prediction method that is based on previous engine and fan vehicle data. The agreement is very good at all frequencies other than the peak. As can be seen the predicted peak frequency is somewhere between the 2000 Hz and 2500 Hz 1/3-octave-band frequencies. This results in a filter split which could tend to cause the peak measured suppression level being lower than it would have otherwise been.

5.2.2 Variable-Depth Treatment Configurations

5.2.2.1 Constant Porosity

The variable-depth treatment configurations consisted of panels having four different depths with equal treated lengths. The suppression and a sketch of the treatment configuration is given in Figure 59. The suppression data are for fan speeds of 70% and 100% $N/\sqrt{\theta}$ at the maximum aft acoustic angle. At 100% $N/\sqrt{\theta}$ the 12% porosity gives the better suppression at higher frequencies (3150 Hz to 8000 Hz); the 27% porosity configuration, however, offers more peak suppression by 2 to 3 dB. The 12% porosity gives more suppression for all frequencies at 70% $N/\sqrt{\theta}$.

5.2.2.2 Mixed Porosity

The two treatment configurations shown in Figure 60 have variable-depth panels with one having a constant 12% faceplate porosity and the other having panels with 12% and 27% porosities. The configuration with the mixed porosity is also different in that the 3.81 cm (0.25 in.) and 1.27 cm (0.5 in.) panel positions are interchanged.

Suppression spectra for the two configurations are shown in Figure 61. The suppression is given for fan speeds of 70% $N/\sqrt{\theta}$ and 100 $N/\sqrt{\theta}$ at the maximum at the maximum aft acoustic angle. Suppression comparison for the two configurations shows little difference at the higher frequency values. Figure 62 shows suppression spectra measured for single sections of treatment with a treated L/H of 1.15. Spectra are given for 100% $N/\sqrt{\theta}$ at the maximum aft acoustic angle. The four liner depths give four tuning frequencies, which enables a comparison of peak suppression versus the acoustic parameter (H/λ_0). The results show that for H/λ_0 values of 1.94, 1.22, and 0.97 the 12% porosity gives more peak suppression. However, as the H/λ_0 value is reduced to 0.78 with the 3.81 cm (1.5 in.) panel, the 27% porosity has the higher peak suppression. This result is strong evidence that for the lower H/λ_0 's a lower resistance value is required for best suppression. This fact does not suggest that 27% porosity is optimum, but that relative to 12% the resulting acoustic resistance is nearer optimum for these H/λ_0 and L/H values.

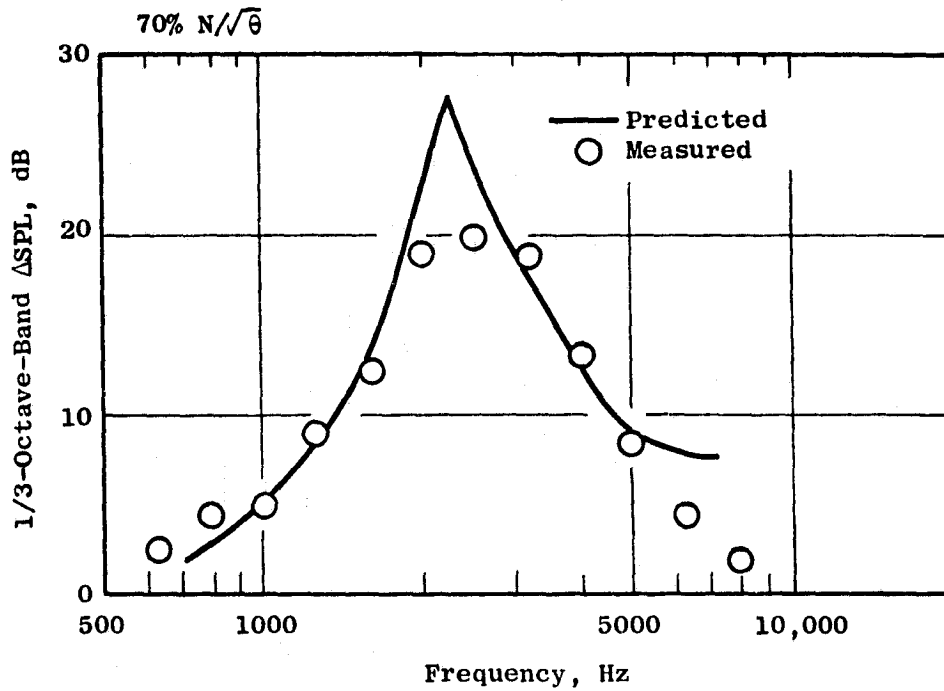
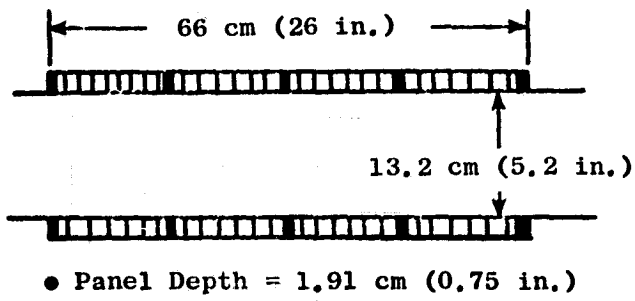
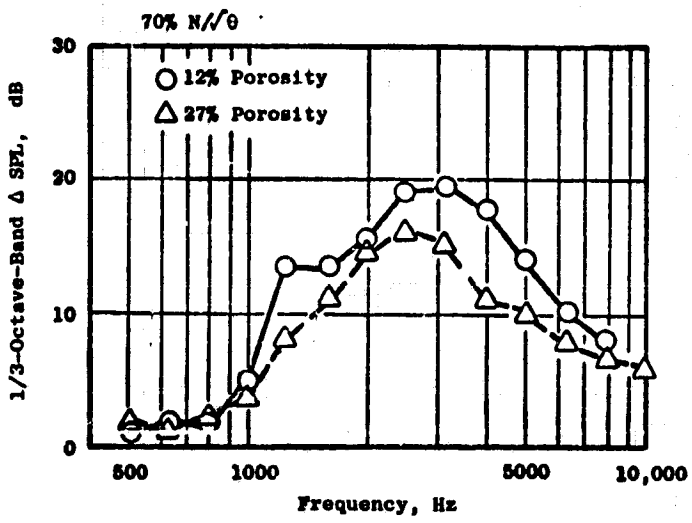
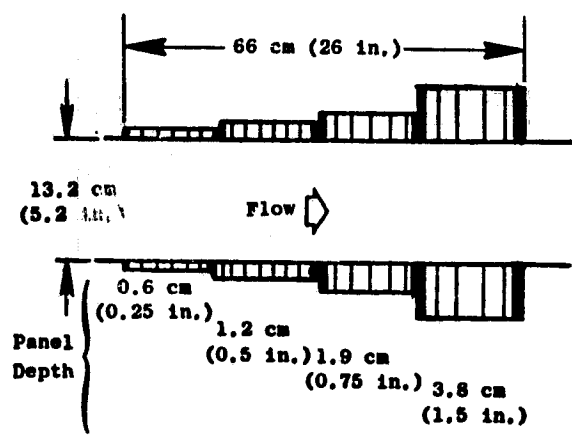


Figure 58. Predicted Vs. Measured Suppression Spectra: Constant Depth, 12% Porosity Panels.

C-2



• Maximum Aft Angle

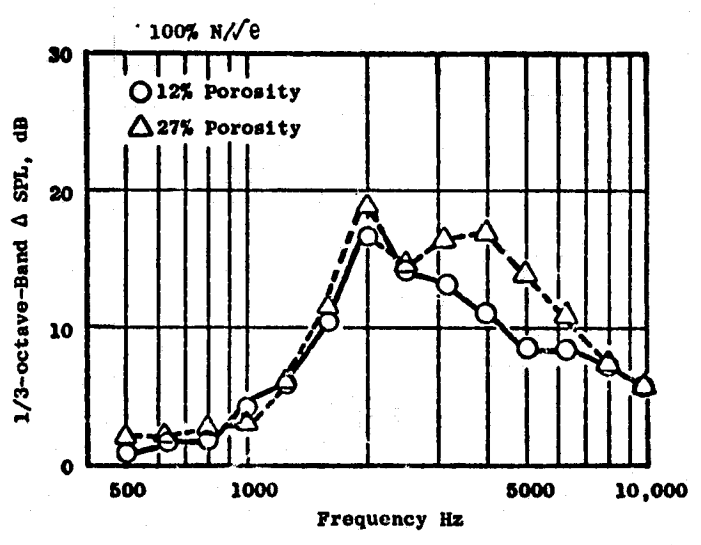
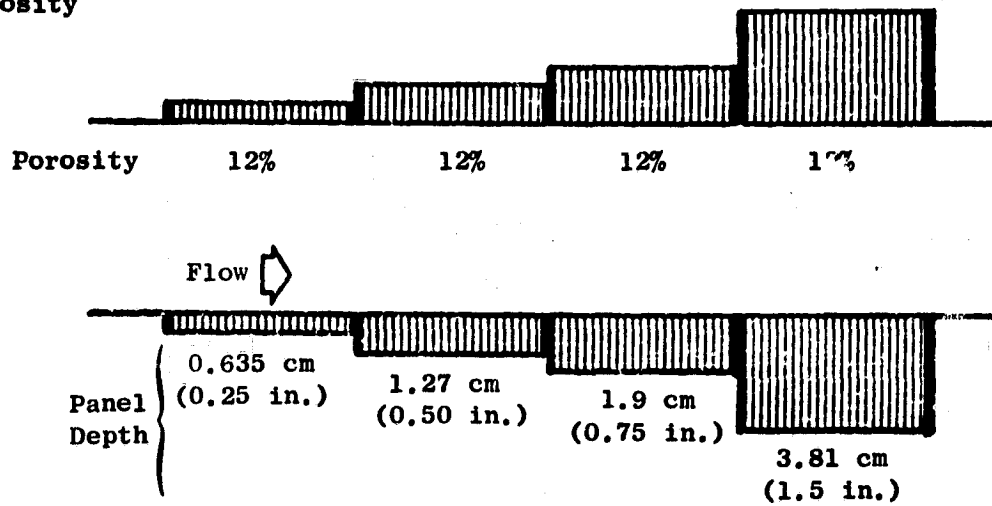


Figure 59. Measured Suppression Vs. Porosity for Variable-Depth Liner.

Configuration No. 1

- Variable Depth
- 12% Porosity



Configuration No. 2

- Variable Depth
- Mixed Porosity

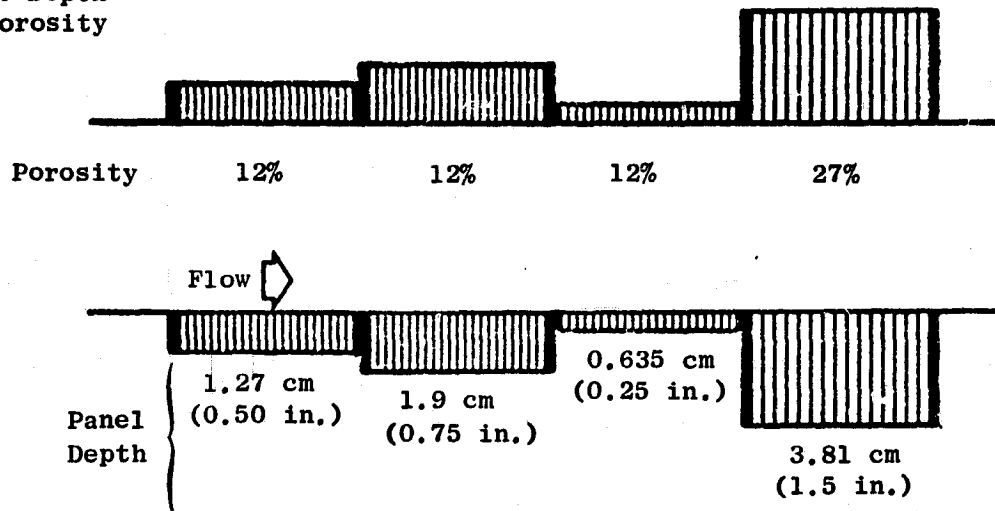


Figure 60. Variable-Depth, Constant-Porosity and Variable-Depth, Variable-Porosity Configurations.

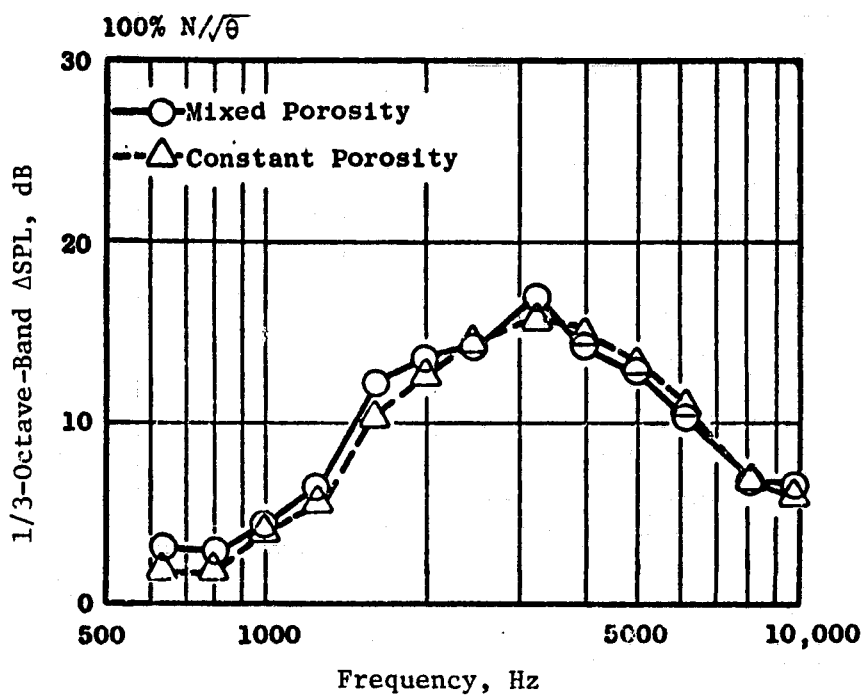
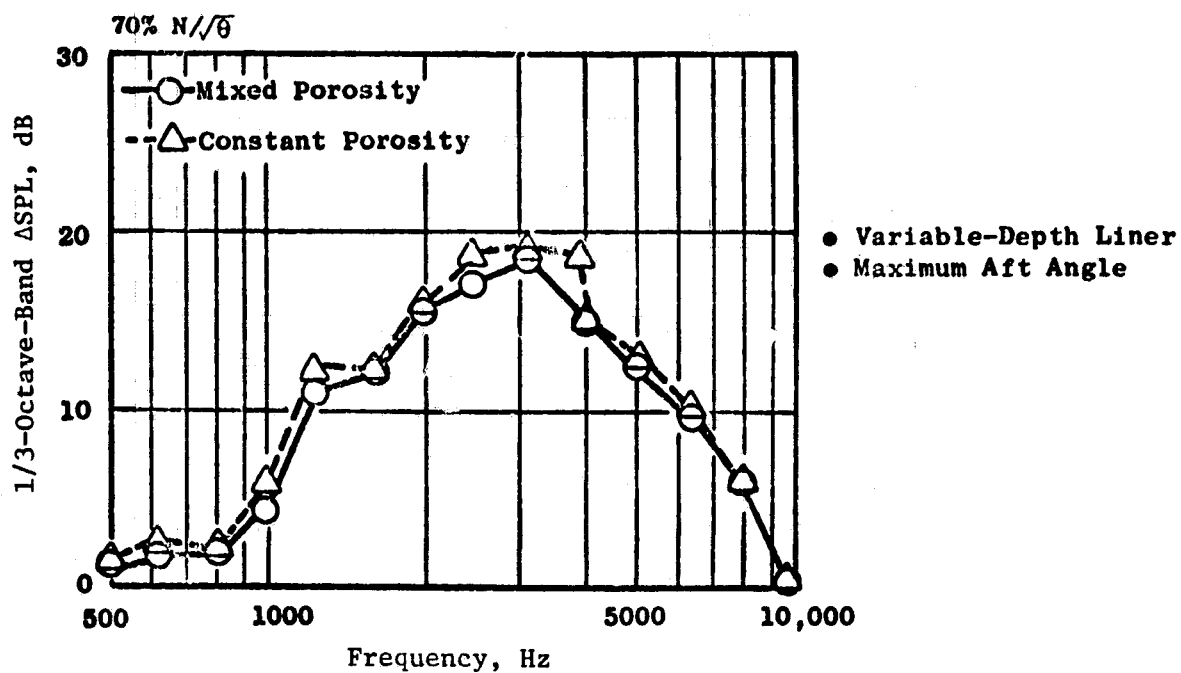


Figure 61. Measured Suppression with Constant Vs. Variable Porosity.

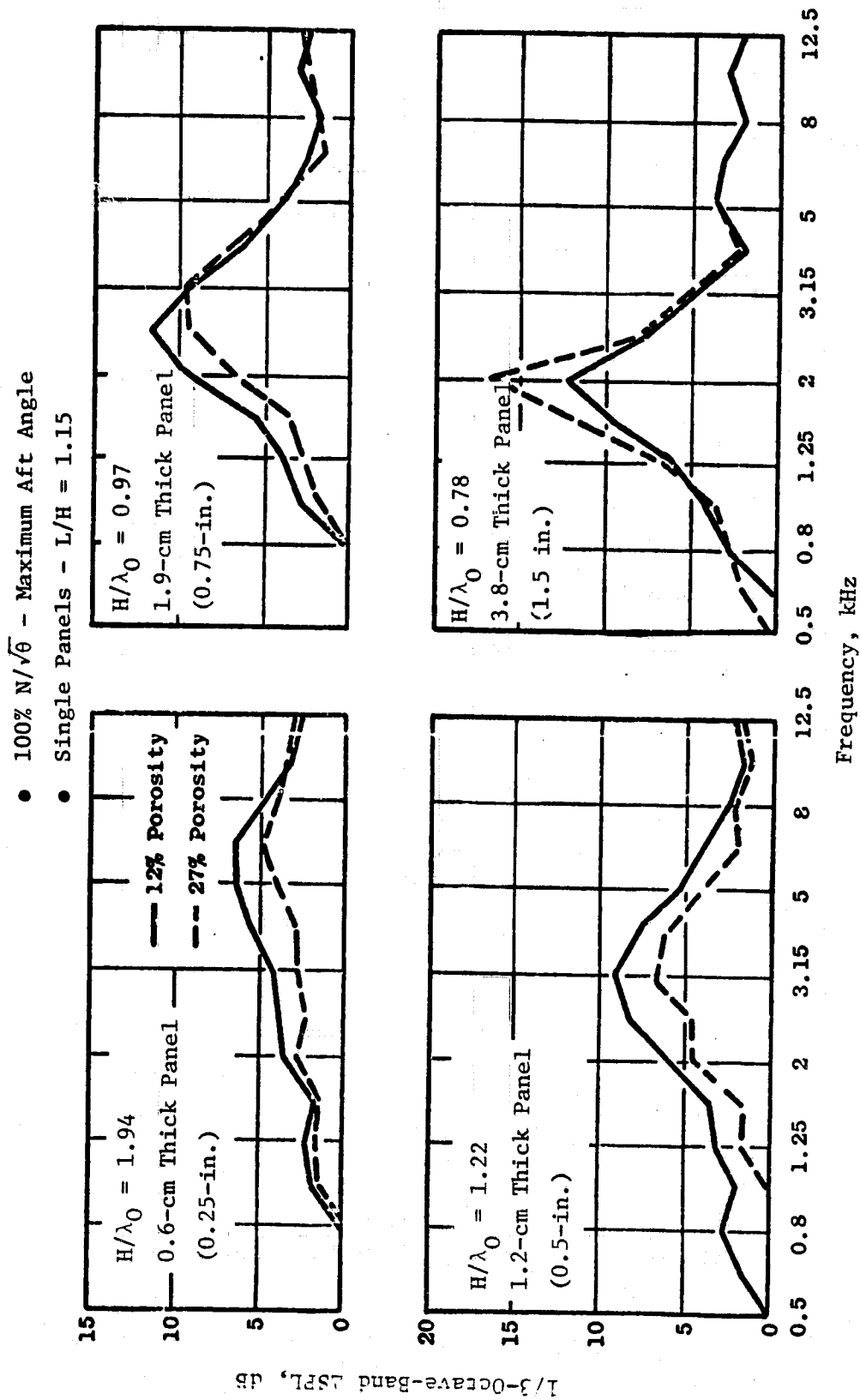


Figure 62. Suppression Spectra for Individual Panels Vs. H/λ_0 .

5.2.3 Comparison of Variable- and Constant-Depth Panel Suppression Results

Suppression spectra comparisons for the variables versus the constant depth treatment configurations as defined in Figure 63 are compared in Figure 64. The data are for a fan speed of $100\% N/\sqrt{\theta}$ at the maximum aft acoustic angle. The variable-depth treatment shows a wider suppression bandwidth, with the constant-depth treatment giving more peak suppression. These suppression characteristics are expected since the variable-depth treatment gives four different tuning frequencies, spreading the suppression out over a broader frequency range. The constant-depth treatment has one design frequency which gives the higher suppression level.

The suppression performance for the variable-depth configuration can be evaluated by comparing the suppression results with previous suppression data. Figure 65 gives the predicted and measured suppression for a variable-depth mixed-porosity configuration at $100\% N/\sqrt{\theta}$. The porosity values and the treatment orientation are indicated in the sketch shown on Figure 65. The prediction method used in calculating the suppression spectrum is from a correlation based on engine data, with the treatment consisting of single-phase constant-depth treatment designs with constant porosity. The predicted suppression level is lower than the measured levels at all frequencies higher than 3150 Hz. The suppression improvements in bandwidth can be attributed to the different tuning frequencies which give a system capable of spreading the suppression out over a broader frequency range. Also the improvement could be a result of a "phased-treatment effect" as observed in the duct data; however, the suppression level improvement from this phenomenon is small when compared to the suppression increase measured in the acoustic duct facility.

5.2.4 Acoustic Splitter Simulation

Fan exhaust suppression requirements in many cases can be satisfied by wall treatment plus an acoustic splitter. Thickness restrictions on the splitter are not compatible with the range of treatment thicknesses usually permissible on the outer and inner flowpaths. Thus, one of the treatment configurations was designed to simulate a splitter condition. A sketch depicting the treatment design is shown in Figure 66. The outer wall treatment has variable-depth panels with the inner wall treatment having a constant thickness. Also shown in Figure 66 are the predicted and measured suppressions. The splitter simulation configurations are discussed later in this report. Here, as was the case for the variable-depth treatment on both walls, the predicted suppression in the higher frequencies is less than measured. However, the difference for the splitter simulation is less than for the variable-depth mixed-porosity design.

A comparison of the suppression spectra for the three different configurations defined in Figure 67 is seen in Figures 68 and 69. These configurations are as follows:

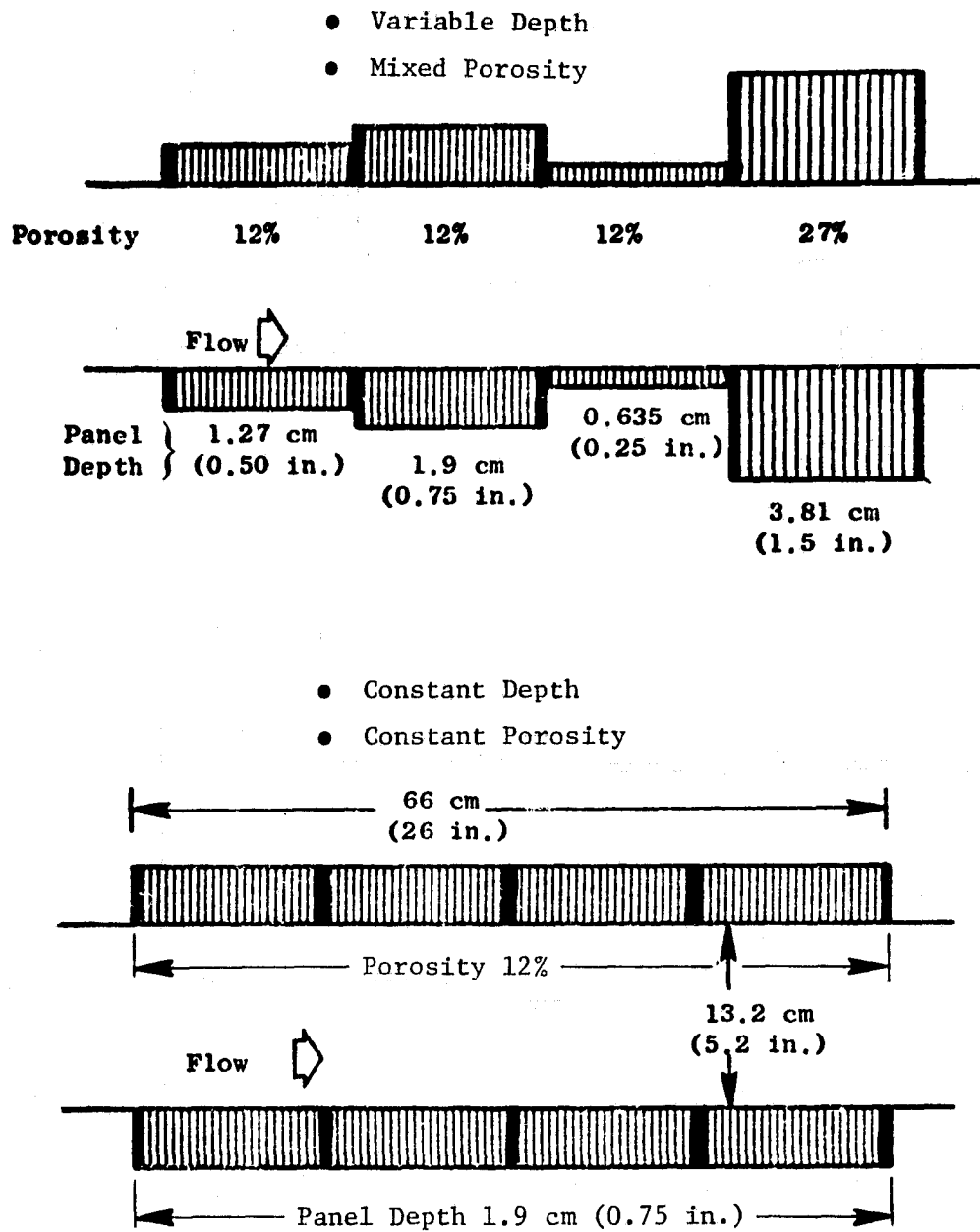


Figure 63. Constant-Depth and Variable-Depth Treatment Configurations.

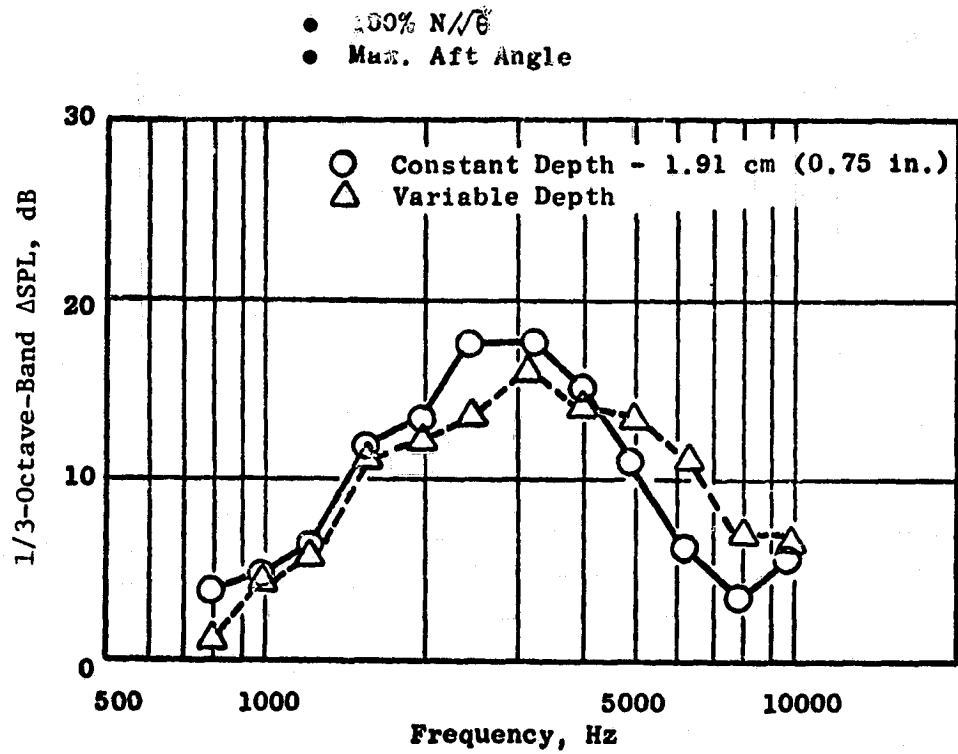


Figure 64. Measured Suppression Spectra for Constant Vs. Variable Panel Depth.

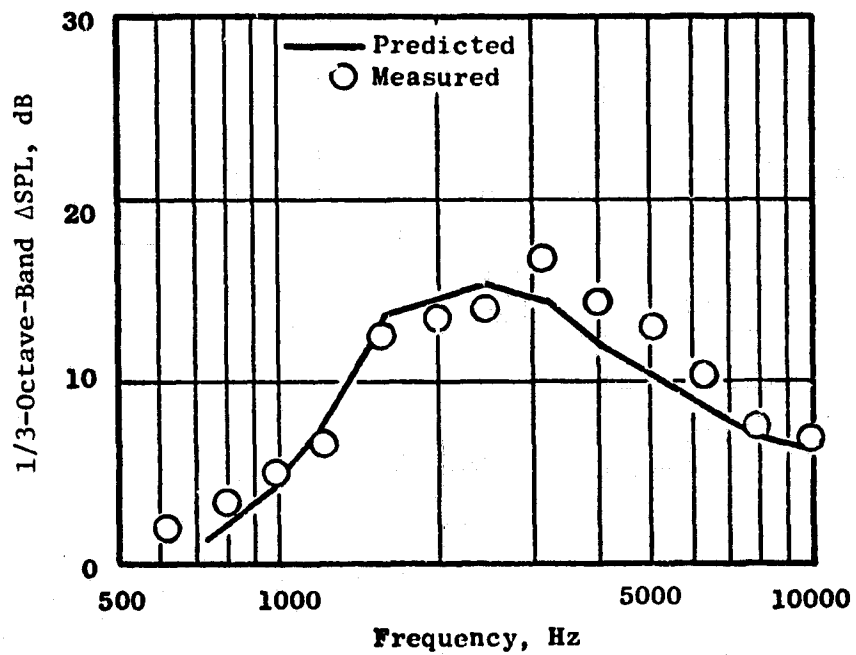
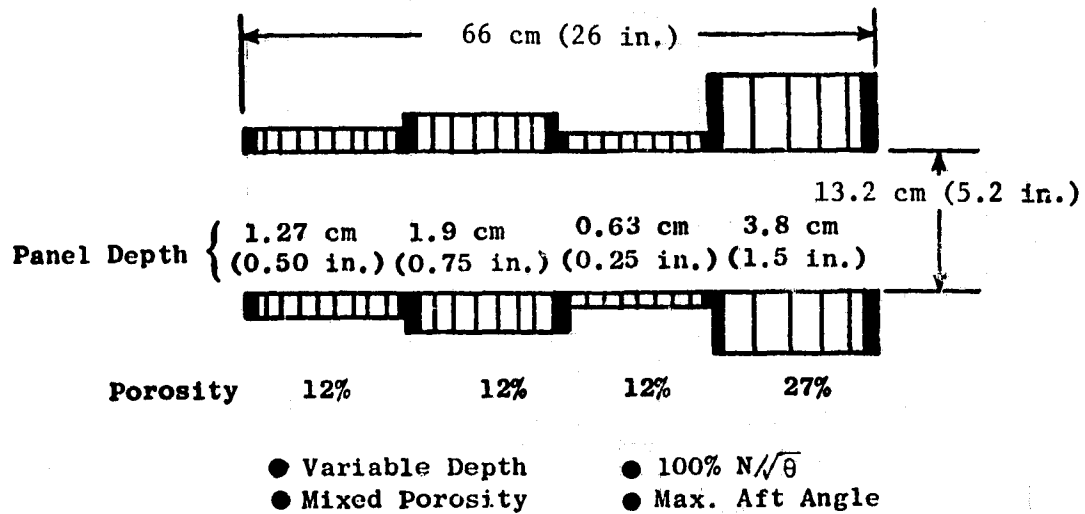
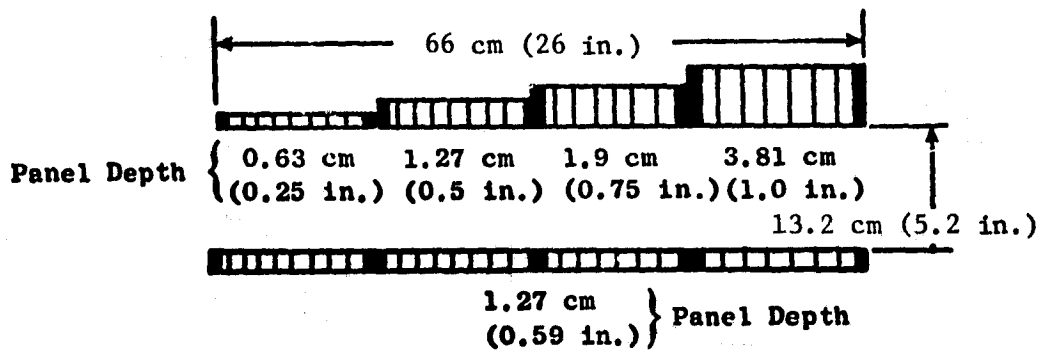


Figure 65. Predicted Vs. Measured Suppression Spectra: Variable-Depth, Mixed-Porosity Panels.



● Splitter Simulation

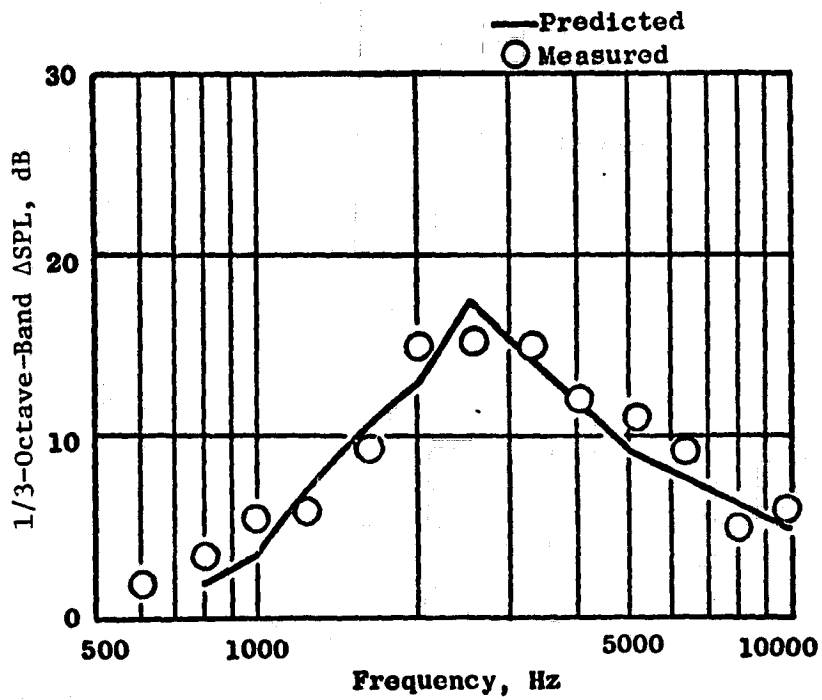
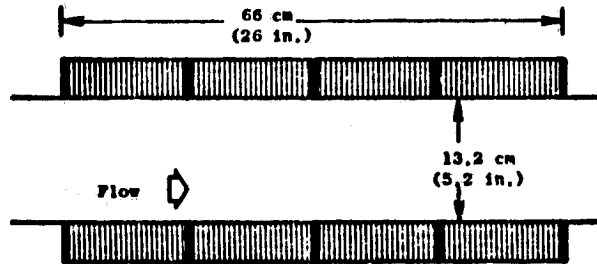


Figure 66. Predicted Vs. Measured Suppression Spectra, Splitter Simulation, 12% Porosity Panels.

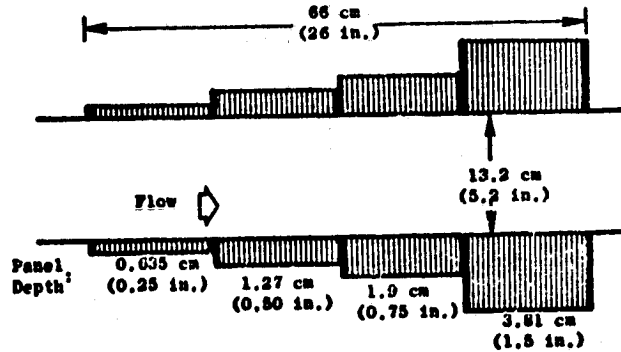
Configuration No. 75-3

- 12% Porosity
- Constant Depth,
1.9 cm (0.75 in.)



Configuration No. 75-4

- 12% Porosity
- Variable-Depth Treatment
(Both Walls)



Configuration No. 7

- 12% Porosity
- Splitter Simulation

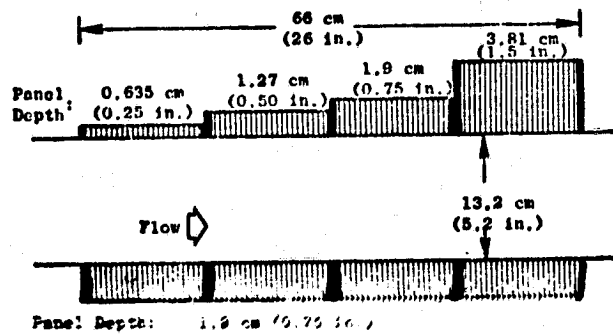
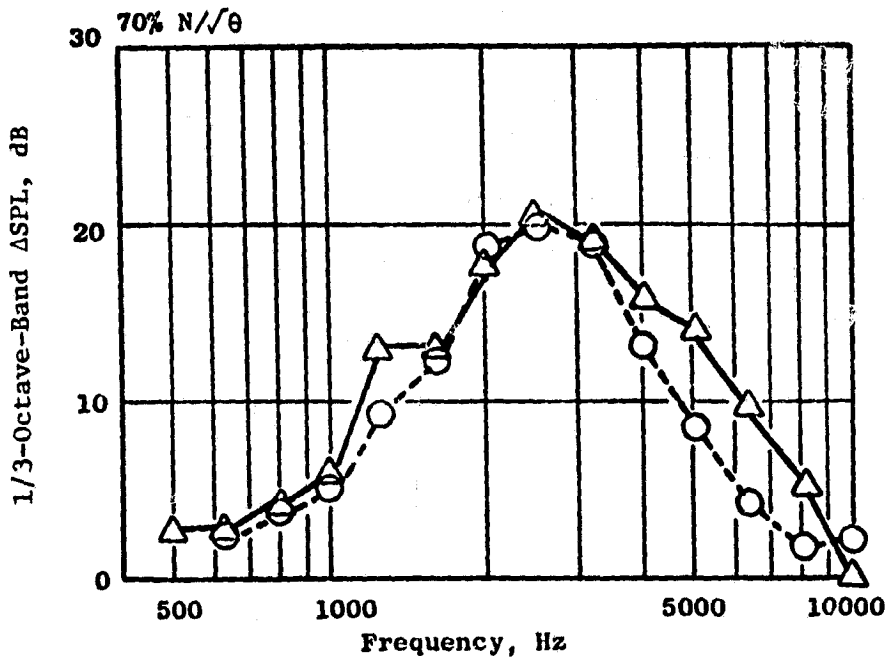


Figure 67. Constant Thickness, Variable-Depth, and Splitter Simulation Treatment Configurations.



- 12% Porosity
- Max. Aft Angle
- Constant Depth
- △ Splitter Simulation

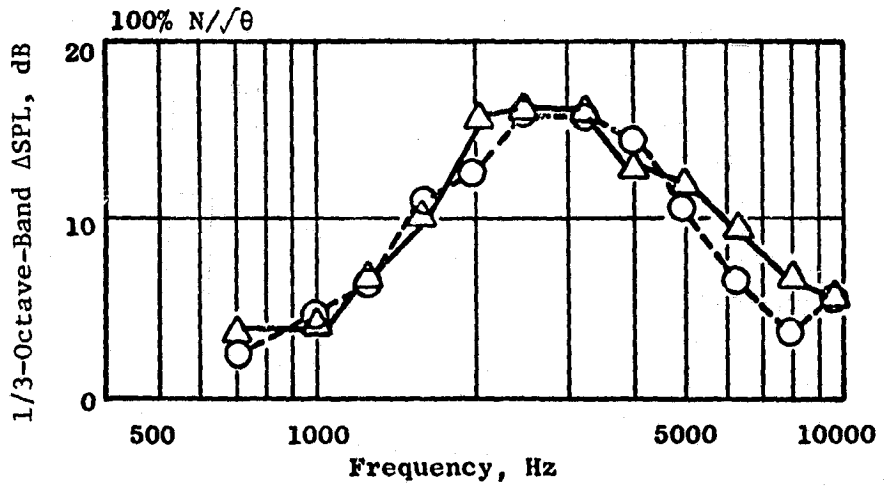


Figure 68. Splitter Simulation Vs. Constant-Depth Wall Treatment.

- Splitter Simulation
- Max. Aft Angle
- △ Variable Depth
- 12% Porosity

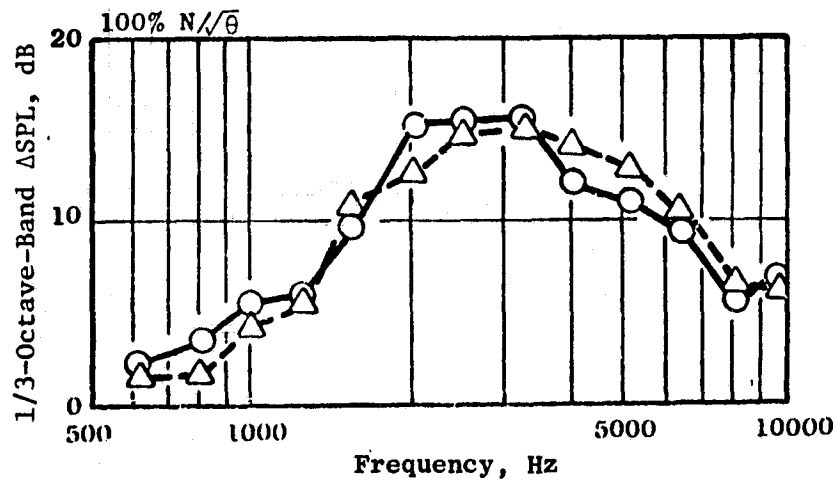
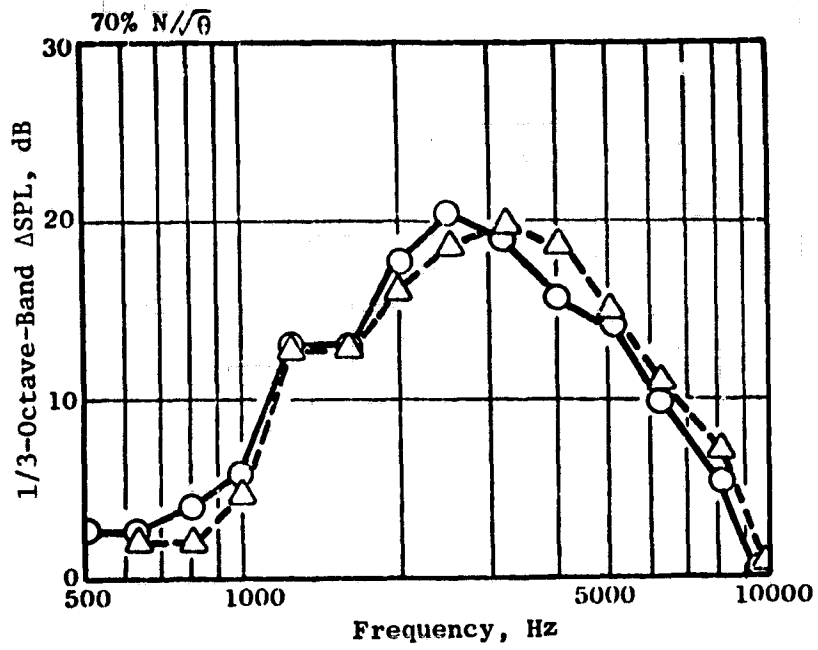


Figure 69. Splitter Simulation Compared to Treatment with Variable Depth on Both Walls.

- Constant-depth treatment on both walls.
- Variable-depth treatment on both walls.
- Splitter simulation: variable-depth treatment on one wall with constant-depth treatment on the other.

Figure 68 compares the suppressions measured for the "simulated splitter" and the constant-depth configuration at fan speeds of $70\% N/\sqrt{\theta}$ and $100 N/\sqrt{\theta}$. The splitter configuration has the wider suppression bandwidth although the peak suppression levels are approximately the same. Figure 69 compares the "splitter-simulation" spectrum with the suppression spectrum measured for the treatment configuration having variable-depth treatment on both walls, for fan speeds of $70\% N/\sqrt{\theta}$ and $100\% N/\sqrt{\theta}$. The configuration with variable-depth treatment on both walls has a somewhat better suppression bandwidth than the splitter case; however, the splitter configuration has a slightly higher peak suppression.

5.2.5 Treatment Area Effectiveness

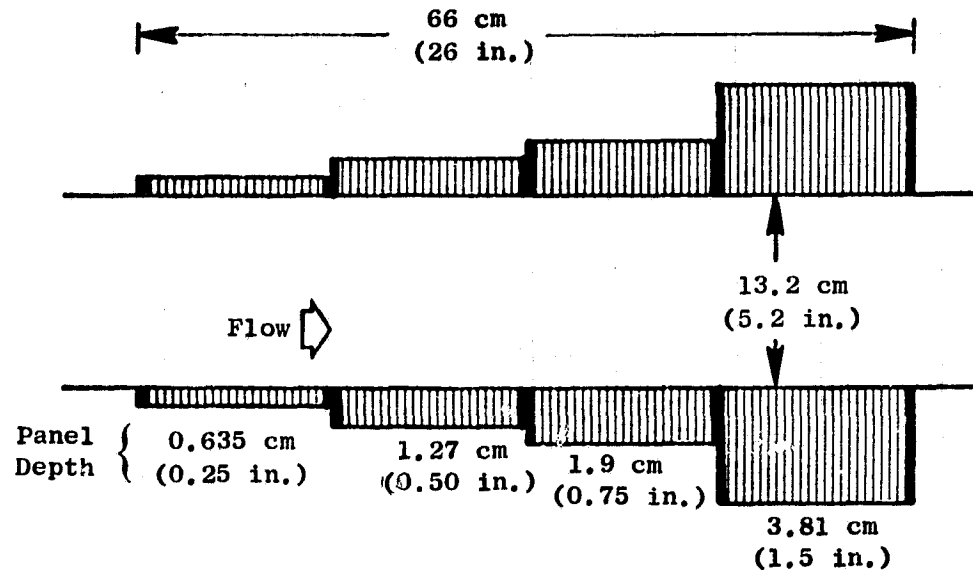
Treatment area losses are usually unavoidable in real engine hardware due to flanges, instrumentation, and faceplate hole blockage. A simulation of this blockage was made by taping approximately 20% of the treated surface area of each of four panels on the inner and outer walls. The fan exhaust treatment configurations tested are shown in Figure 70. The configuration without taping has an effective L/H of 4.6, and a L/H of 3.7 with taping. This would result in a 20% predicted loss of treatment effectiveness if suppression in ΔdB varies linearly with treatment area.

The suppression spectra for the two configuration values are shown in Figure 71 for fan speeds of $70\% N/\sqrt{\theta}$ and $100\% N/\sqrt{\theta}$. Data are given at the maximum aft angle as measured on a 5.18-m (17-ft) arc. Suppression decreases for each fan speed with the reduced treatment area. This reduction occurs primarily over the 1,600-10,000-Hz frequency range. No significant change in suppression is noted at frequencies below 1,600 Hz.

Figure 72 provides a comparison of the suppression loss measured using the reduced treatment area, and the suppression loss predicted using a linear relation between treatment area and suppression. Approximately 1/4 to 1/2 of the predicted suppression loss was measured for the configuration with treatment blockage. This result shows that a linear relation between treatment area and suppression did not hold in the case tested.

The correlation given in Figure 73 first shows the peak suppression in terms of the actual L/H value and in the second graph shows the peak suppression rate ($\Delta dB/L/H$) versus the actual L/H value. This correlation shows that the effectiveness of the treatment decreases as the L/H parameter is increased. With this situation a linear prediction method would not be expected to give good agreement. The suppression rate used in making suppression estimates is based on a data bank with treated L/H values in the 2.0 to

- $L/H = 5.0$
(Actual Length)
- $L/H = 4.6$
(Effective Length)



- $L/H = 3.7$
(Effective Length)

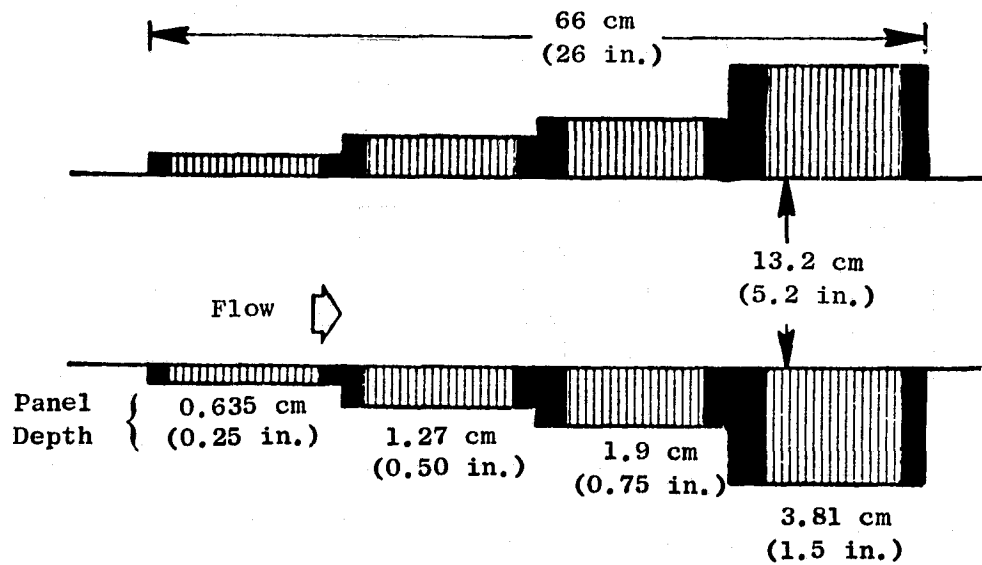


Figure 70. Configurations With and Without Reduced Treatment Area.

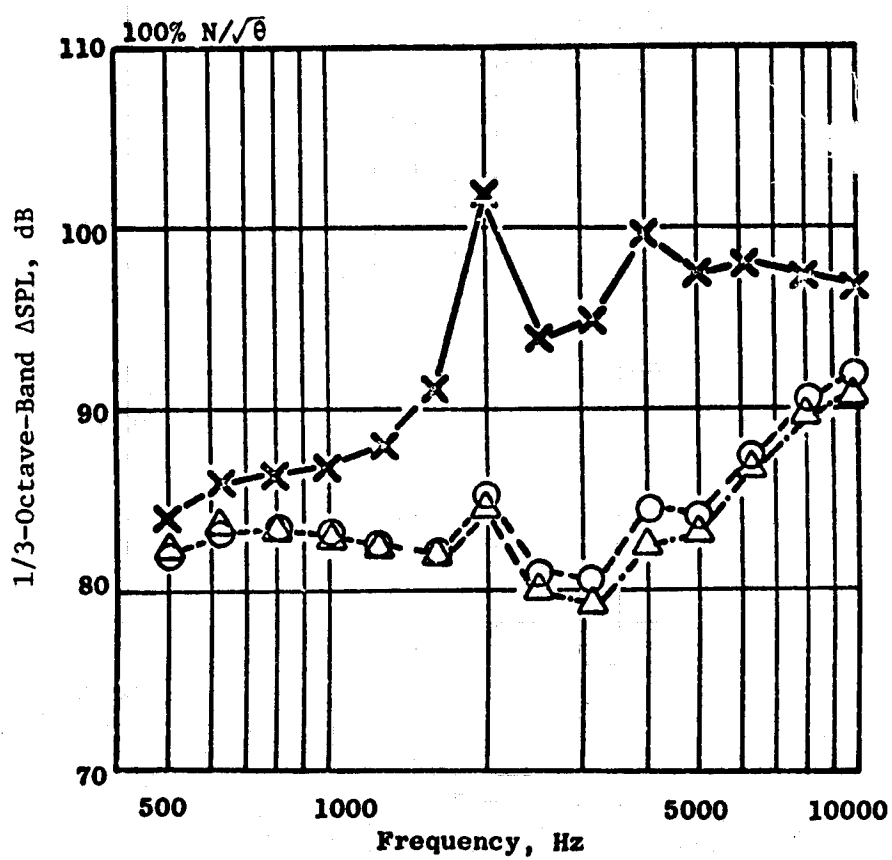
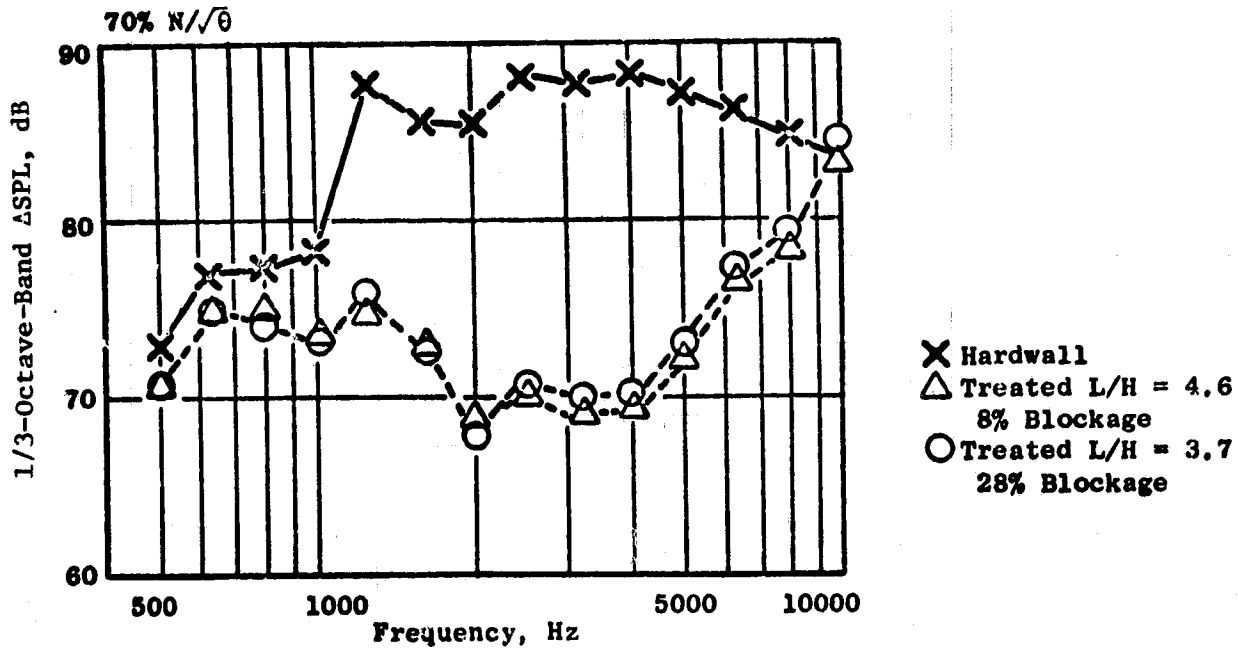


Figure 71. Suppressed and Unsuppressed Spectra for Different Treatment Areas.

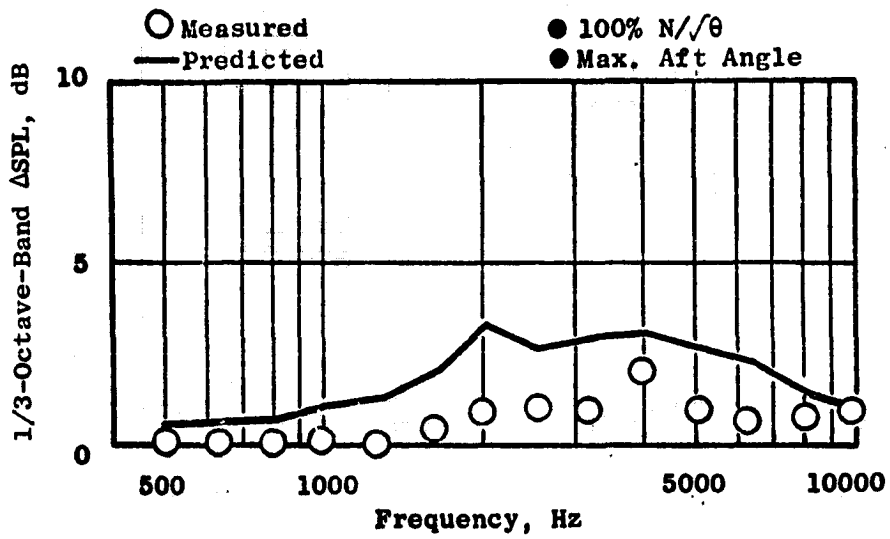


Figure 72. Predicted Vs. Measured Suppression Loss Resulting from Reduced Treatment Area.

- 12% Porosity - Constant-Depth Treatment
- 12% Porosity - Variable-Depth Treatment

$H/\lambda = 1.24$ for All Data

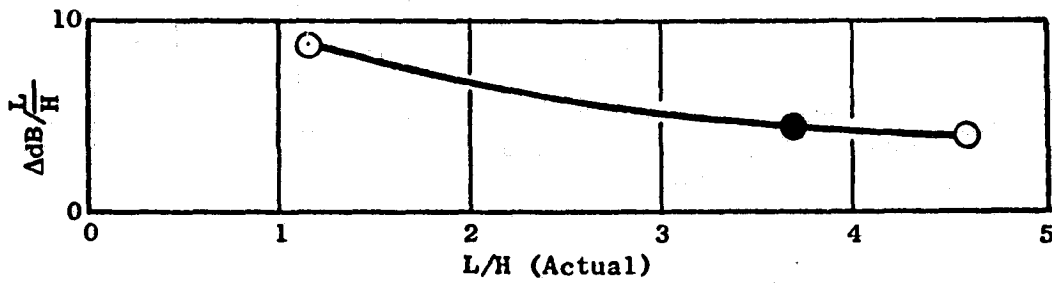
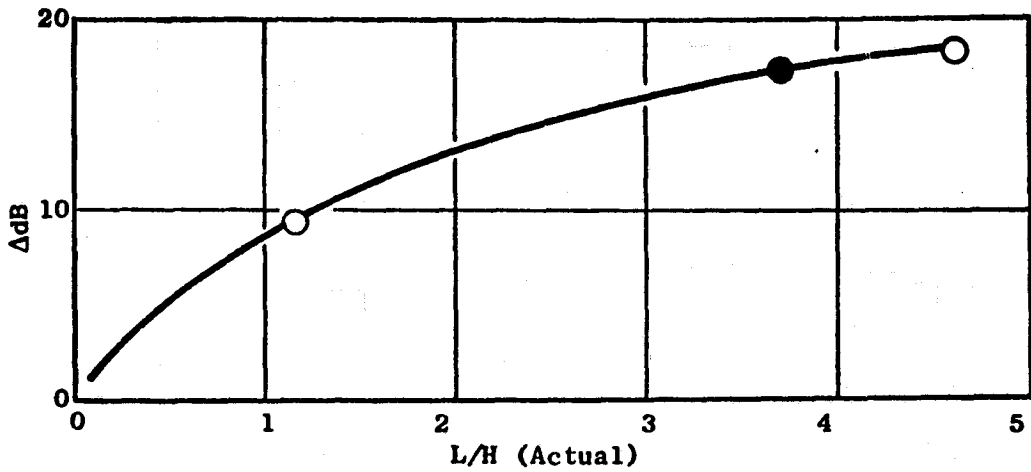


Figure 73. Suppression Vs. L/H (Actual).

4.0 range. Thus for higher L/H values, as is the case for these configurations (L/H values of 3.7 and 4.6), the reduction in suppression resulting from treatment area loss would be overestimated. However, if the same method for smaller L/H values is used (L/H values <2.0) then the penalty would be underestimated.

Rotor-OGV Treatment

Acoustic treatment was placed between the fan rotor and OGV's along the outer flowpath only. The type of treatment used was a single-degree-of-freedom (SDOF) resonator with the honeycomb cell slanted in the circumferential direction. The resonator cavity and faceplate dimensions of the design are as follows:

- Straight cavity depth, 2.54 cm (1.0 in.)
- Slant cell length, 3.81 cm (1.5 in.)
- Faceplate porosity, 28%
- Hole diameter, 0.083 cm (0.033 in.)
- Faceplate thickness, (0.048 cm (0.019 in.)

The panel was designed to have a tuning frequency of about 2000 Hz, the blade passing frequency at 100% $N/\sqrt{\theta}$.

The rotor-OGV treatment was evaluated for two fan exhaust configurations. The first test was with an untreated fan exhaust configuration to determine the effectiveness of treatment in this region. The second test was run with a fully treated fan exhaust configuration to determine if the suppression measured for the first configuration is additive with treatment in the fan exhaust.

The suppression for the configuration having rotor-OGV treatment without the fan exhaust treatment is given in Figure 74 for fan speeds of 70% $N/\sqrt{\theta}$ and 100% $N/\sqrt{\theta}$. All data are for the maximum aft acoustic angle measured on a 5.18-m (17-ft) arc. The data in Figure 74 show that the rotor-OGV treatment achieved both tone and broadband suppression. The tone suppression level increased from 2.5 dB at 70% $N/\sqrt{\theta}$ to 5 dB at 100% $N/\sqrt{\theta}$. Broadband noise suppression varies from 0.5 to 2.0 dB over the measured frequency range for both fan speed points.

Figure 75 gives the suppression spectra for the fully treated fan exhaust with and without the rotor-OGV treatment at fan speeds of 70% $N/\sqrt{\theta}$ and at 100% $N/\sqrt{\theta}$. The fully treated fan exhaust configuration consisted of:

- Variable-depth treatment with panel depths of 0.63 cm (0.25 in.); 1.27 cm (0.5 in.); 1.9 cm (0.75 in.); and 3.81 cm (1.5 in.) on both walls.

Honeycomb Slanted Circumferentially

- Max. Aft Angle

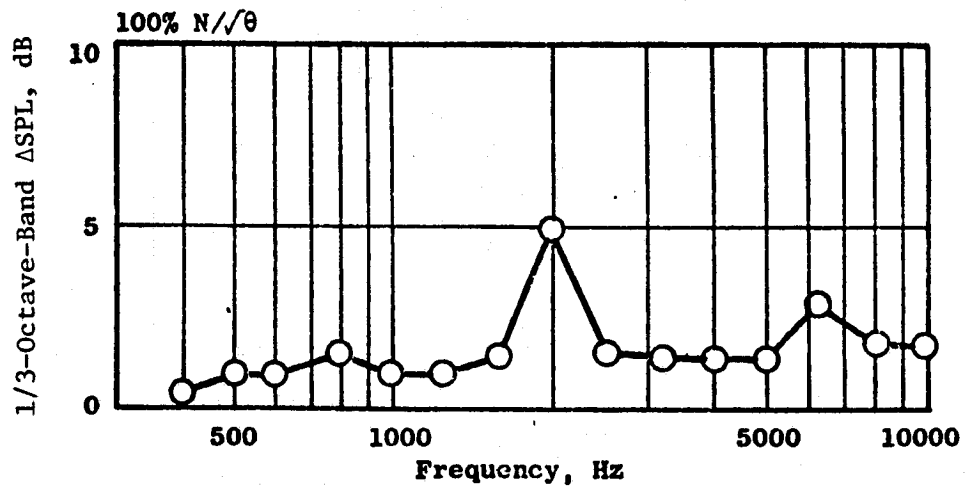
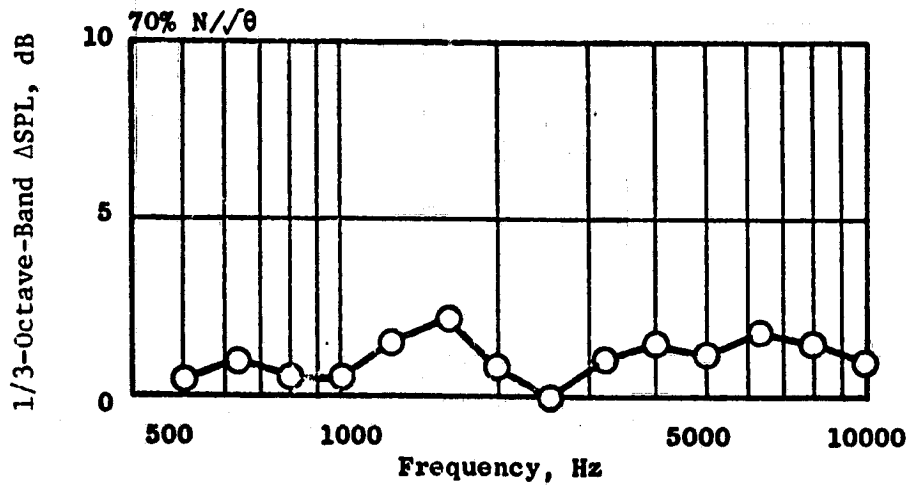
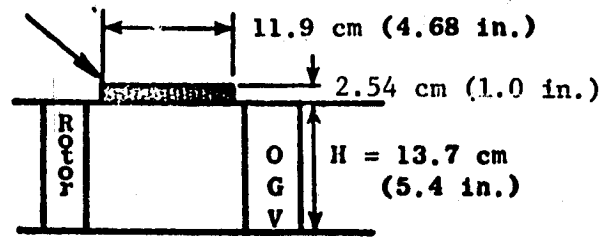


Figure 74. Measured Suppression for Rotor-OGV Treatment.

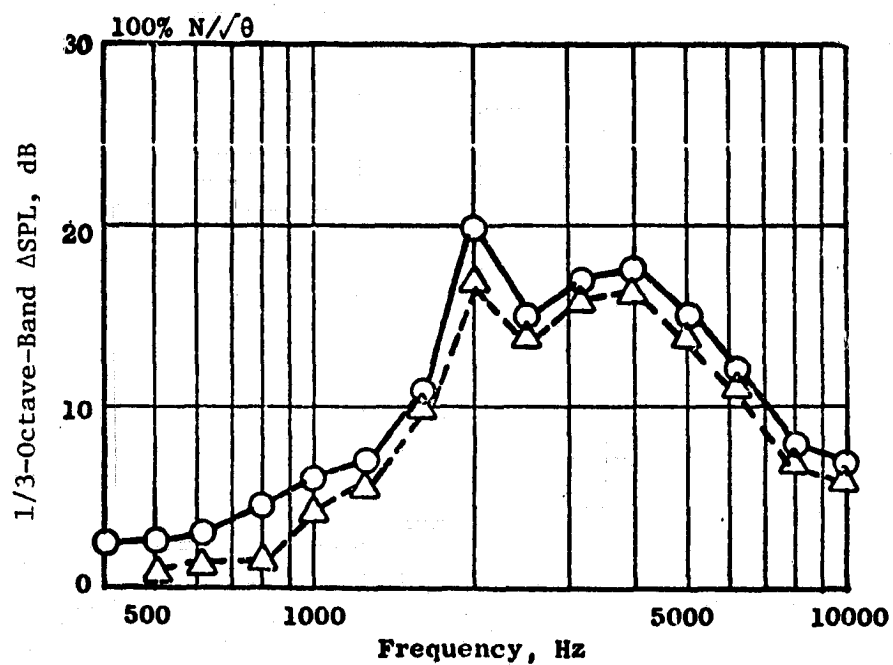
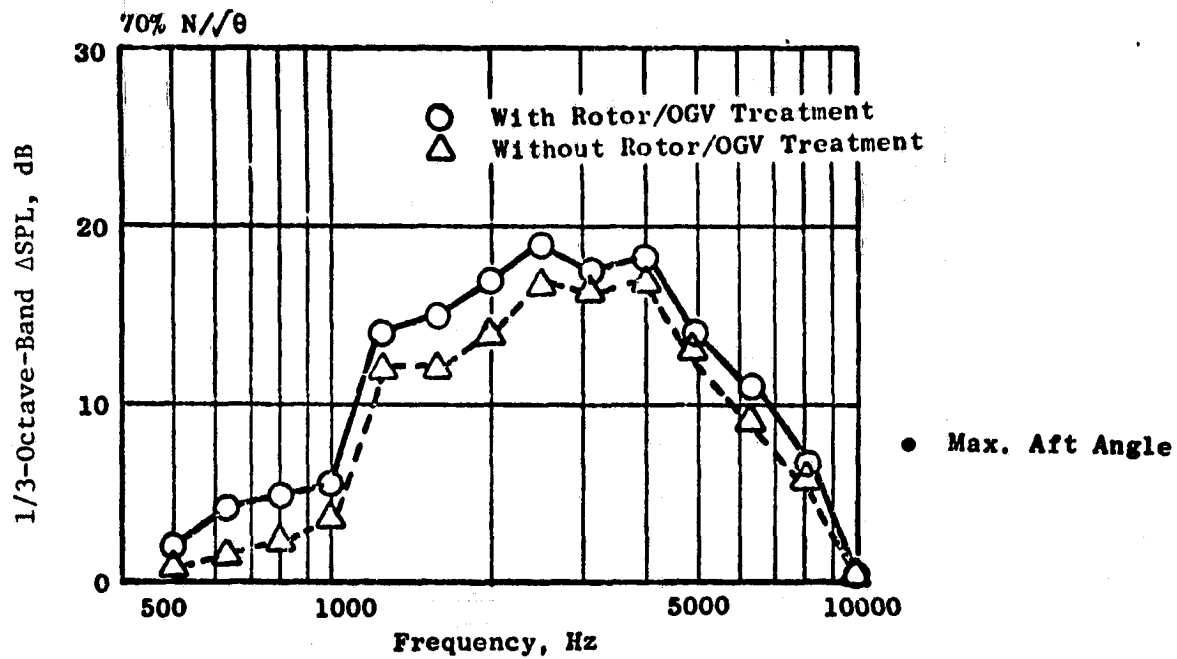


Figure 75. Measured Suppression of Fully Treated Fan Exhaust With and Without Rotor-OGV Treatment.

- 12% porosity

The addition of the rotor-OGV treatment increased the tone and broadband suppression levels at 70% $N/\sqrt{\theta}$. The broadband suppression increased from 1-3 dB while the tone suppression increased some 2-3 dB. The results for the 100% $N/\sqrt{\theta}$ fan speed point show the broadband suppression level increased by 1-3 dB for the rotor-OGV treatment with about a 3-dB increase in the tone suppression level. These data show the rotor-OGV treatment to be effective at both fan speeds and gives suppression even when combined with a fully treated exhaust configuration.

5.2.6 Variable-Depth Treatment Orientation

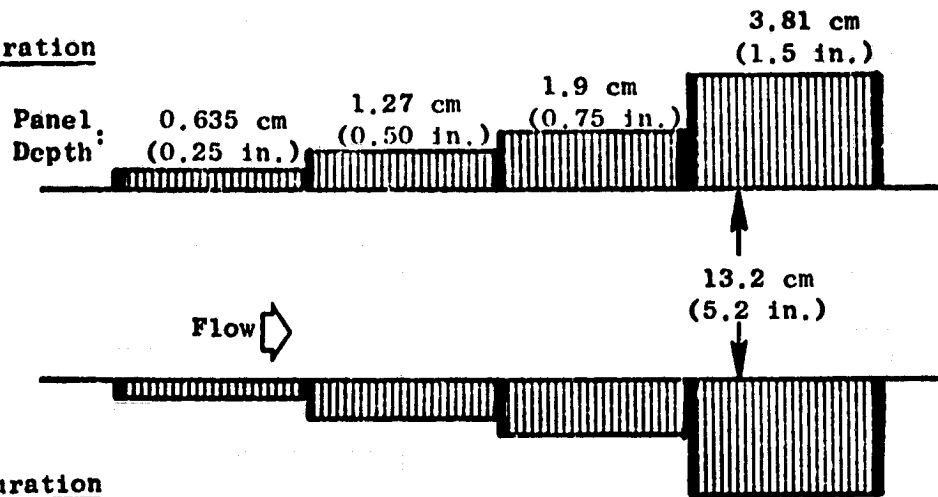
Acoustic rectangular duct data taken prior to the Rotor 55 fan exhaust tests gave indications that suppression levels were strongly influenced by axial treatment depth orientation for a high-porosity (27%) faceplate design; however, the duct data showed suppression to be independent of axial orientation for a 12% faceplate porosity.

Figure 76 shows a schematic of the variable-depth configurations that were run with thin/thick and thick/thin treatment orientation. The suppression for the configuration with 12% porosity is shown in Figure 77 for 70% $N/\sqrt{\theta}$ and 100% $N/\sqrt{\theta}$ fan speeds. These data were taken at the maximum aft acoustic angles on a 5.18-m (17-ft) arc. The 70% $N/\sqrt{\theta}$ fan speed point suppression results show that at frequencies greater than the peak attenuation frequency the thin/thick treatment sequence gives higher suppression. Suppression at frequencies below the peak attenuation is not greatly influenced by the treatment sequence. The same comparison of data at 100% $N/\sqrt{\theta}$ fan speed shows less difference in suppression over the entire frequency range.

Figure 78 gives suppression for the configuration with 27% faceplate porosity. At 70% $N/\sqrt{\theta}$ the thin/thick configuration gave better suppression at the higher frequencies, somewhat less at lower frequencies, than the thick/thin configuration. The results in Figure 78 for 100% $N/\sqrt{\theta}$ likewise show an advantage at higher frequencies for the thin/thick configuration. The low frequencies show no difference in the suppression levels.

The Rotor 55 data show the same trend as the duct data, in that the sensitivity in suppression with respect to treatment arrangement is more notable for the high-porosity (27%) design. However, the difference in suppression level as measured in Rotor 55 is much less than prior duct data had indicated. The total suppression level obtained from the 27% porosity thin/thick configuration is small when compared with other configurations having either constant 12% porosity, or a mixed-porosity design. For the optimum design of the configurations tested here, suppression seems to be independent of the treatment placement. Hence, the thick-to-thin orientation is used in the engine design (which will be discussed later) since the engine nacelle can accommodate this arrangement more readily.

Thin/Thick Configuration



Thick/Thin Configuration

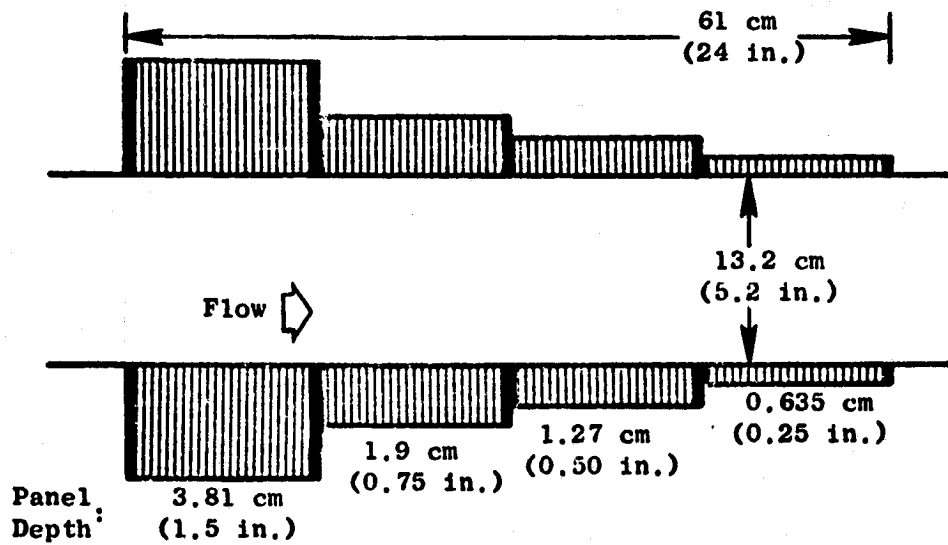


Figure 76. Thin/Thick Vs. Thick/Thin Variable-Depth Treatment Configurations.

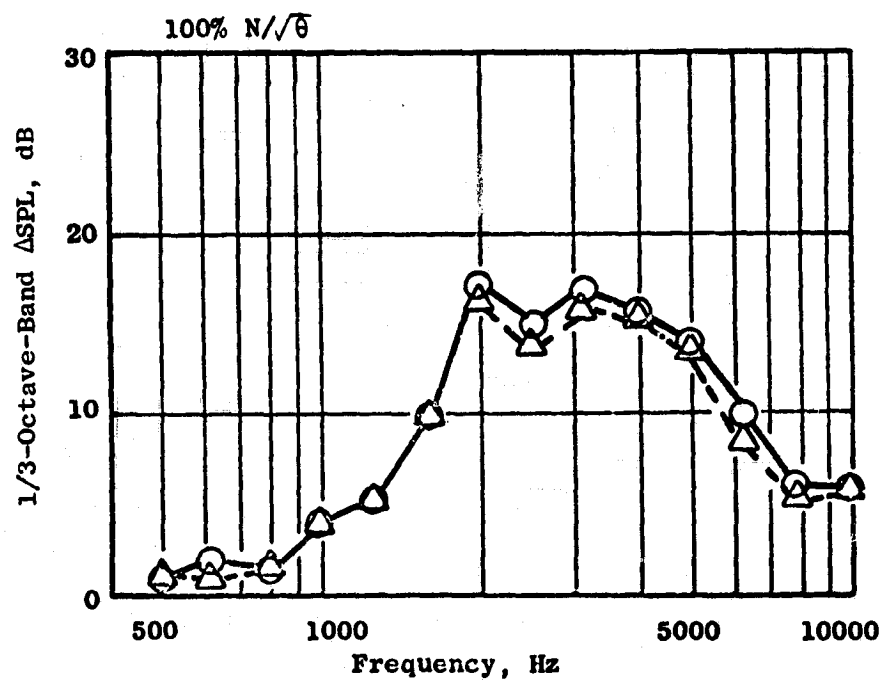
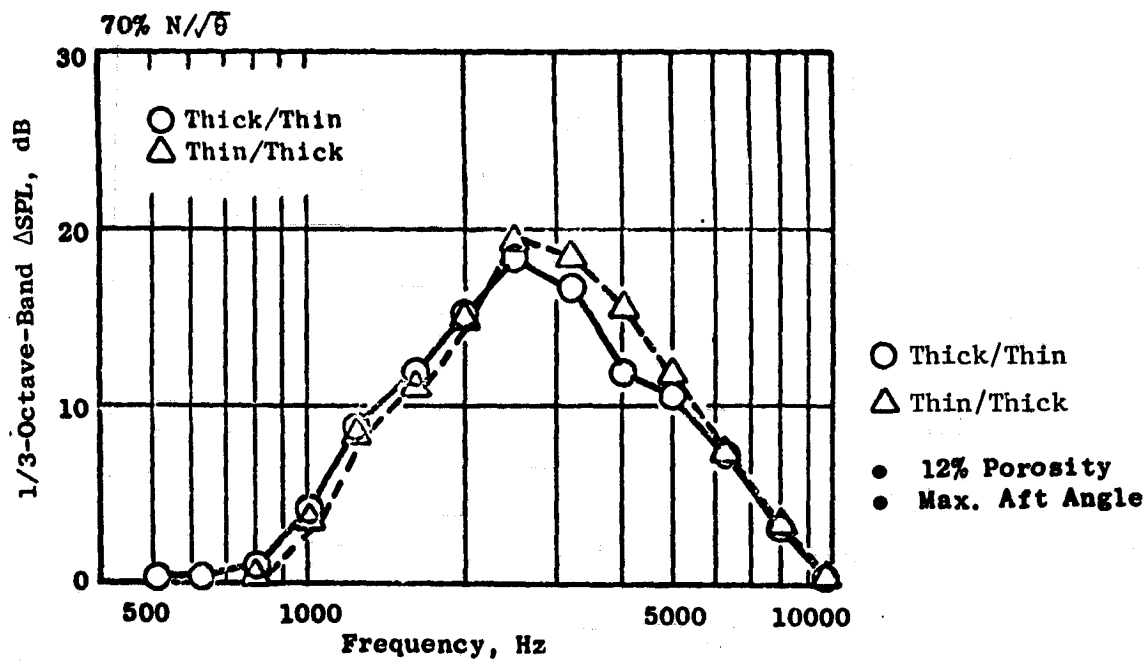
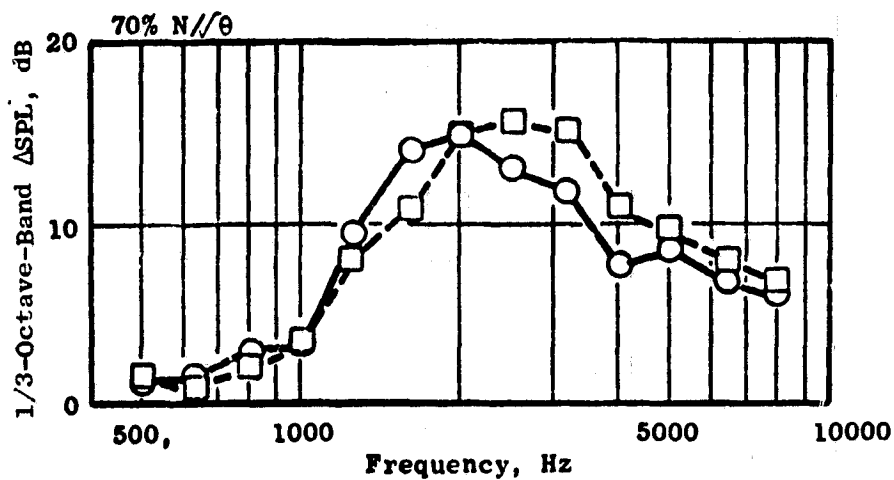


Figure 77. Effect of Treatment Orientation on Suppression.



- Max. Aft Angle
- 27% Porosity
- Thick to Thin
- Thin to Thick

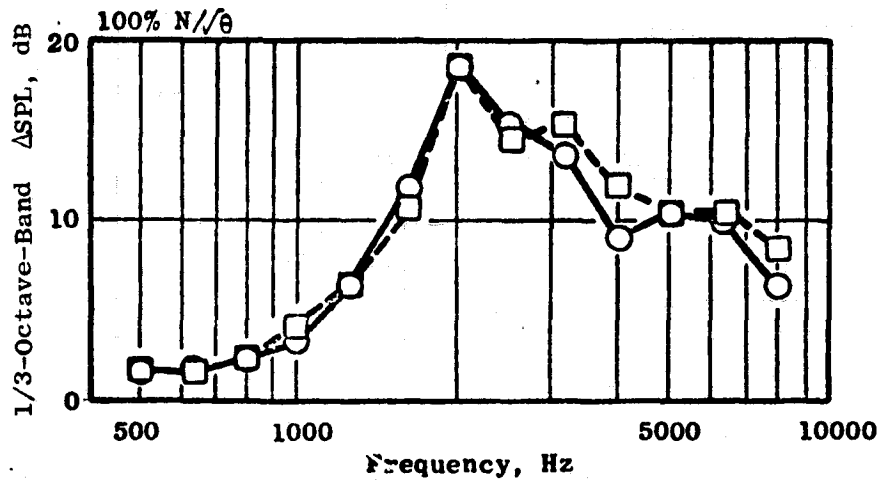


Figure 78. Suppression Spectra for Thin/Thick Vs. Thick/Thin Treatment.

5.3 ENGINE BOILERPLATE TREATMENT DESIGN AND SUPPRESSION ESTIMATES

Suppression results from the rotor-OGV and the fan exhaust series of tests were utilized in the design of the QCSEE UTW engine Boilerplate No. 1 fan exhaust treatment configuration. The design features that showed desirable suppression (based on the data as presented herein) were maintained in the aft duct treatment design whenever possible. The design approach is to use variable-depth treatment with mixed porosity aimed at optimizing the acoustic resistance for each treatment panel. These two considerations are necessary for maximum suppression bandwidth and peak suppression.

Figure 79 depicts the rotor-OGV treatment design for Rotor 55 and for the UTW engine. The acoustic parameter L/H is given for each of the configurations and is calculated from the average length of the inner and outer walls relative to the duct height. The engine has more treatment in this area than was tested in Rotor 55. A straight cell geometry with 10% porosity was used. Treatment on the inner wall was also included in the engine design, giving a greater amount of treatment area. Data from other test vehicles show that the amount of damping offered by the lower 10% porosity is very effective in the rotor-OGV region.

Figure 80 gives a sketch of the engine aft duct outer wall treatment and the Rotor 55 configuration that was used to simulate the engine design. One notable difference in the two designs is the orientation of the outer wall treatment, being thick/thin rather than thin/thick. Such a design was more adaptable to the engine configuration, and was selected because the data results (as previously discussed) showed no penalty in suppression for low-porosity designs. The acoustic parameters L/H and H/λ_0 are also given. The L/H value is slightly higher for the engine (5.5 versus 5.2). The H/λ_0 values are for the measured maximum-attenuation frequency from Rotor 55 and the calculated peak-attenuation frequency for the engine.

The previously used GE prediction method was adjusted to give better agreement with the Rotor 55 measured suppressions. The adjustment in the prediction method resulted in increasing the suppression bandwidth in the higher frequency range above the peak attenuation frequency. The original predicted levels were increased by a factor of 10% for all frequencies having a H/λ value greater than 1.0. The procedure also accounted for treatment area losses not depicted in engine drawings used in preliminary design estimates. Previous procedure had been to use a linear relation between treatment area reduction and the predicted decrease in suppression levels. This procedure was modified based on the results discussed previously herein, which show the measured suppression loss to be 1/4 to 1/2 the predicted level. Thus, in the modified procedure, only 50% of the treatment area loss is assumed.

Figure 81 shows a comparison of the predicted and measured suppression (using the modified prediction procedure) for the configurations as defined in the sketch. The configuration has variable-pitch treatment and a mixed-porosity design. The measured and predicted suppression are seen to have

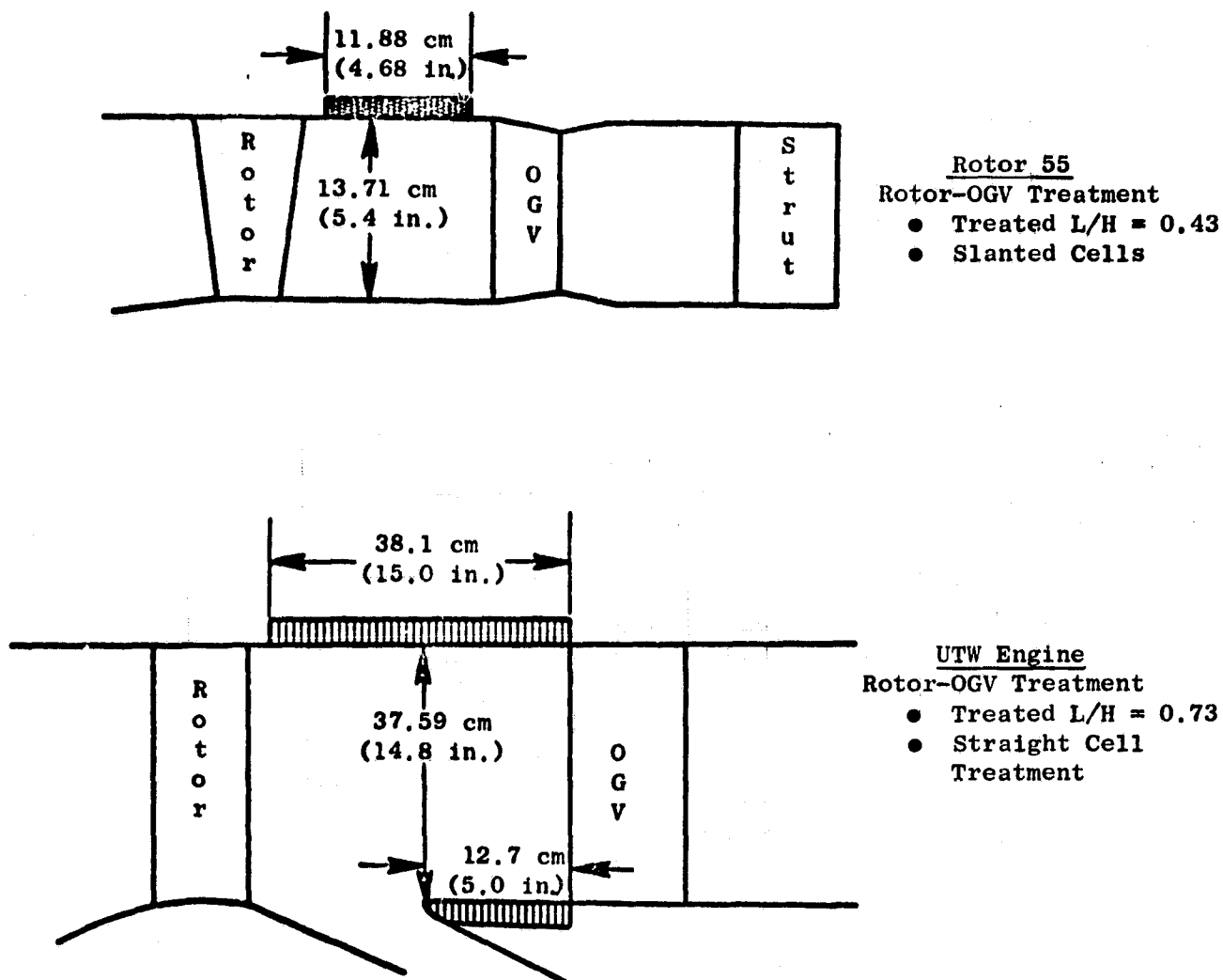
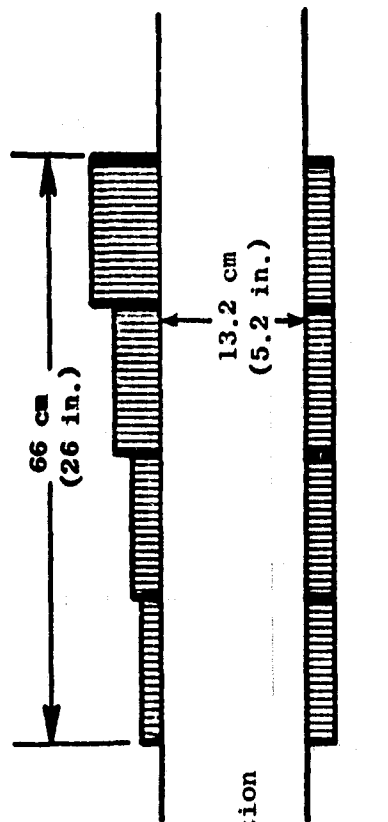
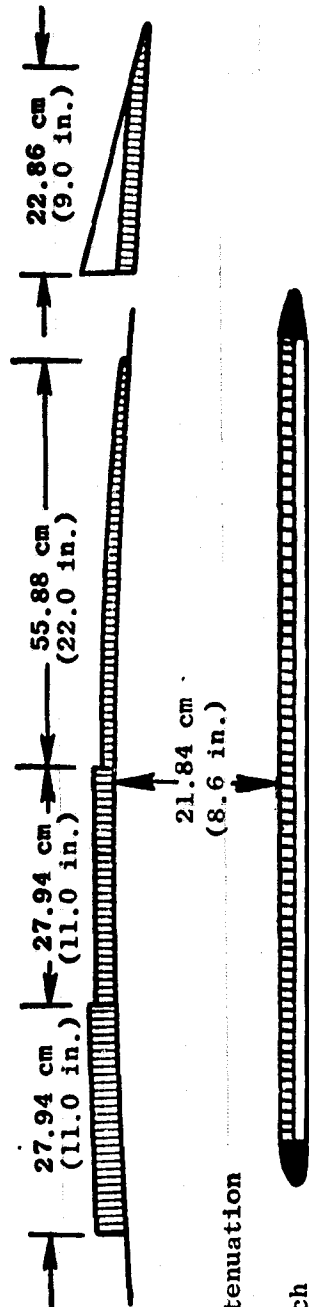


Figure 79. Rotor 55 and QCSEE UTW Rotor-OGV Treatment.



Rotor 55

- $L/H = 5.2$
- H/λ_0 at Peak Attenuation Frequency = 1.22
- Average Duct Mach Number = 0.42 at Takeoff Power



UTW Boilerplate No. 1

- $L/H = 5.5$
- H/λ_0 at Peak Attenuation Frequency = 1.6
- Average Duct Mach Number = 0.47 at Takeoff Power

Figure 80. Model and Engine Aft Duct Treatment Configurations.

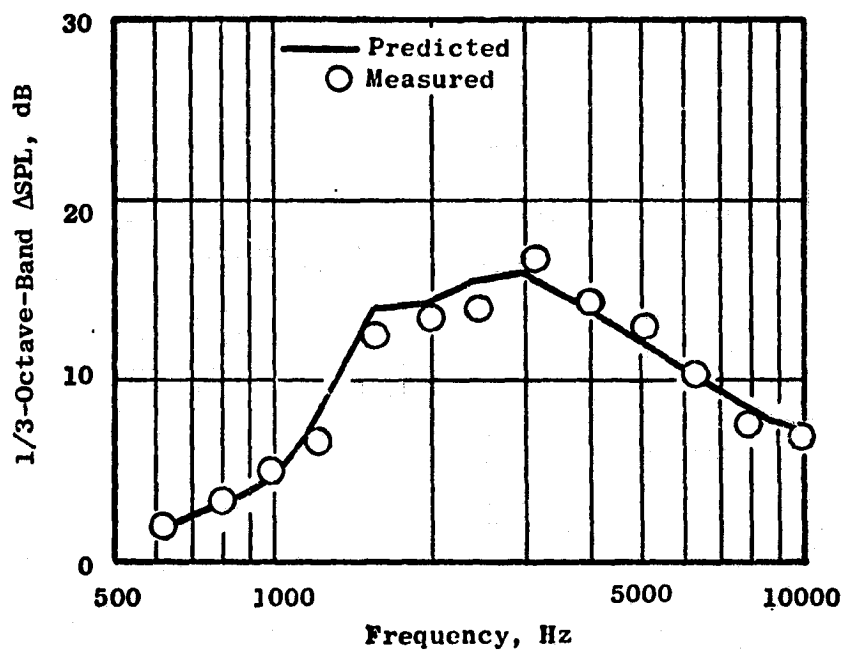
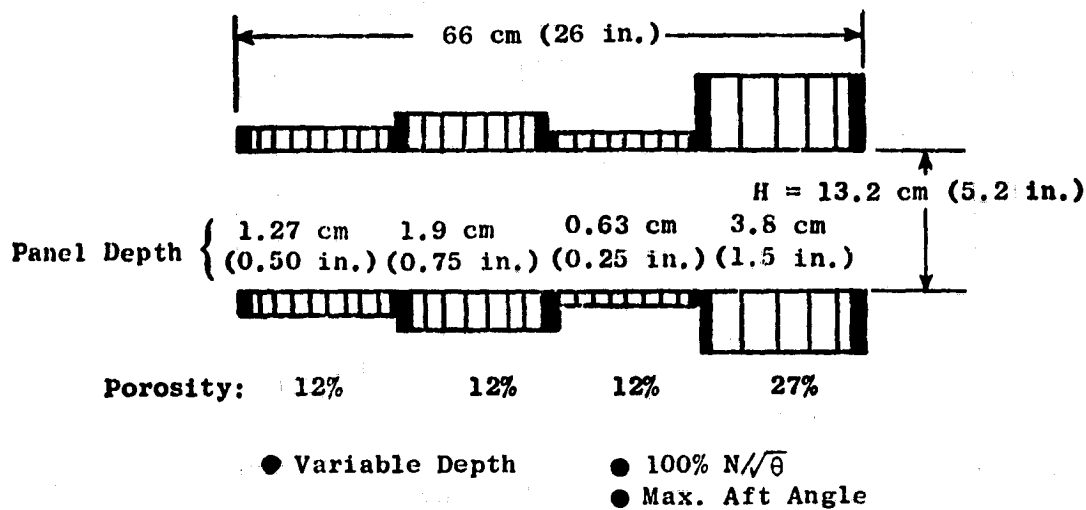


Figure 81. Adjusted Predictions Vs. Measured Suppression Spectra, Variable-Depth, Mixed-Porosity Panels.

good agreement. Figure 82 gives a comparison of the predicted and measured data for the configuration used in simulating the engine splitter configuration. The predicted value is higher than the measured peak suppression; however, good agreement is indicated at most of the other 1/3-octave-band frequencies.

Figure 83 shows the UTW Boilerplate No. 1 treatment configuration, and gives a summary of the treatment design details, including the rotor-OGV, vane, and fan exhaust treatment. The porosity values were defined based on acoustic duct tests where optimum suppression values were correlated with H/λ_0 . The prediction procedure as described above was used in arriving at this design.

Suppression calculations were made for several different combinations of treatment lengths and tuning frequencies until a balanced design was achieved. The Noy-weighted suppressed fan spectrum given in Figure 84 illustrates that a balanced design was achieved. To further increase the suppression in terms of PNL requires additional suppression in both the high and low frequencies. The predicted suppression for the recommended design is 13.4 PNdB. This level of fan exhaust-radiated noise suppression, when combined with the other noise constituents, is expected to allow the total engine system level of 95 EPNdB to be met.

This same fan exhaust duct treatment design was used for the OTW engine as a "first cut" design for that engine as well; the same procedure was also used for the core treatment (combustor and turbine) in which the same hardware was intended for use on both engines.

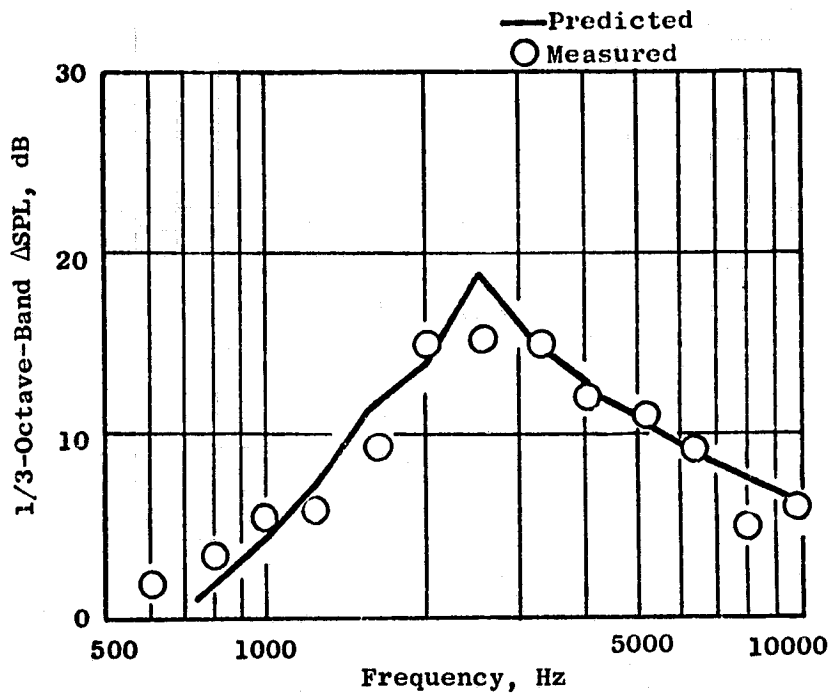
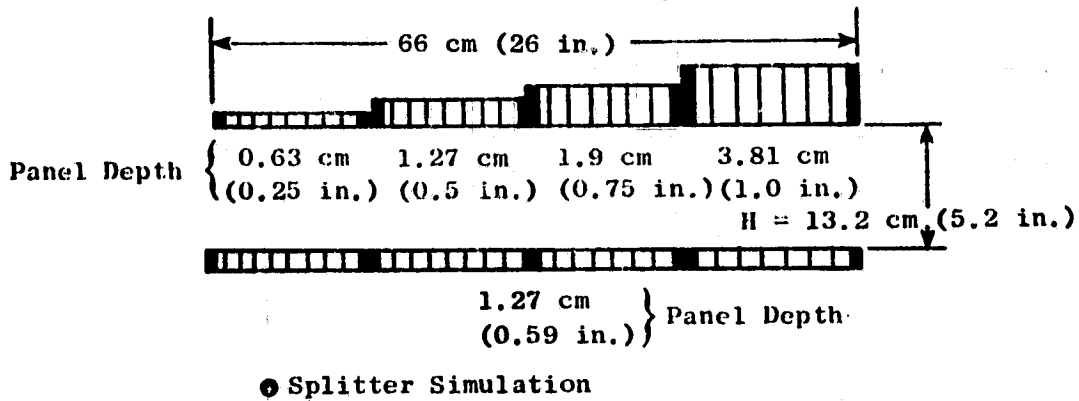
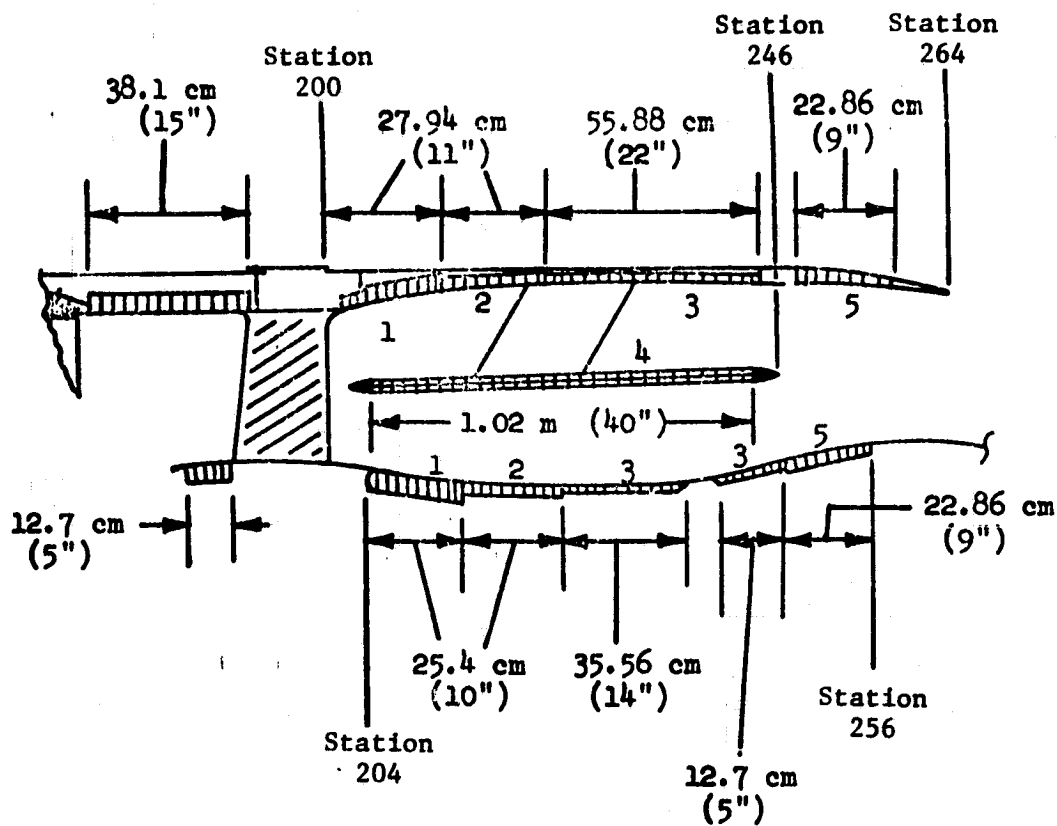


Figure 82. Adjusted Predictions Vs. Measured Suppression Spectra, Splitter Simulation, 12% Porosity Panels.



	<u>Depth</u>	<u>Porosity, %</u>	<u>Tuning Frequency, Hz</u>
Fan Frame Treatment	5.08 cm (2 in.)	10.0	1000
Treated Vanes	0.762 cm (0.3 in.)	10.0	4000
Fan Exhaust Treatment			
Section 1	5.08 cm (2 in.)	22.0	1250
Section 2	2.54 cm (1 in.)	15.5	2000
Section 3	1.90 cm (0.75 in.)	15.5	2500
Section 4	1.27 cm (0.5 in.)	11.5	2500
Section 5	2.54 cm (1 in.)	15.5	1600

Figure 83. UTW Boilerplate No. 1 Treatment Configuration.

- Max. Aft Angle
- 152.4 m (500 ft) Sideline at
61 m (200 ft) Altitude
- Takeoff Power

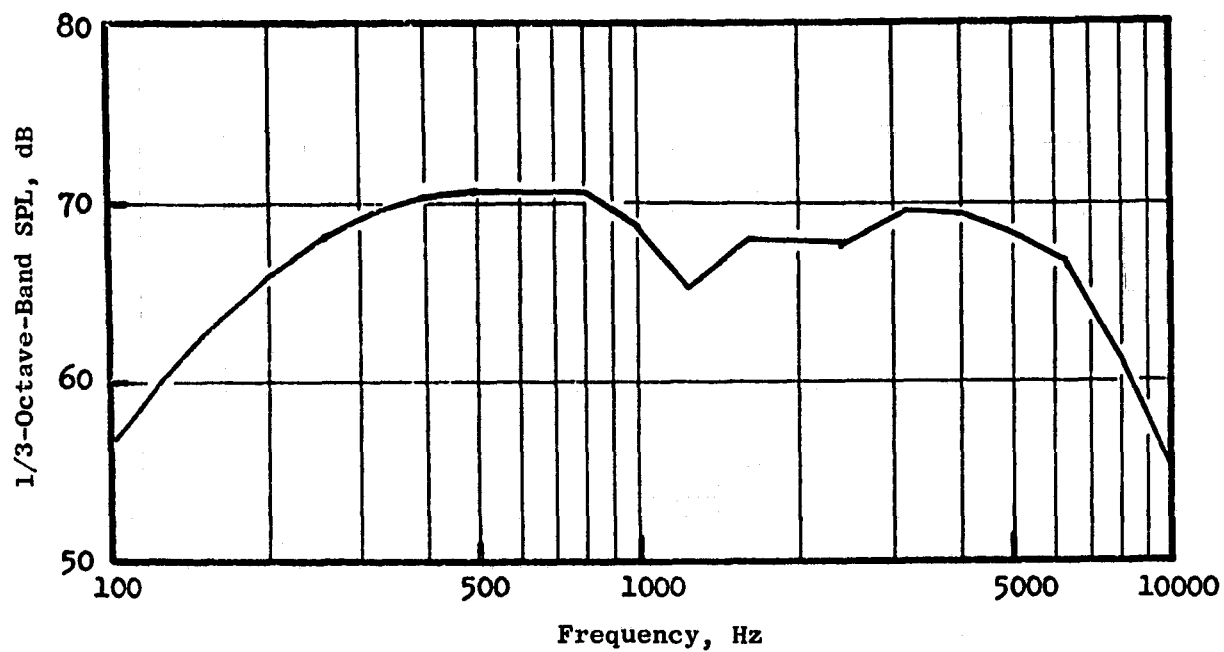


Figure 84. UTW Boilerplate No. 1 Noy-Weighted Suppressed Fan Exhaust Spectrum.

6.0 FAN INLET TREATMENT DEVELOPMENT AND DESIGN

6.1 SCALE MODEL INLET TESTS

The UTW 50.8-cm (20-in.) diameter scale model fan was used to evaluate the effectiveness of several inlet treatment configurations and to identify a design capable of meeting the engine noise suppression goal. The overall inlet suppression objectives for the system at different operating conditions were:

	<u>ΔPNdB</u>
Takeoff	13
Approach	8
Reverse Thrust	3

Two types of inlets were evaluated in scale model testing. The first type was an accelerating inlet, with inlet noise obtained from a combination of high inlet flow throat Mach number at takeoff power and acoustic treatment. Suppression at approach and reverse thrust operation is obtained from the acoustic treatment only. The second inlet evaluated in the tests was a conventional low Mach inlet design, with suppression obtained from treatment at all system operating conditions.

6.1.1 Description of Inlet Treatment Configuration

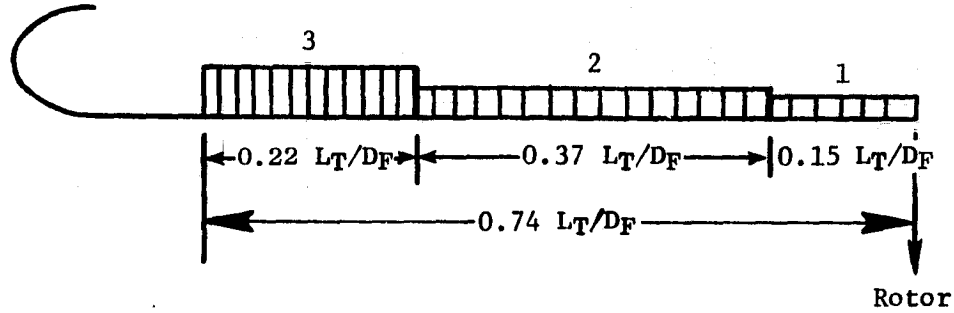
6.1.1.1 Accelerating Inlets

Four different inlet treatment configurations for the accelerating inlet are defined in Table V. Each of the treatment configurations had a treated length-to-fan-diameter ratio (L_T/D_f) of 0.74 with the total treatment length consisting of three sections having different panel depths. All of these configurations employed resonator-type treatment which was designed for the reverse thrust condition. Table VI gives the treatment faceplate definition for each treatment configuration. Included are the faceplate hole diameter, porosity, and thickness. The design-objective values of each panel's tuning frequency are shown in Table V; the actual tuning frequencies predicted for each panel are shown in Figures 86 through 89 for inlets A and B and C and D in reverse thrust and forward thrust, respectively. The panel reactance values were predicted using the analytical relations given in Reference 5. The optimum reactance values were determined by the analytical model presented by E.J. Rice in Reference 4.

6.1.1.2 Low Mach Inlets

The low Mach inlet treatment configurations are defined in Table VII. The configurations have (L_T/D_f) ratios of 0.825 and 0.85 with the total treated

Table V. Accelerating Inlet Treatment Designs.



	Section	Cavity Depth		Open Area, %	Tuning Frequency, Hz	
		cm	(in.)		Full-Scale	Scale-Model
Treatment A	1	0.312	(0.123)	24.0	3150	11182
	2	0.570	(0.225)	24.0	2000	7100
	3	1.720	(0.680)	24.0	1000	3550
Treatment B	1	0.312	(0.123)	9.2	3150	11182
	2	0.570	(0.225)	9.2	2000	7100
	3	1.720	(0.680)	9.2	1000	3550
Treatment C	1	0.134	(0.053)	3.6	3150	11182
	2	0.325	(0.128)	3.6	2000	7100
	3	1.420	(0.560)	3.6	1000	3550
Treatment D	1	0.246	(0.097)	7.2	3150	11182
	2	0.744	(0.293)	14.4	2000	7100
	3	2.060	(0.812)	28.0	1000	3550

Table VI. Accelerating Inlet Designs, Acoustic Treatment Faceplate Definitions.

<u>Inlet</u>	<u>Hole Diameter</u>		<u>Porosity, %</u>	<u>Thickness</u>	
	<u>cm</u>	<u>(in.)</u>		<u>cm</u>	<u>(in.)</u>
A. All Sections	0.0240	(0.0600)	24.0	0.0320	(0.0810)
B. All Sections	0.0450	(0.1100)	9.2	0.0200	(0.0508)
C. All Sections	0.0625	(0.1580)	3.6	0.0200	(0.0508)
 <u>Inlet D</u>					
1	0.0330	(0.0830)	7.2	0.0200	(0.0508)
2	0.0220	(0.0550)	14.4	0.0200	(0.0508)
3	0.0450	(0.1140)	28.0	0.0320	(0.0508)

- 60° Acoustic Angle
 - 152.4 m (500 ft) Sideline
 - 86% N_{FC} , 35% of Takeoff Forward Thrust
 - QF9 Data Scaled to Full-Size
-
- Unsuppressed
 - - - Unsuppressed Noy-Weighted

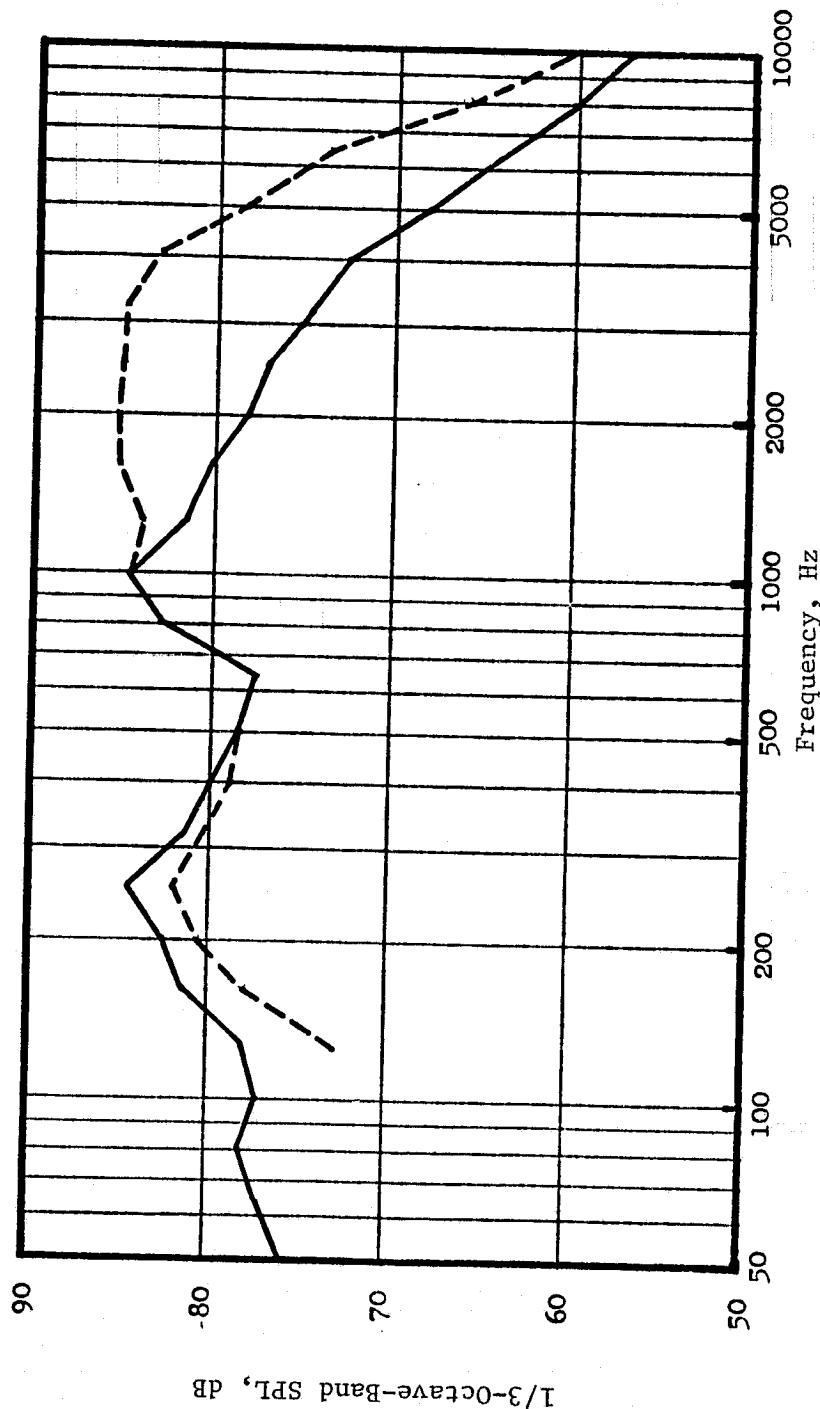


Figure 85. Predicted Reverse Thrust UTW Engine Noise Spectra at 86% N_{FC} , (60°) to Inlet.

* See Table V for
Definitions of Treatment
Sections ①, ②, and ③

ACCELERATING INLETS

— TREATMENT A

- - - TREATMENT B

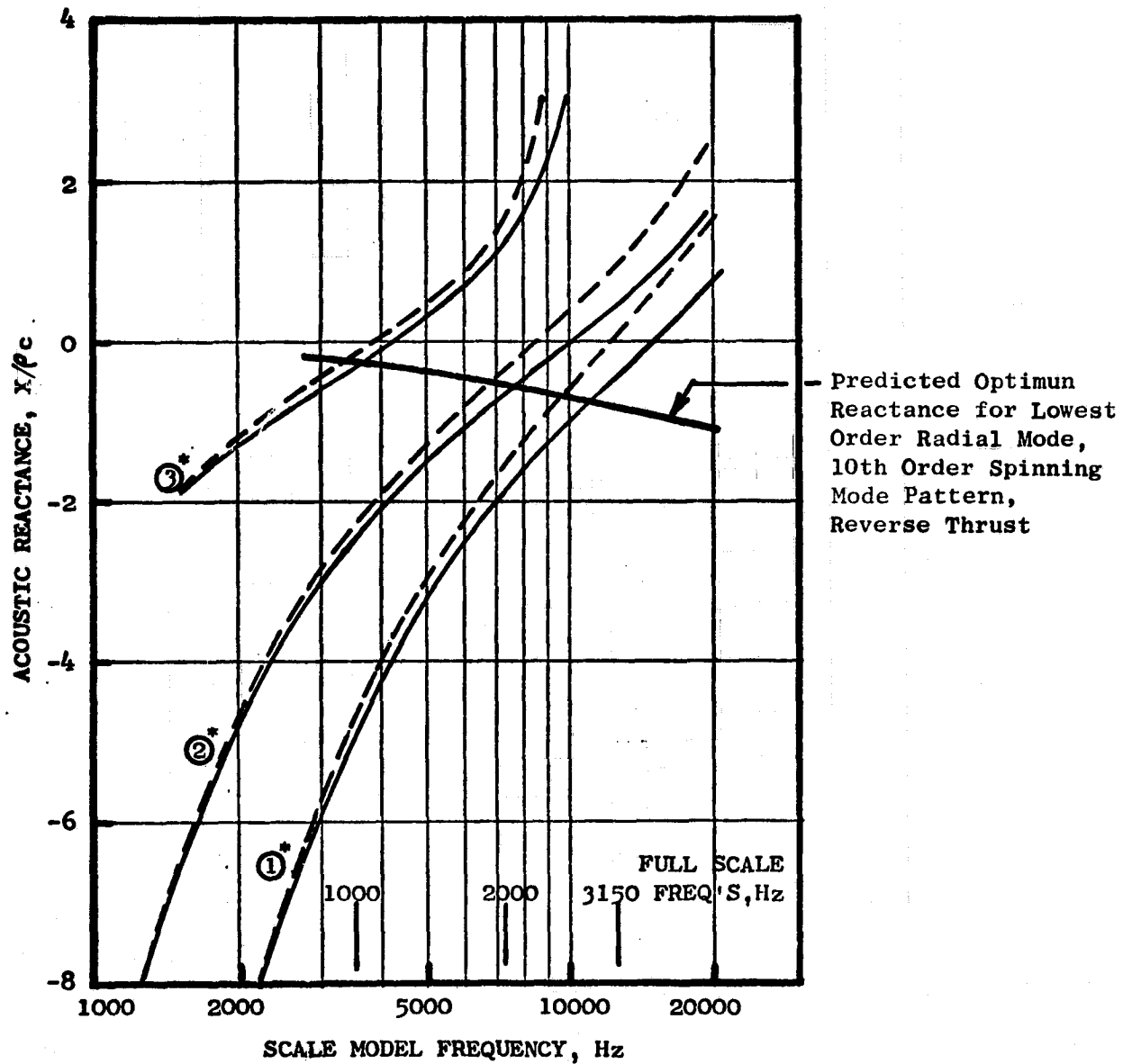


Figure 86. Reverse Thrust Acoustic Reactance Vs. Frequency for Accelerating Inlet Treatments A and B.

* See Table V for
Definitions of Treatment
Sections ①, ②, and ③

ACCELERATING INLETS

—— TREATMENT C

- - - - TREATMENT D

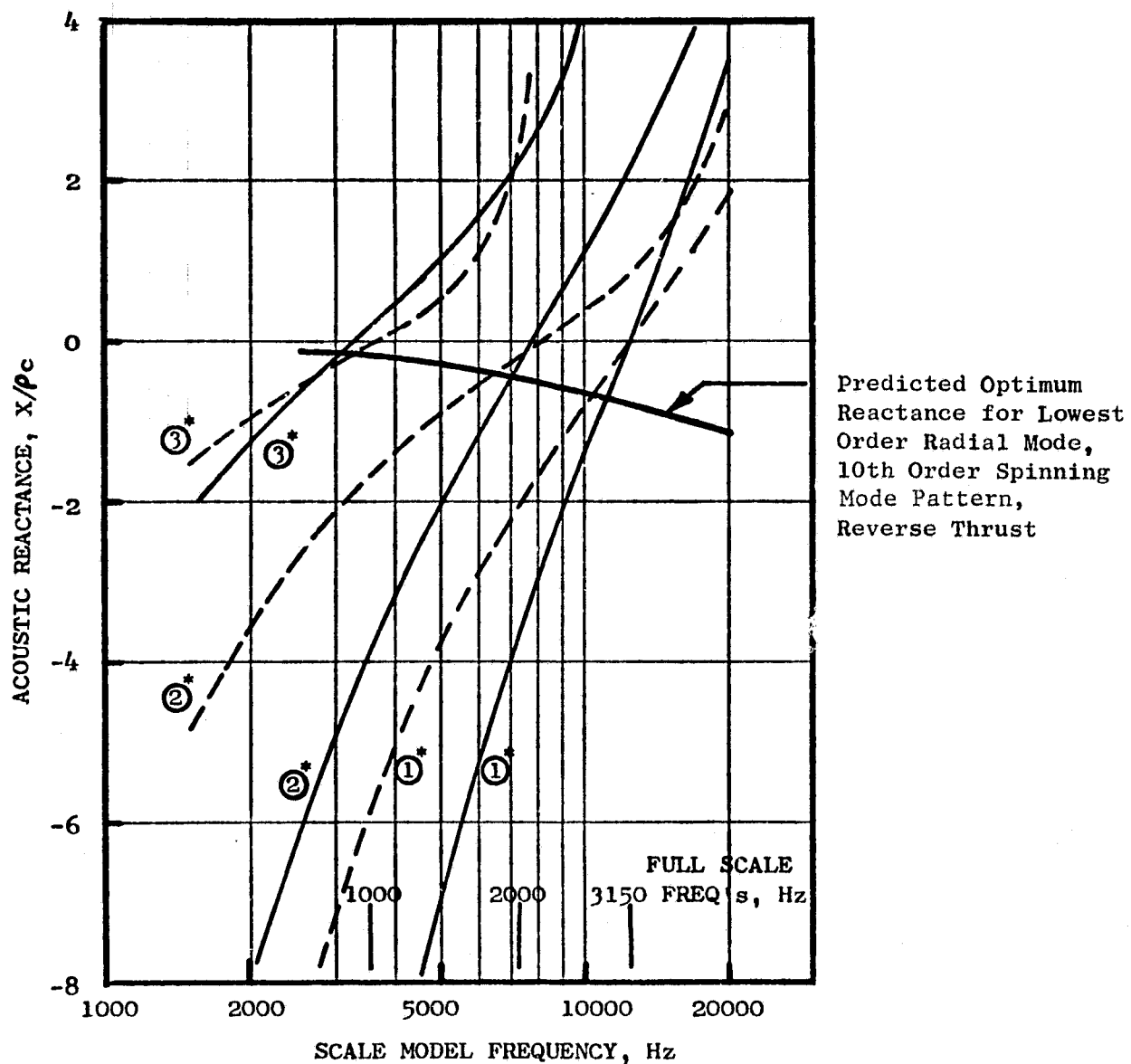


Figure 87. Reverse Thrust Acoustic Reactance Vs. Frequency for Accelerating Inlet Treatments C and D.

* See Table V for
 Definition of Treatment
 Sections ①, ②, and ③

ACCELERATING INLETS

—— TREATMENT A

- - - TREATMENT B

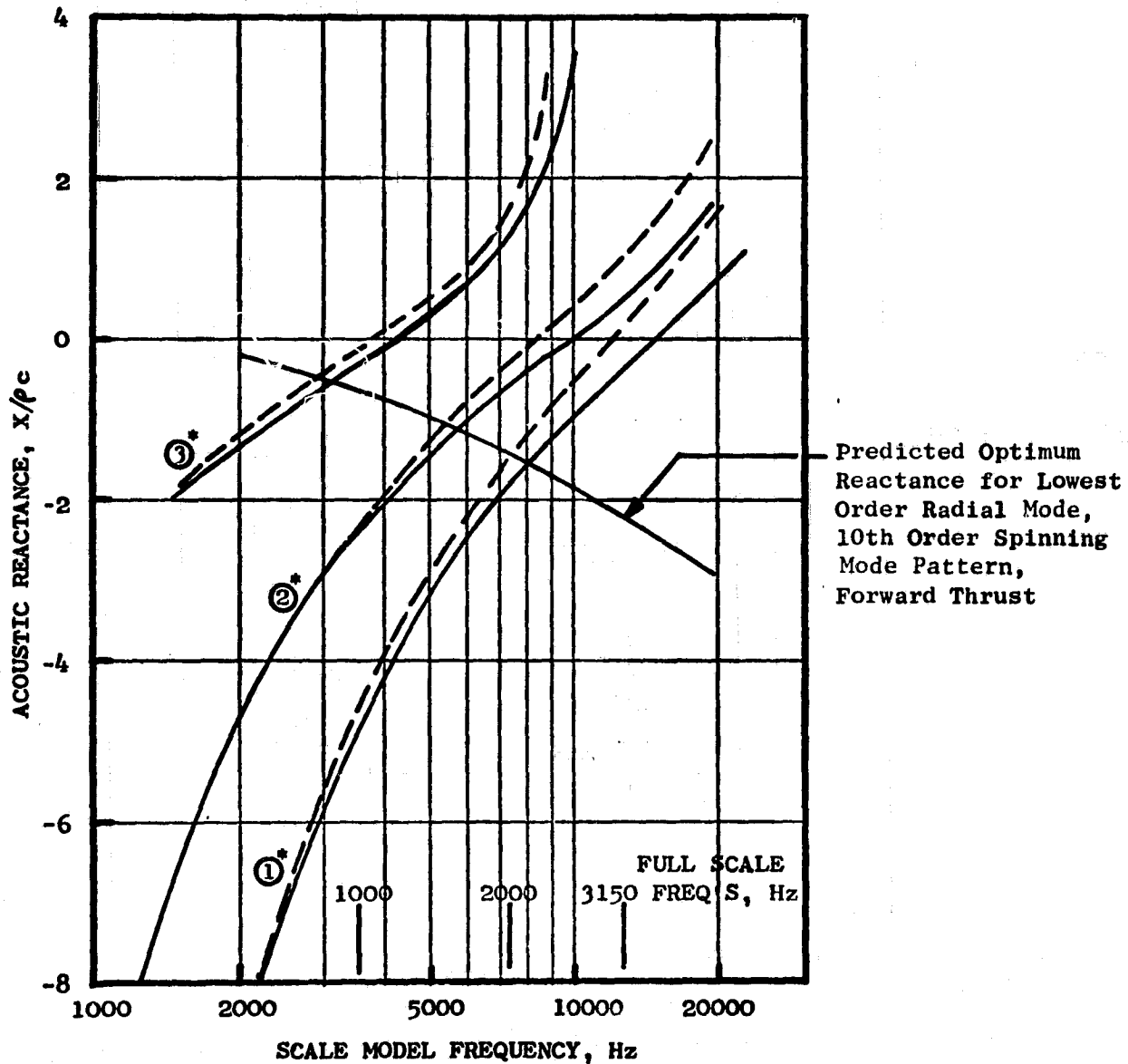


Figure 88. Forward Thrust Acoustic Reactance Vs. Frequency for Accelerating Inlet Treatments A and B.

* See Table V for Definition
of Treatment Sections
①, ②, and ③

Accelerating Inlets

— Treatment C
- - - Treatment D

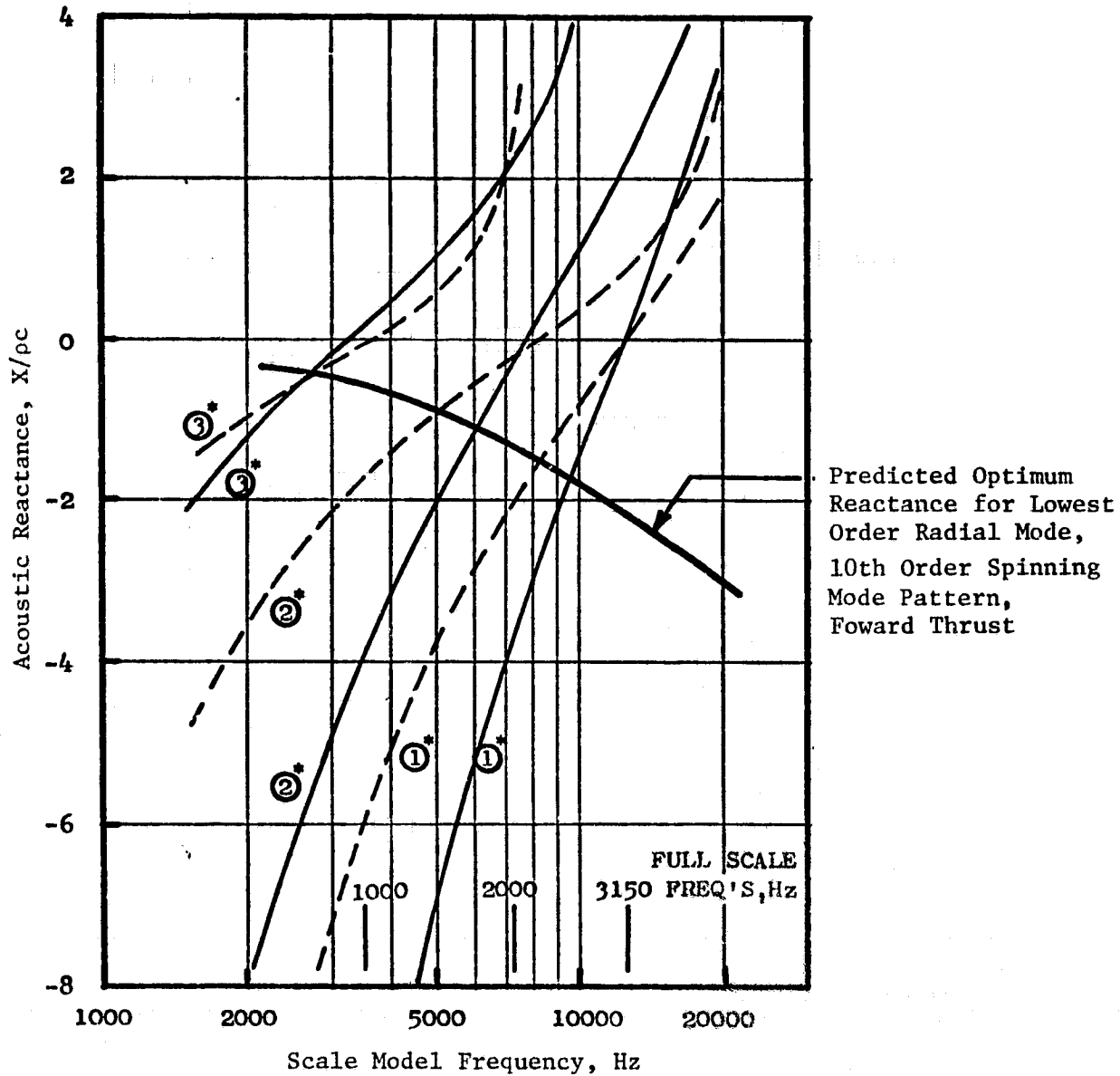
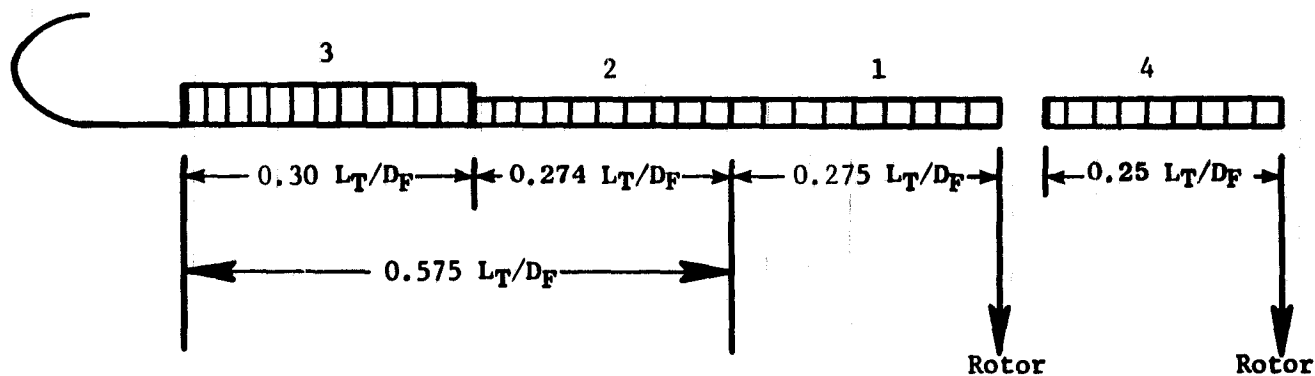


Figure 89. Forward Thrust Acoustic Reactance Vs. Frequency for Accelerating Inlet Treatments C and D.

Table VII. Low Mach Inlet Treatment Designs.



	Section	Cavity Depth		Open Area, %	Tuning Frequency, Hz	
		cm	(in.)		Full-Scale	Scale Model
Treatment A	2	0.381	(0.150)	10.0	2000	7100
	3	1.420	(0.560)	10.0	1000	3550
	4	1.147	(0.058)	10.0	3150	11182
Treatment B	1	1.270	(0.500)	28.0	} Broadband Characteristics }	
	2	1.270	(0.500)	28.0		
	3	1.270	(0.500)	28.0		
Treatment C	2	0.134	(0.053)	3.6	2800	9940
	3	0.393	(0.155)	3.6	1550	5500
	4	0.200	(0.080)	3.6	2253	8000

length consisting of three sections, each of which has a different panel depth. Two of the configurations, A and C, are resonator-type treatments and the other configuration, B, is a bulk absorber design. The faceplate for each of the treatments is defined in Table VIII. The same methods for panel reactance and optimum reactance were used here as for the accelerating inlets (see Section 6.1.1.1). Estimates of the resistance were made per Reference 14.

6.1.2 Treatment Designs

6.1.2.1 Accelerating Inlet Treatment

The treatment designs presented in Table V for the accelerating inlet configurations were designed for reverse thrust operation, because the desired suppression levels at takeoff power were assumed to be achievable primarily from the high throat Mach number accelerating inlet design. This assumption was based on previous high Mach inlet test data. The suppression requirements at approach power were also considered. Preliminary estimates indicated that the suppression requirements could be obtained from the treatment designed for the reverse thrust conditions. The predicted noise spectrum for the reverse thrust mode is given in Figure 85. The spectrum is based on QF9 data (Reference 13) and is scaled to the full-size UTW engine. The Noy-weighted unsuppressed spectrum is also given and indicates that the spectrum requires broadband suppression characteristics in order to obtain significant suppression in terms of Δ PNdB. Thus, the inlet treatment of each configuration has three thicknesses to provide the various tuning frequencies as defined in Table V. The Noy-weighted unsuppressed spectrum indicates that tuning at these frequencies is necessary to provide a balanced design. The full-scale and scale model tuning frequencies are given in Table V.

The required treatment depths and faceplate parameters needed to give the tuning frequencies were determined by using analytical methods to predict the acoustic reactance of the treatment and the optimum reactance required in designing for the reverse thrust mode. Treatments A, B, and C were designed for the lowest order radial mode, with a 10th order spinning lobe pattern. Treatment D was designed for the 15th order spinning lobe pattern. The analytical model used for determining the optimum reactance is presented by E.J. Rice in Reference 4. The predicted panel reactance values were made using the analytical relations given in Reference 5.

Figure 86 shows the predicted optimum reactance for the 10th order lobe pattern as a function of frequency for reverse thrust plus the predicted reactance for treatments A and B. Figure 87 depicts the same type of information for treatments C and D. The intersection of the optimum reactance curve with the predicted reactance curve determines the tuning frequencies for each section of treatment. A comparison of the predicted optimum reactance versus the predicted panel reactance shows that the panel designs have the optimum reactance within the previously defined 1/3-octave-band tuning frequencies for reverse thrust operation.

Table VIII. Low Mach Inlet Faceplate Definitions.

	<u>Hole Diameter</u>		<u>Faceplate Thickness</u>		<u>Porosity, %</u>
	<u>cm</u>	<u>(in.)</u>	<u>cm</u>	<u>(in.)</u>	
Treatment A	0.158	(0.0625)	0.0508	(0.020)	10.0
Treatment B	0.114	(0.0450)	0.0810	(0.032)	28.0
Treatment C	0.158	(0.0625)	0.0508	(0.020)	3.6

The faceplate porosities for treatments A, B, and C were selected to give a wide range of acoustic resistance values. The cavity depths were adjusted as required to maintain the same tuning frequencies for each design. The results from this type of test matrix provide essential data for the optimization of acoustic liner faceplates.

Treatment D is not a part of the above matrix. The faceplate porosity is different for each of the three treatment sections. The idea here was to optimize the resistance for each of the different tuning frequencies corresponding to each section of treatment. The treatment was, however, designed to have resonant frequencies corresponding to those selected in the other inlet designs.

The predicted reactance and the optimum reactance for the forward thrust operating conditions for the four accelerating inlet configurations are shown in Figures 88 and 89. The predictions are based on the analytical procedure presented in Reference 4. The prediction is for the lowest order radial mode/10th order spinning mode pattern. The tuning frequencies for the forward thrust operation for each treatment configuration are given below.

<u>Treatment Configuration</u>	<u>Predicted 1/3-Octave-Band Tuning Frequencies (Full-Scale)</u>		
	<u>Section</u>		
	<u>1</u>	<u>2</u>	<u>3</u>
A	2000	1600	800
B	2000	1600	800
C	2500	1600	800
D	2500	1250	800

The Noy-weighted unsuppressed spectrum for takeoff given in Figure 90 shows the spectrum PNL to be controlled at 1000 Hz and at 3150 Hz, with a smaller contribution at 2000 Hz. At approach the Noy-weighted unsuppressed spectrum peaks at 3150 Hz. Hence, the tuning frequencies given above are not optimized for the forward thrust condition.

6.1.2.2 Low Mach Inlet Treatment

The low Mach inlet treatment configurations are presented in Table VII. These configurations were designed to give maximum suppression in the forward thrust operating conditions. The Noy-weighted spectrum presented in Figure 91 was used to determine the treatment design frequencies. From Figure 91 it can be seen that the unsuppressed spectrum is controlled at 1000 and 3150 Hz, with a significant contribution also at 2000 Hz. Thus, with the PNdB level controlled by these three frequencies, treatment designs are required that yield broadband suppression characteristics in order to meet the suppression goal.

- 60° from Inlet Axis
 - 152.4 m (500 ft) Sideline
at 61 m (200 ft) Altitude
- Unsuppressed
 - - - Noy-Weighted

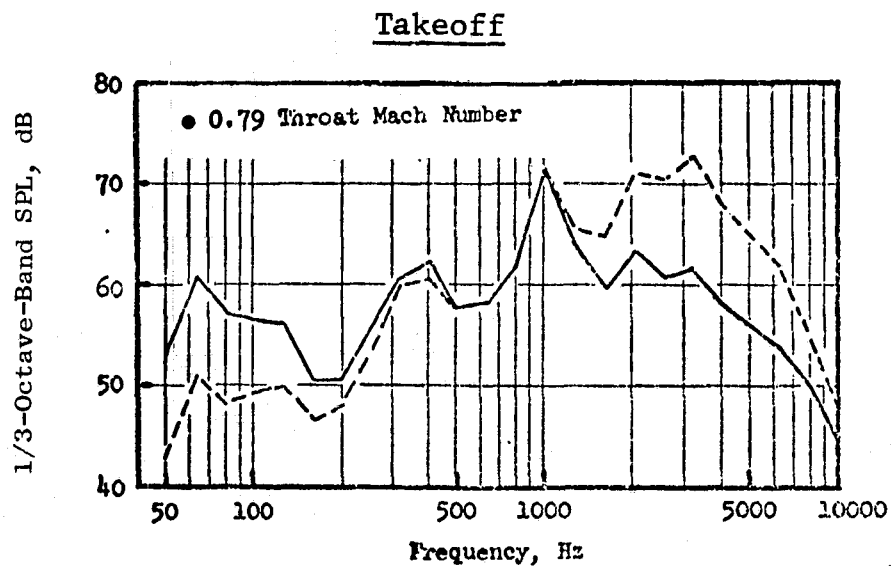
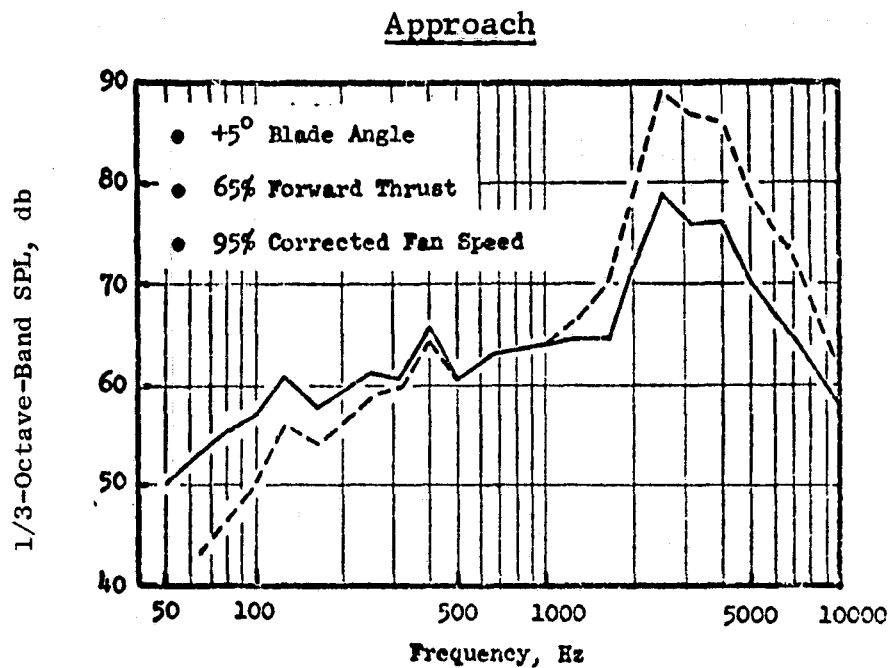


Figure 90. UTW Takeoff Fan Inlet Spectra, Hard-Wall Accelerating Inlet.

- 60° Acoustic Angle
- 152.4 m (500 ft) Sideline
at 61 m (200 ft) Altitude
- 100% N_{FC}
- Full-Scale Data

— Unsuppressed
 - - - Unsuppressed Noy-Weighted

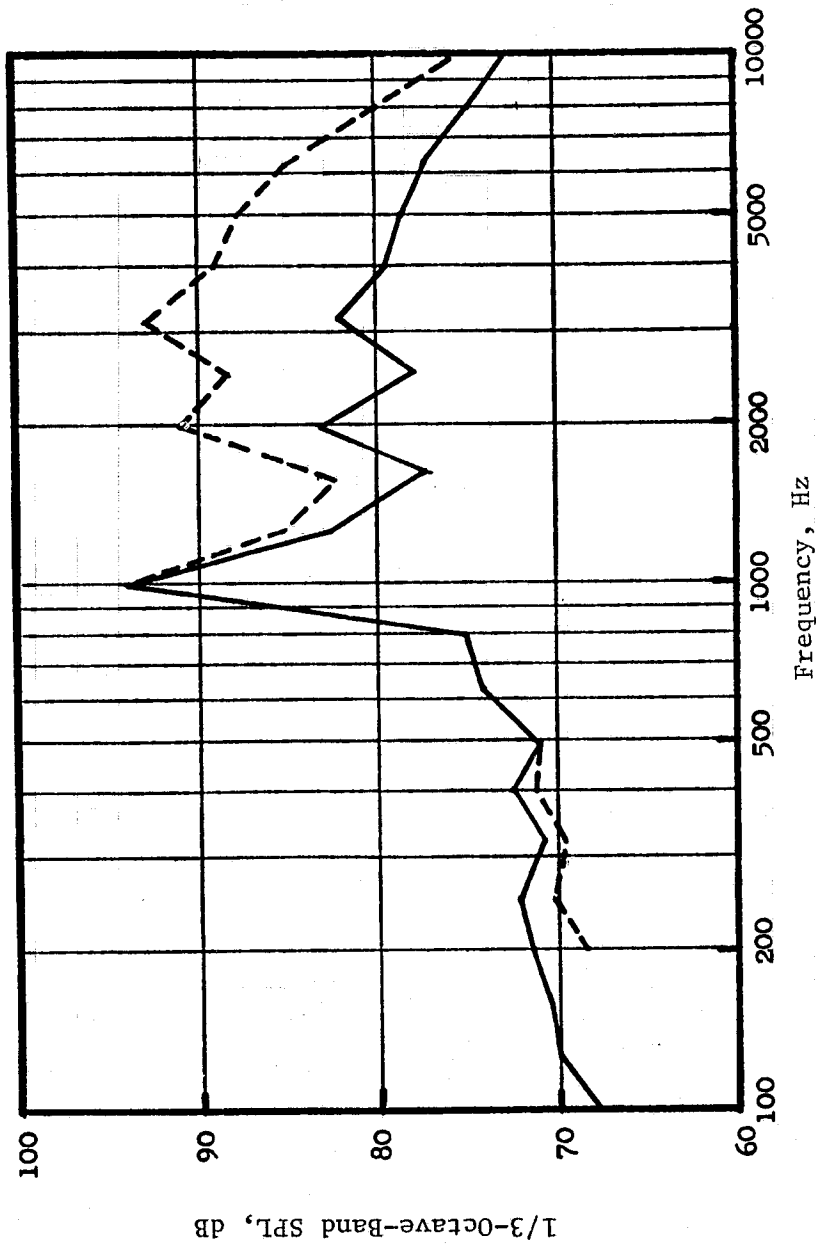


Figure 91. Predicted Unsuppressed Forward Thrust UTW Fan Spectra at 100% N_{FC} , 60° to Inlet for the Low Mach No. Inlet.

Two inlet treatments were designed with the resonator concept to give suppression bandwidth. The three tuning frequencies for the different treatment sections are given in Table VII. The same procedure was followed as for high Mach inlets except that one of the inlet treatments consists of a constant-depth 1.27-cm (0.5-in.) bulk absorber material. The selection of the bulk absorber design was made using previous data from engine configurations that have demonstrated that bulk absorber materials do give wide suppression bandwidth characteristics. The basic information and design procedure for the bulk absorber configuration is given in Appendix B.

Figure 92 gives the predicted acoustic reactance for the A and C inlet liner designs described in Table VII. Also shown in Figure 92 is the predicted optimum reactance versus frequency for the lowest order radial mode and 10th order spinning lobe pattern. The intersection of the reactance lines with the predicted optimum reactance curve determines the frequency tuning for each liner section for treatments A and C. The desired tuning frequencies for the liner sections, as determined from the Noy-weighted spectrum in Figure 91, are 1000 Hz, 2000 Hz, and 3150 Hz. Inlet A design gives these tuning frequencies; however, treatment C tuning is higher (1600 Hz, 2500 Hz, and 3150 Hz) because of the low porosity used in the inlet A design.

Inlets A and C have constant faceplate porosities of 10% and 3.6%, respectively. These porosity values were selected on the basis of previous fan data showing good suppression results for the liner designs. The initial planning was to test inlets A and C and then "drill out" the faceplates to higher porosities, thereby giving a test matrix to identify the optimum porosity.

The low Mach inlet treatment predicted acoustic reactance versus frequency, the optimum reactance for the lowest order radial mode, and the 10th order spinning lobe pattern at reverse thrust conditions are presented in Figure 93. The predictions were made using the procedure found in References 4 and 5. The predicted tuning frequencies for the different configurations in reverse thrust operation are:

<u>Treatment Configuration</u>	<u>Predicted 1/3-Octave-Band Tuning Frequencies (Full-Scale)</u>		
	<u>1</u>	<u>Section 2</u>	<u>3</u>
A	4000	2500	1250
C	3150	2500	1600

* See Table VII for Definition of Treatment Sections ①, ②, and ③.

Low Mach Inlets

— Treatment A
 - - - Treatment C

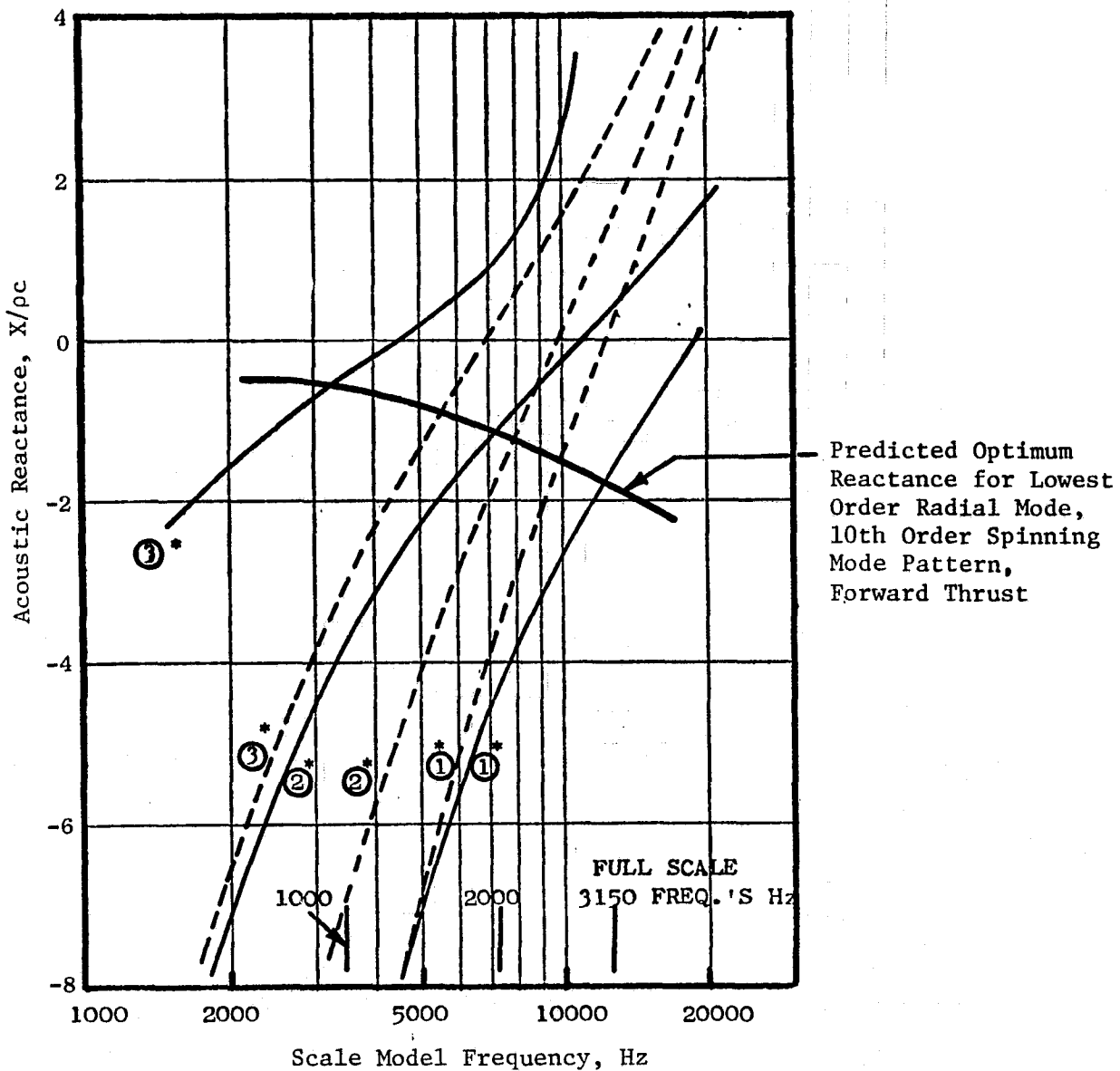


Figure 92. Forward Thrust Acoustic Reactance Vs. Frequency for Low Mach No. Inlet Treatments A and C.

* See Table VII for Definition of Treatment Sections ①, ②, and ③.

Low Mach Inlets

— Treatment A
 - - - Treatment C

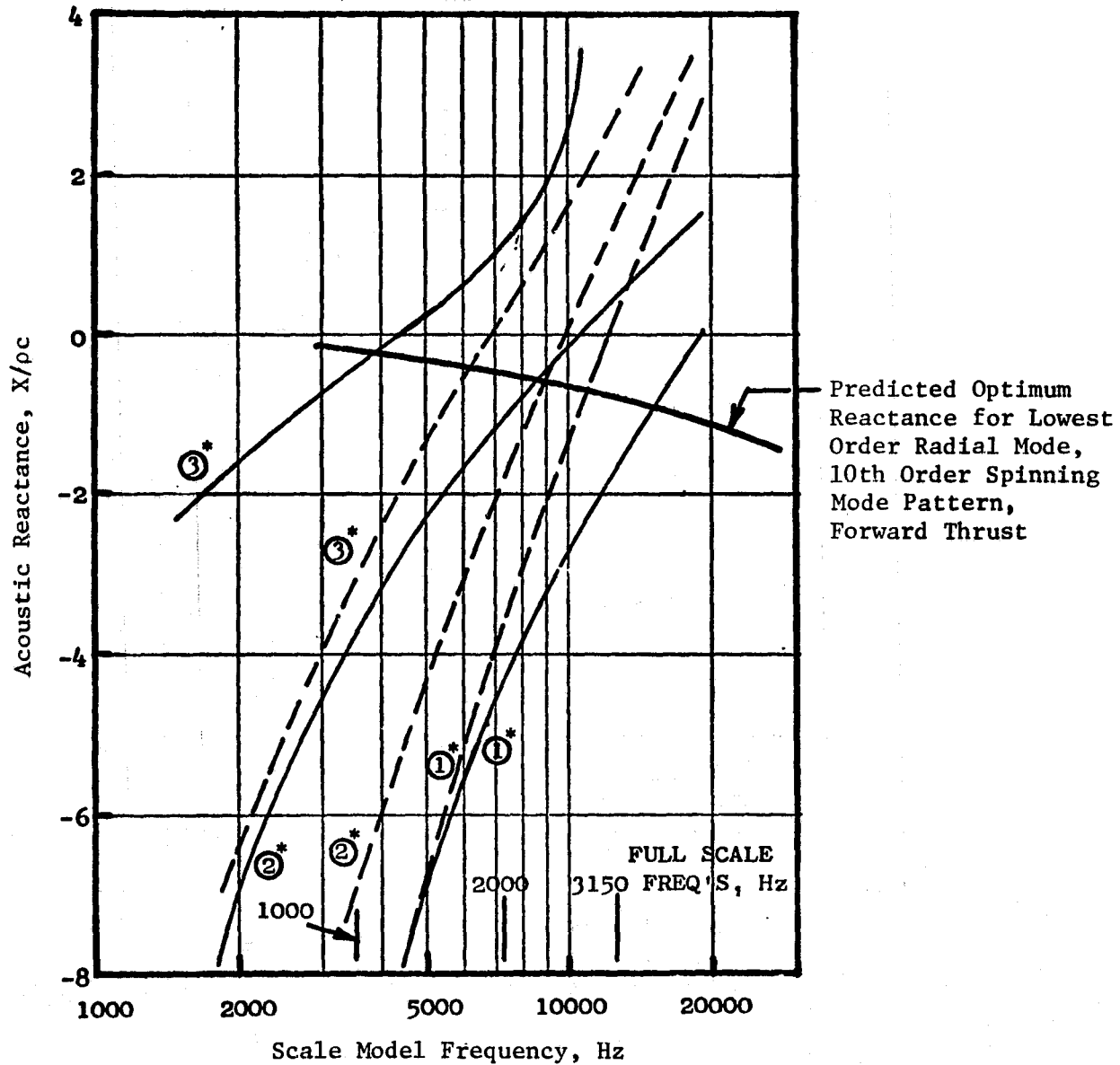


Figure 93. Reverse Thrust Acoustic Reactance Vs. Frequency for Low Mach No. Inlet Treatments A and C.

6.1.3. Suppression Results

6.1.3.1 Accelerating Inlet Suppression

Reverse Thrust

Suppression data for accelerating inlet treatment configurations at reverse thrust operation are presented in Figure 94. The data gives suppressed and unsuppressed levels in PNdB versus acoustic angle with the engine operating at 35% of the available thrust level. The figure reveals that treatment configurations D and B give the greatest suppression at all acoustic angles. The unsuppressed directivity pattern shows the noise level to be somewhat flat from 60° through 80°, with the suppressed noise levels peaking at 60°. Suppression levels at 60° show inlet D giving the highest suppression (approximately 5 PNdB) and inlet B as the next best (approximately 4 PNdB).

The unsuppressed and suppressed spectra comparisons are demonstrated in Figure 95. The same suppression trends are reflected in Figure 95 as in Figure 94 to compare the different treatment configurations. The peak suppression frequency is at the fan fundamental tone of 800 Hz, with treatment D giving approximately 8 dB. The comparison shows all configurations providing broad suppression bandwidth with approximately 5-dB suppression for 1000-6300 Hz for treatment D and lesser amounts for all other treatments.

The better performance of treatment D relative to other treatment designs is a result of the variable porosity for the three sections of treatment (chosen in general accordance with the methods stated in Reference 4). In the case of a constant porosity the value of 10% for treatment B provides more suppression than for either inlet A or C, which have respective porosity values of 24% and 3.6%.

Forward Thrust

The hard-wall and suppressed PNdB levels for accelerating inlets operating in forward thrust are delineated in Figure 96. The PNdB levels are given as a function of percent corrected fan speed for the baseline bellmouth, and for the accelerating inlet with hard-wall and with treatment configurations B and D. The results are for a 152.4-m (500-ft) sideline distance and for a 60° acoustic angle.

Suppressed noise levels are given in Figure 96 for inlet treatment configurations B and D. Other inlet configurations were not run in the forward thrust mode due to test-time constraints. Treatment B was selected over treatment A and C on the basis of previous test data that showed good suppression with liner designs having 10% faceplate porosity. The selection of treatment D for forward thrust testing was based on the good suppression characteristics exhibited during reverse thrust tests.

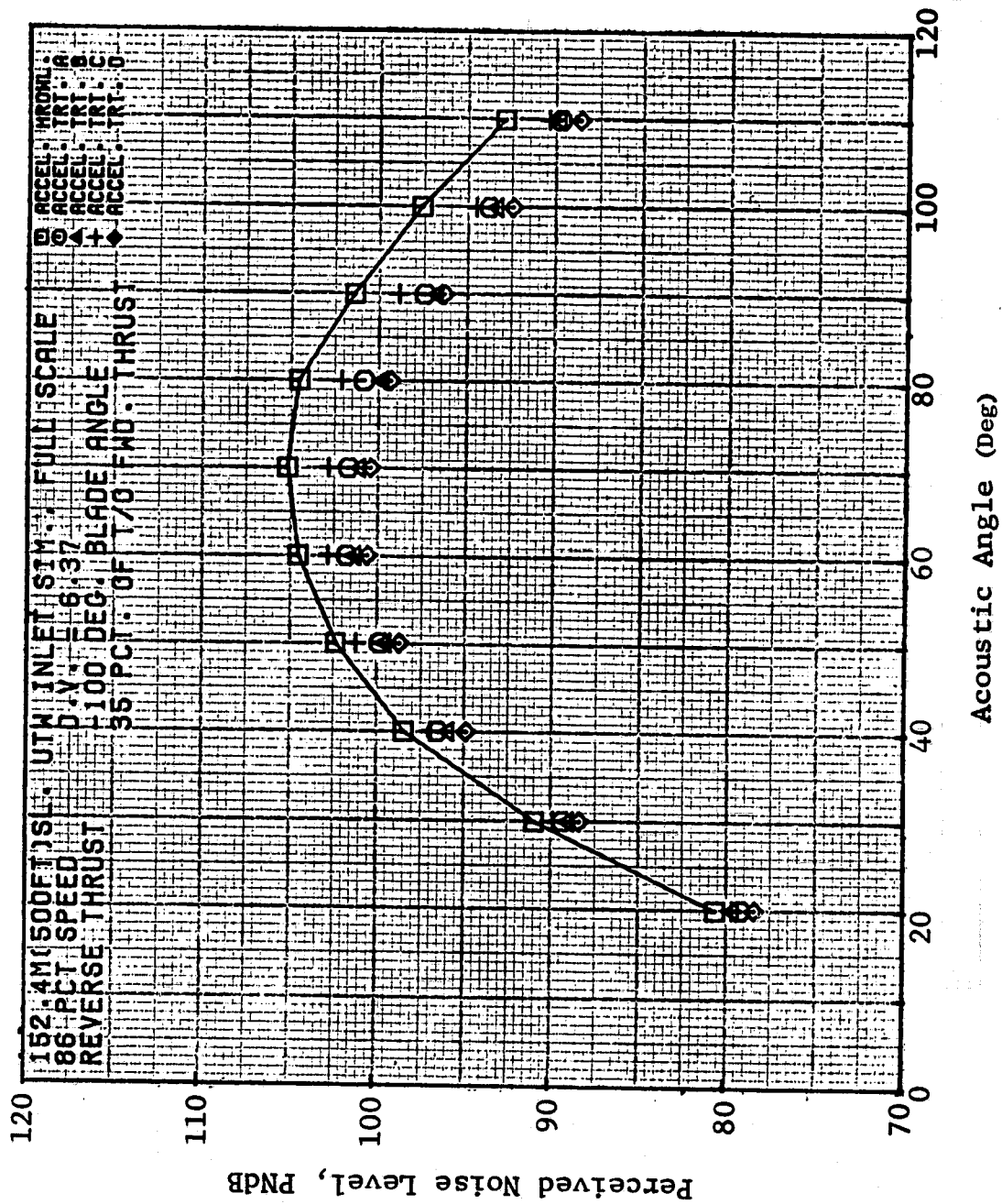


Figure 94. Reverse Thrust PNL Directivity, All Accelerating Inlets at 86% N_{FC}.

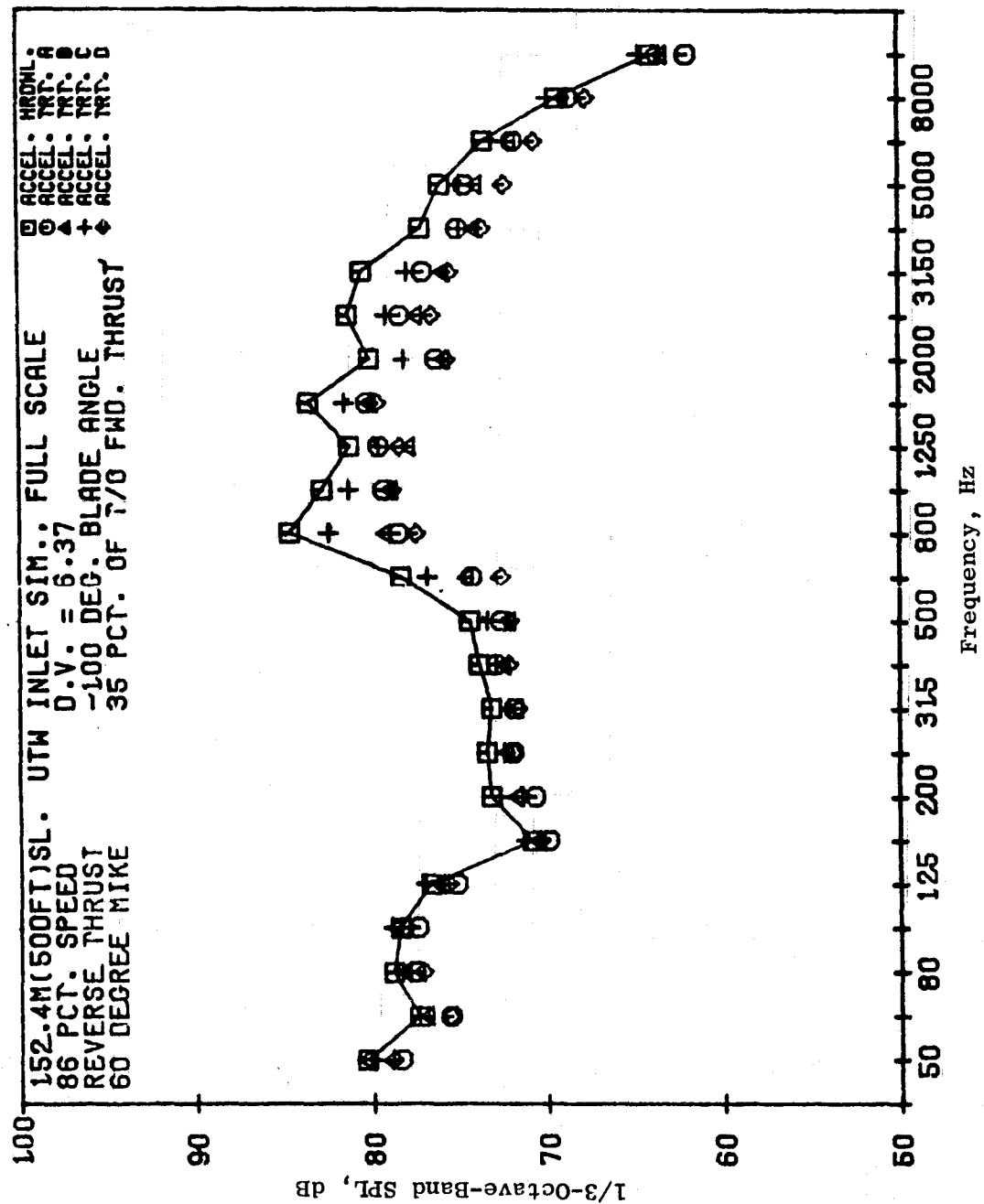


Figure 95. Reverse Thrust 1/3-OBSPL Spectra, All Accelerating Inlets at 86% N_{FC}, 60° to Inlet.

- 60° Acoustic Angle
- 152.4 m (500 ft) Sideline
- 0° Blade Angle
- Full-Scale Data
- ◇ Baseline Bellmouth Inlet Tests
- Average of Baseline Bellmouth Tests
- Accelerating Inlet - Hard Wall
- Accelerating Inlet - Treatment B
- △ Accelerating Inlet - Treatment D

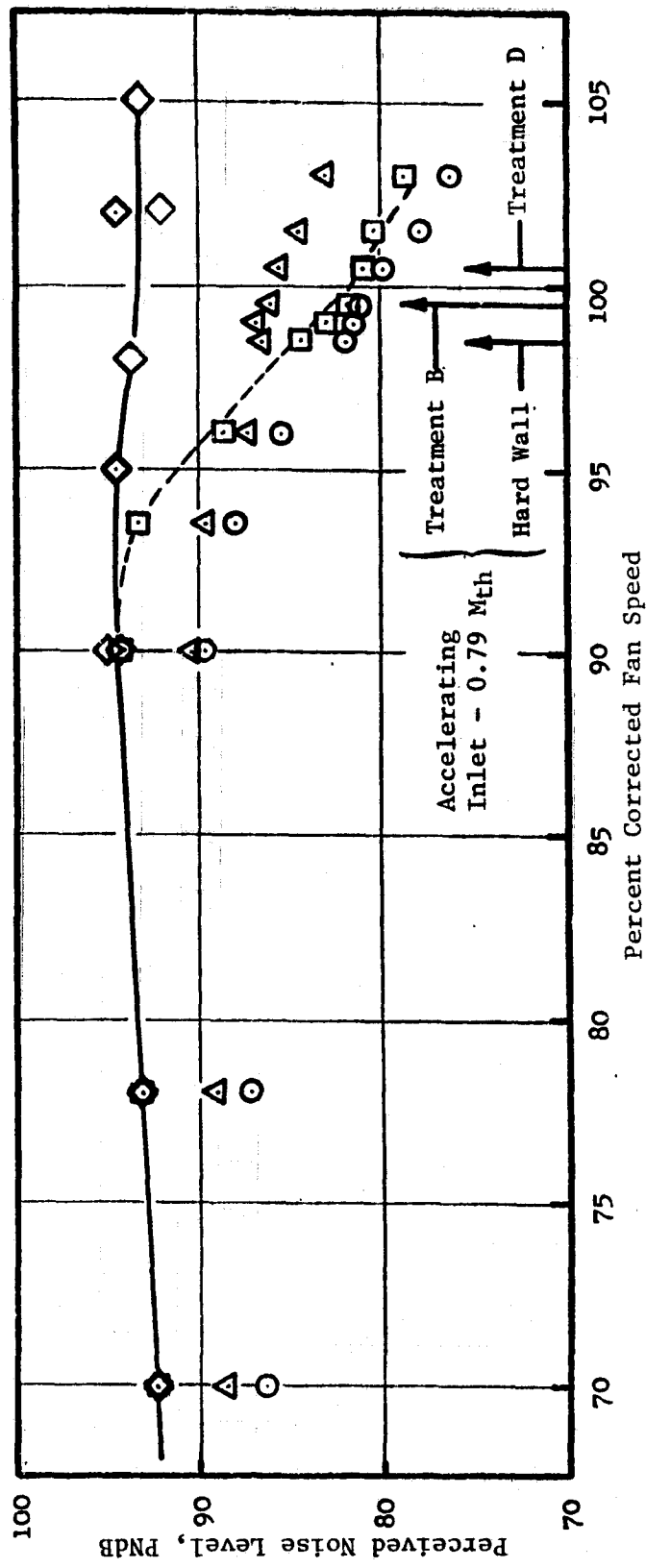


Figure 96. Forward Thrust PNL Vs. Percent Fan Speed, Baseline Bellmouth Inlet and Accelerating Inlets, Hard Wall, Treatments B and D.

The comparison of treatments D and B indicate that the latter shows increased suppression relative to the hard-wall accelerating inlet at the higher fan speeds, whereas treatment D shows an unexpected and surprising increased noise level relative to hard wall. For a throat Mach number of 0.79, inlet B treatment gives an additional 3-PNdB suppression. Comparing inlet D to the hard wall at 0.79 throat Mach number shows the surprising result that the noise level increased with the acoustic treatment by about 1.0 PNdB.

Treatment B also gives more suppression than inlet D at the lower fan speeds. The suppression measured at 70% N_{FC} for treatment B is 6 PNdB while for inlet D the suppression is approximately 4.0 PNdB relative to the hard-wall accelerating inlet.

The forward radiated fan noise levels in PNdB versus acoustic angle are given in Figure 97 for the accelerating inlet hard wall and fan treatments B and D. The data are for 0.79 throat Mach number on a 152.4-m (500-ft) sideline. Inlet treatment B gives the additional noise reduction as noted in Figure 96 at most of the forward acoustic angles. Treatment D shows a noise increase for angles 50° through 90°.

Spectral comparisons for a 0.79 throat Mach number are shown in Figure 98 for the accelerating inlet hard wall and inlet treatments B and D. The data are for an acoustic angle of 60° on a 152.4-m (500-ft) sideline. A noticeable reduction in noise level occurs for the treatment B configuration relative to the other inlets from the fan BPF (blade passing frequency) at 1,000 Hz and upward through 10,000 Hz. No particular trend in suppression is evident for frequencies below 1000 Hz for any of the configurations. The accelerating inlet and treatment D have approximately the same general noise level at all frequencies except at 1250 Hz, where for treatment D the level is about 6 dB higher. This increase undoubtedly contributes significantly to the 1.0-PNdB level increase measured on inlet D.

The inlet B configuration gives a total tone suppression level of approximately 20 dB at 1000 Hz; 8 dB of the 20-dB suppression are from the acoustic treatment. Comparatively, treatment D gives a total suppression of 15 dB of which only 3 dB result from the addition of acoustic treatment.

Figures 99 and 100 give the spectra discussed above for the 70° and 50° acoustic angles. A comparison of the data at the 50, 60 and 70° angles reveals that the suppression characteristics noted at the 60° angle are relatively independent of acoustic angle.

Figure 101 describes noise levels in PNdB at 70% speed for the hard-wall inlet and treatments B and D as a function of acoustic angle. The unsuppressed noise peaks at 60°. The suppressed noise level also peaks at 60°. However, the directivity pattern is somewhat flatter than for the unsuppressed noise levels. The suppressed level as a function of angle is rather constant for angles of 50° and is greater but decreases significantly for smaller angles.

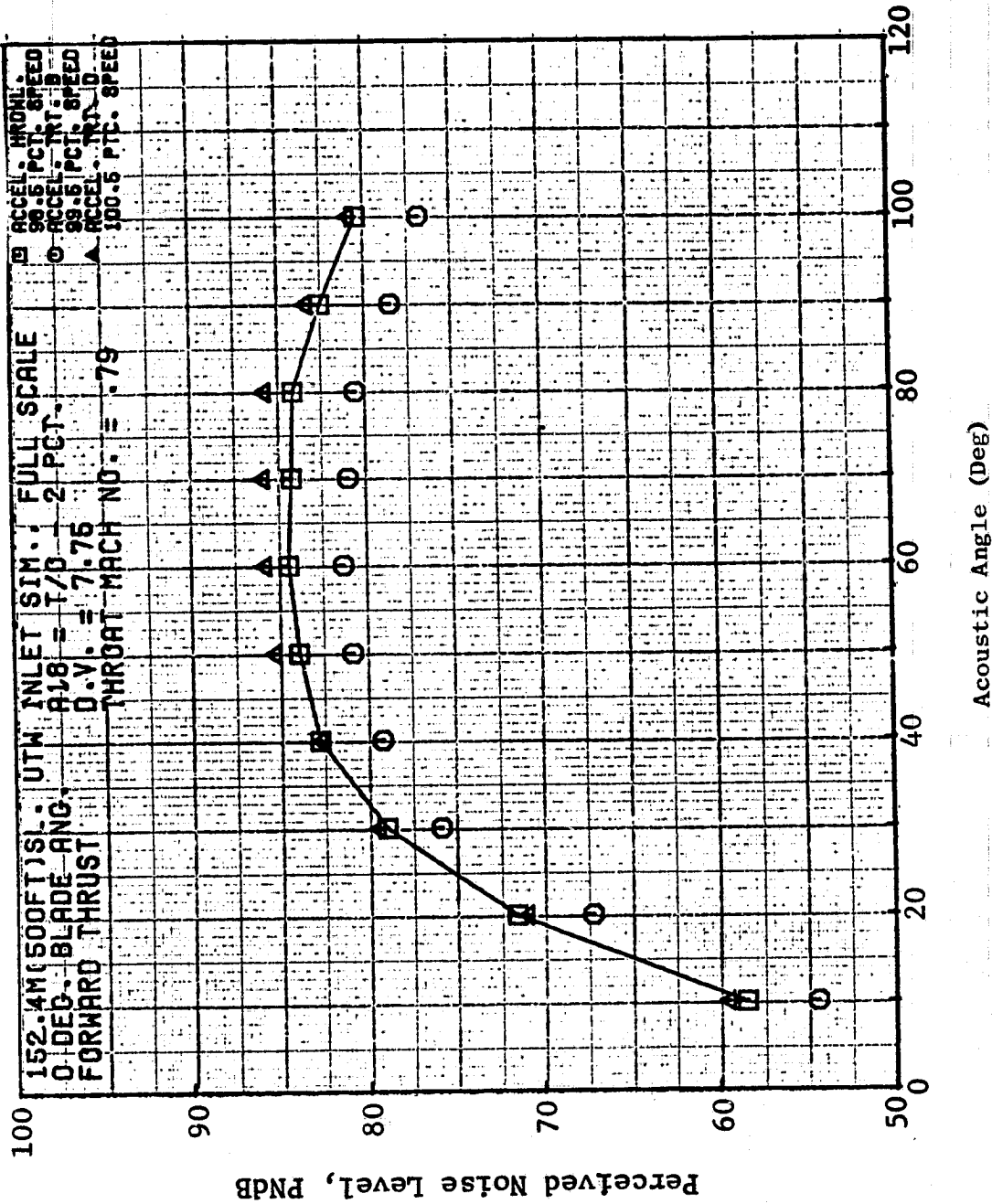


Figure 97. Forward Thrust PNL Directivity, Accelerating Inlet Hard Wall, Treatments B and D at 0.79 (Takeoff) Throat Mach No.

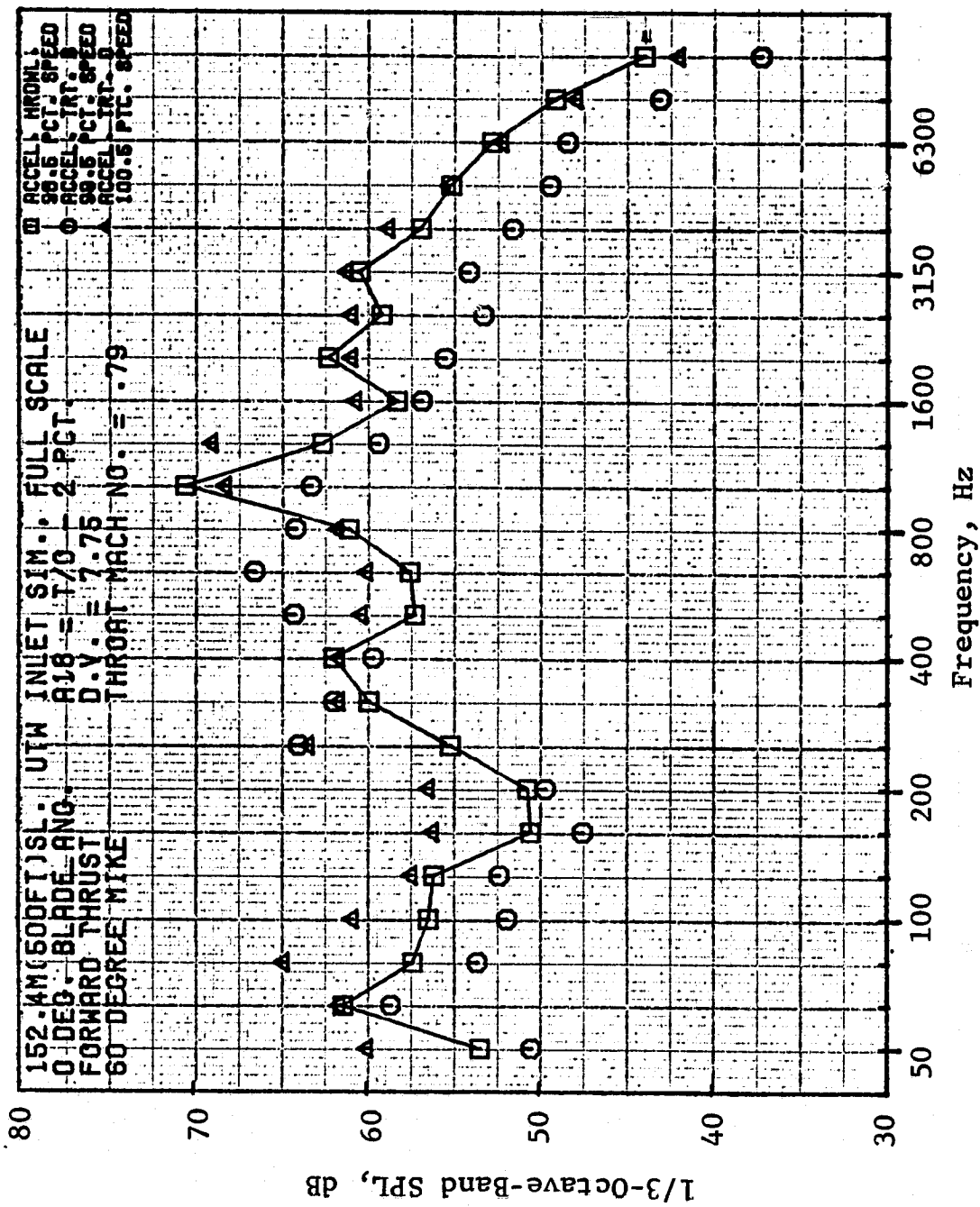


Figure 98. Forward Thrust 1/3-OBSPL Spectra, Accelerating Inlet Hard Wall, Treatments B and D at 0.79 (Takeoff) Throat Mach No., 60° to Inlet.

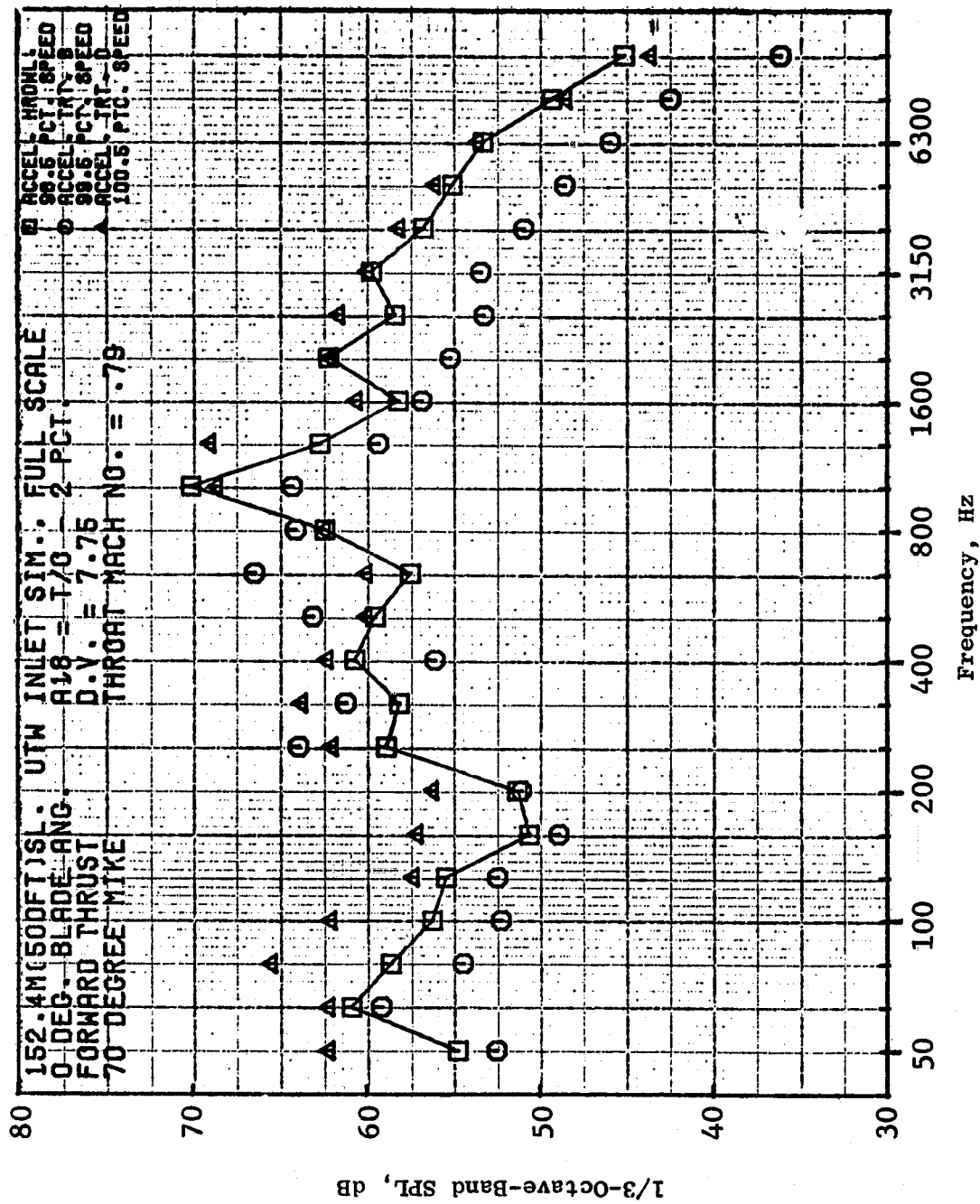


Figure 99. Forward Thrust 1/3-OBSPL Spectra, Accelerating Inlet Hard Wall, Treatments B and D at 0.79 (Takeoff) Throat Mach No., 70° to Inlet.

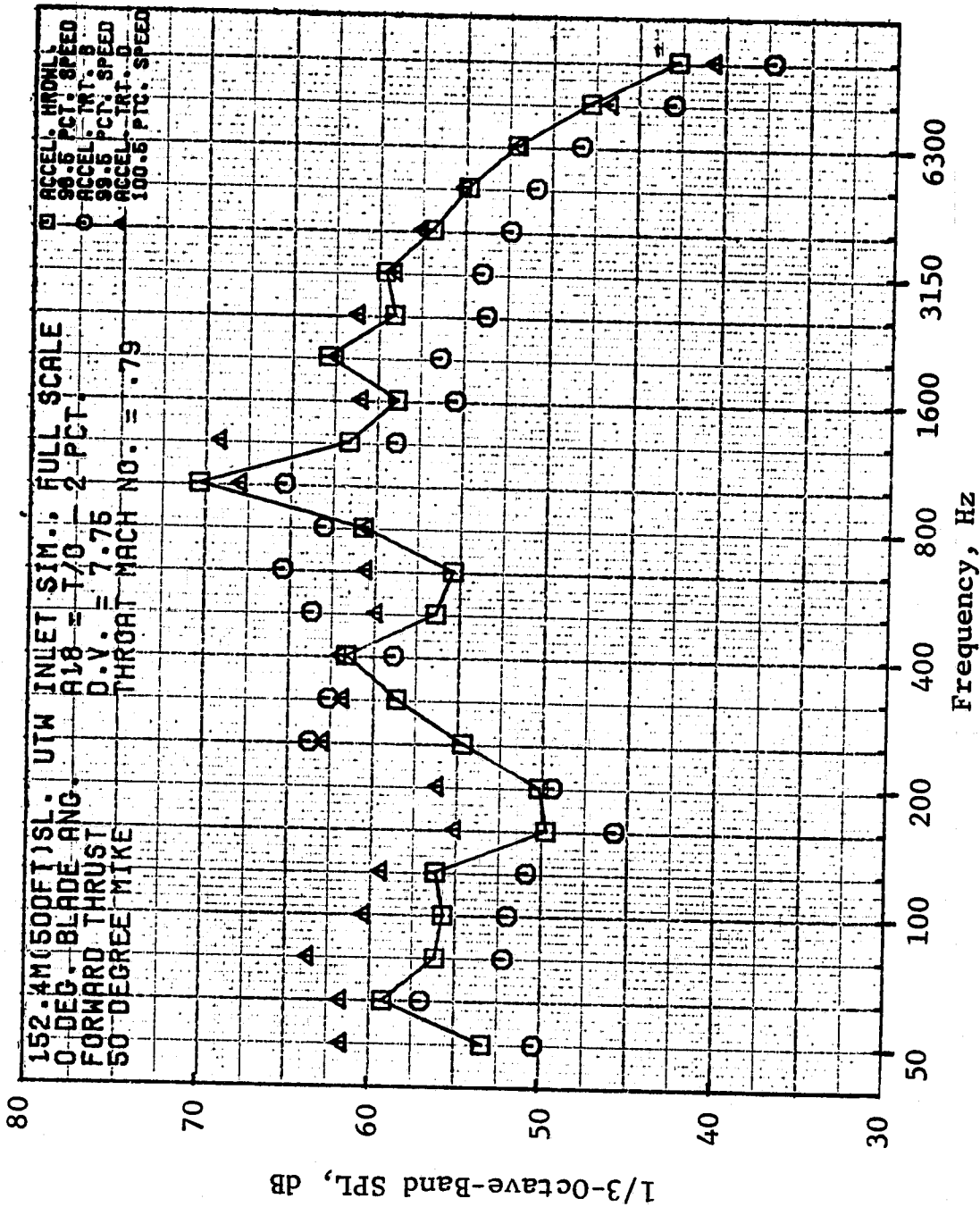


Figure 100. Forward Thrust 1/3-OBSPL Spectra, Accelerating Inlet Hard Wall, Treatments B and D at 0.79 (Takeoff) Throat Mach No., 50° to Inlet.

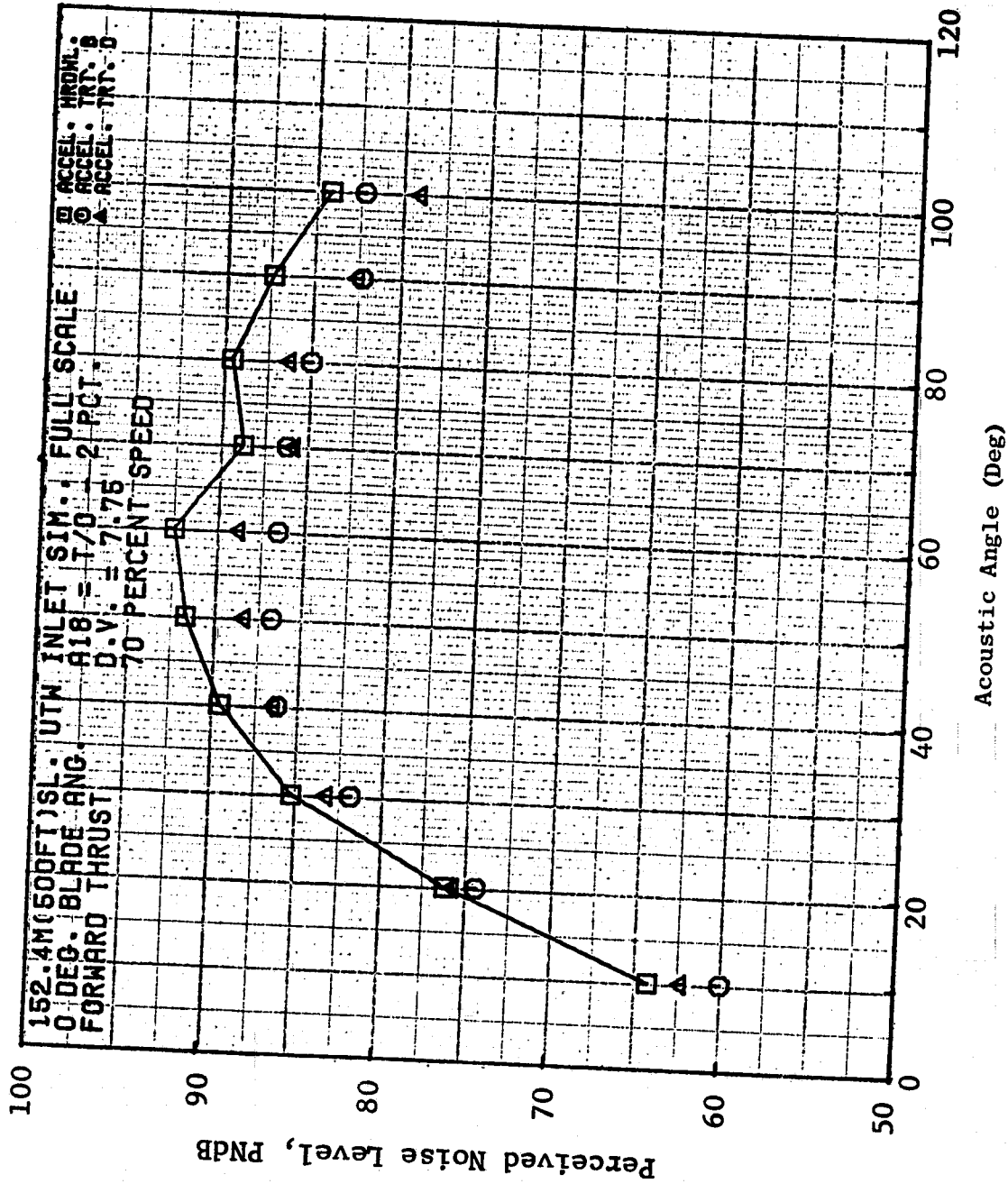


Figure 101. Forward Thrust PNL Directivity, Accelerating Inlet Hard Wall, Treatments B and D at 70% N_{FC}.

Figure 102 offers spectral comparisons for 70% speed at 60° to the inlet. At this low fan speed there is practically no suppression resulting from inlet Mach number. The spectral results for treatments B and D show that the treatment B configuration suppression levels at frequencies of 800 through 3150 Hz are significantly higher than for inlet D. Tone suppression level comparisons at 630, 1250, and 2500 Hz show treatment B giving from 2 to 5 dB greater suppression. The suppression is small at frequencies greater than 3150 Hz, with little difference seen for either treatment configuration.

6.1.3.2 Low Mach Inlet Suppression

Forward Thrust

The low Mach inlet unsuppressed and suppressed noise levels in terms of PNL on a 152.4-m (500-ft) sideline at 60° are shown in Figure 103 as a function of fan speed. At the lower fan speeds the treatment configuration utilizing the bulk absorber treatment yields the higher suppression. At the lowest fan speed (70%) the suppression approaches 8.5 PNdB, which is a 4-PndB improvement over the other two treatment configurations.

For fan speeds above 90%, bulk absorber suppression decreases with little difference between inlets A and B; total suppression for the bulk absorber design is near 4.5 PNdB. Total suppression for the resonator inlet approximates that measured at the lower fan speed points.

The hard-wall and suppressed inlet noise levels in PNL versus acoustic angle are given in Figure 104 for 70% fan speed. The hard-wall level peaks at 60°. Treatments A and C also peak at 60°; for treatment B, however, the peak is shifted to 50°. Suppression is fairly constant for 60° angles and greater, but decreases for lower acoustic angles. At 20°, inlets A and C show negligible suppression; inlet B gives about 4-PNdB reduction.

The hard-wall and treated spectra are shown in Figure 105. The treatment B suppressed level is lower than the other inlet levels at all 1/3-octave-band frequencies, and thus provides increased tone and broadband suppression relative to the resonator treatments. The maximum tone suppression occurs at the second fan harmonic where 12 dB is measured. Suppression at the fan fundamental tone is 8 dB.

In comparing resonator treatments for inlets A and C, the spectra indicate that inlet A with the 10% faceplate porosity yields much higher suppression at most of the 1/3-octave-band frequencies. The data at frequencies greater than 4000 Hz show no suppression for either inlet A or C and are not a function of acoustic angle.

Data for 98.5% fan speed are given in Figures 106 and 107. Figure 106 gives the hard-wall and suppressed inlet noise levels in PNdB versus acoustic angle. The hard-wall and suppressed noise directivity patterns peak at 60°. Suppression level versus acoustic angle is constant for all of the treated in-

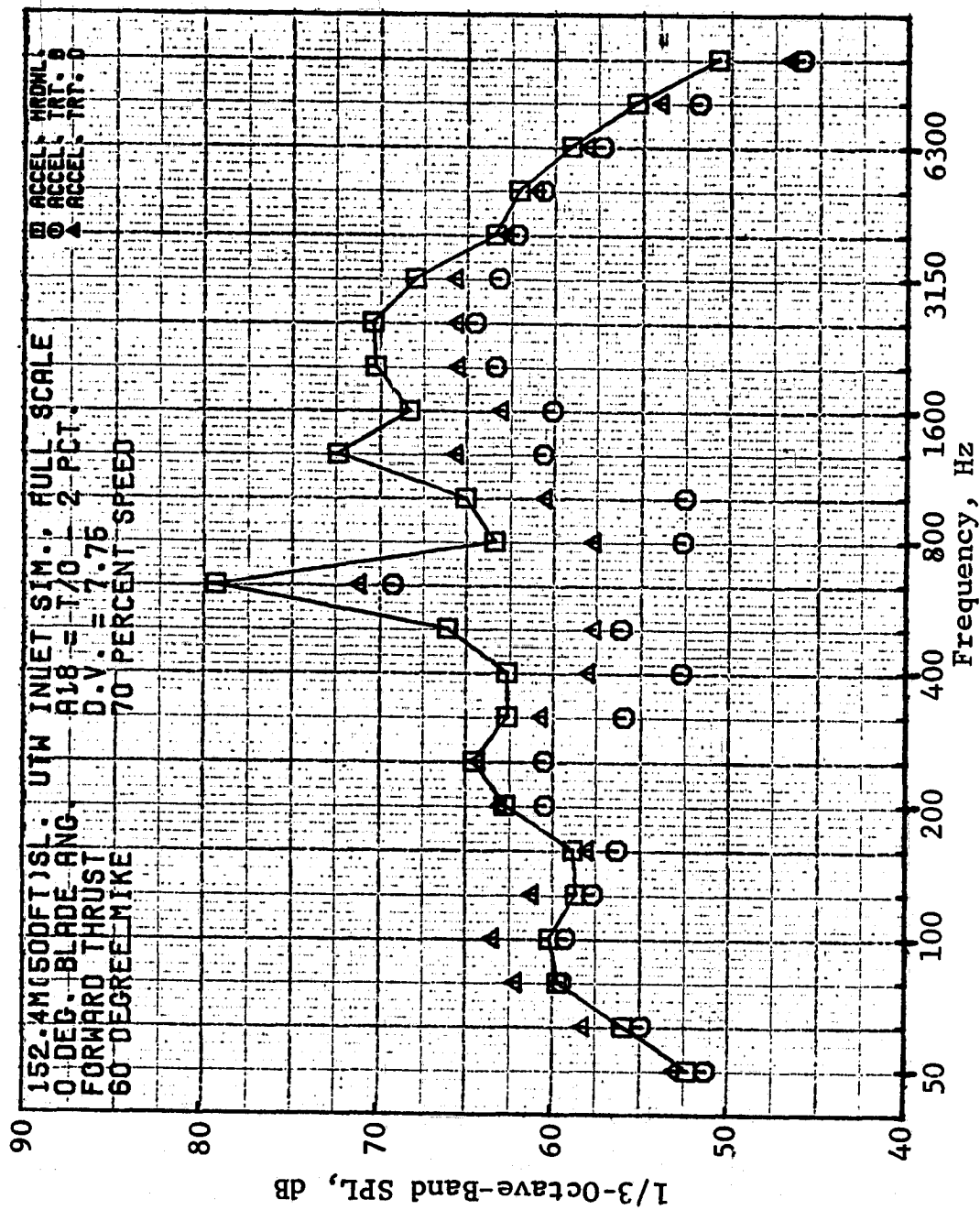


Figure 102. Forward Thrust 1/3-OBSPL Spectra, Accelerating Inlet Hard Wall, Treatments B and D at 70% N_{FC}, 60° to Inlet.

- 60° Acoustic Angle
- 152.4 m (500 ft) Sideline
- 0° Blade Angle
- Full-Scale Data

Low Mach Inlets

- Hardwall
- Treatment A
- △ Treatment B (Scottfelt)
- ⊕ Treatment C

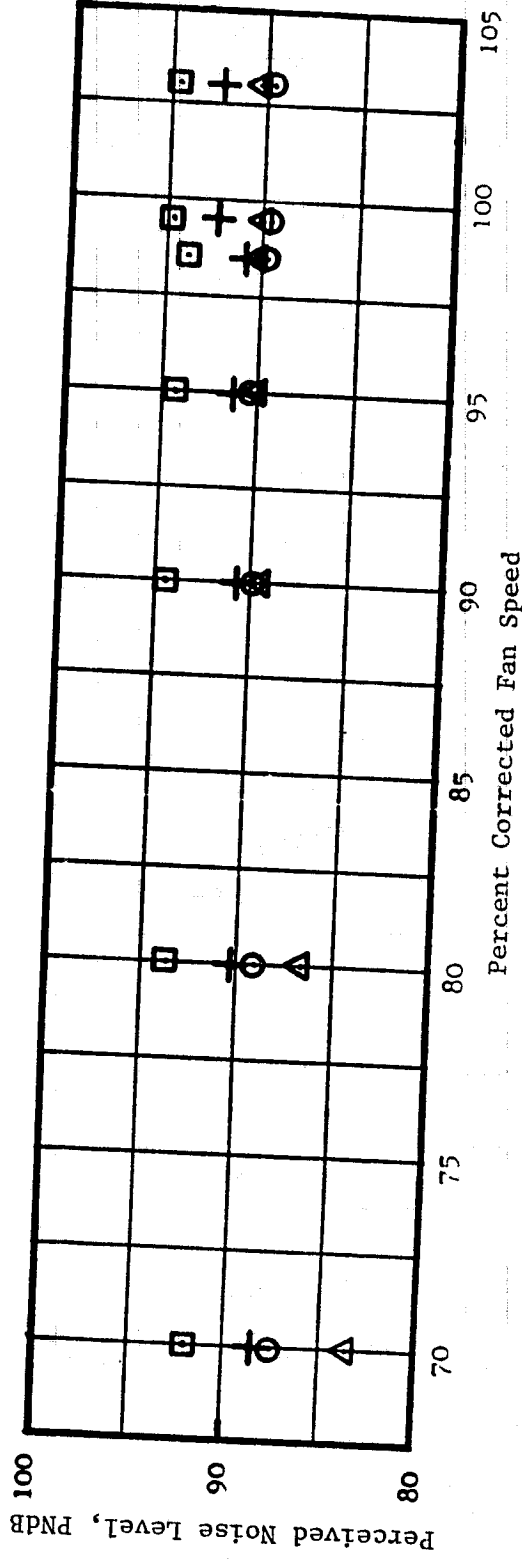


Figure 103. Forward Thrust PNL Vs. Percent Fan Speed, All Low Mach No. Inlets.

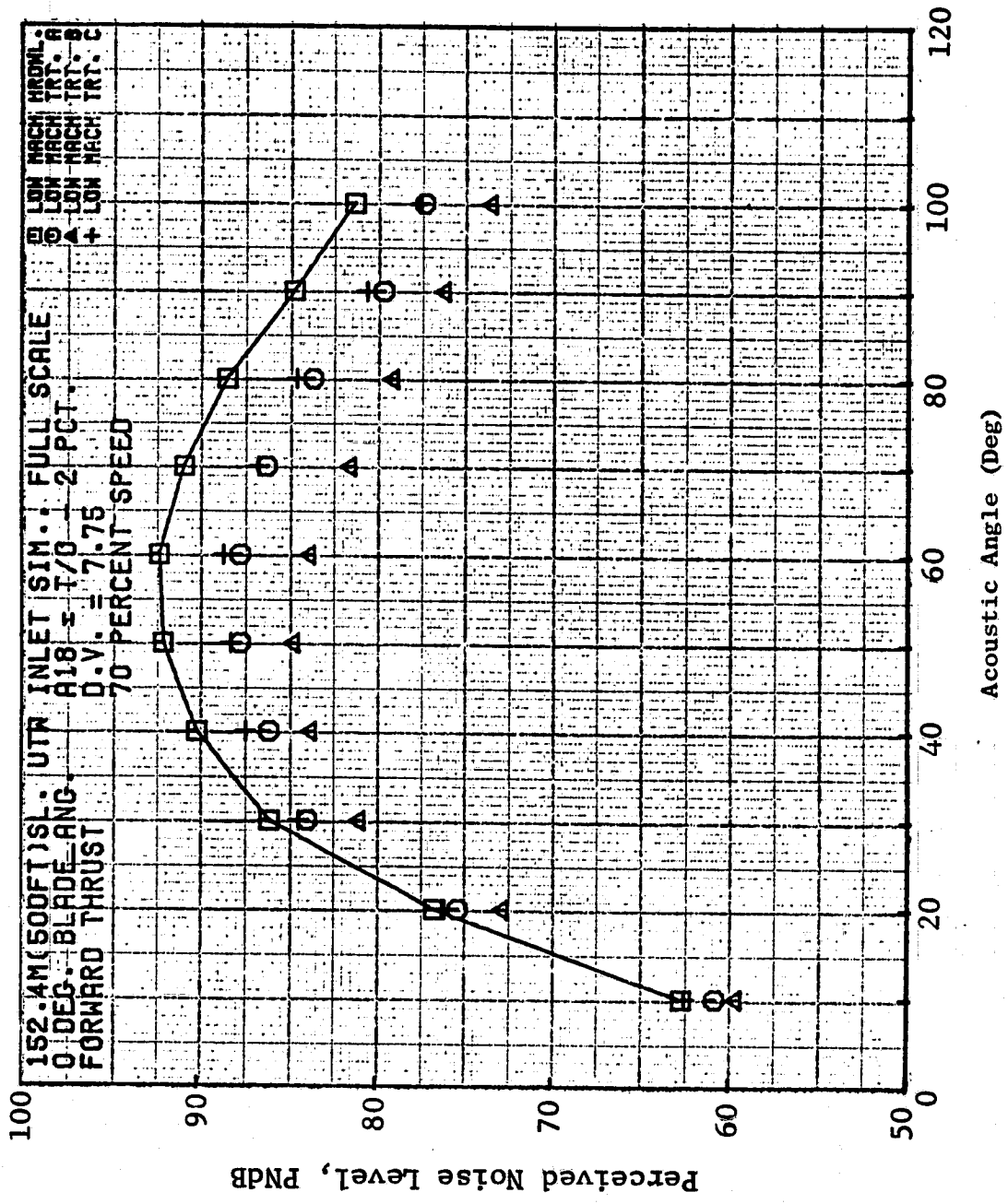


Figure 104. Fwd Thrust Directivity, All Low Mach No. Inlets at 70% NFC.

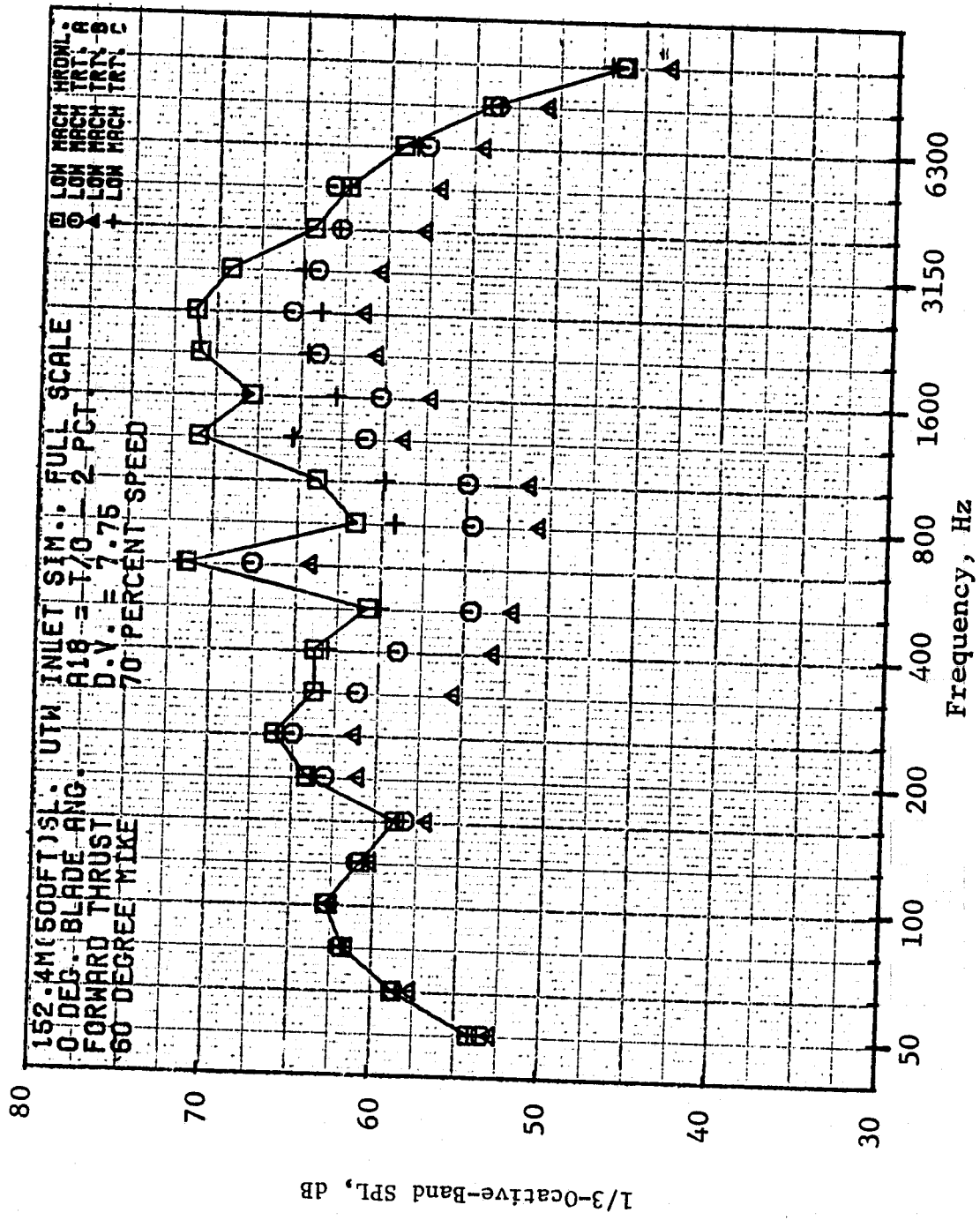


Figure 105. Forward Thrust 1/3-OBSPL Spectra, All Low Mach No. Inlets at 70% MFC, 60° to Inlet.

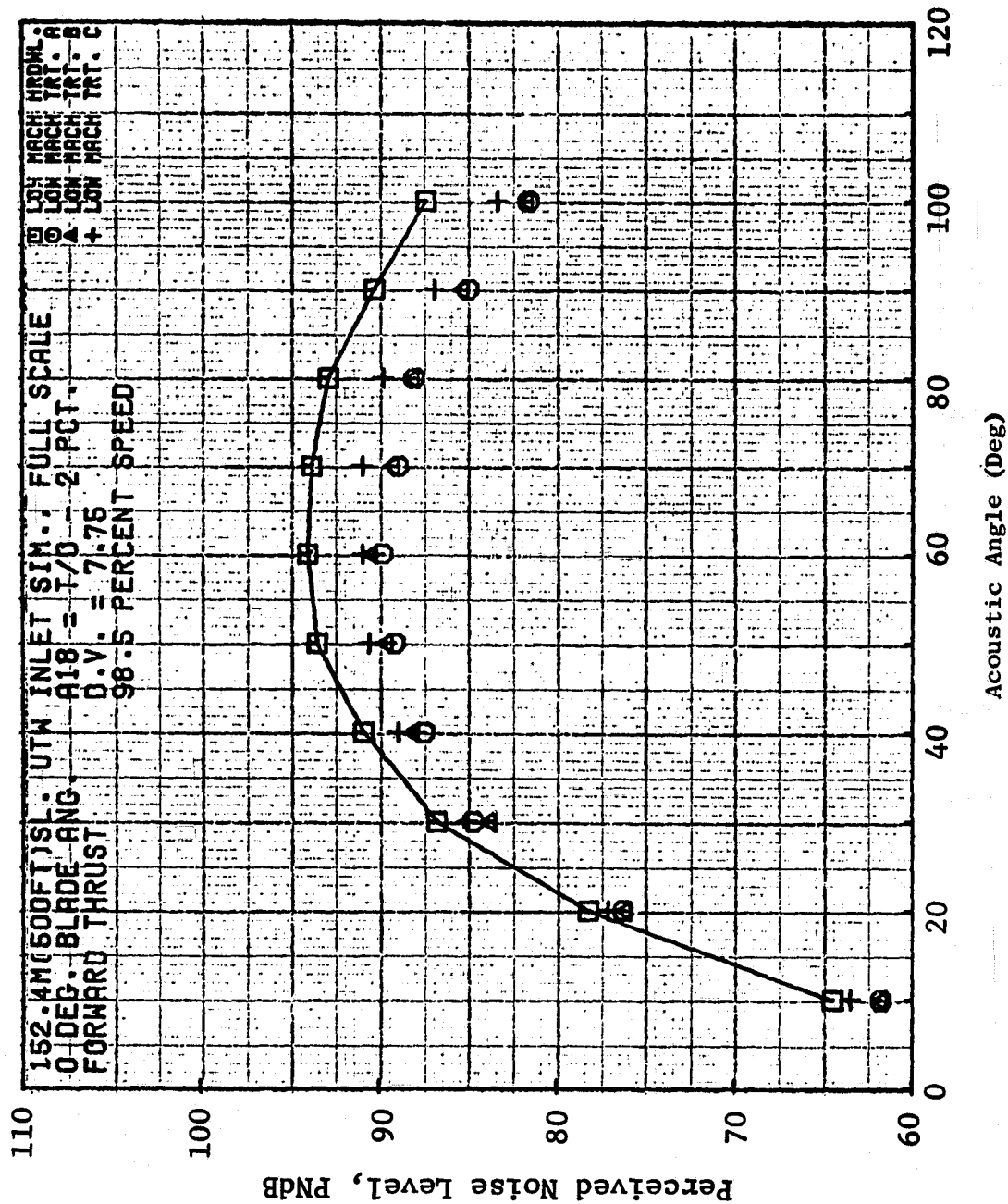


Figure 106. Forward Thrust PNL Directivity, All Low Mach No. Inlets at 98.5% N_{FC}.

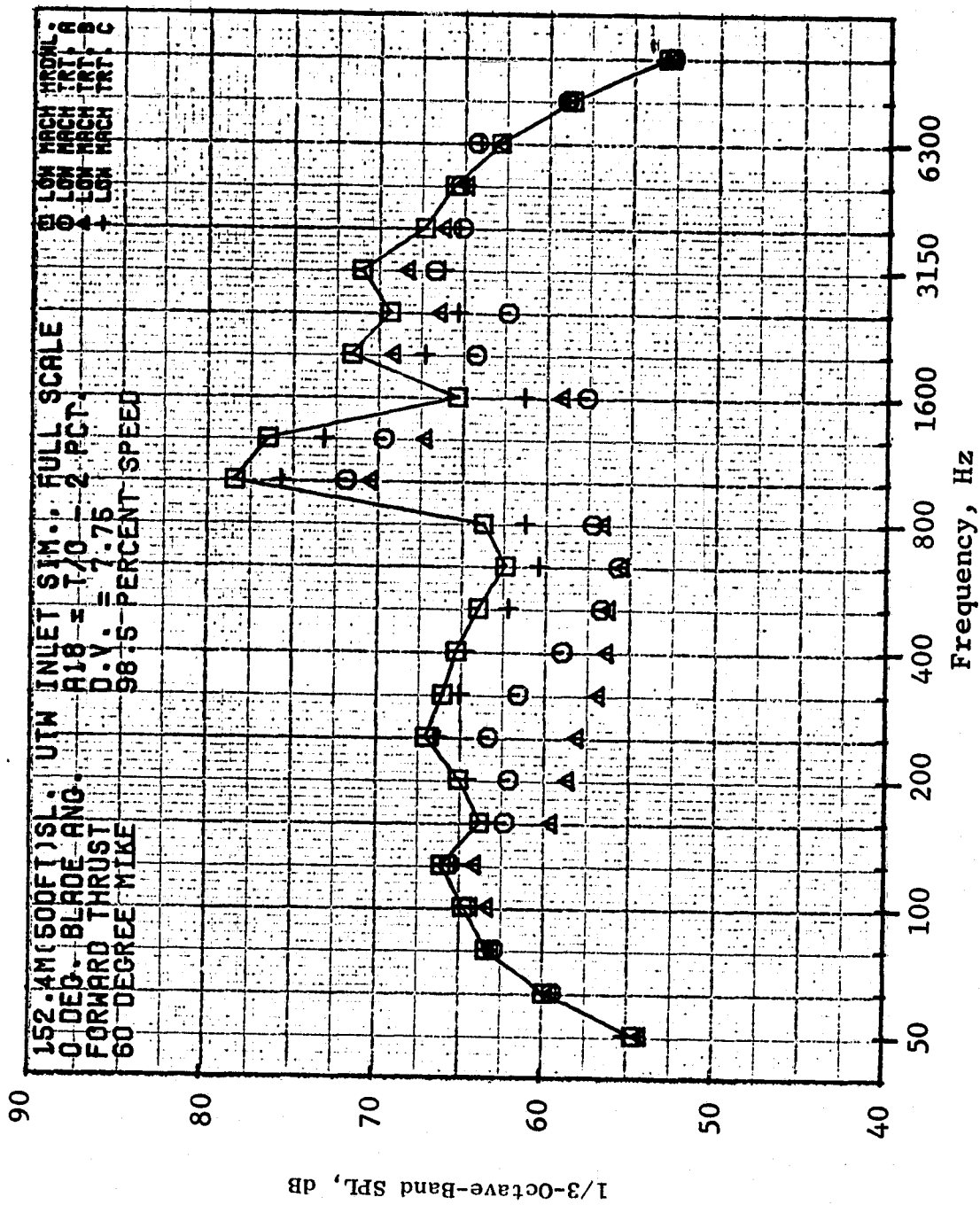


Figure 107. Forward Thrust 1/3-OBSPL Spectra, All Low Mach No. Inlets at 98.5% Nfc, 60° to Inlet.

lets at angles equal to or greater than 60° . However, for angles less than 60° , the suppression level decreases. This characteristic was also noted for the lower fan speed discussed above.

A spectral comparison for the hard-wall and treatment configurations for 98.5% fan speed is given in Figure 107 for an acoustic angle of 60° . The treatment B bulk absorber configuration gives higher levels of suppression at most 1/3-octave-band frequencies.

The suppression spectra for the three inlet configurations for the 70% and 98.5% fan speeds are presented in Figures 108 and 109. Comparison of these two sets of data shows the suppression decrease for the bulk absorber inlet in the higher frequencies at the higher fan speed. Also, the decrease in suppression for the low porosity inlet treatment, inlet C, is depicted for the increased fan speed. The inlet A configuration with 10% porosity offers approximately the same suppression at both low and high fan speeds.

The poor suppression performance for inlet configurations at a high fan speed of 98.5% is unexpected, especially for the bulk absorber treatment. Analysis of these data has not as yet produced an explanation of this suppression behavior.

Reverse Thrust

The unsuppressed and suppressed low Mach inlet noise levels in PNL for reverse thrust operation are delineated in Figure 110 for fan speeds 60% through 100%. These data are for a fan blade angle of -100° . The results show that treatment B (the bulk absorber configuration) gives higher suppression than the two resonator configurations at all fan speeds. The bulk absorber gives a suppression of ≈ 6 PNdB at 60% N_{FC} while the best resonator configuration delivers approximately 3.5 PNdB. The suppression level for the bulk absorber treatment decreases to about 4 PNdB as fan speed is increased to 100% N_{FC} . Suppression levels for the resonator inlets treatment are approximately constant as a function of fan speed; the best resonator, treatment A, provides close to 3.5-PNdB reduction at all fan speeds.

Resonator inlet Configurations A and C have different faceplate porosity values. The results show that treatment A, with a 10% porosity faceplate, yields significantly more suppression at all fan speeds than treatment C with a 3.6% porosity faceplate. The lower porosity has an overall acoustic resistance much higher than optimum for reverse thrust conditions.

Figure 111 gives the low Mach hard-wall and treated inlet PNL versus acoustic angle for 86% fan speed (35% of design forward thrust), the reverse thrust operating conditions. The peak unsuppressed and suppressed noise levels occur at 60° . The suppression versus acoustic angle is seen to increase by a small amount for angles greater than 60° but decreases at angles less than 60° .

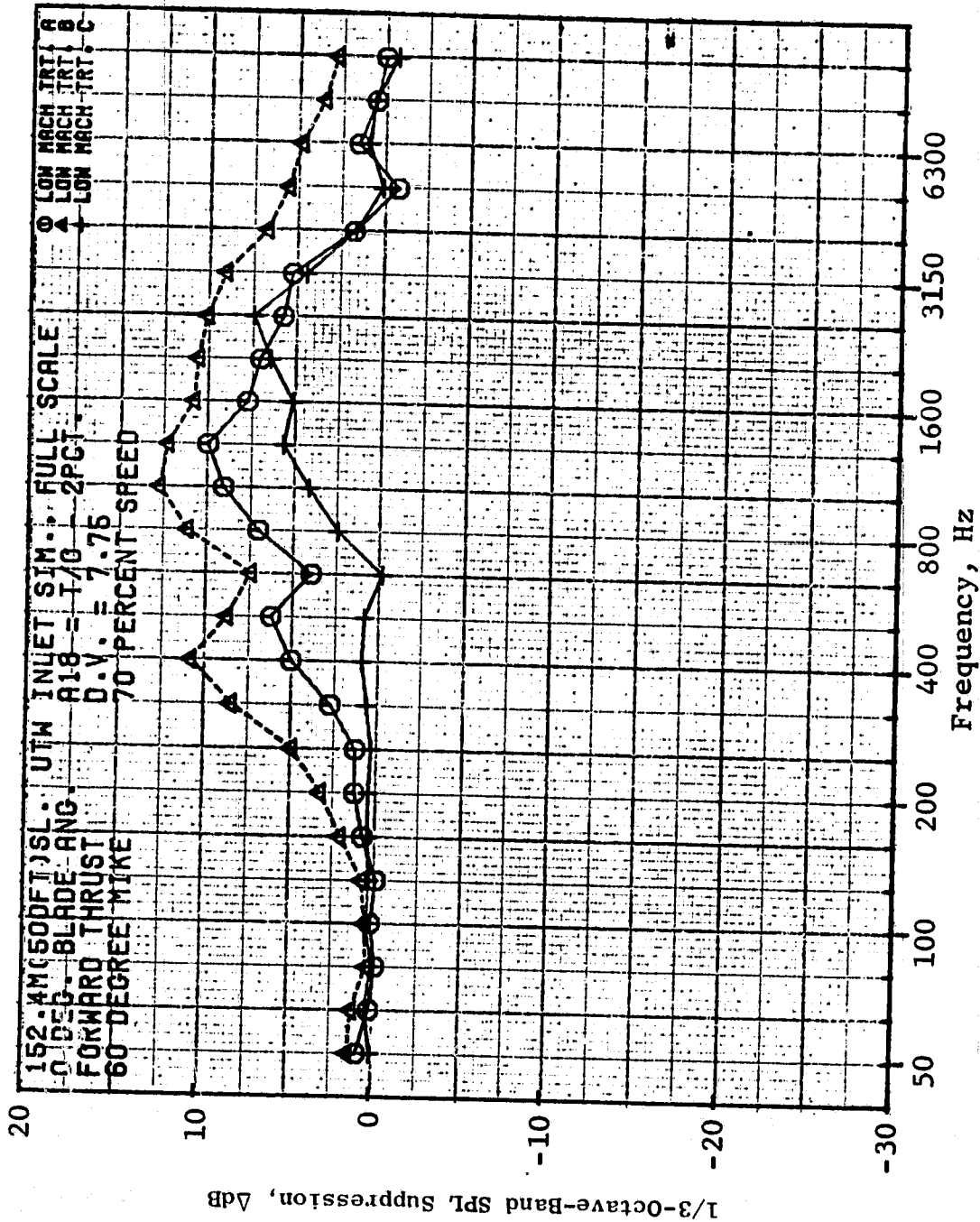


Figure 108. Forward Thrust 1/3-OBSPL Suppression Spectra, Low Mach No. Inlet Treatments A, B, and C at 70% N_{FC} , 60° to Inlet.

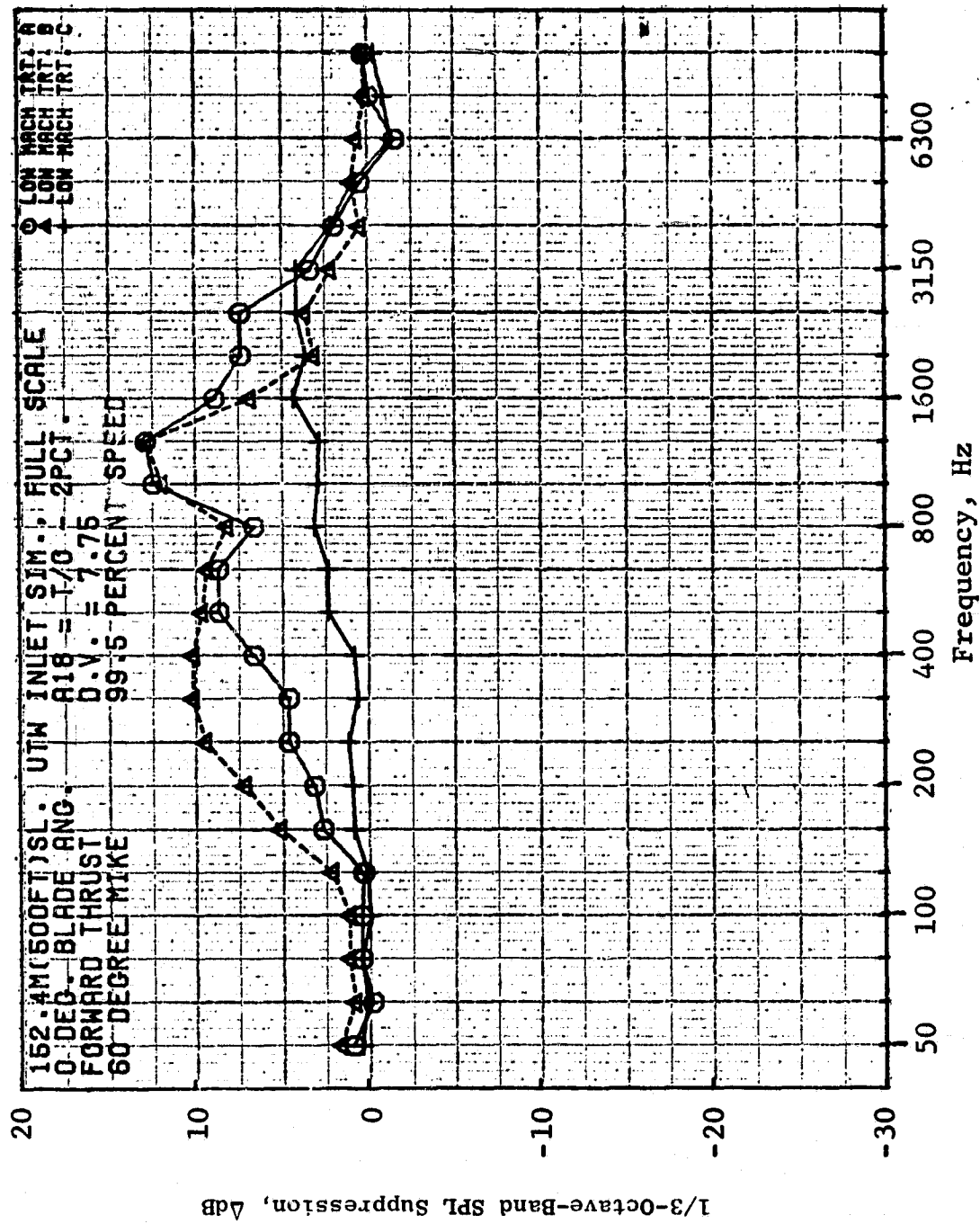


Figure 109. Forward Thrust 1/3-OBSPI. Suppression Spectra, Low Mach No. Inlet Treatments A, B, and C at 99.5% N_{FC} , 60° to Inlet.

- 60° Acoustic Angle
- 152.4 cm (500 ft) Sideline
- -100°, Blade Angle
- Full-Scale Data

- Low Mach Inlets
- Hard Wall
 - Treatment A
 - △ Treatment B (Scottfelt)
 - + Treatment C

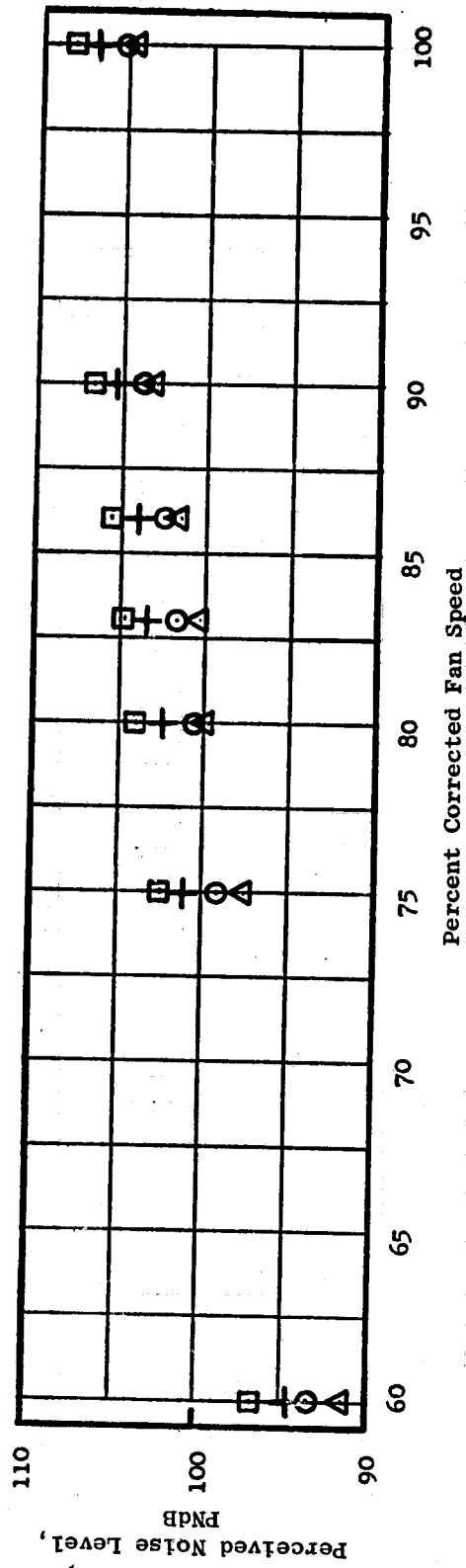


Figure 110. Reverse Thrust PNL Vs. Percent Fan Speed, All Low Mach Inlets.

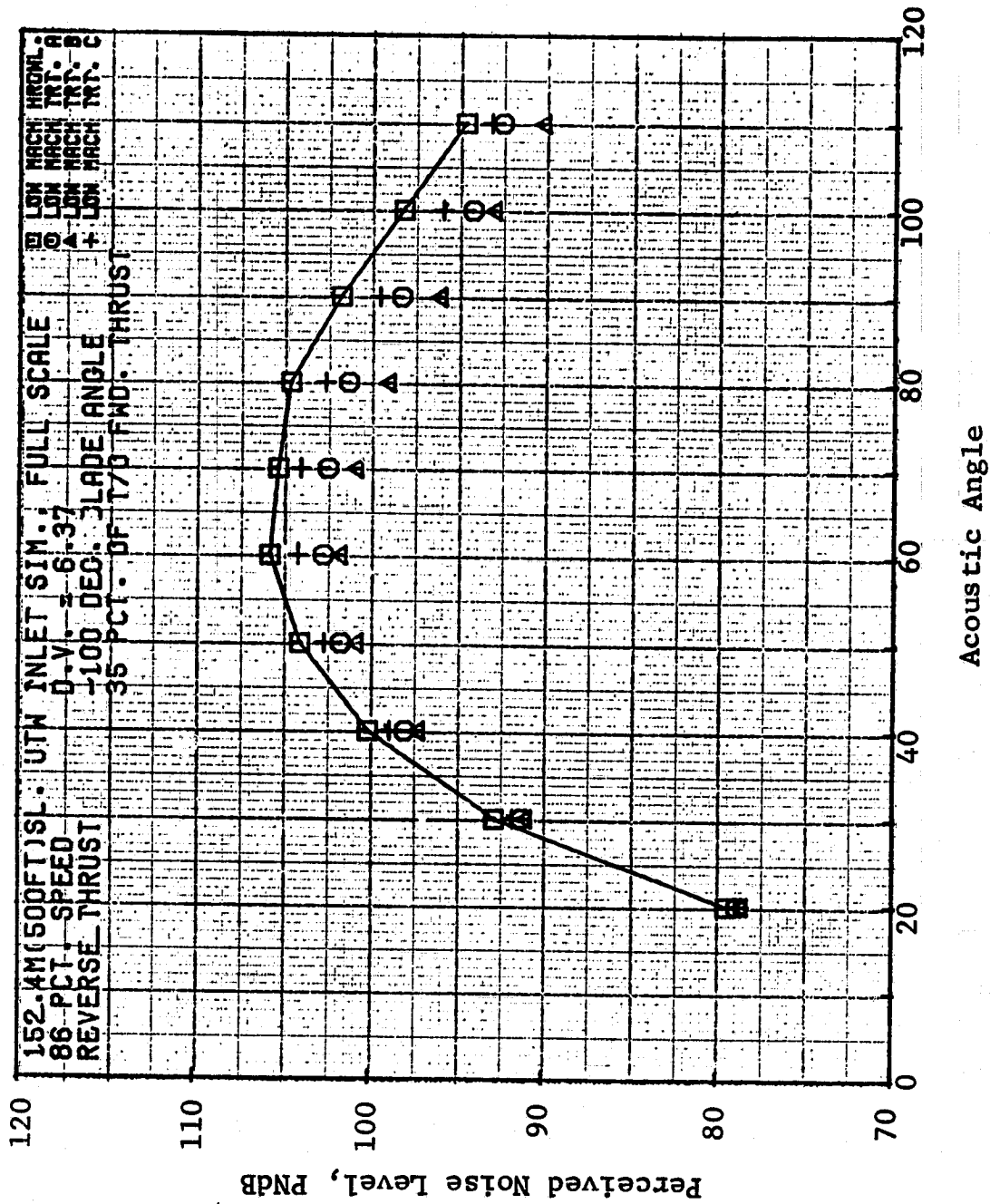


Figure 111. Reverse Thrust PNL Directivity, All Low Mach No. Inlets at 86% NFC.

The measured spectra for the hard-wall and treated inlet configurations are shown in Figure 112. The spectra are for 86% speed (35% thrust) at an acoustic angle of 60° on a 152.4-m (500-ft) sideline. The bulk absorber configuration suppressed levels are lower at all the 1/3-octave-band frequencies relative to the two resonator inlet configurations. Inlet A, which has 10% faceplate porosity, gives suppression over a wide range of frequencies; however, treatment C with 3.6% porosity gives little suppression at frequencies below 2000 Hz. Neither of these inlets provides suppression at the 8,000-Hz and 10,000-Hz 1/3-octave-band frequencies.

Figures 113 and 114 give spectral comparisons for the hard-wall and treated inlet configuration for fan speeds of 60% and 100% $N/\sqrt{\theta}$ at an acoustic angle of 60°. The 60% speed data show the same spectral characteristics as previously observed for 86% speed. But the results of 100% speed in Figure 114 show the bulk absorber inlet giving little greatly reduced suppression at the higher fan speed. Suppression in almost all the frequency bands, including tones, is significantly reduced in relation to suppression at 60% $N/\sqrt{\theta}$ fan speed.

The suppressed spectra for all inlet configurations indicate that to obtain additional suppression in terms of PNdB requires more high-frequency suppression. In fact, a large amount of the low-frequency suppression measured for each of the inlet tested contributed little toward reducing the PNL. A design with more of the treatment length tuned to the higher 1/3-octave-band frequencies would be desirable.

6.2 ENGINE BOILERPLATE INLET TREATMENT DESIGN AND SUPPRESSION ESTIMATES

The approach used to design the engine inlet treatment configuration was to design for the reverse thrust mode condition. This decision was based on results from the 50.8-cm (20-in.) scale model test results, which show the unsuppressed noise levels to be much higher than preliminary estimates, thus increasing the suppression level requirement for the reverse thrust condition.

6.2.1 Unsuppressed Spectra and Tuning Requirements

6.2.1.1 Unsuppressed Spectra

The UTW reverse thrust unsuppressed noise spectrum is shown in Figure 115. The data are at an acoustic angle of 60° on a 152.4-m (500-ft) sideline. The engine is operating at a thrust level of 35% of the thrust available at takeoff power with a blade angle of -100°. The data are shown scaled to the full-size UTW engine. A comparison is shown for the spectrum measured versus that predicted in preliminary design studies. The comparison was based on the NASA Q Fan 1 (Reference 13) data scaled to the UTW engine size. The measured levels are significantly higher than the predicted levels at frequencies greater than 1250 Hz. At frequencies below 1000 Hz the measured levels are significantly

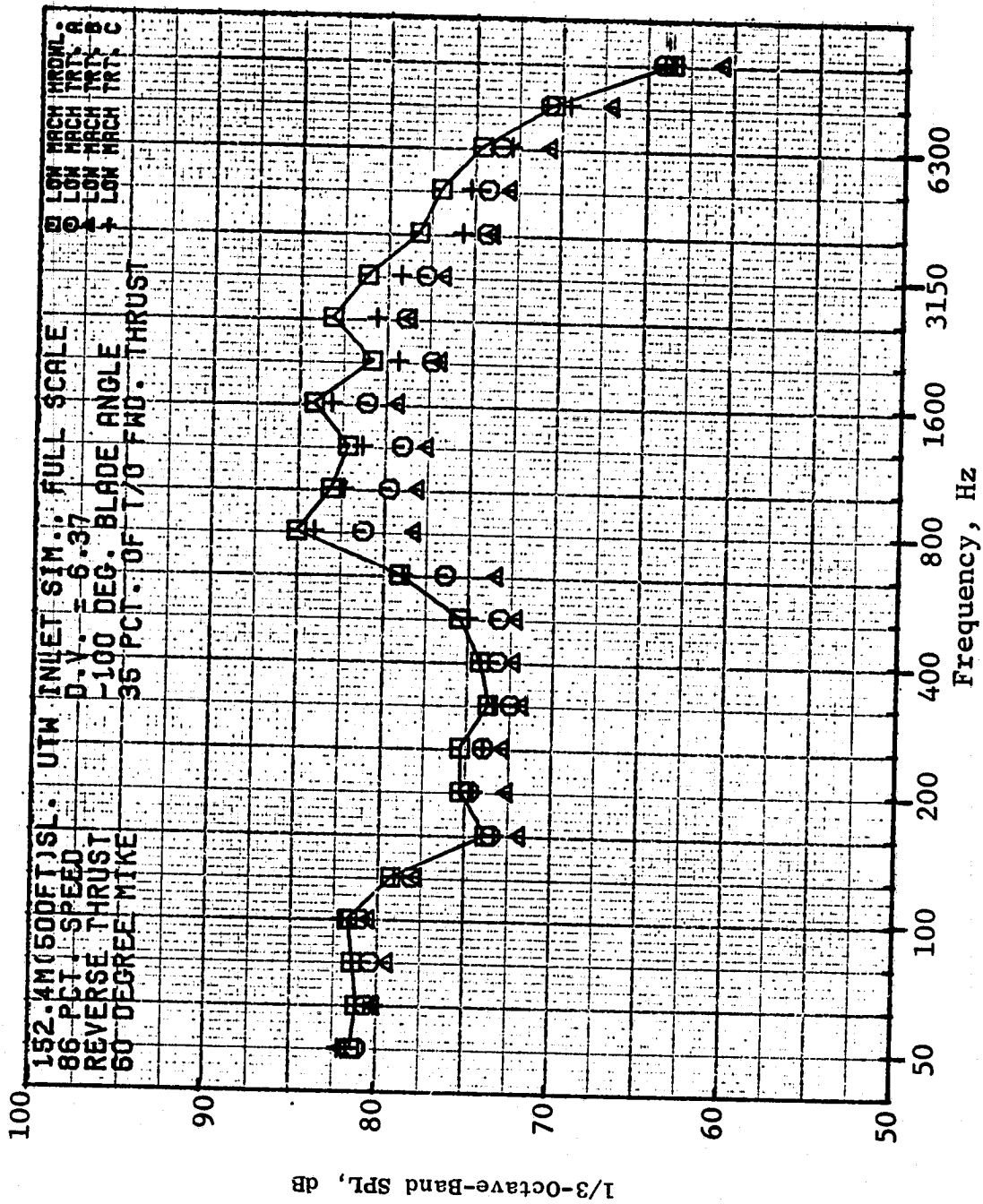


Figure 112. Reverse Thrust 1/3-OBSPL Spectra, All Low Mach No. Inlets at 86% N/C, 60° to Inlet.

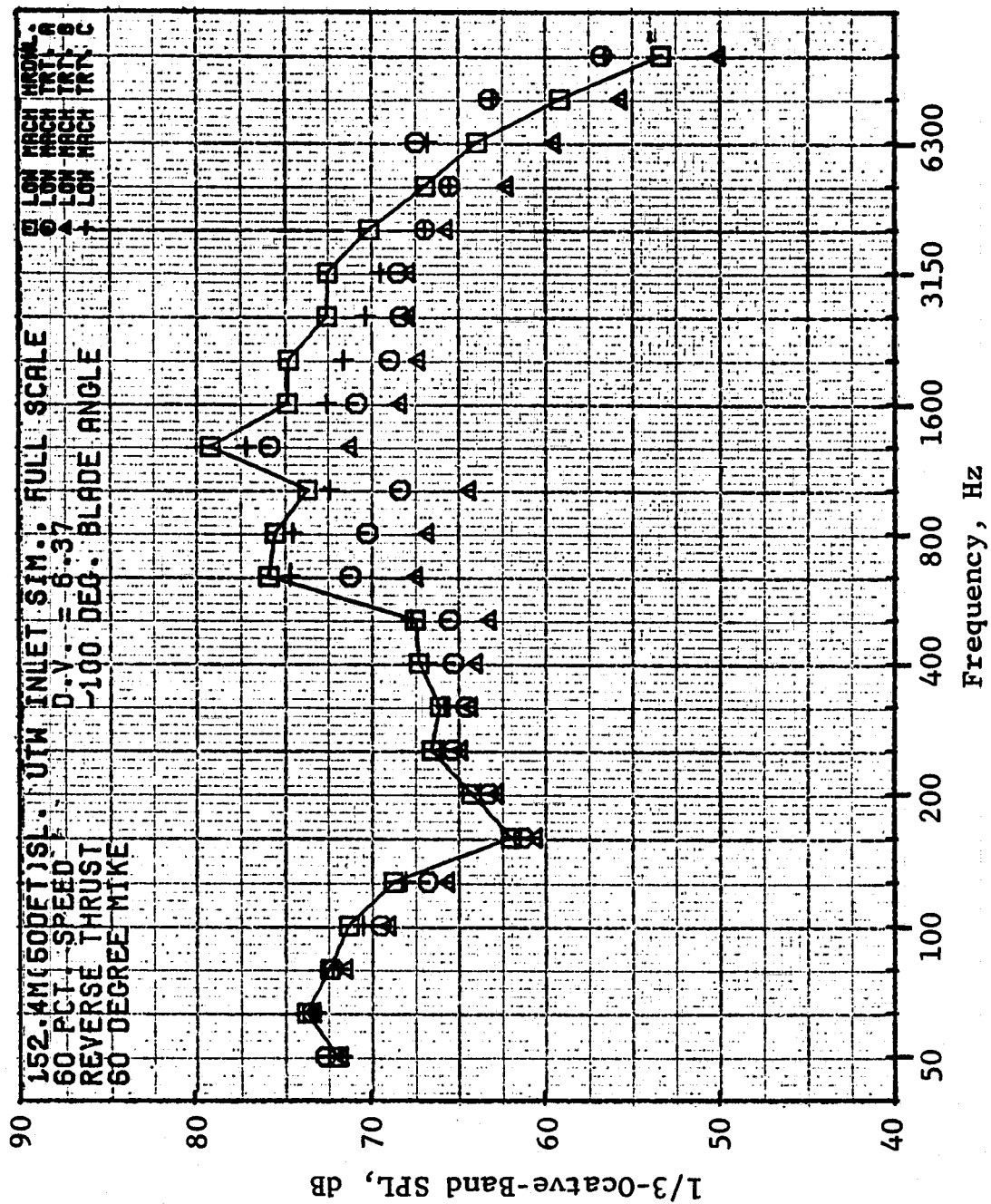


Figure 113. Reverse Thrust 1/3-OBSPL Spectra, All Low Mach No. Inlets at 60% N_{FC}, 60° to Inlet.

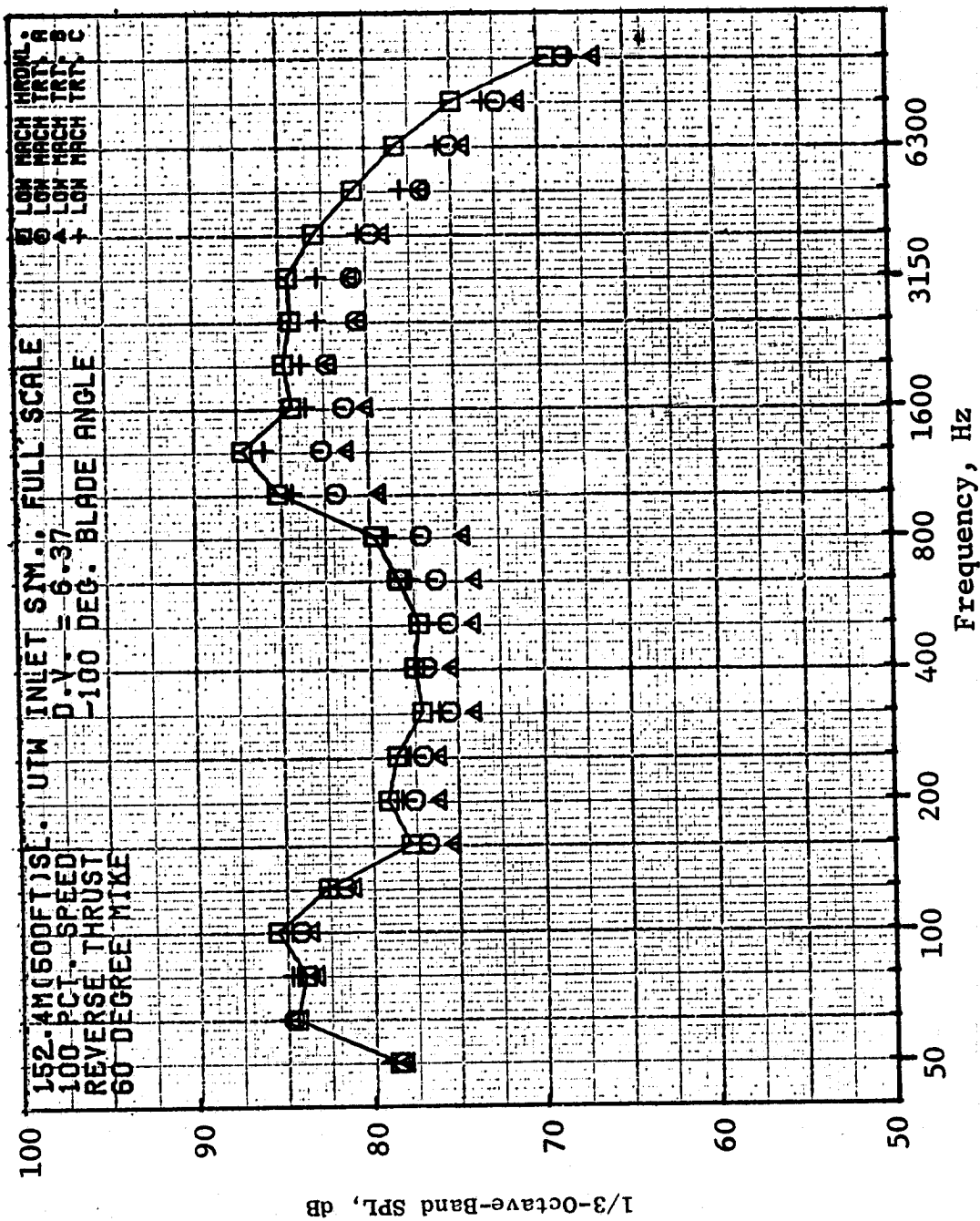


Figure 114. Reverse Thrust 1/3-OBSPL, All Low Mach Inlets at 100% Nfc, 60° to Inlet.

- 152.4 m (500 ft) Sideline at 60° Acoustic Angle
- 35% of Thrust Available at Takeoff Power
- -100° Blade Angle

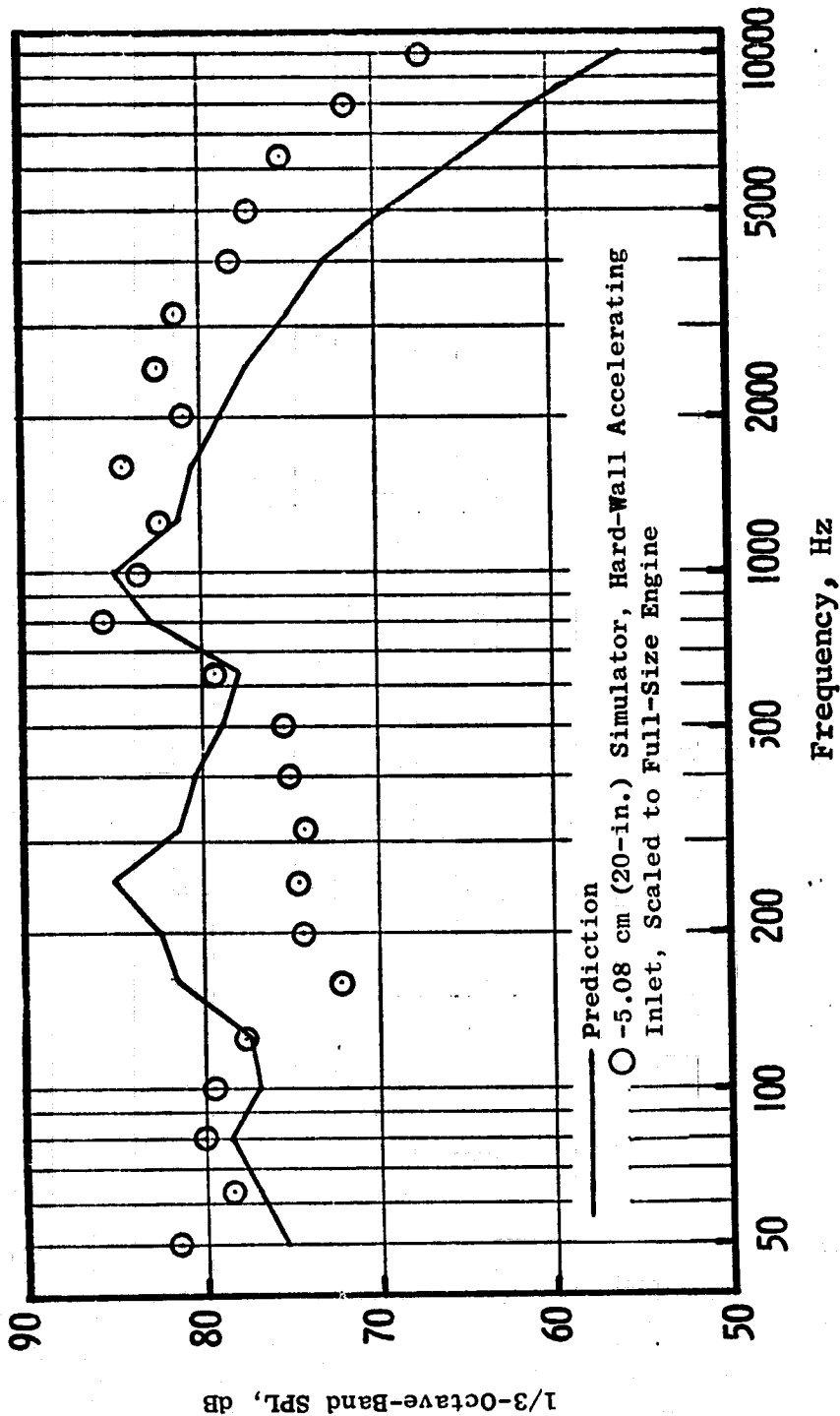


Figure 115. Unsuppressed UTW Reverse Thrust Fan Spectra, Prediction Vs. Measured.

lower than those predicted. However, the levels in the higher frequency range are the more significant since these levels contribute more greatly to the spectrum PNL. The PNL for the measured spectrum is approximately 5-PNdB higher than predicted.

The forward thrust unsuppressed spectrum is described in Figure 116. The data are for 100% thrust at 152.4-m (500-ft) sideline and 61-m (200-ft) altitude for an acoustic angle of 60° . Here the measured 50.8-cm (20-in.) scale model fan results are scaled to the UTW engine size and compared with the predicted level, which was based on previous fan data corrected to the UTW engine. The comparison of the predicted versus measured 1/3-octave-band SPL values shows very good agreement. The levels for the predicted versus measured in terms of PNdB also agree well.

The forward thrust unsuppressed spectra for the approach conditions are given in Figure 117. The data are for an engine thrust of 65% of that available at takeoff power with a $+5^\circ$ blade angle and are taken on a 152.4-m (500-ft) sideline at an altitude of 61-m (200-ft) and at an acoustic angle of 60° . The predicted spectrum is compared with the measured 50.8-cm (20-in.) scale model fan data scaled to the UTW engine size. This comparison shows very good agreement at the fan fundamental, at the second harmonic, and at all frequencies lower than the second harmonic. However, the measured levels at frequencies greater than the second harmonic are significantly higher than the predicted levels. This difference increases the unsuppressed noise level by about 5 PNdB. The cause for the increased noise in the higher frequencies has not been identified.

6.2.1.2 Noy-Weighted Spectra - Treatment Tuning Frequency Requirements

The measured reverse thrust spectra from the scale model fan configuration scaled to the UTW engine are given in Figure 118. The spectra include the unsuppressed Noy-weighted, suppressed, and suppressed Noy-weighted. These spectra show that in terms of PNdB the reverse thrust noise level is controlled at 2500 Hz-3150 Hz and that the suppressed spectrum Noy-weighted also peaks at 2500 Hz. This indicates that in order to improve the treatment design in terms of achieving more Δ PNdB, the treatment tuning should be at or near 2500 Hz.

The hard-wall accelerating inlet, 0.79 throat Mach number spectrum, is given in Figure 119. The data are for an acoustic angle of 60° on a 152.4-m (500-ft) sideline at an altitude of 61-m (200-ft). The noise reduction resulting from the high throat Mach number is in the spectrum as shown. Thus the Noy-weighted spectrum indicates where the acoustic treatment tuning would be the most effective in achieving suppression in terms of Δ PNdB. The Noy-weighted spectrum indicates that the level is controlled at frequencies of 1000, 2000, and 3150 Hz in terms of PNdB. Hence, a wide suppression bandwidth,

- 152.4 m (500 ft) Sideline
- 61 m (200 ft) Altitude At 60° Acoustic Angle
- 100% Thrust
- Baseline Bellmouth, 0° Blade Angle

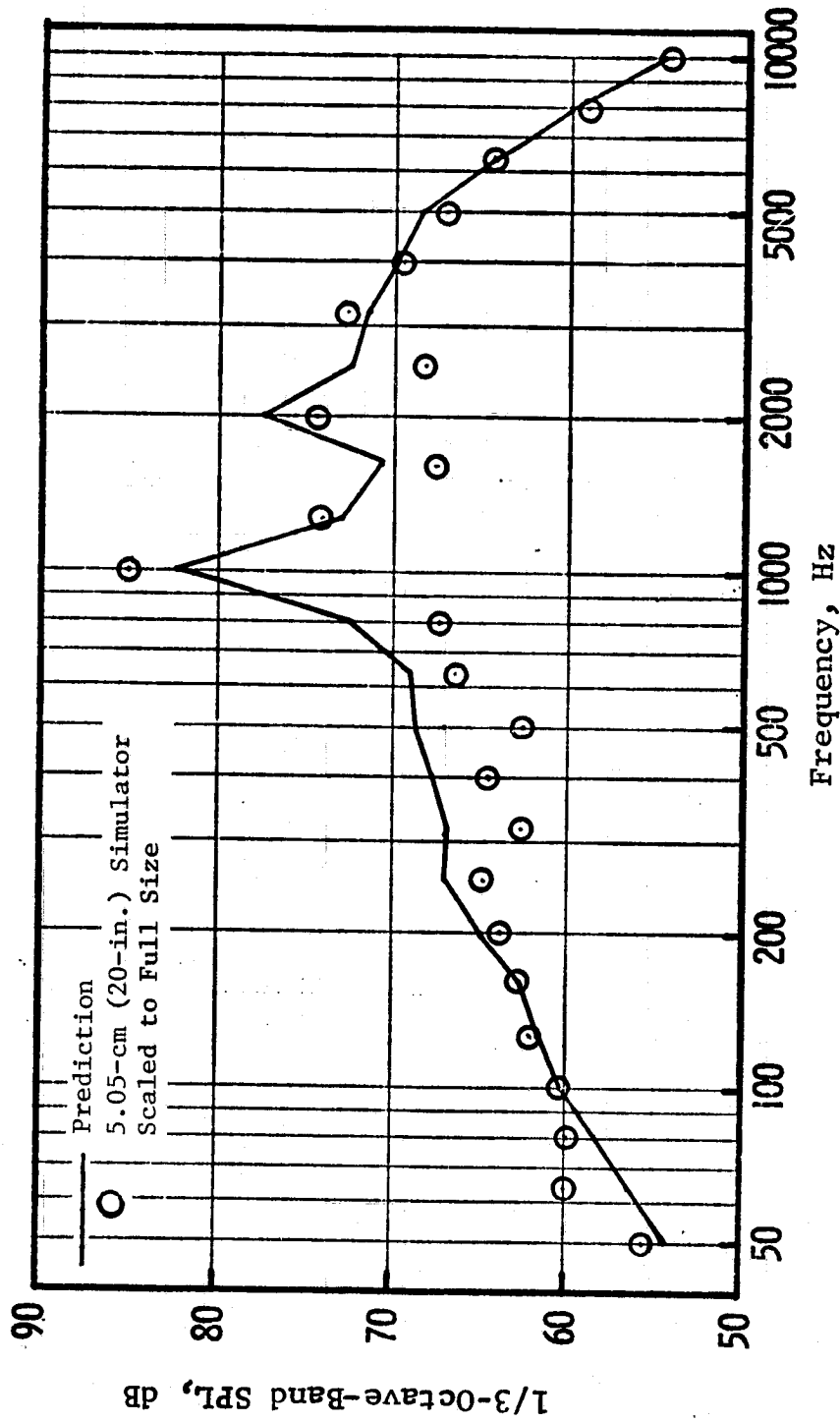


Figure 116. Unsuppressed UTW Takeoff Thrust Fan Spectra, Prediction Vs. Measured.

- 152.4 m (500 ft) Sideline
- 61 m (200 ft) Altitude At 60° Acoustic Angle
- 65% of Thrust Available at Takeoff Power
- Baseline Bellmouth, 5° Blade Angle

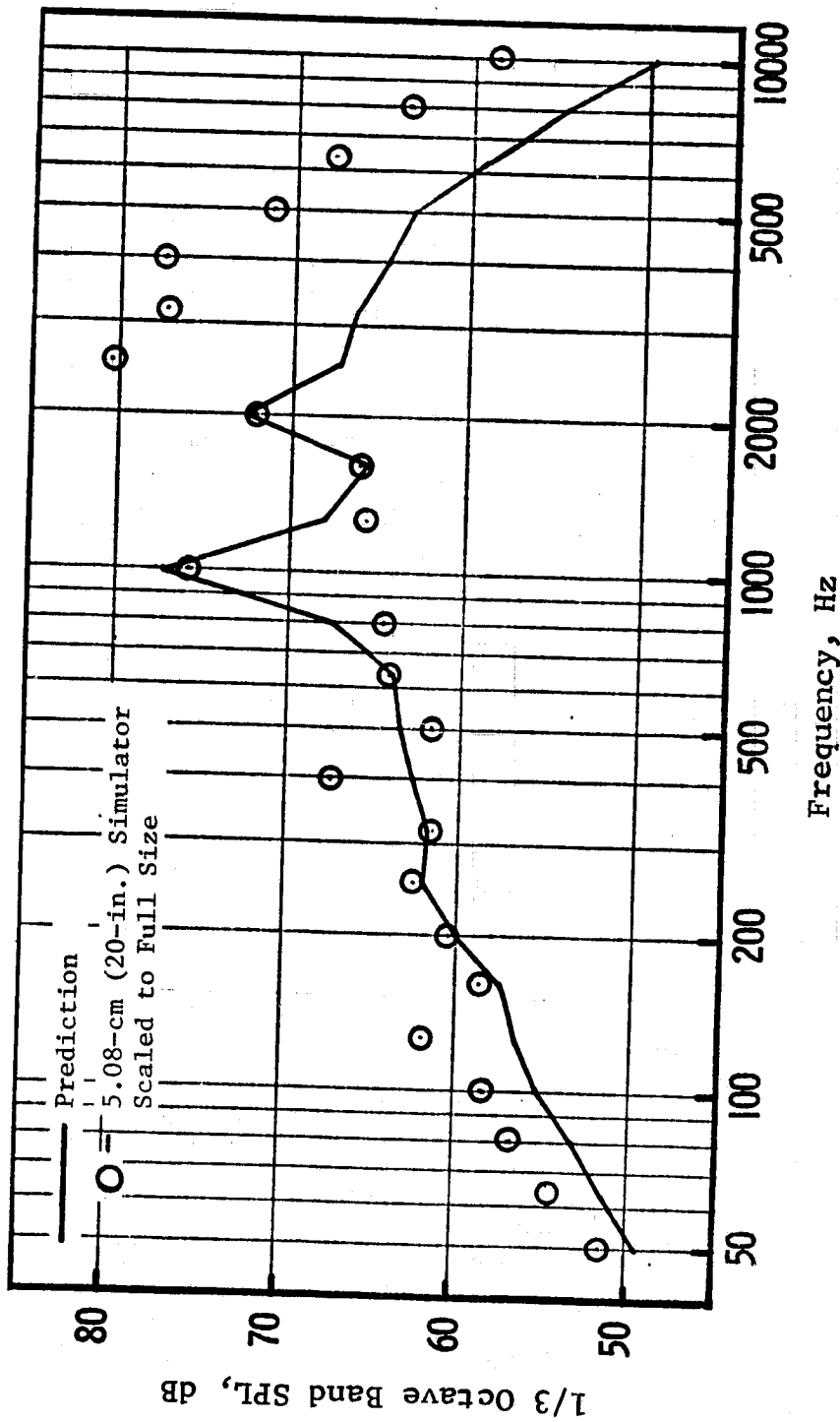


Figure 117. Unsuppressed UTW Approach Thrust Fan Spectra, Prediction Vs. Measured.

- Reverse Thrust 35% F_n - 86% N/θ
- 100° Blade Angle
- 152.4 m (500 ft) Sideline, Full-Scale Data
- 60° Acoustic Angle

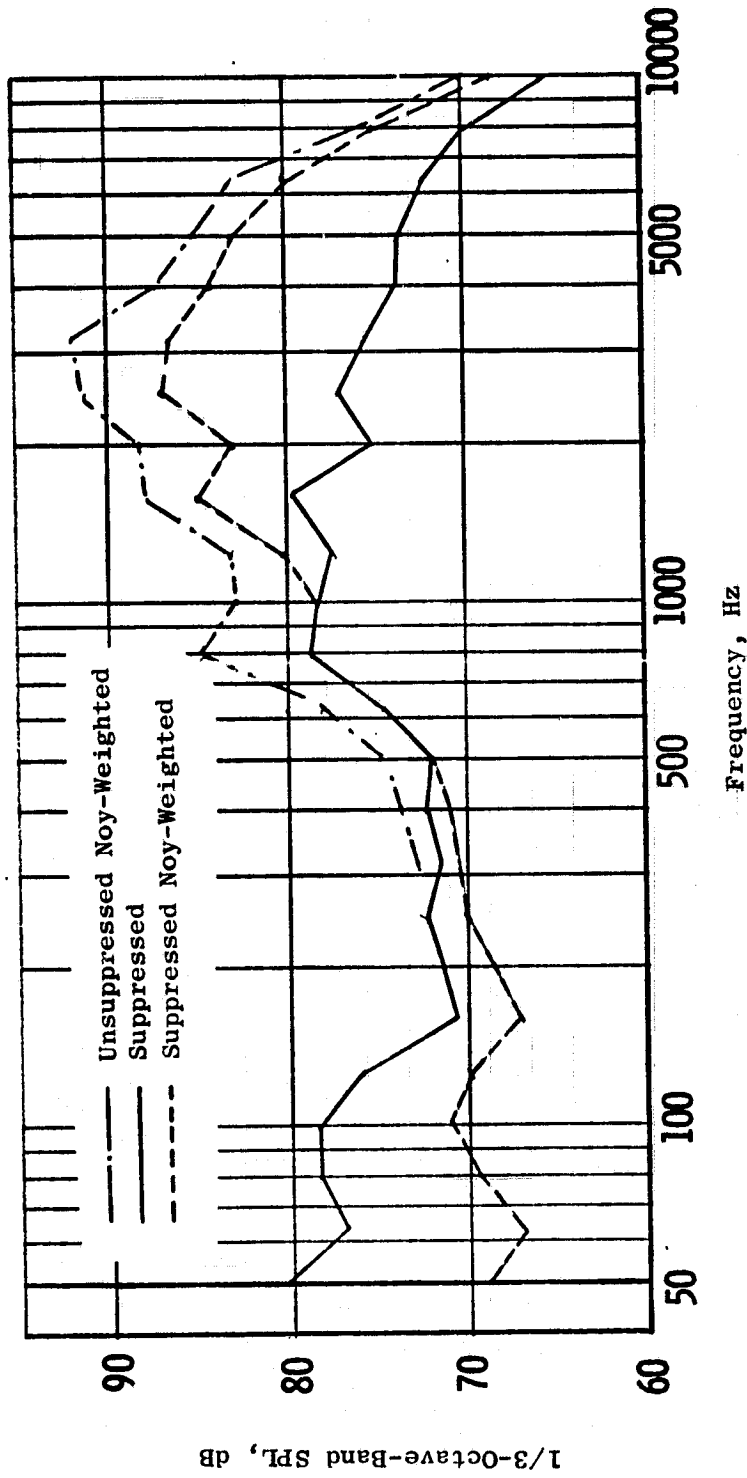


Figure 118. Reverse Thrust Spectra.

- 0.79 Throat Mach Number
- 152.4 m (500 ft) Sideline, 61 m (200 ft) Altitude
- Full-Scale Data
- 60° Acoustic Angle

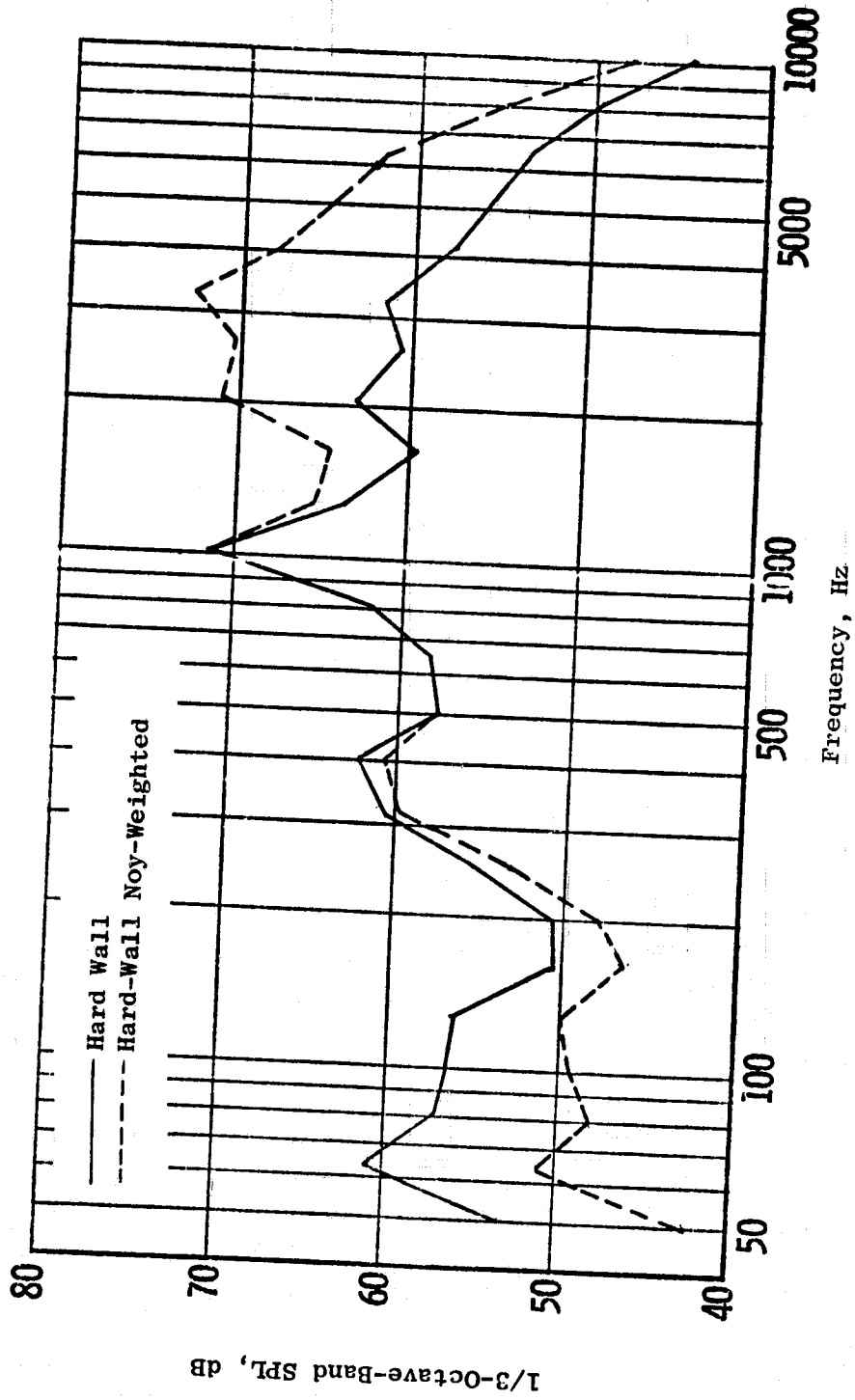


Figure 119. Hard-Wall Accelerating Inlet Spectra.

which can be achieved by tuning the treatment to different 1/3-octave-band frequencies, is required in order to achieve a significant reduction in terms of PNdB.

The unsuppressed and unsuppressed Noy-weighted spectra based on the scale model fan results are given in Figure 120. The data are for a +5° blade angle, 65% of takeoff thrust, 95% $N/\sqrt{\theta}$ operating conditions. The data are for an acoustic angle of 60° on a 152.4-m (500-ft) sideline at an altitude of 61-m (200-ft). The unsuppressed Noy-weighted spectrum shows the spectrum is controlled at 2500 Hz and drops off rather fast at all frequencies above and below 2500 Hz. Thus a treatment configuration with a single tuning frequency at 2500 Hz would be effective in reducing the PNL at this approach condition.

Based on the Noy-weighted unsuppressed spectra as shown in Figures 118 through 120 the tuning frequency requirements for the three operating conditions can be summarized as follows:

Reverse Thrust

1600 Hz 2500 Hz 3150 Hz

Forward Thrust

at Takeoff

1000 Hz 2000 Hz 3150 Hz

at Approach

2500 Hz

Since the decision was to design for the reverse thrust mode, the total treatment length should be divided into three segments, with treatment tuning frequencies corresponding to the reverse thrust frequencies as given above. This design approach favors a wide suppression bandwidth required for suppression in terms of Δ PNdB.

6.2.2 Definition of Inlet Design and Predicted Suppression

Extensive use was made of the scale model suppression data in the definition of the inlet treatment design for the UTW engine. The suppression spectra for the accelerating inlet treatment configuration B are shown in Figure 121. This configuration was selected from the series of inlet configurations since in reverse thrust mode the design was one of the two best configurations tested. This design also gave the highest suppression in the forward thrust condition of the inlets tested. The treatment D configuration which gave from 0.5 to 1.0 PNdB better suppression than inlet B in reverse thrust performed poorly at the forward thrust condition. One of the reasons

- 65% F_n - 95% $N/\sqrt{\theta}$ - Forward Thrust
- 5° Blade Angle, 60° Acoustic Angle
- 152.4 m (500 ft) Sideline, 61 m (200 ft) Altitude
- Full-Scale Data

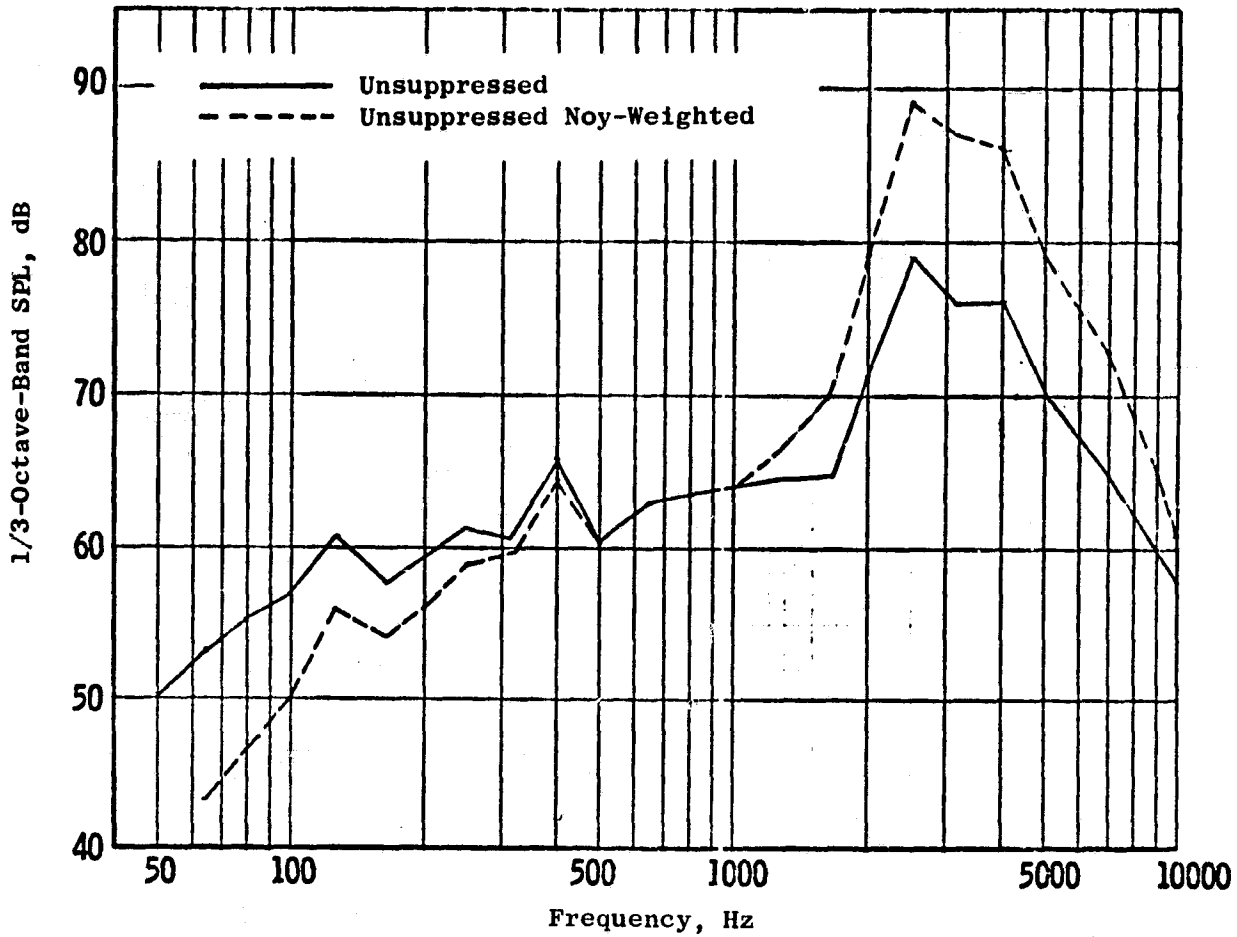


Figure 120. Unsuppressed Spectra, Bellmouth Inlet.

- 35% $F_n - 86 N/\sqrt{\theta}$
- -100° Blade Angle
- 60° Acoustic Angle
- 61 m (200 ft) Sideline, Full-Scale Data
- Treatment B
- 10% Porosity

— Total Suppression
 - - - Suppression per Section of Treatment

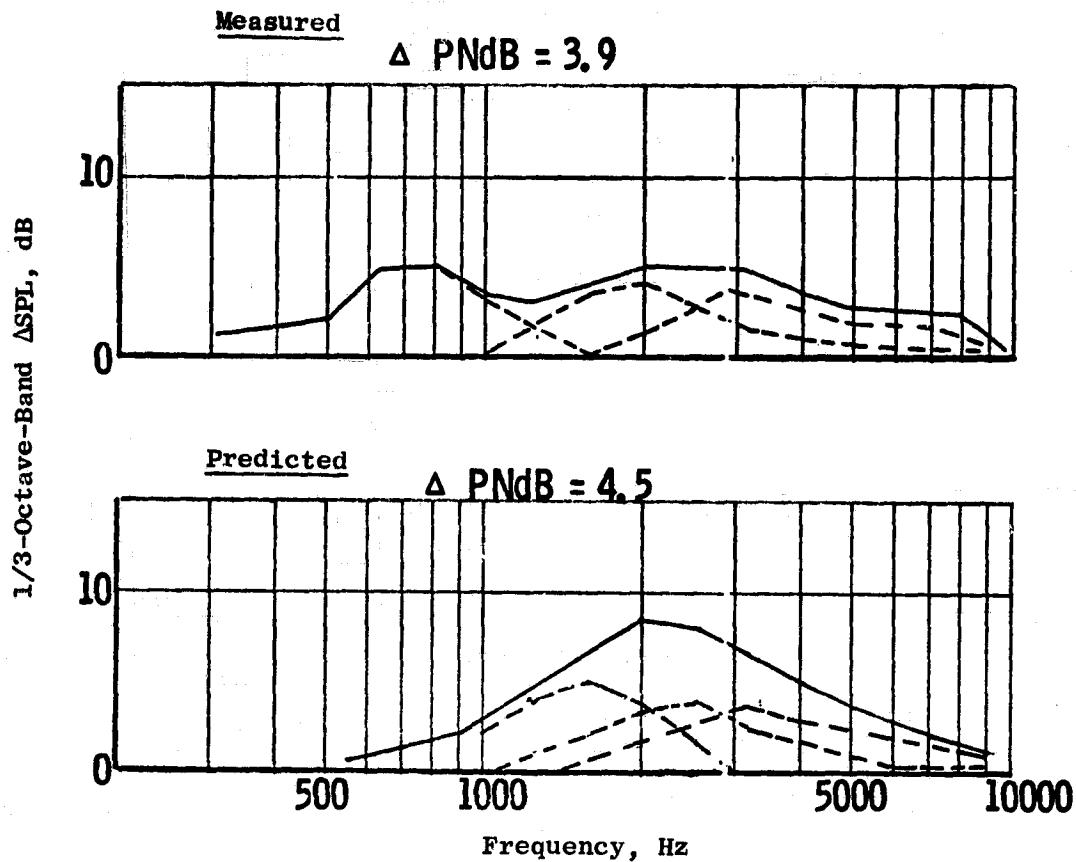


Figure 121. UTW Reverse Thrust Suppression Spectra.

believed to contribute to inlet D's poor performance was the fact that a relatively high faceplate porosity (28%) was situated in the inlet throat high Mach number region which could possibly be generating noise and therefore eliminating the treatment effectiveness. Thus in selecting treatment B a constant porosity of 10% was used in all sections of the treatment length.

Figure 121 also shows the estimated suppression for the UTW inlet at reverse thrust conditions calculated from the scale model results. In estimating the UTW suppression spectrum the scale model results were corrected as follows:

- The total suppression as measured for the scale model fan was split into three spectra. The peak frequencies of those spectra correspond to the predicted tuning frequencies for the three sections of treatment found in inlet B. The suppression bandwidths of the three spectra are adjusted such that their sum is equal to the total suppression measured.
- The three sections of treatment for the UTW inlet were assumed to have the three tuning frequencies previously defined as optimum for the reverse thrust condition. The measured peak and adjusted bandwidth were made to correspond with the UTW design frequencies with the same peak frequency level and bandwidth. The total suppression is the sum of these three spectra.

From Figure 121 it is seen that by retuning the treatment the suppression can be increased from 3.9 Δ PNdB to a level of 4.5 Δ PNdB. The suppressed Noy-weighted spectrum given in Figure 122 shows that in order to improve the suppression in terms of Δ PNdB additional suppression at both 3150 Hz and 800 Hz is required.

The suppression estimate for the accelerated inlet in forward thrust at or near takeoff power was made using the same procedure as outlined for the reverse thrust condition. The suppression spectra are shown in Figure 123. The data are for a fan speed of $90\% N/\sqrt{\theta}$, which is close to the fan speed at takeoff but does not have the high throat Mach number suppression effects. The peak suppression of each section is based on that predicted for reverse thrust with corrections for the changing airflow direction. The performance of the inlet design at takeoff power is expected to be equal to the scale model design which gave a total suppression of 13 PNdB of which 10 is a result of the high throat Mach number, 3 PNdB being obtained from the inlet treatment.

Figure 124 gives the suppression for approach power. The same procedure was followed in estimating the suppression. The predicted suppression for the UTW design is about 1.0-PNdB less than that measured on the scale model configuration.

- Noy-Weighted, Reverse Thrust
- 60° Acoustic Angle
- 61 m (200 ft) Sideline
- 35% F_n - 86% N/θ - 100° Blade Angle

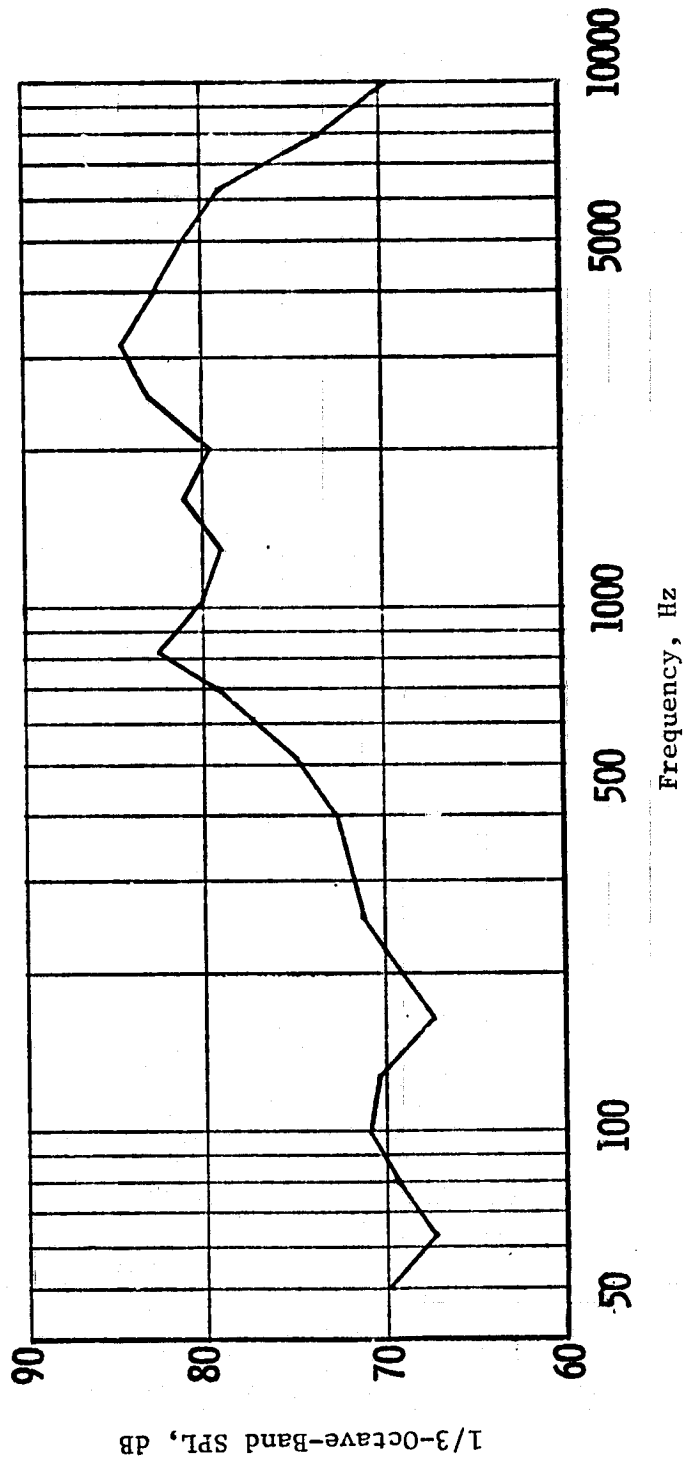


Figure 122. UTW Predicted Suppression Spectrum.

- 90% N/√θ
 - 60° Acoustic Angle
 - 61 M (200 ft) Sideline, Full Scale Data
- Treatment B
10% Porosity

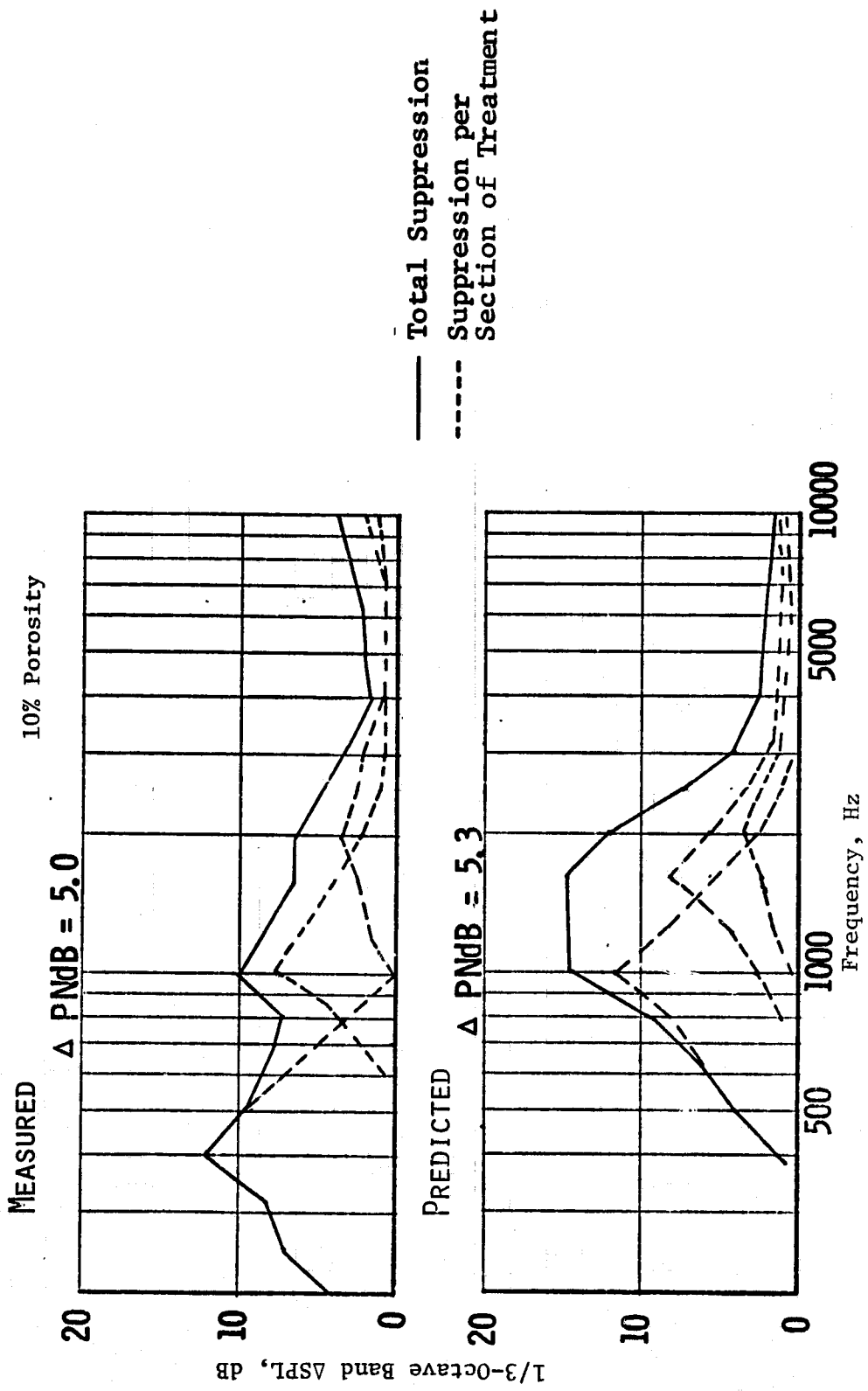


Figure 123. UTW Forward Thrust Suppression Spectra.

- 65% F_n - 95% N/θ
- 5° Blade Angle, 60° Acoustic Angle
- 61 M (200 ft) Sideline, Full-Scale Data

Treatment B
10% Porosity

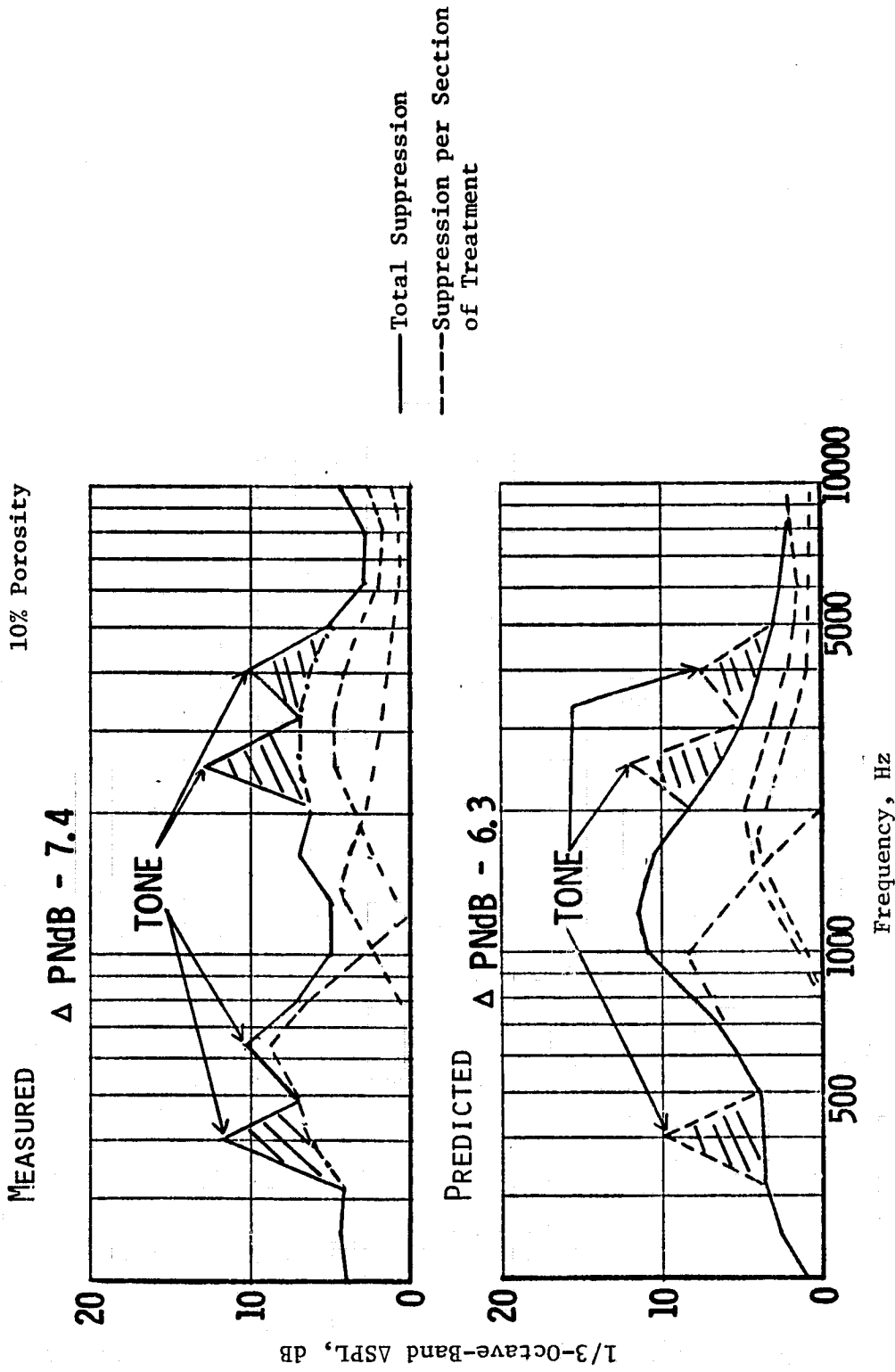


Figure 124. UTW Suppression Spectra.

Inlet Design

The UTW Boilerplate No. 1 inlet treatment configuration is defined in Figure 125. The total treatment length-to-fan-diameter ratio is 0.74. A definition of the faceplate dimensions and the cavity depth requirements to give the desired tuning frequencies are given in Table IX. The predicted tuning frequencies for the reverse thrust and the forward thrust conditions for the inlet design are summarized in Table X.

The panel depth requirements were determined using the predicted acoustic reactance versus optimum reactance curves given in Figure 126. The optimum reactance was determined for the inlet using the analytical model presented by E.J. Rice in Reference 4. The panel reactance values were predicted using the analytical relations given in Reference 5. The predictions were made for the lowest order radial mode, 10th order spinning mode pattern. The intersection of the two curves, optimum and predicted reactance in Figure 126, determine the tuning frequency for each section of acoustic treatment.

• Treated $L_T/D_F = 0.74$

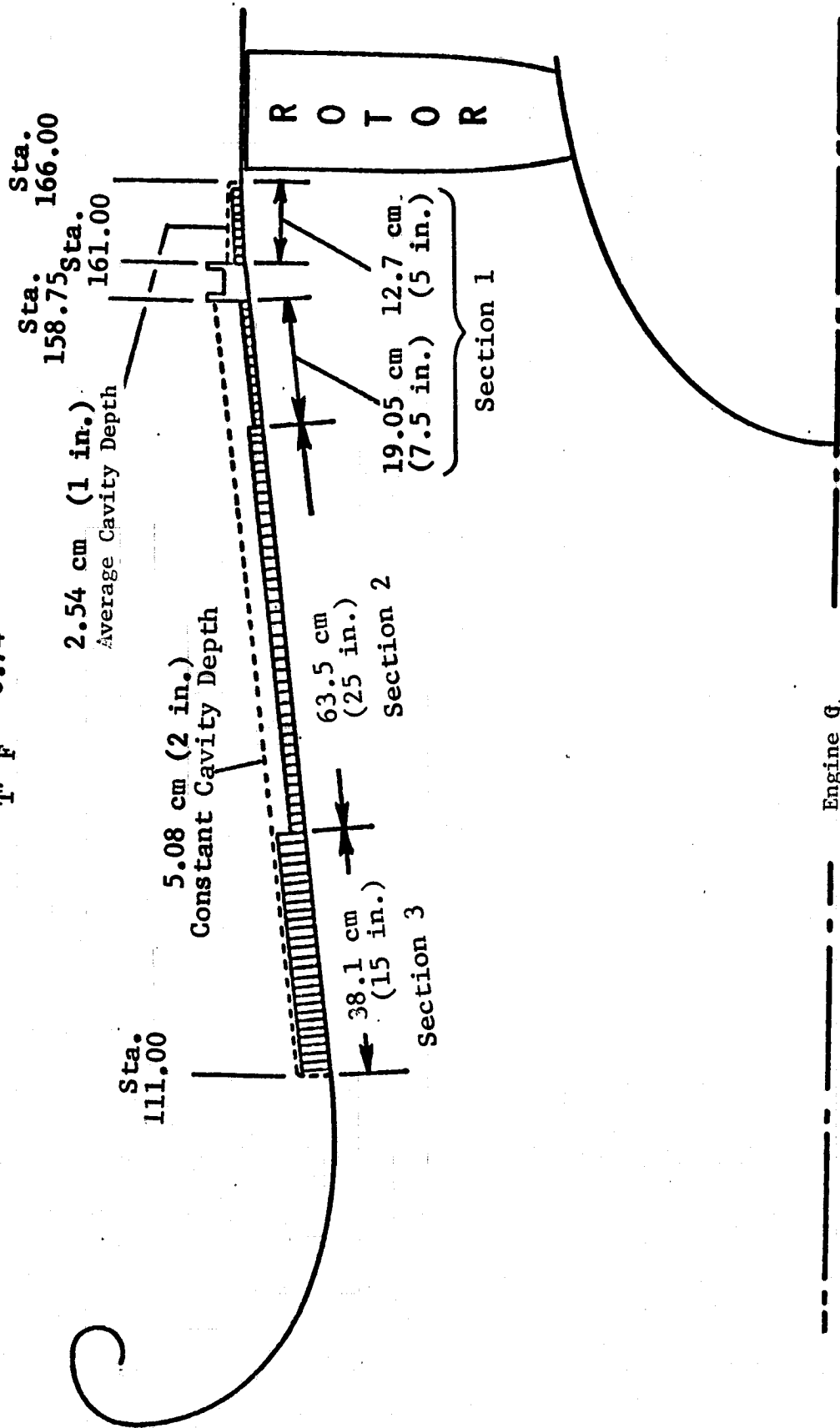


Figure 125. UTW Boilerplate No. 1 Fan Inlet Treatment Design.

Table IX. Treatment Design Details.

<u>Section</u>	<u>Hole Size</u>		<u>Porosity, %</u>	<u>Cavity Depth</u>		<u>Faceplate Thickness</u>	
	<u>cm</u>	<u>(in.)</u>		<u>cm</u>	<u>(in.)</u>	<u>cm</u>	<u>(in.)</u>
1	0.158	(0.0625)	10	1.27	(0.50)	0.076	(0.03)
2	0.158	(0.0625)	10	1.90	(0.75)	0.076	(0.03)
3	0.158	(0.0625)	10	3.81	(1.50)	0.076	(0.03)

Table X. Design Frequencies.

<u>Section</u>	<u>Frequency, Hz</u>	
	<u>Reverse Thrust</u>	<u>Forward Thrust</u>
1	3150	2000
2	2500	1600
3	1600	1000

- ① Treatment Section
- ② Treatment Section
- ③ Treatment Section

See Table IX for
Definition of Each
Section

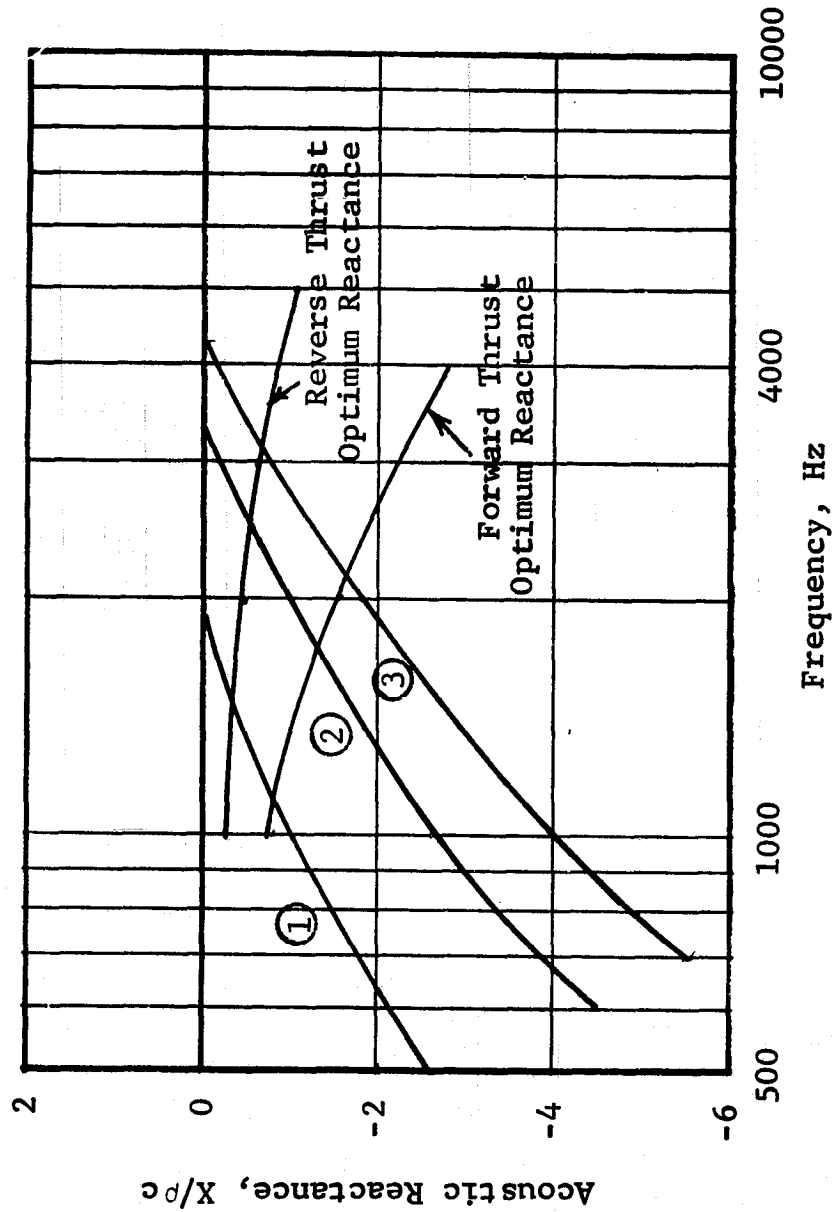


Figure 126. Predicted Acoustic Reactance Vs. Optimum Reactance.

7.0 CORE EXHAUST SUPPRESSOR DESIGN

7.1 DEFINITION OF CONCEPTS TO BE EVALUATED

The core exhaust noise suppression requirements for both QCSEE engines (UTW and OTW) are such that both high-frequency turbine noise and low-frequency combustor noise suppression are required. This is evident from the core noise Noy-weighted spectrum in Figure 127. Because of engine dimensional constraints the core noise suppressor must be very compact. Suppressor design concepts not previously evaluated for this type of application were identified and evaluated during the test phase of this program. The concepts evaluated all have one thing in common; they are compact compared to the more conventional designs. These designs, with their short treatment length and thin panel requirements, are able to satisfy the engine envelope constraints.

Three illustrations of the evaluated concepts are given in Figure 128. The concepts are defined as:

- Dual-Layer Single-Degree-of-Freedom (SDOF) Dissipative Treatment
- Dual-Layer SDOF and Side-Branch Resonator Reactive Treatment
- Dual-Layer SDOF and Folded Quarter-Wave Reactive Treatment

Each of these concepts combine thin, high-frequency single-degree-of-freedom (SDOF) treatment with the deeper panel low-frequency-type treatment which is either dissipative or reactive. The compactness of the suppressors is achieved by stacking the thinner high-frequency treatment on top of the thicker low-frequency panel. Communication to the low-frequency panel is provided by cutouts in or removal of some of the high-frequency thin panel treatment area. Figure 129 defines the engine envelope within which the core treatment must be contained.

The low-frequency dissipative treatment was designed based upon the principles involved in absorbing the sound via the frictional losses in the apertures connecting the duct with the treatment partitions, using distributed point-reaction Helmholtz resonator cavities; the two low-frequency reactive treatments were designed based upon the principles involved in reflecting the sound energy back toward the source, using local impedance discontinuities such as in transmission-line theory.

7.2 ACOUSTIC DUCT TESTS

All three concepts defined above were evaluated using both cold flow and high temperature acoustic duct data. The cold flow acoustic tests were used to develop and evaluate the candidates for testing in the General Electric High Temperature Acoustic Duct facility (HITAD). The purpose of the

- UTW at Takeoff Power
- 152.4 cm (500 ft) Sideline
- 120° Acoustic Angle
- 61 m (200 ft) Altitude

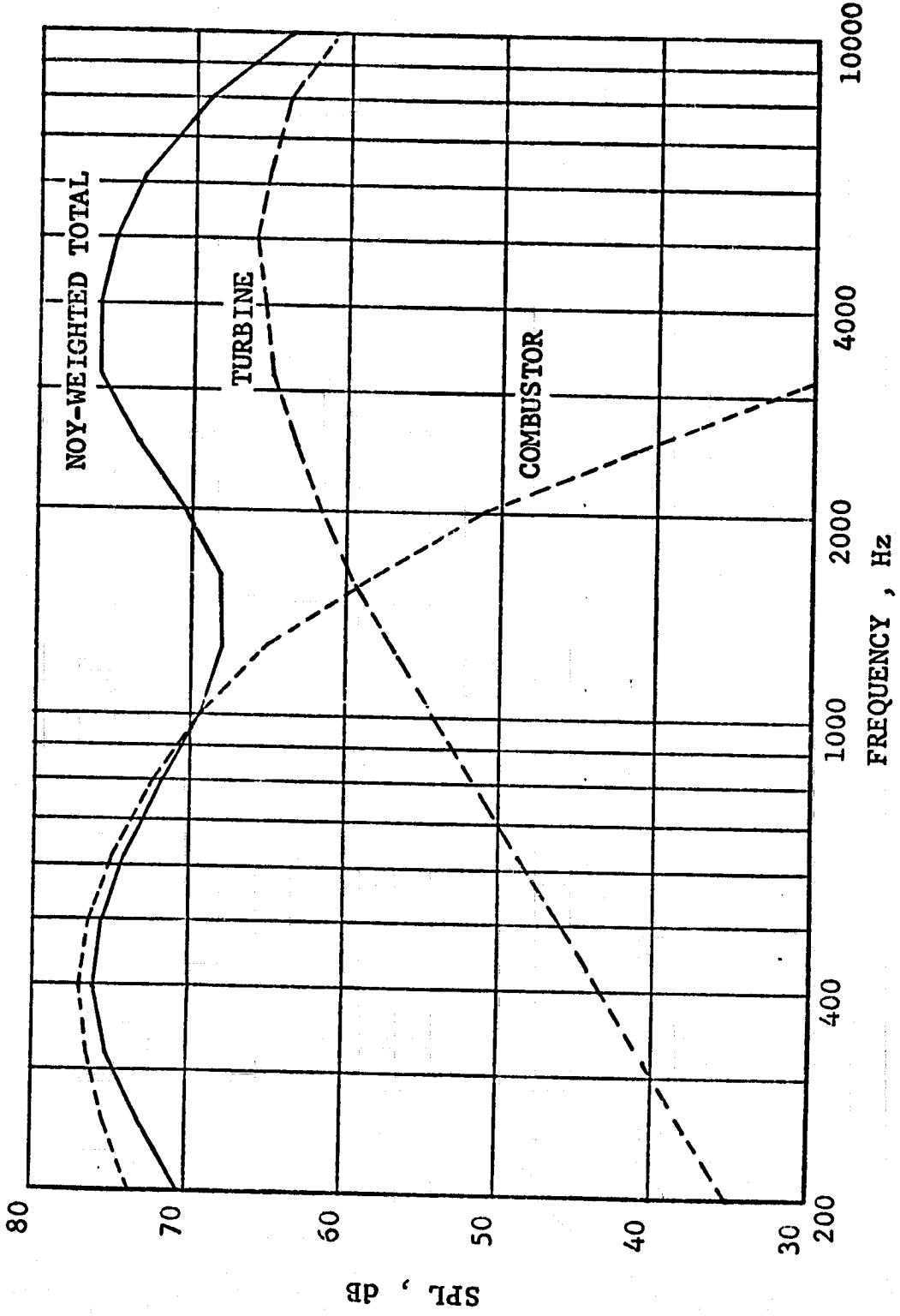
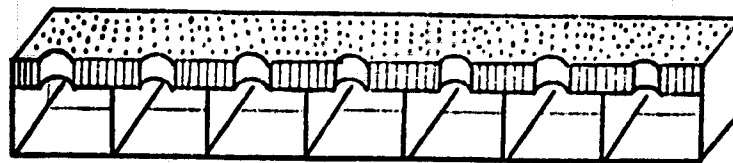
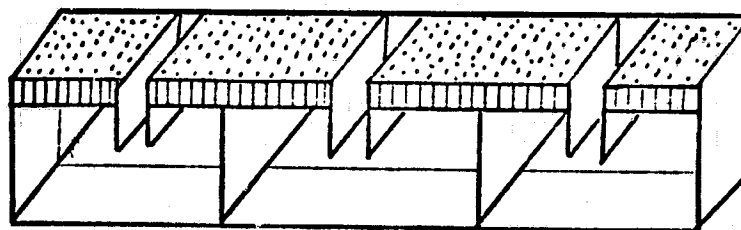


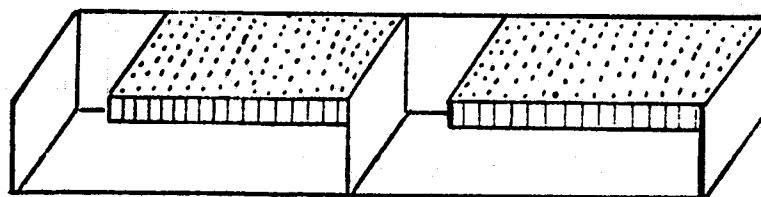
Figure 127. Predicted Core Noise Spectra.



(a) Dual-Layer SDOF Dissipative Treatment



(b) Dual-Layer SDOF and Side-Branch Resonator Reactive Treatment



(c) Dual-Layer SDOF and Folded Quarter-Wave Reactive Treatment

Figure 128. Compact Suppressor Concepts.

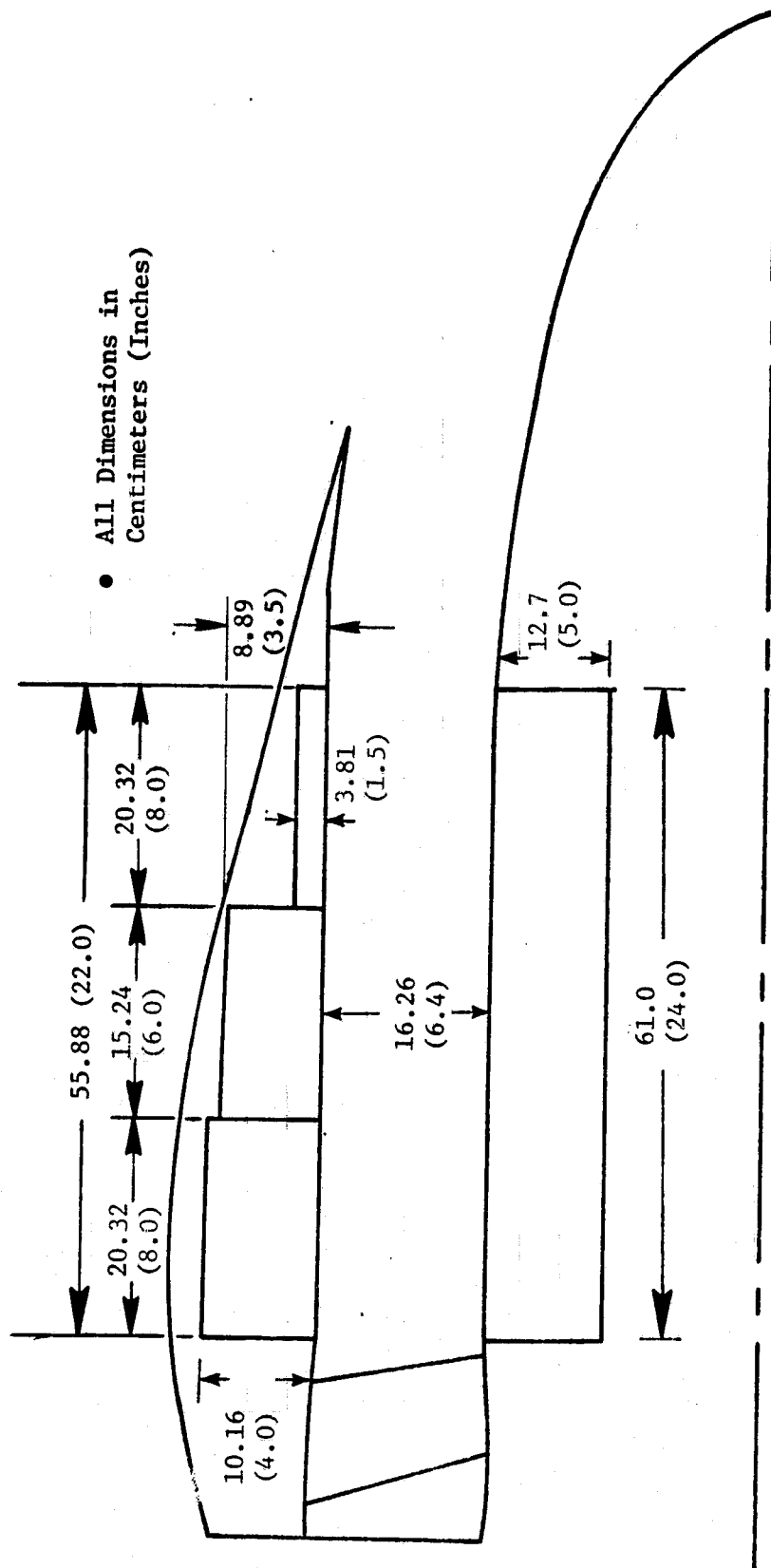


Figure 129. Suppressor Envelope Definition.

high temperature duct testing was to demonstrate the suppressor performance at engine temperature and Mach number conditions.

7.2.1 Test Facilities

The cold flow rectangular duct is six feet long and four inches wide, and has an adjustable duct height. The height between the treated walls can be set at any value up to 44.45 cm (17.5 in.). For this core exhaust testing, the duct height was 12.7 cm (5 inches). A schematic of the duct facility is shown in Figure 130. The duct is capable of handling various treatment materials up to 15.24-cm (6-in.) thick and is equipped with the instrumentation needed to monitor test effects. Figure 131 depicts the acoustic probe instrumentation used to evaluate treatment effectiveness and flow effects. In operation, the duct is secured by a rectangular-circular transition section to a plenum chamber through which up to 20-lb/sec air can be supplied from the central air supply. A Ling 200 is used to provide high-intensity noise that propagates with or against the flow to simulate a high-intensity noise source connected in either the inlet or exhaust modes.

A schematic of the HITAD test facility is given in Figure 132. The HITAD facility is capable of obtaining Mach numbers up to 0.5 for temperatures up to 1200° F. Acoustic treatment configurations are mounted in a 10.16-cm (4-in.) by 20.32-cm (8-in.) rectangular duct cross section with the treated surfaces 20.32-cm (8-in.) apart. Configurations up to 91.44-cm (36-inches) long and 15.24-cm (6-in.) deep can be tested. The instrumentation, as shown in Figure 133, includes a pitot-static probe and thermocouples for monitoring flow conditions and far-field microphones for collecting acoustic data. In operation, test conditions are maintained by regulating the air and fuel supplied to the burners and preburner upstream of the test section. A siren acts as the noise source. Its fundamental frequency can be varied from 200 Hz to 2,000 Hz, and its harmonics can be used as high as 10,000 Hz, enabling measurement of treatment suppression over the frequency range of interest.

7.2.2 Data Results

7.2.2.1 Cold Flow Duct

Preliminary testing of the folded quarter-wave low-frequency suppressor concept was completed first, measuring the suppression from 315 to 2500 Hz for duct flow velocities of Mach 0.0, 0.2, 0.3, and 0.4. The test sections consisted of an upper and lower 36-in. tray with cavities, as shown in Figure 134.

For the preliminary testing, 0.635-cm (0.25-in.) aluminum plate was substituted for the high-frequency treatment. All cavity dimensions except length were held constant, as shown in Figure 134. Length was tested at 7.62 cm (3 in.), 10.16 cm (4 in.), and 12.7 cm (5 in.) to vary the tuning frequency from 500 to 700 Hz. These treatments were tested, singly and

CB

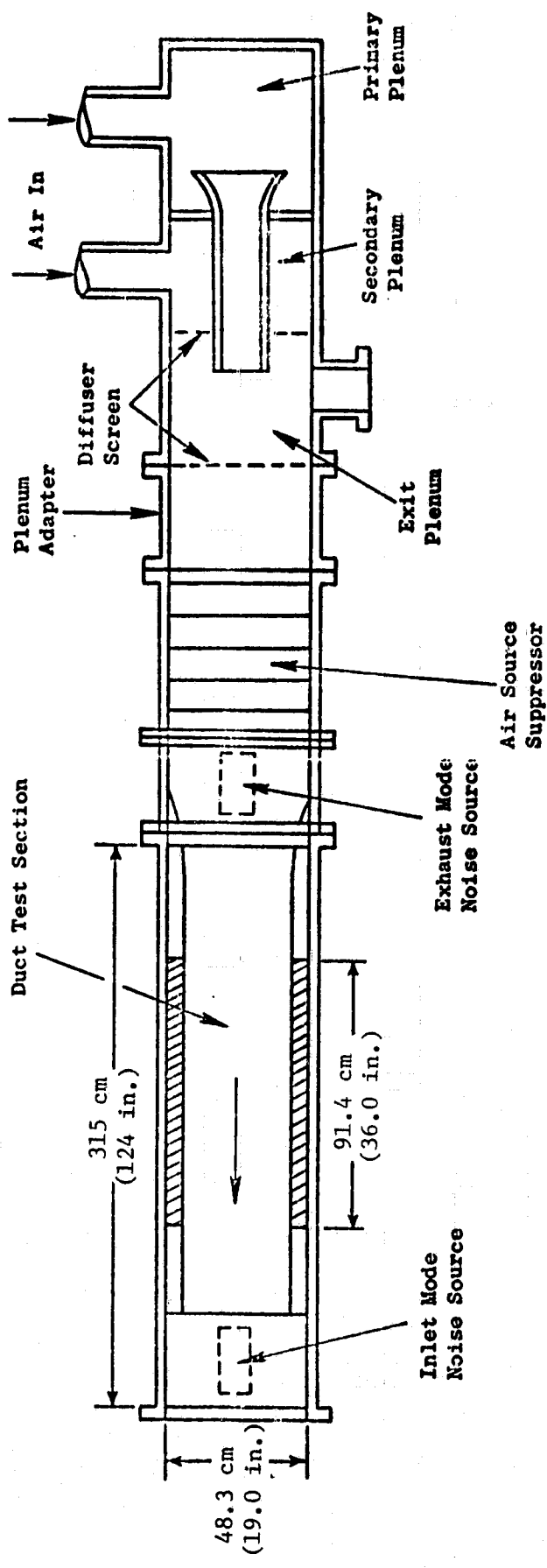


Figure 130. Schematic of Rectangular Cold Flow Duct Facility.

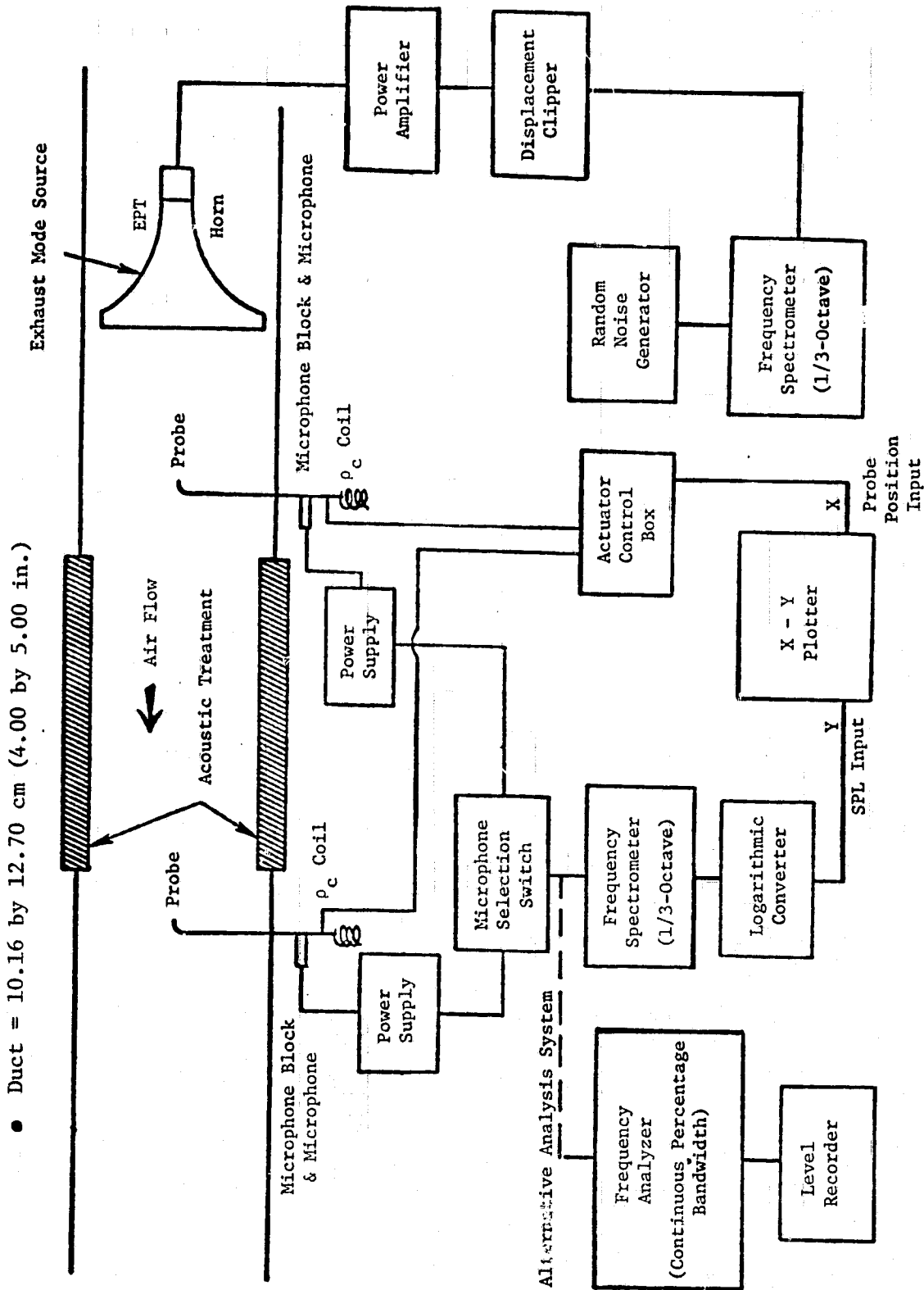


Figure 131. Instrumentation of Rectangular Cold Flow Duct Facility.

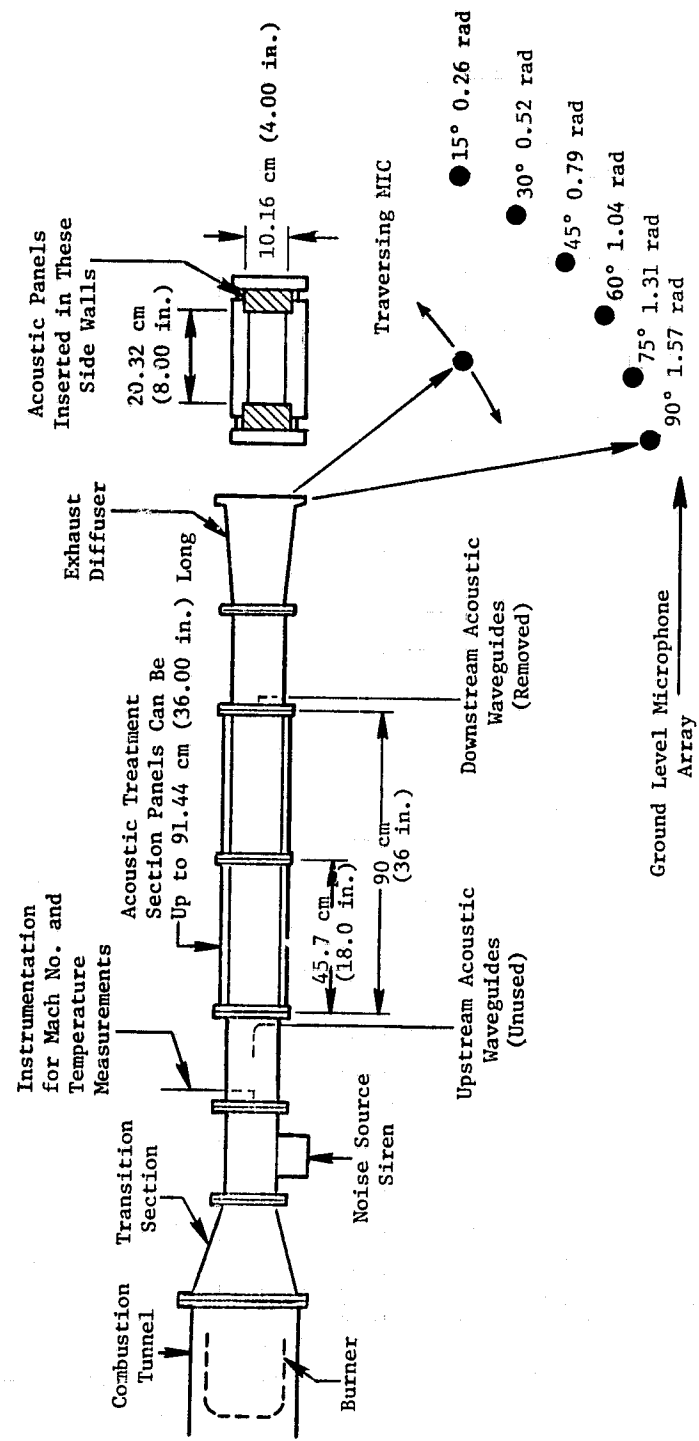


Figure 132. Schematic of High-Temperature Acoustic Duct Facility.

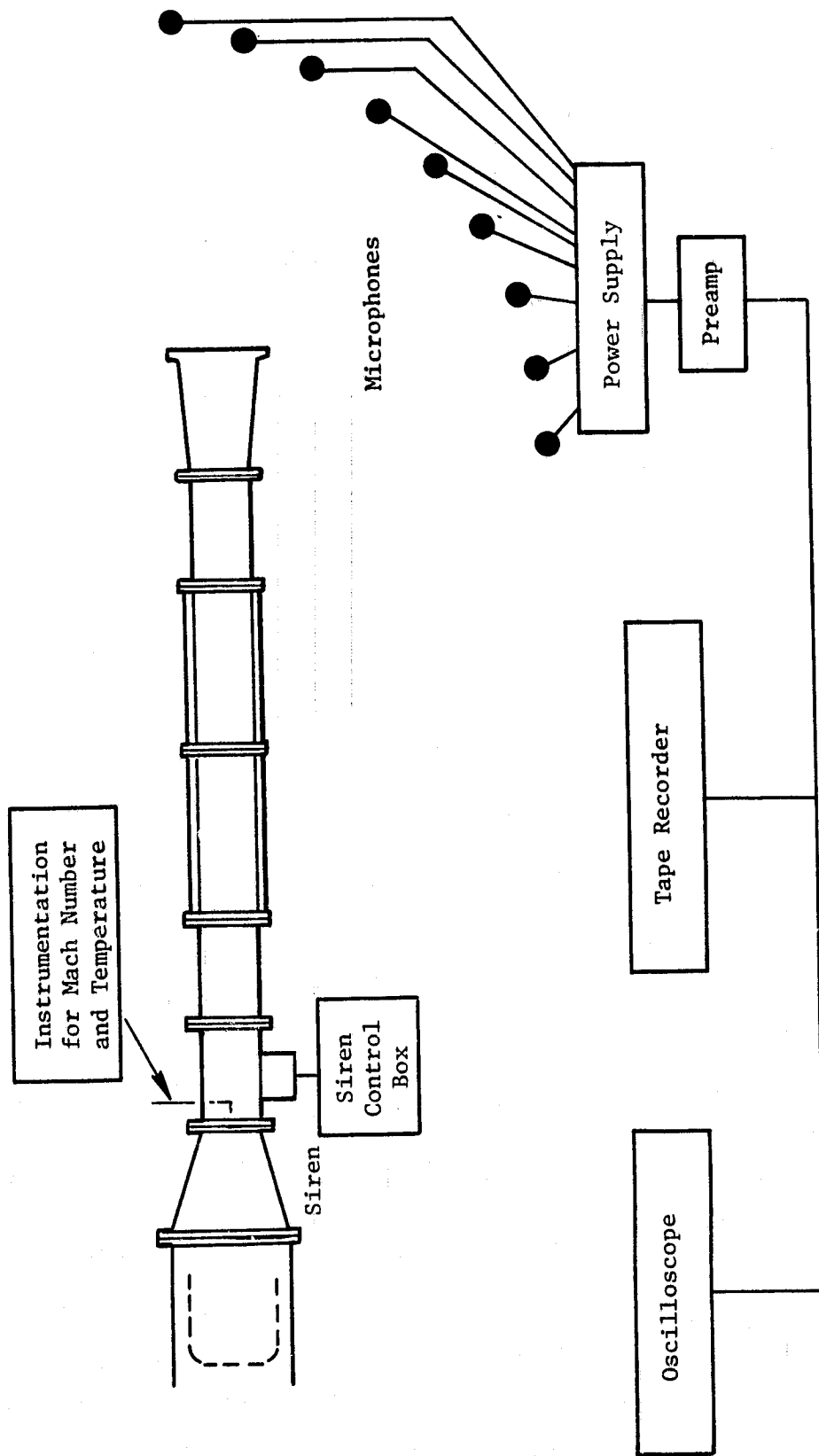
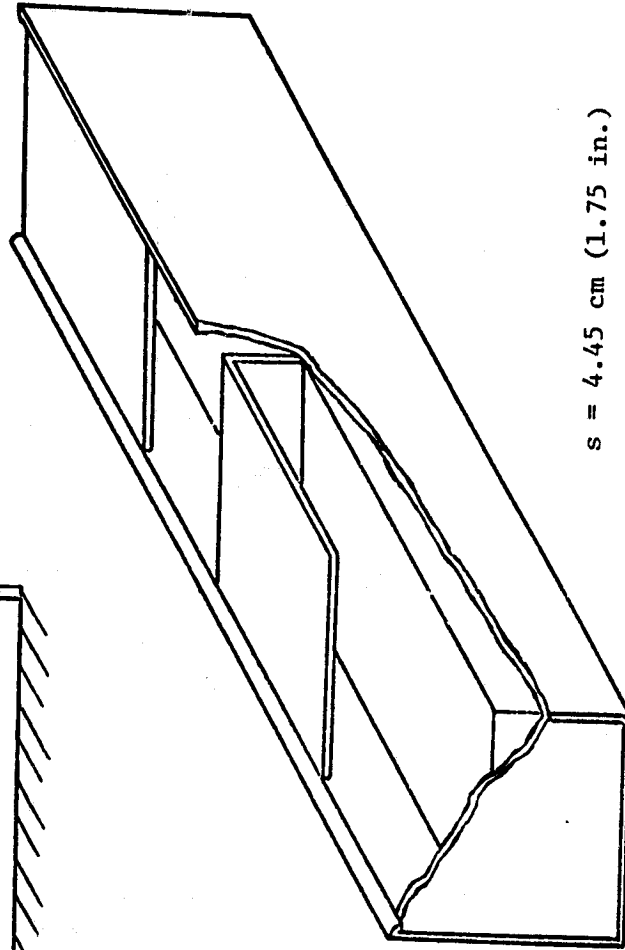
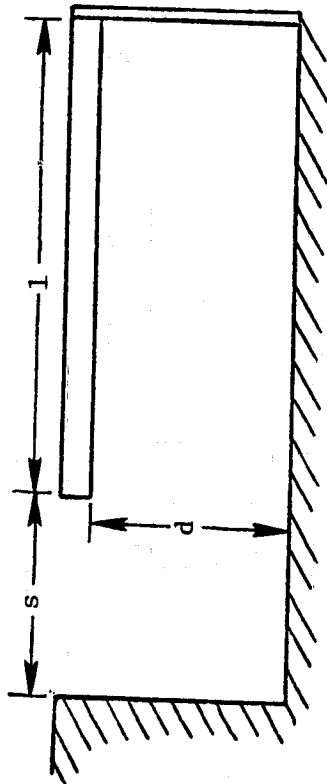


Figure 133. Instrumentation of High-Temperature Acoustic Duct Facility.



$s = 4.45 \text{ cm (1.75 in.)}$

$d = 4.45 \text{ cm (1.75 in.)}$

$l = 76.62 \text{ cm, } 10.16 \text{ cm, } 12.7 \text{ cm}$
 $(3.0 \text{ in.}), (4.0 \text{ in.}), (5.0 \text{ in.})$

Figure 134. Sketch of Quarter-Wave Suppressor Test Trays.

mixed, as a function of treated duct length/height; when only one side of the duct was treated, the value of H was taken to be twice the actual duct height. Various length/height configurations were tested for the 12.7-cm (5-in.) lengths by installing hard-wall sections in the remainder of the 91.44-cm (36 in.) trays. Tests were also run mixing 12.7-cm (5-in.) and 7.62-cm (3-in.) lengths in an alternating arrangement. Figure 135 defines the exact configurations tested. The corrected transmission loss results for these configurations are presented in Figures 136 through 142.

Figure 136 gives the corrected transmission loss spectra for the hard-wall configuration - the configuration used as the reference baseline in determining the corrected transmission loss spectra for each of the treatment configurations. Figure 137 gives the corrected transmission loss spectra for configuration 2 from Figure 135. The data results show a peak suppression at 500 Hz for the four different duct Mach numbers, with a maximum suppression of 22 dB for 0.3 Mach number. Figure 138 gives the suppression data for configuration 3 which is the same design of Configuration 2 but has the amount of treatment doubled by having treatment located on both duct walls. The increased treatment gives an increase in the peak frequency of about 9 dB; however, the peak occurs for a duct Mach number of 0.2 rather than the 0.3 shown in Configuration 2. The peak tuning frequency remained at 500 Hz.

The data shown in Figure 139 are for Configuration 4 which differs from Configuration 3 in that the slot orientation is reversed. The peak frequency is at 500 Hz; however, the peak suppression levels relative to those given in Figure 138 are significantly reduced for the 0.2 and 0.3 flow Mach number tests.

Figure 140 gives data results for Configuration 5. This configuration is the same design as Configuration 3 but has reduced treatment lengths on each of the duct walls, giving an L/H of 4.05 versus the 6.75 value for Configuration 3. Compared with the suppression levels given in Figure 138 the peak frequency suppression is significantly reduced for most of the Mach numbers. No change, however, is seen in the peak attenuation frequency at the higher Mach number.

In order to vary the suppressor tuning frequency the "l" dimensions of the panel were varied. Configuration 6 has an "l" value of 10.17 cm (4 in.) versus the 12.7 cm (5 in.) value for the previously described configurations. Data results for this configuration are given in Figure 141. The peak suppression is shown to have shifted from 500 to 630 Hz as a result of the shorter "l" length. The tuning frequency, f, is given by $f = c/4l$ where "c" is the speed of sound and "l" is the axial cavity length. The peak suppression levels are compared with the results in Figure 140 and are uniformly higher at all duct Mach numbers probably due to the slightly higher L/H value.

The design for Configuration 7 shows the "l" value reduced from 10.16 cm (4 in.) to 7.62 cm (3 in.), a reduction which should shift the peak attenuation to a higher frequency. Figure 142 giving the data results shows

Configuration	Description*	* All Dimensions in Centimeters (Inches)	
1	Hard Wall Base Configuration		
2	Hard Wall 12.7 (5.0) Slots L/H = 3.38		
3	12.7 (5.0) (Slots Forward) L/H = 6.75		
4	12.7 (5.0) (Slots Aft) L/H = 6.75		
5	12.7 (5.0) (Slots Forward) L/H = 4.05		
6	10.2 (4.0) (Slots Forward) L/H = 4.6		
7	7.6 (3.0) (Slots Forward) L/H = 3.8		
8	12.7 (5.0) & 7.6 (3.0) (Slots Forward), L/H = 4.6		

Figure 135. Definition of Quarter-Wave Suppressor Configurations.

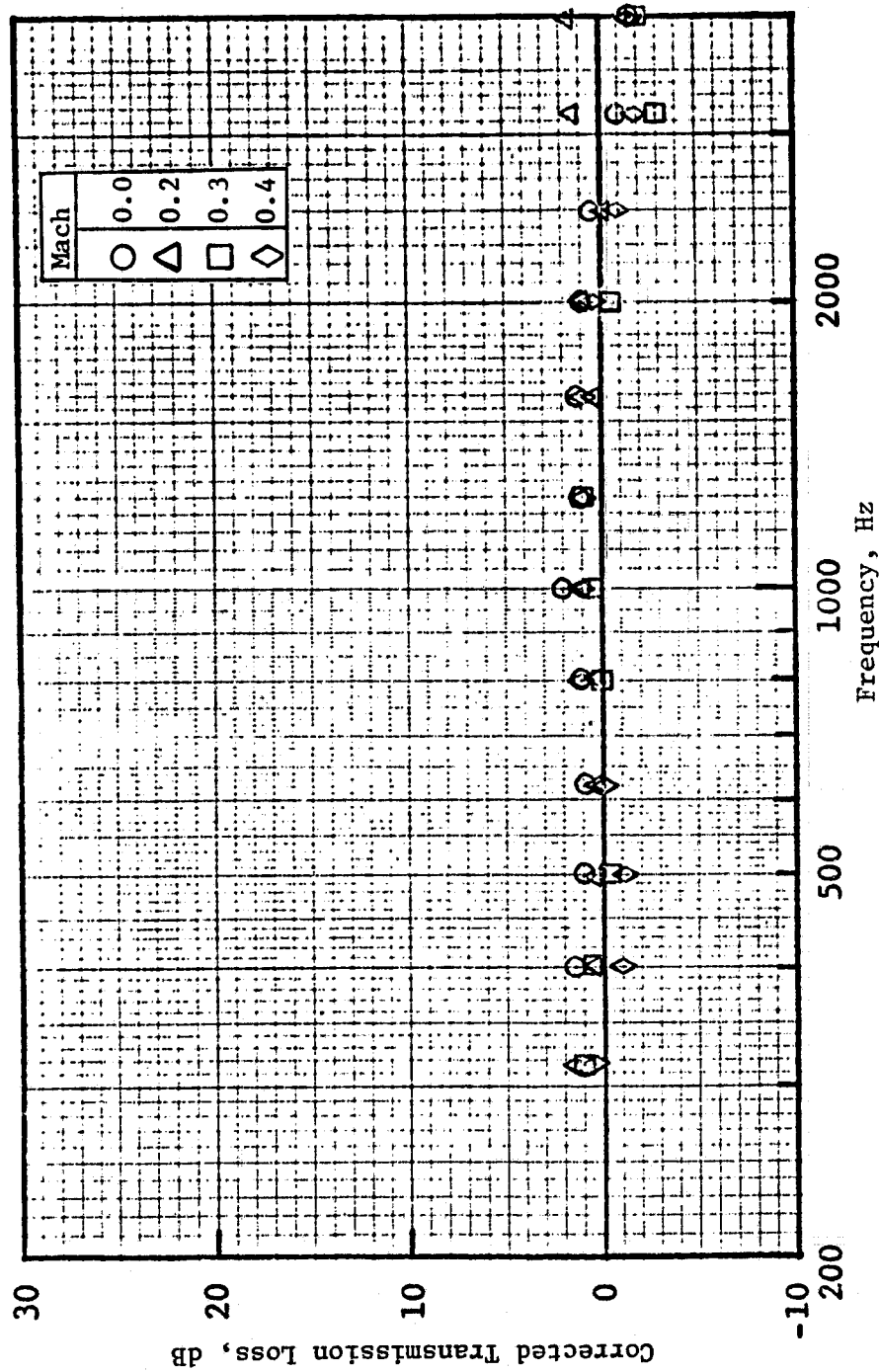


Figure 136. Cold Flow Acoustic Duct Data, Hard-Wall Baseline Configuration 1.

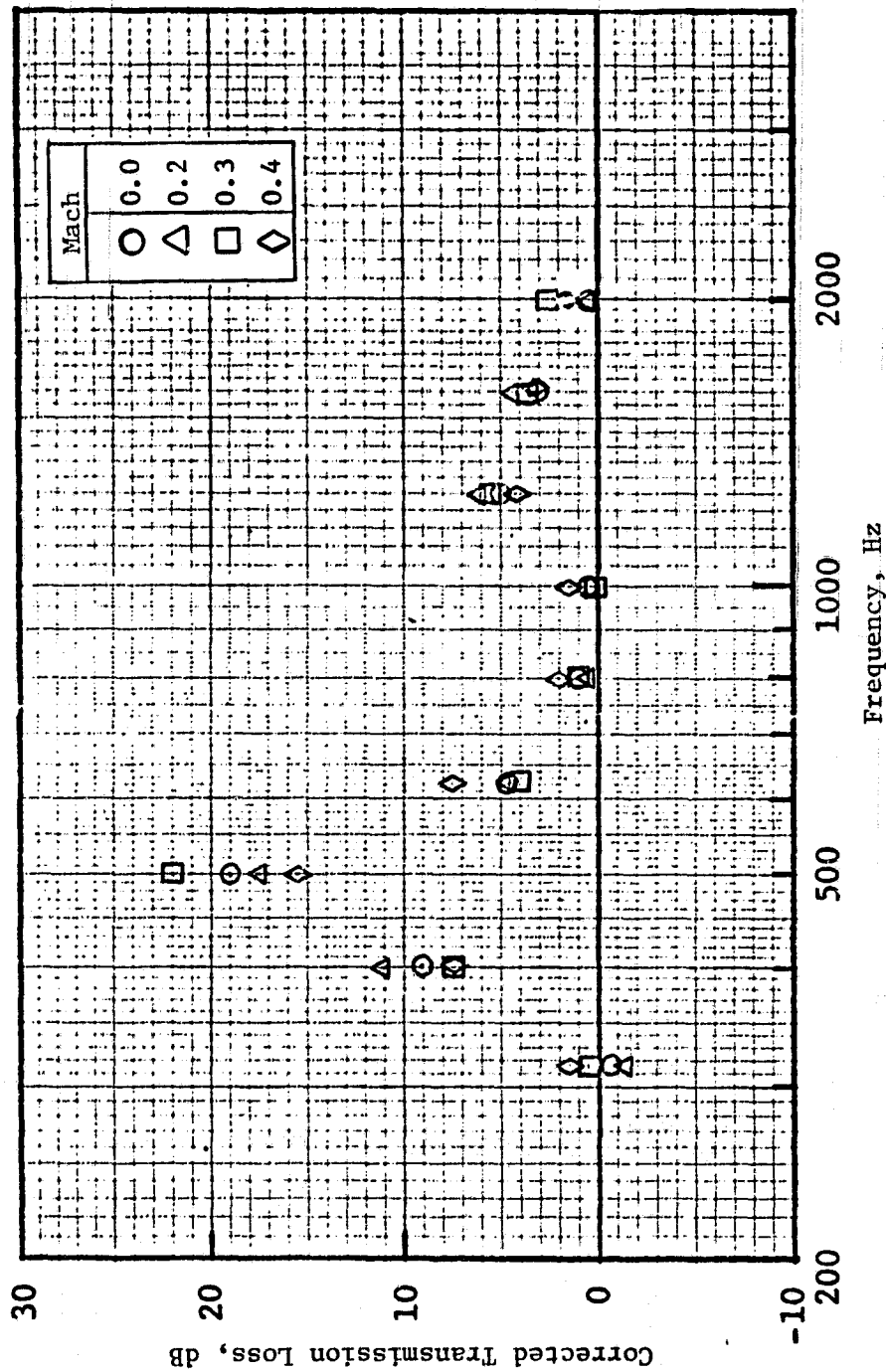


Figure 137. Cold Flow Acoustic Duct Data, Configuration 2 Folded Quarter-Wave Resonator, 12.7 cm (5 in.) Slots on One Side, $L/H = 3.38$.

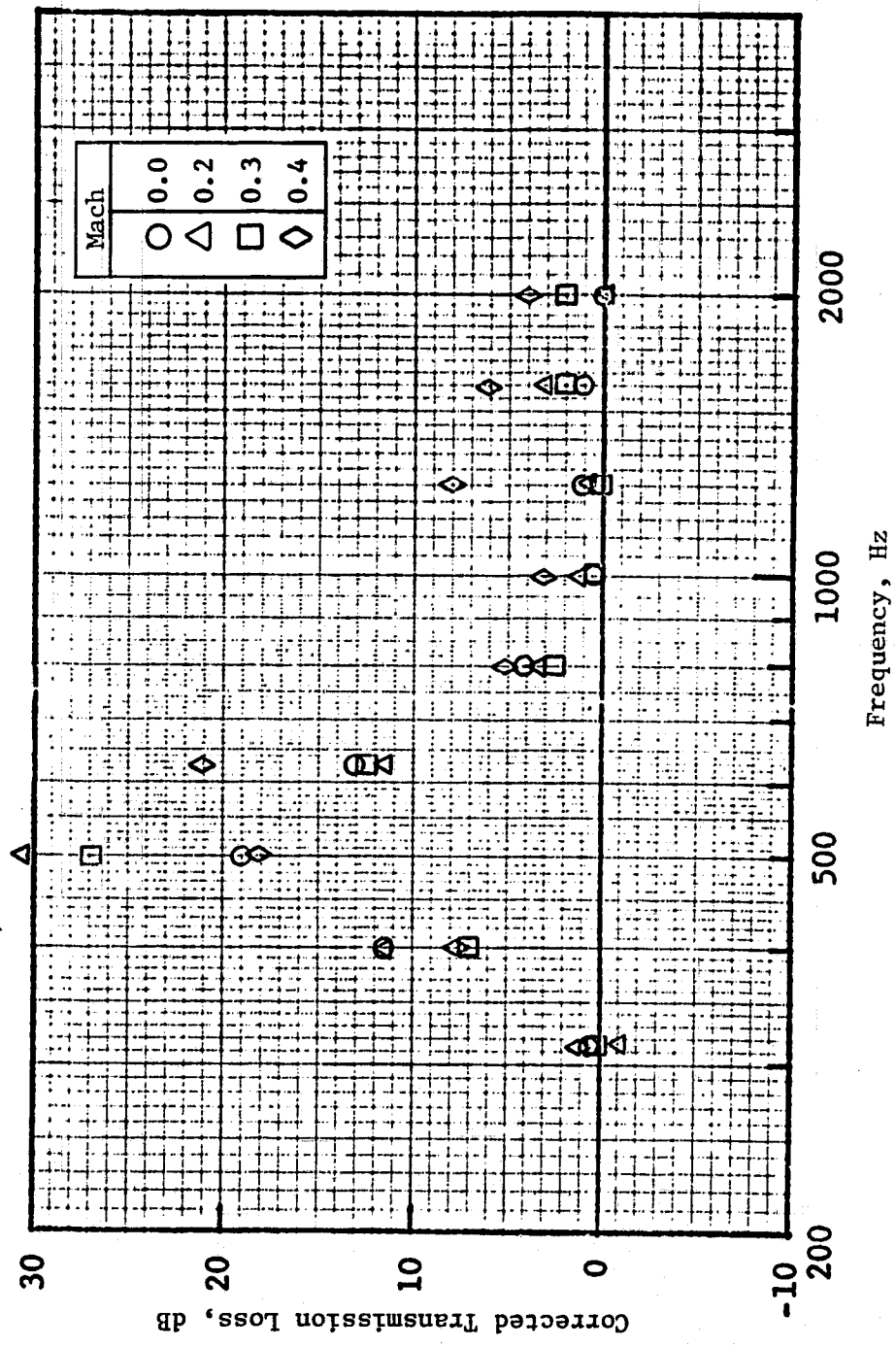


Figure 138. Cold Flow Acoustic Duct Data, Configuration 3 Folded Quarter-Wave Resonator, 12.7 cm (5 in.), Slots Forward, L/H = 6.75.

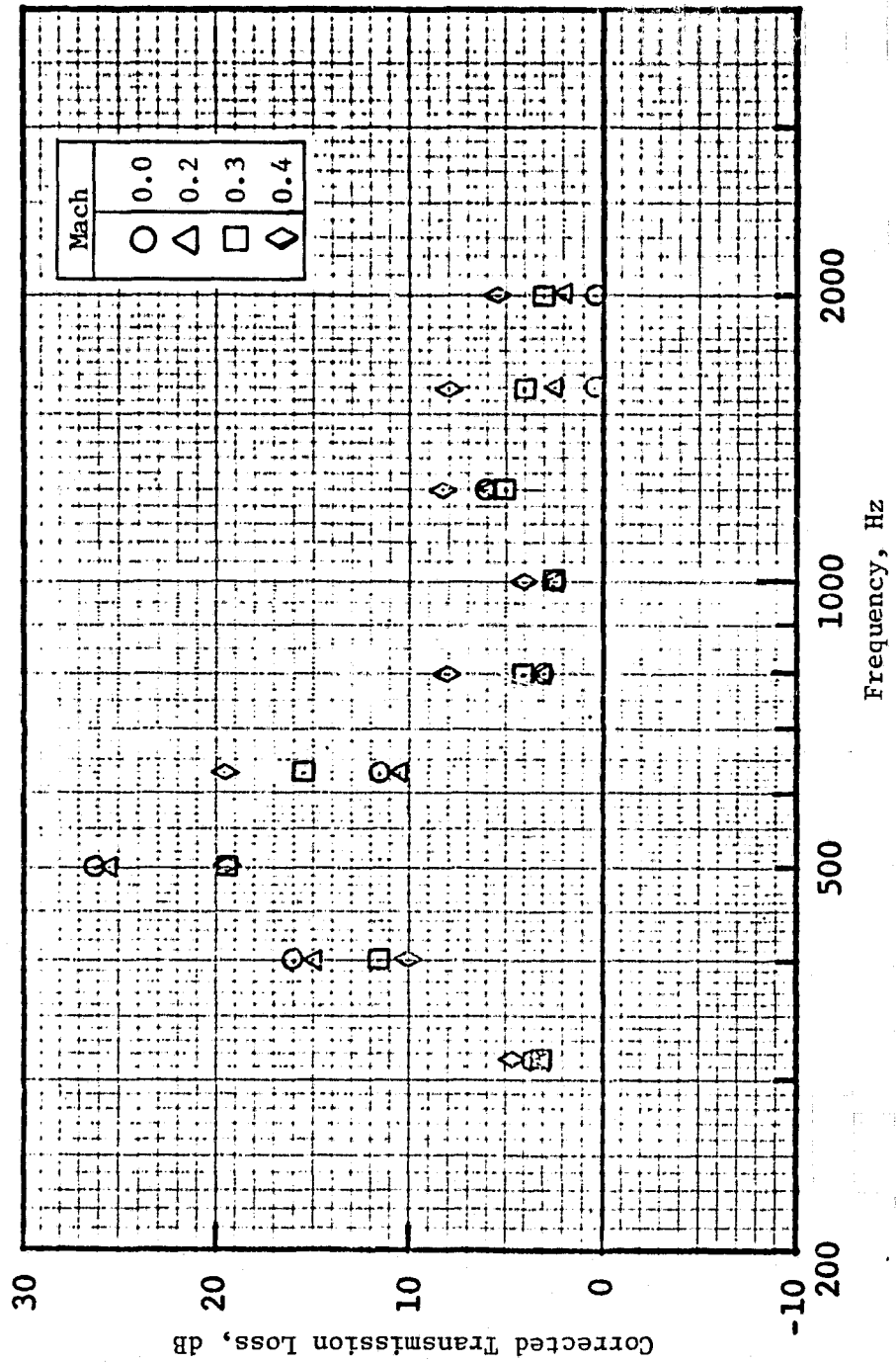


Figure 139. Cold Flow Acoustic Duct Data, Configuration 4 Folded Quarter-Wave Resonator, 12.7 cm (5 in.), Slots Aft, L/H = 6.75.

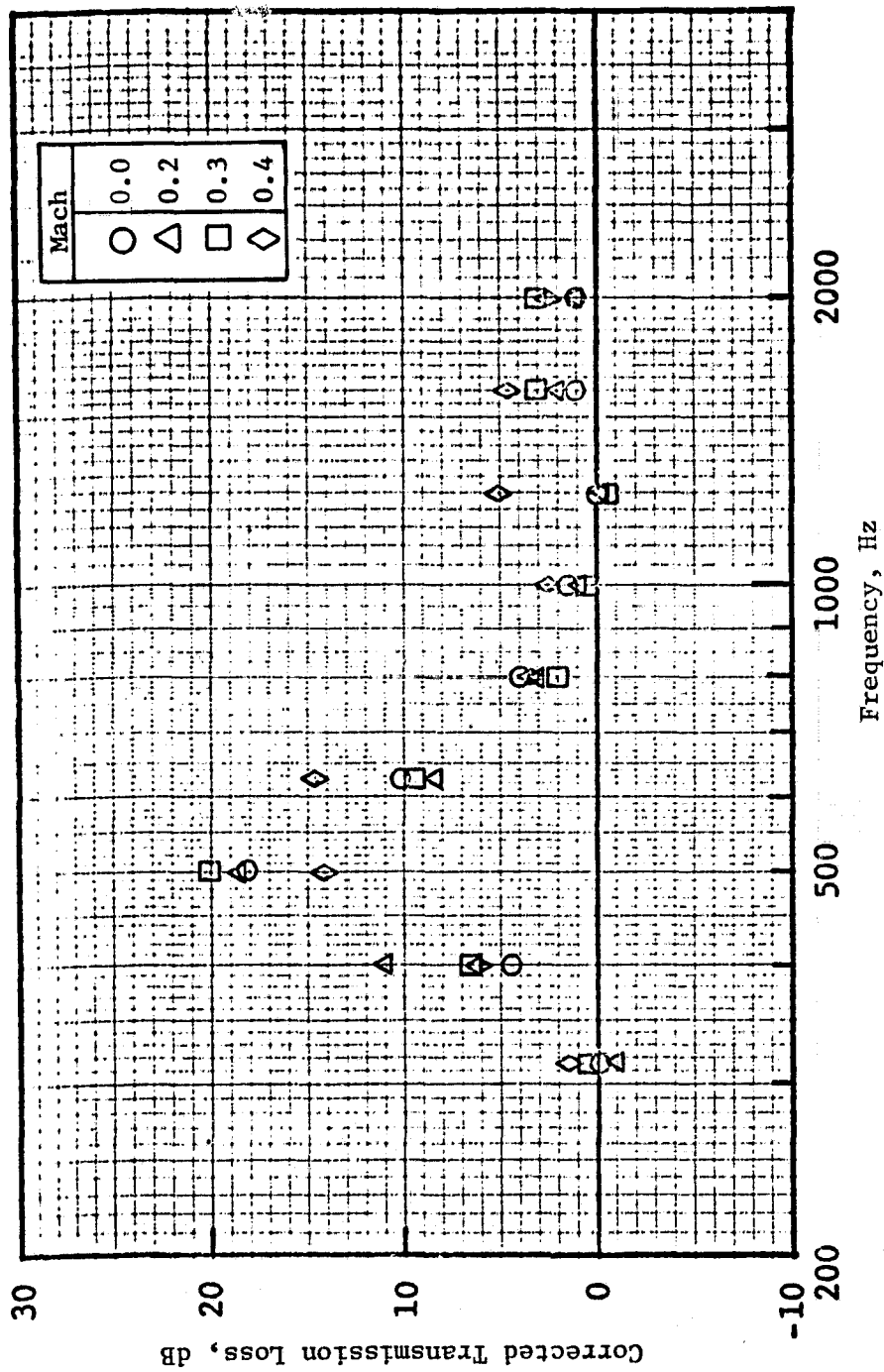


Figure 140. Cold Flow Acoustic Duct Data, Configuration 5 Folded Quarter-Wave Resonator, 12.7 cm (5 in.), Slots Forward, $L/H = 4.05$ in.

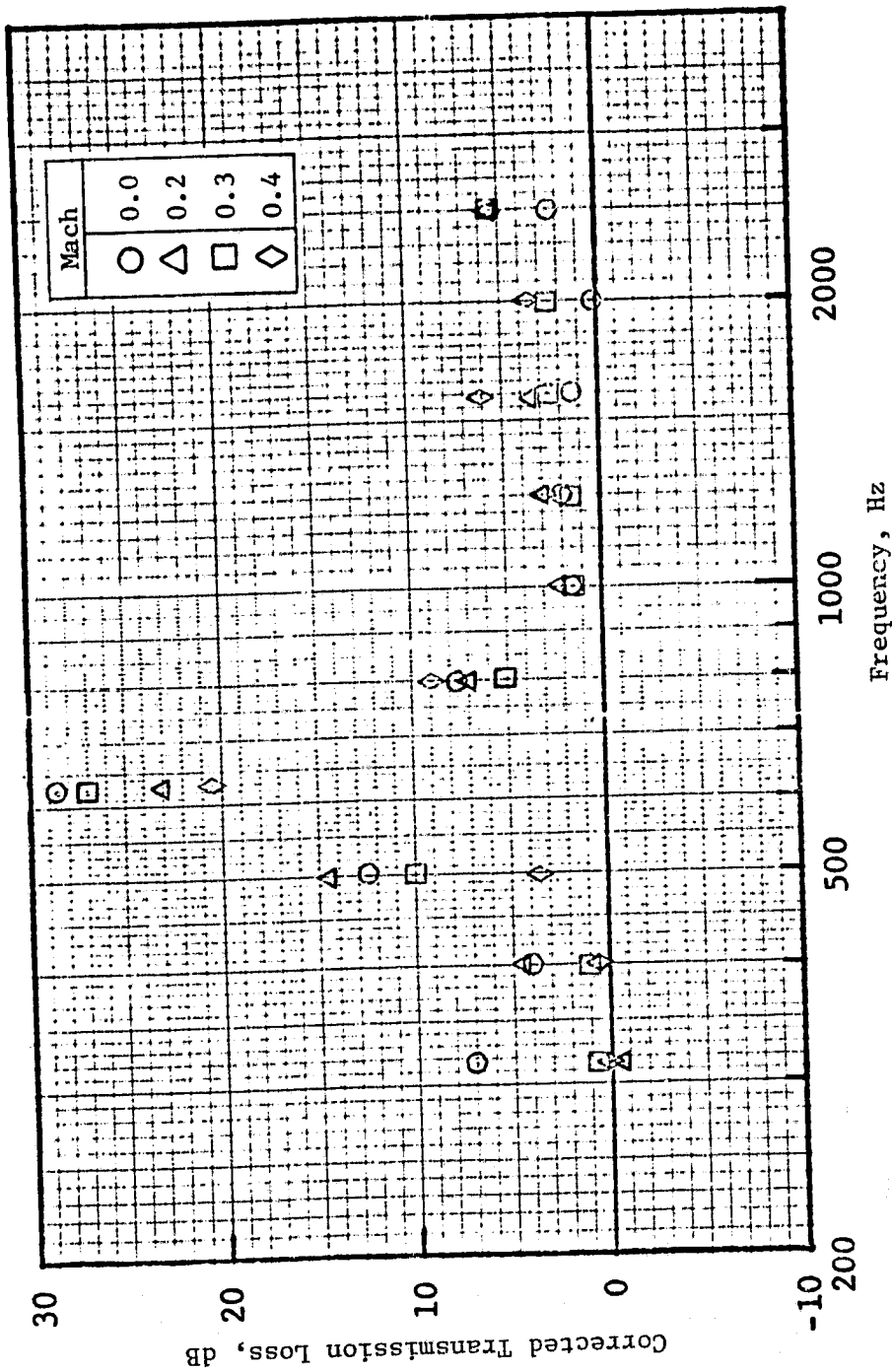


Figure 141. Cold Flow Acoustic Duct Data, Configuration 6 Folded Quarter-Wave Resonator, 10.2 cm (4 in.), Slots Forward, L/H = 4.6.

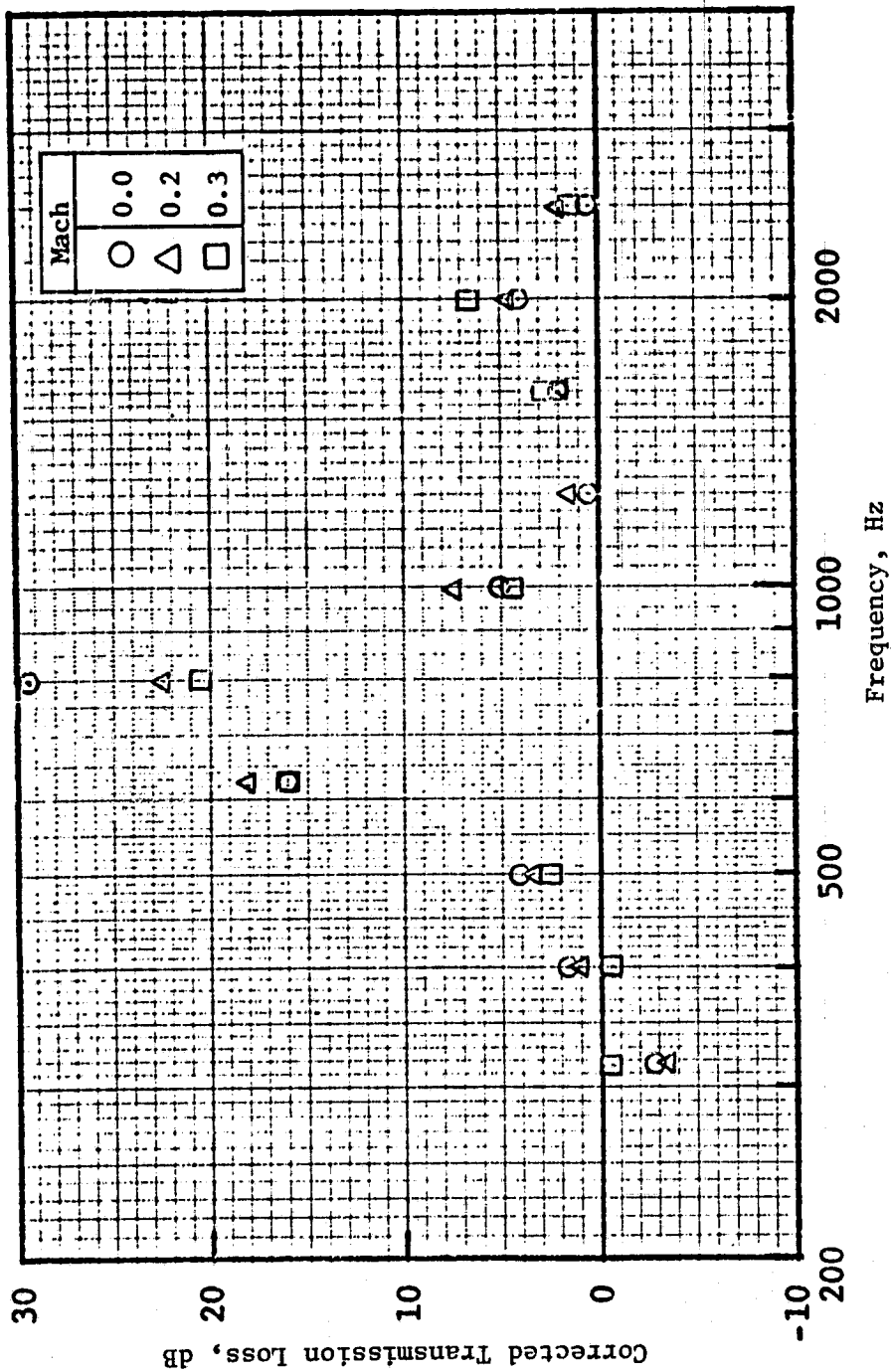


Figure 142. Cold Flow Acoustic Duct Data, Configuration 7 Folded Quarter-Wave Resonator, 7.62 cm (3 in.), Slots Forward, $L/H = 3.8$.

the peak frequency to occur at 800 Hz. The peak suppression level is approximately the same as shown for Configuration 6 in Figure 141.

Since the data have shown that this suppressor concept can be designed with different frequencies of peak-attenuation by varying the panel "L" length, Configuration 8 was designed with panels having "L" lengths of 12.7 cm (5 in.) and 7.62 cm (3 in.) in an effort to improve the suppression bandwidth. The data for the configuration shown in Figure 143 do not indicate a significant bandwidth improvement. In fact, the peak attenuation frequency of 630 Hz is not surprising since the two panels when tested independently showed peak suppression frequencies of 500 and 800 Hz.

Dual-Layer SDOF Dissipative Suppressor

The next series of tests was performed to evaluate the dual-layer SDOF dissipative low-frequency suppressor concept. Figure 144 defines the exact configurations tested, which were installed in test trays similar to the folded quarter-wave samples. Each configuration was constructed to maintain a peak suppression around 800 Hz by varying the porosity and cavity depth (as shown on Figure 144) while holding the faceplate thickness constant at 1.01 cm (0.4 in.). The tuning frequency was determined by the equations in Reference 5. Testing was conducted for various L/H's and both sides versus one side of the duct treated. Figures 145 through 152 present the corrected transmission loss results. Data are shown for duct Mach numbers of 0, 0.3, and 0.4.

Data for Configuration 2 (defined in Figure 144) are given in Figure 145. The suppression peaks at 800 Hz give 12 dB at zero Mach number.

Figure 146 gives data for Configuration 3 that are also defined in Figure 144. The panel design differs from Configuration 2 in that the porosity is increased from 5% to 10% and the cavity depth increased from 2.54 to 4.06 cm (1.0 to 1.6 in.). Also the hole diameter was increased from 0.87 to 1.27 cm (0.3438 to 0.5 in.). The results show the tuning frequency to be at 800 Hz. The peak suppression level relative to that given for Configuration 2 increased significantly, advancing to about 20 dB from the roughly 12 dB of Configuration 2.

Figure 147 gives data for Configuration 4. The design for this configuration utilizes an increased porosity of 15% instead of 10%, an increased cavity depth from 5.58 cm versus the earlier 4.06 cm (2.2 versus 1.6 in.) and a larger hole diameter. The suppression for this design peaks at 630 Hz rather than 800 Hz; however, a high suppression level is seen also at 800 Hz. The peak suppression level is about the same as that measured for Configuration 3.

Configuration 5 has yet an additional increase in cavity depth and faceplate porosity. The results for this configuration are given in Figure 147. In Configuration 6 the panel design of Configuration 5 is maintained,

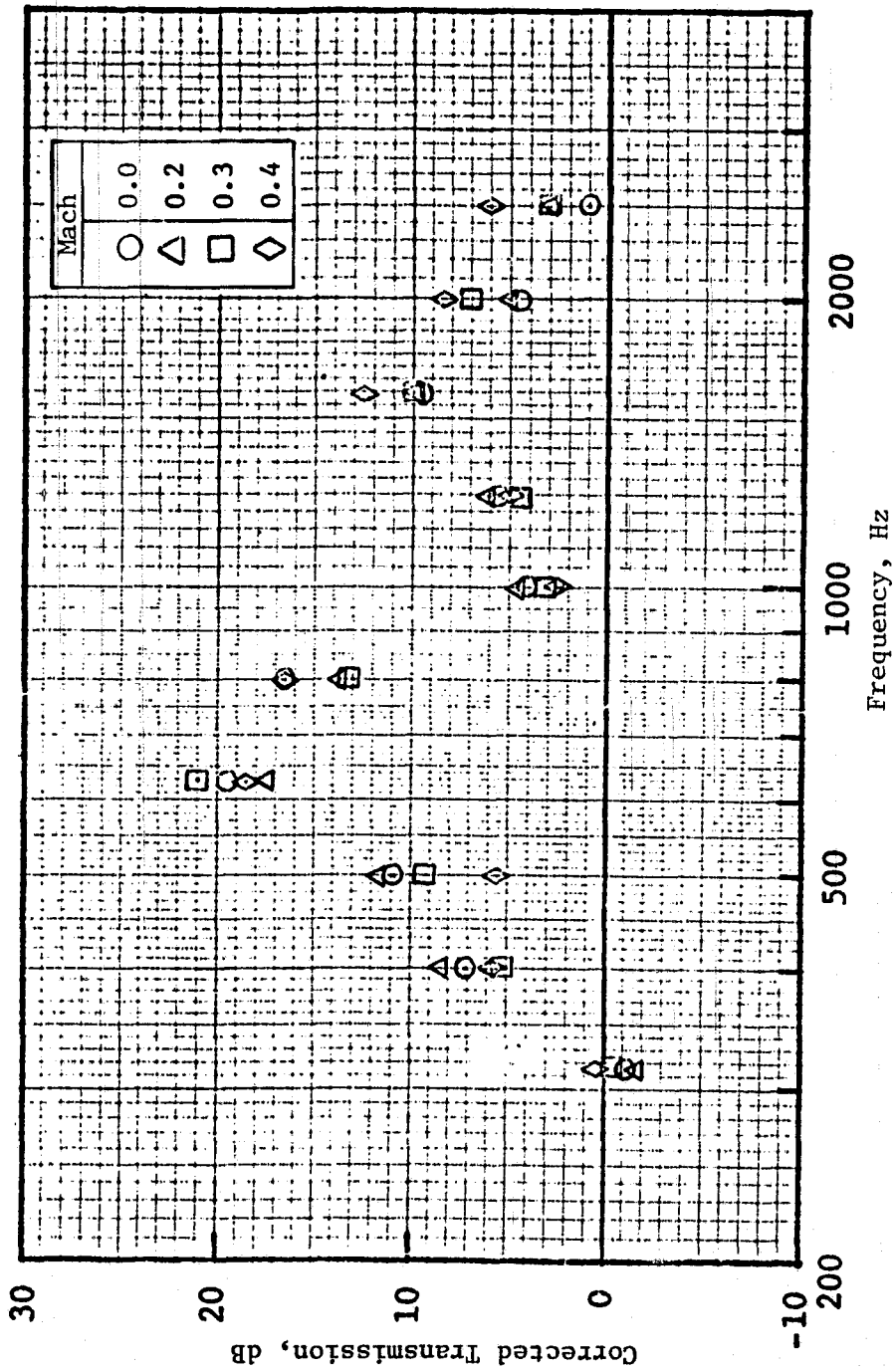







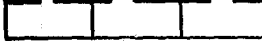



Figure 143. Cold Flow Acoustic Duct Data, Configuration 8 Folded Quarter-Wave Resonator, 7.62 cm (3 in.) and 12.7 cm (5 in.), Slots Forward, $L/H = 4.6$.

- All Dimensions are cm (inch)
- OA = Open Area
- L/H = Length-to-Height-Ratio

1. Hard Wall Base Configuration		
2. 5% OA, L/H = 3.6 Both Sides	Cavity Depth = 2.54 (1.0)	Hole Diam = 0.87 (0.3438) 
3. 10% OA, L/H = 3.6 Both Sides	Cavity Depth = 4.06 (1.6)	Hole Diam = 1.27 (0.5) 
4. 15% OA, L/H = 3.6 Both Sides	Cavity Depth = 5.6 (2.2)	Hole Diam = 1.51 (0.5938) 
5. 20% OA, L/H = 3.6 Both Sides	Cavity Depth = 7.1 (2.8)	Hole Diam = 1.75 (0.6875) 
6. 20% OA, L/H = 2.4 Both Sides	Cavity Depth = 7.1 (2.8)	Hole Diam = 1.75 (0.6875) 
7. 26.5% OA, L/H = 3.6 Both Sides	Cavity Depth = 7.1 (2.8)	Hole Diam = 2.02 (0.7969); 
8. 26.5% OA, L/H = 1.8 Treated One Side Only	Cavity Depth = 7.1 (2.8)	Hole Diam = 2.02 (0.7969) 
9. 20% OA, L/H = 3.6 Three Tuning Frequencies Both Sides	Cavity Depth = 7.1 (2.8) 5.6 (2.2) 4.1 (1.6)	Hole Diam = 1.75 (0.6875) 

All faceplates for low-frequency treatment were 1.02-cm (0.4 in.) thick.
No high-frequency treatment was used.

Figure 144. Definition of Dual-Layer SDOF Dissipative Treatment Test Configurations.

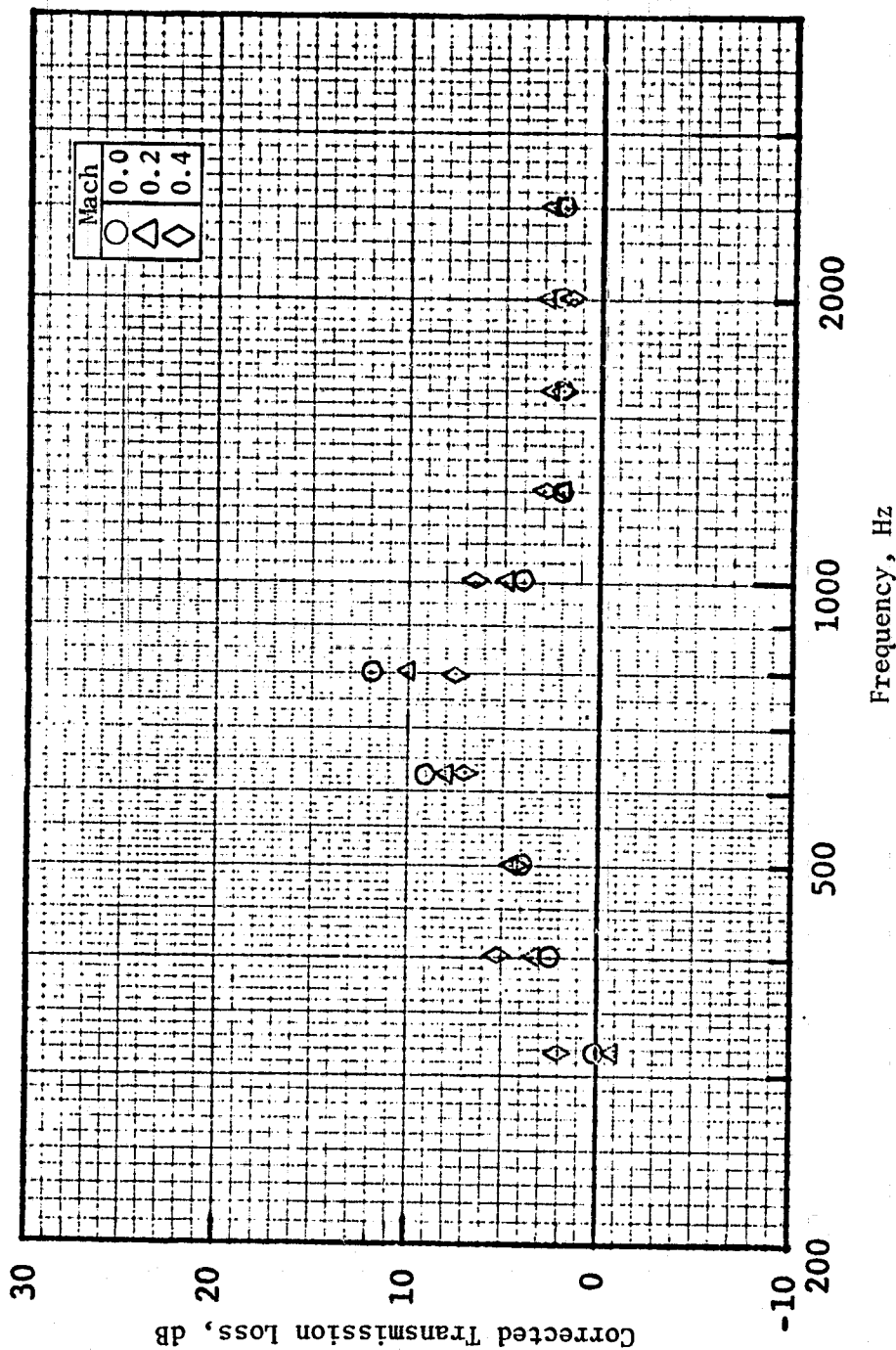


Figure 145. Cold Flow Acoustic Duct Data, Configuration 2
Dual-Layer SDOF Treatment, $L/H = 3.6$.

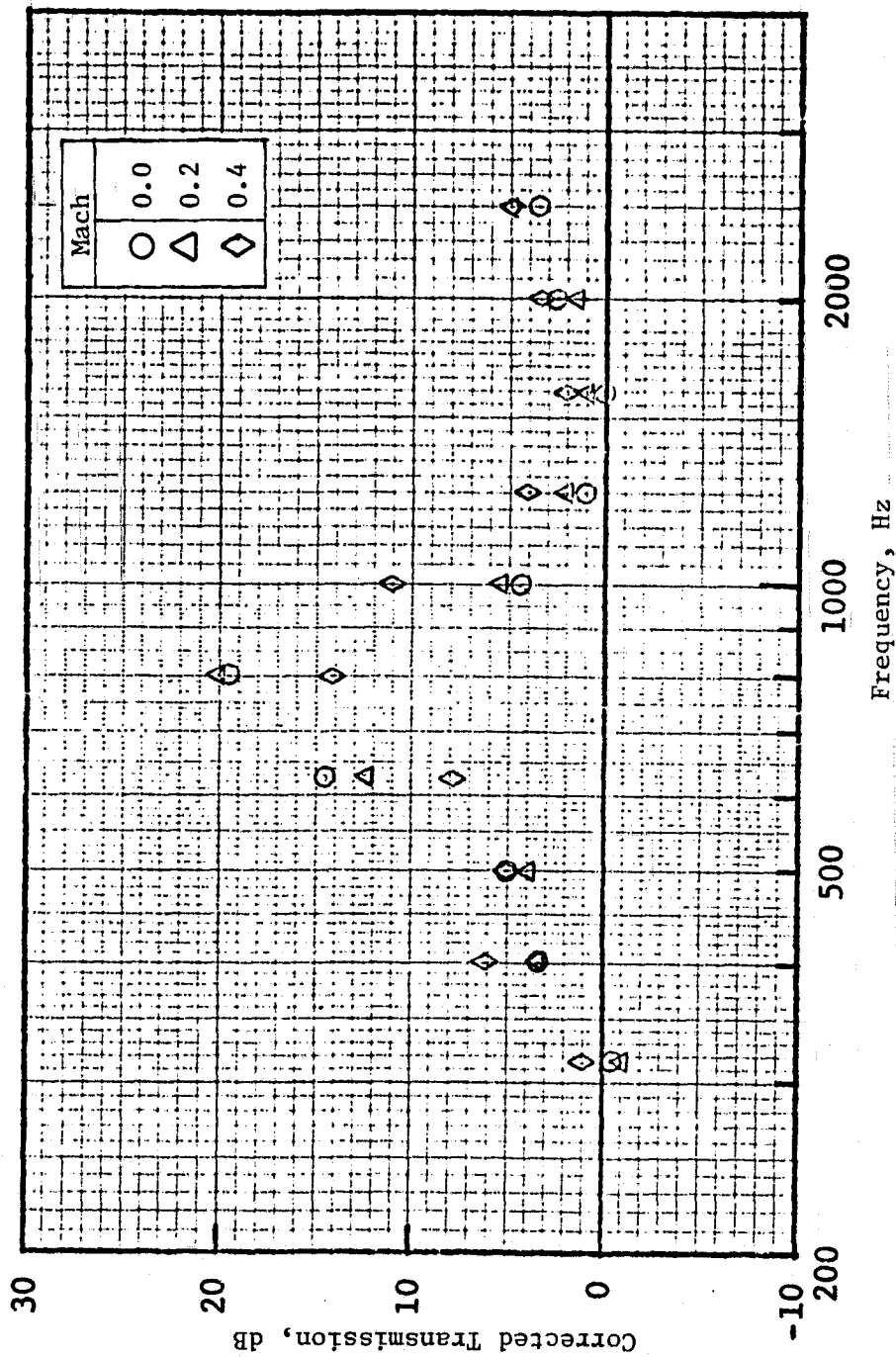


Figure 146. Cold Flow Acoustic Duct Data, Configuration 3 Dual-Layer SDOF Treatment, $L/H = 3.6$.

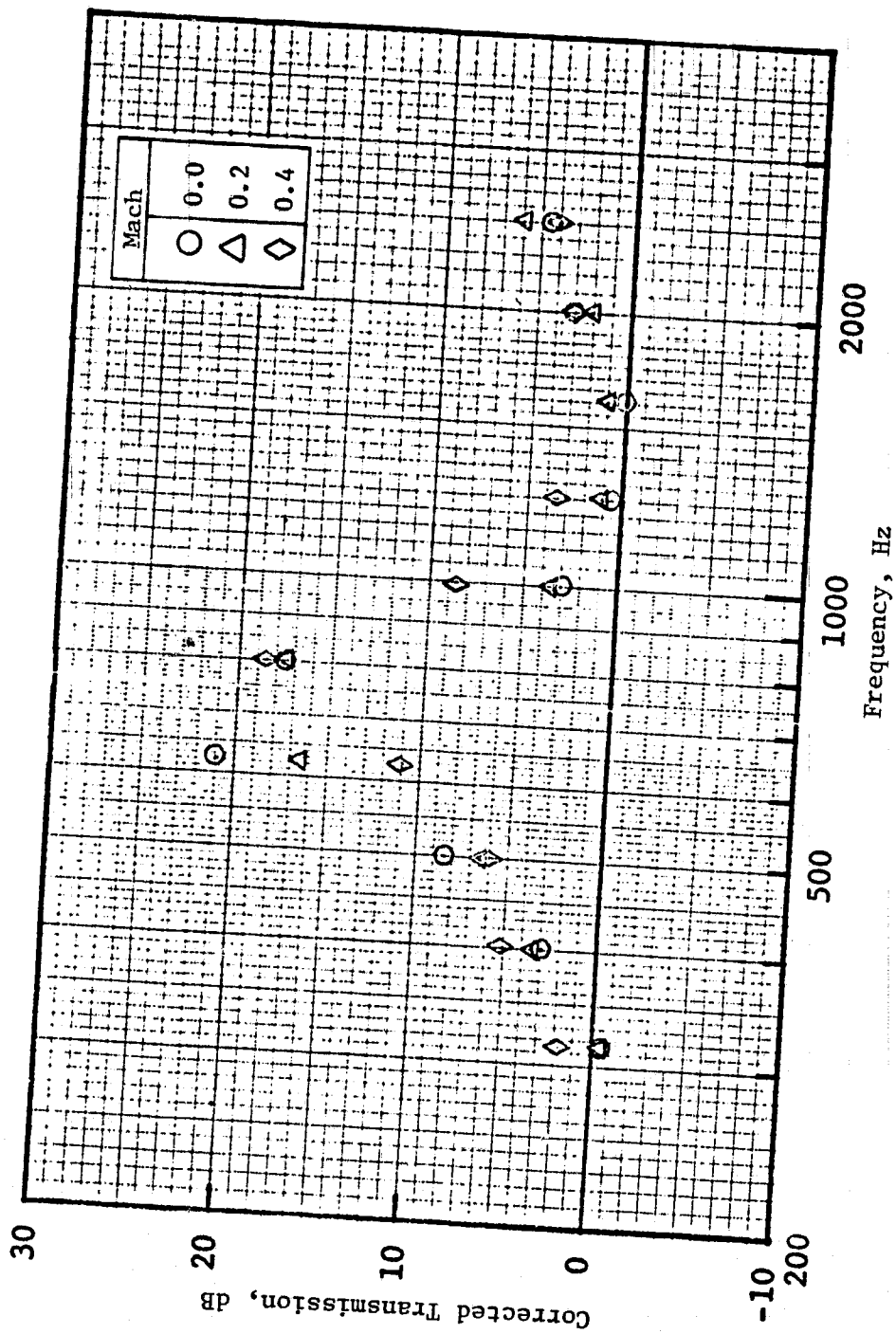


Figure 147. Cold Flow Acoustic Duct Data, Configuration 4 Dual-Layer SDOF Treatment, $L/H = 3.6$.

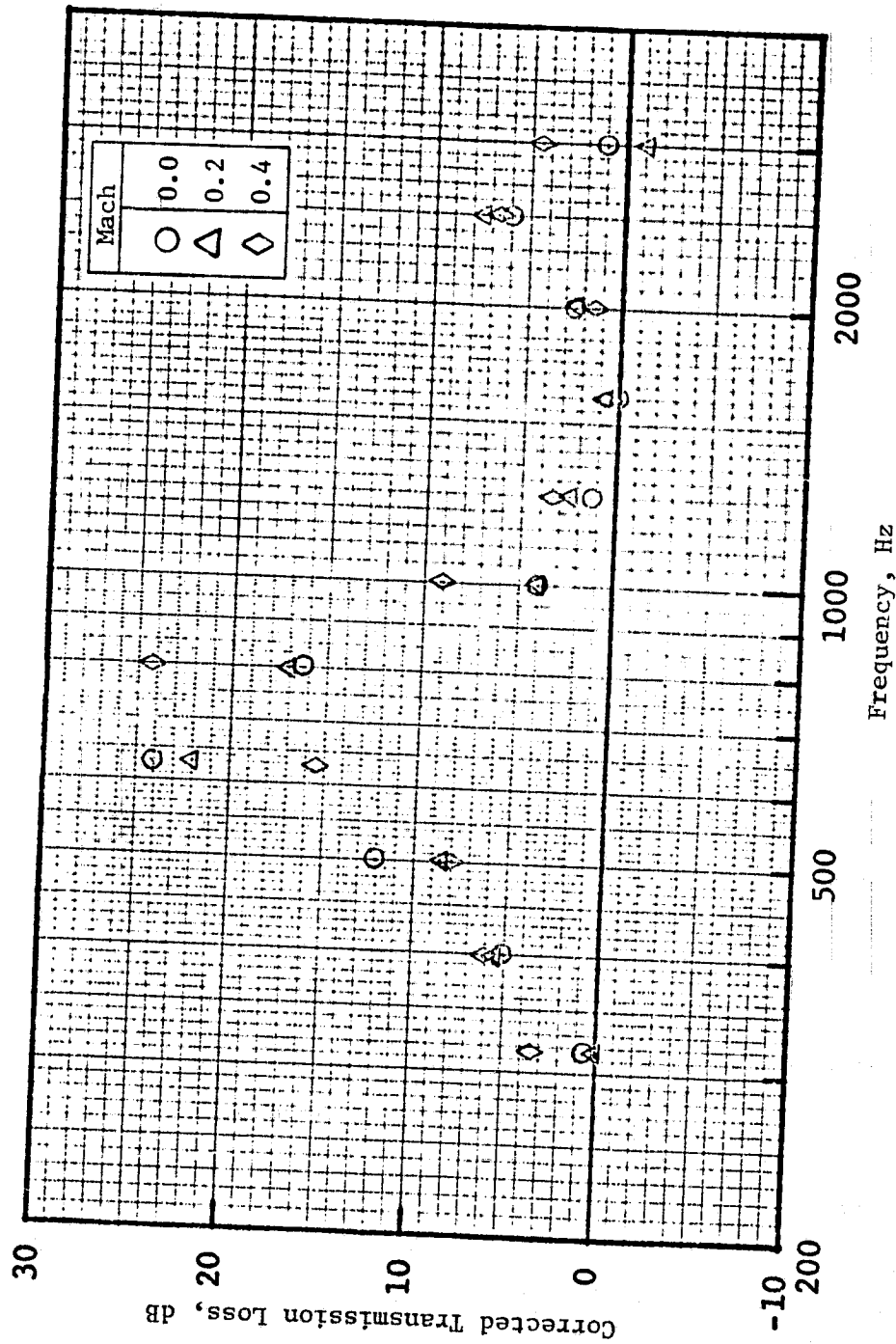


Figure 148. Cold Flow Acoustic Duct Data, Configuration 5 Dual-Layer SDOF Treatment, $L/H = 3.6$.

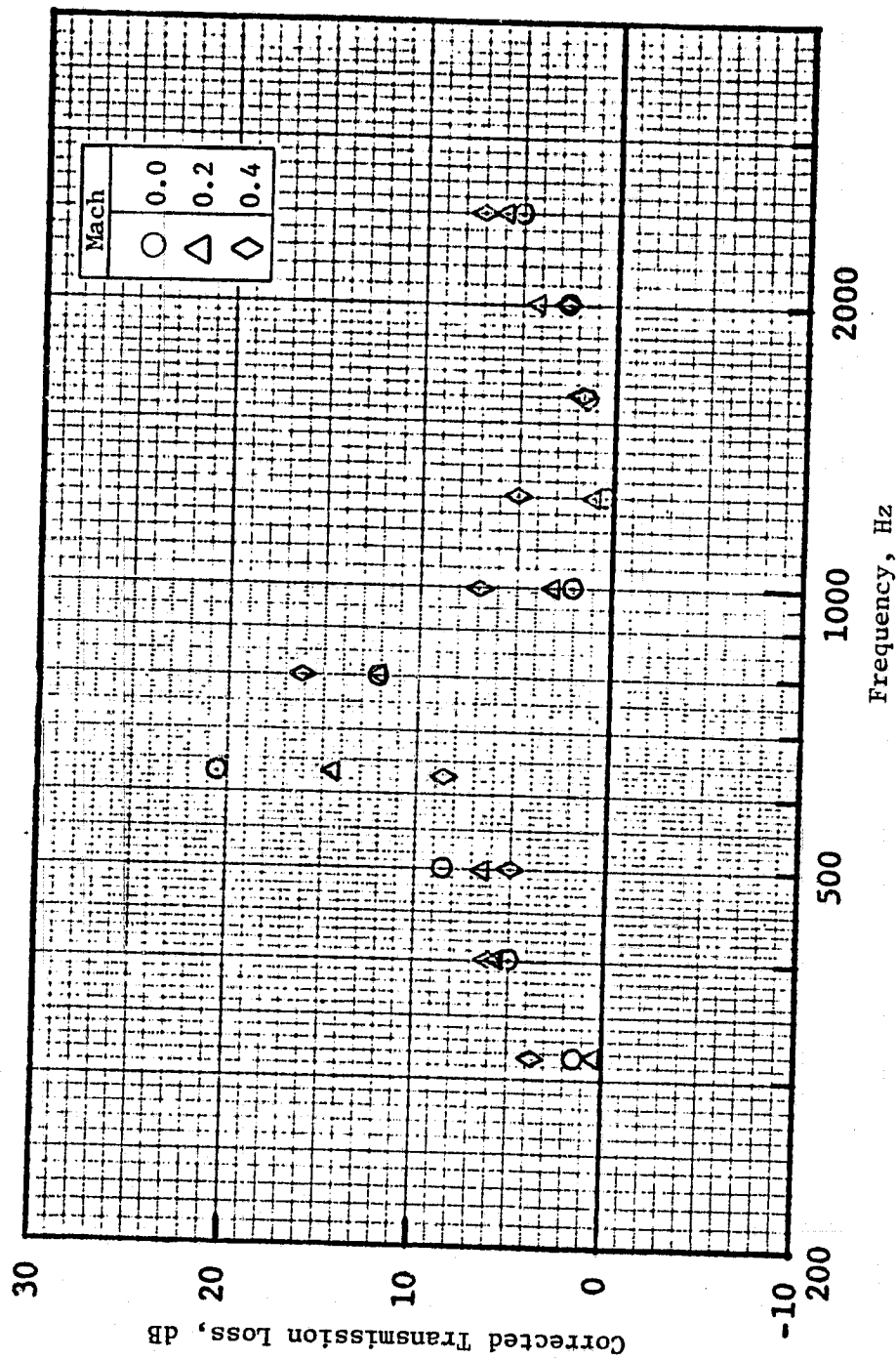


Figure 149. Cold Flow Acoustic Duct Data, Configuration 6 Dual-Layer SDOF Treatment, $L/H = 2.4$.

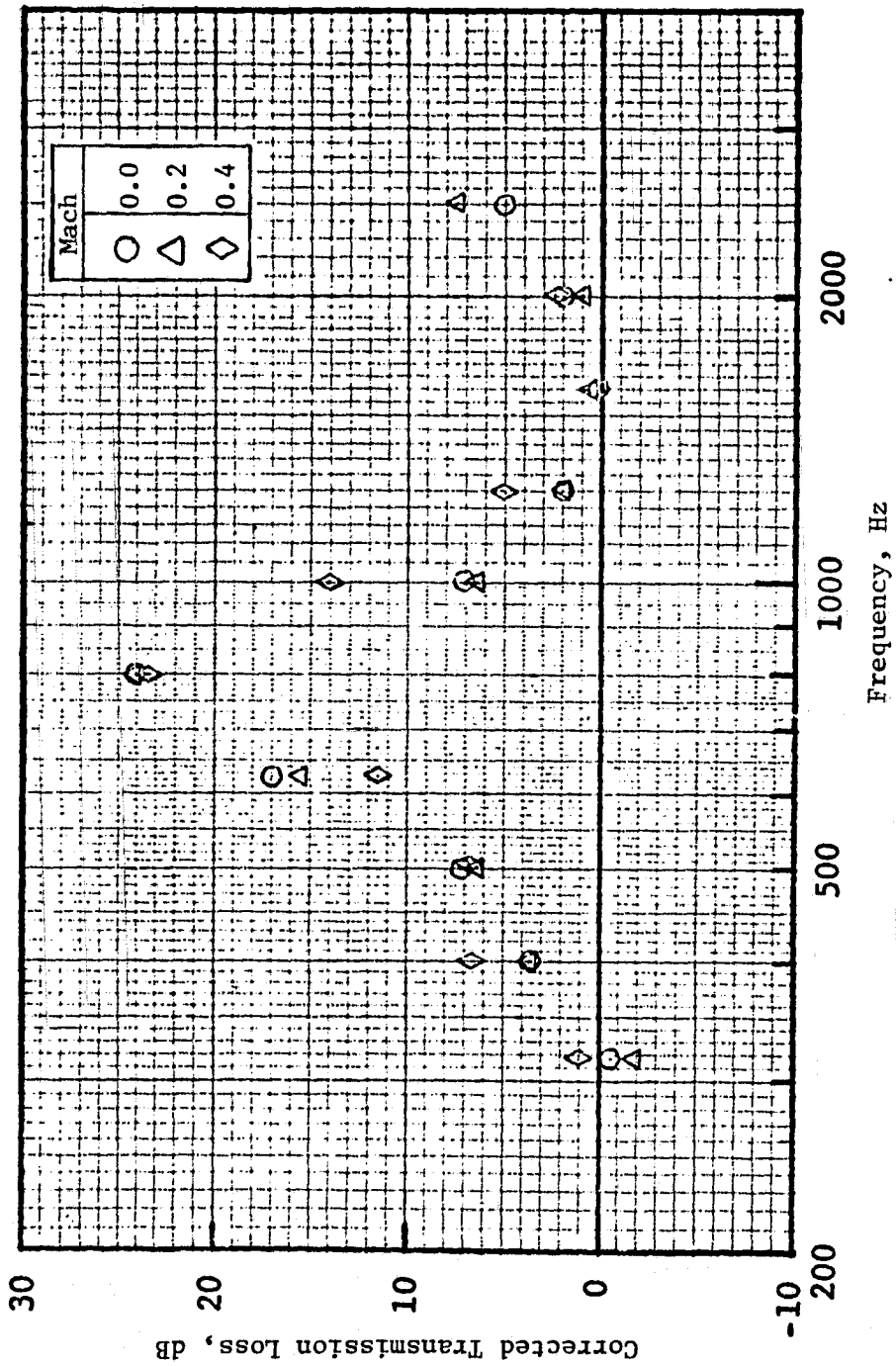


Figure 150. Cold Flow Acoustic Duct Data, Configuration 7 Dual-Layer SDOF Treatment, L/H = 3.6.

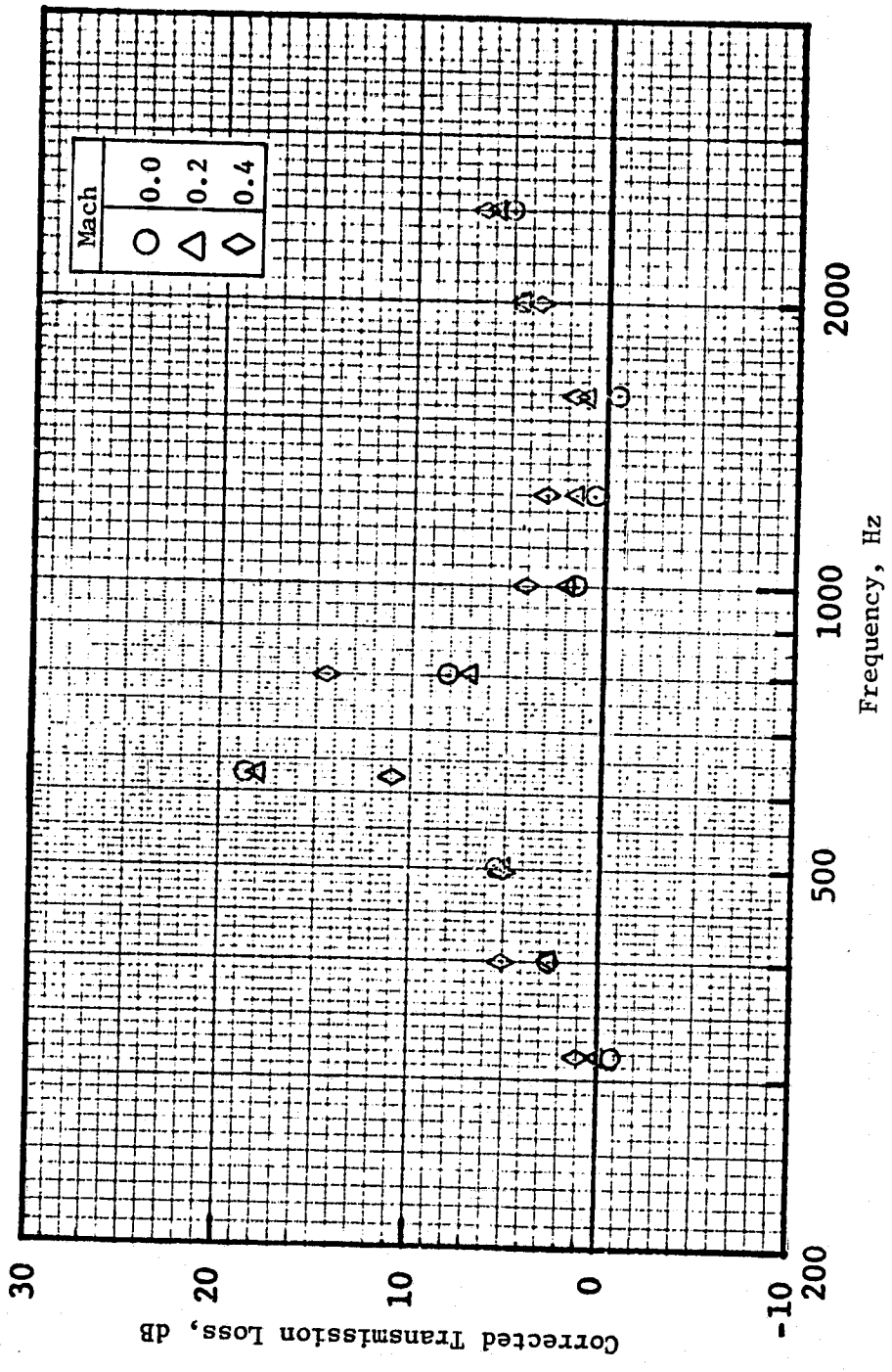


Figure 151. Cold Flow Acoustic Duct Data, Configuration 8 Dual-Layer SDOF Treatment, L/H = 3.6.

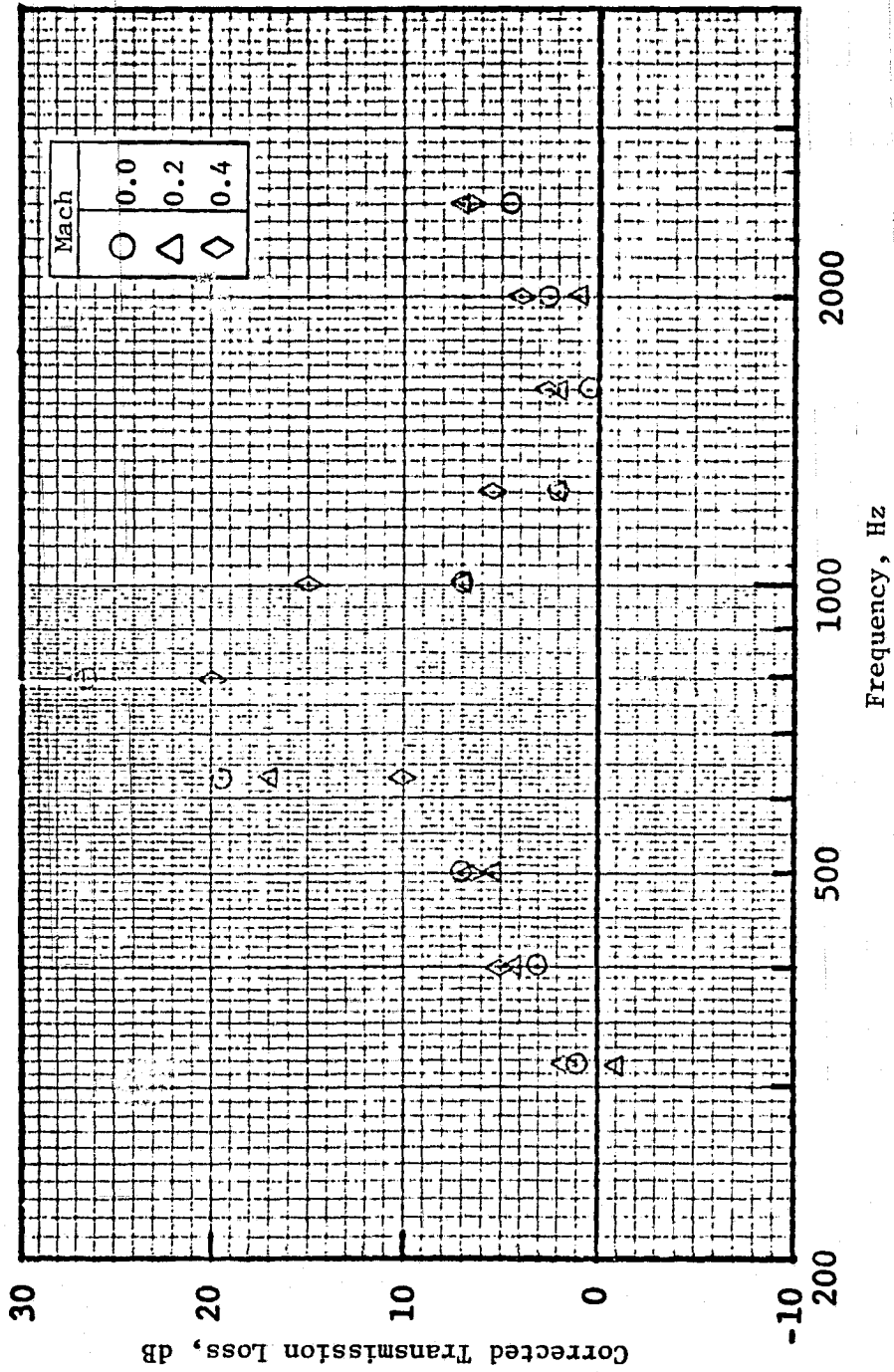


Figure 152. Cold Flow Acoustic Duct Data, Configuration 9 Dual-Layer SDOF Treatment, L/H = 3.6.

but the L/H parameter is reduced. A comparison of the suppression spectra, which are given in Figure 149, shows that the reduced L/H for Configuration 6 has resulted in better suppression.

Configurations 7 and 8 are for a panel design with 26.5% faceplate porosity and a cavity depth of 7.11 cm (2.8 in.). Configuration 8 has all the treatment on one wall of the duct while Configuration 7 has equal amounts on each wall. Comparison of the data given in Figures 150 and 151 shows a shift in frequency and a decrease in suppression level for the configuration with one wall only treated. No significant changes are noted in the suppression bandwidth.

The final configuration tested in this series of tests is Configuration 9. This design consists of three tuning frequencies obtained by varying the panel depth over three equal segments of treatment length. The faceplate porosity of 20% was held constant for each of the treatment sections. Data for this configuration are shown in Figure 152. The suppression bandwidth is somewhat broader than that for the configurations with single tuning frequencies, demonstrating that an increased bandwidth can be obtained. This increase in bandwidth, however, entails a reduction in the peak suppression level.

The suppression data as measured for each of the panels described in Figure 144 are summarized in Figure 153. Data are given for faceplate porosity variations from 5 through 26% as measured at a duct Mach number of 0.4. All the data were taken for an L/H of 3.6. The results show that the peak suppression is a maximum for the 20 and 26.5% porosity values. Therefore the optimum porosity for these conditions is probably somewhere between these two values. The comparison shows little if any impact of porosity on suppression bandwidth.

Low-Frequency Design Concepts Combined with High-Frequency Panel Design

The remainder of cold flow rectangular duct testing combined both the low-frequency suppressor concepts and the high-frequency turbine treatment to determine if the combination improved or deteriorated the overall treatment performance.

The folded quarter-wave suppressor, one section or cavity of which is shown on Figure 154, was constructed of six L-shaped cavities, three on each side of the 12.7-cm (5-in.) duct. The results for Mach number = 0.0, 0.2, and 0.3, and 0.4 are shown in Figures 154 through 157. The dual-layer SDOF Treatment suppressor is schematically shown in Figure 158 and was constructed with similar high-frequency treatment. Figures 158 through 161 show the testing results and comparisons with low-frequency treatment only.

- Mach = 0.4
- L/H = 3.6
- 10.2 by 12.7 cm (4.0 by 5.0 in.) Rectangular Duct

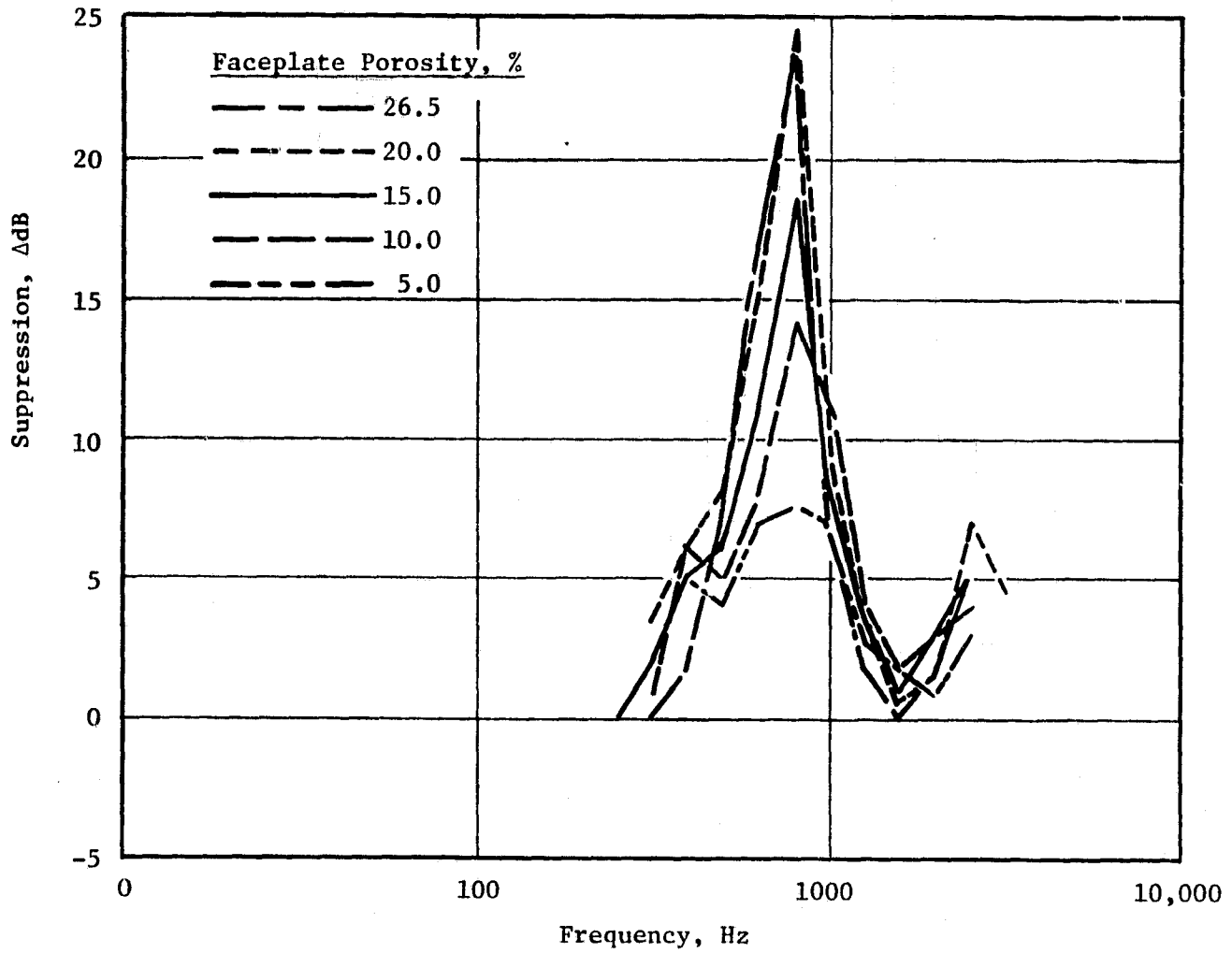


Figure 153. Summary of Dual-Layer SDOF Treatment Suppression Vs. Porosity.

High-Frequency Treatment

- Open Area = 7.5%
- Hole Diam = 0.16 (0.062)
- Faceplate Thickness = 0.08 (0.032)
- Cavity Depth = 0.64 (0.25)

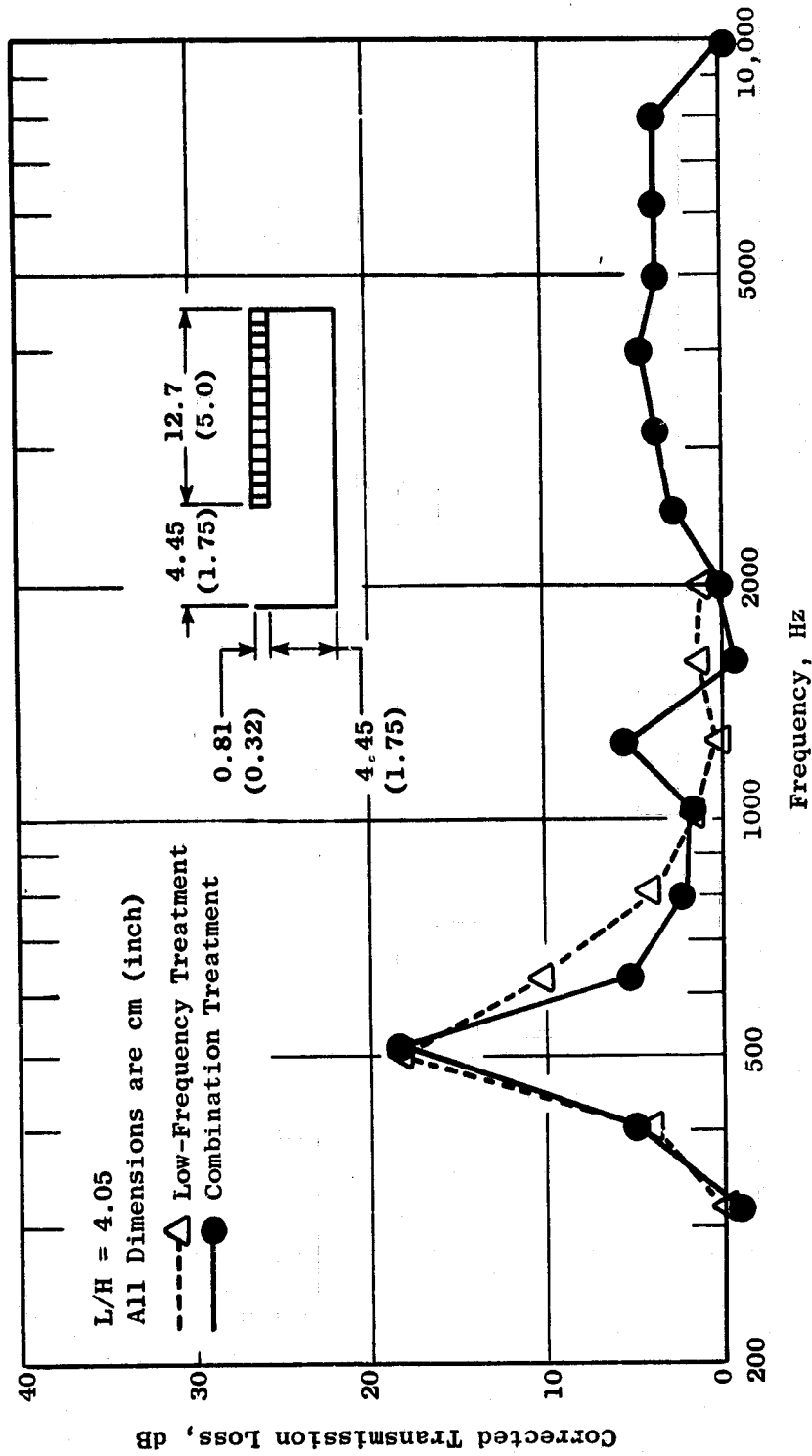


Figure 154. Cold Flow Acoustic Duct Data, Folded Quarter-Wave Suppressor (Two Sides Treated), Mach No. = 0.

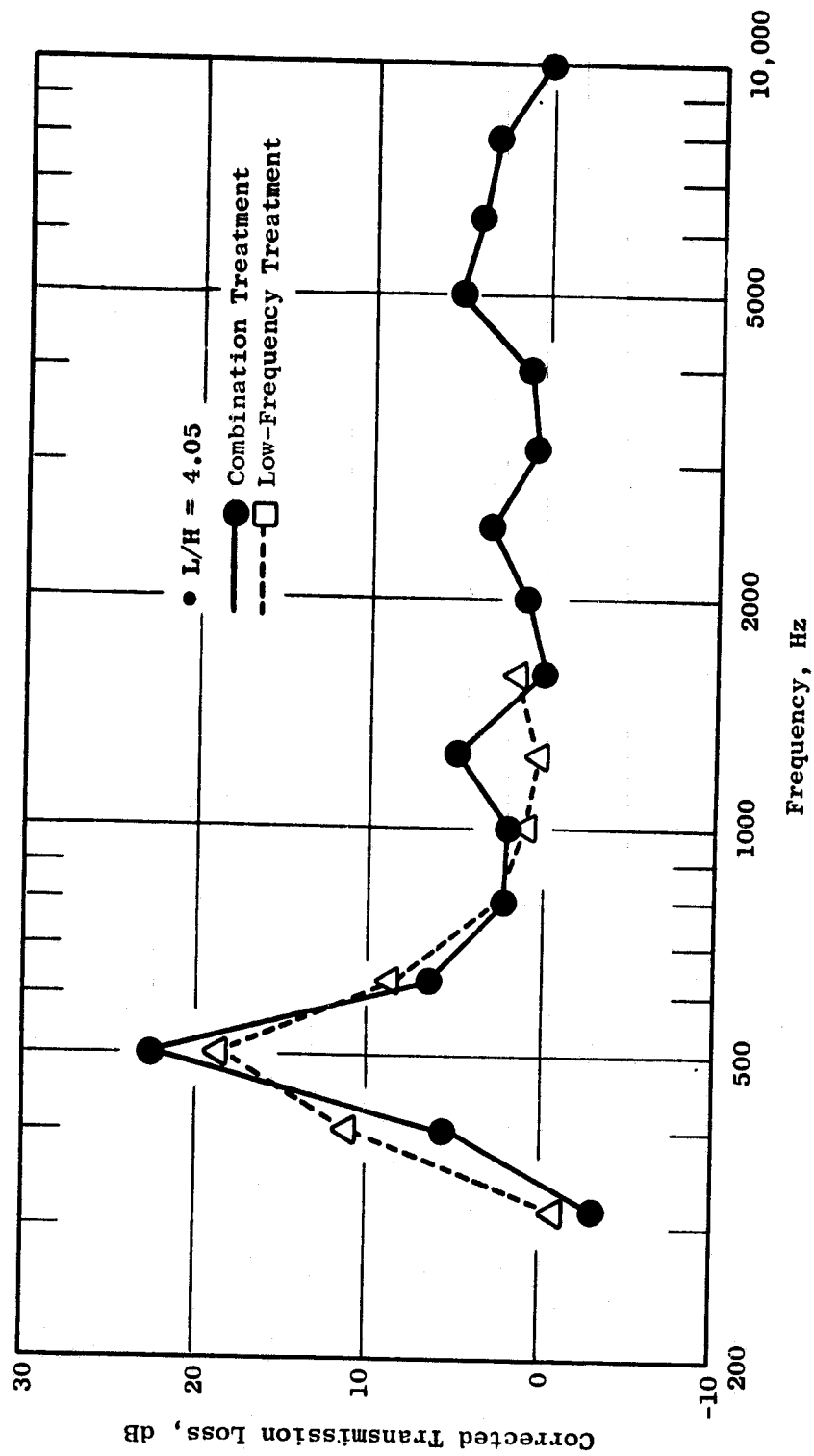


Figure 155. Cold Flow Acoustic Duct Data, Folded Quarter-Wave Suppressor (Two Sides Treated),
 Mach No. = 0.2.

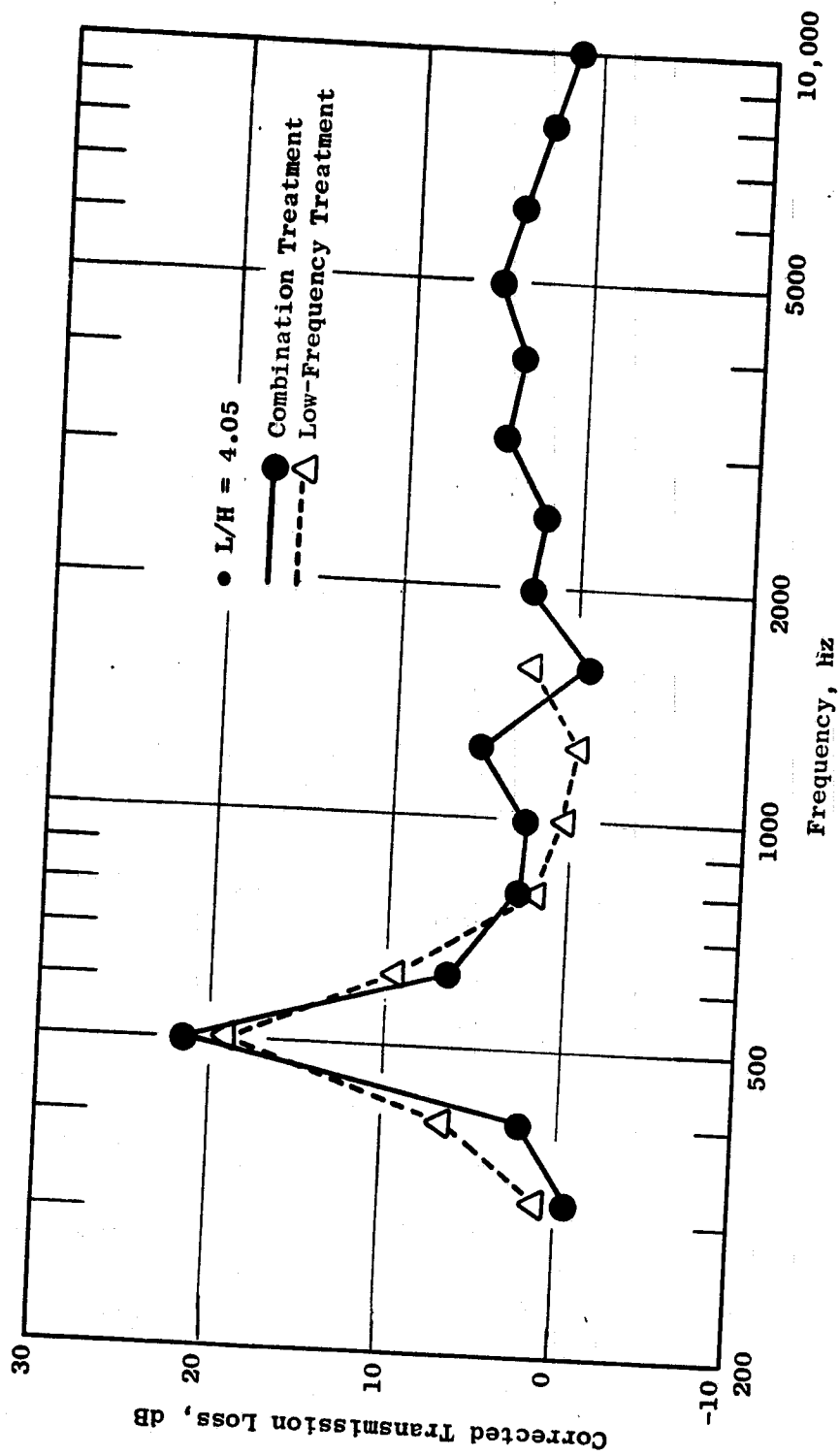


Figure 156. Cold Flow Acoustic Duct Data, Folded Quarter-Wave Suppressor (Two Sides Treated), Mach No. = 0.3.

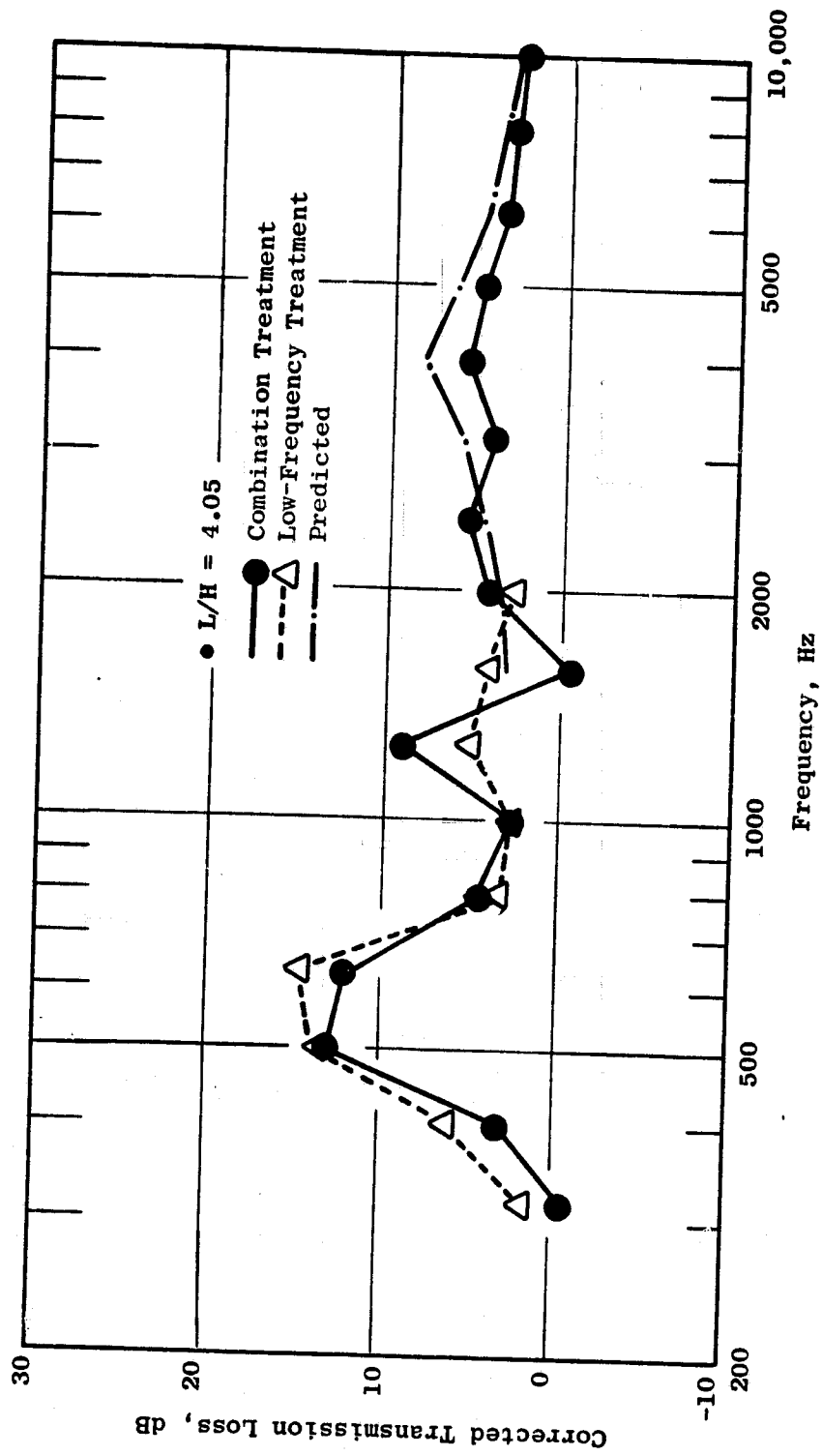


Figure 157. Cold Flow Acoustic Duct Data, Folded Quarter-Wave Suppressor (Two Sides Treated), Mach No. = 0.4.

High-Frequency Treatment

- Open Area = 7.5%
- Hole Diam = 0.16 (0.0625)
- Faceplate Thickness = 0.08 (0.032)
- Cavity Depth = 0.64 (0.25)

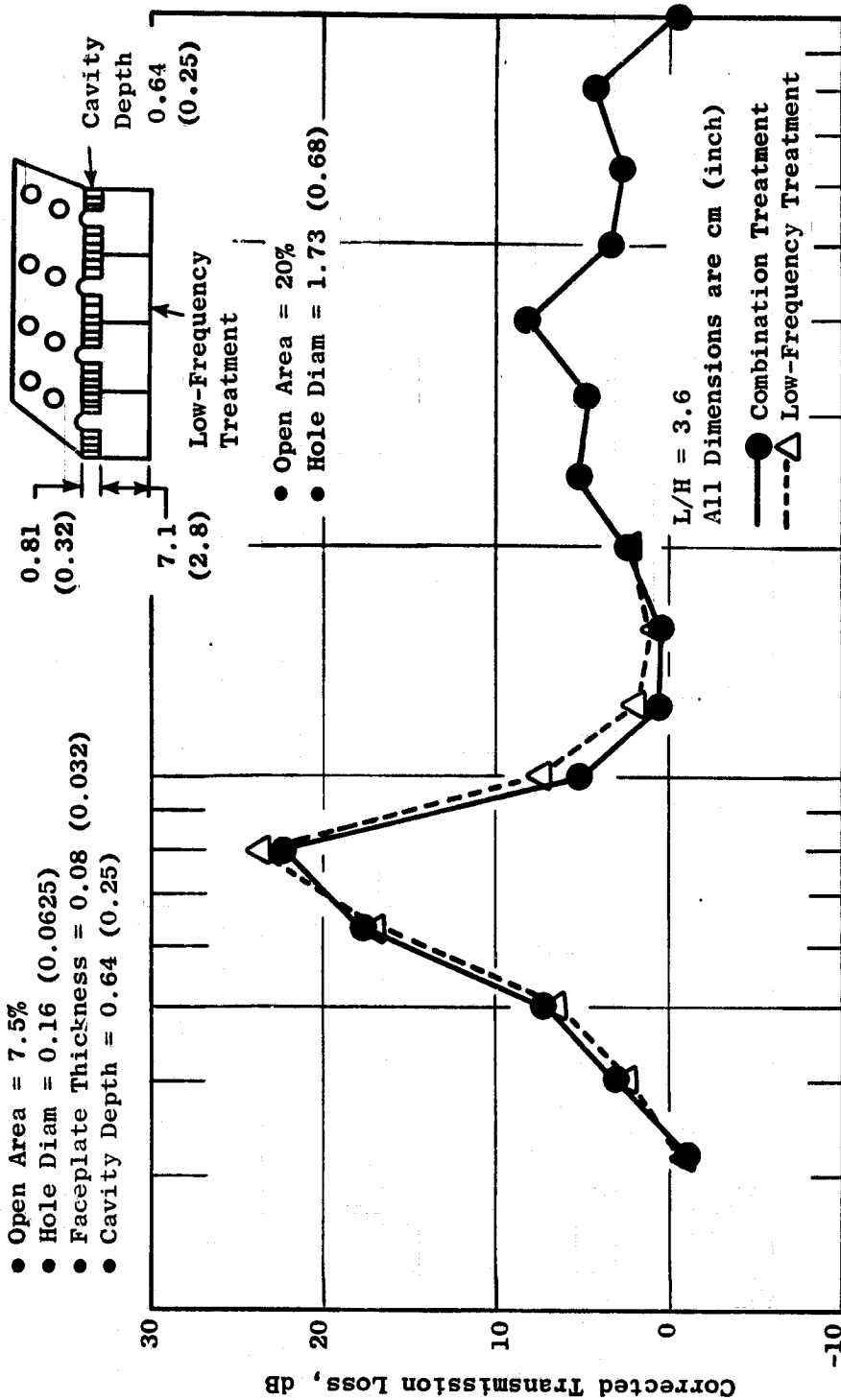


Figure 158. Cold Flow Acoustic Duct Data, Dual-Layer SDOF Treatment (Two Sides Treated), Mach No. = 0.

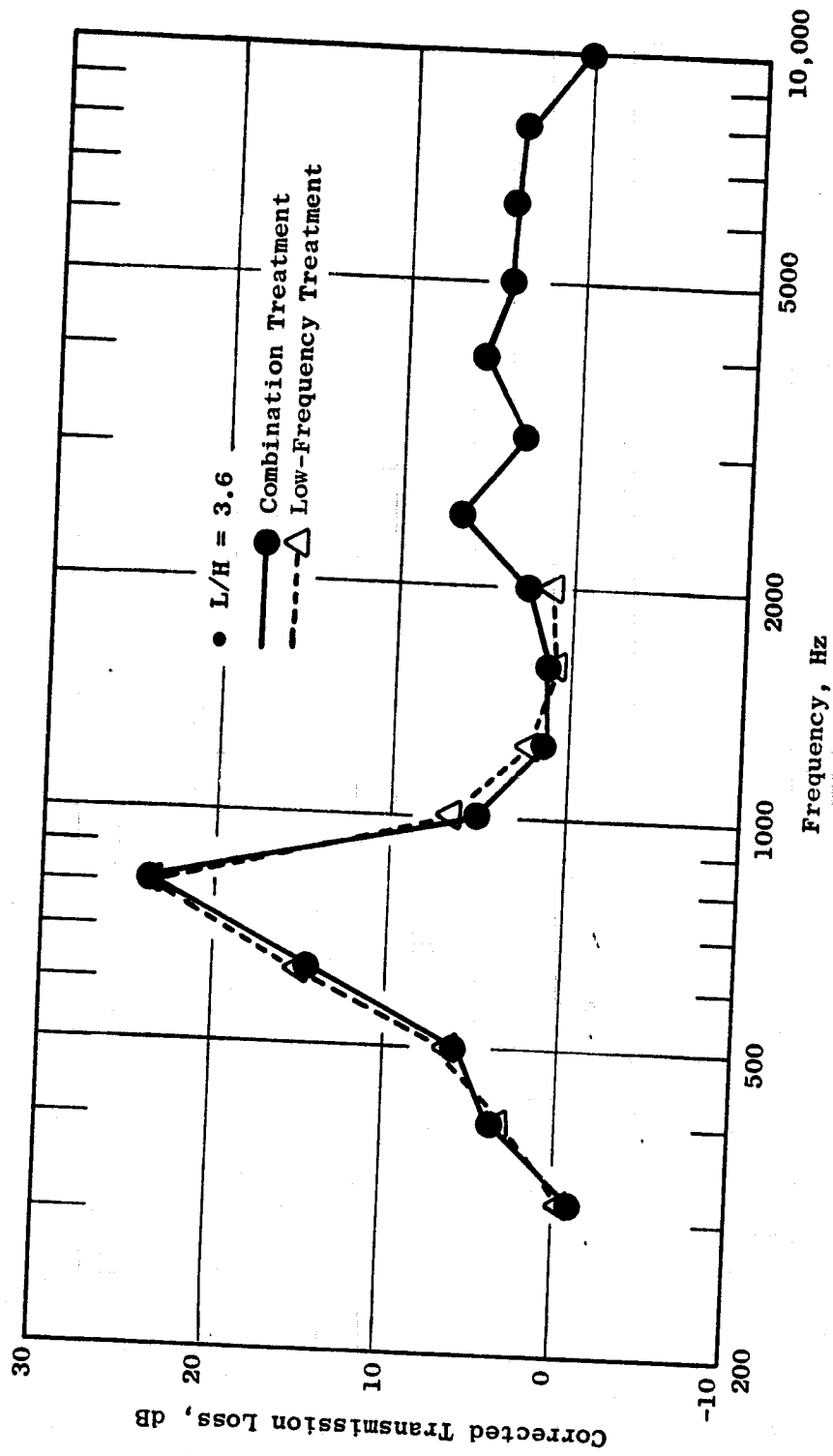


Figure 159. Cold Flow Acoustic Duct Data, Dual-Layer SDOF (Two Sides Treated),
 Mach No. = 0.2.

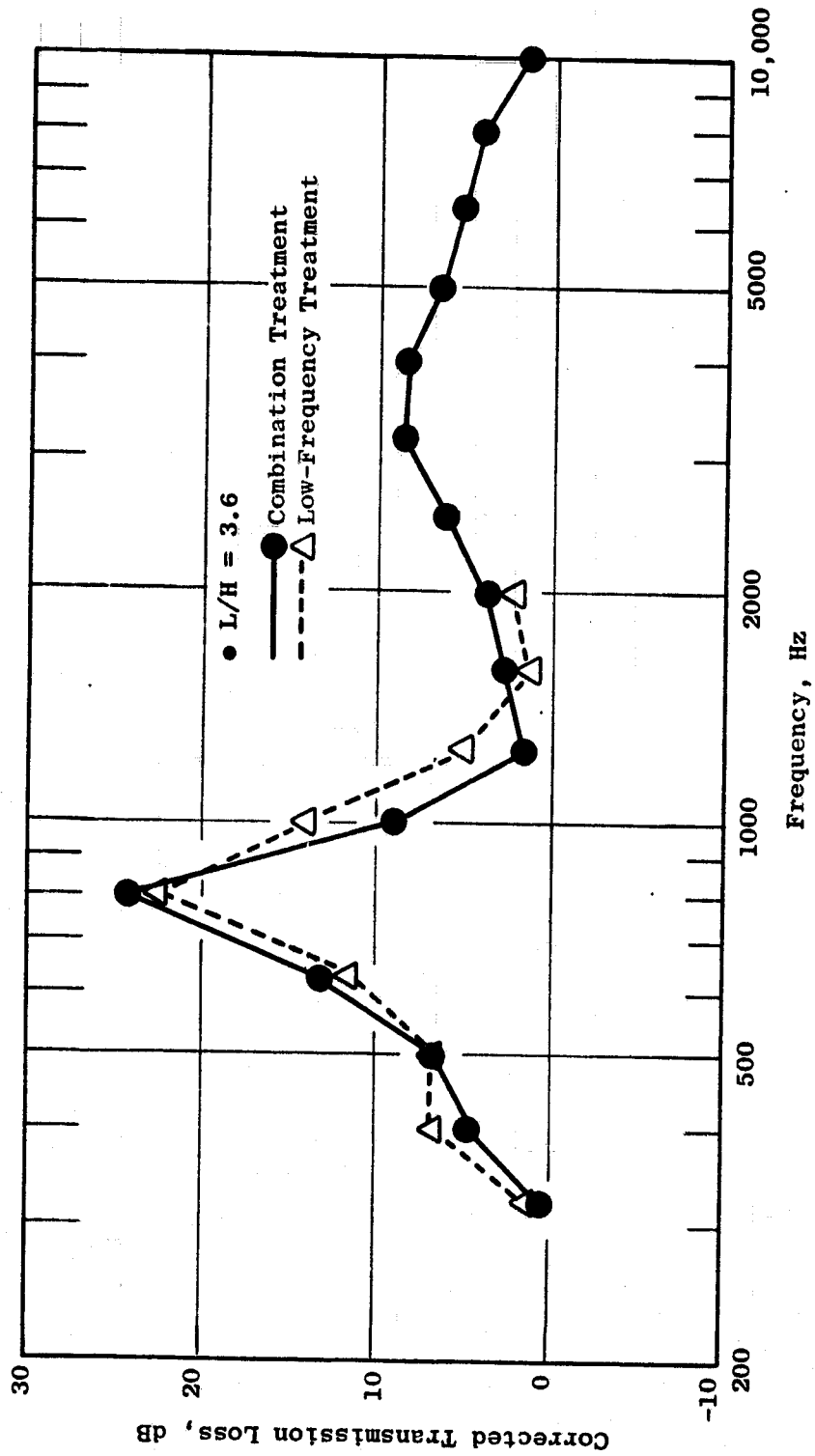


Figure 160. Cold Flow Acoustic Duct Data, Dual-Layer SODF Treatment (Two Sides Treated), Mach No. 0.3.

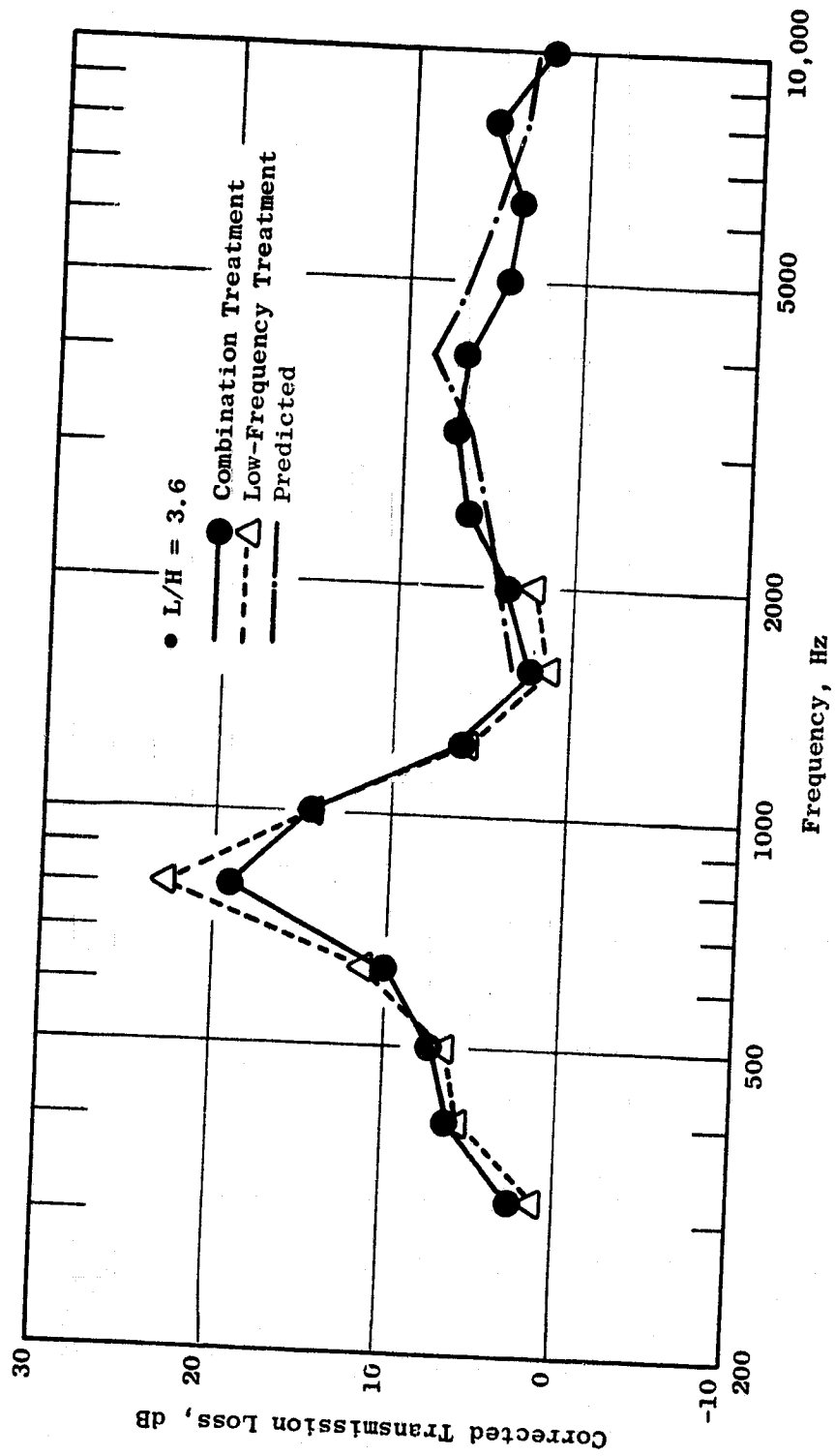


Figure 161. Cold Flow Acoustic Duct Data, Dual-Layer SDOF Treatment (Two Sides Treated),
 Mach No. = 0.4.

The last concept tested, the side-branch resonator, is schematically shown in Figure 162. This concept had not been previously tested and was included in this set of tests to test two hypotheses. First, the side-branch resonators would in practice give acceptable suppression; and second, that they could be tuned to low frequencies for combustor noise suppressor. The tuning frequencies were determined by the methods given in Reference 15, Chapter 21. The 1/3-octave data shown in Figures 162 through 165 support both of these hypotheses.

Figures 154 through 157 give the folded quarter-wave plus high-frequency treatment suppression results for Mach numbers of 0, 0.2, 0.3, and 0.4. The results are compared with the data obtained for the design without the high-frequency treatment. The comparison shows little change in the low-frequency suppression but shows greater high-frequency suppression, the result of the treatment tuned to the high-frequency range. Figure 157 shows the high-frequency results versus predicted suppression based on previous duct data. This comparison indicates that the measured levels are somewhat lower than predicted.

Figures 158 through 161 give results for the dual-layer SDOF treatment equipped with a high-frequency suppressor. Data are shown for duct Mach numbers of 0, 0.2, 0.3, and 0.4. The results are compared with the data obtained for the configuration having low-frequency treatment only. As was the case for the folded quarter-wave suppressor, little suppression difference is seen in the low frequencies. Figure 161 shows the predicted high-frequency suppression versus measured suppression for a duct Mach number of 0.4. The overall agreement between predicted and measured data is good.

The combined high-frequency and low-frequency results for the side-branch resonator are shown in Figures 162 through 165. Data are given for duct Mach numbers of 0, 0.2, 0.3, and 0.40. Since no data were obtained for the low-frequency treatment alone, these are the only data for this design concept. The results for this design are encouraging. The data given in Figure 165 for a duct Mach number of 0.4 show good suppression levels in both the high and low frequencies. Figure 165 gives a comparison of the predicted versus measured high-frequency suppression. The results show good agreement, which indicates that the combination of high- and low-frequency suppressors does not penalize the effectiveness of the high-frequency suppressor.

7.2.2.2 High-Temperature Duct

The High-Temperature Acoustic Duct (HITAD) testing was performed to evaluate viable core suppressor concepts under engine temperature and airflow conditions and to demonstrate the desired QCSEE suppression. Two concepts, the side-branch resonator and the dual-layer SDOF Treatment, were chosen as the most promising engine candidates for testing on the HITAD facility, based on the cold flow duct test results.

High-Frequency Treatment

- Open Area = 7.5%
- Hole Diam = 0.16 (0.0625)
- Faceplate Thickness = 0.08 (0.032)
- Cavity Depth = 0.64 (0.25)

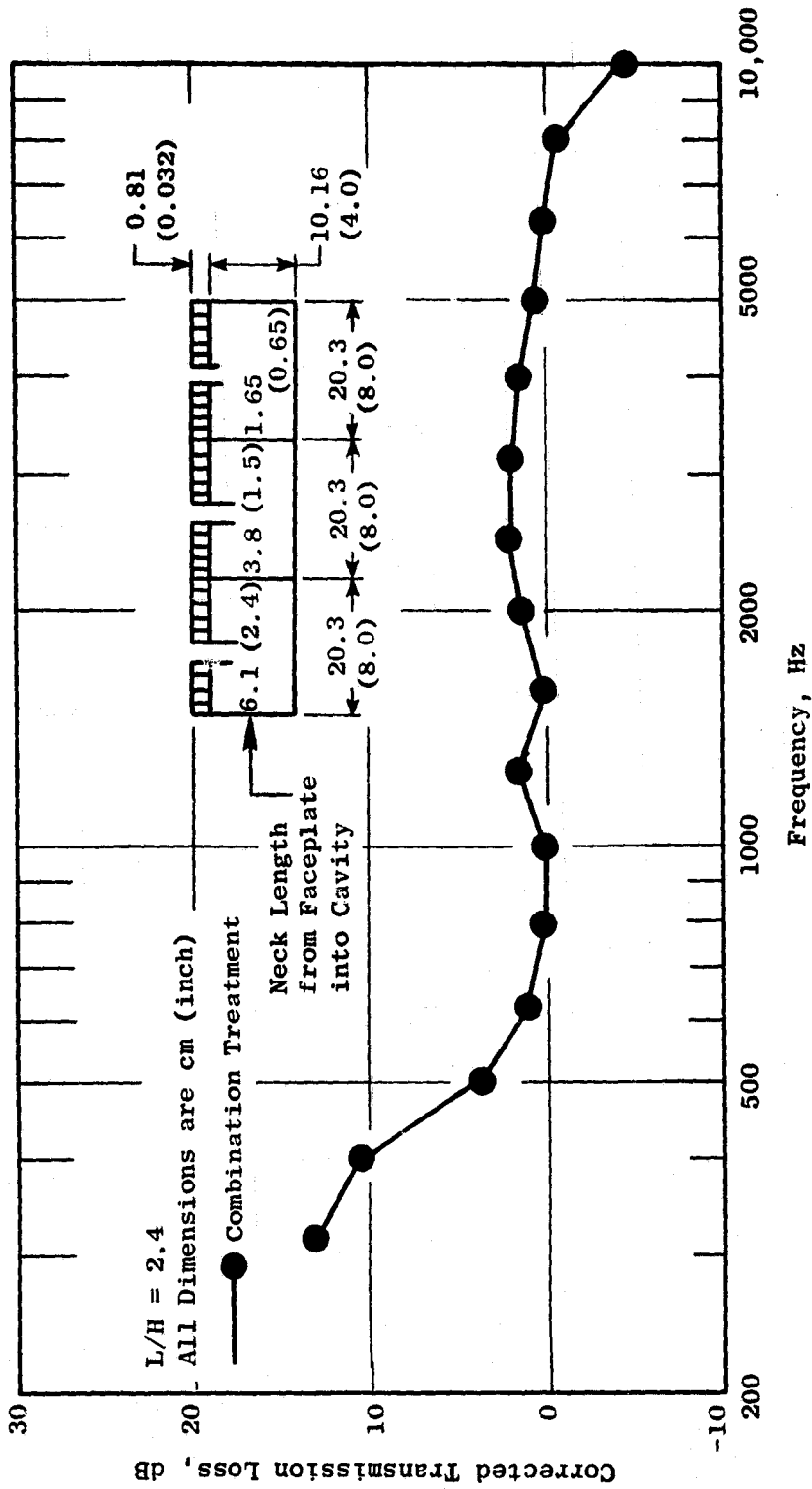


Figure 162. Cold Flow Acoustic Duct Data, Side-Branch Resonator (Treated on One Side), Mach No. = 0.

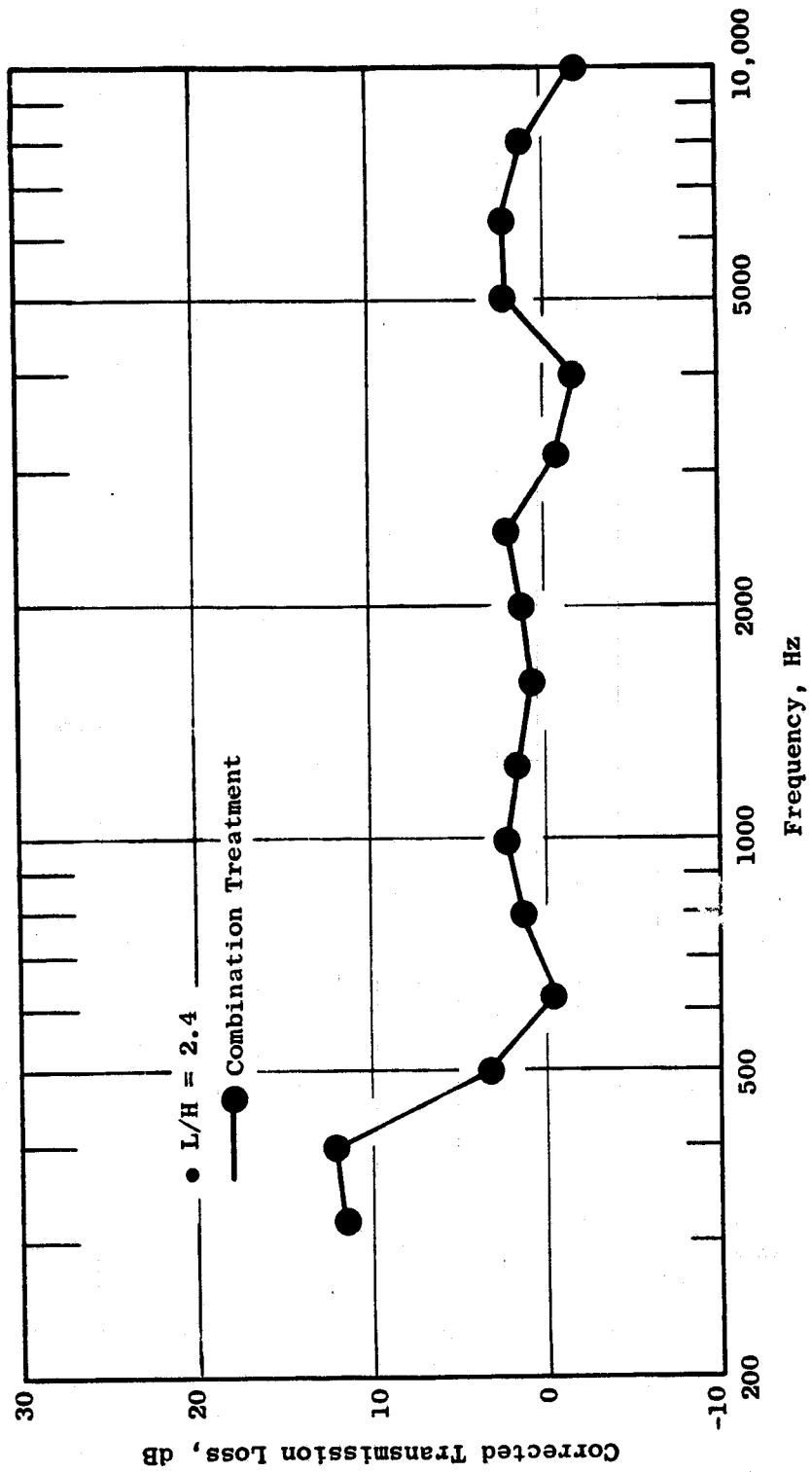


Figure 163. Cold Flow Acoustic Duct Data, Side-Branch Resonator (Treated on One Side), Mach No. = 0.2.

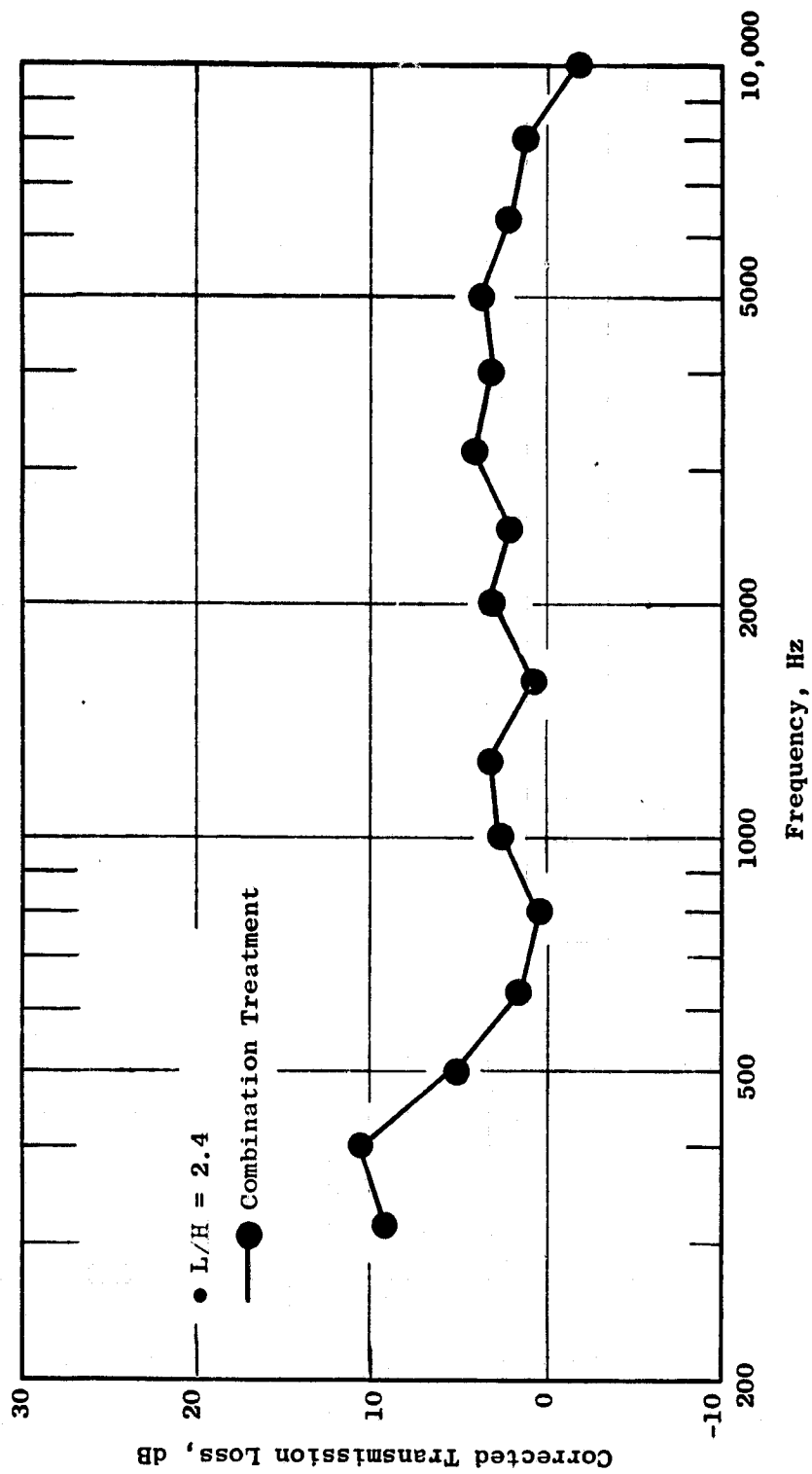


Figure 164. Cold Flow Acoustic Duct Data, Side-Branch Resonator (Treated on One Side), Mach No. = 0.3.

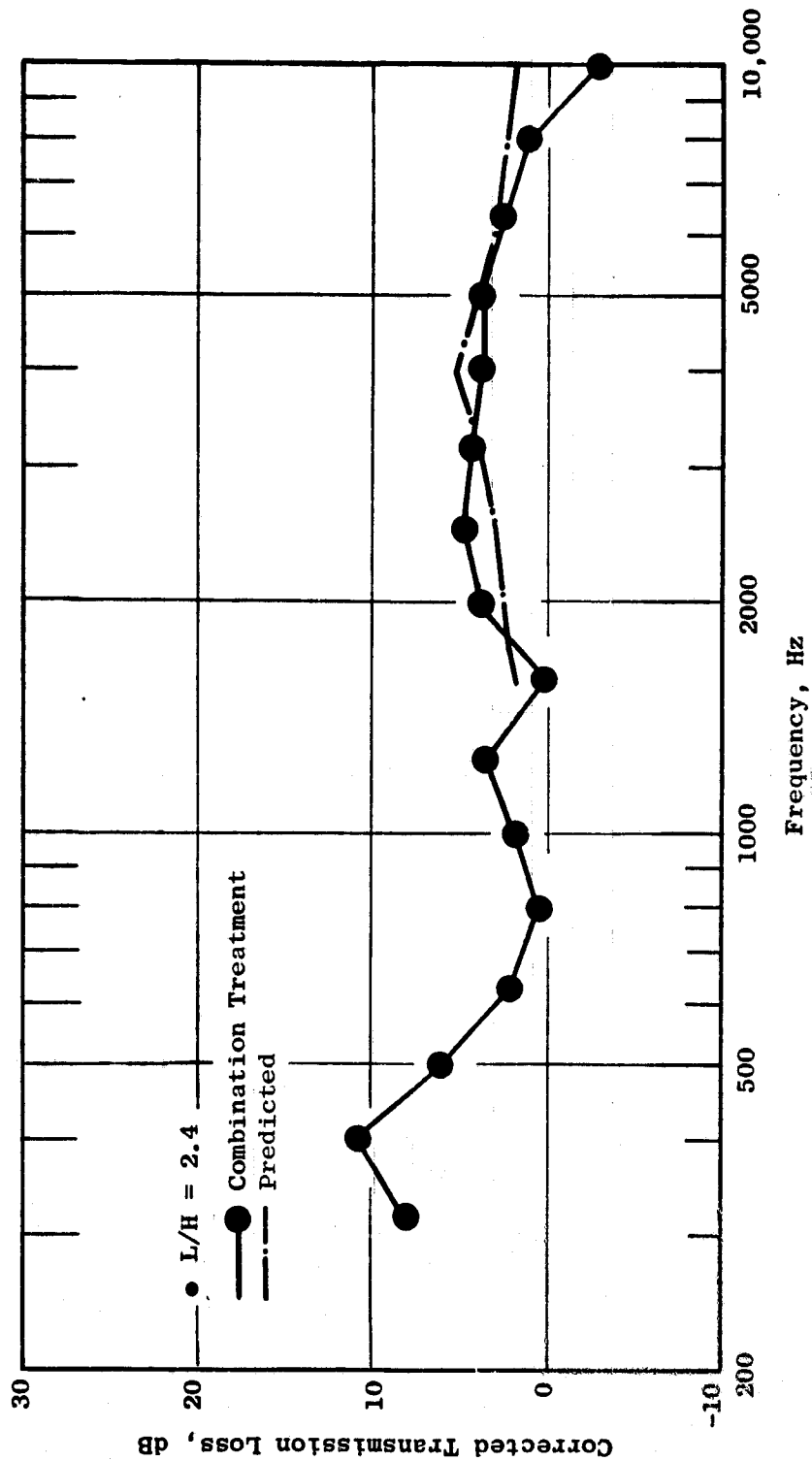


Figure 165. Cold Flow Acoustic Duct Data, Side-Branch Resonator (Treated on One Side), Mach No. = 0.4.

Side-Branch Resonator Design

The side-branch resonator suppressor was constructed as shown in the sketch on Figure 166. The configuration simulated the engine plug treatment having both low- and high-frequency panels; however, only the thinner treatment was mounted on the opposite wall of the treated duct section. The low-frequency treatment yielded an L/H of 2.85 and an effective turbine treatment area of 90% due to the low-frequency treatment suppressor cutouts.

The total treatment length of the inner wall treatment simulating the engine core plug is 57.91 cm (12.8 in.) and is divided into three segments of equal length, each tuned to a different frequency. These frequencies are 300, 400, and 500 Hz. The multiple-frequency design was selected because its suppression bandwidth is more effective in giving the required suppression in terms of PNdB.

The turbine treatment on both the inner and outer walls has a constant panel depth of 2.54 cm (1.0 in.) and a faceplate porosity of 10%. The panel tuning frequency is 3150 Hz.

Dual-Layer SDOF Treatment Design

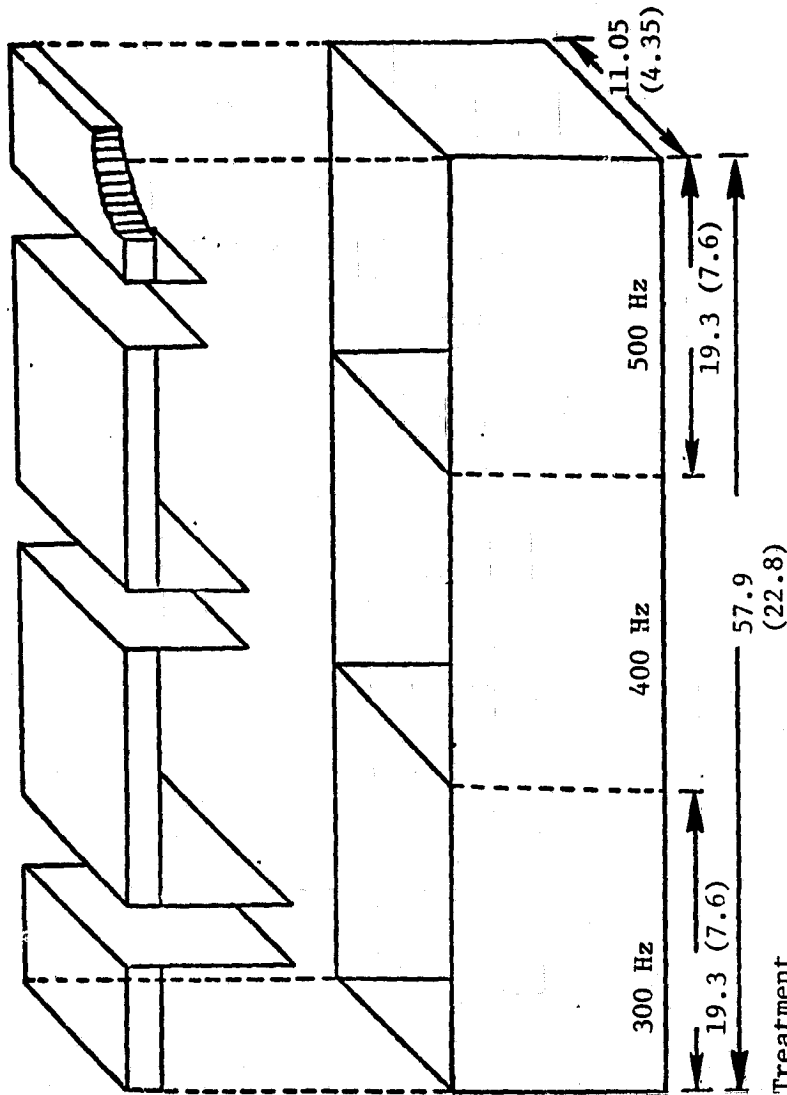
The dual-layer SDOF treatment suppressor was constructed as shown in Figure 167. The combined high- and low-frequency treatment was installed on both walls of the duct treatment section. The configuration gives a low-frequency L/H of 3.0 and has an effective turbine treatment area of 90%.

The low-frequency treatment length was divided into three segments, each 20.32-cm (8-in.) long. Each segment had a different panel depth and neck length which gave tuning frequencies of 300, 400, and 500 Hz. The dimensions of the test panels were determined by the impedance equations in Reference 5. The objective here with the multiple tuning frequencies, is, as with the side-branch resonator, an effort to improve the suppression bandwidth. The turbine treatment had a constant treatment thickness on each wall and a constant faceplate porosity of 22.5%; the panel is tuned to the 3150-Hz 1/3-octave band.

Measured Suppression, Side-Branch and Dual-Layer SDOF Treatment Designs

Data contained in Figures 168 through 174 give the HITAD results using both PWL and SPL measurements for the side-branch and dual-layer SDOF treatment design concepts. The corrected transmission loss spectra given are based on a PWL insertion loss determined from the 3.04-m (10-ft) and 7.62-m (25-ft) arc spectra shown in Figures 168 through 170. Figure 168 gives the measured spectrum for the hard-wall (untreated) configuration; Figure 169, the side-branch resonator; and Figure 170, dual-layer SDOF treatment.

• All Dimensions are cm (in.)



Turbine Treatment

Tuning Frequency, Hz, 3150

Porosity, %, 10

Hole Diameter, 0.16 (0.0625)

Faceplate Thickness, 0.08 (0.032)

Cavity Depth, 2.54 (1.0)

Combustor Treatment

Tuning Frequency, Hz, 300

Porosity, %, 20

Neck Length, 10.2 (4.0)

Cavity Depth, 12.7 (5.0)

400

20

7.6 (3.0)

12.7 (5.0)

500

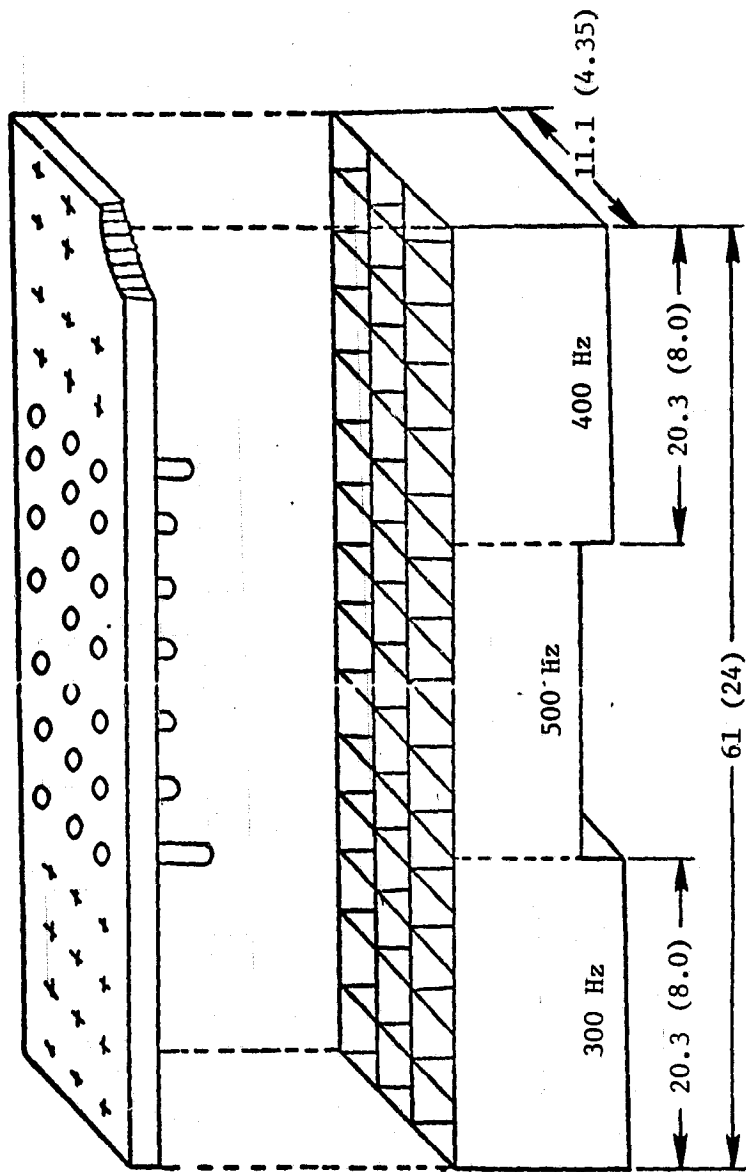
20

5.1 (2.0)

12.7 (5.0)

Figure 166. Schematic of Side-Branch Resonator Treatment Panel.

• All Dimensions are cm (inch)



Turbine Treatment

Tuning Frequency, Hz, 3150
 Porosity, %, 22.5
 Faceplate Thickness, 0.08 (0.032)
 Hole Diameter, 0.16 (0.062)
 Cavity Depth, 2.54 (1.0)

Combustor Treatment

Tuning Frequency, Hz, 300
 Porosity, % 10
 Neck Length 6.4 (2.5)
 Cavity Depth 10.2 (4.0)
 Hole Diameter 1.52 (0.6)

400
 10
 5.1 (2.0)
 9.5 (3.8)
 1.52 (0.6)

500
 10
 4.5 (1.75)
 7.6 (3.0)
 1.52 (0.6)

Figure 167. Schematic of Dual-Layer SDOF Treatment Panel.

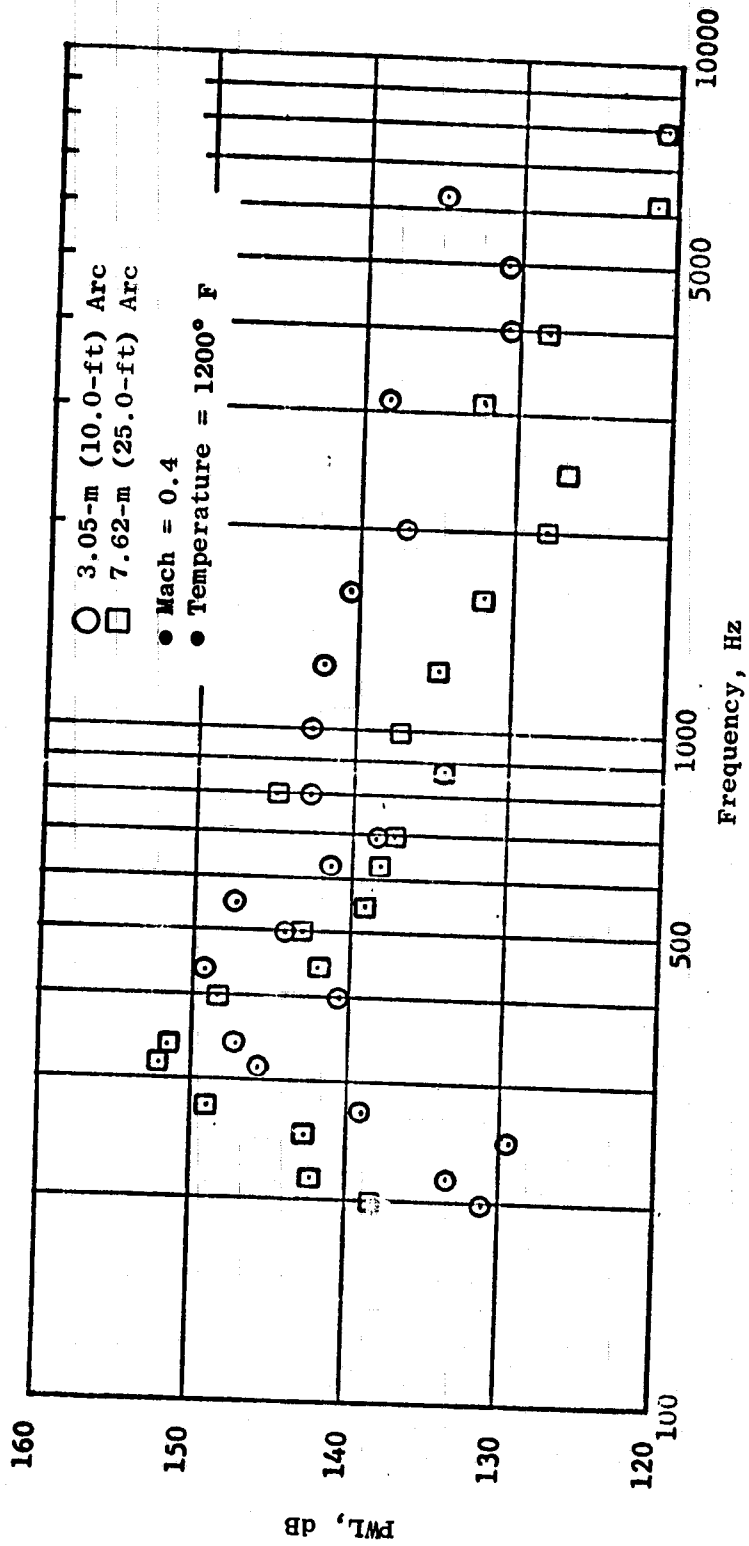


Figure 168. PWL Spectrum for Duct Hard-Wall Configuration.

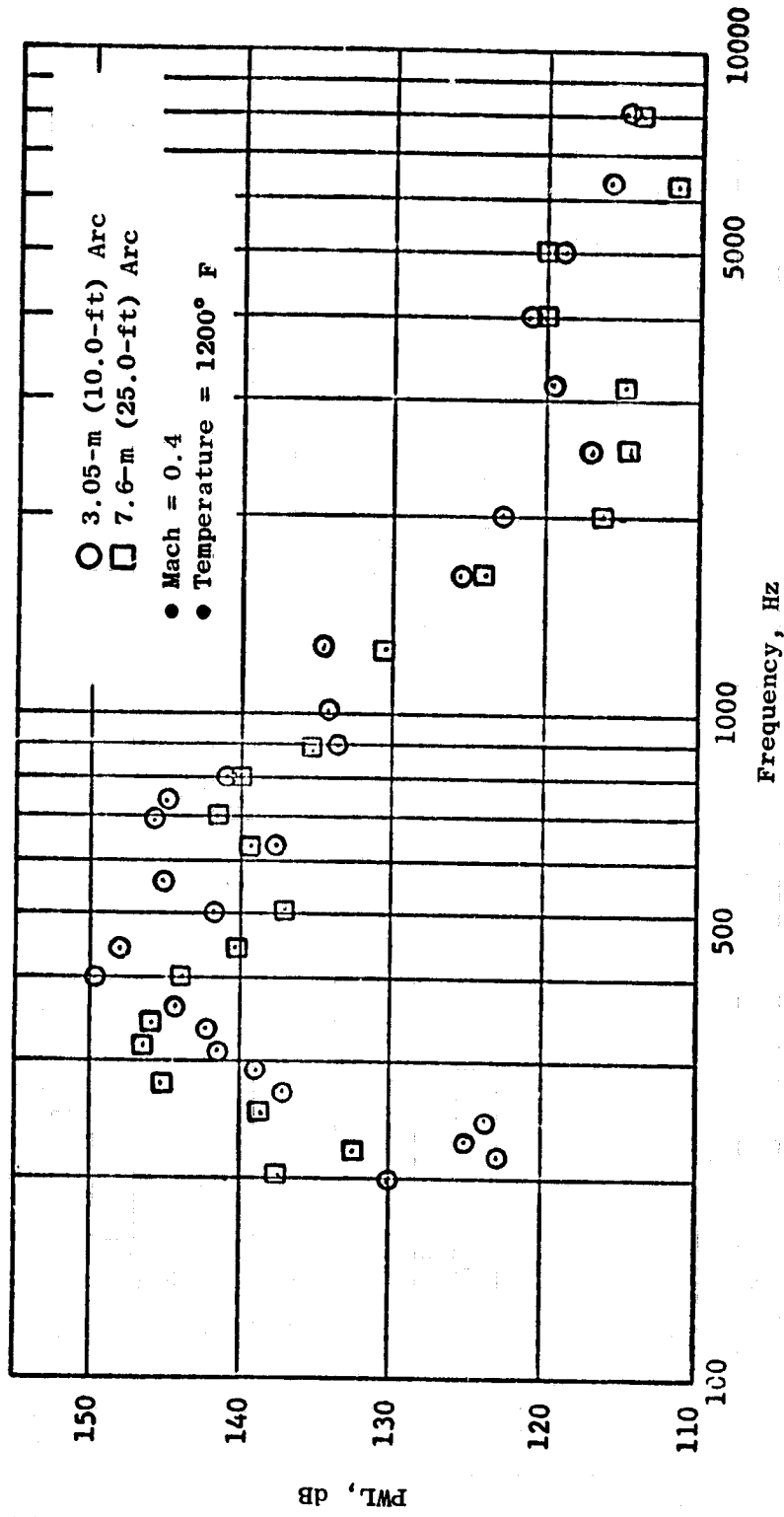


Figure 169. PWL Spectrum for Side-Branch Resonator Configuration.

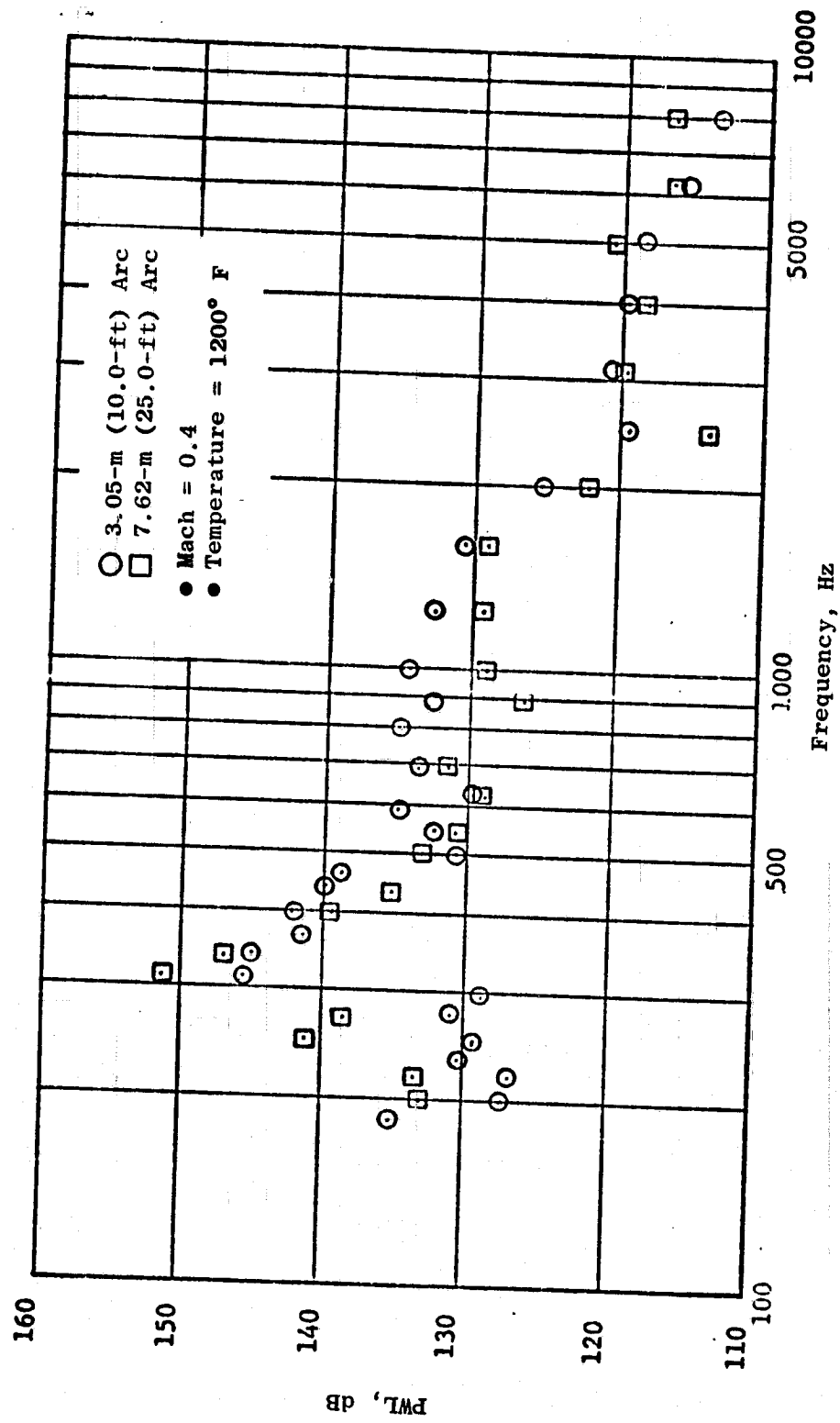
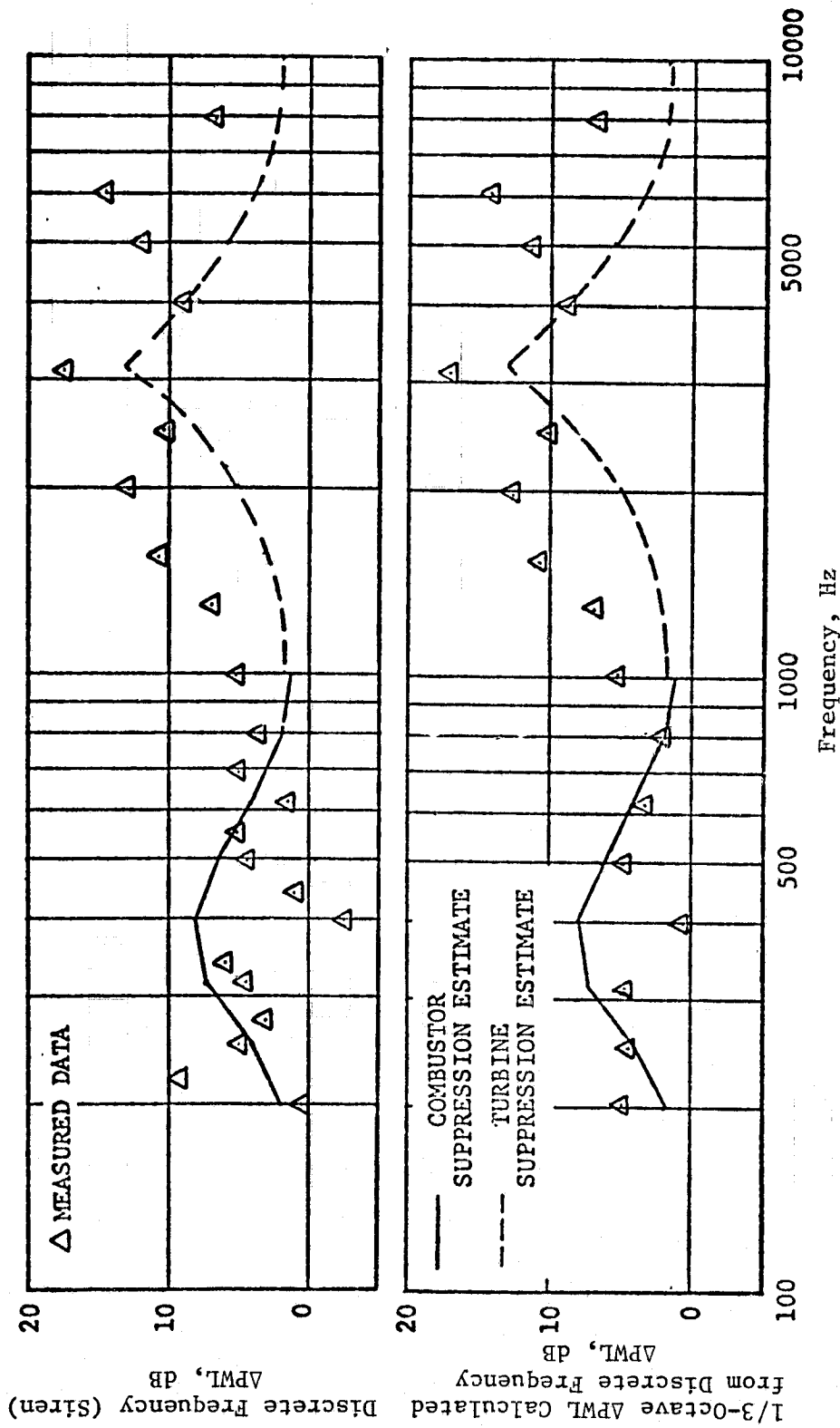
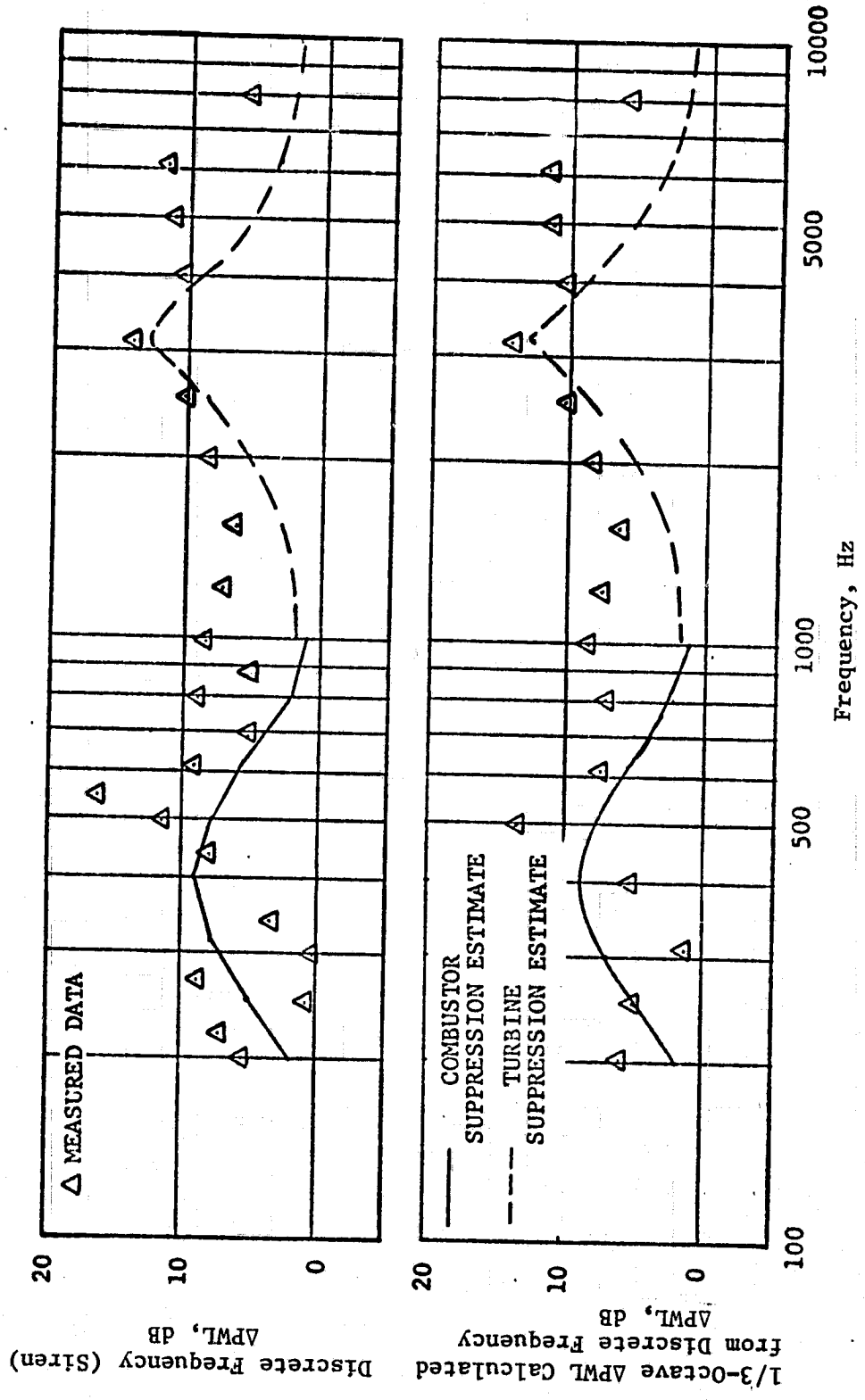


Figure 170. PWL Spectrum for Dual-Layer SDOF Treatment Configuration.



- 3.05 m (10 ft) and 7.62 m (25 ft) Arcs
- Mach = 0.4, Temperature = 1200° F

Figure 171. Suppression in Δ PWL for Side-Branch Resonator Treatment Configuration.



- 3.05 m (10 ft) and 7.62 m (25 ft) Arcs
- Mach = 0.4, Temperature = 1200° F

Figure 172. Suppression in Δ PWL for Dual-Layer SDOF Treatment Configuration.

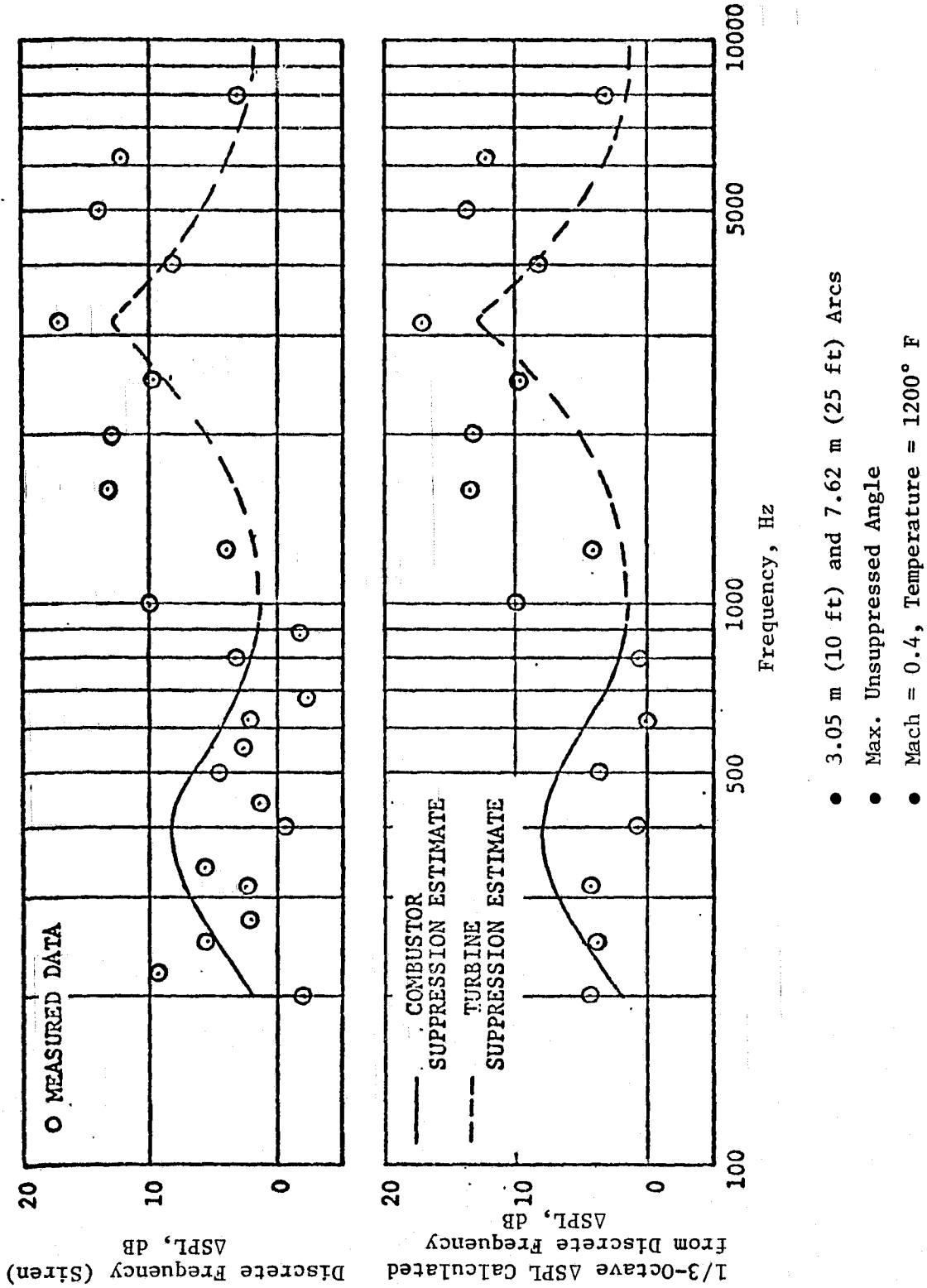


Figure 173. Suppression in Δ SPL for Side-Branch Resonator Treatment Configuration.

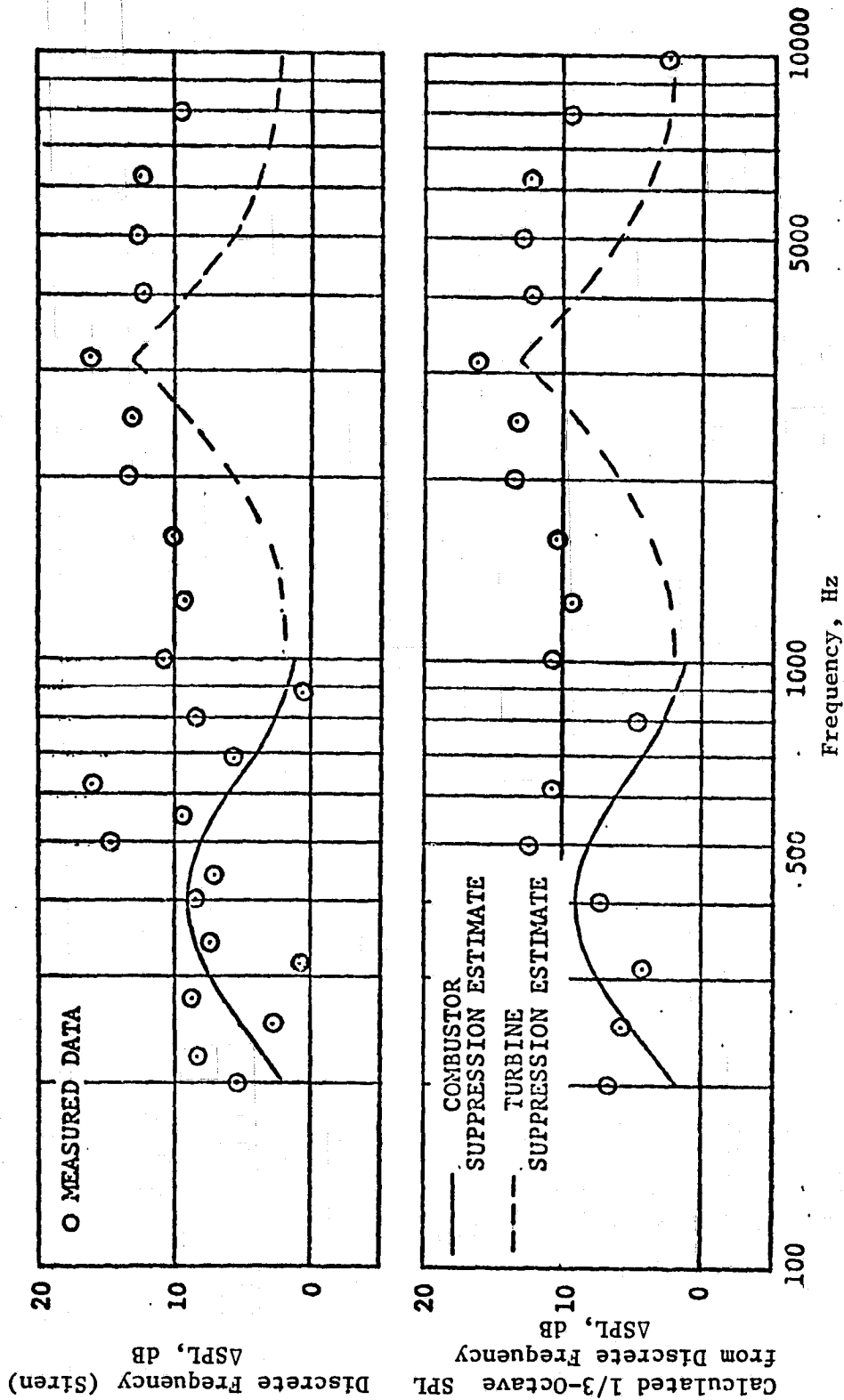


Figure 174. Suppression in ASPL for Dual-Layer SDOF Treatment Configuration.

Suppression spectra in terms of Δ PWL are given in Figures 171 and 172 for the two treatment concepts. Figure 173 gives the SPL suppression for the side-branch resonator treatment and suppression for the dual-layer SDOF treatment is given in Figure 174. The suppression represents the average of the 7.62-m (25-ft) and 3.04-m (10-ft) arc data, for a duct Mach number of 0.4 and a temperature of 1200° F. The suppression levels were calculated by subtracting the SPL values of the treated spectra from those of the spectra measured for the hard-wall configuration. Since the noise source was a discrete-frequency siren, a number of frequencies within a 1/3-octave band were sometimes used. (See the individual frequencies in Figures 168, 169, and 170.) Because we are interested in 1/3-octave-band suppression, two spectra are given in Figures 171 through 174. The upper figure gives data at the frequencies at which the suppression was measured, whereas the spectrum in the lower figure is calculated for a 1/3-octave bandwidth using the data measured within each 1/3-octave band. For these lower figure calculations it was assumed that the unsuppressed noise is uniform over the 1/3-octave bandwidth.

Also given with the measured suppression spectra are the predicted levels, determined during the preliminary design phase of the treatment development, which represent the suppression required to meet the total system noise goal of 95 EPNdB. Comparison of measured versus predicted suppression levels shows that the measured high-frequency suppression in Δ PWL is greater than the predicted levels. The comparison in the low frequencies shows that the desired suppression is obtained at most of the frequencies, with the dual-layer SDOF treatment having an advantage over the side-branch resonator.

Figures 173 and 174 show the suppression as determined in Δ SPL for the maximum unsuppressed acoustic angle. These results also show the dual-layer SDOF treatment to give significantly higher suppression levels in the lower frequencies; Figure 174 shows that it gives the required combustor noise suppression at most frequencies. Both the dual-layer SDOF and the side-branch resonator designs give higher suppression levels than predicted in the higher frequencies.

7.3 DEFINITION OF ENGINE CORE TREATMENT DESIGN AND SUPPRESSION ESTIMATES

7.3.1 Suppression Concept Selection

Acoustic data for two design concepts were presented and discussed in the preceding section of this report. The data were obtained from the HITAD facility, where the expected engine geometric and environmental conditions were closely simulated. These two concepts, the dual-layer SDOF treatment and the side-branch resonator, both gave good suppression results. In order to determine which of the suppressor concepts has the higher suppression potential in an engine application, the results were further analyzed.

A comparison of the suppression spectra for the two design concepts is shown in Figure 175. The results of this comparison show the dual-layer SDOF treatment giving higher levels of suppression in the low frequencies but show little difference at the higher frequencies. The suppression spectra given in Figure 175 were applied to the predicted turbine and combustor noise spectra. A summary of the calculated results is given in Table XI. The suppression is given in terms of Δ PNdB and shows the dual-layer SDOF treatment giving 2.7 PNdB more suppression than the side-branch resonator design. Thus, on the basis of this difference and the fact that the combustor suppression level from the side-branch resonator was below that required, the dual-layer SDOF treatment concept was selected for engine application.

7.3.2 Suppressor Design Definition

The predicted suppressed Noy-Weighted core noise spectrum is given in Figure 176. The spectrum illustrates the need for both low- and high-frequency suppression in order to suppress the total core radiated noise in terms of PNdB. The low-frequency suppression requirement is centered at 400 Hz, while the high-frequency noise is controlled at about 3150 to 4000 Hz. The spectra also show that suppression bandwidth is of importance since the spectrum is rather flat over several 1/3-octave-band frequencies in the low- and high-frequency ranges. In order to meet the low-frequency requirements, suppression is needed for 200 through 1000 Hz. The high-frequency suppression needed covers the 2000 to 8000-Hz frequency band.

The parameters governing the treatment tuning for the low-frequency design are as follows:

- Cavity Depth
- Tube length
- Porosity
- Hole Diameter

The method used in determining the optimum acoustic reactance for each panel is illustrated by the curves given in Figure 177 for the low-frequency treatment and in Figure 178 for the high-frequency treatment. The optimum reactance is defined as:

$$X/\rho c = -0.77 H/\lambda_p$$

where:

$$X/\rho c = \text{specific reactance}$$

$$H = \text{duct height}$$

$$\lambda_p = \text{phase wavelength at tuning frequency}$$

- Avg of 3.05 m (10 ft) and 76.2 m (25 ft) Arcs
- Max. Unsuppressed Angle
- Mach = 0.4, Temperature = 1200° F

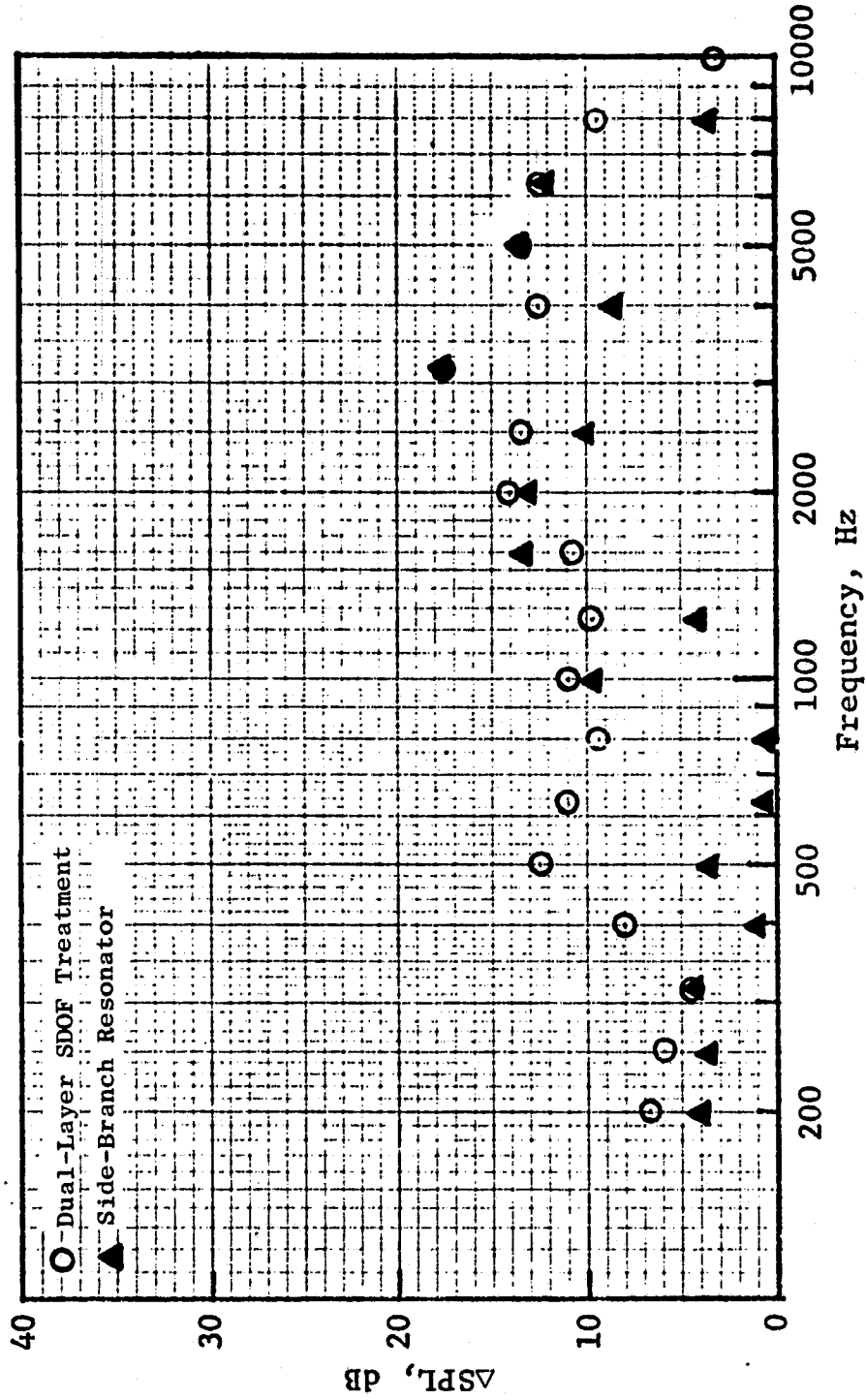


Figure 175. Suppression Spectra for Dual-Layer SDOF Vs. Side-Branch Resonator Treatment.

Table XI. QCSEE Core Suppression Estimates.

- 152.4-m (500-ft) Sideline at 61-m (200-ft) Altitude
- Max. Aft Acoustic Angle

	<u>ΔPNdB</u>		<u>System EPNdB</u>
	<u>Combustor</u>	<u>Turbine</u>	
Core Noise Design Suppression Requirements	4.6	5.0	94.2
Engine Suppression Based on Duct Data			
● Dual-Layer SDOF Treatment	5.1	9.8	93.9
● Side-Branch Resonator	2.4	9.4	94.1

- Noy-Weighted Total (Turbine & Combustor)
- UTW Engine at Takeoff
- 120° Acoustic Angle
- 152.4 m (500 ft) Sideline, 61 m (200 ft) Altitude

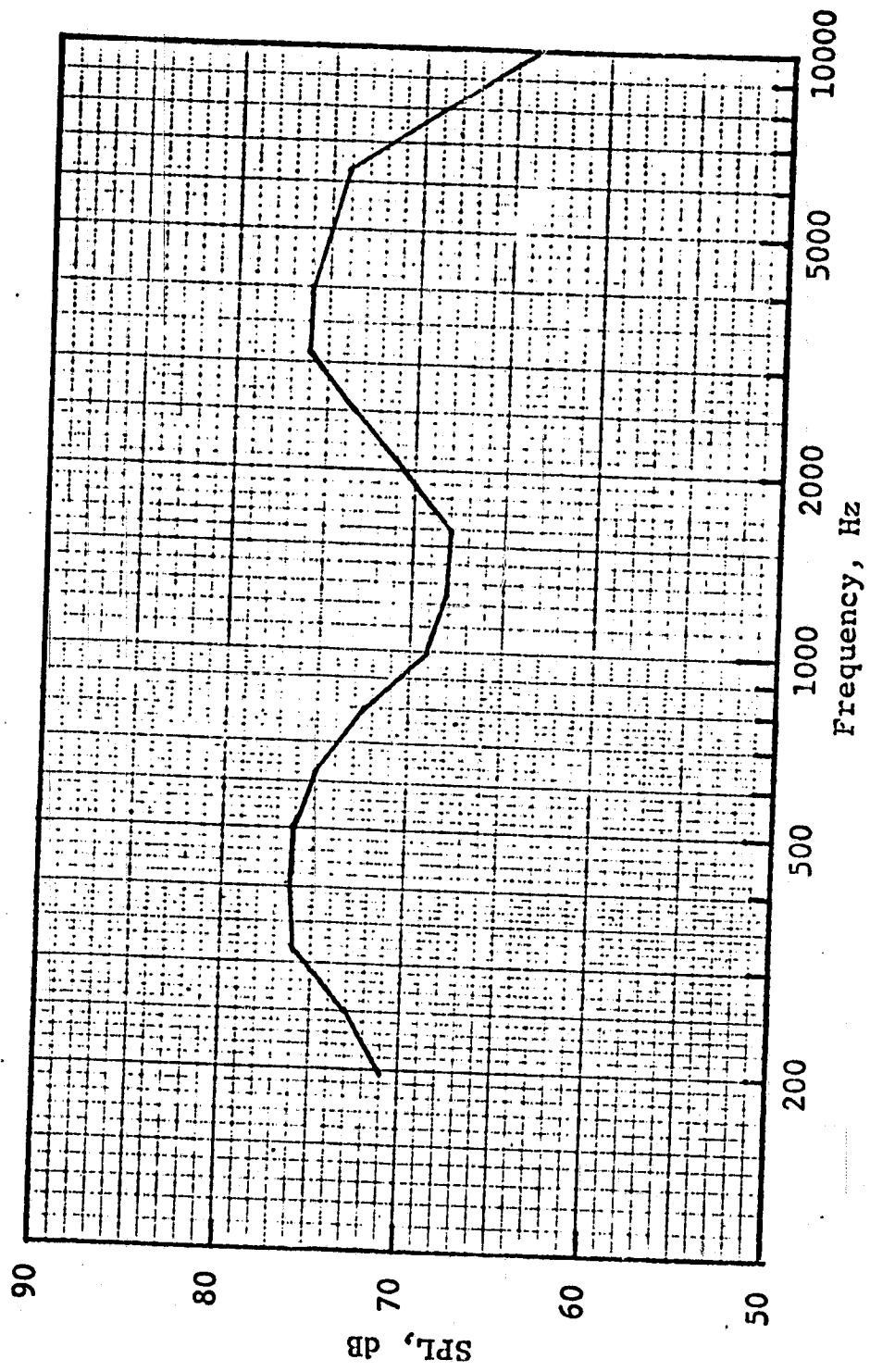


Figure 176. Predicted Core Noise Spectra.

- Mach = 0.40
- 1000° F

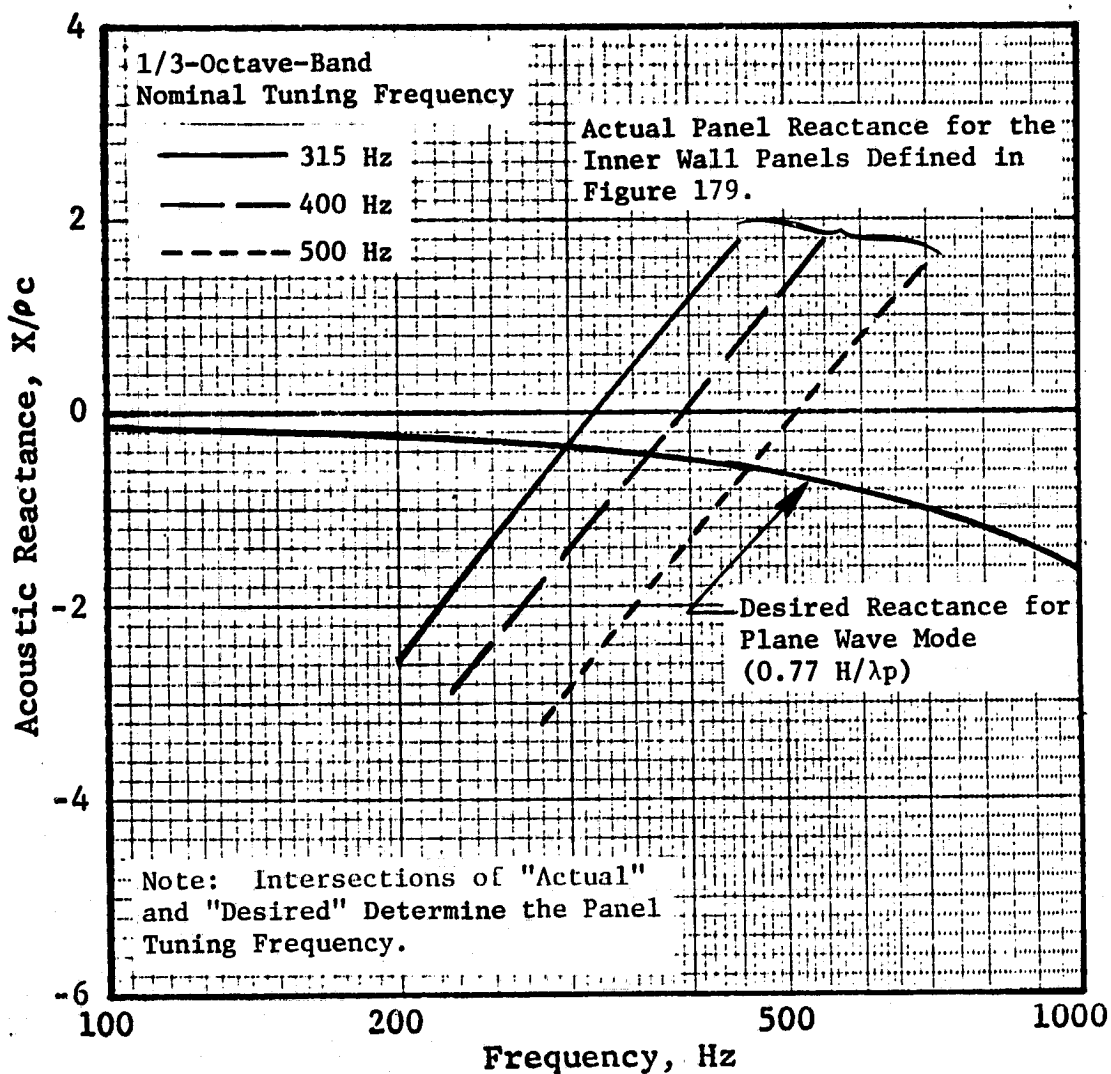


Figure 177. QCSEE Core Suppressor Tuning Frequencies Low-Frequency Combustor Treatment.

- Mach = 0.40
- 1000° F

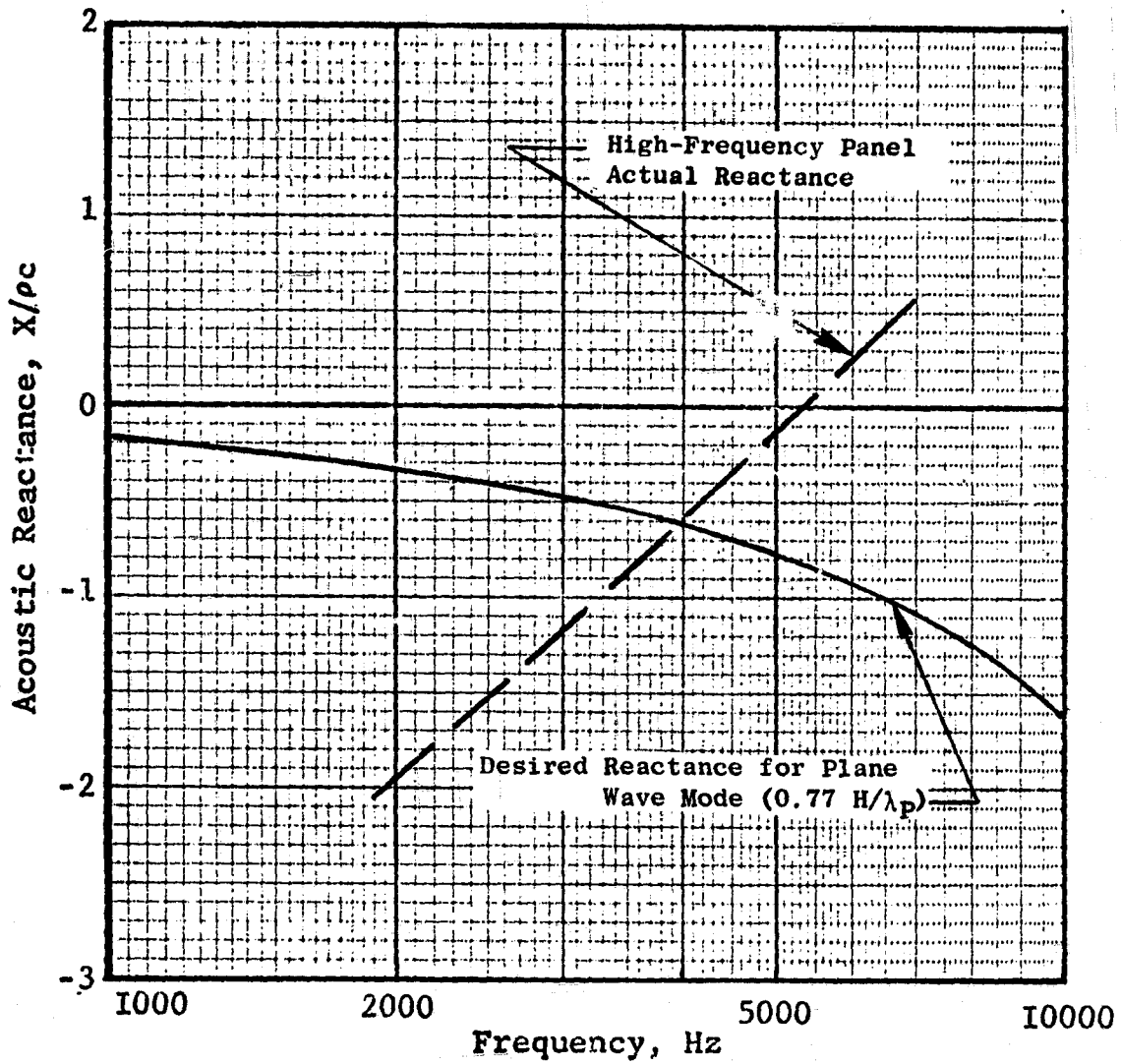


Figure 178. QCSEE Core Suppressor Tuning Frequencies High-Frequency Turbine Treatment.

The predicted reactance for panels of three different depths is shown in Figure 177. The intersection of the predicted reactance curve with the optimum reactance curve determines the desired tuning frequency. The panel reactances given in Figure 177 correspond to the inner wall treatment design for the engine treatment defined in Figure 179. The intersection of the predicted-versus-optimum reactance shows that these designs offer tuning frequencies that fall within the 315, 400, and 500-Hz 1/3-octave bands. This same procedure was followed in designing the low-frequency panels on the outer wall. Different design frequencies are indicated for the three segments of treatment. The higher tuning frequencies indicated for the aft treatment segment are a result of the unavailability of sufficient panel depth for lower frequency tuning. This range of tuning frequencies should give the required bandwidth in the lower frequencies.

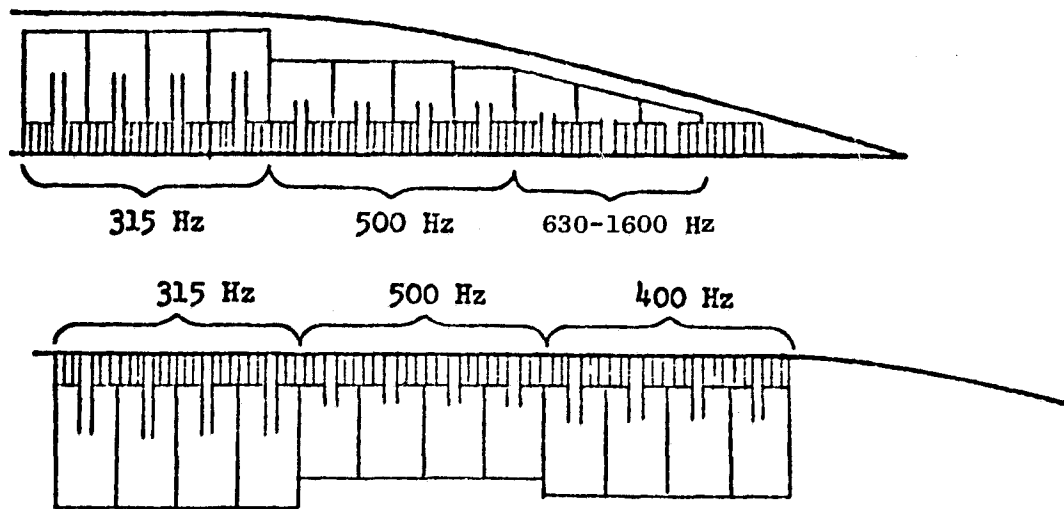
Figure 178 gives the optimum-versus-predicted reactance for the thin high-frequency turbine treatment. The predicted reactance is for the design defined in Figure 179 with both inner and outer walls having the same high-frequency treatment. The intersection of the two reactance curves shows the panel is designed for 4000 Hz which is desirable based on the unsuppressed Noy-weighted spectrum given in Figure 176.

The detailed design of the high- and low-frequency treatment panels is given in Figure 179. The engine hardware is shown in the photos given in Figures 180 through 183.

7.3.3 Engine Suppression Estimates

The final predicted core exhaust suppression spectrum for the actual engine core treatment design is given in Figure 184. The potential engine core noise suppression in PNdB was calculated by applying this spectrum to the predicted unsuppressed turbine and combustor spectra.

A summary of these results plus suppression estimates for other engine noise constituents are given in Table XI. These suppression levels when applied to the predicted unsuppressed noise source levels give a total system suppressed EPNdB level meeting the QCSEE noise goal.



	Combustor						Turbine Both Walls
	Inner Wall			Outer Wall			
Tuning Frequency, Hz	315	400	500	315	500	630-1600	3150
Neck Length, cm (in.) (Faceplate Thickness)	6.99 (2.75)	5.72 (2.25)	4.45 (1.75)	6.99 (2.75)	4.45 (1.75)	3.56-2.54 (1.4)-(1.0)	0.08128 (0.032)
Cavity Depth, cm (in.)	10.2 (4.0)	8.89 (3.5)	7.62 (3.0)	7.62 (3.0)	4.32/ 5.08 (1.7/ 2.0)	4.06-0.51 (1.6)-(0.2)	1.095 (0.750)
Porosity	10%	10%	10%	7%	7%	7%	10%
Treatment Length, cm (in.)	20.32 (8.0)	20.32 (8.0)	20.32 (8.0)	20.32 (8.0)	15.24/ 5.08 (6.0/ 2.0)	20.32 (8.0)	60.96 (24.00)
Hole Diameter, cm (in.)	1.52 (0.6)	1.52 (0.6)	1.52 (0.6)	1.52 (0.6)	1.52 (0.6)	1.52 (0.6)	0.1575 (0.062)

Figure 179. UTW Boilerplate No. 1 Core Exhaust Treatment Definition.

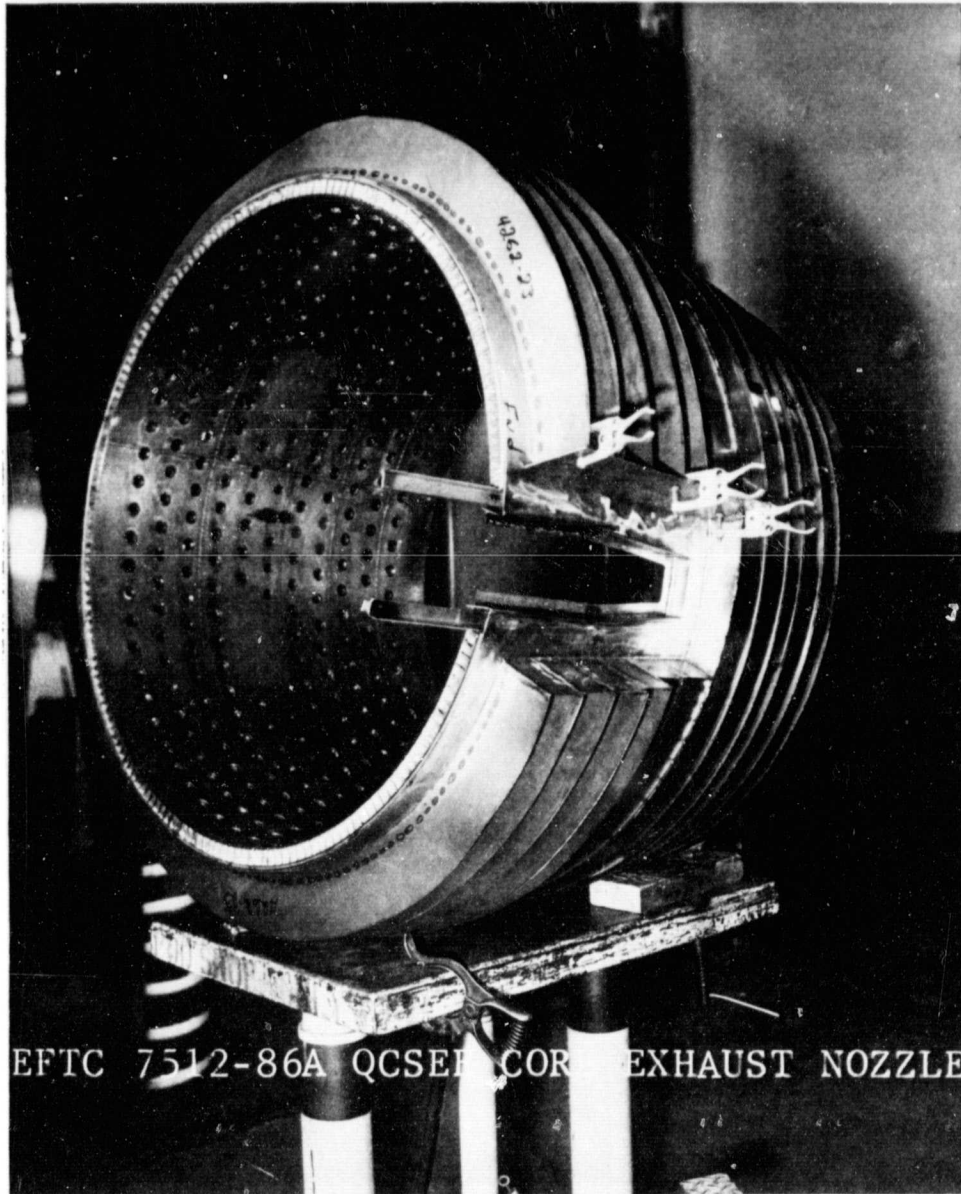


Figure 180. QCSEE Core Exhaust Outer Wall Acoustic Treatment.

REPRODUCIBILITY OF THE
ORIGINAL PAGE IS POOR

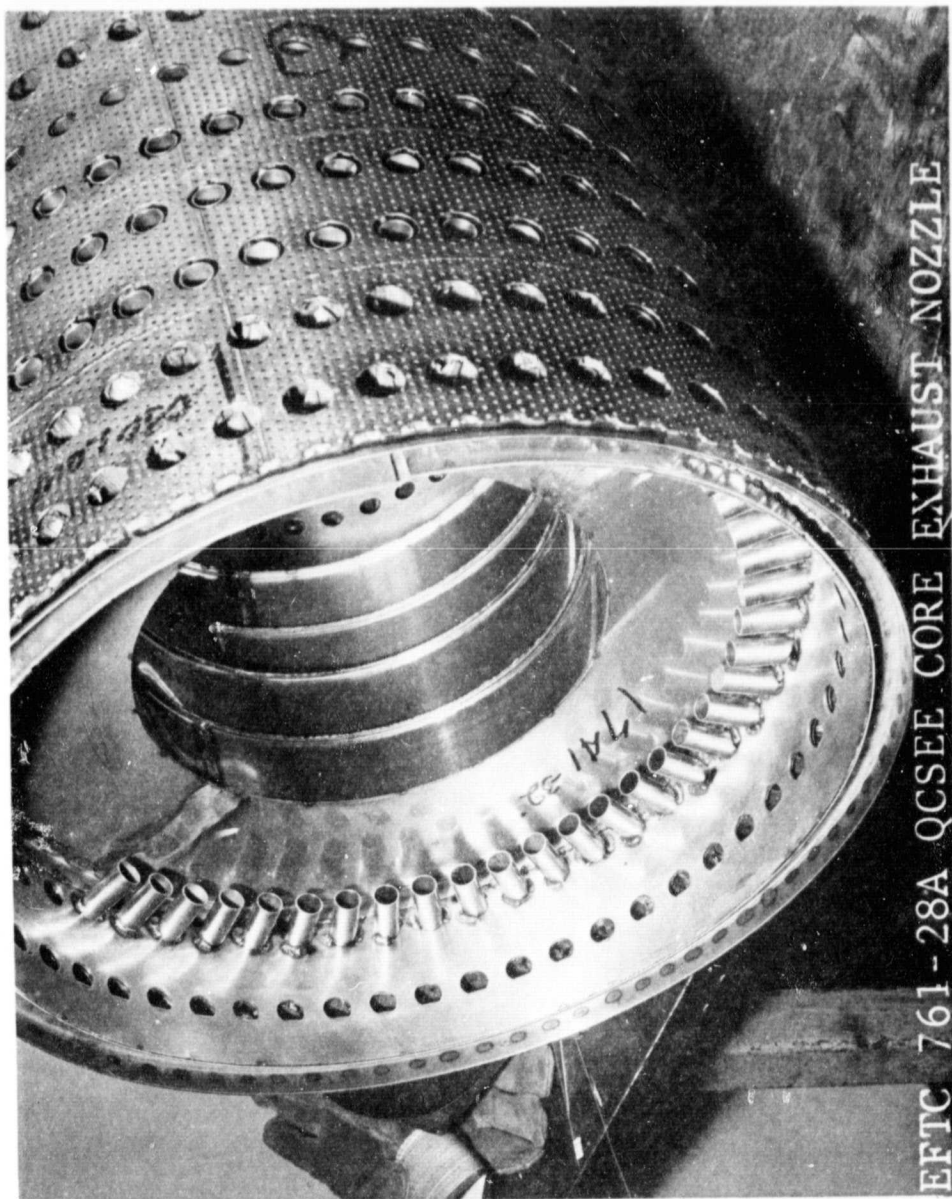


Figure 181. QCSEE Core Exhaust Inner Wall Acoustic Treatment.

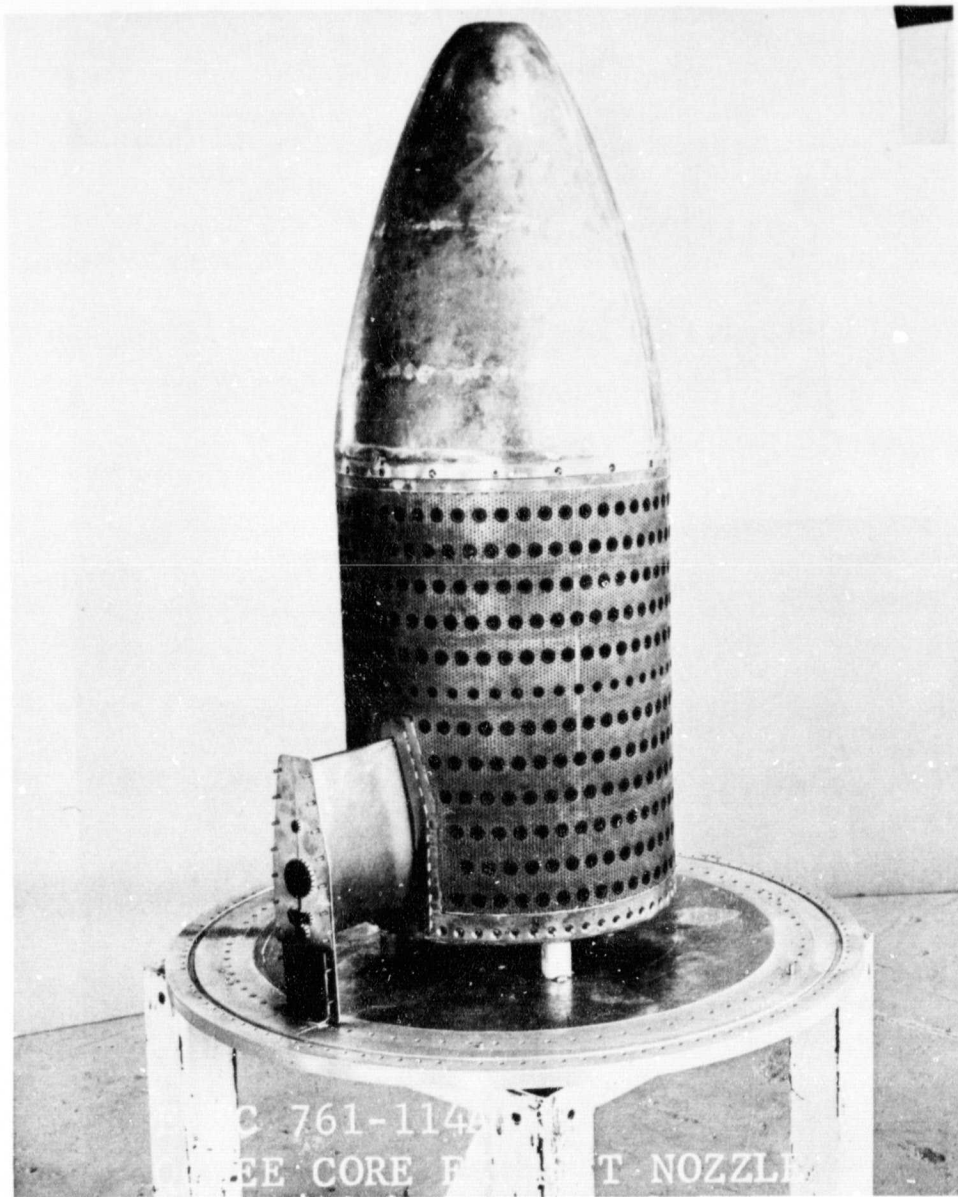


Figure 182. QCSEE Core Exhaust Plug Nozzle Assembly.

REPRODUCIBILITY OF THE
ORIGINAL PAGE IS POOR

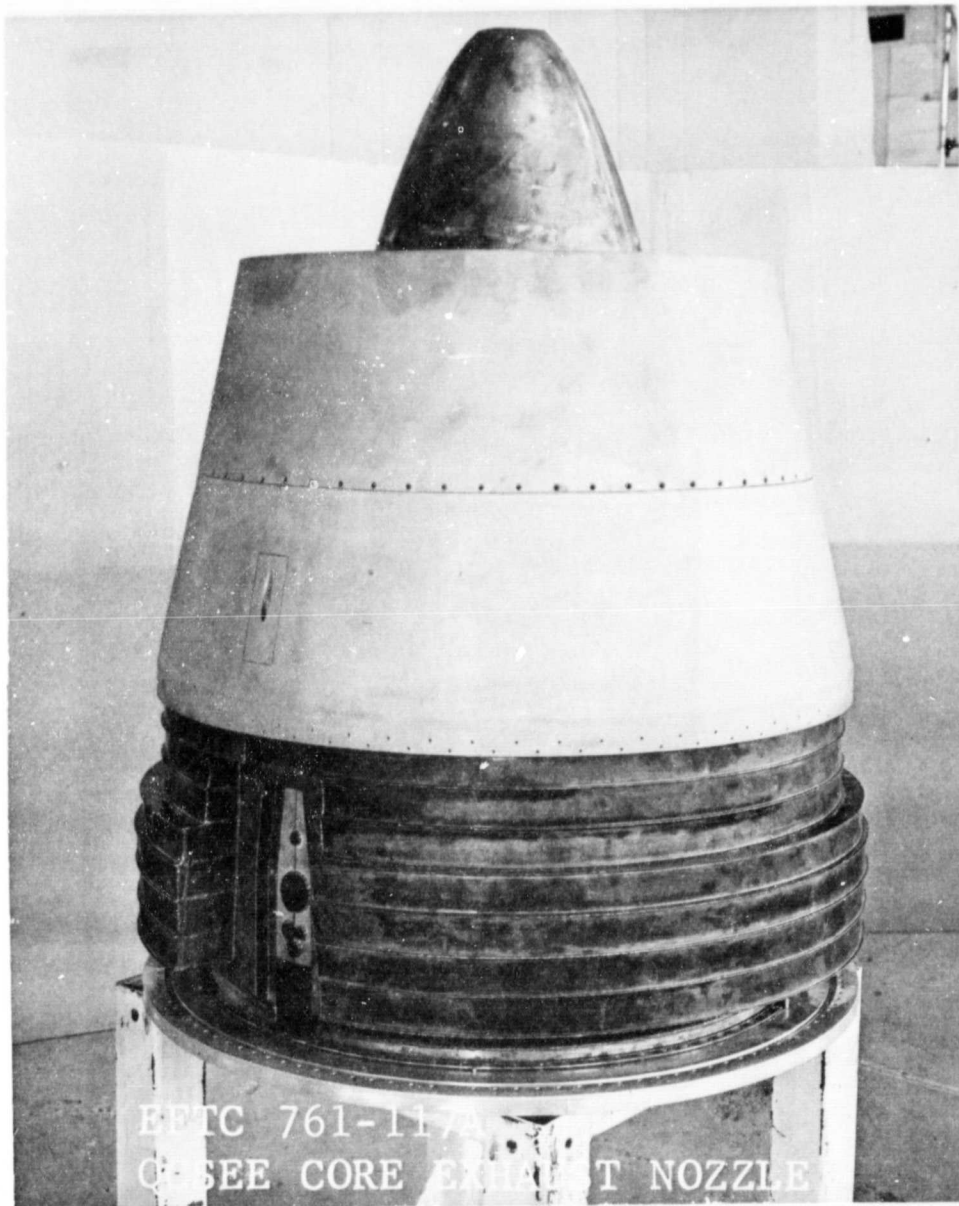


Figure 183. QCSEE Core Exhaust Nozzle Assembly.

● Based on Laboratory Duct Test Results

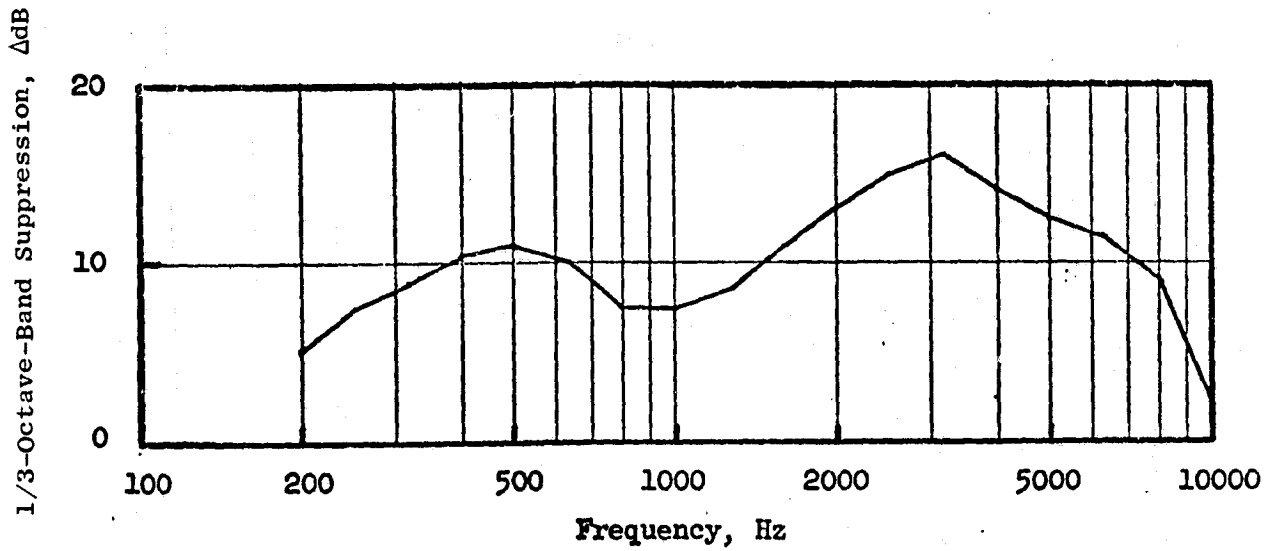


Figure 184. UTW Boilerplate No. 1 Core Exhaust Dual-Layer SDOF Treatment Suppression.

8.0 ADDITIONAL SUPPORTING INVESTIGATIONS

8.1 Flow Noise Regeneration

8.1.1 Preliminary Analysis

During the preliminary phase of the acoustic treatment development program attention was given to the noise floor in the fan exhaust duct. The concern was that with the demanding high fan exhaust suppression requirements, the noise floor could prevent the full effectiveness of the treatment. The noise floor level consists of strut noise, splitter trailing edge noise, and treatment flow regenerated noise. The models as described below were used in the early stages of the treatment development to estimate the floor noise sound power level (PWL) for the UTW and OTW engines.

Strut Noise

The strut noise estimate is based on an overall power level (OAPWL) formulation, derived from a series of laboratory tests of obstructions in flow. The tests were performed under the core noise program (Reference 6), and the prediction method is documented in Reference 2. The overall strut noise power level is given by the following expression:

$$\text{OAPWL} = 16.8 + 10 \log (c \cdot t_{\max} \cdot h \cdot u^5) + 4 \log C_D + 10 \log N$$

dB re 10^{-13} watts

where

- c = chord, cm/30.48
- t_{\max} = maximum strut thickness, cm/30.48
- h = strut length, cm/30.48
- u = upstream flow velocity, cm/(30.48 sec)
- C_D = profile drag coefficient
- N = number of struts

The spectral shape of the strut noise is shown in Figure 185. The suppression due to treatment aft of the six struts was applied in the UTW and OTW engines.

The following values were assumed for the estimates of the unsuppressed strut noise shown in Figure 186 (after applying the suppression of the treatment aft of the struts):

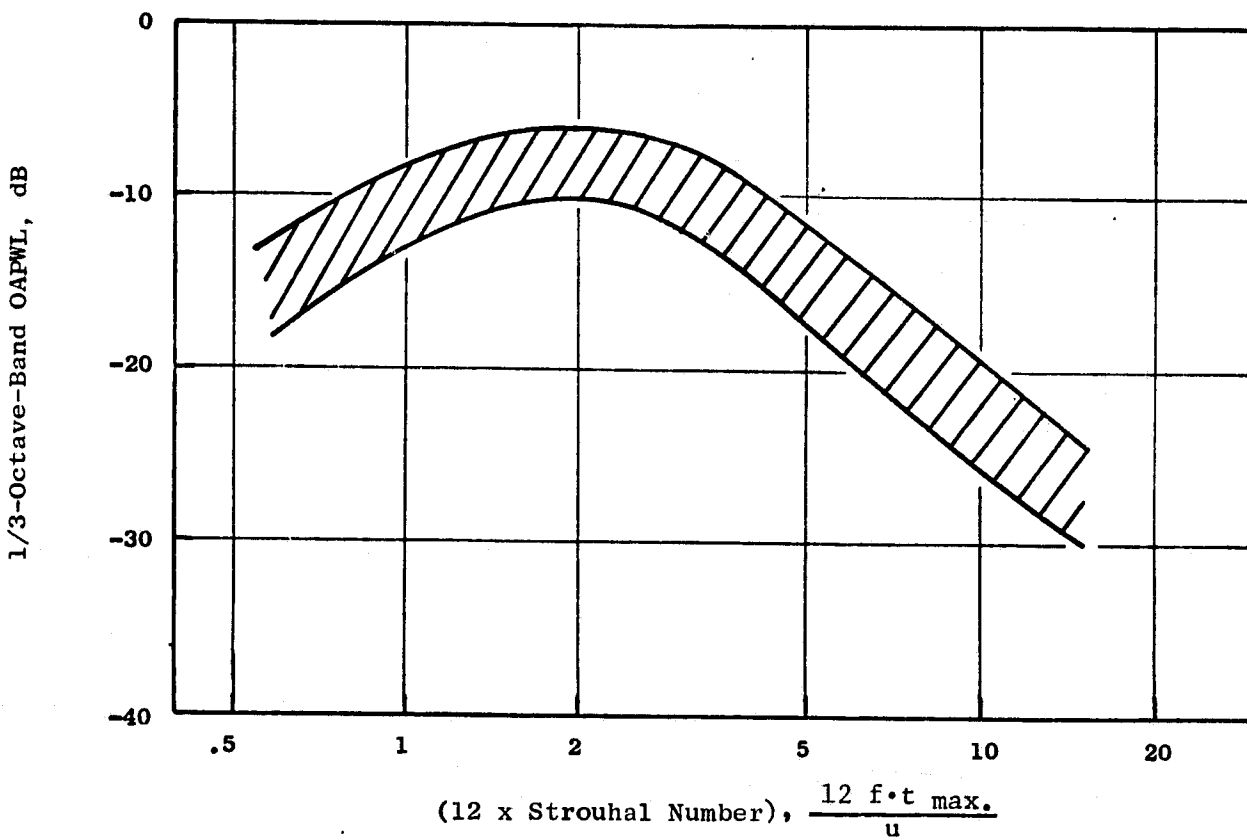


Figure 185. Normalized Spectrum of Strut Noise.

• Takeoff Power

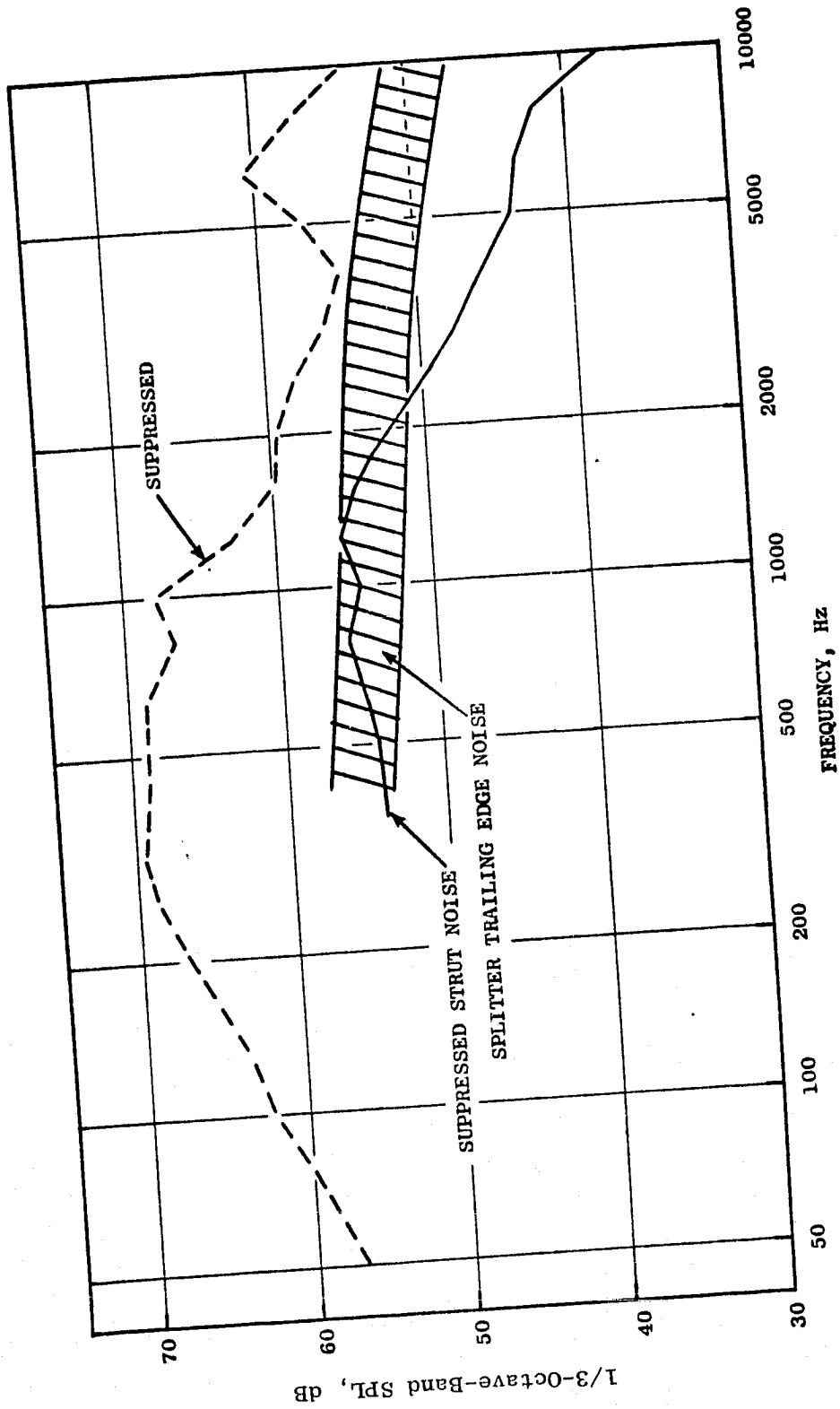


Figure 186. UTW Suppressed Fan- and Flow-Generated Noise Spectra.

Strut Noise

Chord (c)	= 25.08 cm (0.82 ft)
Max. Strut Thickness ($t_{\max.}$)	= 1.58 cm (0.05 ft)
Strut Length (h)	= 30.48 cm (1.0 ft)
Profile Drag Coefficient (C_D)	= 0.086
Number of Struts (N)	= 6
Upstream Flow Velocity (u)	= 161 m/sec (530 ft/sec)

Splitter Trailing Edge Noise

The splitter trailing edge noise estimate is based on a semiempirical formulation by I.L. Ver (Reference 7) and is as follows (for any 1/3-octave band):

$$PWL = 126 + 55 \log M + 10 \log A - 45 \log (P/100) + 7.5 \log (T/530)$$

where

$$PWL = 1/3\text{-octave power level, dB re } 10^{-13} \text{ watt}$$

and

M	= surface Mach number
A	= surface area, ft^2
P	= percent open area of cross section of flow passage area
T	= air temperature, ° R

The following values were used in the calculation of splitter trailing edge noise:

Surface Area (A)	= 4.63 m^2 (20.75 ft^2)
Percent Open Area of Cross Section of Flow Passage Area (P)	= 92%
Temperature (T)	= 294.3 K (530° R)
Trailing Edge Mach Number (M)	= 0.48

8.1.2 Rotor 55 Flow Noise Investigation

One of the objectives in the Aft Noise Suppression Test series was to determine levels of treatment regenerated flow noise by varying the Mach number in the aft duct, since in highly suppressed fan exhaust ducts there is a possible noise floor which may limit the achievable suppression. The noise floor is thought to be a function of the duct Mach number; therefore, the Mach number was varied in these tests over a range representative of the QCSEE engine to determine whether a significant suppression decrease at Mach numbers above 0.4 occurred. The configurations involved are shown in Figure 187 and provided three Mach numbers at a given fan speed. The lowest Mach numbers were achieved with the nominal nozzle configuration without a splitter

- HARD ROTOR-OGV
- TREATMENT L/H = 4.6

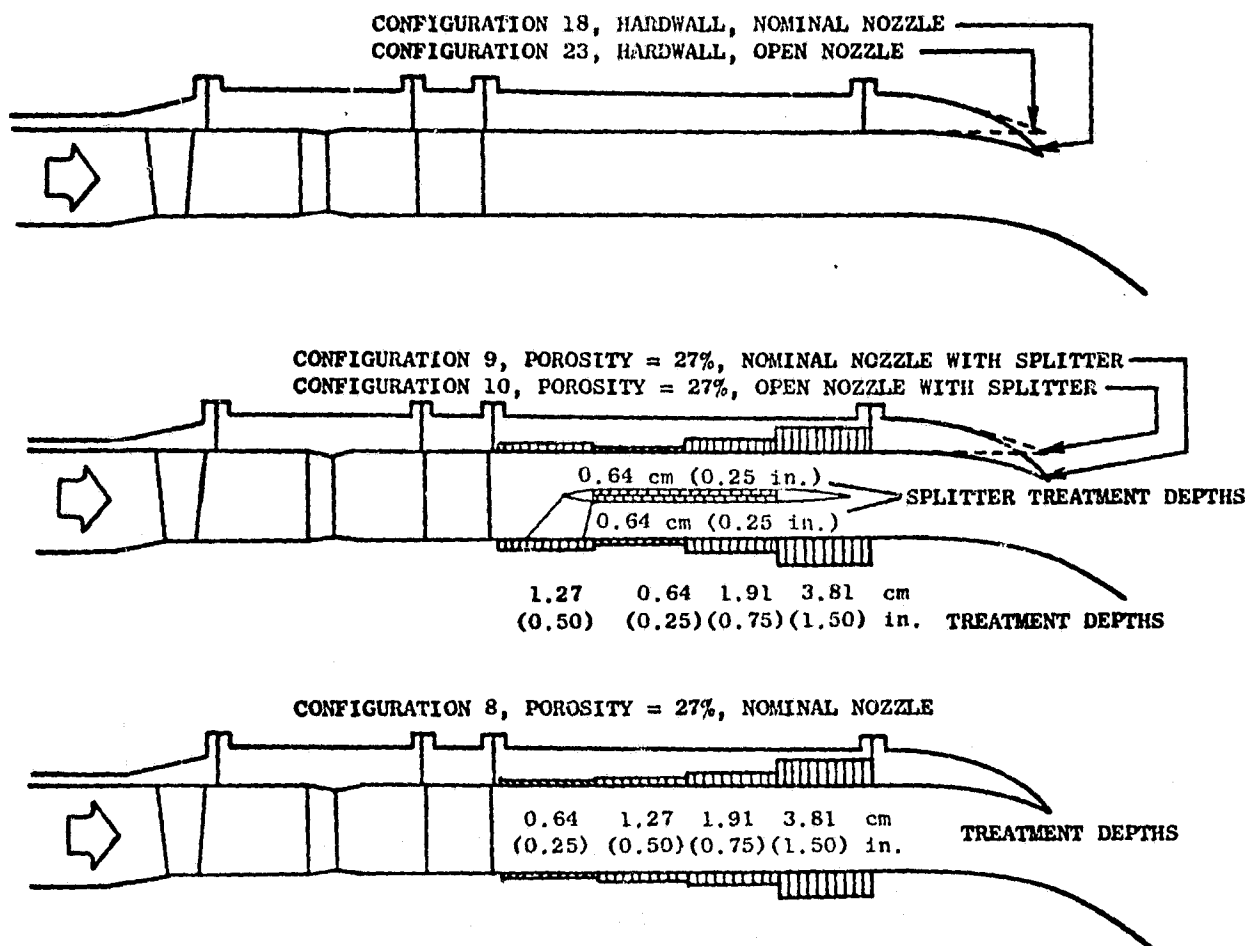


Figure 187. Treatment Regenerated Flow Noise Configurations.

installed. Installing the splitter increased the Mach numbers. A further increase to the highest Mach numbers was achieved by opening the nozzle.

The suppression levels achieved with the three different Mach numbers are shown in Figure 188 at 100% fan speed and at acoustic angles of 1.94 and 12.13 radians (111 and 122°). An average duct Mach number for the configurations is shown below:

<u>Configuration</u>	<u>M_{Duct}</u>
Nominal nozzle without splitter	0.40
Nominal nozzle with splitter - outer channel	0.50
- inner channel	0.46
Open nozzle with splitter - outer channel	0.56
- inner channel	0.52

Looking at the suppression levels we see that installation of the splitter resulted in an increase in suppression peaking at 6300 Hz which was the tuning frequency of the splitter. There is a degradation in suppression below 3150 Hz, but whether this is due to a flow noise floor or a decrease in bandwidth cannot be established. Opening the nozzle with the splitter installed did not result in any significant change in the suppression levels. One would expect a decrease in suppression if a treatment-regenerated noise floor were being reached at the higher Mach numbers.

Using the results with the 0.52 Mach number and assuming that a noise floor had been reached, the impact of flow noise on the suppressed engine noise was estimated. The Rotor 55 levels were extrapolated to a 152.4-m (500-ft) sideline at a 61-m (200-ft) altitude with an adder of 10 log (treatment area) applied. No frequency shift was made.

The results for the takeoff and approach conditions are given in Figures 189 and 190. At takeoff this "worst case" assumption does not show the flow noise as a problem. The results at approach show that the floor noise level would raise the total engine system noise from its 87.8-PNdB level to 88.5 PNdB.

8.2 COMPOSITE FACEPLATE MATERIALS

A series of studies were conducted to determine the acoustic characteristics of the composite-type faceplate material, Kevlar, which will be used in the QCSEE engine composite nacelle. The results were compared with the characteristics found for the more conventional metal material used for acoustic treatment faceplates to determine if any differences exist.

The following list summarizes the tests conducted to obtain pertinent data in evaluating the acoustic characteristics of the composite faceplate material.

- 5.2 m (17 ft) Arc
- 100% Fan Speed

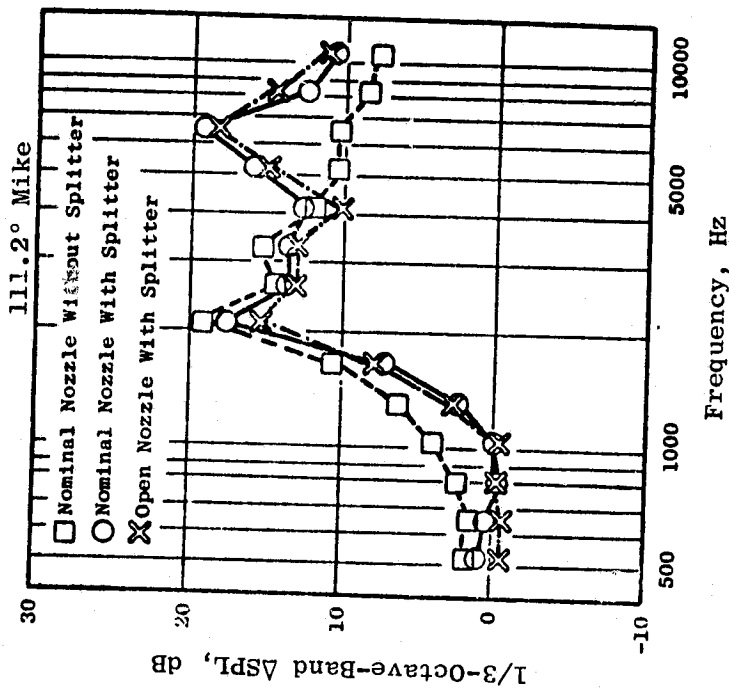
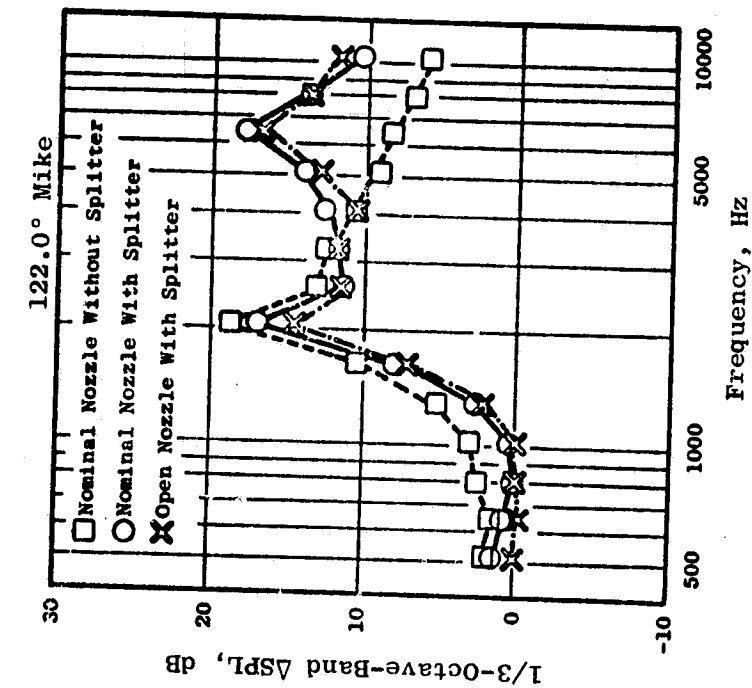


Figure 188. Aft Suppression Spectra Change with Duct Mach Number Change.

- Takeoff Power
- Single Engine
- Max. Aft Angle, 120°
- 152.4 m (500 ft) Sideline at 61 m (200 ft) Altitude

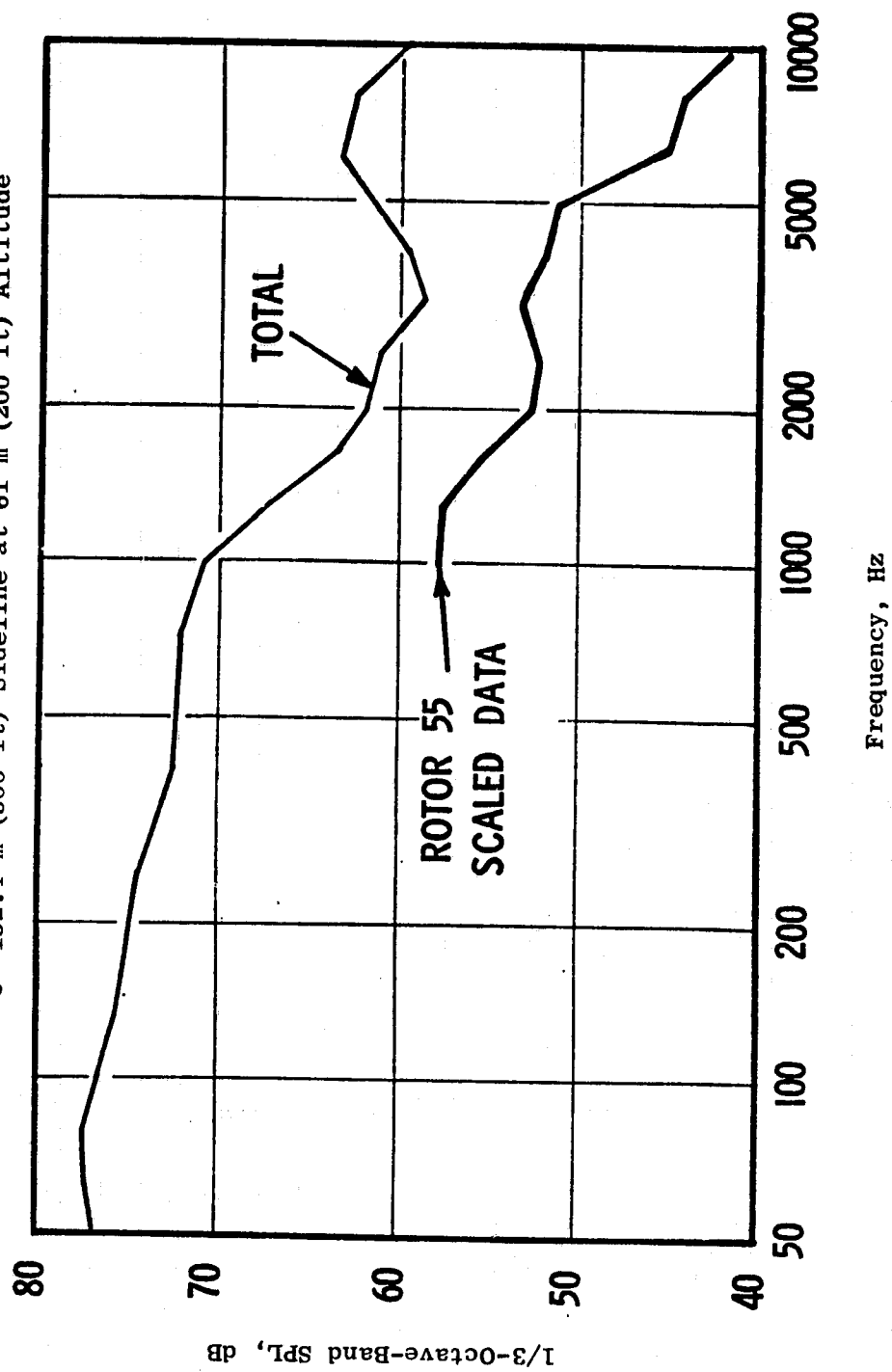
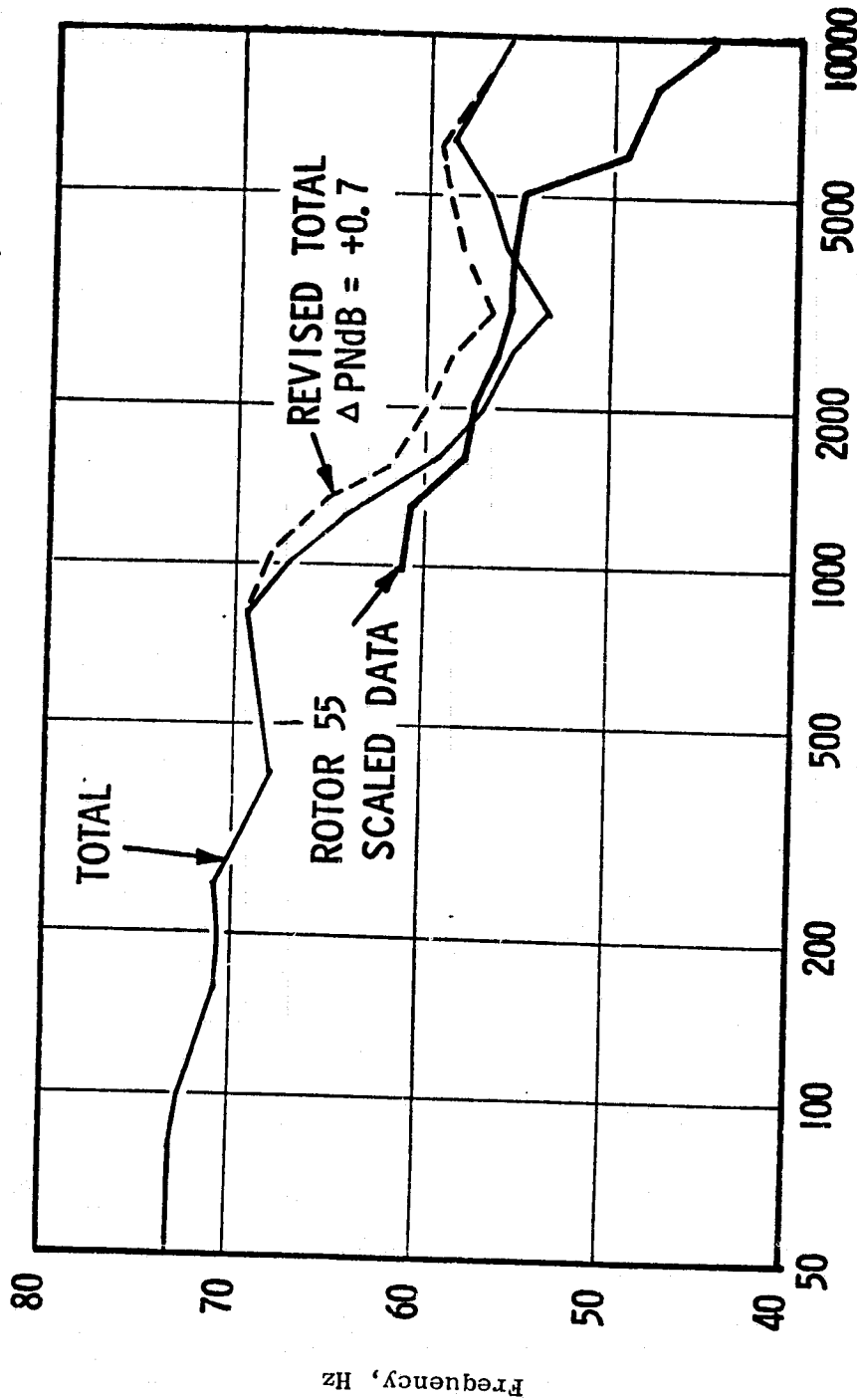


Figure 189. UTW Engine Total System Noise Suppressed Level Vs. Predicted Flow Noise Floor, Takeoff Power.

- Approach Power
- Single Engine
- Max. Aft Angle 120°
- 152.4 m (500 ft) Sideline at 61 m (200 ft) Altitude



1/3-Octave-Band SPL, dB

Figure 190. UTW Engine Total System Noise Suppressed Level Vs. Predicted Flow Noise Floor, Approach Power.

- D.C. Flow Resistance Tests
- Acoustic Duct Transmission Loss Tests
- Normal Impedance Tests

8.2.1 Composite Materials Tested

Two composite faceplate samples were tested and compared with a metal perforate faceplate in the duct cavity flow apparatus. The first was the molded three-ply Kevlar faceplate planned for use in the QCSEE inlet. The second sample was a laser-drilled four-ply graphite faceplate which is planned for use in the fan exhaust. Specifications for these faceplates and the metal perforate faceplate are as follows:

Composite Kevlar Faceplate

Porosity = 10%
 Hole Diameter = 0.158 cm (0.0625 in.)
 Staggered Hole Pattern
 3-Ply Thickness = 0.86 cm (0.034 in.)
 Coated Thickness = 0.177 cm (0.070 in.)

Laser-Drilled Graphite Faceplate

Porosity = 10%
 Hole Diameter = 0.158 cm (0.0625 in.)
 Square Hole Pattern
 Thickness = 0.1 m (0.04 in.)

Metal Perforate Faceplate

Porosity = 10%
 Hole Diameter = 0.158 cm (0.0625 in.)
 Staggered Hole Pattern
 Thickness = 0.08 cm (0.0375 in.)

Due to the current manufacturing methods, tapered holes exist in both composite faceplates. These tapered holes appear as shown in the sketch given in Figure 191.

8.2.2 Test Results

Both normal impedance tube and D.C. flow resistance tests were run on all three faceplate materials. Duct transmission loss tests were run on the composite Kevlar and metal perforate faceplates in a rectangular duct treated on both sides with a treated length of 11.43 cm (4.5 in.) and a duct height of 20.32 cm (8 in.).

Composite Kevlar Faceplate

Laser-Drilled Graphite Faceplate

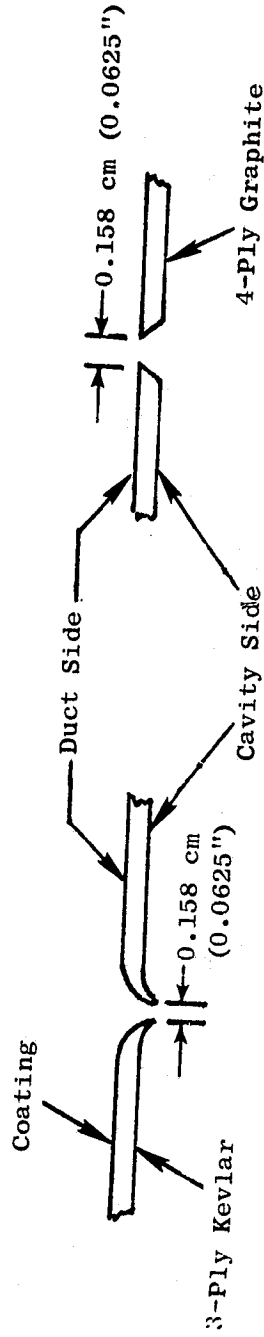


Figure 191. Sketch of Composite Kevlar and Laser-Drilled Graphite Faceplate Materials.

The D.C. flow tests on the QCSEE composite faceplates were conducted to identify possible differences in acoustic resistance between composite and metal perforate faceplates.

Two test cases were run to check the accuracy and repeatability of the data. These results, compared with the predicted and previous results are shown in Figure 192. The predicted resistance is based on the following equation derived in earlier D.C. flow work with metallic perforate sheet:

$$R = 0.862 \frac{\rho u}{\sigma^2}$$

where

R = resistance	mks rayls
ρ = air density	kg/m ³
u = flow velocity	m/sec
σ = porosity	dimensionless

Figure 192 shows good agreement with both the previous D.C. flow test data and the correlation equation.

Test results for the composite faceplates are shown in Figures 193 and 194, and also are compared with the predicted resistance. The results indicate that the D.C. flow resistance does differ with the flow direction through the tapered holes for both composite faceplates. These D.C. flow differences, however, are reasonably small. The dashed lines on the figures indicate a two percent change in porosity to show the magnitude of the changes.

The duct transmission loss tests were run to check the suppression characteristics and identify differences between the composite Kevlar and metal perforate faceplates. Figures 195, 196, and 197 show the measured rectangular duct results for Mach numbers 0.0, 0.3, and 0.4. Note that the thicker composite Kevlar faceplate shifts the peak suppression down approximately 1/3 octave and does not appear to change the amount of peak suppression. The shifting of the peak suppression frequency can be attributed to the differences in faceplate thickness. No correlation on the amount of peak suppression can be obtained from these results, since 10% porosity is over-damped and the peak frequency shifts with no adjustment being made to maintain an optimum porosity. However, these results do indicate the corrections necessary to a treatment design to maintain comparable suppression.

The final tests were conducted to determine the normal impedance characteristics of the various samples. These results are presented in Figure 198. For each sample, the resistance results were nearly identical. The reactance,

- 10.0% Porosity
- Hole Diam = 0.158 cm (0.0625 in.)
- Thickness = 0.083 cm (0.0325 in.)
- 22.7% Porosity
- Hole Diam = 0.158 cm (0.0625 in.)
- Thickness = 0.1 cm (0.041 in.)

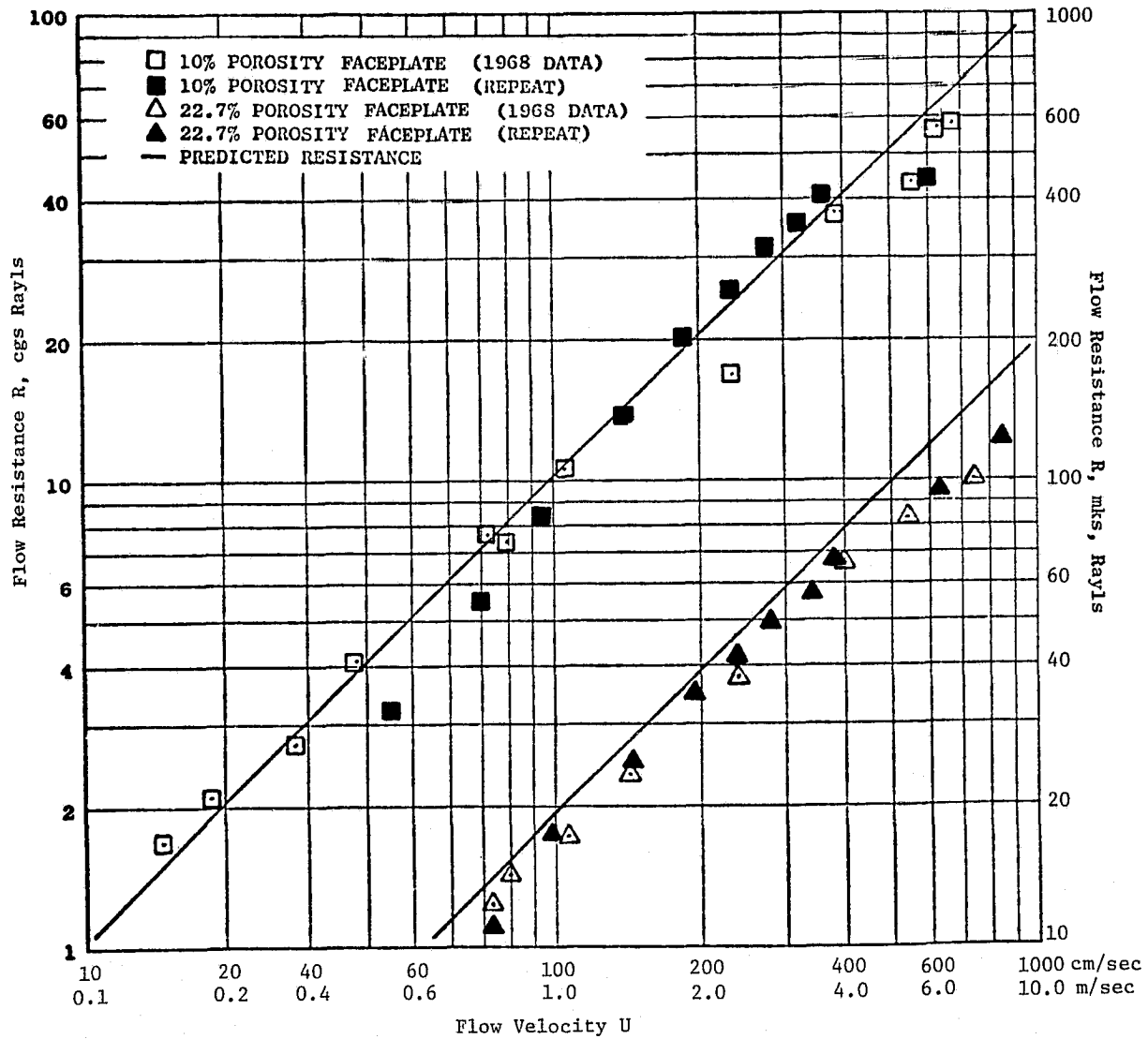


Figure 192. Duct Cavity Flow Resistance, Metal Perforate Faceplate.

- Hole Diam = 0.158 cm (0.0625 in.)
- Thickness = 0.086 cm (0.034 in.)

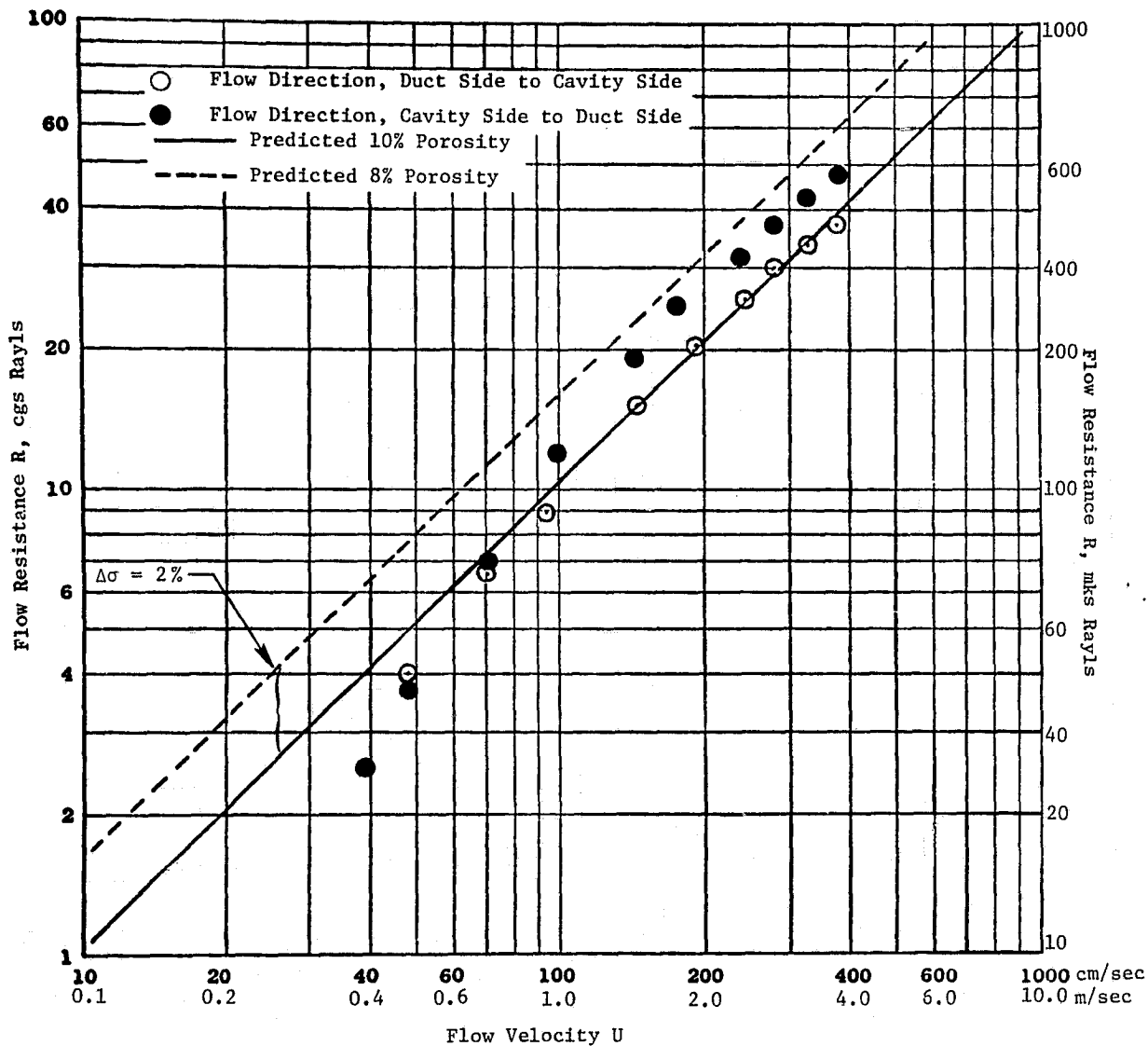


Figure 193. Duct Cavity Flow Resistance, Kevlar 3-Ply Composite Faceplate.

- Porosity = 10%
- Hole Diam - 0.158 cm (0.0625 in.)
- Thickness - 0.1 cm (0.04 in.)

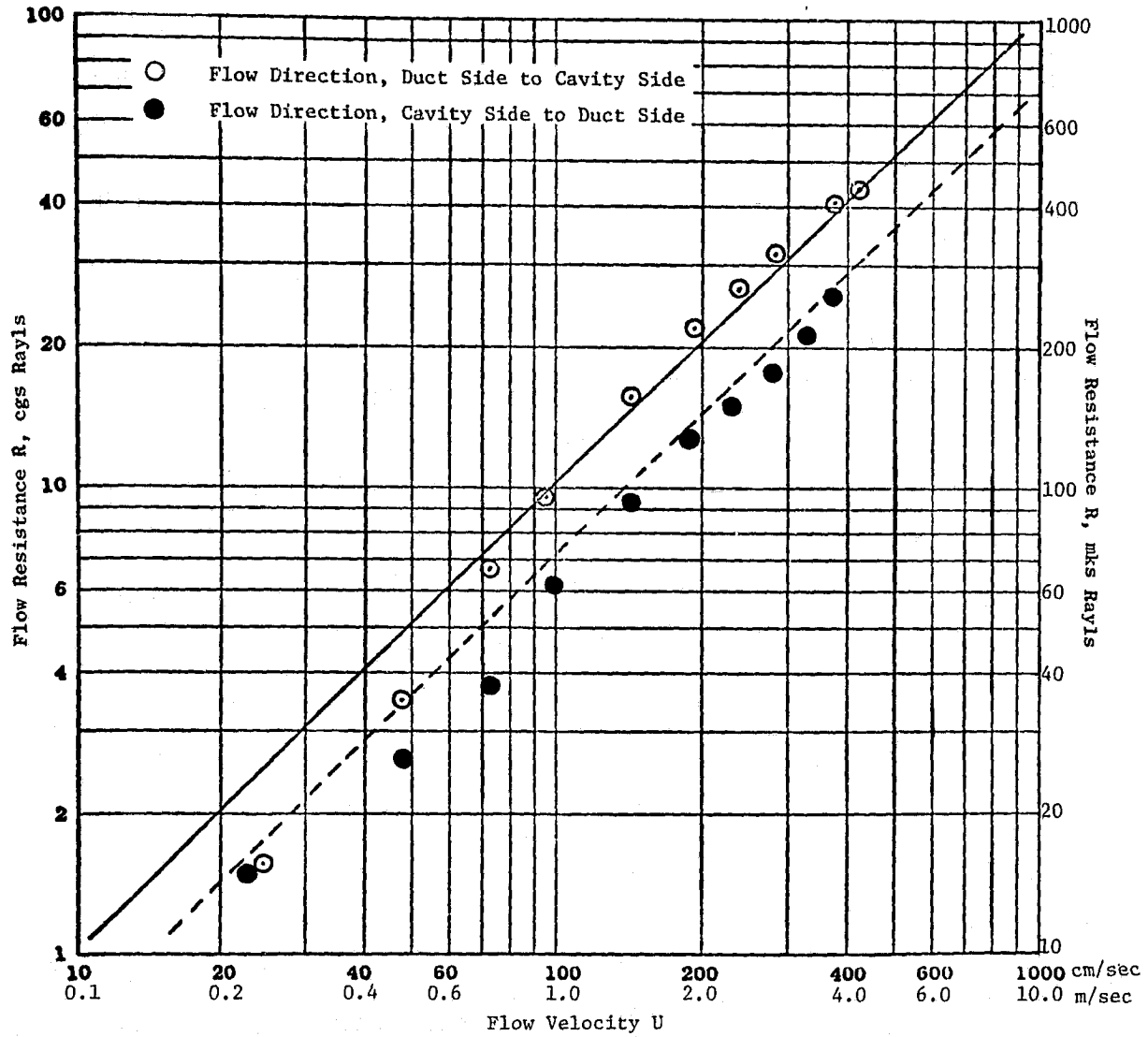


Figure 194. Duct Cavity Flow Resistance, Graphite 4-Ply Composite Faceplate.

- $L/H = 4.5$, $H = 20.32$ cm (8.00 in.)
- Core Depth = 1.9 cm (0.75 in.)

--- Composite Kevlar Faceplate
 — Perforated Metal Faceplate

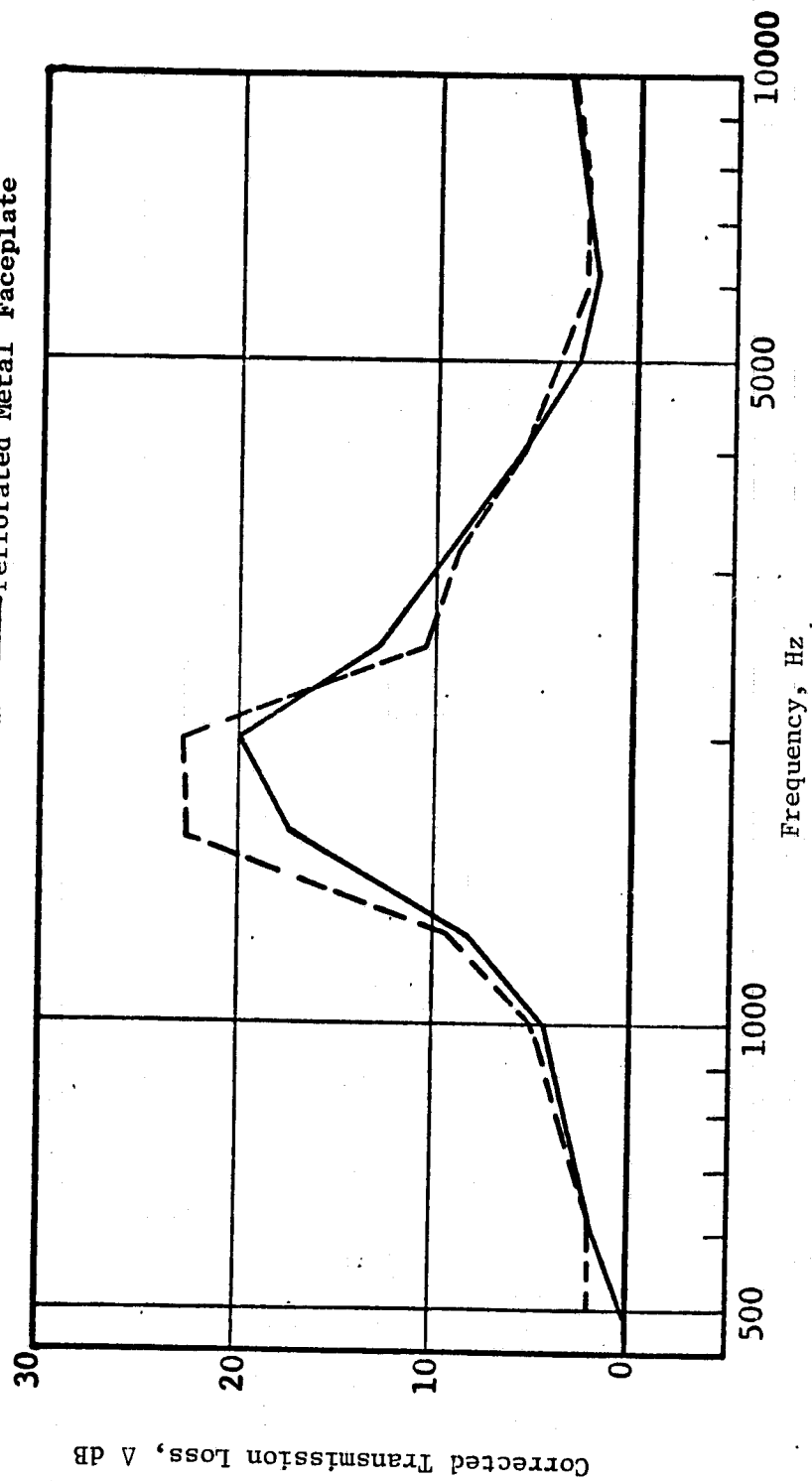


Figure 195. Duct Transmission Loss Results, Mach No. = 0.

- $L/H = 4.5$, $H = 20.32$ cm (8.00 in.)
- Core Depth = 1.9 cm (0.75 in.)

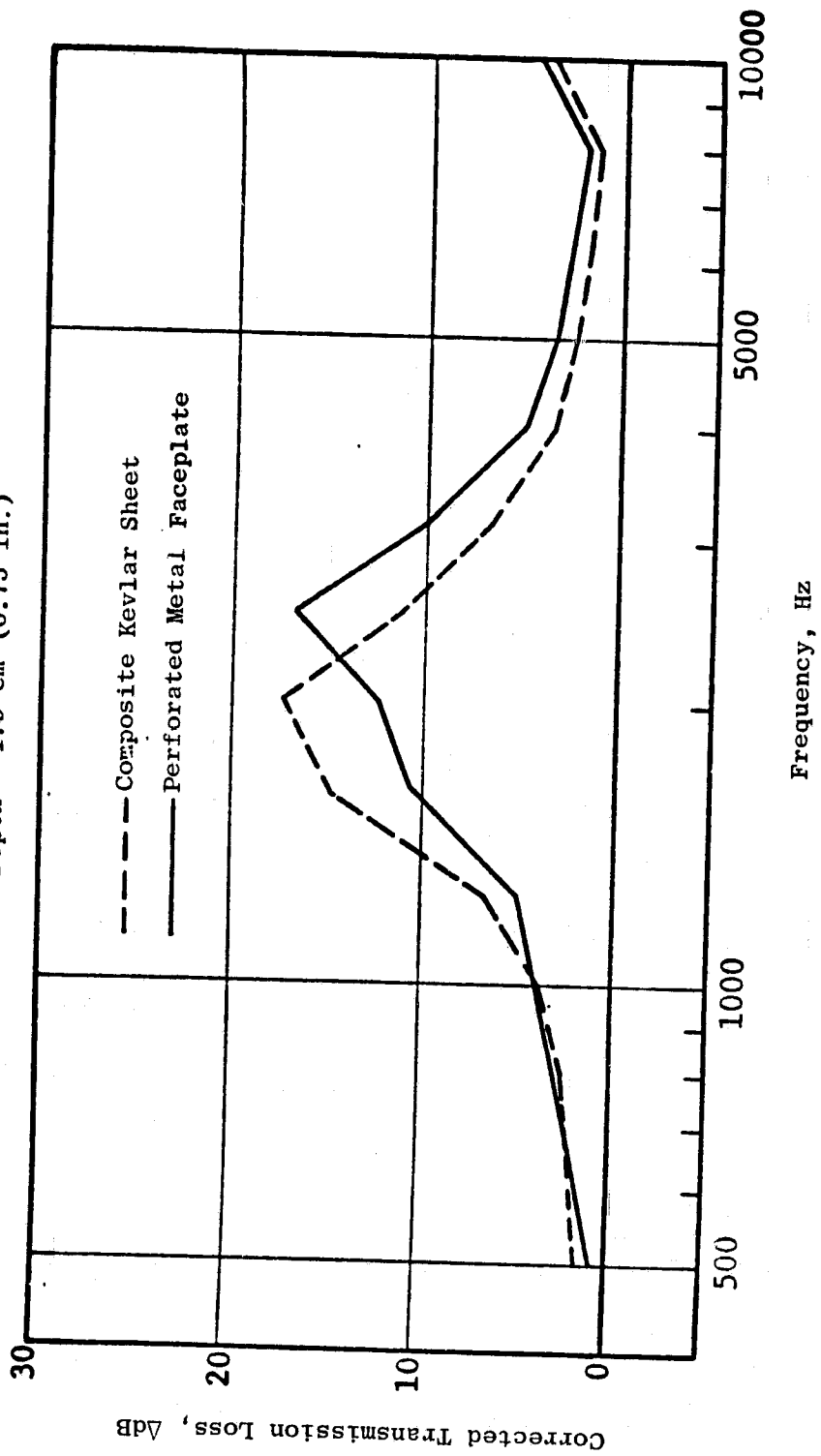


Figure 196. Duct Transmission Loss Results, Mach No. = 0.3.

- $L/H = 4.5$, $H = 20.32$ cm (8.00 in.)
- Core Depth = 1.9 cm (0.75 in.)

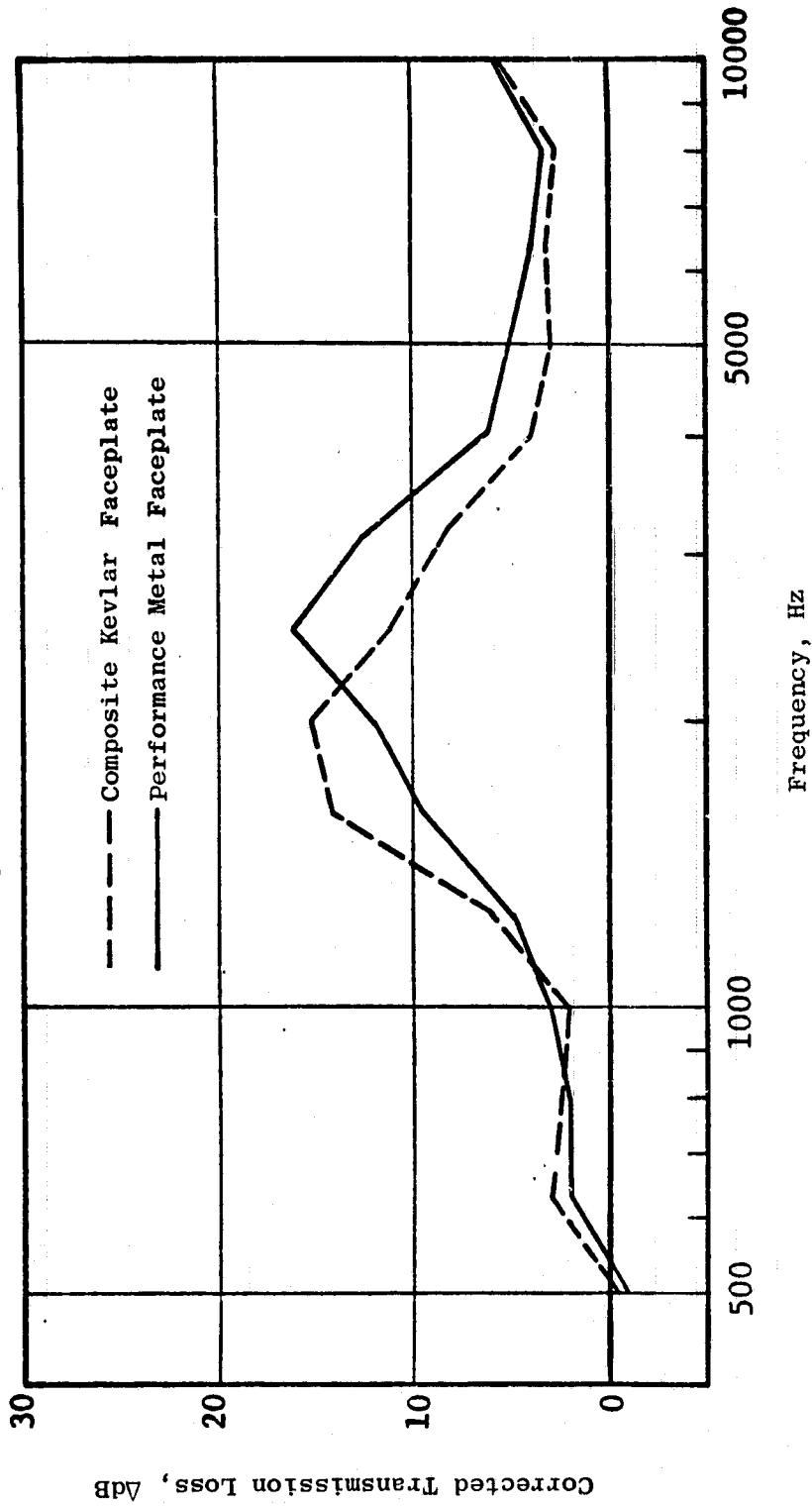


Figure 197. Duct Transmission Loss Results, Mach No. = 0.4.

- Laser-Drilled Graphite Faceplate
- Composite Kevlar Faceplate
- Perforated Metal Faceplate

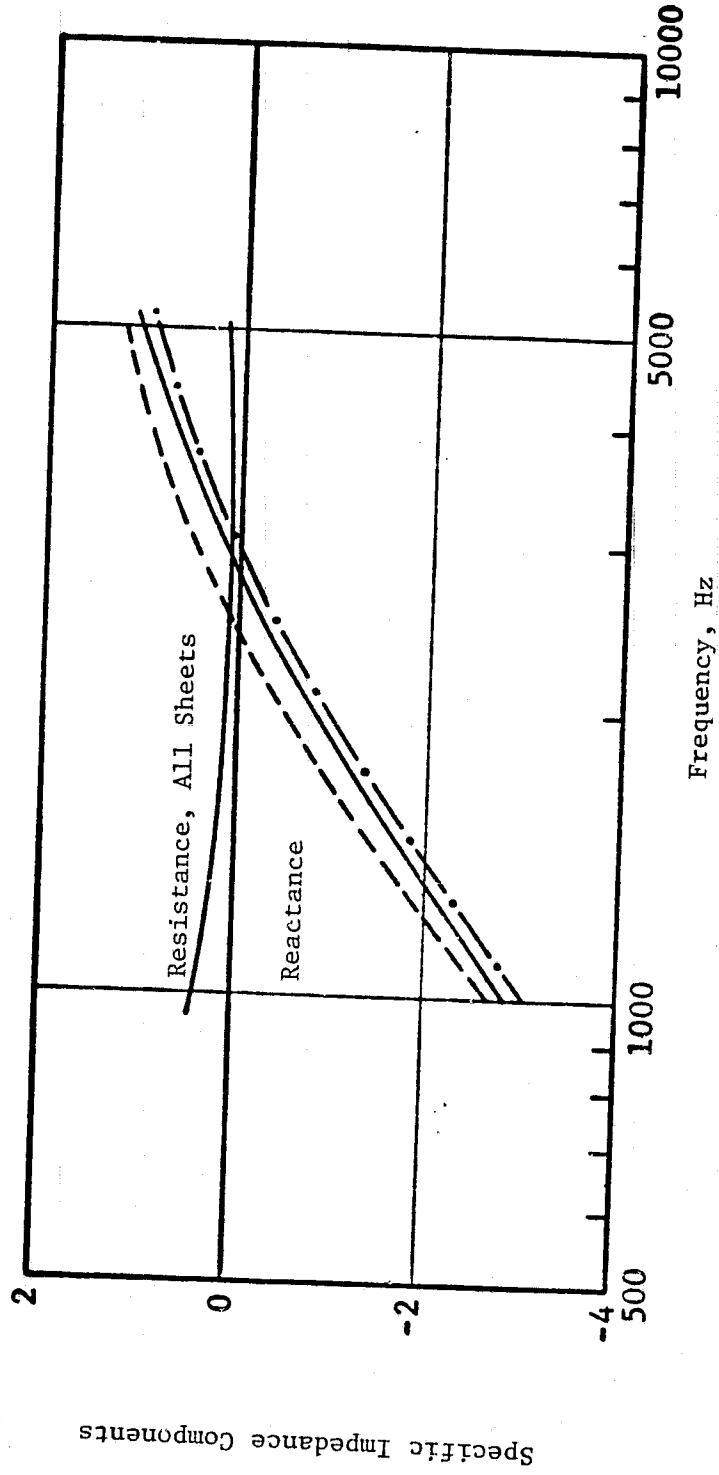


Figure 198. Normal Impedance Test Results.

however, does differ and agrees with the peak frequency shift, as seen in the transmission loss results.

Therefore, from the data presented here, the proper adjustments can be defined and the corrections incorporated into a composite faceplate treatment design equivalent to a conventional design.

8.3 COMPOSITE NACELLE FLEXIBLE JOINT TRANSMISSION LOSS STUDY

The QCSEE composite nacelle will utilize chevron seals at a number of flexible joint locations to aerodynamically seal access panels and doors. Since the chevron seal is designed to withstand chemicals and engine aerodynamic conditions, its suitability for containing the high sound pressure levels were unknown. To answer this question, a series of tests were defined in which a test panel typical of the engine nacelle was built and tested with a number of seal configurations using standard transmission loss procedures. The test results were analyzed to determine whether the seals were a problem and if so, whether the problem could be corrected. These results are presented and discussed below.

8.3.1 Identification of Nacelle Flex Joints

Preliminary analysis of the QCSEE composite nacelle considered the six seal joints shown in Figure 199 and identified the most critical areas subject to noise leakage. Figures 200 through 203 are detailed views showing the construction at the seal locations designated at 1, 2, 5, and 6 in Figure 199. Seal Locations 3 and 4 were omitted from further consideration due to their remote location relative to the noise source. Seal Location 3 can only radiate or leak noise to the inner engine structure, causing no far-field noise leakage problem. Seal Location 4 would only short-circuit the flap treatment; to be a problem, the seal would have to have a very small transmission loss. Seal Locations 1 and 2 (shown in Figures 200 and 201) are circumferential seals located forward and aft of the fan and are considered to be possible problem areas since they are subjected to the unsuppressed noise levels. Of the two seal locations, Seal Location 1 appears to be the most prone to noise leakage, because it has no positive interlocking surface.

Figures 202 and 203 show Locations 5 and 6, which are axial seals located either side of the pylon and along the bottom of the engine. A comparison of these figures indicates that Seal Location 6 would be most prone to noise leakage. Therefore, Seal Locations 1 and 6 were identified as possible problem areas, with Seal Location 6 selected to be lab tested, since when compared to Seal Location 1 it is the more prone to noise leakage, due to its small joint thickness and slot offset.

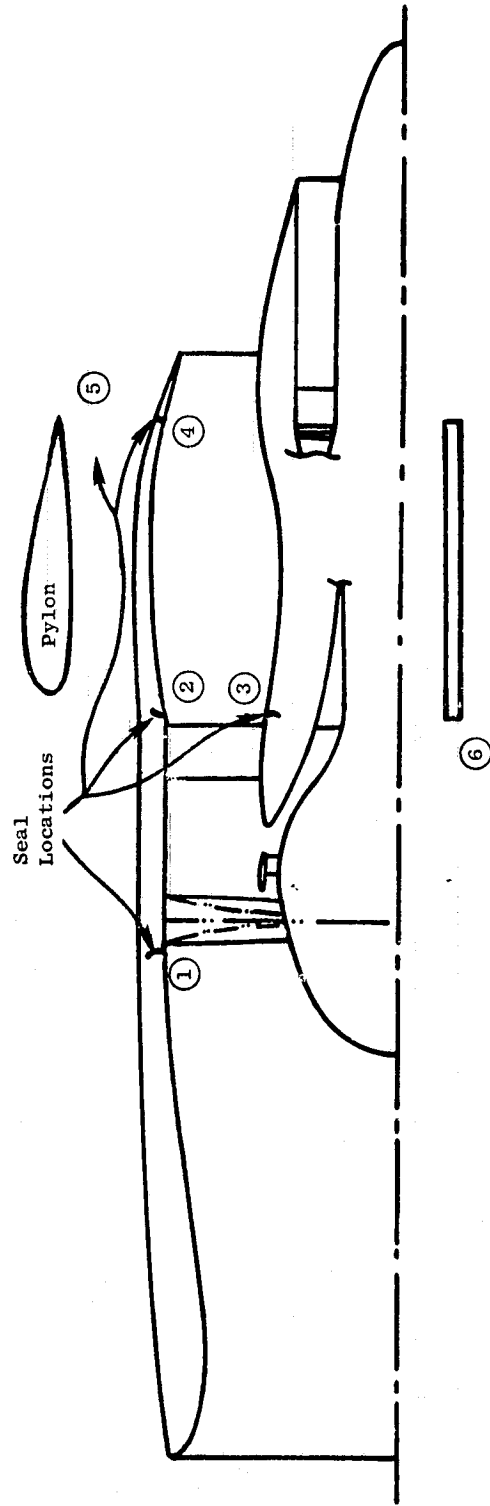


Figure 199. Engine Seal Locations.

● Location 1 in Figure 199.

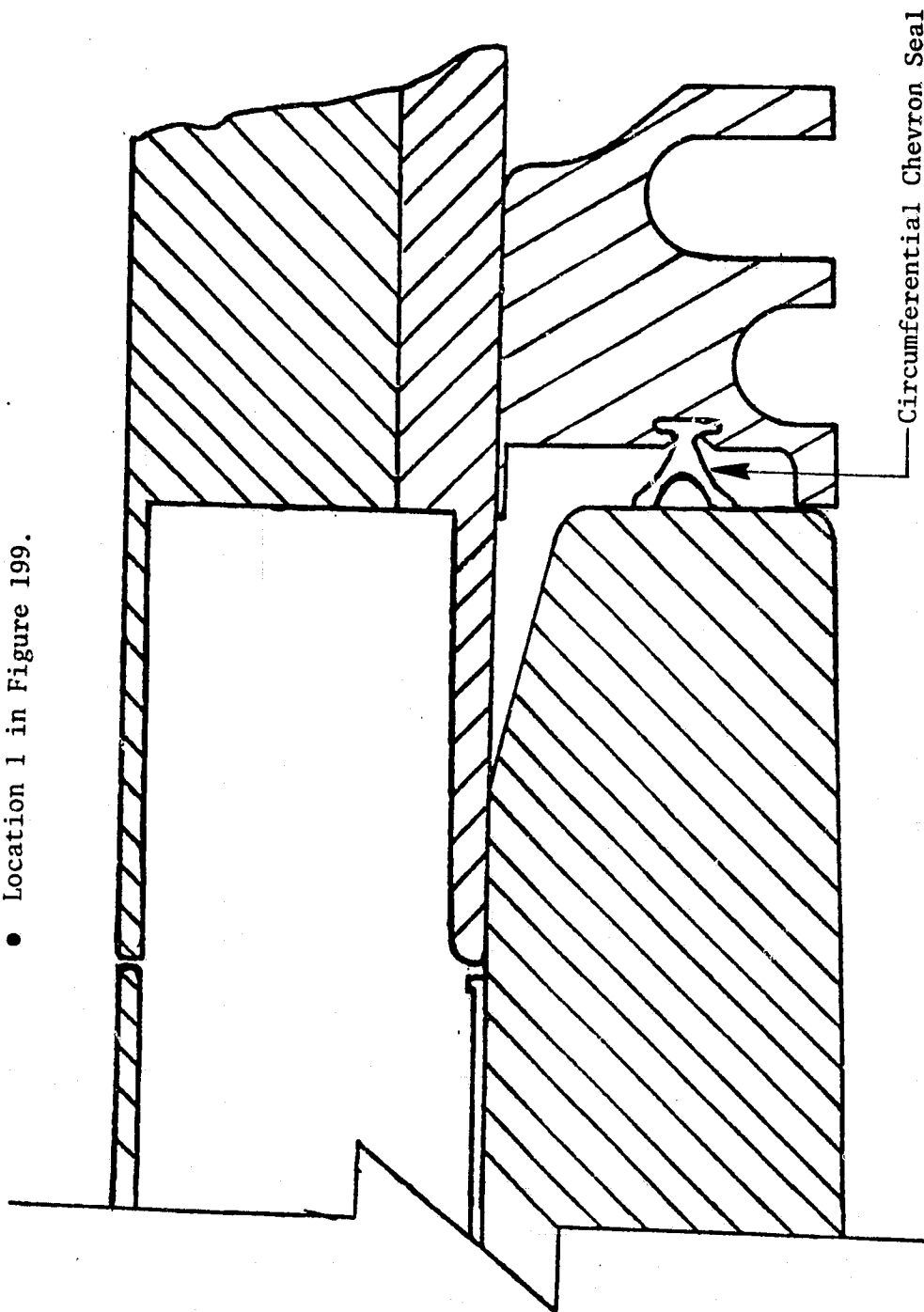


Figure 200. Outer Cowl/Inlet Attachment Forward of Fan Frame.

● Location 2 in Figure 199.

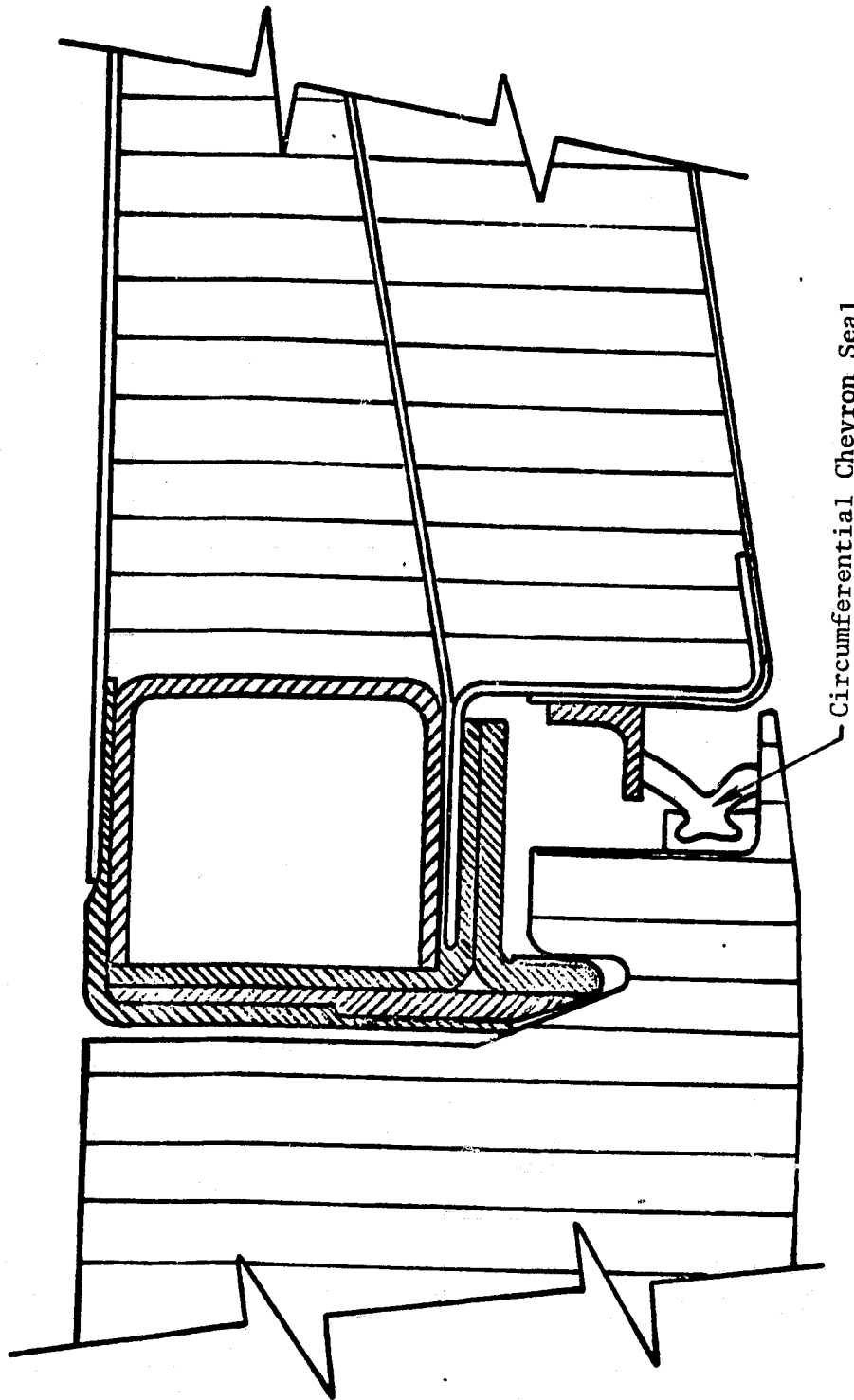


Figure 201. Outer Cowl/Fan Frame Attachment Aft Fan Frame.

● Location 5 in Figure 199.

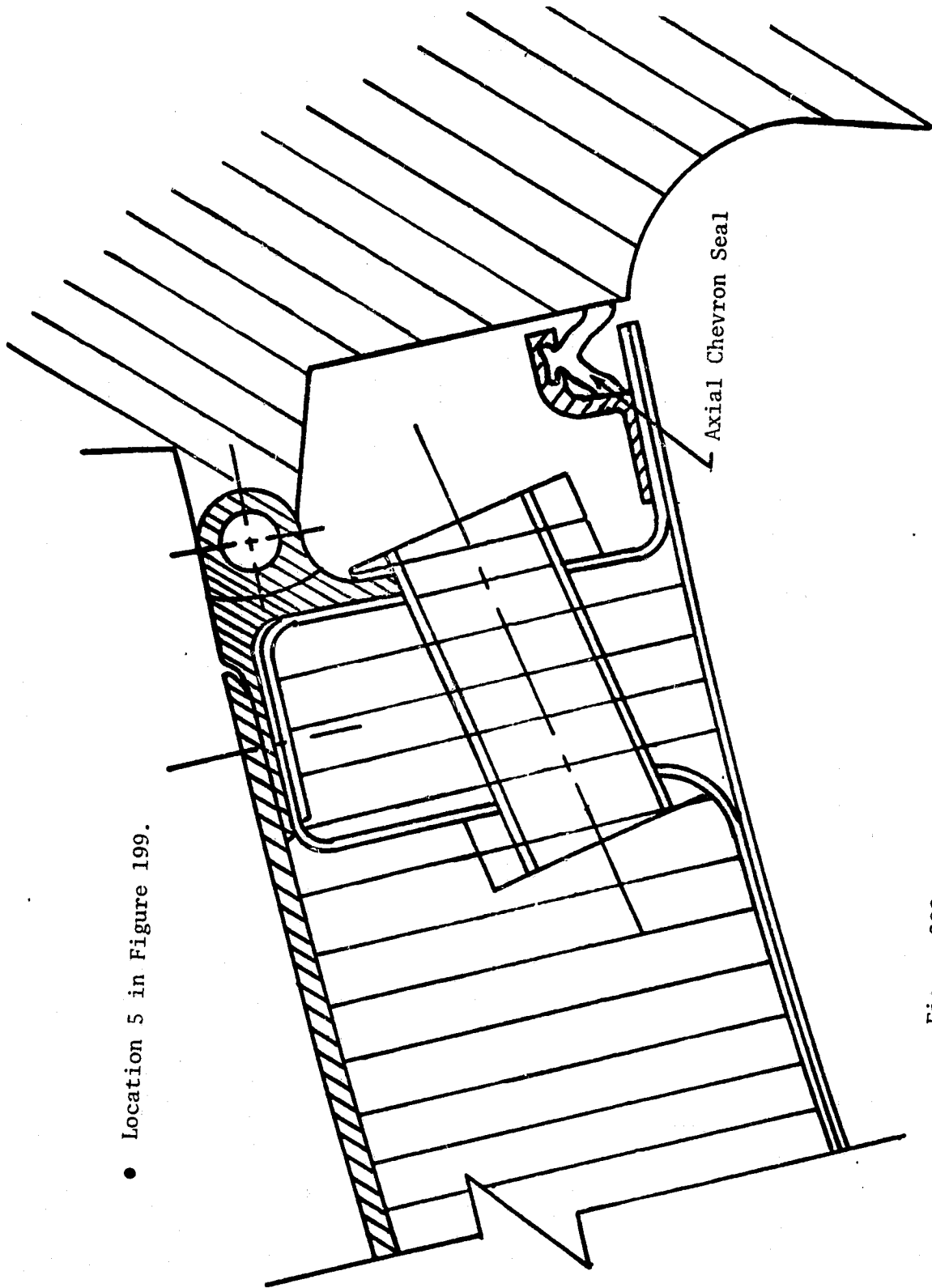


Figure 202. Nacelle/Pylon Hinge Seal Outer Cowl.

- Location 6 in Figure 199

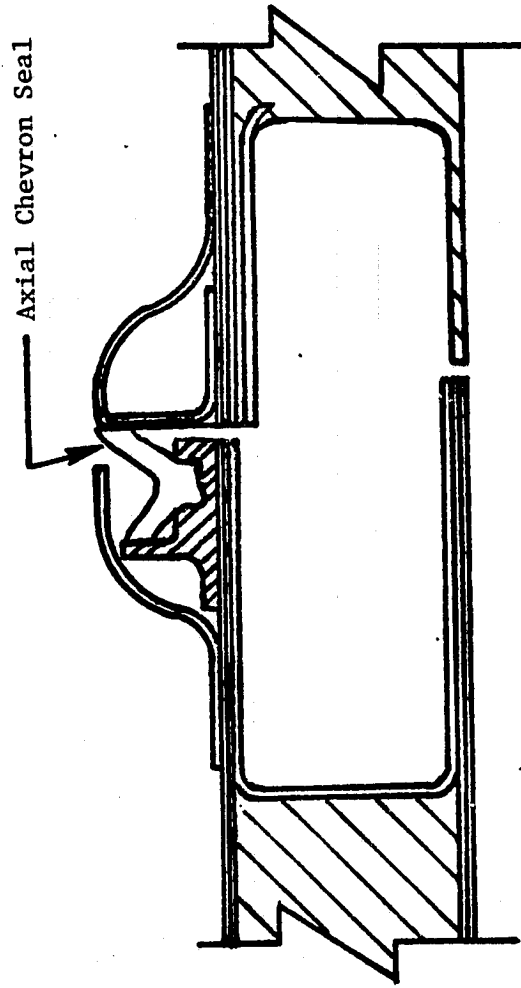


Figure 203. Outer Cowl Rotary Latch Seal.

8.3.2 Transmission Loss Test Arrangement

The 0.91-m (3-ft) by 2.13-m (7-ft) test panel was composed of two composite structures aligned by pins, as shown in Figure 204. The construction was typical of composite nacelle engine hardware in that the materials, densities, and dimensions resembled engine seal locations. A perforated Kevlar faceplate to model engine treatment was not tested for reasons of cost, the possibility of obscuring the seal performance, and violating ASTM transmission loss standards. The chevron seal was chosen for use in the composite nacelle and is presently in use on the GE CF6 production engines. The seal is composed of a polyester dacron core molded into a fluorosilicone rubber seal; it was tested in the configuration shown in Figure 204. A second seal, the bulb seal shown in Figure 205, was tested for comparison purposes to determine a possible means for increasing the acoustic performance of the seals. Limiting test cases, represented by no seal and a solid test panel, were also tested so as to identify the joint characteristics. The solid test panel serves as a reference case and the seal configuration shows the effect of an offset leakage path. The frequency range was 125 to 10,000-Hz 1/3-octave bands and the source sound power was as large as the lab could reasonably obtain.

8.3.3 Transmission Loss Test Results

Test results were obtained for the configurations below.

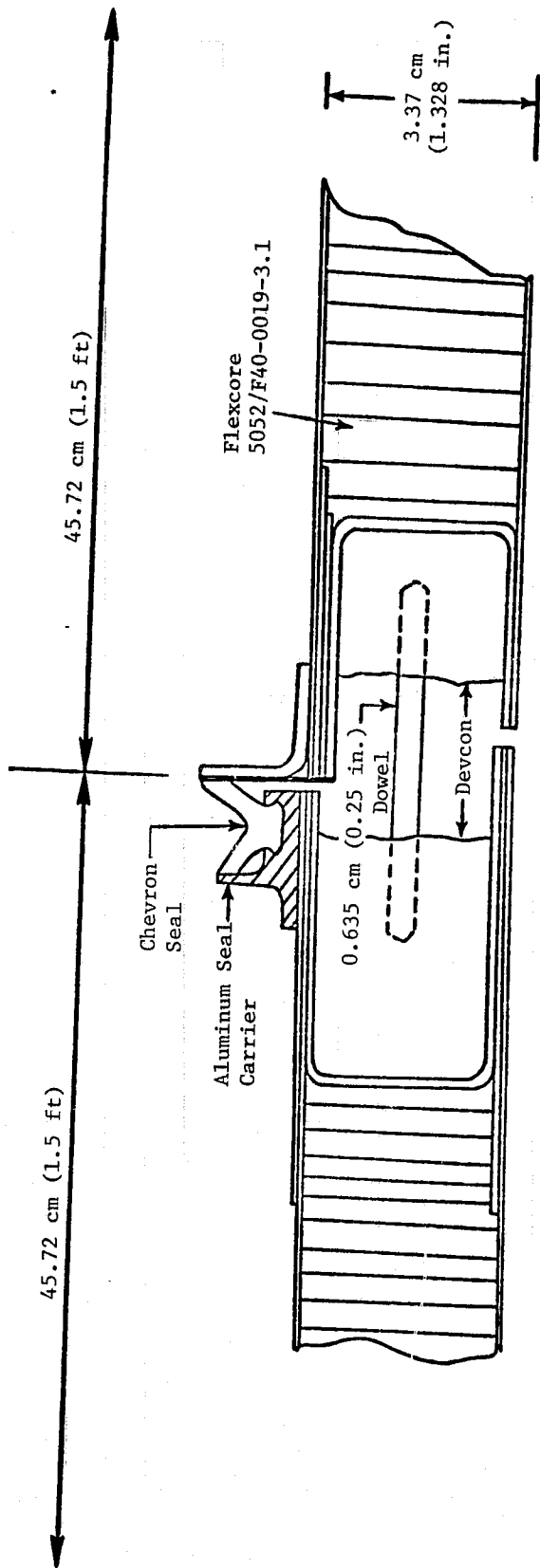
Summary of Test Configuration Definitions

1. Base Structure - 1/8-in. vertical gap sealed (7-ft direction)
2. Chevron Seal - 1/8-in. vertical gap with chevron seal
3. Bulb Seal - 1/8-in. vertical gap with bulb seal at 50% compression
4. No Seal - 1/8-in. vertical open gap; no seal present.

The lab report can be found in Appendix A. From those results the comparisons shown in Figures 206 through 208 were plotted, comparing the base structure results with the chevron, the bulb, and the no-seal results. These comparisons show the seal and gap configurations' relative transmission loss effects on the base structure for the panel tested. These are not absolute levels, since an engine configuration would have different seal-to-base structure area ratios. Figure 209 compares the bulb and chevron seal configurations and indicates the respective effects of the two seals.

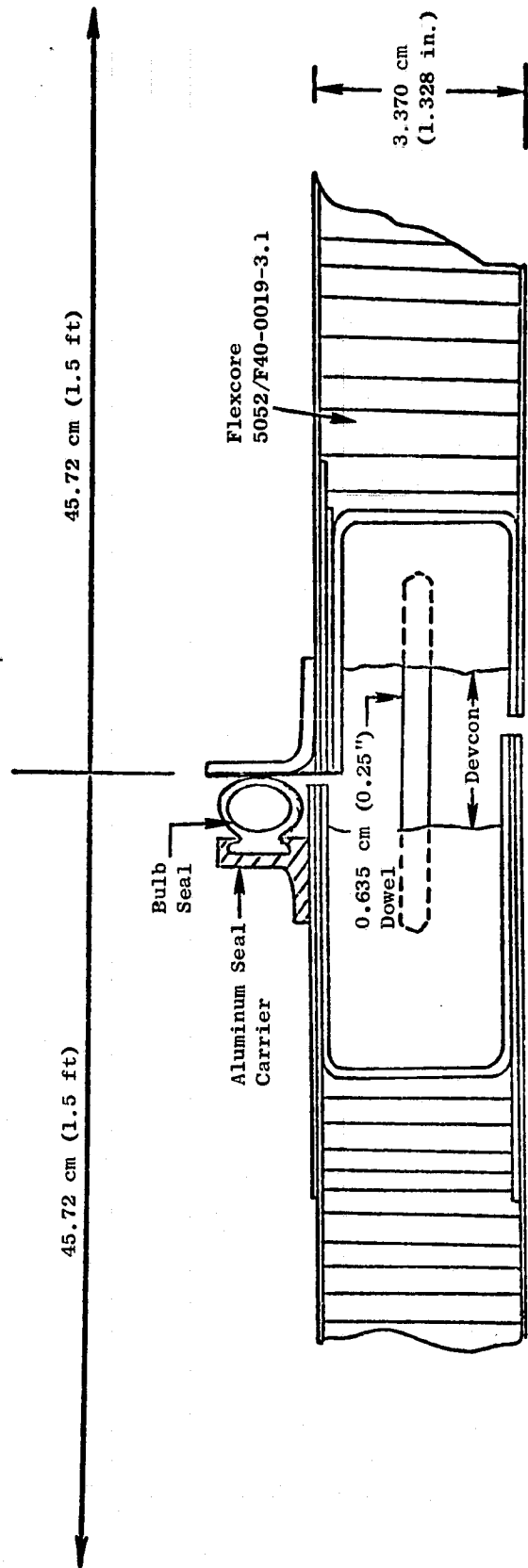
8.3.4 Data Analysis and Application to Engine Configuration

The engine flexible seal joint performance was estimated by evaluating the seal effects on the far-field engine spectra for the critical transmission



- All Material Is 3-Ply Kevlar Except Where Noted.
- Each Panel Is 2.13-m (7.0 ft) Long in Seal Direction.
- 0.635 cm (0.25 in.) Dowel Pins to Simulate Latches Potted-in at Approximately Every 19.05 cm (7.5 in.)

Figure 204. Chevron Seal Test Configuration.



- All Material Is 3-Ply (Kevlar) Except Where Noted
- Each Panel Is 2.13 m (7.00 ft) Long in Seal Direction
- 0.635 cm (0.25") Dowel Pins to Simulate Latches Potted-in at Approximately Every 19.05 cm (7.5")

Figure 205. Bulb Seal Test Configuration.

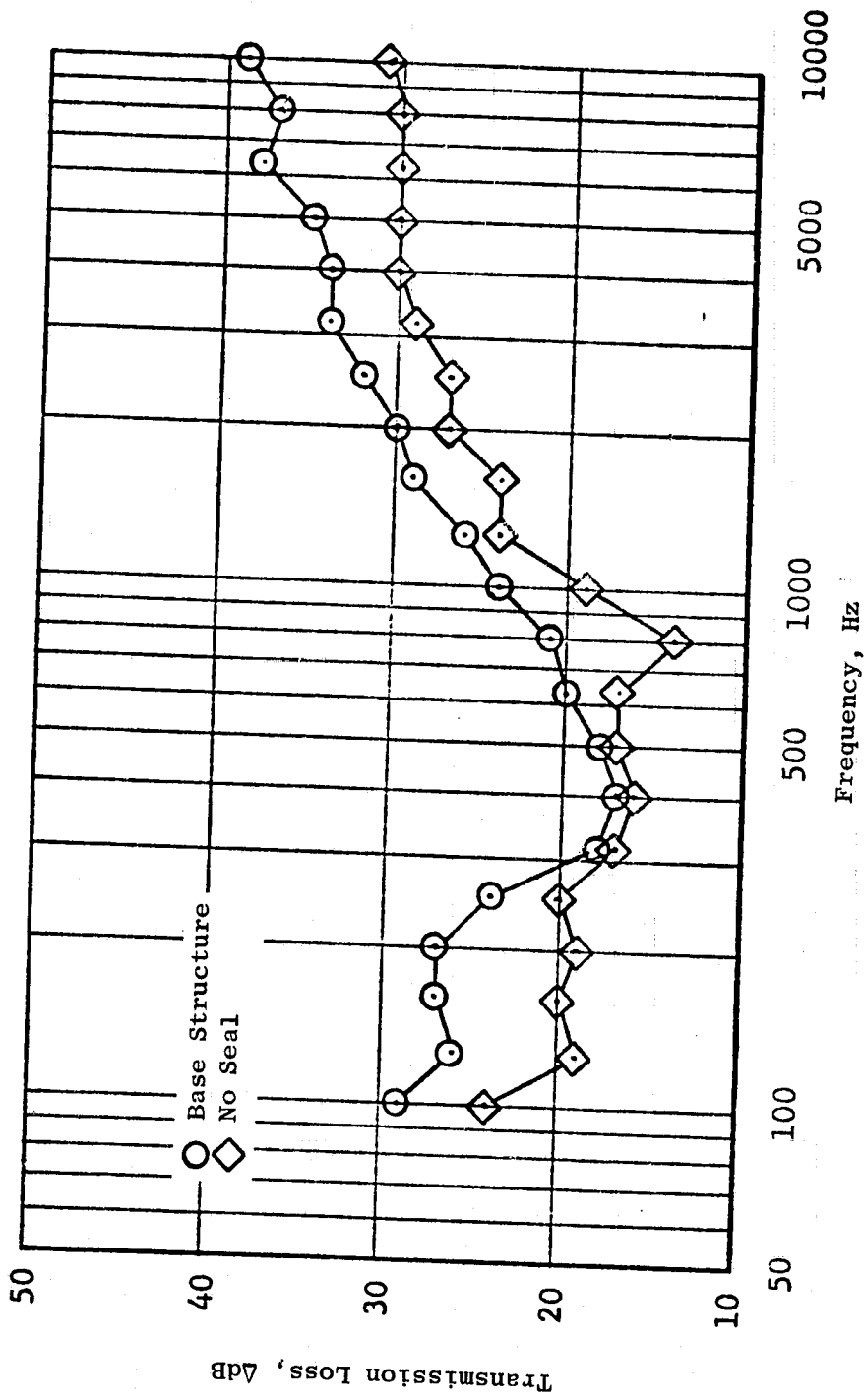


Figure 206. Base Structure Vs. No Seal Transmission Loss.

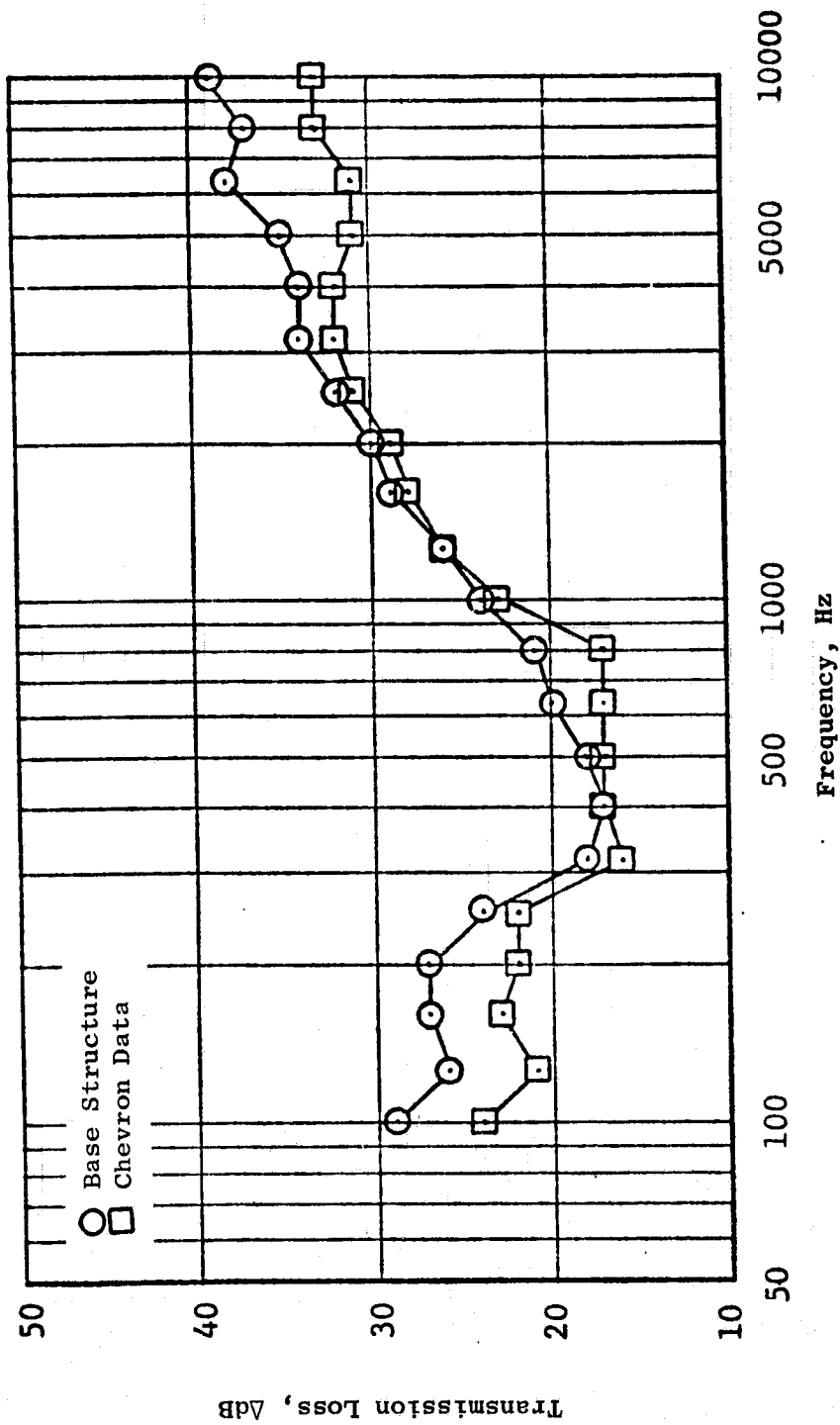


Figure 207. Base Structure Vs. Chevron Seal Transmission Loss.

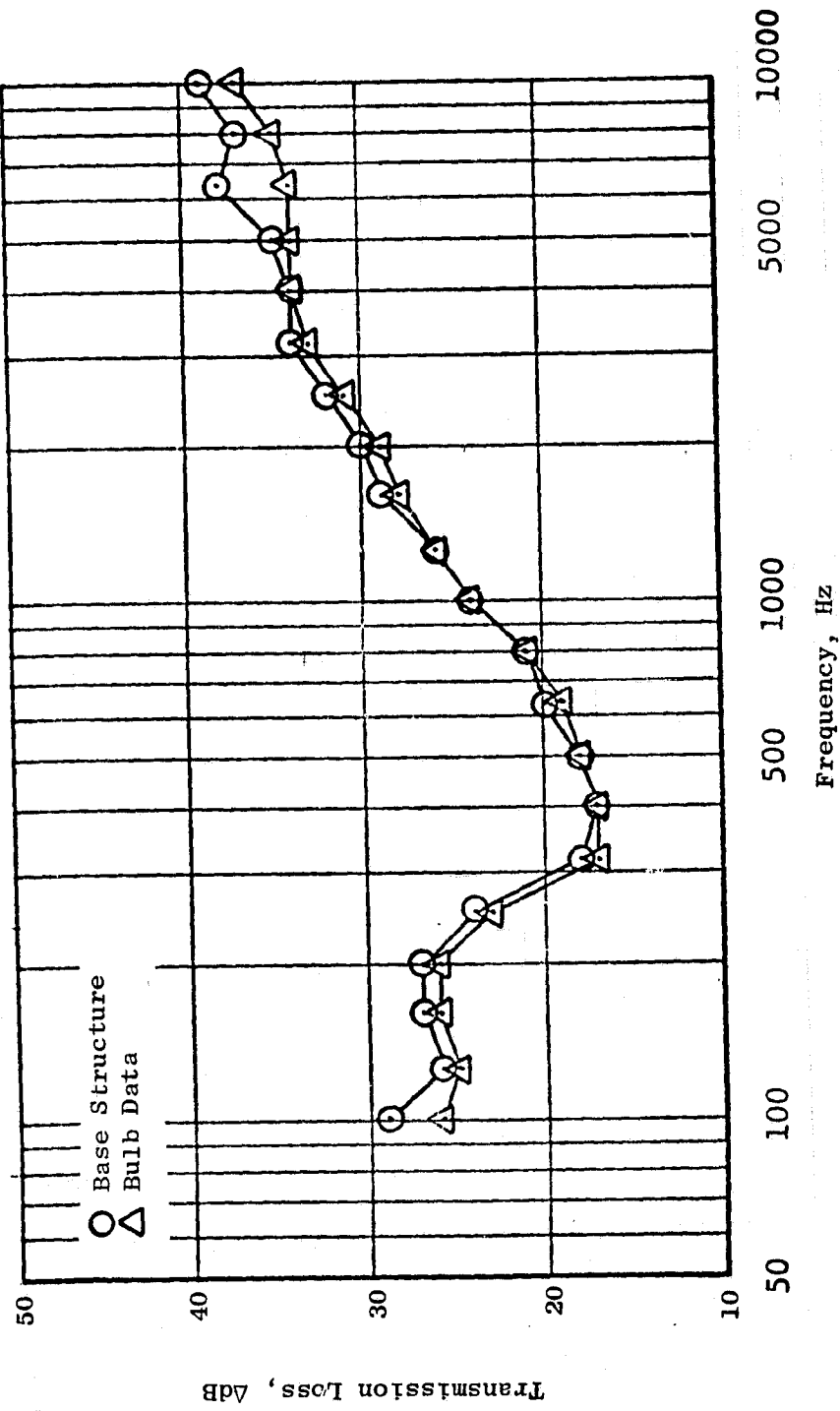


Figure 208. Base Structure Vs. Bulb Seal Transmission Loss.

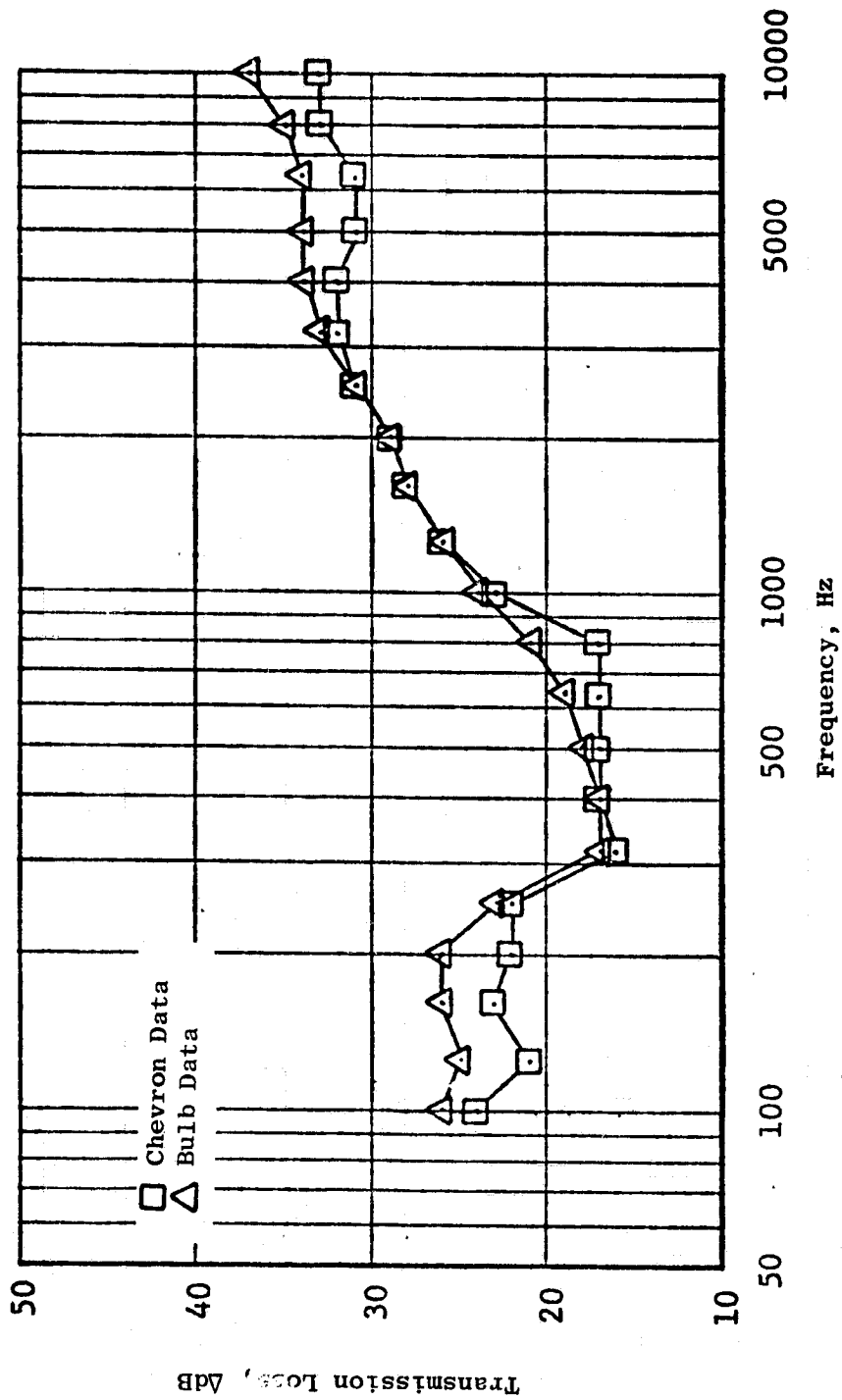


Figure 209. Chevron Seal Vs. Bulb Seal Transmission Loss.

paths. The results showed small increases in the critical sound pressure levels, increases that result in very small perceived noise level (PNL) changes when applied to the proper spectra. The following paragraphs show how the test data were corrected and applied to the engine to analyze the far-field affects.

The test data presented in Figures 206 through 209 apply to the configurations tested, which have panel areas of 1.95 m² (3024.0 in.²) and gap or seal areas of 0.0068 m² (10.5 in.²). These two areas represented the possible sound transmission paths as shown in Figure 210(a). By application of the following equation the contribution of the seal addition was determined.

$$\Delta \text{SPL} = 10 \text{ Log}_{10} \left[1 + 10 \left\{ \frac{(\text{TL}_1 - \text{TL}_2) - 10 \text{ Log}_{10} \frac{A_1}{A_2}}{10} \right\} \right]$$

where: ΔSPL = Difference in transmission loss of the test panel with and without the seal (dB)

TL_1 = Transmission loss of just the base structure (dB)

TL_2 = Transmission loss of the seal only (dB)

A_1 = Area of the base structure m² (in.²)

A_2 = Area of the seal m² (in.²)

The ΔSPL and TL_1 were obtained from the measured data and then combined with the known areas, A_1 and A_2 , to yield the seal transmission loss, TL_2 , through the seal alone. This seal transmission loss was then used to make the engine evaluation.

The engine seal areas that seemed the most critical were defined earlier herein as the axial seals on the fan cowling. Supplementing this knowledge with the high fan exhaust suppressions expected, as shown in Figure 211, it appeared that there might be a noise leakage problem at 1000 or 2000 Hz. Therefore, the engine configuration was analyzed, and we judged the fan cowling seals and the fan exhaust duct to be the two transmission paths (see Figure 210(b)). For the engine configuration, the fan exhaust area was 30 m² (4651.0 in.²) and the seal area, 1.34 m² (20.7 in.²). The far-field results - again using the equation given above - indicated that the engine sound pressure levels for the chevron seal configuration would increase about 0.3 dB at both 1000 and 2000 Hz. Similarly, the bulb seal data resulted in no engine far-field sound pressure level increase at 1000 Hz (0.0 dB) and an increase of 0.3 dB at 2000 Hz. Running the engine with no seal (that is, with gap only) would yield sound pressure level increases of 1.9 and 1.2 dB at 1000 and 2000 Hz. Note that in all the above cases the source was assumed constant for both the fan exhaust and seal area, when in fact the source varies along the seal area because of the treatment. This means the above numbers are a little pessimistic.

Applying the new sound pressure level changes to a predicted fan exhibit spectrum shown in Figure 212 yields the following PNL numbers.

C-4

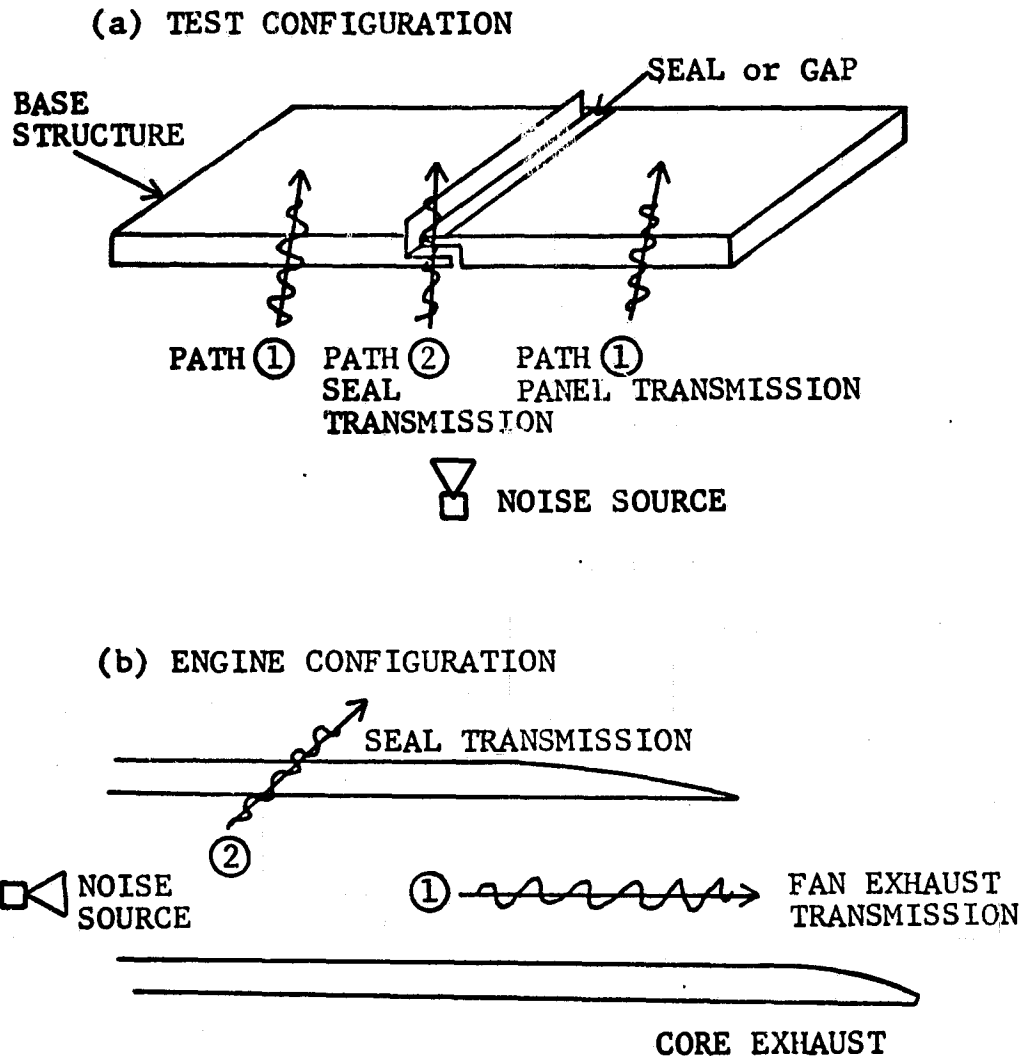


Figure 210. Test Panel and Engine Sound Transmission Paths.

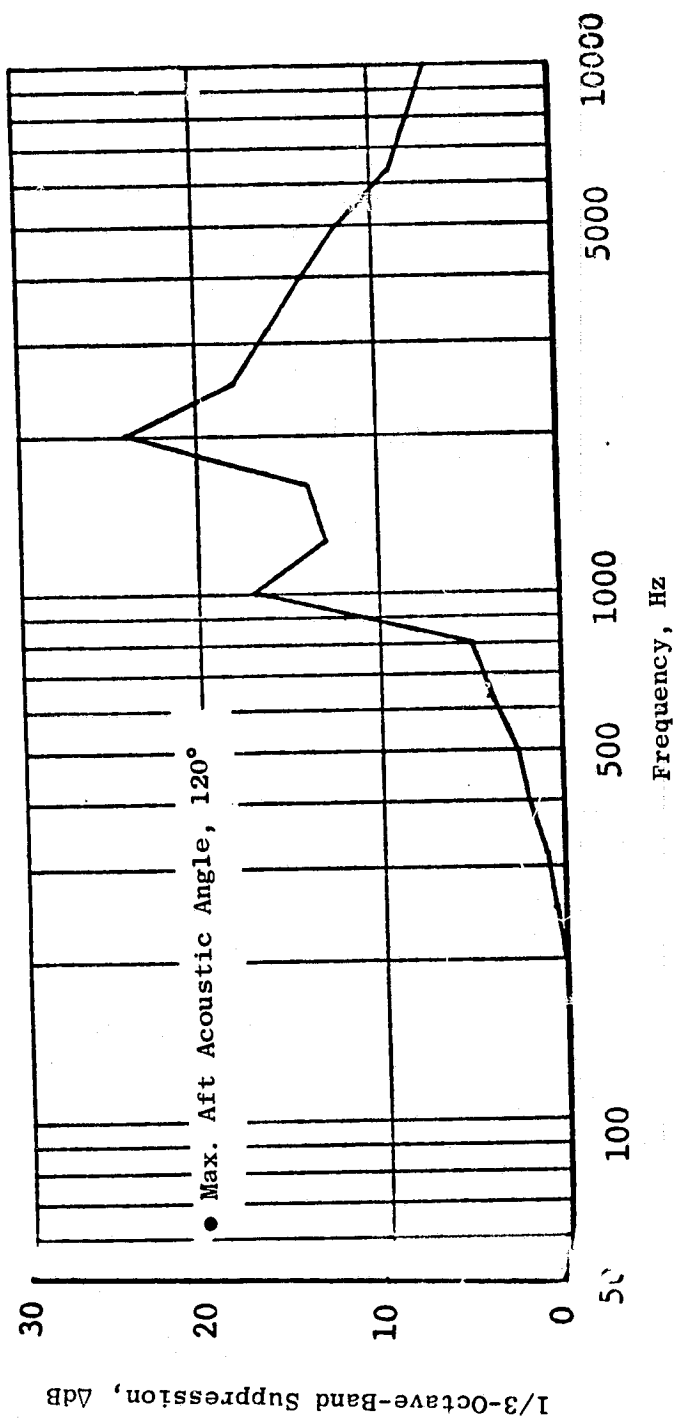


Figure 211. OCSEE Fan Exhaust Suppression.

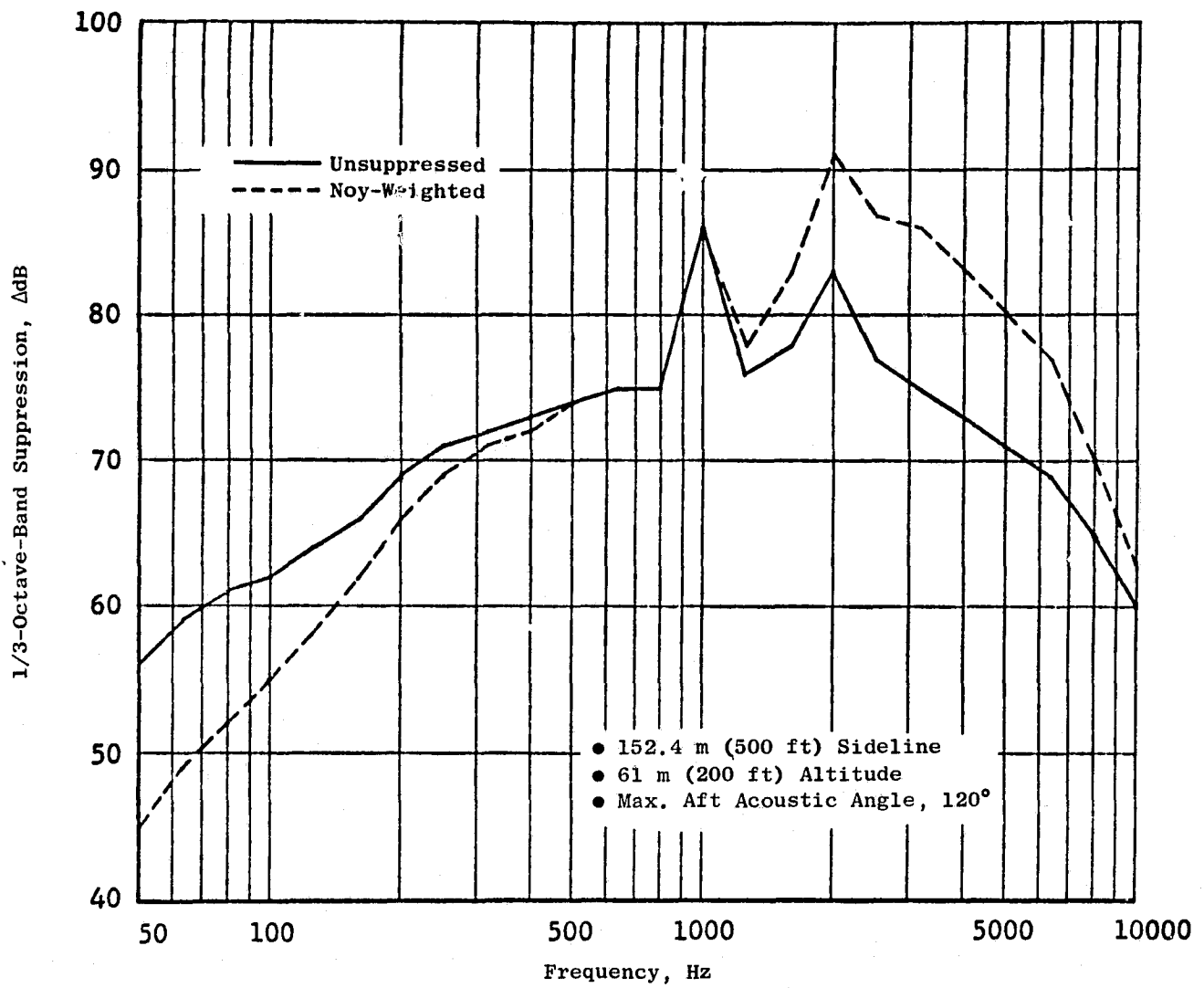


Figure 212. QCSEE UTW Fan Exhaust Spectrum.

Seal Effects on Far-Field Fan Exhaust Noise Levels

<u>Configuration</u>	<u>PNL (PNdB)</u>	<u>Δ</u>
Base Structure	88.3	---
Chevron Seal	88.4	+0.1
Bulb Seal	88.4	+0.1
No Seal	88.5	+0.2

The flexible joint sound transmission loss study as presented herein points to the following conclusions.

1. The noise transmitted through the flexible joints on the QCSEE composite nacelle does not significantly change the far-field noise measurements as shown by the ΔPNL's in Table XI.
2. Comparison of the chevron and bulb seals has shown that the flexible joint noise leakage could, if necessary, be improved by another choice of seals.
3. The study has shown that even if the seal fails to close the expected 3.2-mm (1/8-inch) gap, the far-field measurements will not appreciably be changed.

9.0 NOMENCLATURE

D_F	Fan Diameter
F_N	Net Thrust
H	Duct Height
L/H	Treated-Duct-Length to Duct-Height Ratio
L_T	Treatment Length
M, M_n	Duct Airflow Mach Number
N_{FC} $N/\sqrt{\theta}$	} Corrected Fan Speed
σ	Faceplate Porosity
λ_o	Wavelength of Sound at the Tuning Frequency, f_o , of the Treatment
λ_p	Phase Wavelength
$Z/\rho c$	Normalized Complex Acoustic Impedance = $R/\rho c + iX/\rho c$
$R/\rho c$	Normalized Acoustic Resistance
$X/\rho c$	Normalized Acoustic Reactance
ρc	Characteristic Impedance of Air (41.5 cgs rayls)

APPENDIX A
SOUND TRANSMISSION LOSS TESTS
LAB REPORT

RIVERBANK ACOUSTICAL LABORATORIES

OF IIT RESEARCH INSTITUTE

1512 BATAVIA AVE., BOX 189
GENEVA, ILLINOIS 60134
312/232-0104

FOUNDED 1918 BY WALLACE CLEMENT SABINE

REPORT

FOR: General Electric

Sound Transmission Loss
Tests TL 76-3, 4, 5, 6

ON: $1\frac{1}{2}$ Inch (31.75 mm) Thick
Honeycomb Panel With Simulated
Joint Conditions

Page 1 of 7

CONDUCTED: 18 September 1978

TEST METHOD

Unless otherwise designated, the measurements reported below were made with all facilities and procedures in explicit conformity with the American Society for Testing and Materials Designations E 90-70 and E413-73, as well as other pertinent standards.

DESCRIPTION OF THE SPECIMEN

The test specimen was composed of 2 panels, each approximately $1\frac{1}{2}$ inch (31.75 mm) thick, 18 inches (0.46 m) wide and 84 inches (2.13 m) high. The two panels were held together at the center with pins for alignment and as a spacer to provide a slat $\frac{1}{8}$ inch (3.18 mm) wide and 84 inches (2.13 m) long. The rest of the panel was held with wood stops on both sides of the perimeter of the test frame and then caulked to the specimen. This center gap was modified to the conditions as listed below. The specimen had an actual thickness of 1.33 inches (33.8 mm) and weighed 31 pounds (14.1 kg) an average of 1.5 pounds per ft² (7.32 kg/m²). The panel was identified as a Flexcore 5052/F40-0019-3.1. The transmission area, S, used in the computations was 2.0 ft² (1.95 m²).

- TL 76-3 Vertical gap sealed.
- TL 76-4 Chevron seal.
- TL 76-5 Bubble seal 50% compression.
- TL 76-6 No seal, open gap.

RESULTS OF MEASUREMENTS

Sound transmission loss values are tabulated at the eighteen standard frequencies. An explanation of the sound transmission class rating, a graphic presentation of the data, and additional information appear on the following pages.

THE RESULTS REPORTED ABOVE APPLY ONLY TO THE SPECIFIC SAMPLE SUBMITTED FOR MEASUREMENT. NO RESPONSIBILITY IS ASSUMED FOR PERFORMANCE OF ANY OTHER SPECIMEN.

RIVERBANK ACOUSTICAL LABORATORIES

OF IIT RESEARCH INSTITUTE

1512 BATAVIA AVE., BOX 189
GENEVA, ILLINOIS 60134
312/232-0104

FOUNDED 1918 BY WALLACE CLEMENT SABINE

REPORT

General Electric
18 September 1975

TL 76-3, 4, 5, 6
Page 2 of 7

RESULTS OF MEASUREMENTS (con't)

FREQUENCY, Hertz (cps)	100	125	160	200	250	315	400	500	630	800	1000	1250	1600	2000	2500	3150	4000	5000	6300	8000	10000
---------------------------	-----	-----	-----	-----	-----	-----	-----	-----	-----	-----	------	------	------	------	------	------	------	------	------	------	-------

TL 76-3

TRANSMISSION LOSS, dB	29	26	27	27	24	18	17	18	20	21	24	26	29	30	32	34	34	35	38	37	39
DEFICIENCIES						2	6	6	5	5	3	2									

SOUND TRANSMISSION CLASS 24

TL 76-4

TRANSMISSION LOSS, dB	24	21	23	22	22	16	17	17	17	17	23	26	28	29	31	32	32	31	31	33	33
DEFICIENCIES						2	4	5	6	7	2										

SOUND TRANSMISSION CLASS 22

TL 76-5

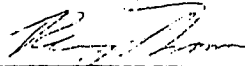
TRANSMISSION LOSS, dB	26	25	26	26	23	17	17	18	19	21	24	26	28	29	31	33	34	34	34	35	37
DEFICIENCIES						3	6	6	6	5	3	2									

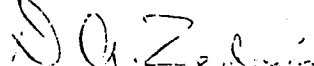
SOUND TRANSMISSION CLASS 24

TL 76-6

TRANSMISSION LOSS, dB	24	19	20	19	20	17	16	17	17	14	19	24	24	27	27	29	30	30	30	30	31
DEFICIENCIES							3	3	4	8	4										

SOUND TRANSMISSION CLASS 20

Approved 
Dr. Renny S. Norman
Manager

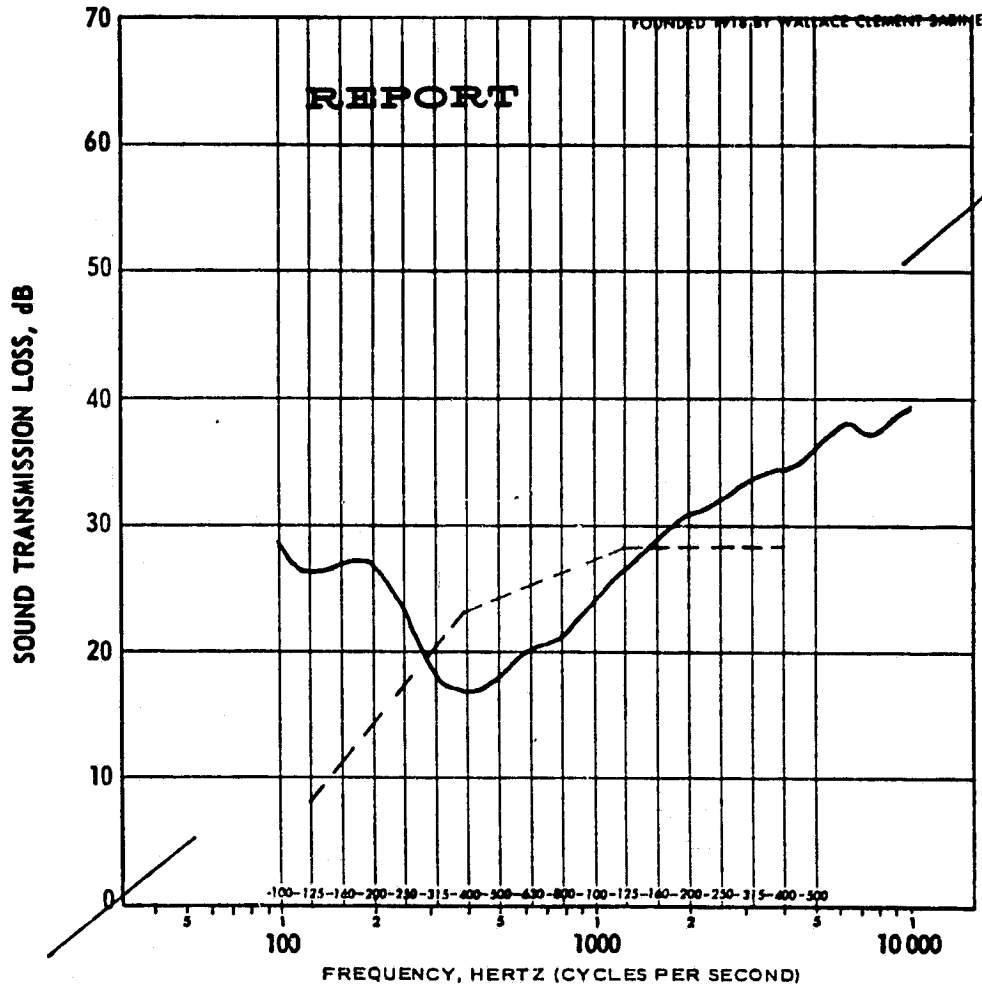
Submitted by 
D. A. Zedonis
Assistant Research Engineer

THE RESULTS REPORTED ABOVE APPLY ONLY TO THE SPECIFIC SAMPLE SUBMITTED FOR MEASUREMENT. NO RESPONSIBILITY IS ASSUMED FOR PERFORMANCE OF ANY OTHER SPECIMEN.

RIVERBANK ACOUSTICAL LABORATORIES

OF IIT RESEARCH INSTITUTE

1512 BATAVIA AVE., BOX 189
GENEVA, ILLINOIS 60134
312/232-0104



PAGE 3 OF 7, TL 76-3 THIS PAGE ALONE IS NOT A COMPLETE REPORT

THE SOUND TRANSMISSION LOSS OF THE TESTED SPECIMEN IS SHOWN BY THE CURVED LINE IN THE ABOVE GRAPH. THE BROKEN LINE IS THE LIMITING SOUND TRANSMISSION CLASS CONTOUR. THE GRAPH WAS PREPARED ON CODEX PAPER NO. 31, 462.

THE THEORETICAL TRANSMISSION LOSS OF THAT LIMP MASS HAVING THE SAME WEIGHT PER SQUARE FOOT AS THE SPECIMEN CAN BE LOCATED BY DRAWING A STRAIGHT LINE BETWEEN THE TWO SLASH MARKS ON THE EDGES OF THE GRID. THIS WAS DERIVED FROM THE EQUATION: $TL = 20 \log W + 20 \log F - 33$, WHERE W IS WEIGHT IN POUNDS PER SQUARE FOOT, AND F IS FREQUENCY IN HERTZ (CYCLES PER SECOND).

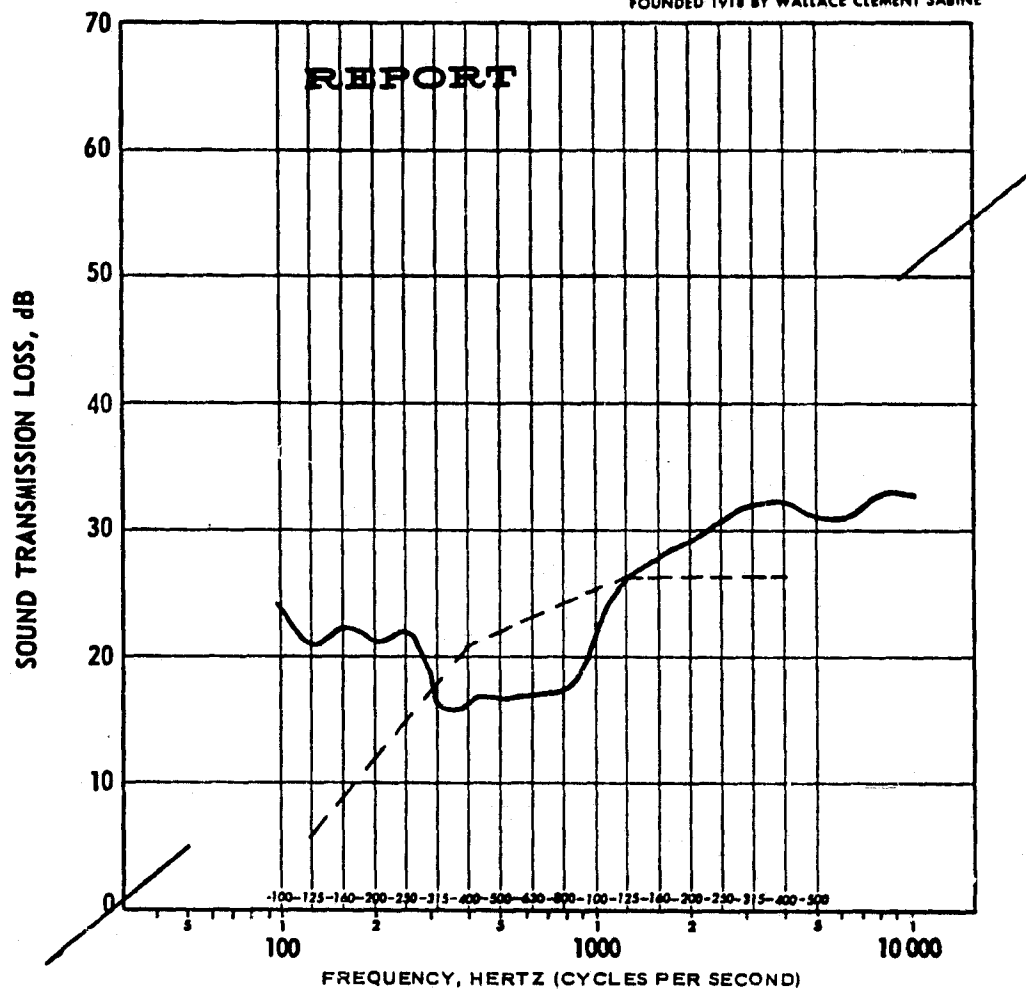
THE RESULTS REPORTED ABOVE APPLY ONLY TO THE SPECIFIC SAMPLE SUBMITTED FOR MEASUREMENT. NO RESPONSIBILITY IS ASSUMED FOR PERFORMANCE OF ANY OTHER SPECIMEN.

RIVERBANK ACOUSTICAL LABORATORIES

OF IIT RESEARCH INSTITUTE

1512 BATAVIA AVE., BOX 189
GENEVA, ILLINOIS 60134
312/232-0104

FOUNDED 1918 BY WALLACE CLEMENT SABINE



PAGE 4 OF 7, TL 76-4 THIS PAGE ALONE IS NOT A COMPLETE REPORT

THE SOUND TRANSMISSION LOSS OF THE TESTED SPECIMEN IS SHOWN BY THE CURVED LINE IN THE ABOVE GRAPH. THE BROKEN LINE IS THE LIMITING SOUND TRANSMISSION CLASS CONTOUR. THE GRAPH WAS PREPARED ON CODEX PAPER NO. 31, 462.

THE THEORETICAL TRANSMISSION LOSS OF THAT LIMP MASS HAVING THE SAME WEIGHT PER SQUARE FOOT AS THE SPECIMEN CAN BE LOCATED BY DRAWING A STRAIGHT LINE BETWEEN THE TWO SLASH MARKS ON THE EDGES OF THE GRID. THIS WAS DERIVED FROM THE EQUATION: $TL = 20 \log W + 20 \log F - 33$, WHERE W IS WEIGHT IN POUNDS PER SQUARE FOOT, AND F IS FREQUENCY IN HERTZ (CYCLES PER SECOND).

THE RESULTS REPORTED ABOVE APPLY ONLY TO THE SPECIFIC SAMPLE SUBMITTED FOR MEASUREMENT. NO RESPONSIBILITY IS ASSUMED FOR PERFORMANCE OF ANY OTHER SPECIMEN.

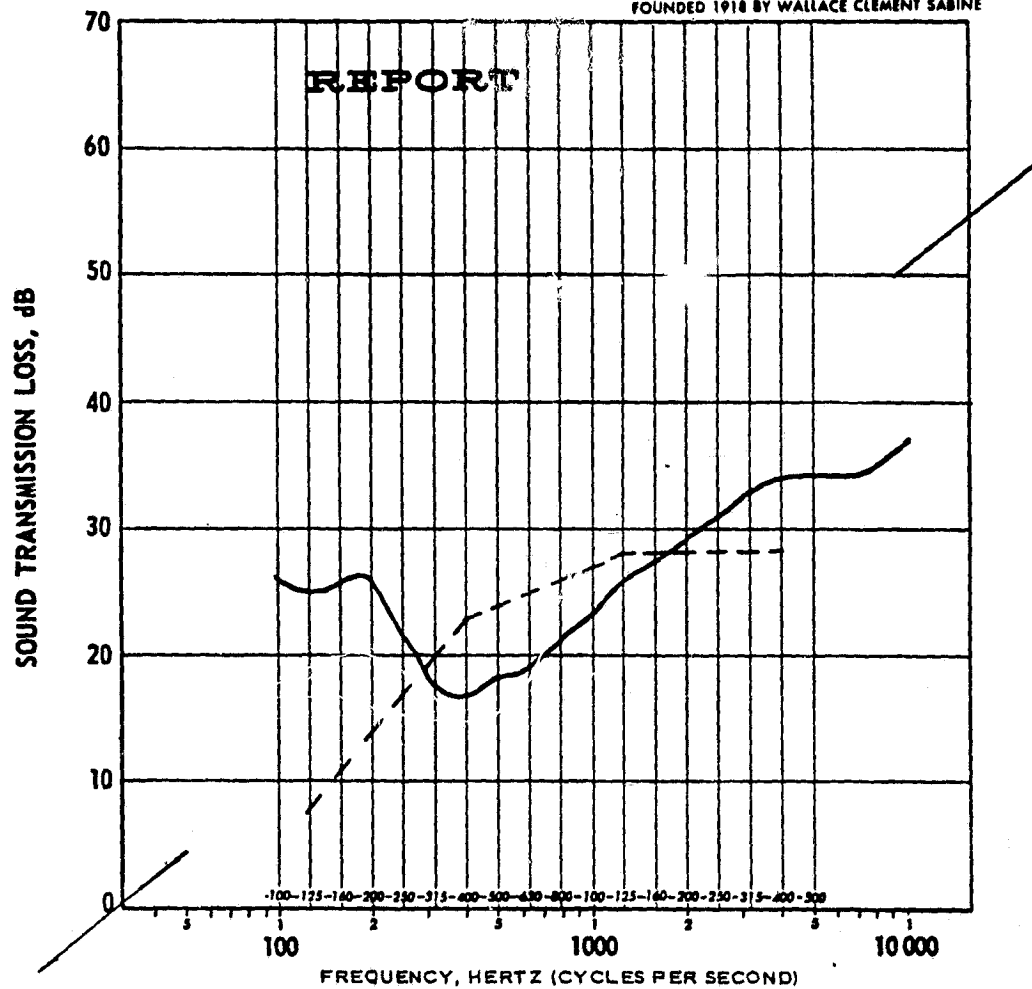
RIVERBANK ACOUSTICAL LABORATORIES

OF IIT RESEARCH INSTITUTE

1512 BATAVIA AVE., BOX 189
GENEVA, ILLINOIS 60134

312/232-0104

FOUNDED 1918 BY WALLACE CLEMENT SABINE



PAGE 5 OF 7, TL 76-5 THIS PAGE ALONE IS NOT A COMPLETE REPORT

THE SOUND TRANSMISSION LOSS OF THE TESTED SPECIMEN IS SHOWN BY THE CURVED LINE IN THE ABOVE GRAPH. THE BROKEN LINE IS THE LIMITING SOUND TRANSMISSION CLASS CONTOUR. THE GRAPH WAS PREPARED ON CODEX PAPER NO. 31, 462.

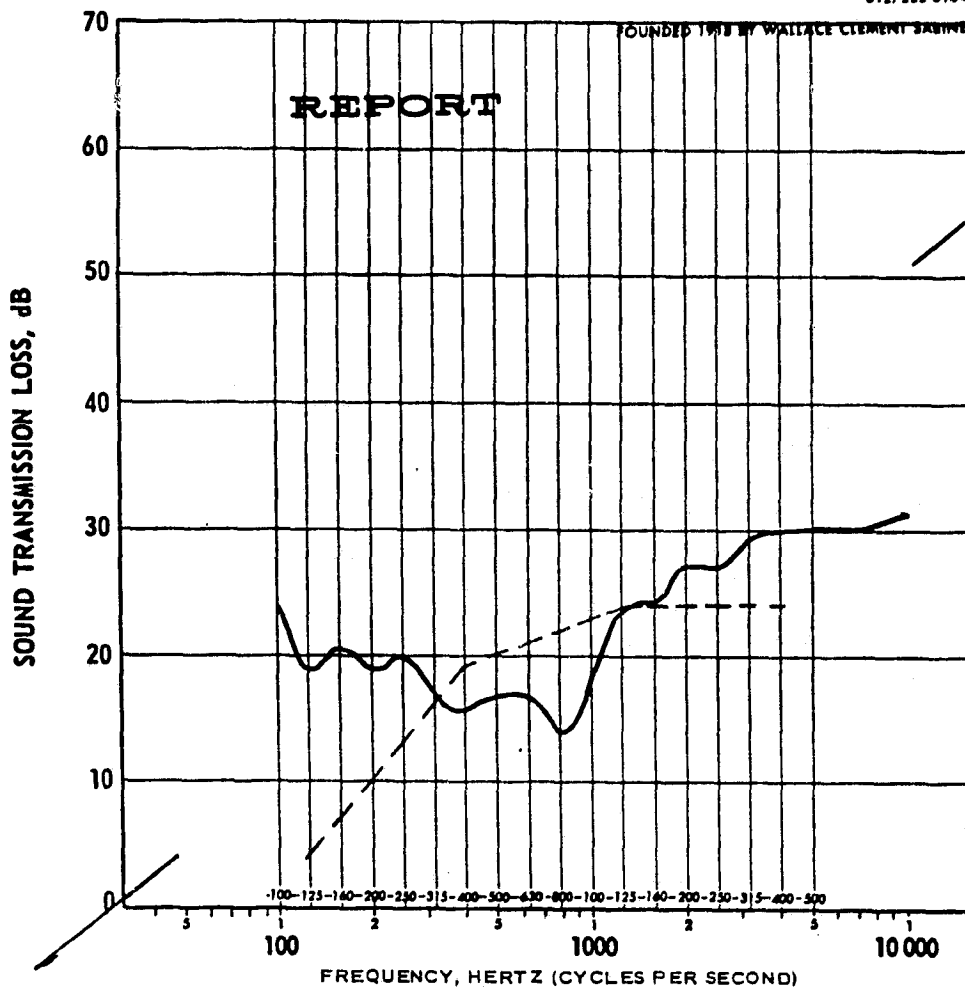
THE THEORETICAL TRANSMISSION LOSS OF THAT LIMP MASS HAVING THE SAME WEIGHT PER SQUARE FOOT AS THE SPECIMEN CAN BE LOCATED BY DRAWING A STRAIGHT LINE BETWEEN THE TWO SLASH MARKS ON THE EDGES OF THE GRID. THIS WAS DERIVED FROM THE EQUATION: $TL = 20 \log W + 20 \log F - 33$, WHERE W IS WEIGHT IN POUNDS PER SQUARE FOOT, AND F IS FREQUENCY IN HERTZ (CYCLES PER SECOND).

THE RESULTS REPORTED ABOVE APPLY ONLY TO THE SPECIFIC SAMPLE SUBMITTED FOR MEASUREMENT. NO RESPONSIBILITY IS ASSUMED FOR PERFORMANCE OF ANY OTHER SPECIMEN.

RIVERBANK ACOUSTICAL LABORATORIES

OF IIT RESEARCH INSTITUTE

1512 BATAVIA AVE., BOX 189
GENEVA, ILLINOIS 60134
312/232-0104



PAGE 6 OF 7 , TL 76-6 THIS PAGE ALONE IS NOT A COMPLETE REPORT

THE SOUND TRANSMISSION LOSS OF THE TESTED SPECIMEN IS SHOWN BY THE CURVED LINE IN THE ABOVE GRAPH. THE BROKEN LINE IS THE LIMITING SOUND TRANSMISSION CLASS CONTOUR. THE GRAPH WAS PREPARED ON CODEX PAPER NO. 31, 462.

THE THEORETICAL TRANSMISSION LOSS OF THAT LIMP MASS HAVING THE SAME WEIGHT PER SQUARE FOOT AS THE SPECIMEN CAN BE LOCATED BY DRAWING A STRAIGHT LINE BETWEEN THE TWO SLASH MARKS ON THE EDGES OF THE GRID. THIS WAS DERIVED FROM THE EQUATION: $TL = 20 \log W + 20 \log F - 33$, WHERE W IS WEIGHT IN POUNDS PER SQUARE FOOT, AND F IS FREQUENCY IN HERTZ (CYCLES PER SECOND).

THE RESULTS REPORTED ABOVE APPLY ONLY TO THE SPECIFIC SAMPLE SUBMITTED FOR MEASUREMENT. NO RESPONSIBILITY IS ASSUMED FOR PERFORMANCE OF ANY OTHER SPECIMEN.

RIVERBANK ACOUSTICAL LABORATORIES

OF IIT RESEARCH INSTITUTE

1512 BATAVIA AVE., BOX 189

GENEVA, ILLINOIS 60134

312/232-0104

FOUNDED 1918 BY WALLACE CLEMENT SABINE

REPORT

Page 7 of 7

The airborne sound transmission loss (TL) of a specimen is the ratio, expressed in decibels, (dB) of the sound power incident upon the specimen to the sound power transmitted through and radiated by the specimen when the sound fields on both sides are diffuse.

These measurements were made using a one-third octave band of pink noise, swept in fifteen minutes from 100 to 5000 Hertz (cycles per second). Two such runs were made, with a system interchange between. During each run the ratio of sound pressure levels in the two rooms is automatically and directly recorded graphically. The final results are obtained with a resultant precision better than a 90% confidence limits of ± 1 decibel.

The Sound Transmission Class (STC) is computed in accordance with ASTM E90-70 and E413-73. This number is intended to be used as a preliminary estimate of the acoustical properties of the specimen. Ultimate decisions should always be based upon the entire TL curve or values at all test frequencies.

Whenever a filler wall is used in mounting a specimen, the sound power transmitted through that wall is calculated and incorporated into the measured results before reporting.

THE RESULTS REPORTED ABOVE APPLY ONLY TO THE SPECIFIC SAMPLE SUBMITTED FOR MEASUREMENT. NO RESPONSIBILITY IS ASSUMED FOR PERFORMANCE OF ANY OTHER SPECIMEN.

APPENDIX B

ACOUSTIC DESIGN PROCEDURE FOR BULK ABSORBER FAN INLET TREATMENT

1.0 INTRODUCTION

Suppression of forward radiated fan noise is essential to attaining a low-noise engine design that will meet future aircraft certification requirements. The amount of acoustic treatment that can be applied to the inlet wall is generally limited by the inlet length, which for a typical wide-body jet in use today is on the order of 0.6 fan diameters or for a future low-noise configuration is on the order of 1.0 fan diameters. Within this constraint of length it is possible to consider the use of acoustic splitters. However, this approach has many drawbacks such as increased inlet total pressure loss, distortion, and anti-icing requirements which penalize the system and lead to the desire for alternate methods of increasing inlet suppression within allowed inlet length.

One means of increasing inlet suppression is to deviate from the typical perforated plate and honeycomb single-degree-of-freedom (SDOF) resonator-type treatment panel design and utilize a bulk absorber panel. The bulk absorber is also covered with a perforated plate but its function is primarily to hold the acoustic treatment in place. Bulk absorber designs have demonstrated on many engine and scale model test programs significant increased suppression relative to SDOF designs. In the past, bulk absorbers have not been considered for flight hardware because of potential problems with the environment (such as accumulation of dirt, grease, fuel, etc., in the fiber), durability of the fiber, and mechanical design of panels which were compatible to the SDOF panels in terms of weight and cost of fabrication. Recent studies by General Electric have answered these questions concerning bulk absorbers and led to their acceptance for potential flight hardware application.

The acoustic design of treatment panels using bulk absorbers has been primarily on a cut-and-try basis; however after several successful full-scale and scale model tests General Electric and NASA have accumulated sufficient data to establish a design procedure which can be substantiated by data. This appendix documents this procedure and provides the substantiated data used to determine each step of the design procedures as well as that used to support the assumptions inherent to the design. Based on experience to date, utilization of the procedure will result in a design which attains more suppression than a well-designed SDOF treatment of equal length. The exact level of suppression will depend upon many factors which are beyond the scope of the analysis and design procedure.

The design procedure is limited to two types of bulk absorber material, Scottfelt and Kevlar, which have been tested on both scale model and full-scale engines. The Scottfelt material has been used in ground static tests but is not considered acceptable for flight hardware. The Kevlar material has been used in static tests and has also been considered for flight hardware application.

2.0 DEVELOPMENT OF ENGINEERING DESIGN PROCEDURE

In order to arrive at a design procedure for bulk absorber inlet treatment, it was first necessary to establish the design parameters which would affect the acoustic characteristics of the treatment panels and then secondly to correlate these parameters with analytical and empirical results to arrive at a set of design curves. Section 2.1 presents the data used to evaluate the various design parameters that could affect the panel impedance and the resulting conclusions as to their impact on the design. Section 2.2 presents the design curves which were developed and the empirical results used to establish the validity of the curves.

2.1 EVALUATION OF DESIGN PARAMETERS

2.1.1 Reactance

The acoustic impedance for a given suppressor system is defined as the complex ratio of sound pressure averaged over the surface to volume velocity through it. Mathematically the impedance can be expressed as:

$$[Z = R + iX]$$

where R equals the real part of the complex quantity and is referred to as the acoustic resistance and X, the reactance, represents the complex part of the impedance expression.

The acoustic reactance is important in the development of a treatment design procedure since this parameter determines the frequency range for which the suppressor system will effectively suppress the incident noise level. For normal incidence sound it can be shown that the maximum suppression is obtained for an acoustic reactance of zero and a resistance value of $1.0 R/\rho c$. However, for conditions with random incidence sound and imposed airflow, as in the engine inlet environment, the peak suppression frequency has been shown to be obtained for a reactance value less than zero.

In order to determine the required reactance for a desired peak suppression frequency the following parameters were evaluated for their impact on the treatment material reactance.

- a. Material density
- b. Panel Thickness
- c. Incident sound pressure level
- d. Flow over the faceplate
- e. Faceplate porosity

For each of these parameters, data are presented which were obtained on Scottfelt and/or Kevlar bulk-absorber-type materials. For the case where data for one material are presented, the assumption is made that the effects are typical of both materials.

2.1.1.1 Material Density

Figures 213 and 214 compare the measured acoustic reactance values for two bulk absorber materials, Scottfelt and Kevlar, at three different density values. The data are for 1.0-in. thick material and were obtained from normal incidence impedance tube.

The measured reactance given in Figure 213 is for the Scottfelt bulk absorber material. The three different samples of material tested are designated as Scottfelt 2-900, 3-900, and 4-900. The numbers 2, 3, and 4 indicate the compressibility or density factor, whereas the 900 indicates that the material has 90 pores per inch. The base material, Scottfoam, is designated as SF 1-900. Therefore Scottfelt 2-900 has a density twice that of the Scottfoam material.

The comparison of the reactance for the different density values, ranging from 3.2 lb/ft^3 to 6.2 lb/ft^3 , shows that for reactance values less than zero, there is little difference in the measured data. Therefore, since the design reactance is always zero or less, variation of the material density within this range is not considered as a primary factor in the selection of material to meet the design reactance value.

Figure 214 gives the same type of comparison for Kevlar material. The type of Kevlar used in these tests is designated as Kevlar 29, Type 973, which was available in the form of a 0.5-in. thickness per layer. The uncompressed density is 0.7 lb/ft^3 .

The results given in Figure 214 are for three different density values, 1.7 lb/ft^3 , 2.38 lb/ft^3 , and 2.72 lb/ft^3 . These values were obtained by placing different amounts of the 0.5-in. layers in a constant 1.0-in. depth core.

The results are similar to those for the Scottfelt material. For reactance values less than zero little difference is seen in the measured data. Therefore the material density is not a significant factor in the reactance.

The data given in Figure 215 compares measured reactance data for the Scottfelt and the Kevlar materials. The data are for a 1.0-in. material depth with the Scottfelt having a density of 3.2 lb/ft^3 while the Kevlar has a density of 2.72 lb/ft^3 .

This comparison shows the different type of materials having little if any effect on the measured reactance. Thus at constant panel thickness neither the material type or density is a significant factor in selecting the panel design reactance for these two bulk absorber materials in the range of densities tested.

- 1.0 in. Material Thickness
- 22.5% Faceplate Porosity

- Scottfelt 2-900, $\rho = 3.2 \text{ lb/ft}^3$
- Scottfelt 3-900, $\rho = 4.8 \text{ lb/ft}^3$
- △ Scottfelt 4-900, $\rho = 6.2 \text{ lb/ft}^3$

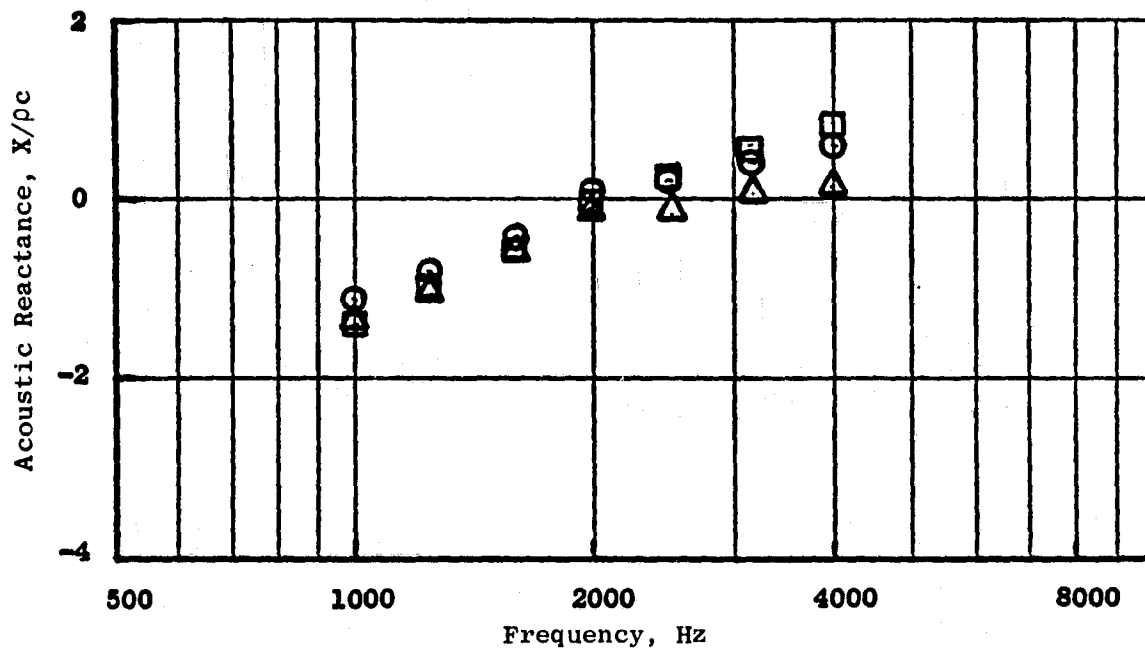


Figure 213. Effect of Material Density on Acoustic Reactance of Scottfelt.

- Type 973 (0.5-in. Thick/Layer Uncompressed)
- 22.5% Faceplate Porosity

Compressed to 1.0 in. Material Thickness

- 5 Layers, $\rho = 1.7 \text{ lb/ft}^3$
- 7 Layers, $\rho = 2.38 \text{ lb/ft}^3$
- △ 8 Layers, $\rho = 2.72 \text{ lb/ft}^3$

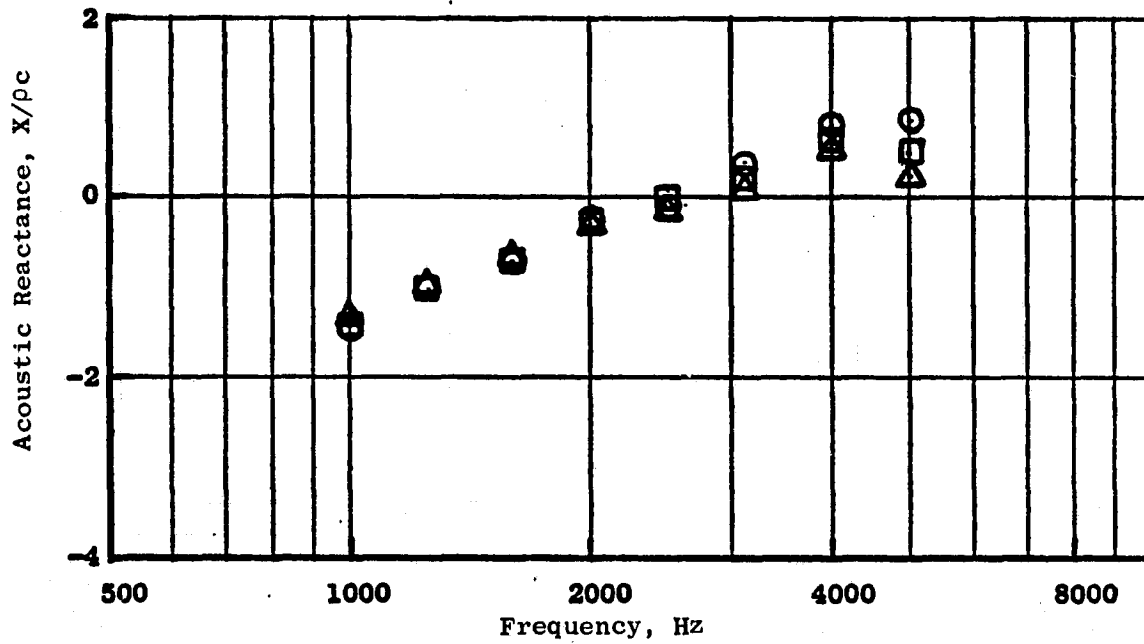


Figure 214. Effect of Material Density on Acoustic Reactance of Kevlar 29.

- 1.0 in. Material Thickness
- 22.5% Faceplate Porosity
- Kevlar = 8 Layers Compressed to 1.0 in. Material Thickness (0.5-in. Thick/Layer Uncompressed)

Kevlar 29, Type 973, $\rho = 2.72 \text{ lb/ft}^3$
 Scottfelt 2-900, $\rho = 3.2 \text{ lb/ft}^3$

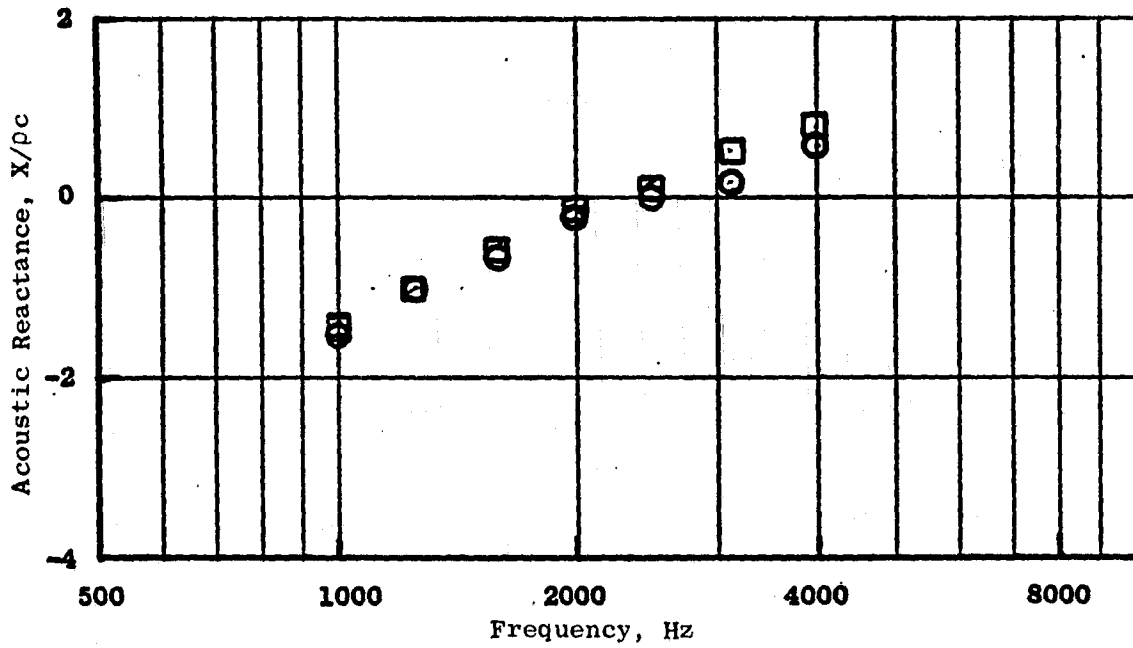


Figure 215. Comparison of Kevlar and Scottfelt Acoustic Reactance.

2.1.1.2 Material Thickness

Panel thickness was thought to have the most significant effect on reactance. The impact that panel depth has on the reactance as a function of frequency is demonstrated by the data given in Figure 216. Shown are the measured reactance values for Scottfelt 3-900 covering a material thickness range from 0.25 to 1.5 in. The thickness is seen to cause a significant change in panel reactance with the reactance curve being shifted toward higher frequencies as the panel depth is decreased. Similar data were obtained on Kevlar materials; these data were used to produce the design curves in Section 2.2.

2.1.1.3 Sound Pressure Level

The inlet treatment panels see varying surface sound pressure levels, both within a given inlet duct as well as from one variable to another. The data given in Figure 217 are the measured reactance for different incident sound pressure levels covering the range of 130 through 160 dB. This comparison of data shows the sound pressure level has little if any effect on the measured reactance.

2.1.1.4 Flow Over the Panel Faceplate

In an engine inlet the treatment panels have airflow passing over the surface which could affect the panel reactance. The expected change in reactance due to the presence of flow is illustrated in Figure 218 for a bulk absorber material with a perforated faceplate. The predicted reactance change, which is seen to be very small, was calculated by assuming the mass reactance term to be a function of the faceplate thickness. The total reactance term is given as follows for a resonator-type configuration:

$$x/\rho c = 2\pi t'/\sigma\lambda - \cot \frac{2\pi h}{\lambda}$$

t = faceplate thickness

$$t' = t + \alpha d$$

d = hole diameter

σ = faceplate porosity

h = cavity depth

λ = wavelength

α = a constant depending upon the duct Mach number

The term $2\pi t'/\sigma\lambda$ is the mass reactance term and is a function of the faceplate thickness, porosity, frequency, and some "end correction factor" which effectively increases the thickness of the faceplate. However, it has been

● 22.5% Faceplate Porosity

Material Thickness, in.

- 0.25
- △ 0.5
- 1.0
- ◇ 1.5

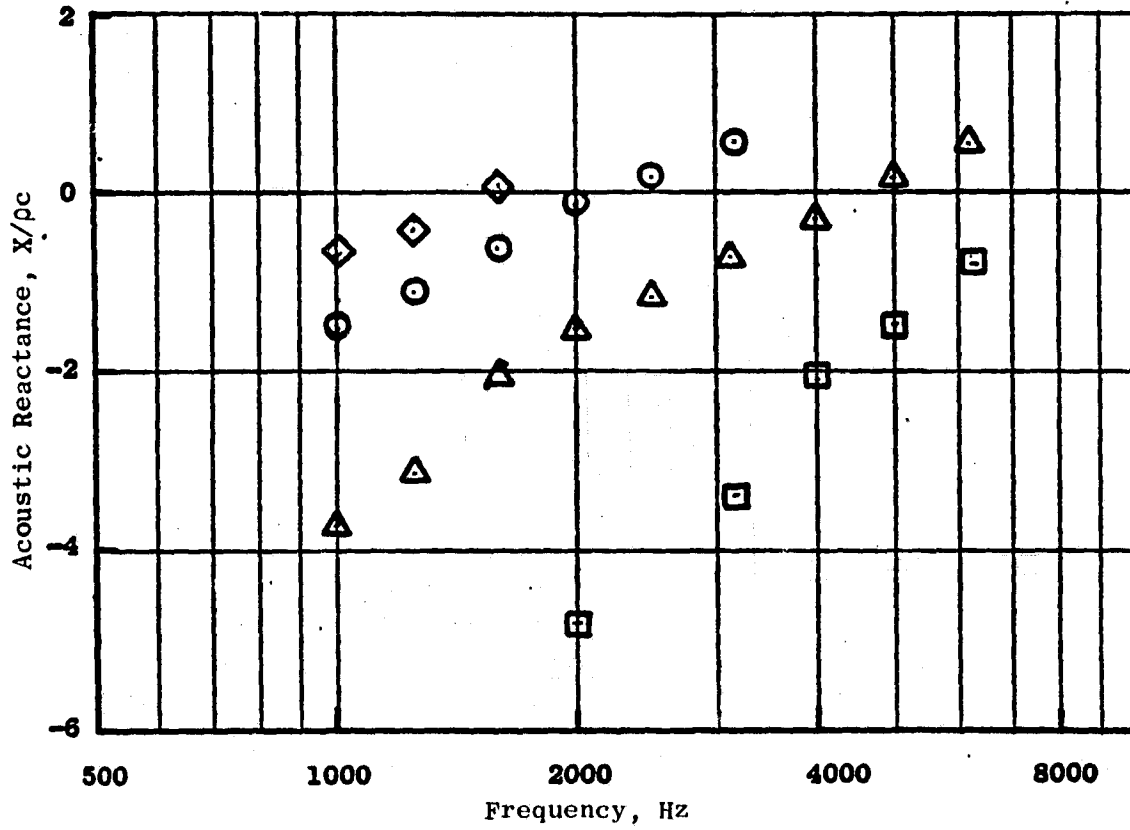


Figure 216. Effect of Thickness on Acoustic Reactance of Scottfelt 3-900.

- 22.5% Faceplate Porosity
- 0.5 in. Material Thickness

Incident Sound Pressure Level, dB

- 130
- 140
- ◇ 150
- △ 160

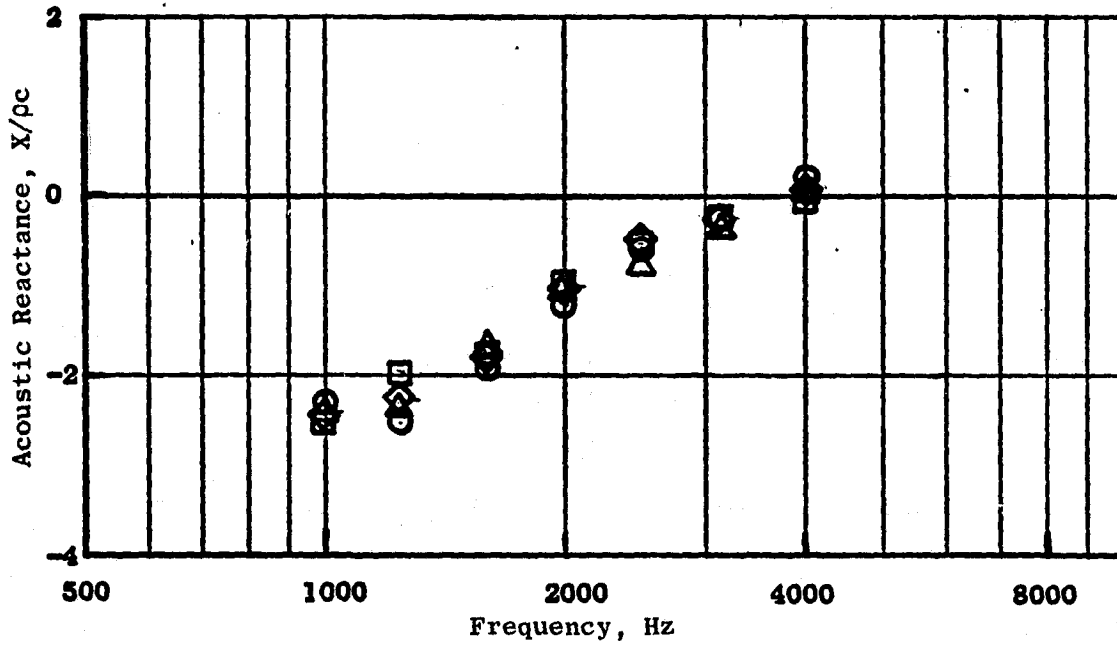


Figure 217. Measured Acoustic Reactance Vs. Frequency at Various Sound Pressure Levels for Scottfelt 3-900.

- 0.5 in. Material Thickness
- 25% Faceplate Porosity

--- Without Flow
— with Flow

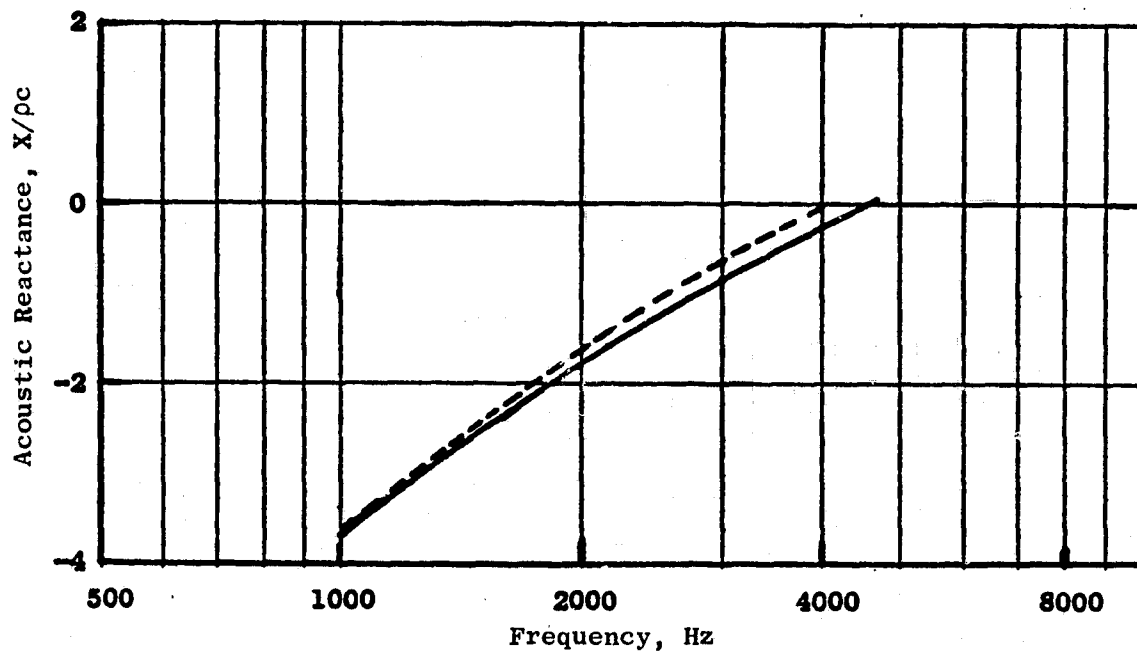


Figure 218. Effect of Flow on Acoustic Reactance of Bulk Absorber Panel.

shown that with the presence of flow this factor is decreased and the effective length becomes simply the faceplate thickness for a duct Mach number greater than approximately 0.35. The reactance difference shown in Figure 218 is the calculated mass term added to the measured bulk absorber reactance. The mass reactance was calculated by assuming the faceplate thickness t , equal to the total thickness t' since the excited particle velocity for a resonator system which introduces the end correction factor is not expected to exist in a bulk absorber suppressor system. Figure 219 compares the calculated reactance with and without flow for a SDOF resonator system. At zero flow the SDOF resonator has the entire end correction in the mass reactance calculation. However at 0.4 Mach number this correction is eliminated which produces the significant shift in the reactance to higher frequencies. The shift seen in Figure 218 for the bulk absorber with faceplate is small when compared with the results for the SDOF system since the end correction factor is not applied.

For the design curves of Section 2.2 it was assumed flow over the faceplate has no significant effect on reactance.

2.1.1.5 Faceplate Porosity

The application of bulk absorber materials in an engine environment necessitates the use of a faceplate material to contain the bulk absorber material. In selecting the faceplate it is important that the facing is acoustically transparent, thereby either eliminating or minimizing the impact of the faceplate on the acoustic characteristics of the bulk absorber. An investigation of the faceplate effects has been made in order to determine a proper faceplate design. The results are given in Figures 220 and 221.

Figure 220 compares the predicted impact of a given faceplate material on the acoustic reactance for a typical resonator treatment design versus that for a bulk absorber. The thickness of the resonator and the bulk absorber is 1.0 in.

The faceplate porosity for the resonator has a significant effect on the panel reactance. The change is due to the difference in the calculated mass reactance resulting from the two different porosity values, 10 versus 25%. The reactance curve shifts to a higher frequency as the porosity is increased from 10 to 25%. The comparison given for the bulk absorber configuration is for a 25% porosity faceplate versus no faceplate. As can be seen, the reactance change is smaller than the resonator change. Here the increase in reactance was determined by calculating and then adding the mass reactance that corresponds to a faceplate having 25% porosity to the measured reactance for a bulk absorber with no faceplate.

Figure 221 compares data for the bulk absorber material Scottfelt with and without a faceplate. This comparison shows little if any difference at most of the frequencies in the measured reactance and substantiates the assumed mass calculation given in Figure 220. Based on this comparison it

- 0.5 in. Core Depth
- 25% Faceplate Porosity

— Without Flow
 - - - with Flow (Mach = 0.40)

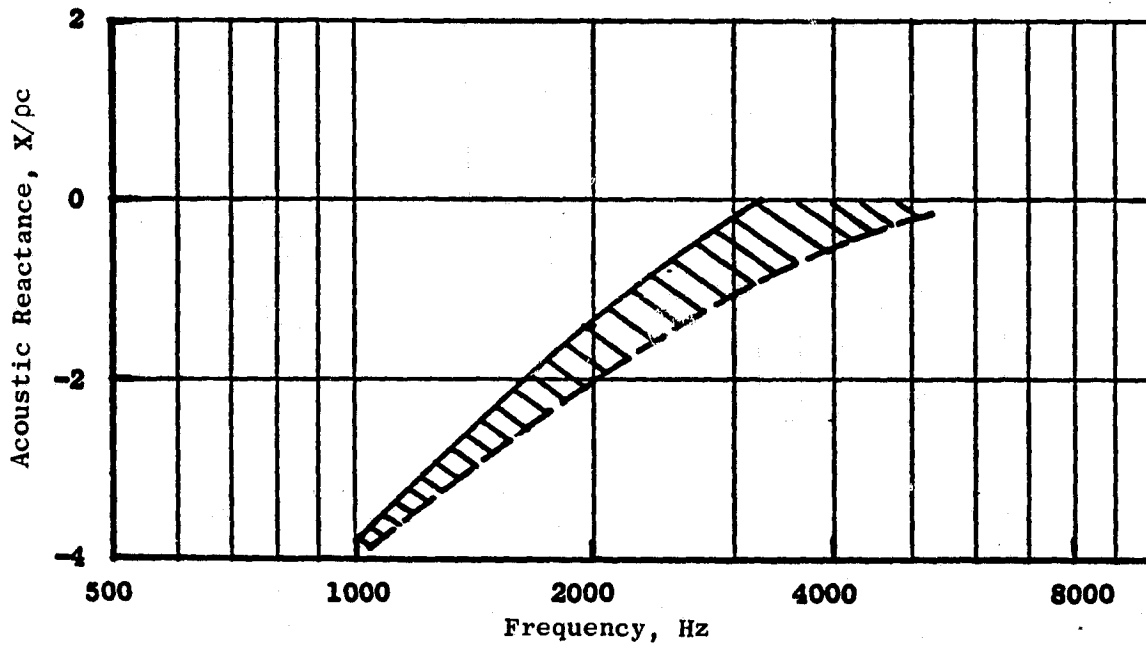


Figure 219. Effect of Flow on Acoustic Reactance of SDOF Panel.

- 1.0 in. Core Depth
- Mach = 0.40

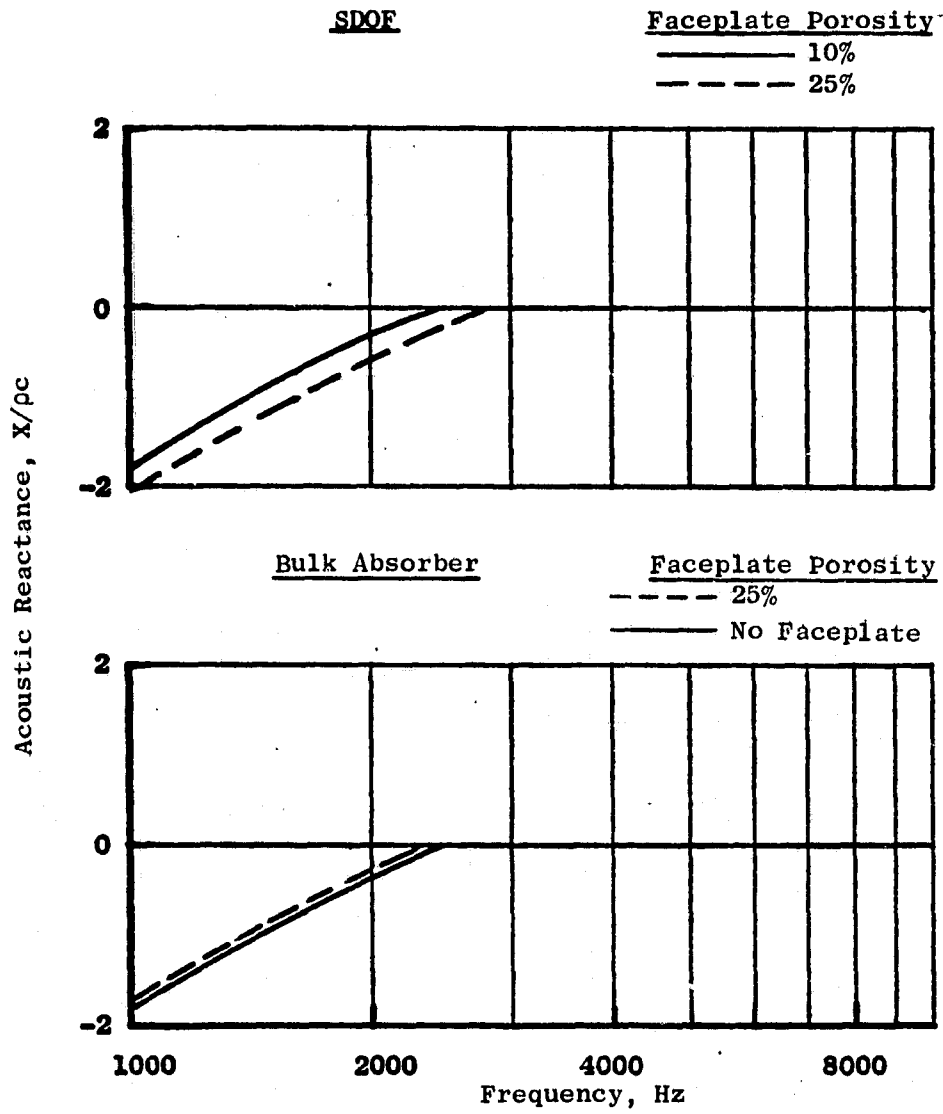


Figure 220. Predicted Effects of Faceplate Porosity on Acoustic Reactance for SDOF and Bulk Absorber Panels.

- 0.5-in. Material Thickness
- 130-dB Incident Sound Pressure Level

- △ No Faceplate
- 22.5% Faceplate Porosity

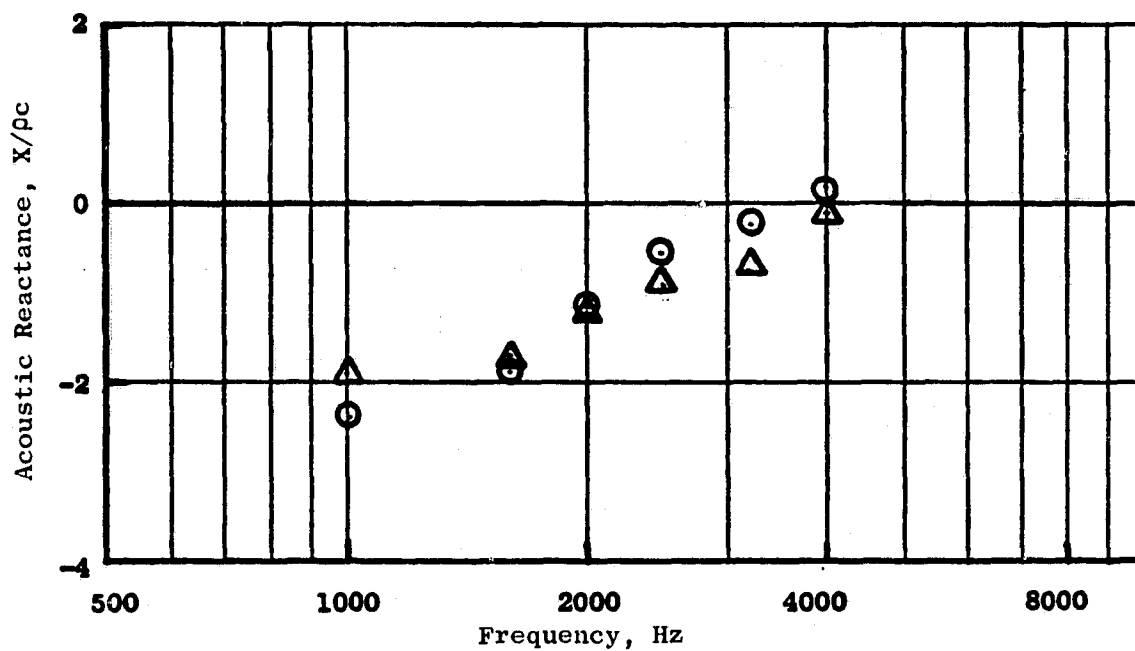


Figure 221. Measured Acoustic Reactance Vs. Frequency for Scottfelt 3-900 With and Without Faceplate.

was assumed that the faceplate porosity is not a factor in the design of the bulk absorber panel reactance.

2.1.2 Resistance

The acoustic resistance is defined as the real part of the acoustic impedance for a given suppressor system. The resistance value is that parameter which primarily determines the level of suppression that can be obtained from a given absorptive-type suppressor system. The parameters felt to have a significant impact on the resistance for the bulk absorber materials Scottfelt and Kevlar have been evaluated and are presented below.

2.1.2.1 Material Density

The measured acoustic resistance as a function of frequency obtained from normal impedance tube data is given in Figure 222. The data are for the bulk absorber Scottfelt having a constant material thickness of 1.0 inch and for a range of material densities from 3.2 lb/ft³ to 6.2 lb/ft³. The density is a significant factor in establishing the acoustic resistance for a given material. In comparing the average resistance values over the frequency range for which data were taken, the resistance is about double that for the higher versus the lower density material.

Figure 223 gives the measured resistance for 1.0-in. deep Kevlar material. The data are for different material densities. Here, as was the case for Scottfelt, the resistance is a function of the Kevlar density. The average resistance over the indicated frequency range increases from about 0.7 R/ ρc to about 1.1 R/ ρc as the density increases from 1.7 lb/ft³ to 2.72 lb/ft³. These data were used in the development of the design curves in Section 2.2.

2.1.2.2 Material Thickness

Resistance versus material thickness is represented in the data shown in Figure 224. The measured resistance values are for the Scottfelt 3-900 material at thicknesses of 0.5 and 1.0 in. The data show that resistance increases with increased material thickness with the increase more significant in the higher frequency bands.

Figure 225 compares the measured resistance for Kevlar-type material at two different treatment depths with approximately the same density. Here, as in the results from the Scottfelt, resistance increases with increasing material thickness with an average value of about 0.8 R/ ρc for 1.0 in. versus 1.3 R/ ρc for a 2.0-in. thick material. These data were used in developing the design curves of Section 2.2.

- 1.0 in. Material Thickness
- 22.5% Faceplate Porosity

- Scottfelt 2-900, $\rho = 3.2 \text{ lb/ft}^3$
- Scottfelt 3-900, $\rho = 4.8 \text{ lb/ft}^3$
- △ Scottfelt 4-900, $\rho = 6.2 \text{ lb/ft}^3$

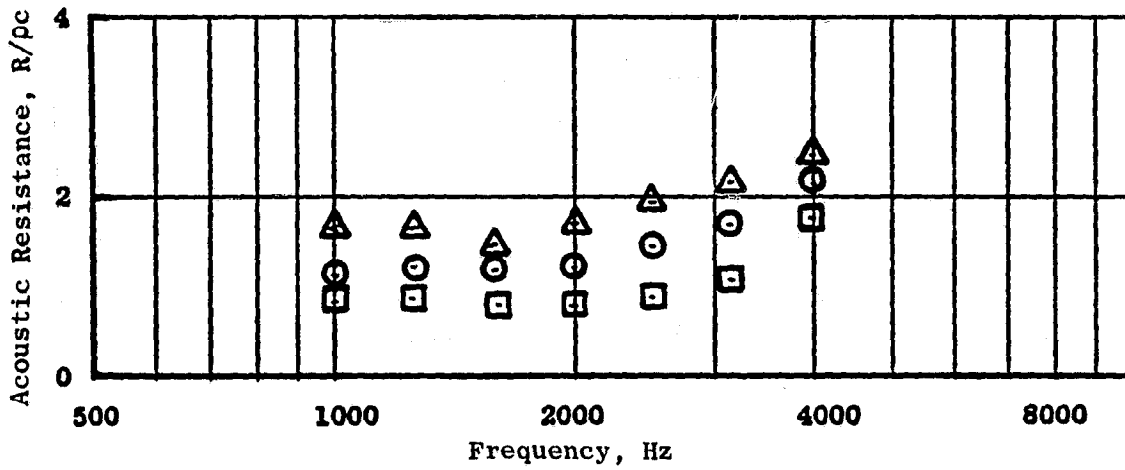


Figure 222. Effect of Material Density on Acoustic Resistance of Scottfelt.

- Type 973 (0.5-in. Thick/Layer Uncompressed)
- 22% Faceplate Porosity

Compressed to 1.0 in. Material Thickness

- 5 Layers, $\rho = 1.7 \text{ lb/ft}^3$
- 7 Layers, $\rho = 2.38 \text{ lb/ft}^3$
- △ 8 Layers, $\rho = 2.72 \text{ lb/ft}^3$

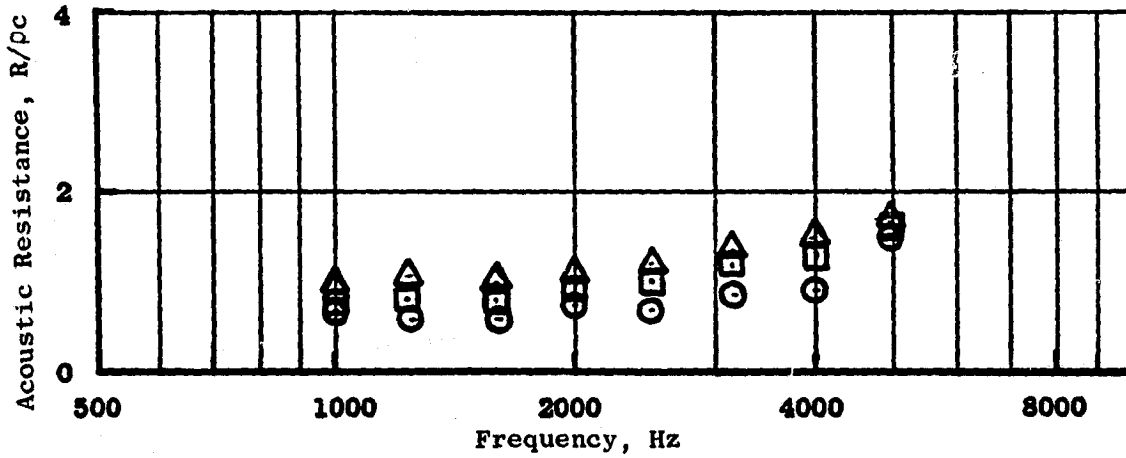


Figure 223. Effect of Material Density on Acoustic Resistance of Kevlar 29.

● 22.5% Faceplate Porosity

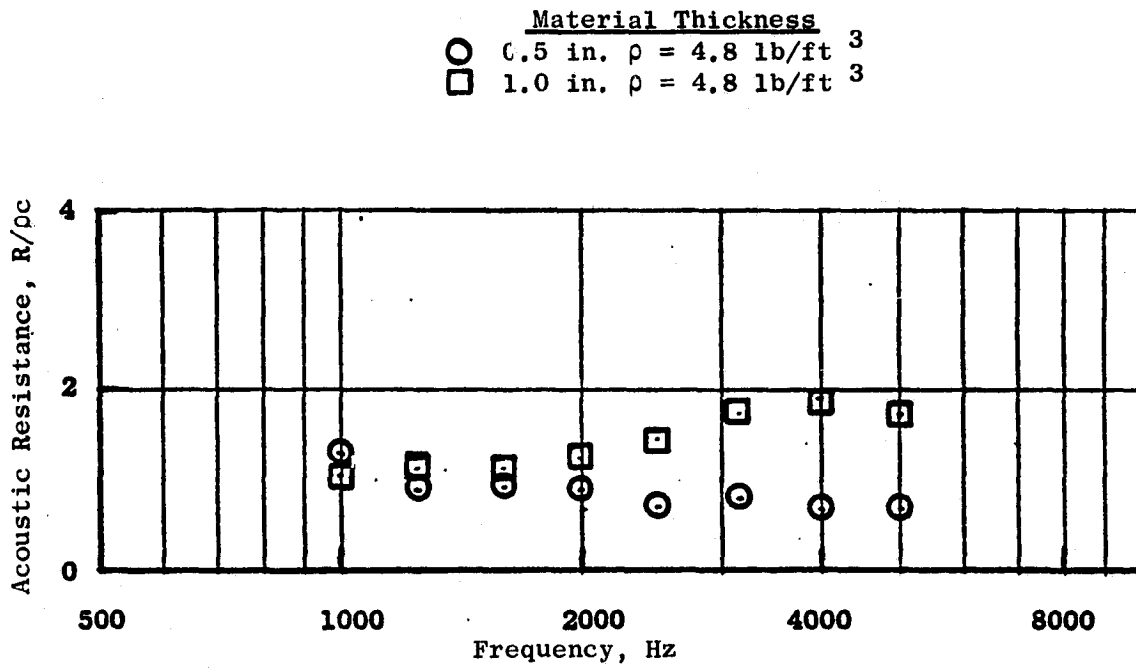


Figure 224. Effect of Thickness on Acoustic Resistance of Scottfelt 3-900.

- Type 973 (0.5-in. Thick/Layer Uncompressed)
- 22% Faceplate Porosity

Compressed Material Thickness

- 1.0 in., 6 Layers, $\rho = 2.40 \text{ lb/ft}^3$
- 2.0 in., 12 Layers, $\rho = 2.1 \text{ lb/ft}^3$

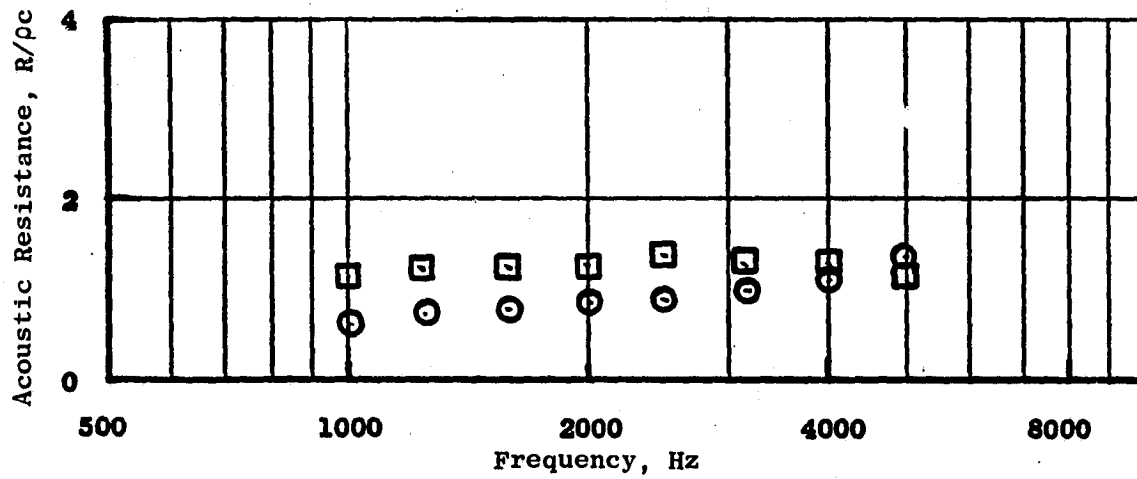


Figure 225. Effect of Thickness on Acoustic Resistance of Kevlar 29.

2.1.2.3 Faceplate Porosity

Figure 226 compares resistance data for the bulk absorber Scottfelt 3-900. The data were taken at an incident sound pressure level of 160 dB. The data are for the material having no faceplate and with a faceplate of 22.5%. The results show little difference in the measured resistance levels.

2.2 DEVELOPMENT OF DESIGN CURVES

2.2.1 Reactance

A correlation of the required versus the measured acoustic reactance for determining the frequency of peak suppression for broadband noise is presented in Figure 227. This correlation is made up of two parts:

- The predicted required reactance as a function of frequency
- The bulk absorber reactance as a function of frequency

The predicted required reactances are based on the assumption that in an inlet configuration the high D_F/λ values (usually 10 or greater) have higher order mode numbers. The functional form of required reactance has been well established analytically as:

$$\frac{x}{\rho c} = -K \frac{D_F}{\lambda_p}$$

where K = proportionality constant

D_F = fan diameter

λ_p = phase wavelength = $(1-M_N)\lambda_0$

λ_0 = wavelength with no flow

M_N = Mach number

The proportionality constant, K , has been determined from General Electric's experience in the use of bulk absorbers on the inlets of fan vehicles and engines to be equal to 0.04.

Using the above relation with a constant of 0.04, the predicted reactance curves versus frequency at various fan diameters were generated for a 0.4 Mach number flow.

- 0.5-in. Material Thickness
- 160-dB Incident Sound Pressure Level

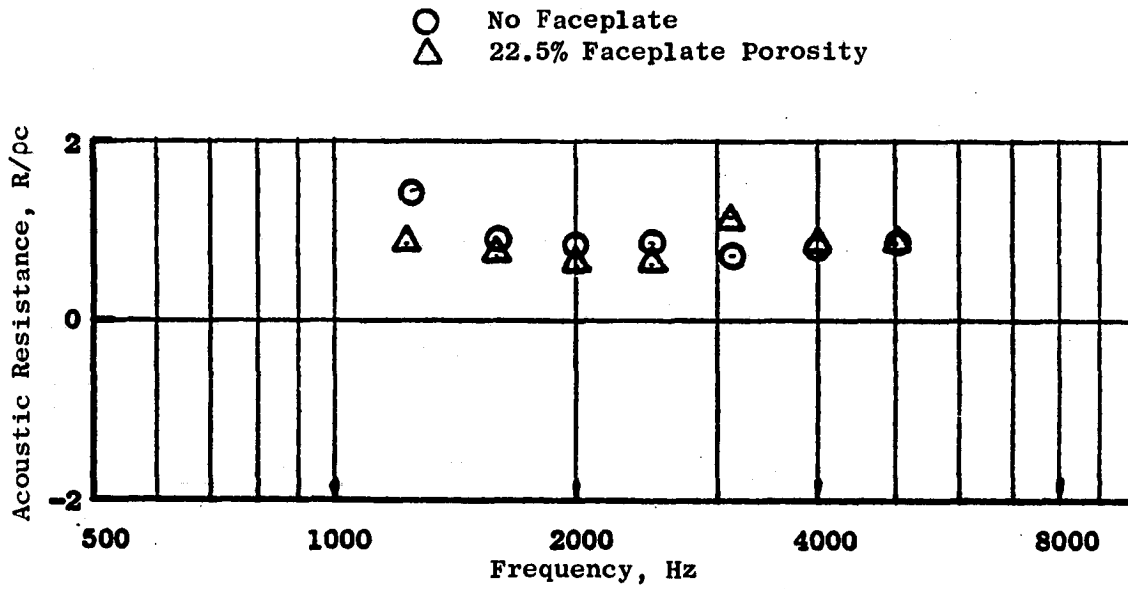


Figure 226. Measured Acoustic Resistance Vs. Frequency for Scottfelt 3-900 With and Without Faceplate.

• Mach = 0.40

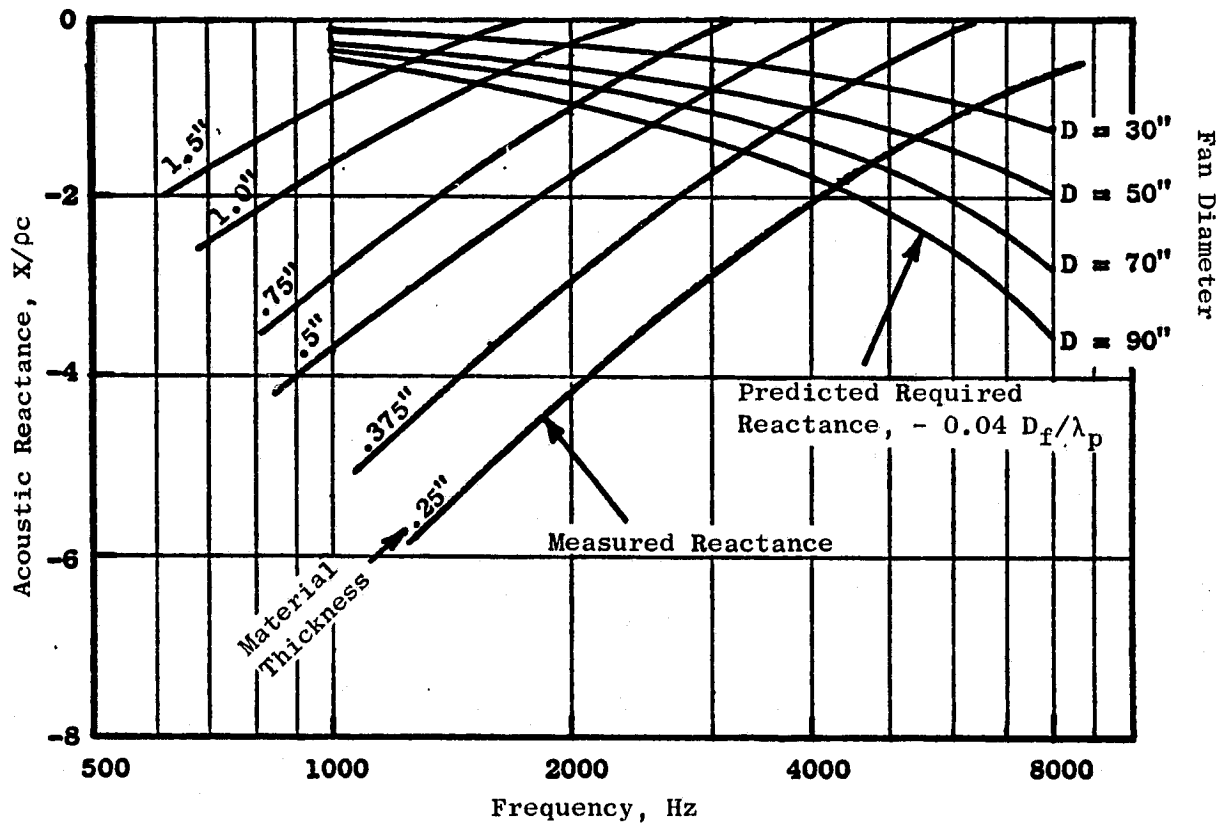


Figure 227. Correlation of Required and Measured Reactance for Bulk Absorber Treatment Panel.

The bulk absorber reactance values are data from Section 2.1. As Shown in Section 2.1 the panel thickness has the only significant effect on reactance, thus these data represent all materials and panel designs.

The frequency of peak attenuation for a given set of conditions is determined from Figure 227 as follows:

- Select the required reactance curve that corresponds to the given fan inlet diameter. Linear interpolation is made for conditions that fall between the given curves.
- The intersection of the required and actual bulk absorber reactance curves occurs at the frequency of peak suppression.

Using the information in Figure 227 and similar figures for other Mach number values, the correlation shown in Figure 228 was obtained. From Figure 228 the frequency of peak suppression is given as a function of fan diameter for a range of material thicknesses and inlet Mach number values. A linear interpolation can be made for Mach number and material thickness values that fall between the given curves.

A comparison was made of the peak suppression attained by various bulk absorber panel designs and that predicted by Figure 228. The bulk absorber materials and designs used in the comparison are defined below.

<u>Configuration</u>	<u>Type Material</u>	<u>Material Thickness</u>	<u>Faceplate Porosity, %</u>
Full-Scale Engine No. 1	Scottfelt 3-900	1.0 in.	22.5
Full-Scale Engine No. 2	Kevlar	0.75 in.	23.0
Scale Model Fan No. 1	Scottfelt 3-900	0.5 in.	28.0
Scale Model Fan No. 2	Scottfelt 3-900	0.25 in. (compressed to 0.18 in.)	30.0

Figure 229 shows the agreement between the predicted and the measured frequency of peak attenuation. The boxes cover the frequency range contained in each of the different 1/3-octave-band frequencies. That is, if the predicted and the measured frequency values fall within the same box then the measured and the predicted 1/3-octave-band frequency of peak suppression are in agreement. The four comparisons given show that the predicted and the measured frequencies are in agreement and substantiate the design curve in Figure 228.

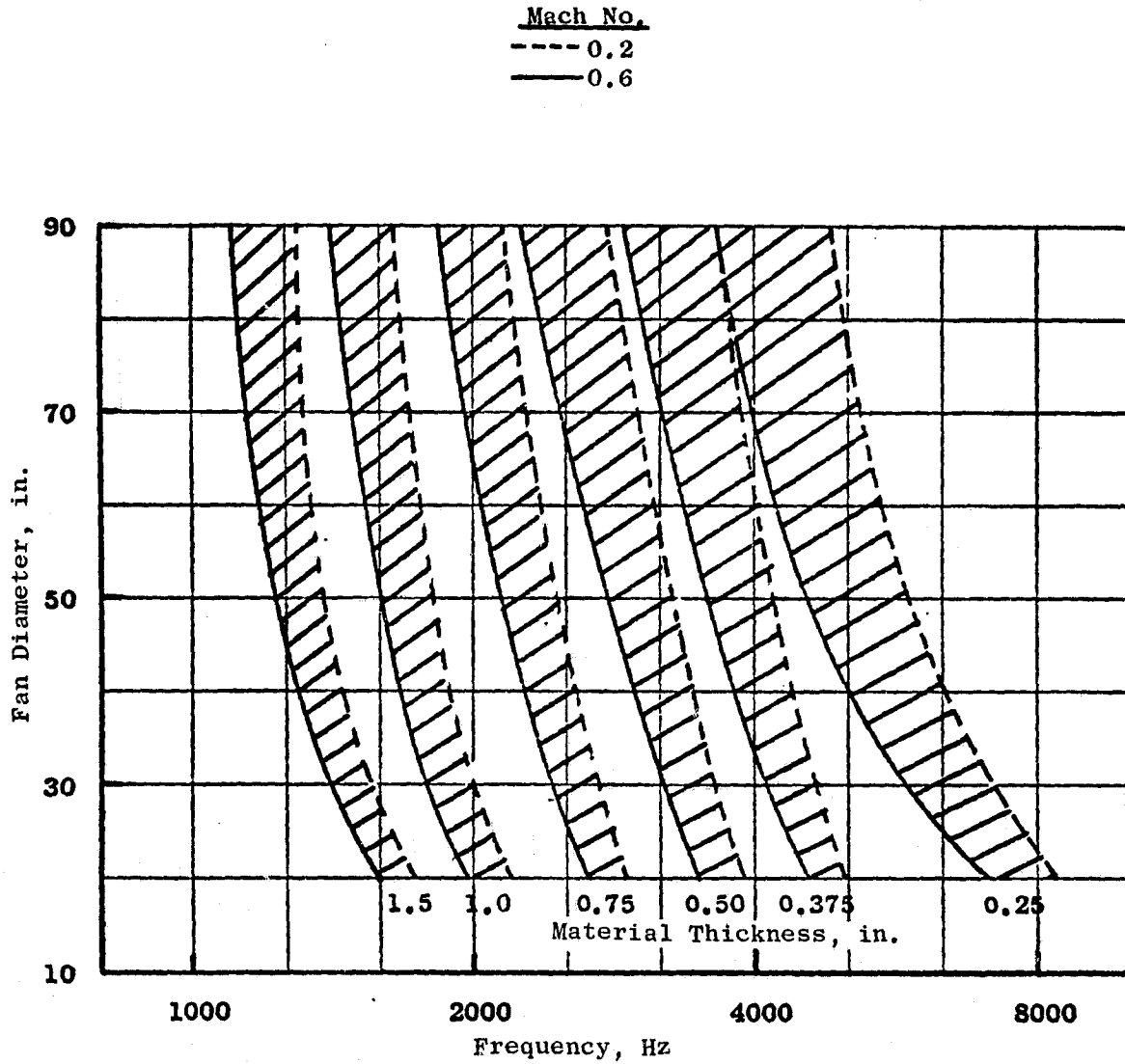


Figure 228. Bulk Absorber Thickness Requirement for Peak Suppression as a Function of Fan Diameter, Frequency, and Mach Number.

- Full-Scale Engine No. 1
- △ Full-Scale Engine No. 2
- ◇ Scale Model Fan No. 1
- ◇ Scale Model Fan No. 2

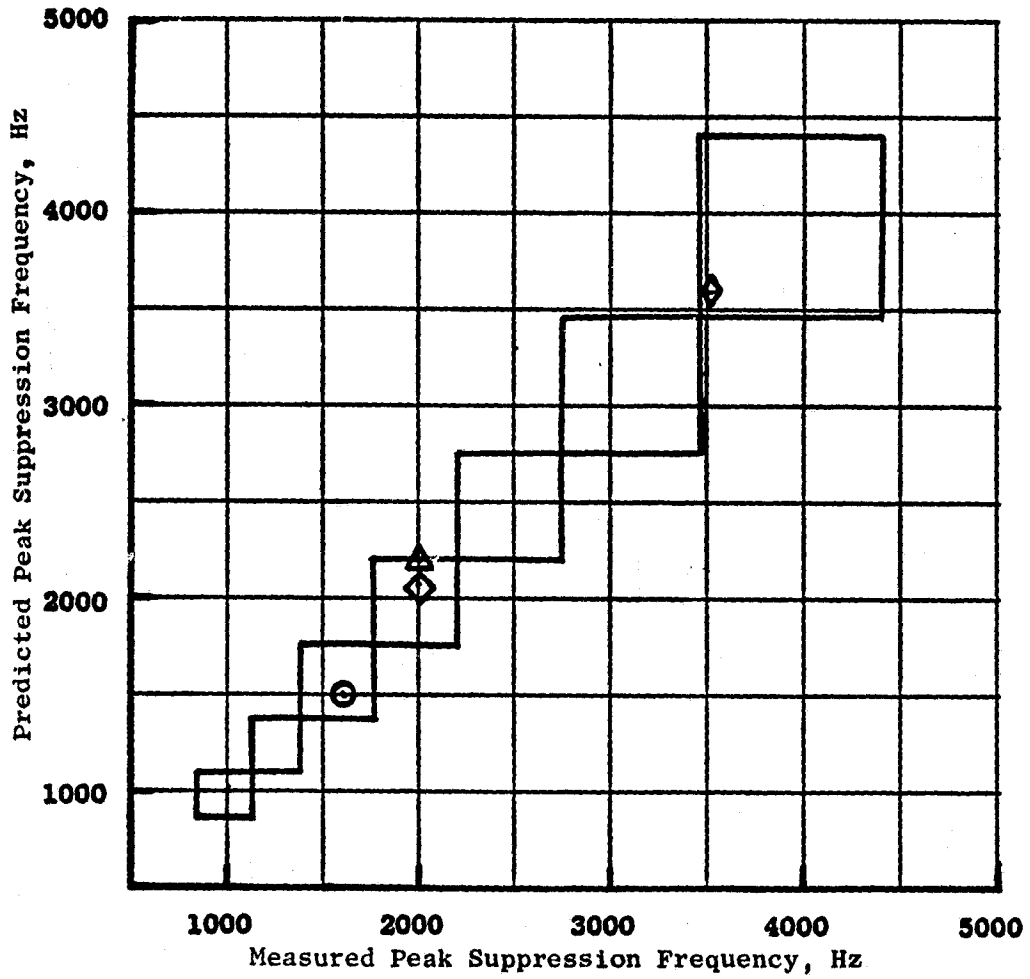


Figure 229. Comparison of Predicted Vs. Measured Frequency of Peak Attenuation.

For each of the configurations compared in Figure 229, Figures 230 through 237 give the actual measured 1/3-octave-band suppression levels and the reactance values from Figure 227 used to establish the predicted peak suppression frequency. Since the tone levels are usually suppressed at a much higher rate than the broadband noise suppression, the increased tone suppression values relative to the broadband suppression rate are indicated when applicable with each of the given suppression spectra. Broadband suppression levels are indicated at each of the tones. The broadband suppression was determined by taking the difference between the estimated broadband level at the tone for the unsuppressed and suppressed spectra.

2.2.2 Resistance

In the design of acoustic liners for engine exhaust ducts, there are some specific criteria for selecting the panel resistance. At the present time there is no such criteria for inlet panel designs. It was thought, based on simple resonator design equations, that an average resistance value of $1 \rho c$ would be a reasonable design objective. Five sets of test data were analyzed to determine if a correlation of resistance and suppression is evident. The five configurations evaluated were:

<u>Configuration</u>	<u>Type Material</u>	<u>Material Thickness</u>	<u>Faceplate Porosity, %</u>
Full-Scale Engine No. 1	Scottfelt 3-900	1.0 in.	22.5
Full-Scale Engine No. 2	Kevlar	0.75 in.	23.0
Scale Model Fan No. 1	Scottfelt 3-900	0.5 in.	28.0
Scale Model Fan No. 2	Scottfelt 3-900	0.25 in. (compressed to 0.18 in.)	30.0
Scale Model Fan No. 3	Scottfelt 3-900	0.775 in.	23.0

The test data were evaluated using peak broadband suppression divided by the ratio of treatment length to fan diameter ($\Delta dB/L_T/D_F$). This parameter was then adjusted for the ratio of fan diameter to peak suppressor frequency wavelength, D_F/λ . The resistance of the treatment panel was obtained from impedance tube data presented in Section 2.1. The resulting correlation is shown in Figure 238. The data show a trend toward peaking between 0.9 and $1.4 \rho c$; however, with this limited data it is not possible to draw a firm

- Scottfelt 3-900
- 60° Acoustic Angle
- 2650 RPM
- 1.0 in. Material Thickness
- $L_T/D_F = 0.47$
- 22.5% Faceplate Porosity

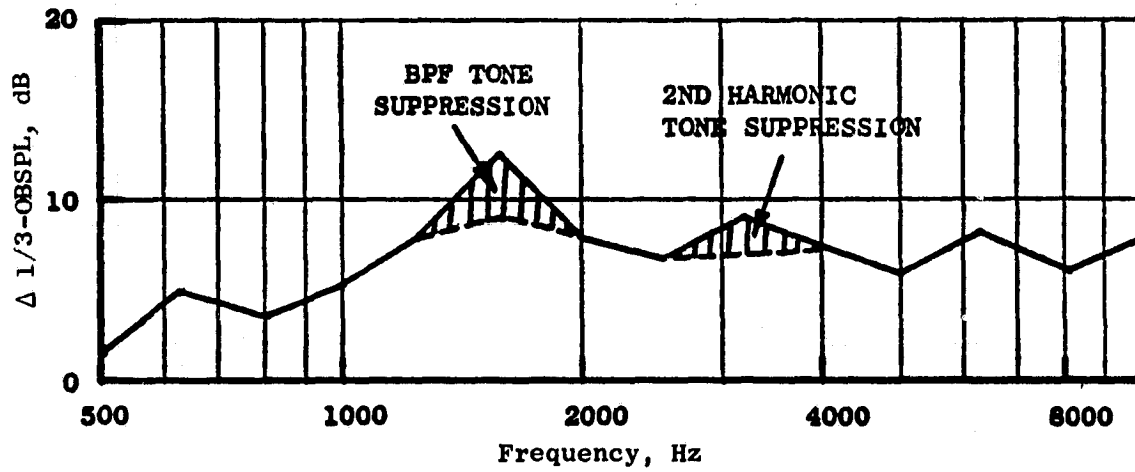


Figure 230. Full-Scale Engine No. 1 Suppression Spectrum.

- Scottfelt 3-900
- 1.0 in. Panel Thickness
- 22.5% Faceplate Porosity

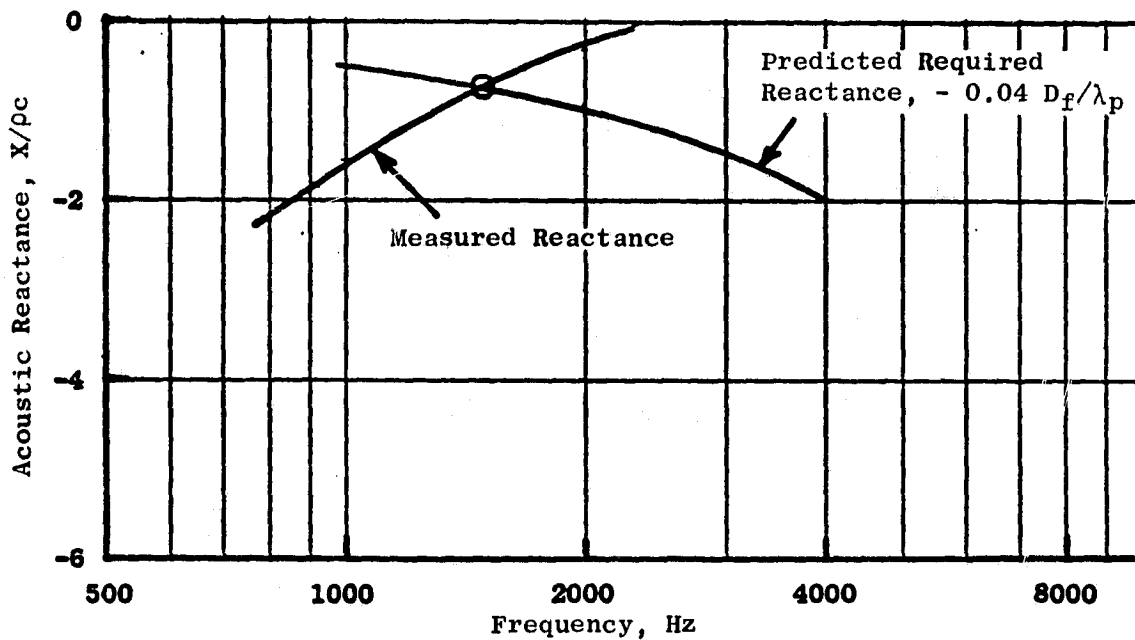


Figure 231. Comparison of Predicted Vs. Measured Peak Suppression Frequencies for Full-Scale Engine No. 1.

- Kevlar 29
- 60° Acoustic Angle
- 60% Corrected Fan Speed
- 0.75 in. Panel Thickness
- $L_T/D_F = 0.80$
- 23% Faceplate Porosity

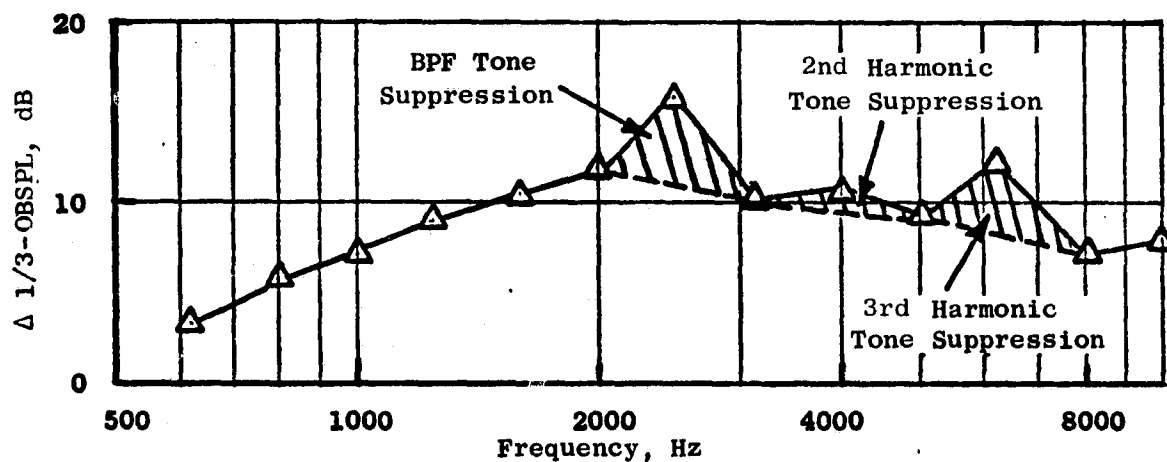


Figure 232. Full-Scale Engine No. 2 Suppression Spectrum.

- Kevlar 29
- 60° Acoustic Angle
- 60% Corrected Fan Speed
- 0.75-in. Panel Thickness
- $L_T/D_F = 0.80$
- 23% Faceplate Porosity

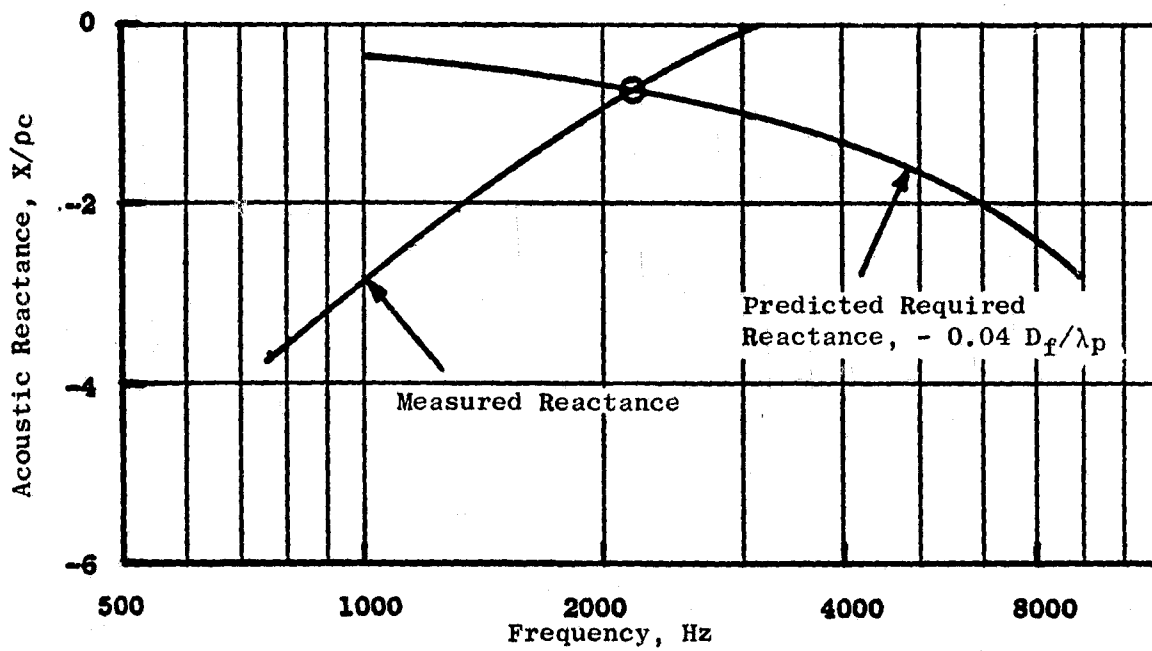


Figure 233. Comparison of Predicted Vs. Measured Peak Suppression Frequencies for Full-Scale Engine No. 2.

- Scottfelt 3-900
- Low Mach Inlet
- 0.5-in. Panel Thickness
- $L_T/D_F = 0.74$
- 70% Corrected Fan Speed
- 28% Faceplate Porosity

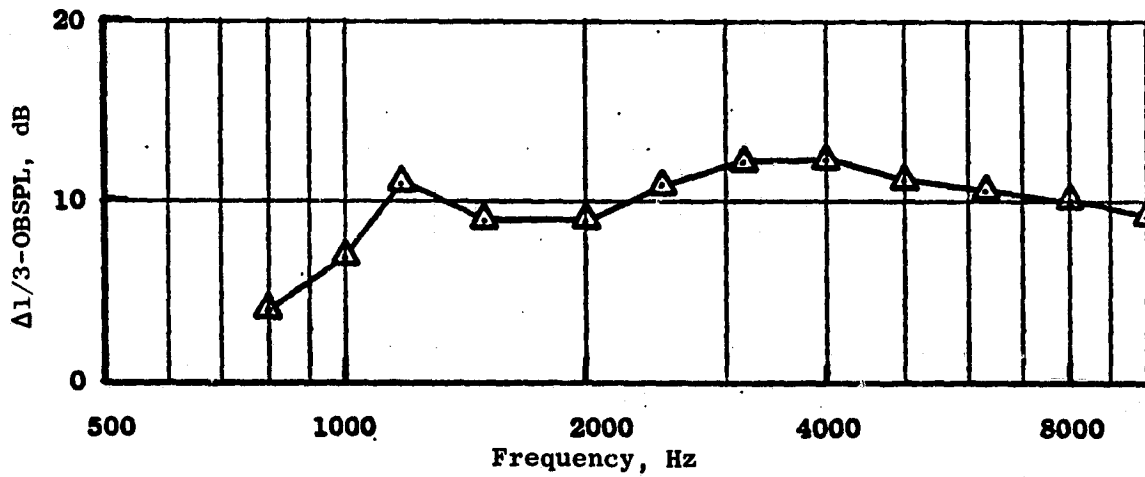


Figure 234. Scale Model Fan No. 1 Suppression Spectrum.

- Scottfelt 3-900
- Low Mach Inlet
- 60° Acoustic Angle
- 70% Corrected Fan Speed
- 0.5 in. Panel Thickness
- $L_T/D_F = 0.85$
- 28% Faceplate Porosity

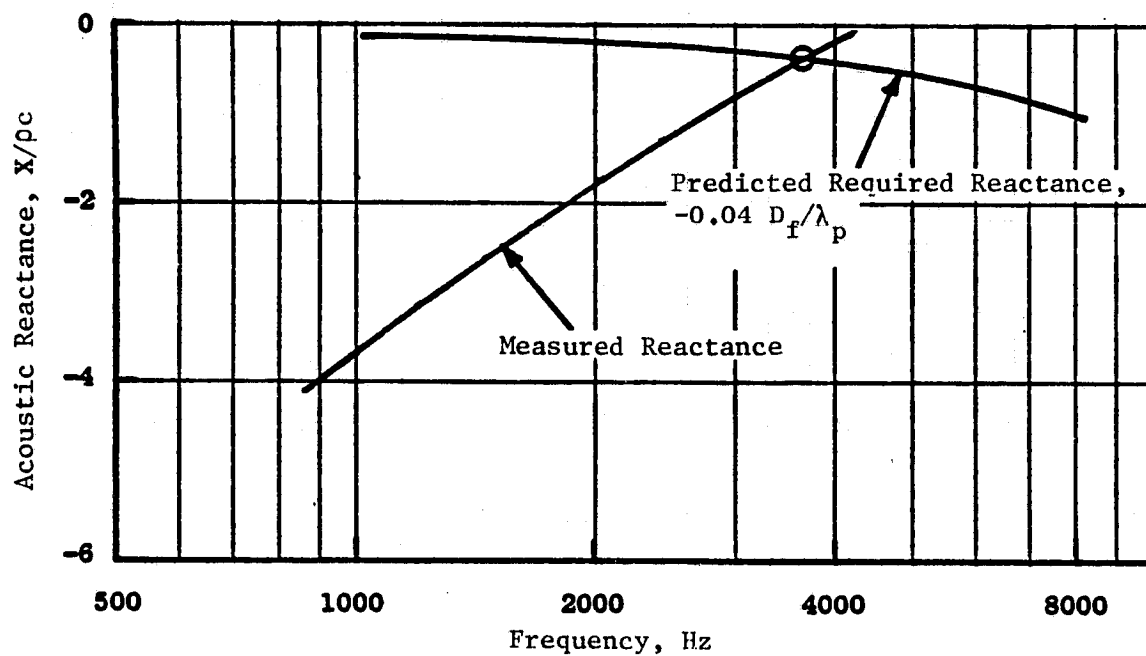


Figure 235. Comparison of Predicted Vs. Measured Peak Suppression Frequencies for Scale Model Fan No. 1.

- 60° Acoustic Angle
- 70% Corrected Fan Speed
- Scottfelt 3-900
- 30% Faceplate Porosity
- 0.25-in. Thick Material Compressed to Fit in 0.18-in. Depth Cavity
- $L_T/D_F = 0.57$

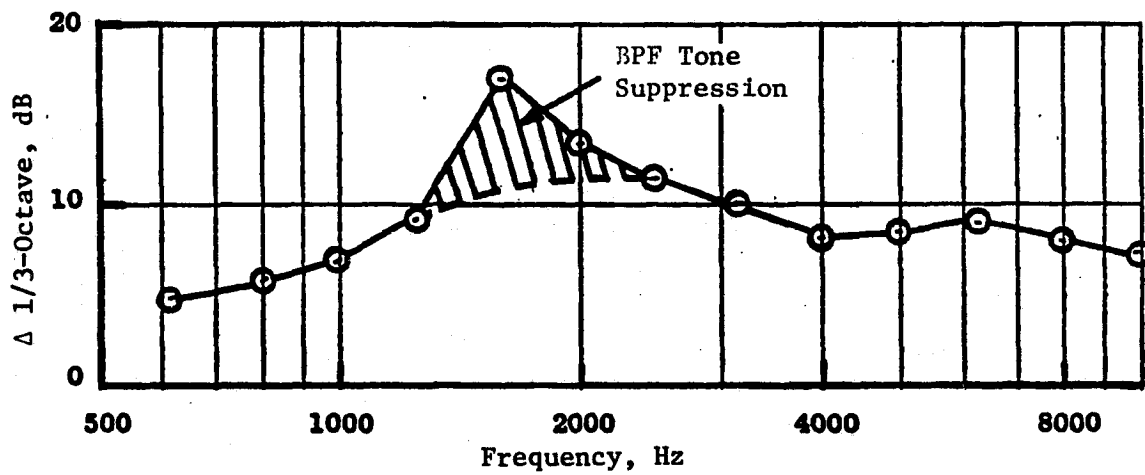


Figure 236. Suppression Spectrum for Scale Model Fan No. 2 Data Scaled to Full-Scale Engine No. 1 Size.

- 70% Corrected Fan Speed
- Scottfelt 3-900
- 30% Faceplate Porosity
- 0.25-in. Thick Material Compressed to Fit in 0.18-in. Depth Cavity
- $L_T/D_F = 0.58$

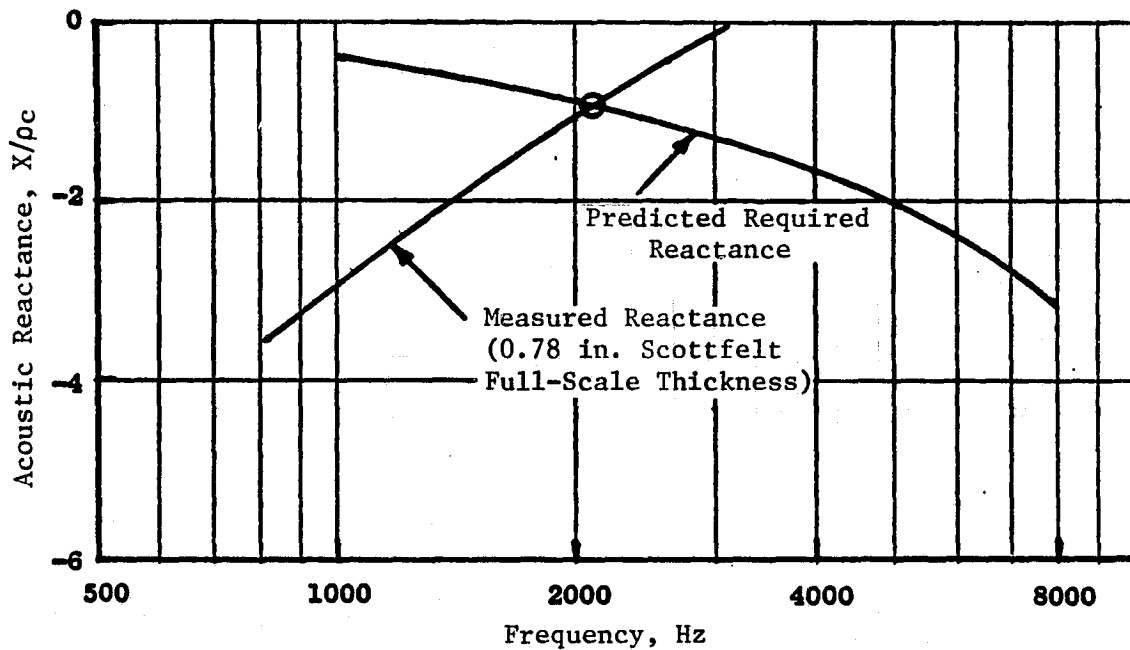


Figure 237. Comparison of Predicted Vs. Measured Peak Suppression Frequencies for Scale Model Fan No. 2 Data Scaled to Full-Scale Engine No. 1 Size.

- Scale Model Fan No. 3, Scottfelt
- △ Scale Model Fan No. 1, Scottfelt
- Scale Model Fan No. 2, Scottfelt
- ◇ Full-Scale Engine No. 1, Scottfelt
- ◻ Full-Scale Engine No. 2, Kevlar

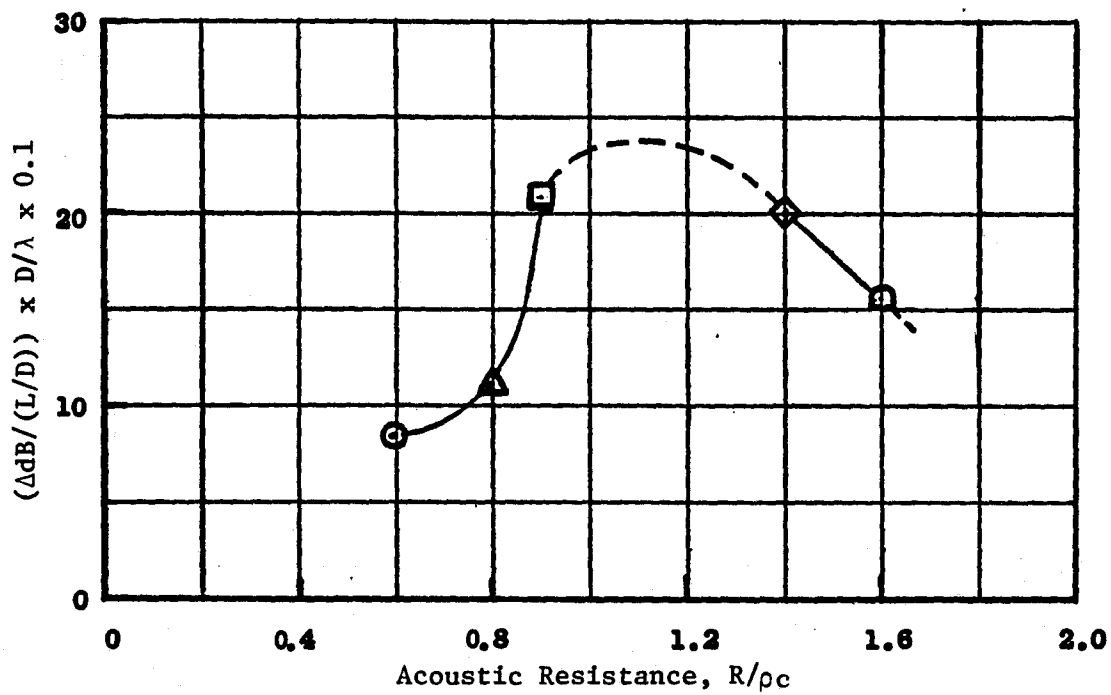


Figure 238. Inlet Treatment Suppression Rate Vs. Acoustic Resistance.

conclusion. The two test configurations with 0.9 and 1.4 ρc did provide more peak suppression than the other three, but other differences in the test configurations may be significant. Until further data can be obtained it is recommended that a design objective of 1.0 ρc be used for acoustic resistance.

Using 1 ρc as a design objective, Figures 239 and 240 were developed from the impedance tube data of Section 2.0 for Scottfelt and Kevlar, respectively. From these figures it is possible to select the material density for a given panel thickness. A band of resistance values from 0.8 to 1.2 ρc is shown, and designs falling within the band would be expected to perform as well as the data shown on Figure 238.

A compressibility factor is designated on Figures 239 and 240. In Figure 239 the compressibility scale indicates that the 0.5-in. thick uncompressed Kevlar material has a factor of 1.0 and a density of 0.7 lb/ft³. Two layers of 0.5-in. thick material fitted into a 0.5-in. core depth would have a factor of 2.0 and a corresponding density value of 1.44 lb/ft³. The compressibility for Scottfelt is shown on Figure 240. Here a compression factor of 1.0 represents the base material Scottfoam which has a density of 1.6 lb/ft³. This material can be obtained in different thicknesses having the density values shown and designated as SF 2-900, 3-900, etc.

- Type 973 (0.5 in. Thick/Layer Uncompressed)
- 22.5% Faceplate Porosity

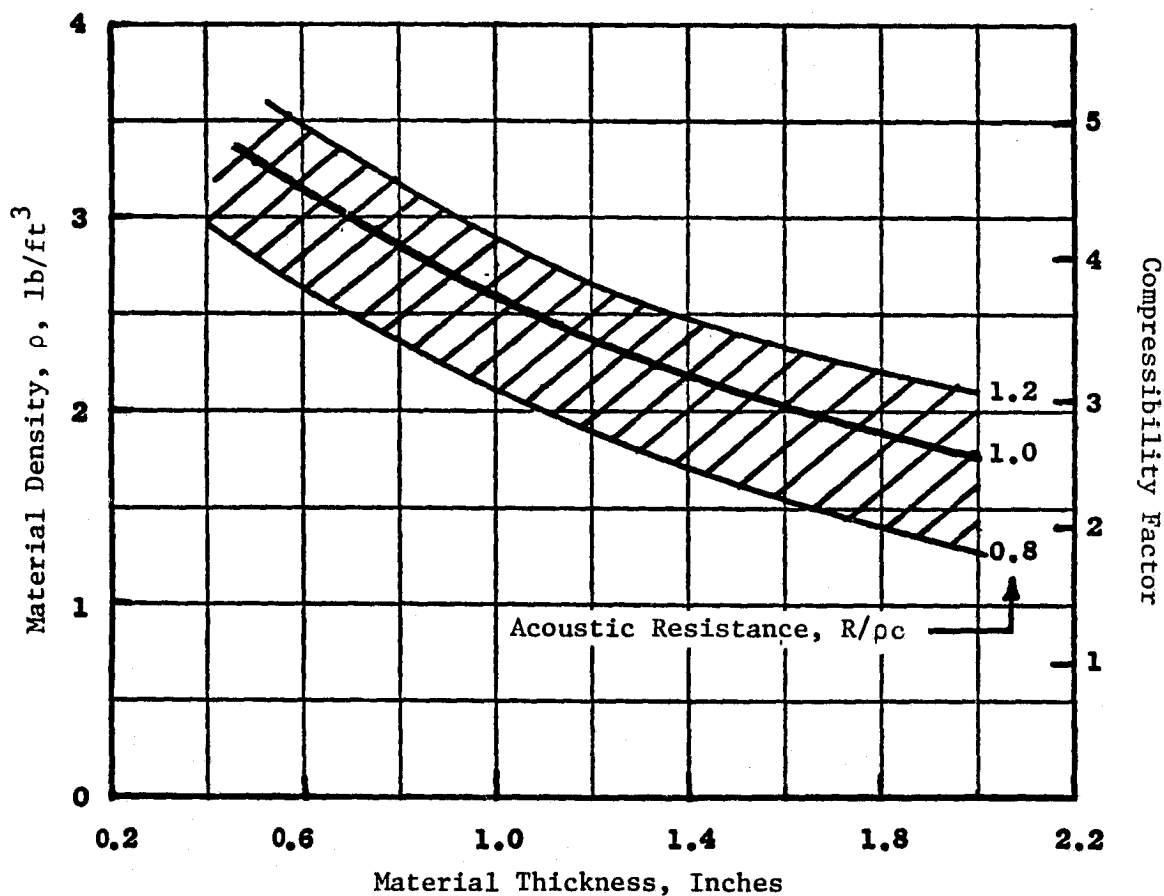


Figure 239. Acoustic Resistance as a Function of Material Thickness and Density for Kevlar 29.

● 22.5% Faceplate Porosity

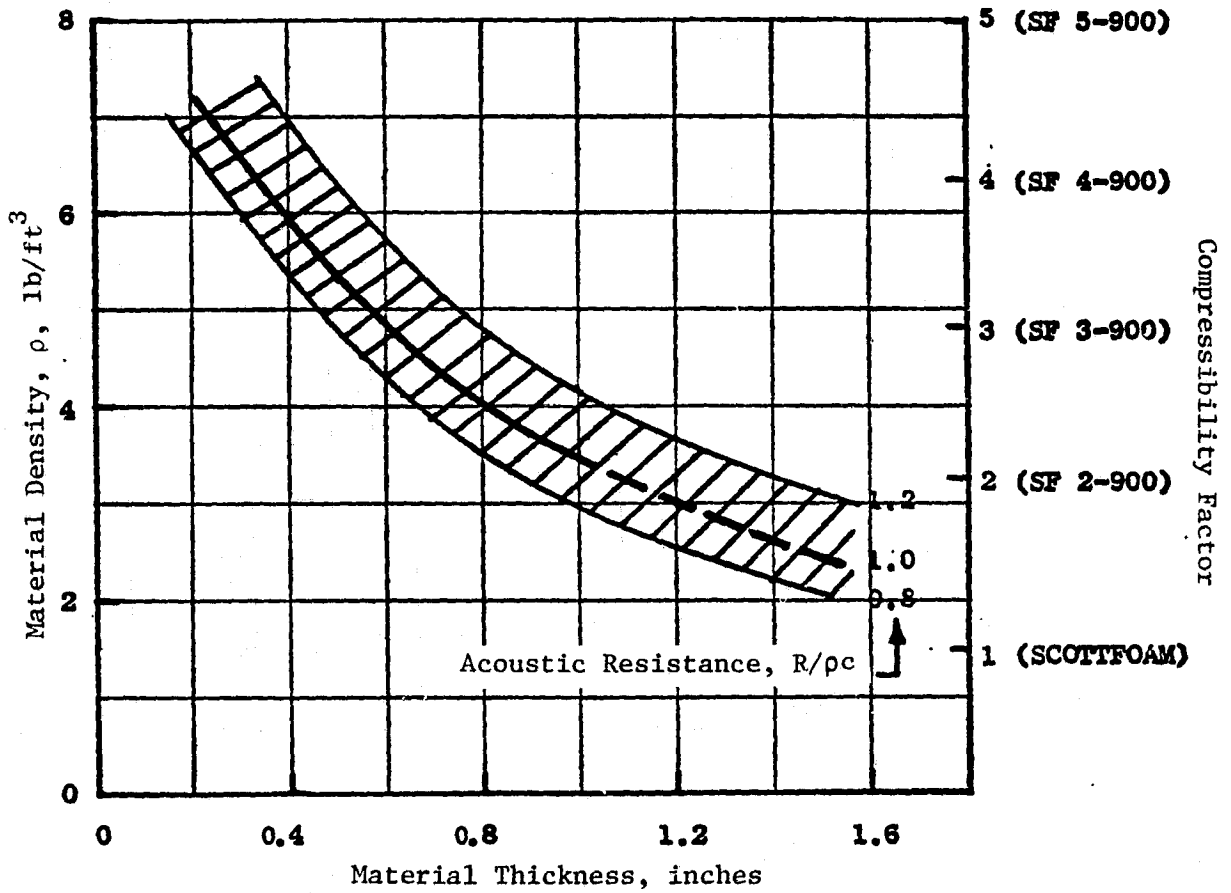


Figure 240. Acoustic Resistance as a Function of Material Thickness and Density for Scottfelt Materials.

3.0 DESIGN PROCEDURE

3.1 SUMMARY

A design procedure for bulk absorber inlet configurations has been evolved and is presented herein. The design method is based on the curves developed in Section 2.0. The procedure gives the information needed to define bulk absorber treatment designs consisting of Scottfelt or Kevlar-type materials.

A sketch depicting a typical bulk absorber treatment panel is given in Figure 241. Note that the material and panel thicknesses are not the same since the faceplate and backing thicknesses are included in the total panel depth. Previous design experience has shown that bulk absorber material should be compressed to fit within the panel. This keeps the material firmly in place and adds stiffness to the faceplate. Thus when selecting the material it should be thicker prior to installation than the final installed material thickness. The faceplate dimensions as given are typical examples of those used in previous panel designs.

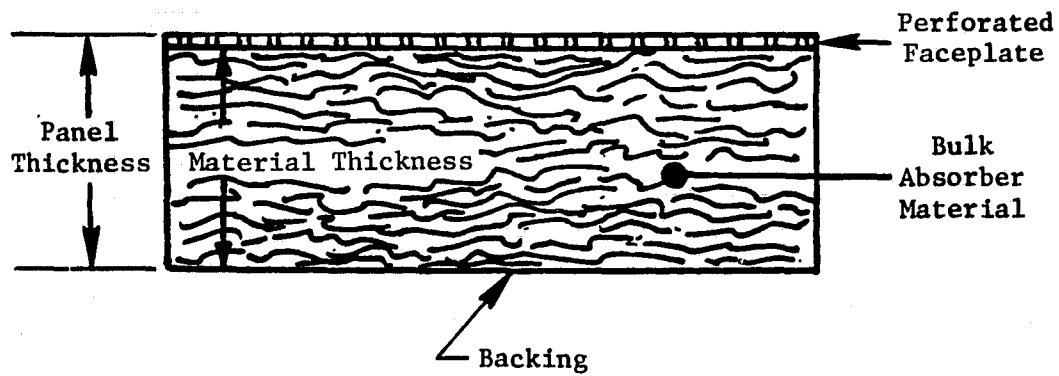
A summary of the steps that will be followed in the design procedure are as follows:

- Step 1: Determine the design frequency from the Noy-weighted unsuppressed spectrum.
- Step 2: Determine the treatment panel thickness.
- Step 3: Select the material density.
- Step 4: Define the faceplate porosity.

3.2 DETERMINATION OF FREQUENCY OF PEAK SUPPRESSION

It is essential in any treatment design procedure to know the spectral characteristics of the noise source that is to be suppressed. Jet engine noise levels are evaluated in terms of PNdB. Therefore, the suppressor system should be designed to effectively reduce the noise source at the highest weighted frequency in the PNdB calculation.

Figure 242 gives the PNdB Noy-weighting factors as a function of frequency that are to be added to the unsuppressed noise spectrum to define the frequency or frequencies that most control the noise level in terms of PNdB. An example of an unsuppressed fan noise spectrum with and without the Noy-weighting corrections are shown in Figure 243. The Noy-weighted spectrum shows the spectrum level being dominated at 2500 Hz. Thus the treatment design for this particular case would be the most effective in terms of suppression in PNdB if it is designed to give its peak attenuation at 2500 Hz.



Nominal Faceplate Design

- Porosity = 22.5% or Greater
- Thickness = 0.03 in. to 0.05 in.
- Hole Diameter = 0.0625 in.

Figure 241. Typical Bulk Absorber Treatment Panel.

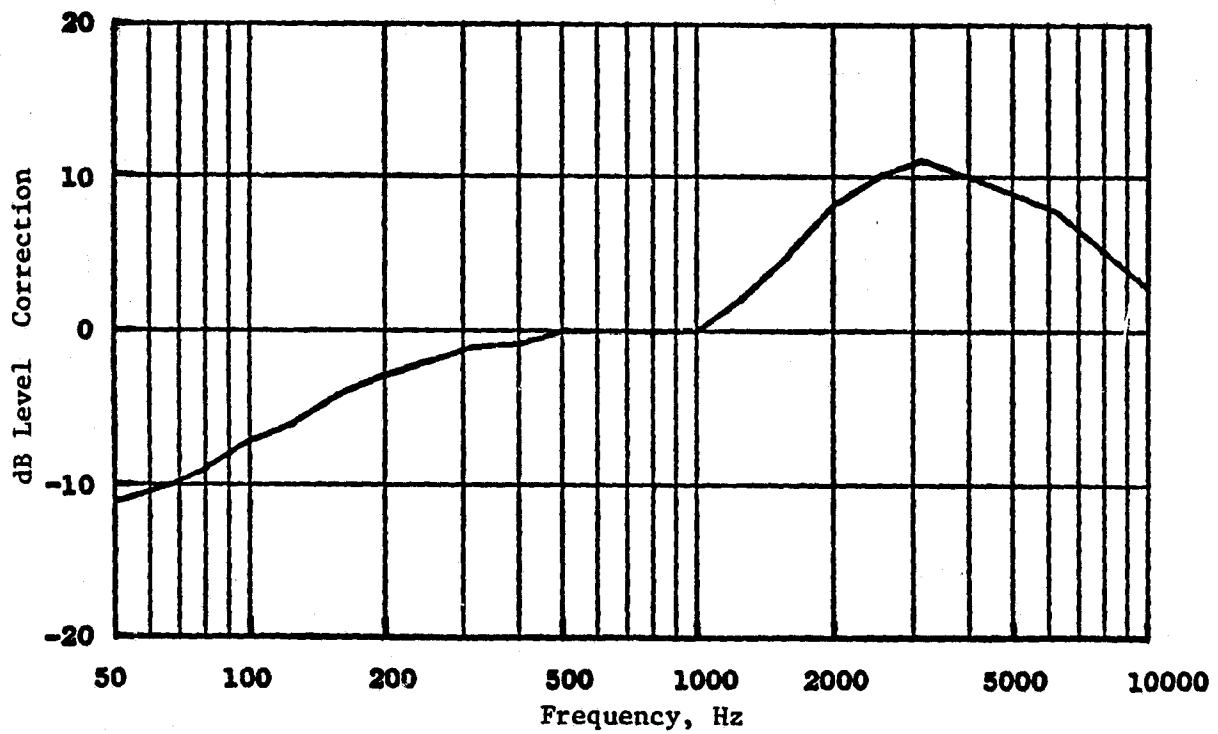


Figure 242. Noise Level Corrections Vs. Frequency for Obtaining Noy-Weighted Spectra.

● Max. Forward Angle

— Unsuppressed

- - - Unsuppressed,
Noy Weighted

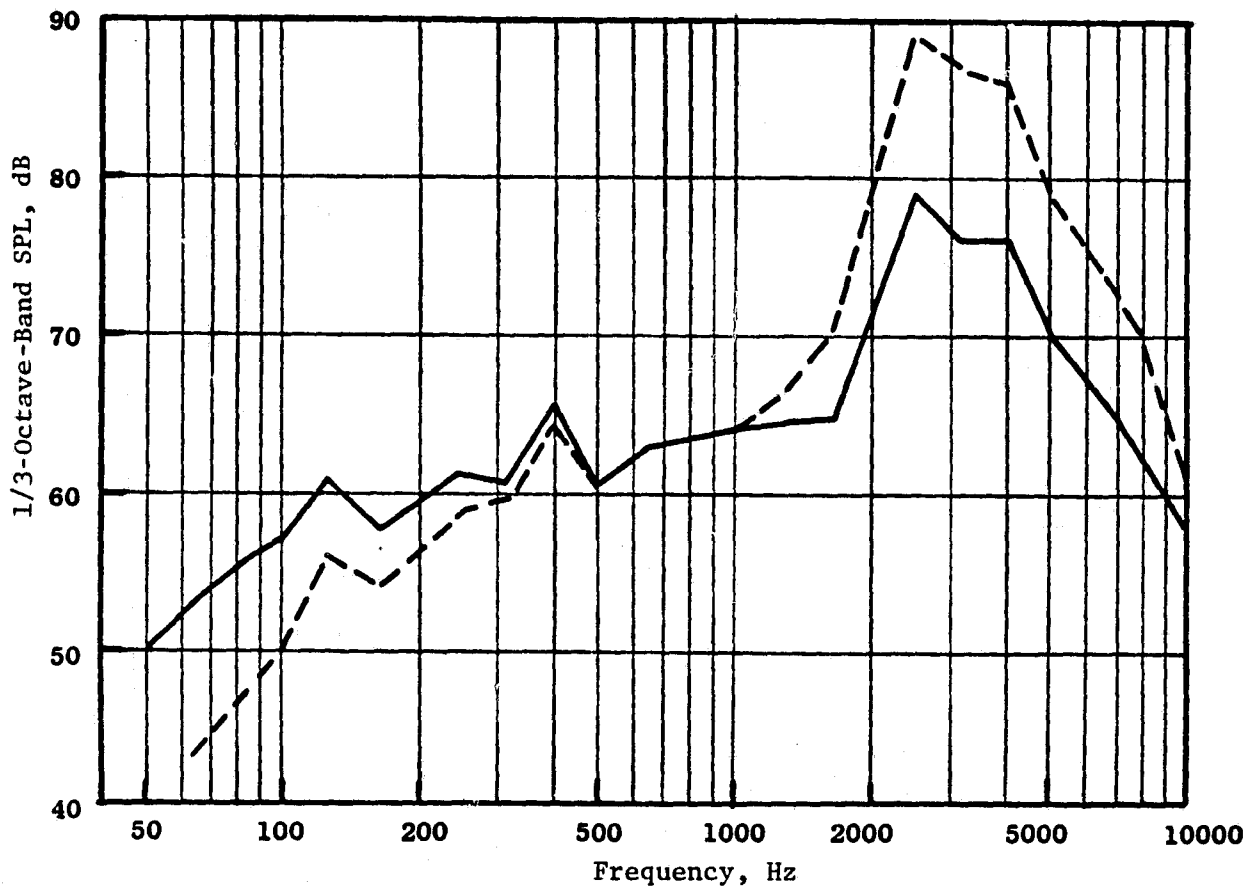


Figure 243. Typical Fan Inlet Noise Spectrum With and Without Noy-Weighted Factors.

3.3 DETERMINATION OF MATERIAL THICKNESS

The correlation given in Figure 244 enables the material thickness to be determined once the design frequency has been selected. The correlation defines the material thickness requirement as a function of:

- Fan Diameter
- Fan Inlet Mach Number

Upon entering Figure 244 with the above parameters identified, plus having selected the design frequency, the material thickness is then determined.

3.4 SELECTION OF MATERIAL DENSITY

Having determined the material thickness required to satisfy the panel tuning requirements, the next procedure in the design is to determine the thickness density combination for either Kevlar or Scottfelt needed to give the selected resistance. Given in Figures 245 and 246 are the acoustic resistance values for Kevlar and Scottfelt for different material density and thickness combinations. These two figures thus allow the density to be defined once the depth requirement has been determined. A range of resistance from 0.8 to 1.2 $R/\rho c$ is given. A nominal averaged resistance value of 1.0 $R/\rho c$ is recommended.

3.5 SELECTION OF FACEPLATE POROSITY

The purpose of the perforated faceplate is to contain the bulk absorber material. The objective is to have the plate fulfill this purpose and to offer an acoustic transparency to the incident sound wave. Based upon data presented and discussed in Section 2.0 of this report a faceplate porosity of at least 22.5% is recommended in all bulk absorber treatment panel designs. Porosity values less than this are not felt to be acoustically transparent and therefore could change the impedance characteristics of the bulk absorber materials.

3.6 SUPPRESSION

Determining the PNdB suppression that will be obtained with a given inlet is dependent upon many factors which cannot be defined in a specific design procedure and some of them are:

- Spectral content of the source
- Tone (blade passing frequency and harmonics) level relative to broadband noise

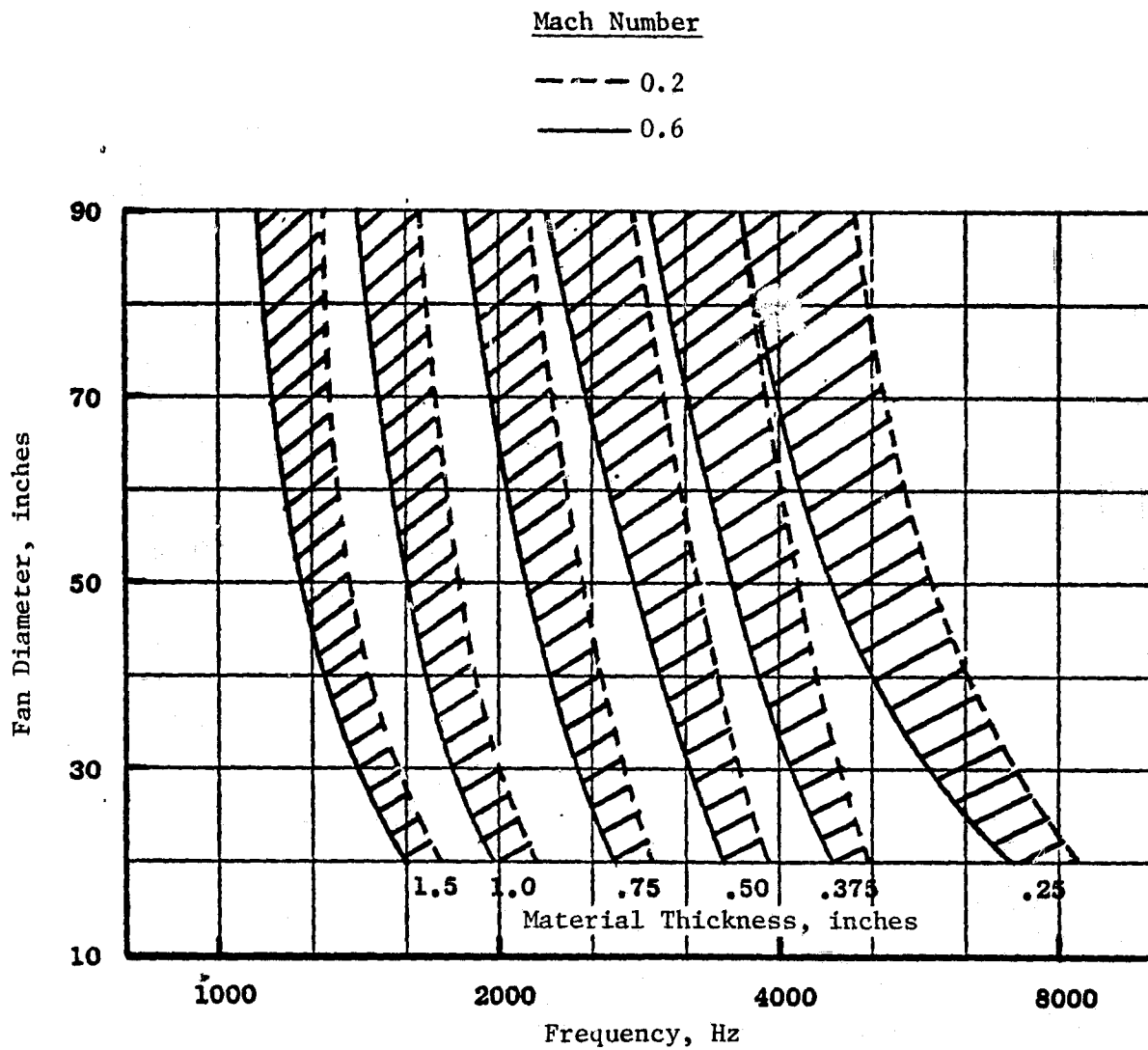


Figure 244. Bulk Absorber Thickness Requirement for Peak Suppression as a Function of Fan Diameter, Frequency, and Mach Number.

- Type 973 (0.5 in. Thick/Layer Uncompressed)
- 22.5% Faceplate Porosity

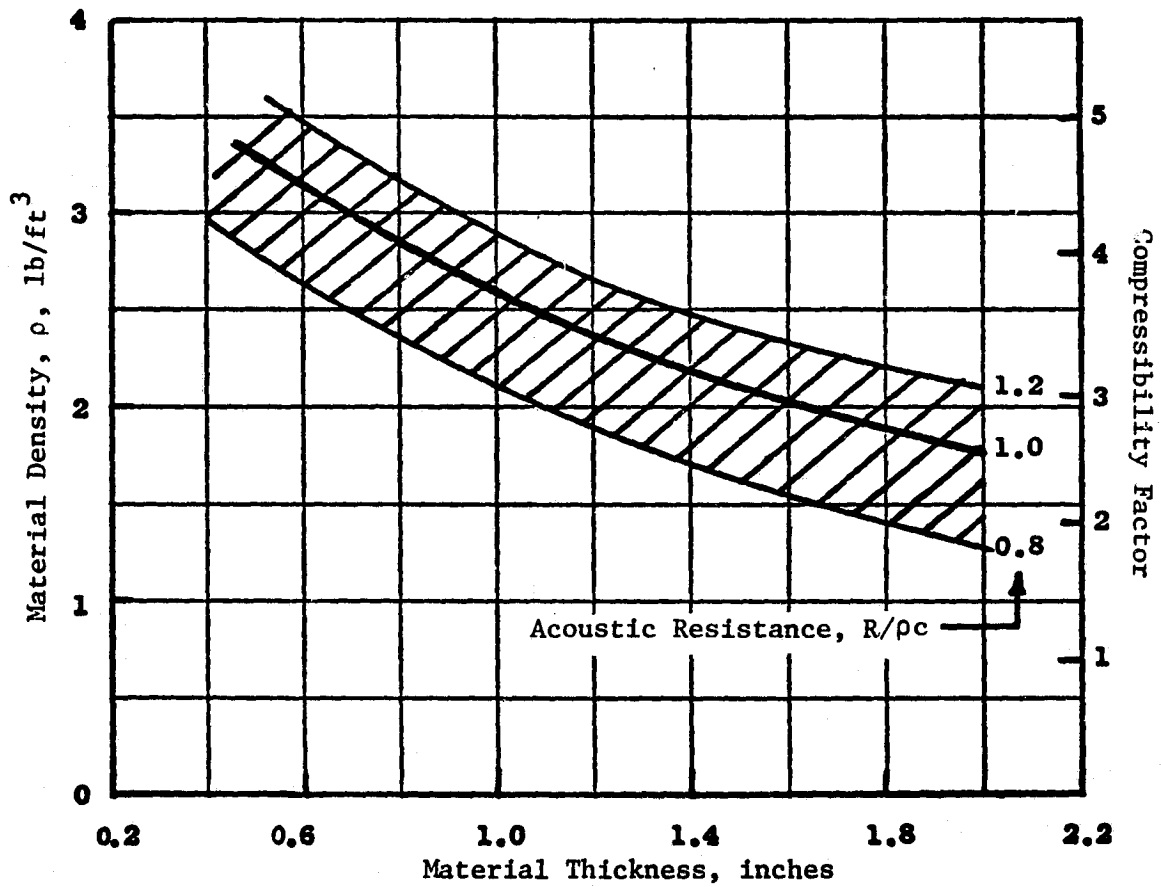


Figure 245. Acoustic Resistance as a Function of Material Thickness and Density for Kevlar 29.

● 2.5% Faceplate Porosity

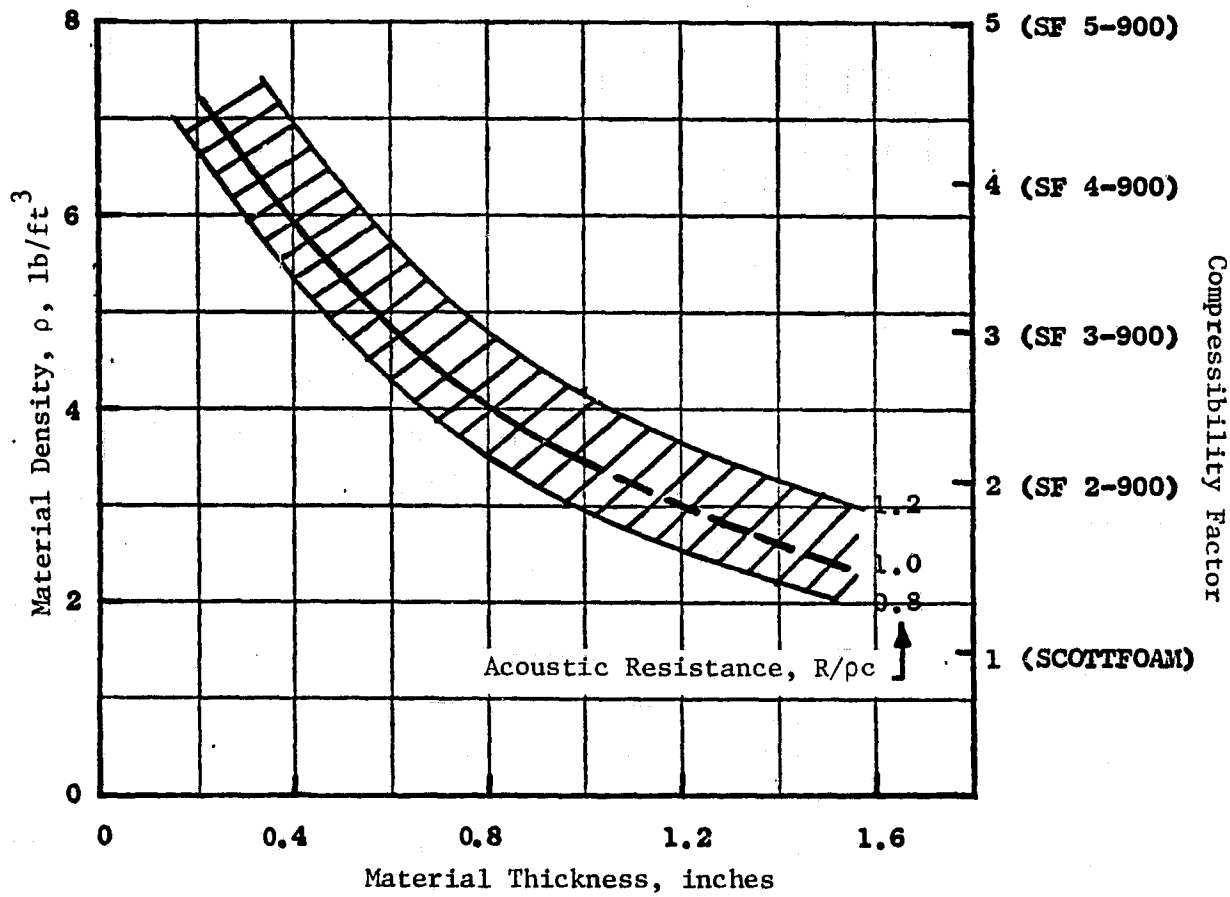


Figure 246. Acoustic Resistance as a Function of Material Thickness and Density for Scottfelt Materials.

- Radial distribution of the source noise in the inlet
- Length of inlet treatment
- Fan speed
- Acoustic angle of interest
- Other engine noise sources

As a general guide, the bulk absorber treatment will provide 2 to 5 PNdB more suppression than an equal length SDOF design. At approach power settings the difference will be larger than that obtained at the higher power settings. Multiple pure tones (MPT's) associated with high tip speed fans will be more affected by the increased suppression than low tip speed fans which do not have MPT's.

This general guideline applies to inlets with between 0.4 and 1.0 fan diameters of treatment length. Shorter lengths will have less increase simply because there is less suppression attainable. For example at 0.2 fan diameters of treatment an SDOF design may attain only 2-PNdB suppression. A bulk absorber design which might attain twice that is still only 2-PNdB more than the SDOF design. At longer treatment lengths the difference in bulk absorber and SDOF treatments decreases because both have such large suppression levels that only the lower order modes remain in the inlet and the wall treatment becomes less effective.

On a sideline basis, the suppression will vary with acoustic angle with the lower angles (relative to inlet axis) such as 20° and 30° having less suppression than that attained at 60° to 90°. The bulk absorber inlet will usually provide more suppression than the SDOF at all angles.

REFERENCES

1. Bilwakesh, K.R., and Clemons, A., "Acoustic Tests on a 50.8-cm (20-in.) Diameter Scale Model (1:3.5) Fan and Inlet for the Under-the-Wing Engine," General Electric Company, NASA CR-135117, to be Published.
2. Matta, R.K., and Kazin, S.B., "Core Engine Noise Control Program, Volume III, Prediction Methods," General Electric Company, FAA-RD-74-125, August 1974.
3. Stimpert, D.L. and McFalls, R.A., "Demonstration of Short-Haul Aircraft Aft Noise Reduction Techniques on a 50.8-cm (20-in.) Diameter Fan," Volume I, GE/NASA-Lewis Research Center, NAS3-18021, April 1975.
4. Rice, Edward J., "Spinning Mode Sound Propagation in Ducts with Acoustic Treatment and Sheared Flow," Paper to Aero-Acoustic Specialists Conference, Hampton, Virginia, March 24-26, 1975.
5. Groeneweg, John F., "Current Understanding of Helmholtz Resonator Arrays as Duct Boundary Conditions," NASA SP-207, 1969.
6. "Identification of Component Noise Sources, Core Engine Noise Control Program - Volume I," General Electric Company, August 1974.
7. "Prediction Scheme for Self-Generated Noise of Silencers," Internoise 72 Proceedings, Washington, D.C., October 4-6, 1972.
8. Adamson, A.F., "Quiet Clean Short-Haul Experimental Engine (QCSEE) Design Rationale," Society of Automotive Engineers, Air Transportation Meeting, Hartford, Connecticut, Paper No. 750605, May 6-8, 1975.
9. "Quiet Clean Short-Haul Experimental Engine (QCSEE), Preliminary Analyses and Design Report," NASA CR-134838 and CR-134839, December 23, 1974.
10. Sowers, H.D., Coward, W.E., "Quiet Clean Short-Haul Experimental Engine (QCSEE) Under-the-Wing (UTW) Engine Acoustic Design," NASA CR-135267, January 1978.
11. Sowers, H.D. and Coward, W.E., "Quiet Clean Short-Haul Experimental Engine (QCSEE) Over-the-Wing (OTW) Engine Acoustic Design," NASA CR-135268, March 1978.
12. Sowers, H.D., and Coward, W.E., "Quiet Clean Short-Haul Experimental Engine (QCSEE) Core Engine Noise Measurements," NASA CR-135160, December 1977.
13. Glaser, F.W., Wazyniak, J.A., and Friedman, R., "Noise Data from Tests of a 1.83-m (6-ft) Diameter Variable-Pitch, 1.2 Pressure Ratio Fan (QF9)," NASA TM X-3181, March 1975.

REFERENCES (Concluded)

14. Rice, E.J., "A Method for the Acoustic Impedance of a Perforated Plate Liner with Multiple Frequency Excitation," NASA TWX-67950, October 1971.
15. Harris, C.M., "Handbook of Noise Control," McGraw-Hill Book Company, 1957.
16. Bilwakesh, K.R., Clemons, A., and Stimpert, D.L., "Quiet Clean Short-Haul Experimental Engine (QCSEE) Acoustic Performance of a 50.8-cm (20-inch) Diameter Variable-Pitch Fan and Inlet, Test Results and Analysis," Volume I, NASA CR-135117, April 1979.